

Sheffield Hallam University

Thermo-analytical and spectroscopic characterisation of pore lining minerals in reservoir rocks.

CLEGG, Francis.

Available from the Sheffield Hallam University Research Archive (SHURA) at:

<http://shura.shu.ac.uk/19479/>

A Sheffield Hallam University thesis

This thesis is protected by copyright which belongs to the author.

The content must not be changed in any way or sold commercially in any format or medium without the formal permission of the author.

When referring to this work, full bibliographic details including the author, title, awarding institution and date of the thesis must be given.

Please visit <http://shura.shu.ac.uk/19479/> and <http://shura.shu.ac.uk/information.html> for further details about copyright and re-use permissions.

CITY CAMPUS, POND STREET,
SHEFFIELD, S1 1WB

101 585 616 0



REFERENCE

ProQuest Number: 10694360

All rights reserved

INFORMATION TO ALL USERS

The quality of this reproduction is dependent upon the quality of the copy submitted.

In the unlikely event that the author did not send a complete manuscript and there are missing pages, these will be noted. Also, if material had to be removed, a note will indicate the deletion.



ProQuest 10694360

Published by ProQuest LLC (2017). Copyright of the Dissertation is held by the Author.

All rights reserved.

This work is protected against unauthorized copying under Title 17, United States Code
Microform Edition © ProQuest LLC.

ProQuest LLC.
789 East Eisenhower Parkway
P.O. Box 1346
Ann Arbor, MI 48106 – 1346

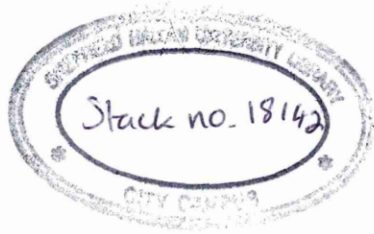
**Thermo-Analytical and Spectroscopic Characterisation
of Pore Lining Minerals in Reservoir Rocks**

Francis Clegg

A thesis submitted in partial fulfilment of the requirements of
Sheffield Hallam University
for the degree of Doctor of Philosophy

July 1998

Collaborating Organisation: Schlumberger Cambridge Research



DECLARATION

The work described in this thesis was carried out by the author in the Materials Research Institute, Sheffield Hallam University, between October 1994 and July 1998. The author declares that this work has not been submitted for any other degree. The work is original except where acknowledged by reference.

Signed:

(Francis Clegg)

Date:

7/10/98

Acknowledgements

Special thanks goes to my academic supervisors Dr C. Breen (mud-master I) and Prof. J. Yarwood (infrared-master) for their help, guidance and contagious enthusiasm throughout the work involved in this thesis. My thanks also goes to the staff at Schlumberger Cambridge Research, particularly Dr T. Hughes whose supervision skills were invaluable.

A big Cheers goes to the many friends I have made throughout my PhD research. The oldies include; Chris (spleech-master), Jason (running-master), Nigel (spurty-master), Reena (beer/smoke-master) and Sohail (unphased-master). The youngies include; Pete (moral-master), Delphine (radio-master), JP (squash-master), Carine (book-master), Claudia (drunk-master), Jane (mud master III), Chris C (Leeds-master), Pierre (chilli-master) and Jeff (mud-master IV).

All the staff at Sheffield Hallam University are also acknowledged for their assistance.

Finally, a whole lot of love and thanks goes to Joanne, whose support and patience has been tremendous.

Abstract

Two methods have been developed for the characterisation of sandstone and carbonate based hydrocarbon reservoir rocks. Particular emphasis has been directed towards determining the surface mineralogy in order to understand the flow of fluids through rocks.

The first method employs Diffuse Reflectance Infrared Fourier Transform Spectroscopy (DRIFTS) to distinguish the constituent minerals of a reservoir rock using characteristic bands in their vibrational spectra. Spectra collected from reservoir rocks that have undergone various sample preparations have shown that the spectra are weighted to the surface mineralogy. Spectra that are specific to the surface mineralogy have been obtained by sedimentation and ultrasonication techniques. The feasibility of applying partial least squares (PLS) modelling to DRIFTS spectra of reservoir rocks for quantitative analysis has been discussed. Application of PLS modelling to mixtures of powdered mineral standards has shown that it is possible to estimate the mineral constituents.

The second method uses organic molecules as chemical probes to elucidate the surface mineralogy of reservoir rocks. Clay mineral standards which have been exposed to certain chemical probes and subsequently heated show desorption profiles (monitored by thermogravimetric analysis (TGA)) that are characteristic for each mineral. The most suitable chemical probe studied so far is Dimethylformamide (DMF). The desorption profiles of DMF from Mg, Ca, Na and K exchanged montmorillonites are characteristic for each of the clays. Characteristic desorption maxima are observed at 420, 330, 220, 190°C, respectively. The desorption of DMF from Mg-SWy-2 within a powdered mixture of mineral standards can only be detected at the 5% level using TGA, whereas using infrared or mass spectrometry 2% can easily be detected with considerable scope for detecting smaller levels.

Extensive studies using Variable Temperature-DRIFTS and Variable Temperature x-ray diffraction on the complexes formed between both DMF and N-Methylformamide (NMF), and, Mg, Ca, Na and K-montmorillonites have shown that molecules retained at higher temperatures are located in the interlayer space and are associated with exchangeable cations via their carbonyl groups. Two layers of DMF and NMF are present in the interlayers at low temperatures which reduces to one upon heating to 50-170°C. NMF is found to be present in hydrogen-bonded clusters.

1) Introduction

1.1) Aims and Objectives	1
1.2) Characteristics of Reservoir Rocks	2
1.2.1) Sandstone rocks	2
1.2.2) Carbonates	5
1.2.3) Shale	6
1.3) Porosity and Permeability	6
1.4) The importance of surface mineralogy	7
1.4.1) Treatment fluids	10
1.5) Classification of minerals	13
1.5.1) Tectosilicates	13
1.5.1.1) Quartz	14
1.5.1.2) Feldspar	14
1.5.2) Phyllosilicates (Clay Minerals)	15
1.5.2.1) Structure	15
1.5.2.2) Clay Mineral Properties and Characteristics	17
1.5.2.2.1) Isomorphous substitution	17
1.5.2.2.2) Hydration/Swelling of a clay	18
1.5.2.2.3) Macroscopic properties	18
1.5.2.3) Clay Minerals of particular interest in this thesis	20
1.5.2.3.1) Kaolinite	20
1.5.2.3.2) Montmorillonite	20
1.5.2.3.3) Illite	21
1.5.2.3.4) Chlorite	22
1.5.3) Carbonates	22

2) Basic theory of techniques used in this thesis

2.1) Infrared Spectroscopy	24
2.1.1) Transmission	26
2.1.2) Diffuse Reflectance Infrared Fourier Transform Spectroscopy (DRIFTS)	27
2.1.2.1) Types of Reflectance	27
2.1.2.2) Instrumental and Optical Geometrics	30
2.1.2.3) Fundamental factors affecting diffuse reflectance	33
2.1.2.4) Quantification in DRIFTS	41
2.1.2.4.1) Reproducing the physical characteristics of a sample	41
2.1.2.4.2) Quantitative relationship between diffuse reflectance and sample concentration	42
2.1.2.5) Variable Temperature-DRIFTS	45
2.2) Multivariate Analysis - Partial Least Squares (PLS)	48
2.3) Thermogravimetric Analysis	51
2.4) Evolved Gas Analysis	
by Thermogravimetric -FTIR and Thermogravimetric -MS	52
2.5) X-ray diffraction and Variable Temperature-X ray diffraction	54
2.6) Scanning Electron Microscopy	55
2.7) X-ray Fluorescence	55

3) Traditional and Current methods of Characterising Minerals

3.1) X-ray Diffraction	57
3.2) Infrared Absorption Spectroscopy	58
3.3) Scanning Electron Microscopy	59
3.4) Chemical Analysis	60
3.5) Thermal Methods	60

4) Literature Survey and Strategy

4.1) Method 1: Characterisation by DRIFTS	65
4.1.1) Review of DRIFTS for Mineral Analysis	65
4.1.2) Advantages over transmission spectroscopy	67
4.1.3) Quantification with DRIFTS	68
4.1.4) Application of DRIFTS in this thesis	72
4.2) Method 2: Characterisation of pore lining minerals using 'Chemical Probes'	76
4.2.1) The 'Chemical Probe' Strategy	76
4.2.1.1) Chemical probe requirements	77
4.2.1.2) Instrumental techniques that could be used to detect a chemical probe	77
4.2.2) Review of organo-mineral interactions	79
4.2.2.1) Types of organo-mineral interactions	80
4.2.2.1.1) Typical smectite and organic molecule interactions	80
4.2.2.1.2) Typical kaolinite and organic molecule interactions	82
4.2.2.1.3) Other organo-mineral interactions	84
4.2.2.1.4) Factors affecting the adsorption of organic molecules onto minerals.	86
4.2.2.2) Methods used to analyse organo-mineral interactions	88
4.2.2.2.1) Thermal methods	88
4.2.2.2.2) X-ray diffraction	90
4.2.2.2.3) Infrared spectroscopy	90
4.2.2.2.4) Other techniques	92
4.2.3) Application of Chemical Probes in this thesis.	93

5) Results - The characterisation of sandstones and reservoir rocks by Scanning Electron Microscopy (SEM) and Diffuse Reflectance Infrared Fourier Transform Spectroscopy (DRIFTS)

5.1) Characterisation of minerals by DRIFTS	97
5.1) Experimental	97
5.1.1) Equipment	97
5.1.2) Mineral Standards preparation	98
5.1.3) Sample preparation	98
5.1.4) Collection of spectra	101

5.1.5) SEM	103
5.2) Interpretation of DRIFTS spectra obtained from ball milled sandstones, reservoir rocks and limestones	104
5.2.1) Berea sandstone	104
5.2.2) Birchover sandstone	115
5.2.3) Clashach sandstone	119
5.2.4) Stancliffe, York stone and Castlegate sandstones	119
5.2.5) Hollington Red sandstone	121
5.2.6) Summary of the components found in sandstones by DRIFTS	123
5.2.7) Reservoir rocks	125
5.2.8) Limestones	127
5.3) Analysis of whole rock as a function of particle size	132
5.3.1) Influence of particle size on the DRIFTS spectrum of Chelford sand	132
5.3.2) DRIFTS spectra of Chelford sand and kaolinite mixtures	133
5.3.3) Influence of particle size on the DRIFTS spectrum of Berea	135
5.3.4) Influence of particle size on the DRIFTS spectra of reservoir rocks	135
5.4) DRIFTS spectra of the minerals released from deconsolidated rocks	137
5.5) DRIFTS spectra of samples derived from ultrasonication of whole rocks	142
5.6) Direct analysis of rocks (cut/fractured surfaces)	145
5.6.1) Cut rock surfaces	145
5.6.2) Fractured rock surfaces	149
5.6.3) SEM studies of the two rock surface types	151
5.6.4) Methods to remove distortions in spectra	157
5.6.5) Effect of oil on the spectra of cut and fractured rock surfaces	161
5.7) Partial Least Squares (PLS)	162
5.7.1) Feasibility of PLS modelling	162
5.7.2) Application of PLS	165
5.7.3) PLS models	166
5.7.4) Summary	178

6) Results - Characterisation of pore lining minerals using chemical probes

6.1) Experimental	180
6.1.1) Chemical probes, mineral standards and sandstones studied	180
6.1.2) Exposure/Intercalation procedures	181
6.1.3) Instrumental Techniques	182
6.2) Thermogravimetric Analysis of untreated minerals	183
6.3) Thermogravimetric Analysis of powdered mineral standards treated with prospective chemical probes	188
6.3.1) TGA of N-Methylformamide/mineral complexes	188
6.3.1.1) Ca, Mg, Na and K-exchanged montmorillonite/NMF complexes	188
6.3.1.2) TGA of kaolinite/NMF complexes	199
6.3.1.3) TGA of illite/NMF complexes	204
6.3.1.4) TGA of chlorite, quartz, feldspar and carbonates exposed to NMF vapour	206
6.3.2) TGA of Dimethylformamide/mineral complexes	207

6.3.2.1) TGA of Ca, Mg, Na and K-exchanged montmorillonite/DMF complexes	207
6.3.2.2) TGA of kaolinite exposed to DMF	216
6.3.2.3) TGA of illite/DMF complexes	218
6.3.2.4) TGA of chlorite, quartz, feldspar and carbonates exposed to DMF vapour	220
6.3.3) TGA of other chemical probe/mineral interactions	221
6.4) Evolved Gas Analysis	225
6.4.1) Evolved Gas Analysis of DMF alone	225
6.4.2) EGA of individual clay mineral and DMF complexes	240
6.4.2.1) SWy-2 and Mg-SWy-2/DMF	240
6.4.2.2) Illite and illite/DMF	249
6.4.3) Mixtures of minerals	253

7.) Results - Characterisation of the chemical probe-clay mineral complexes

7.1) Experimental	266
7.1.1) Variable Temperature-DRIFTS	266
7.1.2) Variable Temperature-XRD	267
7.1.3) Fourier-self deconvolution	268
7.1.4) Molecular modelling	268
7.2) VT-DRIFTS and VT-XRD of the X-SWy-2/NMF and X-SWy-2/DMF complexes	269
7.2.1) VT-DRIFTS analysis of the Ca-SWy-2/NMF complexes.	271
7.2.2) VT-DRIFTS analysis of Mg, Na and K-SWy-2/NMF complexes.	290
7.2.3) Carbonyl stretching region of the X-SWy-2/NMF complexes.	302
7.2.4) VT-XRD analysis of X-SWy-2/NMF complexes.	312
7.2.5) Summary of X-SWy-2/NMF complexes.	317
7.2.6) Molecular modelling of Na and Mg montmorillonite/NMF complexes.	329
7.2.7) VT-DRIFTS analysis of the Ca, Mg, Na and K-SWy-2/DMF complexes.	334
7.2.8) Carbonyl stretching region of the X-SWy-2/DMF complexes.	351
7.2.9) Summary of the X-SWy-2/DMF complexes	357
7.3) The use of infrared spectroscopy to map the surfaces of reservoir rocks.	361

8) Conclusions

8.1) Characterisation of Minerals by DRIFTS	363
8.2) Characterisation of Minerals using Chemical Probes	364
8.3) Considerations for Future Work	365
8.4) Other Methods	367
8.5) Conferences Attended	369

9) References

Appendix 1: A1) DRIFTS spectra of ball milled reservoir rocks	381
--	------------

1) Introduction

1.1) Aims and Objectives

The research in this PhD thesis has been undertaken in collaboration with Schlumberger Cambridge Research (SCR) and is concerned with the characterisation of hydrocarbon reservoir rocks.

A knowledge of the surface properties of reservoir rocks is highly important in the recovery of oil, especially when complex multicomponent treatment fluids are applied to the reservoirs in order to enhance the extraction of oil. One key property of the reservoir rock surface is its mineralogical composition. Previously, the methods of characterising reservoir rocks have focused on the determination of bulk composition. One such technique is X-ray Diffraction (XRD), which is used routinely. An exception is Scanning Electron Microscopy (SEM), which has the ability to distinguish the surface mineralogy from the bulk mineralogy. The work described in this thesis is concerned with the development and evaluation of new characterisation methods which will be able to ascertain the surface mineralogy. The minerals that a fluid can come in contact with when pushed through a rock are termed the surface mineralogy and the whole composition of the reservoir rock is termed the bulk mineralogy.

The main programme of research has focused on developing two characterisation methods. The first method employs an infrared technique, Diffuse Reflectance Infrared Fourier Transform Spectroscopy (DRIFTS), which can distinguish the constituents of a reservoir rock from differences in their vibrational spectra. This technique has been applied to several sandstones which have undergone various sample preparations. The intention is that the spectra obtained can be used to determine the surface mineralogy.

The second method aims to use organic molecules as 'chemical probes' to elucidate the surface mineralogy of the rock. If the 'chemical probe' associates itself with a particular constituent of a sandstone, under certain conditions, then the probe may be used to identify the particular constituent. The first objective of this method is

therefore to find a suitable chemical probe that meets the requirements. A wide range of techniques could be suitable for the detection of the chemical probes, but research in this thesis has considered the following techniques:

- i) Thermogravimetric Analysis,
- ii) Evolved Gas Analysis - Fourier Transform Infrared Spectroscopy (EGA-FTIR),
- iii) Evolved Gas Analysis - Mass Spectrometry (EGA-MS).

SEM, XRD and Infrared Spectroscopy have been employed to provide corroborative evidence to support the DRIFTS work and the chemical probe study.

1.2) Characteristics of Reservoir Rocks.

Petroleum (crude oil and gas) is a naturally occurring complex of hydrocarbons widely distributed in the sedimentary rocks of the earth's crust. Any rock that possesses the ability to contain and to yield oil, or gas, or both in commercial quantities is termed a reservoir rock. Most commercial reservoirs of oil and gas occur in two dominant rock types, namely, sandstones and carbonates. Another less common type is shale. Compositionally and structurally, sandstones and carbonates are two very distinct types of rock. Understanding the differences between them is vital for successful oil/gas exploration.

1.2.1) Sandstone Rocks

The basic descriptive element of all sedimentary rocks is the grain size. Several grain size scales have been proposed but one which is widely used and accepted is that of Udden and Wentworth [1]. According to this scale the dominant grain size of a sandstone should be between 62.5 μ m and 2mm.

Sandstone rocks are classified into three principal types according to their composition:-

- I) those totally dominated by quartz grains,
- II) those containing significant quantities of unweathered feldspar,
- III) those with high contents of clay minerals.

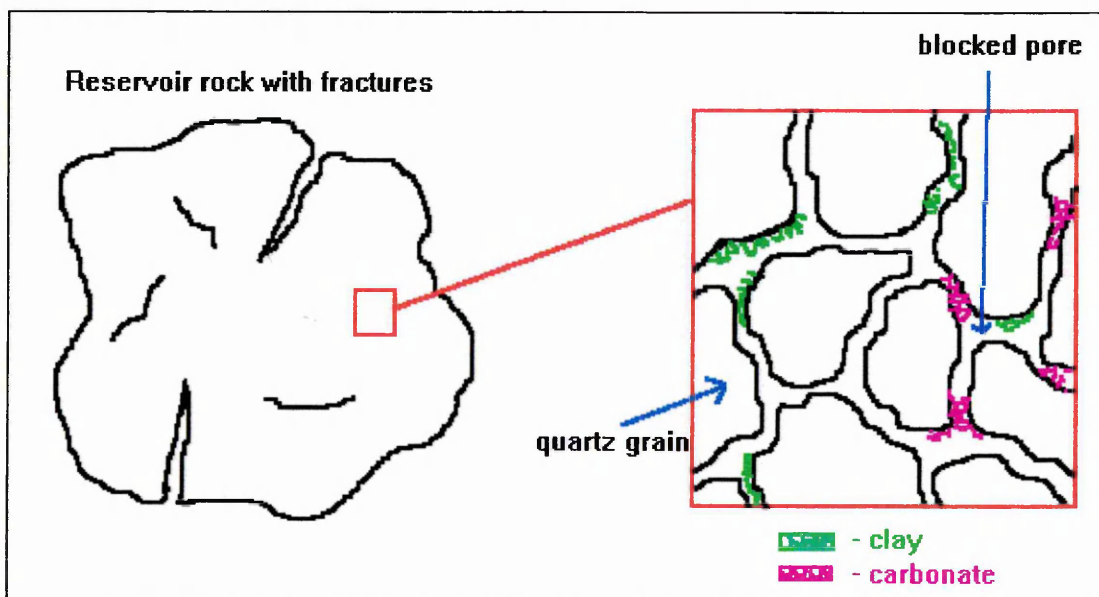
Table 1.1 shows the typical percentage composition of minerals present within each sandstone type.

Table 1.1: Typical mineral percentages in sandstones.

Mineral	Percentage Composition		
	Type I	Type II	Type III
Quartz	100%	75-99%	≈65%
Feldspar	0%	1-25%	5-25%
Clay Minerals	0%	0%	1-20%

Table 1.1 shows that quartz grains are the major building blocks of a sandstone rock. These are present in various irregular shaped sizes. If feldspar grains are present, they will be found mixed in with the quartz grains. When clay minerals and carbonates are present, they hold together the quartz and feldspar grains acting like a cement. There are several types of clay minerals of varying crystal structure. Kaolinite, montmorillonite, illite and chlorite are the most commonly occurring clay minerals found in sandstone rocks. The resulting network of grains, carbonate and clay minerals (figure 1.1) is never sustained because diagenetic processes occurring throughout its life-span constantly modify it.

Figure 1.1: Network structure of sandstones.



Diagenetic processes in reservoir rocks result in either an introduction of material into the pore spaces or creation of pore spaces by removing material from the body of the rock. Some of these processes include; compaction, dissolution and replacement. They are very important since they can affect a rock's porosity and permeability (these are properties that control a sediment's potential as a reservoir for oil or gas, see section 1.3).

Compaction is a physical process arising from the mass of overlying sediment, which basically results in a closer packing of grains, local fracturing and bending of weak grains. Dissolution occurs more commonly to feldspar grains rather than quartz grains because they are chemically less stable and can react with the waters present in the reservoir. The reaction leads to dissolution and breakdown of the grains, which can also happen to unstable quartz grains. The release of ions from the dissolution can result in the formation of clay minerals and cements (carbonates) in the place of, or adjacent to altered grains. Alternatively the ions may be carried in solution until chemical and physical conditions favour their precipitation. Which clay or cement is formed depends on the mineral being altered to it and the character of the altering fluid. For example, the derivation of kaolinite can occur from potassium feldspars by the removal of the soluble bases, or it can derive from mica, a common minor constituent of sandstones. The latter process requires a high throughput of water of low ionic strength and low pH. The further alteration of kaolinite to illite, on the other hand, requires a source of potassium. Clay minerals and silica cements may of course be allogenic rather than authigenic, i.e. introduced into the sandstone from an outside source rather than generated within it.

Individual sandstone bodies are markedly restricted in size, being lenticular or linear in overall shape. Sandstone reservoirs are commonly less than 25m thick and less than 250km² in area. Very large productive reservoirs are necessarily multiple consisting of complexes of interlocking river channels separated from one another by hydraulic barriers of shale.

1.2.2) Carbonates

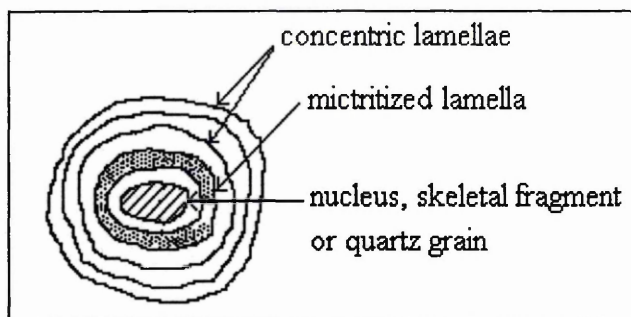
Carbonates are the accumulations of the remains of carbonate-secreting animals and plants and thus biological and biochemical processes dominate their formation. Once deposited, the chemical and physical processes of diagenesis can considerably modify the carbonate sediment.

In carbonates, two calcium carbonate minerals predominate, namely aragonite and calcite. Dolomite ($\text{CaMg}(\text{CO}_3)_2$) may also develop within carbonate sediment. Carbonates are very varied in composition but broadly the components can be divided into four groups:-

- i) non-skeletal grains
- ii) skeletal components
- iii) micrite
- iv) cement

The principle non-skeletal grains in carbonates are ooids, peloids and aggregates. Ooids are spherical-sub-spherical grains consisting of one or more regular concentric lamellae around a nucleus, often a carbonate or quartz grain (figure 1.2).

Figure 1.2: Diagrammatic representation of an ooid.



Although the term ooid has been restricted to grains less than 2mm in diameter, the majority of ooids range from 0.2-0.5mm in diameter. Aggregates consist of several carbonate particles cemented together by a microcrystalline cement or bound by organic matter.

The skeletal components of a carbonate are a reflection of the distribution of carbonate-secreting invertebrates through time and space. The main skeletal contributors to carbonates are discussed in reference [1].

Many carbonates have a fine grained usually dark matrix or are composed entirely of fine grained carbonate. This fine grained material is known as micrite (microcrystalline calcite) and has a grain size generally less than $4\mu\text{m}$.

It is not uncommon to find carbonates that have been dolomitized. This involves the conversion of CaCO_3 minerals into dolomite, $\text{CaMg}(\text{CO}_3)_2$, and may take place either soon after or a long time after deposition. Carbonate rocks are classified on the basis of dolomite content into:-

	% Dolomite
Limestone	0-10
Dolomitic limestone	10-50
Calcitic dolomite	50-90
Dolomite	90-100

1.2.3) Shale

Shale is a widely and often loosely used field term for mudstone which shows a conspicuous fissility on weathering (fissility is the property of splitting into thin sheets). A mudstone is a lithified sediment in which grains of sand ($62.5\mu\text{m}$ or larger) are absent or form an insignificant part. The major constituent is clay, which refers to particles less than $4\mu\text{m}$ in diameter. The typical size of clay minerals is less than $2\mu\text{m}$ but they may reach $10\mu\text{m}$ or more. Typical clay mineral examples will be discussed in more detail in section 1.5.

1.3) Porosity and Permeability

The ability to extract oil or gas from a reservoir rock is governed by its porosity and permeability. An understanding of these properties is therefore highly important. Since the surface mineralogy in a rock is a factor that can change its porosity and permeability a knowledge of this is also highly important.

Porosity arises from the void space in reservoir rocks and provides a place for the accumulation of oil and gas deposits. The porosity in the rock gives the rock its

characteristic ability to absorb and hold fluids. Permeability is the measure of the ease with which a fluid flows through a reservoir rock and is defined using Darcy's law. From Darcy's law permeability (K) depends on the rate (Q) at which fluid flows through a unit cross-section of rock:

$$Q=(K/\mu)(dp/dl),$$

where μ is the fluid viscosity and dp/dl is the pressure gradient in the direction of flow. A fluid can undergo two main routes, it can either go through a fracture in the rock or work its way through the network of grains. When the fluid goes through the network of grains it can encounter blocked pores. A blocked pore is a void within the sandstone that is inaccessible to fluids and can arise from:-

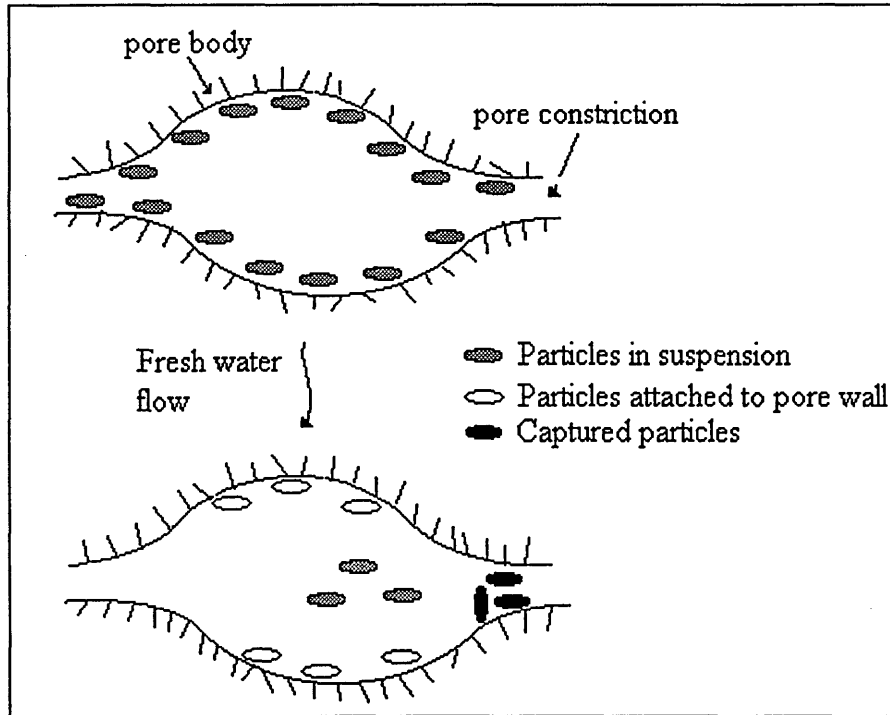
- i) the formation of cement at a pore throat,
- ii) the growth of a clay mineral blocking a pore throat,
- iii) the movement of clay minerals (fines) which then block a pore throat.

The displacement of fines (figure 1.3) can occur by simply replacing the saltwater present in a pore by fresh water [2]. Entrapment of the fines at the pore throats then occurs which can cause the pores to block and hence change the porosity and permeability. This has also been shown by Azari et al. [3] who flushed cores of Berea sandstone with brine. Berea is a quarry sandstone that contains both montmorillonite and illite. It was found that both clay minerals moved even though migration was only expected for montmorillonite. Blocked pores usually account for about 10-20% of the total pore volume and are not accessible to fluids pumped down a well.

1.4) The Importance of the Surface Mineralogy

The aim of this thesis is to develop methods that can determine the surface mineral content of a reservoir rock. In particular, these methods need to be quick, accurate and be able to distinguish between the surface and bulk mineralogy. This research is being undertaken because it forms part of a general strategy (within Schlumberger Cambridge Research) of improving the understanding of fluid flow through reservoir rocks. A knowledge of fluid flow is necessary because when the production of oil from a reservoir begins to decline, complex multicomponent treatment fluids may be used to enhance the recovery. There are many types of treatment fluids [4, 5] and

Figure 1.3: Movement of fines resulting from a change in pore fluid.



each one has a different role (an example will be discussed later in this section). The choice of treatment fluid to be used in the enhancement of oil recovery depends on the nature of the rock in the reservoir. Thus, a knowledge of the type of rock present is a necessity.

Once a method that can determine the surface mineralogy has been devised, the aim is to investigate the relationships between surface mineralogy and several physicochemical properties such as; porosity, permeability, pore size distribution, pore fluid composition and rock structure. It may then be possible to predict these physicochemical properties using only the knowledge of the surface mineralogy from the reservoir rocks. The proof to the connection that this may occur is due to the 'Geochemical Logging Tool' (GLT) [6] which is used to predict certain physicochemical properties (including; permeability, porosity, grain size, cation-exchange-capacity (CEC) and density of reservoir rocks) with a degree of accuracy. The GLT measures the abundance of elements commonly found in reservoir rocks. This is achieved by measuring naturally radioactive elements and neutron activated elements. The elemental concentrations are then used to derive mineral concentrations, which in turn can be converted to reservoir properties such as

porosity, permeability, grain size and CEC. These properties may then be modelled to help oil exploration. The GLT is used down the borehole and monitors elemental concentration as a function of depth. It is used in association with coring programs, i.e. cores taken at depths which are analysed by XRF, etc. and are compared to GLT results. The reason why the GLT method is not routinely used as a single method of analysis is because of the need for calibrations on a well to well basis.

Current methods [7] that are used to determine physicochemical properties of reservoir rocks include:

A) Porosity: this can be determined by assuming the density of the grains and then weighing a sample saturated with a fluid of known density.

B) Permeability: this can be measured (using Darcy's law) by sealing the sides along the length of a cylindrical core, removing any oil in the core with a solvent and forcing air longitudinally through the core. The accuracy is not perfect since when the core is removed from the subsurface the rock surface expands in all directions and thus changes the permeability.

Porosity and permeability can also be estimated by indirect methods based on reservoir characteristics such as grain size, surface area, pore lining mineralogy and pore dimension. These rock characteristics can be obtained by either core or log experiments. Nelson [8] has discussed in detail the effect of the above characteristics on permeability and porosity.

C) Grain size: this is best determined using direct microscopy but may also be achieved by sieve analysis or sedimentation. However, these latter two methods require disassembly of the rock.

D) Bulk Mineralogy: Several methods are available which include FTIR and XRD. These are discussed in more detail in section 3.

E) Pore lining Mineralogy: Electron Microscopy can give qualitative analyses of rocks.

Before investigating the relationships between surface mineralogy and physicochemical properties the following are required:-

- 1) a method to determine surface mineralogy (applicable to typical sandstones and carbonates).
- 2) supporting techniques to confirm if the developed method is determining the surface mineralogy (e.g. XRD, SEM and others).

Given the above, a key question is to consider whether there are any general relationships between the surface and bulk mineralogy.

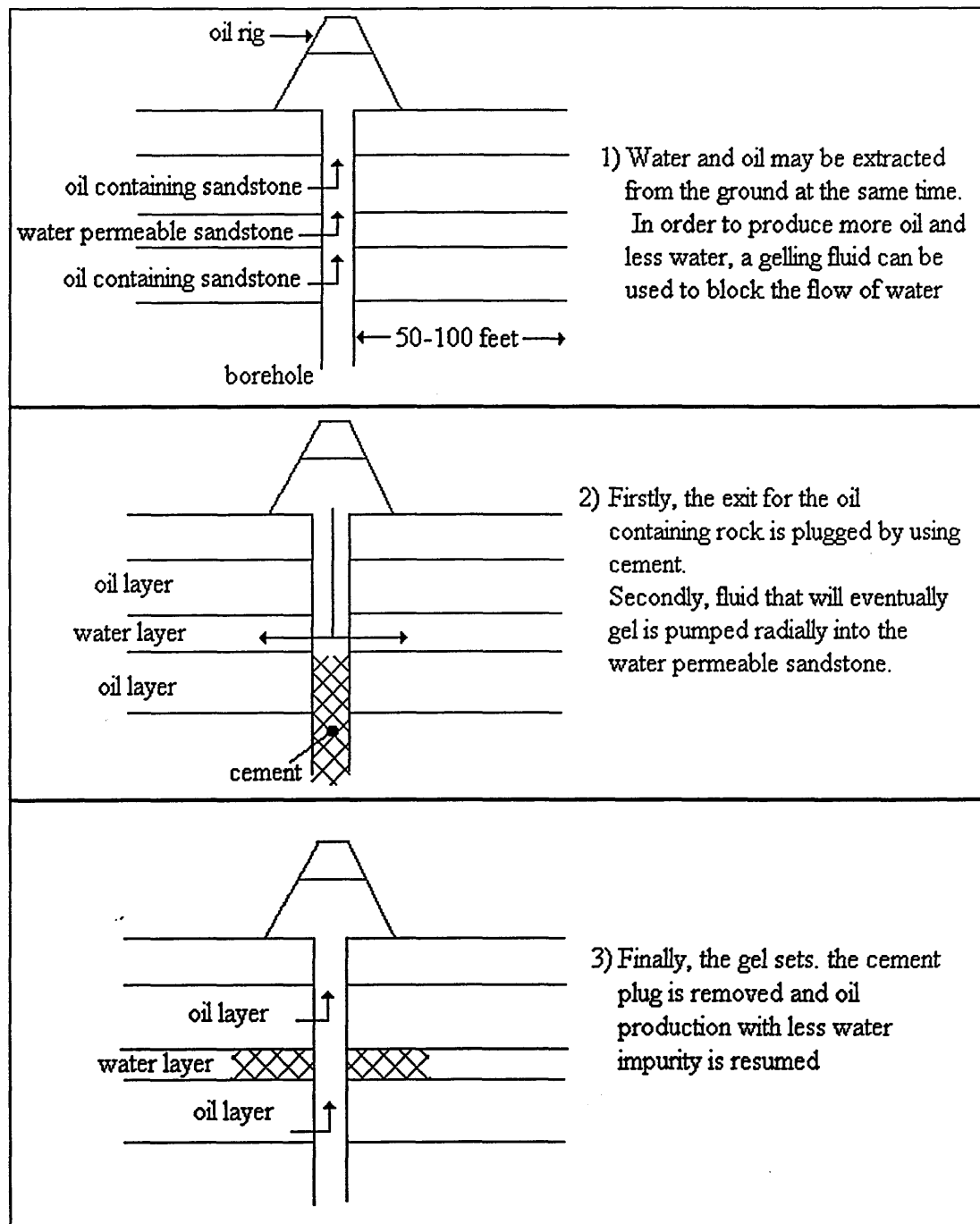
This thesis primarily investigates point 1. It is expected that the surface mineralogy will be different to the bulk mineralogy since direct observation of rock surfaces (prepared by fracturing) by SEM shows that clay minerals cover quartz grains, within the pores. Bulk composition is obtained by crushing rock samples which increases the surface area of quartz and thus a difference should be noted.

1.4.1) Treatment fluids

Clay minerals in hydrocarbon containing sandstone reservoirs play an important role in determining the productivity. The type, abundance and morphology of individual clay mineral particles and aggregates can all impose a profound effect on the quality of the reservoir and the means by which the volume of petroleum in place is evaluated. It is imperative that the pattern of clay mineral abundance throughout the unit of interest is also understood if reservoir performance is to be appraised in accurate and precise terms.

It is not only important to know the surface mineralogy of the oil and gas containing rocks, but also the surface mineralogy of the rocks surrounding them. This is because some treatments involve modifying the surrounding areas so that for example, less water from surrounding rocks is extracted at the same time as oil. This is depicted in figure 1.4

Figure 1.4: An example of a treatment fluid.



There are several types of treatment fluid systems that gel, these include polymer and inorganic gelling systems.

Polymer gel systems comprise of two main components, a high molecular weight polymer (e.g. polyacrylamide) and a cross linker (e.g. Al^{3+} or Cr^{3+}). At some trigger the cross linker attaches itself to two polymer molecules. Further linking occurs and

the result is a 3-dimensional tangle of interconnected polymer molecules that cease behaving like a fluid and eventually constitute a rigid immobile gel.

An example of an inorganic gelling system is the Delayed Gelling System (DGS)TM which has been developed by Schlumberger Dowell (SDR) [9]. The DGS comprises of partially hydrolysed aluminium chloride that precipitates to a gel when an activator responds to temperature and raises the system pH above a certain value. A gel materialises because Al and hydroxyl ions link each other in such a way as to form an amorphous, irregular 3-dimensional network. DGS may be adversely affected by high concentrations of divalent cations such as SO_4^{2-} and CO_3^{2-} . Thus, it is important to know whether sulphate or carbonate minerals are present in the reservoir as these are sources of these anions. Case studies using both these gelling systems are presented in reference [9].

During placement the gelling systems can come into contact with clay minerals or carbonates present in the sandstones. The treatment fluid can react with a large surface area of chemically reactive clay or carbonate. If the clay minerals change the components and/or ratios of a treatment fluid as it is pumped further away from the borehole then the fluid could lose its properties. Before the treatment fluid is employed it would be invaluable to have a knowledge of what clay minerals are present at the surface and what effect they may have on a fluid composition and performance.

It is important to note that reservoir rocks are large three-dimensional networks and there is a need to determine the homogeneity and heterogeneity of them.

A knowledge of the surface mineralogy in rocks is not only important to the oil industry. For example, the presence of clay minerals can contribute to exploration geology in allowing greater precision in stratigraphical correlation where fossils are absent and in the reconstruction of palaeogeographies and diagenetic histories.

1.5) Classification of Minerals

All minerals are divided into several classes, of which the most common found in sandstones is the silicates. The class of silicates is divided into several sub-classes based on the types of linkages between the basic units of their structure (i.e. SiO_4 tetrahedra). The sub-classes found in sandstones and sedimentary rocks are the tectosilicates and the phyllosilicates [10, 11], see table 1.2.

Table 1.2

Class	Subclass	Group	Subgroup
Silicates	Tectosilicates	silica	quartz
		feldspars	alkali series plagioclase series
	Phyllosilicates	smectites	
		kaolinites	
		illites	
		chlorites	
Carbonates		calcite	
		aragonite	
		dolomite	

1.5.1) Tectosilicates (Quartz, Feldspars)

In tectosilicates every SiO_4 tetrahedron shares all its corners with other tetrahedra, giving a three-dimensional network in which the Si:O ratio is 1:2 (i.e. silica). There are several common forms of silica of which the most common is quartz. Substitution of Al^{3+} for Si^{4+} does occur in silica which requires additional positive ions to compensate the resulting negative charge. The most common group of these aluminosilicates is the feldspars.

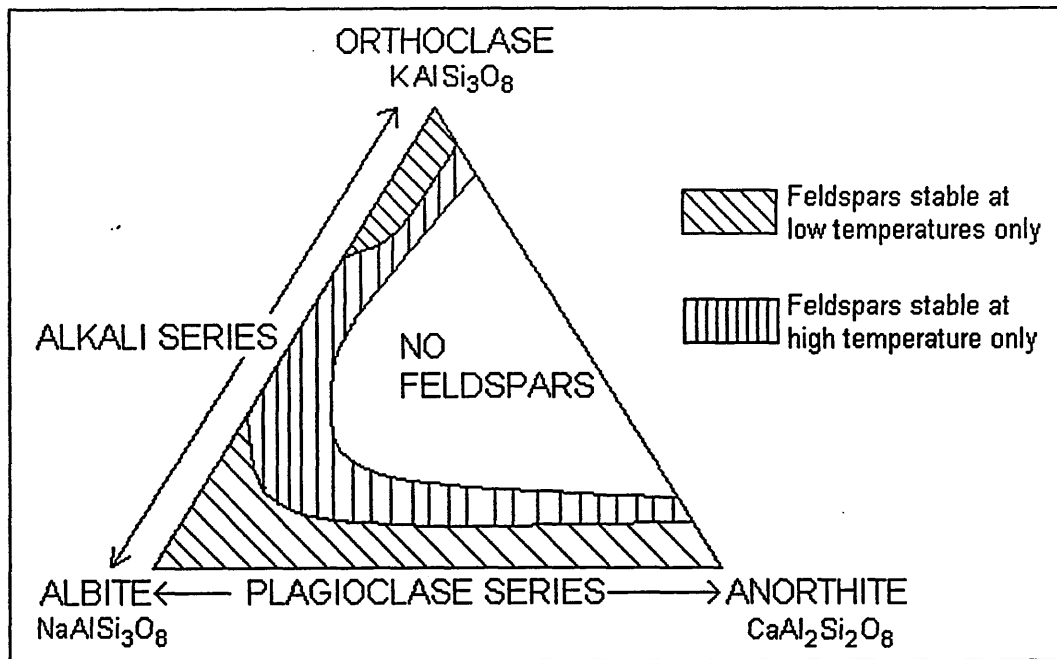
1.5.1.1) Quartz

Quartz is stable over practically the whole range of geological conditions and is therefore the most common mineral found in sandstones and sedimentary rocks. The composition of pure quartz is always close to 100 percent SiO_2 . The quartz structure has very limited space for accommodating extra atoms and thus the silicon cannot be readily replaced by other quadrivalent cations.

1.5.1.2) Feldspars

Feldspars are split into two subgroups namely; the alkali and plagioclase series [11, 12]. These are groups that consists of partly discontinuous solid solutions between the end-member groups. The relation between these series is shown in figure 1.5 in the form of a triangular diagram.

Figure 1.5: Compositions of the feldspars in terms of three end members.



The relationship occurs due to the isomorphism between the end-members orthoclase, albite and anorthite. Isomorphism between albite and orthoclase is continuous only in feldspars stable at high temperatures and is discontinuous in low temperature feldspars, whereas the plagioclase series (albite to anorthite) forms complete solid

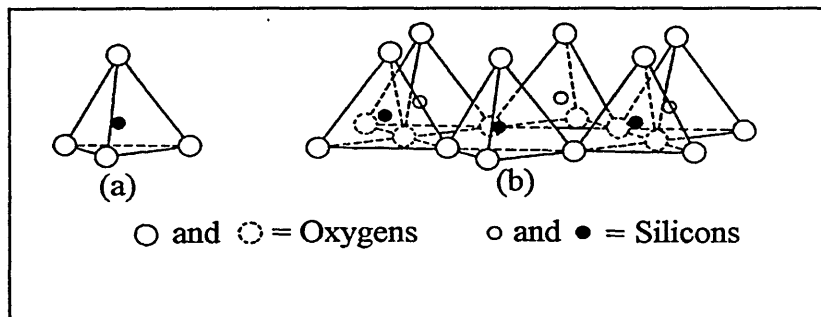
solutions at all temperatures. The general formula for feldspars can be written as $W, Al (Al,Si) Si_2O_3$ in which W may be Na, K or Ca and the variable (Al, Si) is balanced by variation in the proportions of mono- and divalent cations.

1.5.2) Phyllosilicates (Clay Minerals)

1.5.2.1) Structure

The basic structural feature of all minerals in this subclass is the presence of SiO_4 tetrahedra linked by sharing three of the four oxygens, which forms sheets (figure 1.6) with a pseudo-hexagonal network (referred to as the silica-tetrahedral layer).

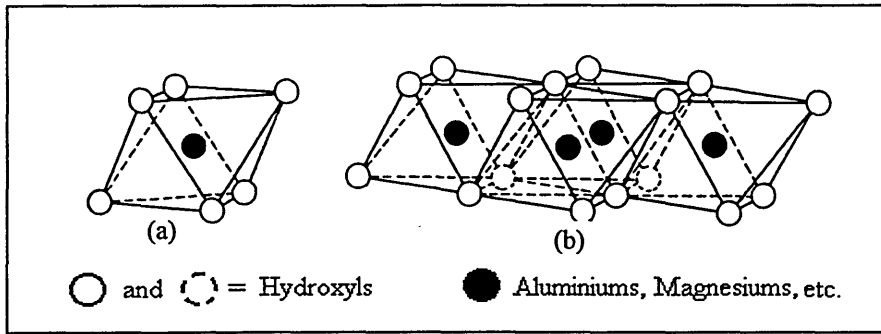
Figure 1.6: Diagrammatic sketch of a single silica tetrahedron (a), and the sheet structure of silica tetrahedra arranged in a hexagonal network (b).



This tetrahedral layer is combined with another sheet-like groupings of cations (mainly Al, Mg and Fe) in six coordination with oxygen and hydroxyl anions. This is referred to as the octahedral-layer since the anions are arranged around the cation in an octahedral pattern. Anions are shared between adjacent octahedra groups and a planar network results (figure 1.7).

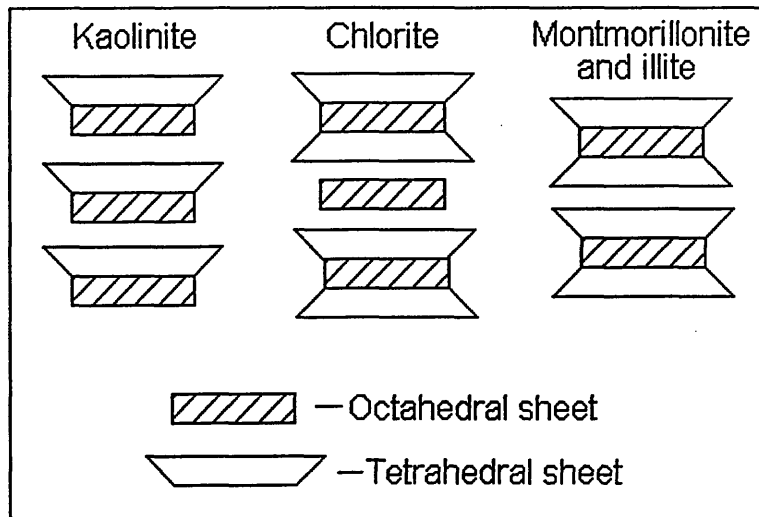
These two sheets can be superimposed on each other. They may share oxygen atoms and thus be essentially fused together in layers by chemical bonds between the two sheets.

Figure 1.7: Diagrammatic sketch showing a single octahedral unit (a), and the sheet structure of the octahedral units (b).



The ratio of tetrahedral to octahedral sheets and the type of cation in the sheets is the basis for the classification system used to assign clays to various groups. For example, if one octahedral sheet and one tetrahedral sheet is shared a 1:1 layered mineral results (e.g. kaolinite), whereas if two tetrahedral and an octahedral sheet is shared a 2:1 layered mineral is obtained (e.g. montmorillonite, illite and chlorite). The sheet-like structures are represented in figure 1.8

Figure 1.8: Sheet-like structures of clays.



Chlorite has an extra sheet and is characterised by a 2:1:1 layer structure. All these structures may be stacked up into successive layers.

Clay minerals may also be subdivided into groups based on their octahedral layer type.

Table 1.3 gives an overview of the main groups of clay minerals

Table 1.3: Classification of clay minerals

Layer type	Group	Di- /Trioctahedral	Subgroups	Species
1:1	Serpentines	trioctahedral	serpentines	chrysotyle
	Kaolinites	dioctahedral	kaolins	kaolinite, dickite
2:1	Smectites	trioctahedral	saponites	saponite, hectorite
		dioctahedral	montmorillonites	montmorillonite, beidellite
	Micas	trioctahedral	trioct. mica	biotite
		dioctahedral	dioc. mica	muscovite
2:1:1	Chlorites	trioctahedral	trioct. chlorite	clinochlore
		dioctahedral	dioc. chlorite	donbassite

1.5.2.2) Clay Mineral Properties and Characteristics

1.5.2.2.1) Isomorphous substitution

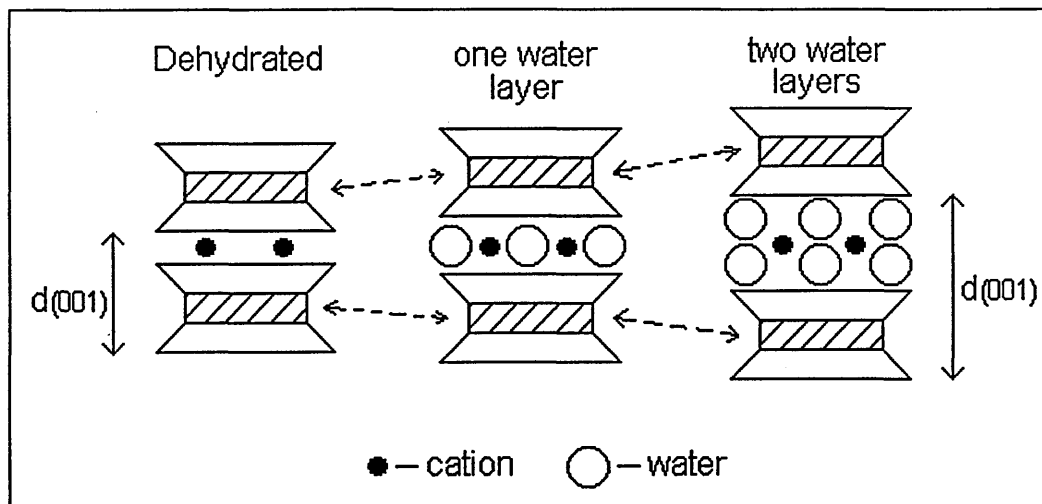
Isomorphous substitution describes a process that modifies the clay structure. It involves the replacement of a cation from the tetrahedral or octahedral sheet by another cation. For example Mg^{2+} for Al^{3+} in the octahedral sheet or Al^{3+} for Si^{4+} in the tetrahedral sheet. Isomorphous substitution occurs most commonly in the octahedral sheet. If substitution by an ion with a lower charge occurs then an excess of electrons will result. This generates a negative charge which is satisfied by the sorption of exchangeable cations. The sharing of these exchangeable cations bonds the clay layers together. The number of cations required to neutralise the lattice is known as the cation exchange capacity (CEC) and is measured in milliequivalents (meq) per 100 grams of clay. Different clays do have different CECs of which some are shown in Table 1.4. These cations can be exchanged by other cations by placing the clay in a solution of the desired ion, e.g. Na, Ca, Mg and K. Incidentally these cations are common in clay minerals found in nature. Exchangeable cations can also

be associated with the edges of silicate layers, where the ions have unsatisfied valences. These are often referred to as broken bonds. Approximately 20% of the CEC is associated with broken bonds and 80% is situated in the interlayer region.

1.5.2.2.2) Hydration/Swelling of a clay

The exchangeable cations are often hydrated and this water may be replaced by polar organic liquids. When water is adsorbed between the layers, the distance between the layers ($d_{(001)}$ -spacing) increases. A phenomenon known as swelling occurs and is represented in figure 1.9. When an organic solvent is adsorbed in between the layers it is referred to as intercalation.

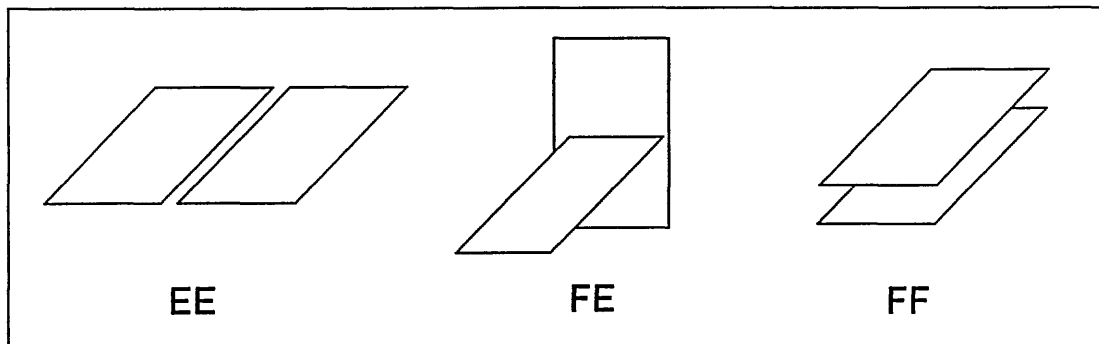
Figure 1.9: Swelling of a clay (e.g. montmorillonite)



1.5.2.2.3) Macroscopic properties

The clay particles can form tactoids as a result of the interactions between their faces and edges. Three possible configurations are known and are shown in figure 1.10.

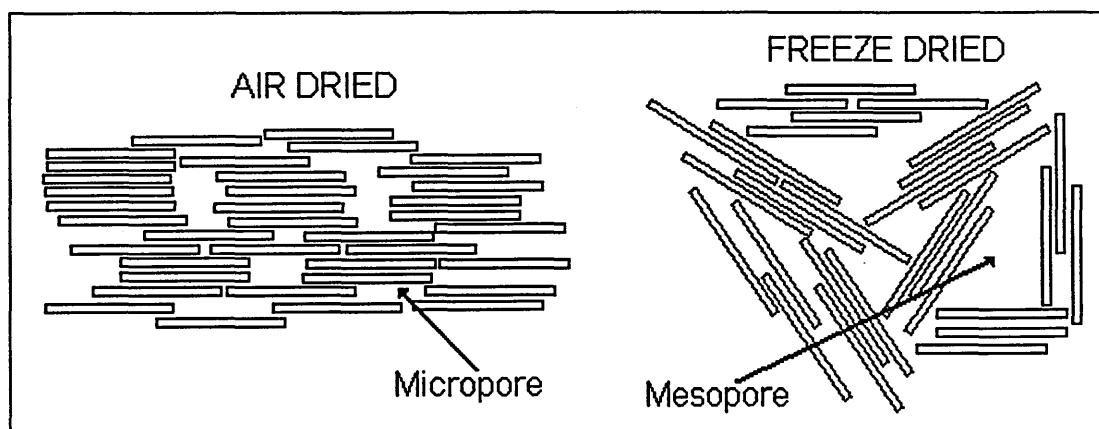
Figure 1.10: The three possible stacking configuration of clay sheets; edge-to-edge (EE), face-to-edge (FE), face-to-face (FF).



FF aggregates are preferentially formed with clays of relatively large particle size, high CEC and exchangeable cations with a high charge density (e.g. Ca^{2+}). FE and EE tend to be formed by clays with small particles sizes.

The drying of clays can change the final porosity of the clay aggregates. If for example montmorillonites are dispersed in water, then the sheets are randomly oriented. If the substrate is air dried the individual clay particles settle down in a homogeneous, parallel orientation which results in many face-to-face stacked layers. If the substrate is dried very fast (e.g. freeze dried) then the clay particles keep their random distribution and a card-house structure is formed. (see figure 1.11)

Figure 1.11: Difference in stacking between an air-dried and freeze dried clay



The crystallinity of the freeze dried clay is lower, but its porosity and surface area are higher.

1.5.2.3) Clay Minerals of particular interest in this thesis

Table 1.4: Table summarising some of the properties of the clay minerals

	Kaolinite	Montmorillonite	Illite	Chlorite
CEC *	3-15	80-150	10-40	10-40
Particle size (microns)	0.5-5	0.1-2	0.1-2	0.1-5
Surface area BET -N ₂ m ² g ⁻¹	15-25	30-80		140
* - [13]				

1.5.2.3.1) Kaolinite

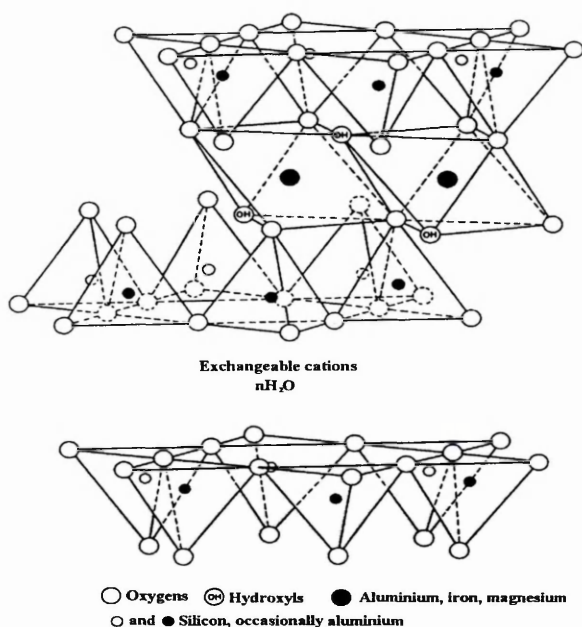
Kaolinite is the most common of four polymorphs, the others being dickite (rare), nacrite (rare) and halloysite (moderately common). The ideal structural formula of kaolinite is $\text{Al}_2\text{Si}_2\text{O}_5(\text{OH})_4$, although Fe, Ti, K and Mg may also be present. Figure 4.3 shows the structure of kaolinite. There is no charge (at the most a very small one) on the lattice due to isomorphous substitution in kaolinite and thus no interlayer cations are present. If exchangeable cations are present these are usually associated with broken bonds at the crystal edges. The layers in kaolinite are held together by hydrogen-bonding and intercalation may occur if this bonding network can be entered into.

1.5.2.3.2) Montmorillonite

The composition of montmorillonite always deviates from the ideal formula, $\text{Al}_2\text{Si}_4\text{O}_{10}(\text{OH})_2 \cdot x\text{H}_2\text{O}$, due to a relatively high amount of isomorphous substitution. An idealised structural formula for montmorillonite is $\text{Na}_{0.3}(\text{Al}_{1.7}\text{Mg}_{0.3})\text{Si}_4\text{O}_{10}(\text{OH})_2$. Figure 1.12 shows the molecular structure of montmorillonite. This model is the most widely accepted and was first proposed by Hofmann, Endel and Wilm [14] and modified by Magdefrau and Hofmann [15], and, Hendricks [16]. The other known

model was proposed by Edelman and Favejee [17]. The outstanding feature of the montmorillonite structure is that water and polar molecules can easily enter between the layers. This is because the electrostatic bonding between the layers and exchangeable cations is weak and the chance of swelling or intercalation is excellent.

Figure 1.12: The 2:1 clay structure of montmorillonite



1.5.2.3.3) Illite

The structure of illite is the same as that for montmorillonite except that some of the silicon ions are always replaced by aluminum ions and the resultant deficiency is balanced by potassium ions. The small size of the potassium ions allows short Van der Waals attractions forces to contribute along with the electrostatic forces to an increased strength in the bonding between the layers. The illite clay layers are held tightly together and therefore illite is very difficult to swell and is difficult to cation exchange. The ideal structural formula for illite is $KAl_2(Si_3Al)O_{10}(OH)_2$, but Mg and Fe may also be present.

1.5.2.3.4) Chlorite

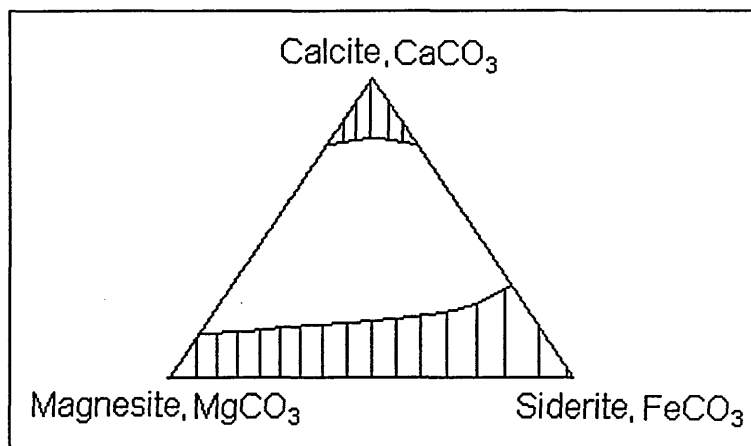
In chlorite, isomorphous substitution of silicon by iron or aluminum ions occur in the tetrahedral sheets, which generates negative charges on the surface. The neutralisation of these charges is accomplished by a magnesium-hydroxide sheet with isomorphous substitution of aluminum ions for magnesium ions. The ideal formula for chlorite is $(\text{Mg, Fe, Al})_6 (\text{Al, Si})_4 \text{O}_{10}(\text{OH})_8$ although some varieties contain appreciable amounts of chromium, nickel or manganese. The octahedral layer of chlorite differs from that of montmorillonite, illite and kaolinite in that it has a trioctahedral rather than a dioctahedral arrangement (i.e. in the former there are two cations for each six OH anions, whereas for the latter clay-type there are three cations for each six OH anions).

1.5.3) Carbonates

The structure of carbonates is based on the fundamental anionic unit $(\text{CO}_3)^{2-}$, which is a planar group with a C at the centre of an equilateral triangle of three O atoms [10]. Carbonates are very common and widespread minerals and are classed in three groups; calcite, dolomite and aragonite. The calcite group consists of the end-members calcite, magnesite and siderite. The compositional variance between these members is shown in figure 1.13. The shaded areas indicate the limits of solid solution observed in nature. The dolomite group results from the regular substitution of alternate calcium ions in calcite by another divalent metal which is usually magnesium, but iron and manganese may also be found.

Aragonite (CaCO_3) is the second most abundant polymorph of calcite.

Figure 1.13: Triangular diagram showing the compositional variations of calcite, magnesite and siderite.



2) Theory of techniques used in this thesis

2.1) Infrared Spectroscopy

Several possible infrared techniques have been discussed [18] in the past for measuring the infrared spectra of powdered samples, these include;

- i) transmission spectroscopy (halide discs and mineral oil mulls)
- ii) diffuse reflectance spectroscopy
- iii) emission spectroscopy [19]
- iv) photoacoustic spectroscopy [19, 20]

The first two techniques have been applied in this thesis for the analysis of minerals and will be discussed further in this chapter.

Infrared radiation is electromagnetic radiation with a wavelength between approximately 10^{-3} and 10^{-6} m. Absorption of particular frequencies of infrared radiation by polyatomic molecules gives rise to a characteristic infrared spectrum.

Absorption of Infrared radiation

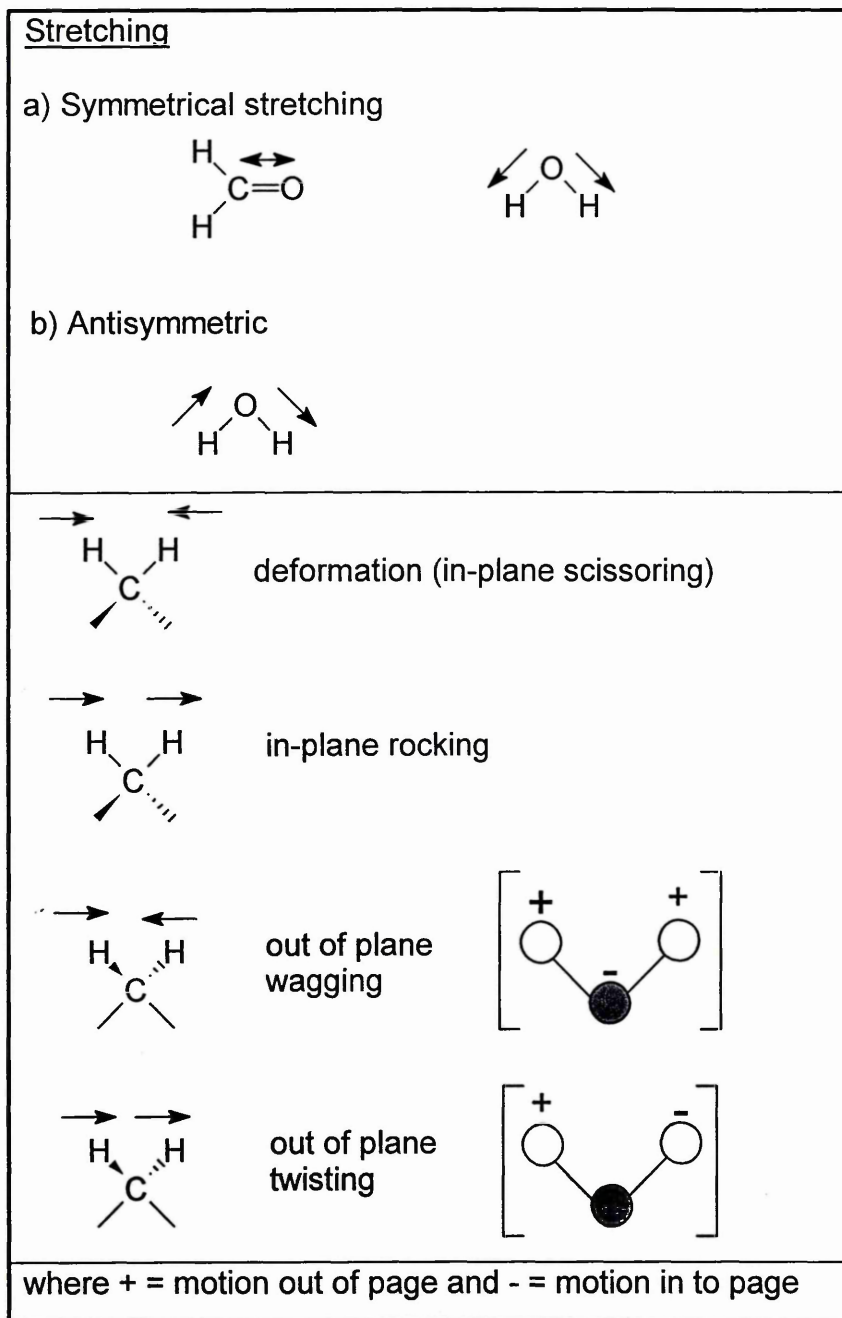
There are two fundamental types of vibration that occur in polyatomic molecules;

- i) stretching of the interatomic bonds, where the length of a bond changes, and,
- ii) bending, where the angle between two bonds changes. Table 2.1 shows a diagrammatic representation of the types of stretching and bending vibrations that occur in molecules.

If a molecule is to absorb infrared radiation it must undergo a net change in dipole moment due to its vibrational motion. A dipole moment is the product of the magnitude of the localised electrical charges within any molecule and the distance separating the positive and negative components of these charges (i.e. atoms). If the frequency of the incident radiation is the same as the frequency of the molecular vibration then a net transfer of energy occurs which results in a change in the amplitude of the molecular vibration, and absorption of the radiation occurs.

The reader is referred to many of the detailed books that are available on the theory of infrared spectroscopy [21, 22].

Figure 2.1: The types of stretching and bending vibrations occurring in molecules



Fourier Transform Infrared Spectroscopy (FTIR)

FTIR spectroscopy is now the preferred method of infrared spectral analysis and has several advantages over the traditional dispersive methods. In a dispersive instrument

a prism or grating is used to resolve the radiation into separate components whereas in a Fourier transform instrument a Michelson interferometer is used. A Michelson interferometer allows all the infrared frequencies of the source to be recorded in the time domain as an interferogram. A Fourier transform (i.e. a mathematical formula) is then used to convert this to the frequency domain. During the mathematical conversion an apodisation function is used to truncate the interferogram which removes unnecessary data. Apodisation can change both the resolution and signal to noise ratio of the spectrum.

Fourier self deconvolution

Fourier self deconvolution can help to determine the number of component bands, the band position and the relative intensities in a poorly resolved infrared spectrum. It is achieved by multiplying the interferogram by an exponentially increasing function. This is employed with an apodisation function and enhances the spatial resolution of the band components (and noise). The extent of deconvolution is determined by the enhancement factor, K . This value is related to the ratio of the bandwidth of the original spectrum to that of the deconvoluted band width. A higher K value results in a more severe deconvolution. During the deconvolution the bandwidth of the component parts in the original spectrum needs to be estimated. This needs to be considered carefully since an overestimation may produce spurious side lobes.

2.1.1) Transmission Spectroscopy

In the classical method of infrared spectroscopy radiation passes completely through the sample. This is known as transmission spectroscopy. A range of appropriate sampling techniques have been developed, which include mulls, KBr discs and free standing films. KBr discs have been used in this thesis and the factors that need to be regulated in order to produce a disc of good quality include;

- i) a thorough mixing of sample and matrix,
- ii) dry KBr needs to be used at all times or the disc will be opaque,
- iii) the weights of both the sample and the matrix need to be accurately weighed.

For a reliable comparison of spectra to be achieved all the experimental procedures need to be carefully performed.

2.1.2) Diffuse Reflectance Infrared Fourier Transform Spectroscopy (DRIFTS)

The most recent literature review concerning DRIFTS in the mid-infrared region was written by Mitchell [23] in 1991. This review covers only the fundamentals of the theory and its application to polymer powders, films and fibres. A more detailed, but older review discussing the theory of DRIFTS was written by Griffiths and Fuller [21] in 1982. Although only a few reviews have been written [19, 24, 25], many papers have been published on the theoretical and practical aspects of DRIFTS. Some of which will be discussed in this chapter.

During a transmission experiment the incident radiation passes through the sample (section 2.1.1), whereas, during a DRIFTS experiment the incident radiation is reflected off the surface of the sample. DRIFTS spectra are calculated by measuring the single beam reflectance spectrum of a sample and ratioing this against a reference single beam reflectance spectrum of a good diffuse reflector (see section 2.1.2.3 for choice of diffuse reflector). The reflectance spectrum is therefore calculated in a manner that is analogous to transmittance:-

$$\% \text{ Reflectance} = (\text{Reflectance sample} / \text{Reflectance reference}) \times 100$$

2.1.2.1) Types of Reflectance

There are three main modes in which the incident radiation can be reflected from a powdered sample. Figure 2.1 shows a schematic diagram describing the three modes of reflection.

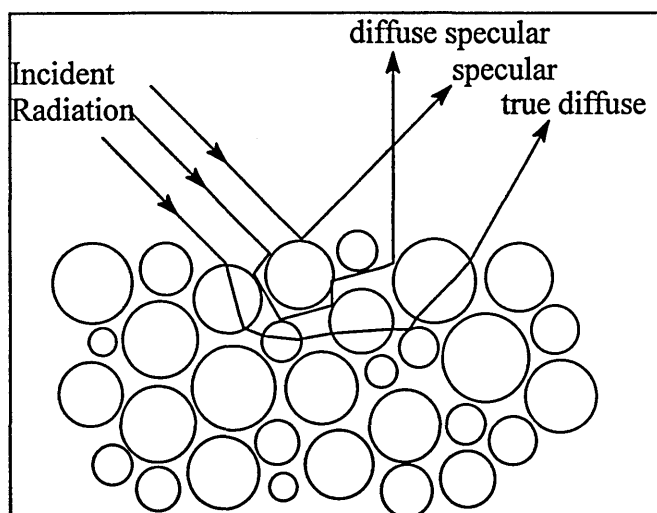
The first mode is where the incident beam is reflected from the sample as if from a mirror (i.e. the angles of incidence and reflectance are equal). This type is governed

by the Fresnel equations [26, 27] and will be called true specular reflectance in this thesis (it is also referred to as front-surface, regular or Fresnel reflectance).

The second mode will be called diffuse specular reflectance (also referred to as diffuse Fresnel reflectance). Here the beam undergoes multiple reflections off particle surfaces without penetrating into the particle. The resulting beam emerges from the sample and is distributed in all directions.

The third mode of reflection is true diffuse reflection, where the beam passes into the bulk of the material and undergoes: absorption, reflection, refraction and scattering before re-emerging at the sample surface. The light reflected in this manner is distributed in all directions.

Figure 2.1 : Schematic diagram showing the three modes of reflection during a DRIFTS experiment.



There are many factors that govern the amount of each type of reflectance collected during an experiment. Some of which include; the optical arrangement of the accessory, and the physical and chemical characteristics of the sample (these and others will be discussed in this chapter).

The major drawback with the DRIFTS technique arises from the specular component (true specular and diffuse specular reflection) of the reflected radiation. When the specularly reflected component is small, the DRIFTS spectrum is similar in

appearance to that of a transmittance spectrum. However, when the specularly reflected component is high, distortions appear in the spectrum as either *anomalous dispersions* or *reststrahlen bands* [28-30].

The amount of specular component in the spectrum is governed by the refractive index, (n'), which is the complex sum of the index of refraction (n) (called the real component) and the absorption index (k') (called the imaginary component):

$$n' = n + ik' \quad (\text{for non-absorbing materials, } k'=0)$$

[26, 27]. Specularly reflected light is well described by Fresnel's equations [26, 27], which express the reflection of radiation at an interface as a function of the refractive indices of the two media that form the interface. The difference in the refractive indices leads to reflection. The differences in refractive index that lead to reflection can be due to the real or imaginary components.

The absorption index, k' , is related to the absorption coefficient, K , i.e.

$$k' = K/4\pi\nu,$$

where ν is the frequency of radiation (cm^{-1}).

The absorption coefficient, K , is related to the absorptivity, a , by:

$$K=2.303ac,$$

where c is the concentration.

If the sample absorbs, the absorption coefficient, K ($\neq k'$) has an effect on the amount of specular reflectance near the wavelength where absorption occurs. The appearance of the features produced in the infrared spectrum depends on the value of the absorption index and hence the absorptivity.

If the absorptivity is very small, very little if any change in the spectrum results. If the absorptivity is intermediate, as is for most organic compounds, the increased specular reflectance can result in an anomalous dispersion feature. This leads to a derivative shaped feature or a shift in the peak maximum to higher wavenumber of the band in question. If the absorptivity is large, such as the strong bands in some minerals, a large reflectance maximum, called a reststrahlen band results. An example of the reststrahlen band is shown in figure 2.4.

The presence of specular reflectance in the radiation collected by the detector leads to much of the non-linearity commonly associated with DRIFTS (which will be discussed in more detail later). Thus, during a DRIFTS experiment all the factors that

produce specular reflectance are minimised in order to collect the maximum ratio of true diffuse to specular reflection.

2.1.2.2) Instrumentation and Optical Geometries

Until about 1976, very little work involving vibrational spectroscopy using diffuse reflectance in the mid-infrared region had been accomplished. This was because it was considered that the intensity of radiation reflected from powders was too low to enable spectra to be measured at medium resolution ($2\text{-}4\text{cm}^{-1}$) and high signal-to-noise ratio. Although this was the case a number of different instrumental arrangements had been employed, which include those designed by Coblenz [31], Gier et al. [32], and Blevin and Brown [33]. All these designs employed either a prism or grating monochromators.

In 1976, Willey [34, 35] described a system which interfaced an FTIR spectrometer to a diffuse reflecting collecting accessory (integrating sphere). Although this system was reported to produce accurate measurements, long signal averaging times were required to produce high quality spectra. Also the resolution was limited to at least 10cm^{-1} which is not sufficient for general analytical use.

In 1978, Fuller and Griffiths [36, 37] described a diffuse reflectance infrared Fourier transform spectrometer which avoided using an integrating sphere. Figure 2.2A shows a schematic diagram of the optical system they constructed. In the system radiation from a Michelson Interferometer is focused onto the sample by a 90° off-axis paraboloid (P). The diffuse reflected light is then collected by the on-axis ellipsoid (E) and focused onto the detector by a second 90° off-axis paraboloid. This system produced good diffuse reflectance spectra with a much higher signal to noise ratio than previously. Nowadays, several companies offer diffuse reflectance accessories for purchase which are compatible with most FTIR spectrometers. The majority of these correspond to one of the two configurations shown in figures 2.2B and C. The former has an optical on-line configuration in which a polariser is used to eliminate the specular component, whilst, the latter has an off-line configuration in which exclusion of the plane of incidence from the collection optics is used to eliminate the specularly reflected component.

Figure 2.2A : Schematic diagram of an optical configuration built by Fuller and Griffiths

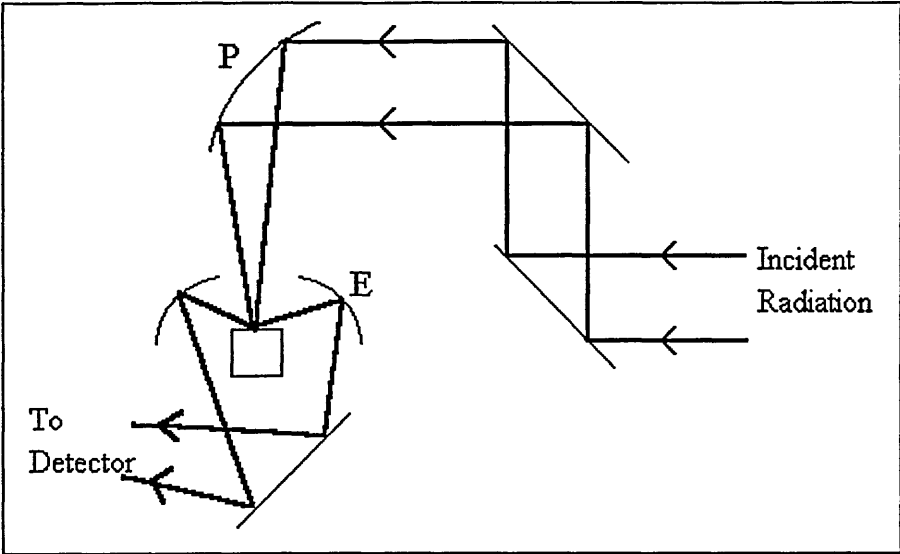


Figure 2.2B : Optical in-line

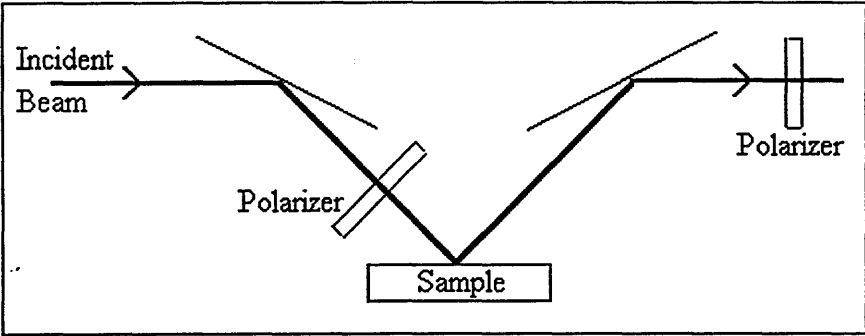
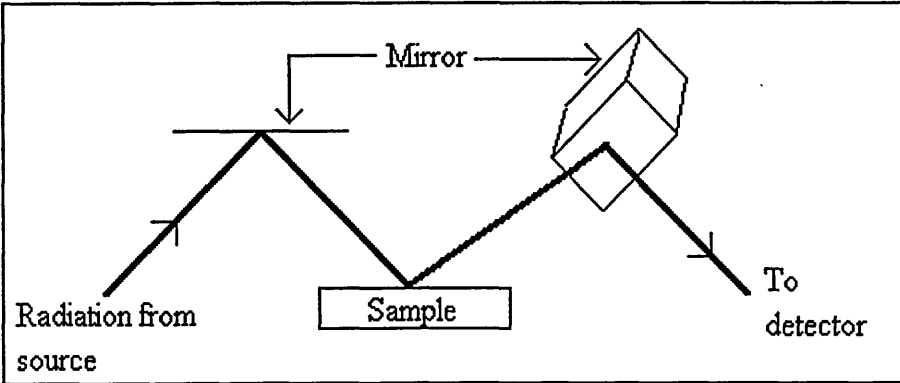


Figure 2.2C : Optical off-line



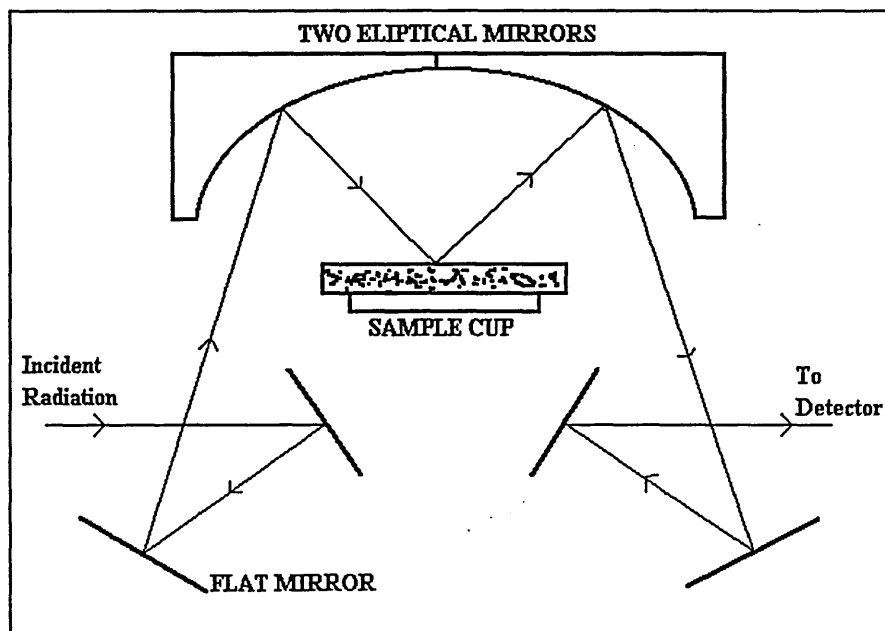
Evaluation of the two common optical configurations has been carried out by Hembree and Smyrl [29]. They showed that without the polariser, the in-line optical configuration essentially collects the total reflectance (i.e. all of the specularly reflected component and part of the diffusely reflected component). The effect of the polariser is to reduce the amount of specular reflectance. Also the optical off-line configuration leads to a better rejection of specular reflectance, but results in a lower efficiency output.

Brimmer et al. [38], investigated the effects of optical arrangement with a specially built spectrogoniophotometer. This allowed diffuse reflectance spectra to be collected via a variety of incident angles and collection geometries. It showed that an off-line configuration greatly minimised specular reflection. They have also shown that the effect is more noticeable for neat rather than dilute samples [28, 39].

These results have been disputed by Yang et al. [40], who concluded that optical geometry had no effect on the amount of specular reflectance collected. This could be a result of using sample particle sizes which were smaller than the wavelength of interest.

Most in-line accessories remove the polarisers and collect the total reflectance via two elliptical mirrors (figure 2.3).

Figure 2.3 : Schematic diagram of the accessory used to collect DRIFTS spectra presented in this thesis.



This type of accessory is used to collect the DRIFTS spectra presented in this thesis. Accessory alignment is very critical because typically, only 10 to 15% of the energy throughput is available for DRIFTS analysis compared to the transmission mode. A screw adjuster allows the sample to be moved up and down so that the surface is positioned at the focal point.

2.1.2.3) Fundamental factors affecting diffuse reflectance

There are many factors which can affect the spectral data. These include:-

- A) Choice of reference powder
- B) Particle size
- C) Absorptivity and refractive index
- D) Depth of sample matrix
- E) Sample packing
- F) Sample homogeneity
- G) Sample height
- H) Polariser
- I) Rotation of sample
- J) Use of a 'Blocker'

A) Reference Powder

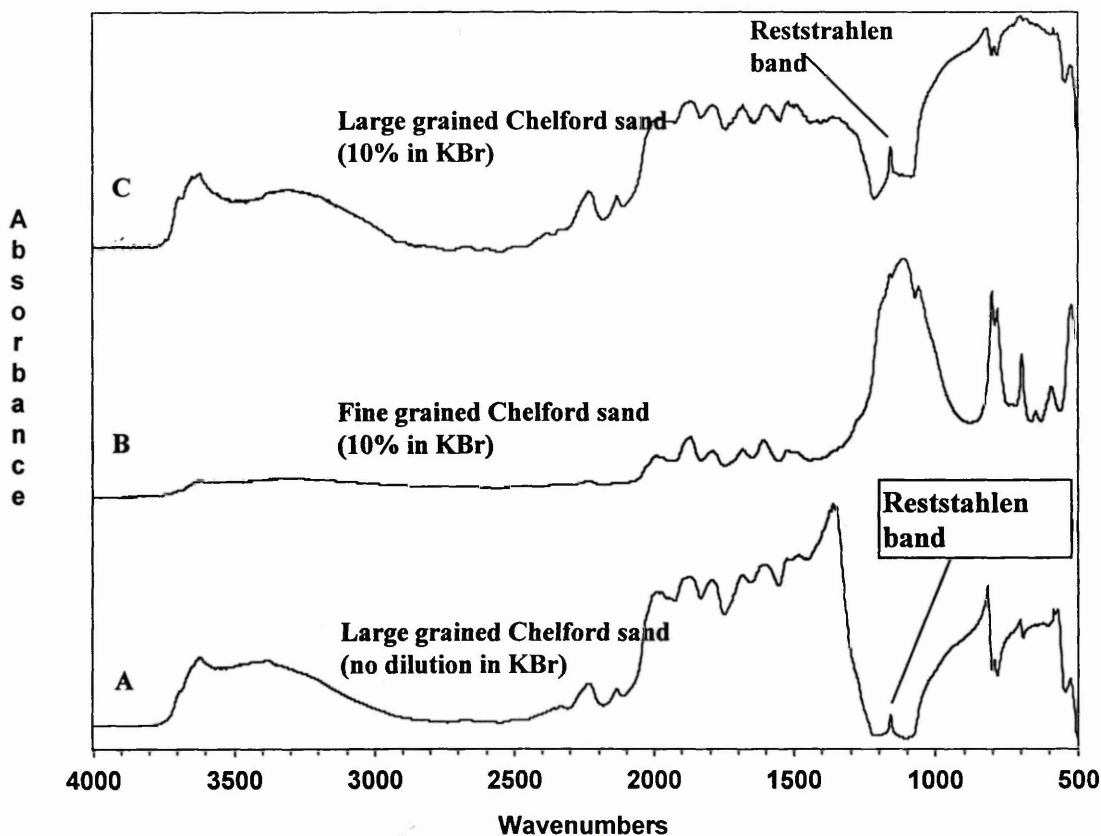
During a DRIFTS experiment the sample single beam spectrum is ratioed against a reference (background) single beam spectrum. It is ideal for the reference to be a good diffuse reflector, non absorbing and a highly scattering material.

Fuller and Griffiths [36, 41] investigated the diffuse reflectance of powdered gold, germanium, silicon and several alkali halides and found that KCl has the fewest interferences and the highest overall reflectance. They also compared [37] the energy reaching a detector using a diffuse reflectance accessory with a transmittance experiment and found about 10-15% of the radiation reaches the detector when KCl is used.

Problems arising from using alkali halides include the presence of adsorbed water and organics causing bands at 3300 and 1640cm^{-1} , and 2950cm^{-1} respectively. It is therefore important that the alkali halide used should be very dry and clean.

Not only is the reference powder used to collect the background single beam spectrum, it can also be used as a diluent within the sample. The effect of this is to decrease the specular component and increase the diffuse component in the reflected radiation. As a result reststrahlen bands and anomalous dispersion effects can be removed or reduced. The amount of dilution required depends on the sample under investigation. For example, a 5-10% dispersion of finely powdered quartz in KBr would result in the removal of the reststrahlen band in its reflectance spectrum (figure 2.4).

Figure 2.4 - The effect of grain size and dilution in KBr on the DRIFTS spectra of Chelford sand



The dramatic difference in the appearance of the reflectance spectra is believed to be due to at least two factors [38]. Firstly, 90-95% of the uppermost surface is KBr and not quartz. Thus, only 5-10% of the incident beam is truly specularly reflected, whilst the remainder penetrates into the sample and undergoes diffuse specular and true diffuse reflection. Secondly, the medium in contact with quartz is no longer air but will now be KBr. The refractive index of KBr is more closely comparable to that of quartz and so less specular reflectance and more diffuse reflectance occurs. An important factor to consider is the mean particle size of both the quartz and KBr, which will be discussed later.

When silicon or germanium is used the overall reflectance is a lot lower than KCl (by about 50%). Also the spectra show strong absorption bands around 1100 and 900 cm^{-1} respectively, which appear to be due to oxide layers on the surface of the powder. Silicon also exhibits a large specular reflectance in comparison to KCl and thus sample penetration would be expected to be low.

When gold is used, the reflectance is only about 50% that of KCl and also the beam does not penetrate deeply into the sample.

An additional advantage of using alkali halides is the ease in which they are crushed into powders. Obviously, it is more difficult to crush gold than silicon or germanium and more difficult for silicon and germanium than alkali halides.

B) Particle Size

It has been shown [36] that the amount and type of reflectance occurring in a diffuse reflectance experiment is greatly dependent on the particle size of both the sample and reference/diluent. The amount of reflectance at high wavenumbers from KCl alone was found to be highest for the smallest average particle size, d , within the range; $d < 10\mu\text{m}$, $10 < d < 75\mu\text{m}$, $75 < d < 90\mu\text{m}$ and $d > 90\mu\text{m}$. For the smallest average particle size a drop in reflectance is observed below 1000 cm^{-1} . This effect presumably occurs when the wavelength of the radiation is approximately equal to the diameter of the particles. Under this condition the scattered radiation presumably undergoes both diffraction and refraction within the sample, resulting in a reduction of the energy reaching the detector and thus causing the observed energy drop.

These results have been compared with those of Moradi et al. [42] and an increase in reflectance was also observed as the particle size of KBr and ZnSe decreased. However, they observed no important variations at the higher wavenumber for the larger particle sizes.

Generally, for pure samples (not dispersed in a non-absorbing matrix), as the particle size decreases the band heights increase and the band widths decrease. Also the relative band intensities change considerably when the particle size changes. This effect has been demonstrated [21, 23 and references therein] for both moderately absorbing organic compounds (e.g. azobenzene) and highly absorbing inorganic compounds (e.g. quartz), and the effect is much greater for the latter.

The change in diffuse reflectance spectra is due mainly to the amount of specular reflectance collected, since the greater the particle size of the sample, the greater is the proportion of specularly reflected component. Also, as the specular component increases, less of the beam penetrates into the powdered sample and thus less refraction, scattering and absorption occurs of which the latter results in loss of information about the sample.

For quartz, in the region below 2000cm^{-1} , where the absorption is high, the shape of the spectrum is caused primarily by specular reflection (figure 2.4). When the particle size of quartz is large, a high amount of specular reflection reaches the detector. This is indicated by the large reststrahlen band. It should be noted that the reststrahlen band is never completely removed whilst investigating pure samples because there is always a high proportion of specular reflectance present.

In regions of low absorption, above 2000cm^{-1} the spectrum has the appearance typical of diffuse reflectance spectra. As the sample size decreases, the amount of diffuse reflectance increases, which is indicated by an increase in the intensity of the bands.

When studying samples dispersed in a non-absorbing matrix (KBr) a similar trend is observed, i.e. a decrease in particle size results in an increase in band height and decrease in band width. For quartz at low concentrations (e.g. 10%) and small particle sizes the reststrahlen band is removed (due to a combination of the small particle size

and the non-absorbing medium) , but at low concentration (10%) and increasing particles sizes the distortions return (figure 2.4).

C) Absorptivity and Refractive Index

As discussed earlier, the absorptivity and refractive index (n) can have a related effect on the types of reflection and thus appearance of the diffuse reflectance spectra.

Moradi et al. [42] studied the behaviour of the diffusely reflected intensity for a given particle size distribution (50-90 μ m) over a wide range of refractive indices. They found that the diffusely reflected energy increases from 0 for $n=1$, to a maximum for n close to 2, and then decreases for higher refractive index values. KBr has a refractive index of 1.54 and is therefore a good choice for the diluting material used in DRIFTS experiments.

D) Depth of Sample Matrix

The depth of the sample matrix is an important factor to consider in diffuse reflectance especially if quantitative analysis is required.

As the depth of any absorbing sample [36] is increased a subsequent increase in its absorption bands will be observed until a certain depth is reached. At this depth, any further increase will result in no change in the diffuse reflectance spectra and the sample is termed to be of 'infinite thickness'. The actual depth depends on both the absorption and scattering coefficients of the sample under investigation [43]. For a pure KCl matrix overlaying a sample , the point of infinite thickness occurs at 5mm, i.e. no bands due to the sample are observed in the spectra. However, the difference in band intensity between 2 and 5mm is not very great.

If a sample is dispersed in KBr (5%) and is weakly absorbing, then the expected depth at which no further change in the diffuse reflectance spectrum occurs will be approximately 3mm. Whilst for strongly absorbing samples, such as coals, the emerging beam will probably originate from less than 1mm below the surface of the sample.

If the sample is insufficiently deep, the incident beam will be reflected off the sample cup bottom and then travel back up through the sample. As a result, part of the radiation will interact twice with the absorbing sample giving rise to increased absorption.

It should be noted that low frequency radiation penetrates more deeply into the sample than high frequency radiation. This was shown [41] by comparing a homogeneous mixture of 1% carbazole in KCl with the same mixture that has a 0.5mm layer of KCl over it. In this set-up the low frequency absorption bands were found to be much more intense relative to the higher frequency bands for the latter.

E) Sample Packing

A powdered sample placed in a sample cup can be levelled by either tapping the side of the cups or by subjecting it to pressure, of which the latter results in a more ordered orientation of the samples crystals. Yeboah et al. [44] studied the effect of pressure on band intensities and showed that as the amount of pressure increased, the amount of scattering occurring in the sample decreased. This was presumably because the particles were packed more efficiently and hence scattered radiation less efficiently. The amount of scatter was determined using the Kubelka-Munk (K-M) function (see section 2.1.2.4.2). Unfortunately, as the pressure increased, the amount of diffuse reflectance decreased and so did the band intensities.

Krivacsy et al. [45] also studied this phenomenon and showed the opposite to occur i.e. scattering increased after pressure was applied. It must be noted that Yeboah's study investigated the pressure range 10-80Mpa whilst Krivacsy studied the range 0-1Mpa.

Although the two studies differ regarding the amount of scattered radiation they both show that as the pressure increases the variability in the scattering coefficient decreases from sample to sample. This helps in reproducing diffuse reflectance spectra and hence better quantification (see later).

Several sample packing accessories have been designed [46, 47] and are simple to build, easy to operate and packing of powdered samples requires only a small amount of time (1-3 minutes).

Another problem associated with packing the sample under pressure is the need to level the sample afterwards. Most groups [48] scrape the excess sample away with a sharp, straight edge (e.g. razor blade). It is thought that this increases the particle orientation at the top surface and enhances specular reflection. Although this effect is only a minor consideration it is very important that when scrapping the sample and background, the height with respect to the incident beam and focal point are the same.

F) Sample Homogeneity

This has been shown [49] to be very important because simply mixing two materials together does not lead to a homogeneous mixture. Thorough mixing is therefore required.

Mixing via the use of a ball mill (with two balls present) is very efficient, it also helps to reproduce particle sizes from sample to sample if milling times are regulated. If samples do not need to be reduced in size, a ball mill with no balls present may mix them efficiently. Care should be taken when using ball mills (either steel, teflon or carbide) because softer components in the mixture may preferentially adhere to the walls of the containers or balls.

G) Sample Height

The sample should be positioned so that maximum radiation throughput is observed. This is extremely important during Variable Temperature-DRIFTS experiments where the sample holder is liable to move due to expansion from the heat (see section 2.1.2.5).

H) Polarisers

The presence of crossed polarisers (one before the sample and one after) [28, 39] for on-line optical geometries reduces the amount of true specular reflectance directed to the detector. This effect is much more noticeable for neat samples but only slightly

noticeable for dilute samples. Also the amount of radiation throughput is decreased which results in a poorer signal-to-noise ratio.

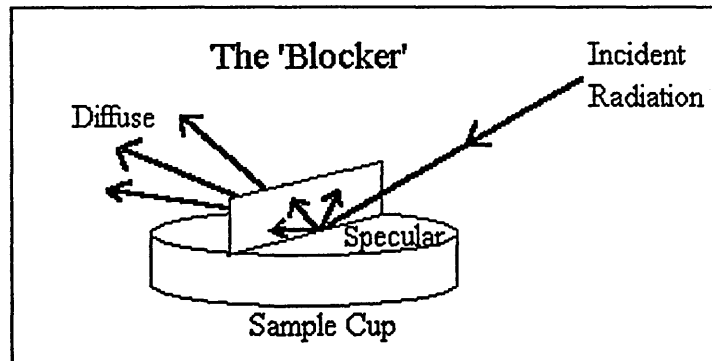
I) Rotation of Sample

Velapoldi et al. [50] designed, built and tested a rotating DRIFTS sample unit. Spectra taken with sample rotation gave data with better reproducibility than without rotation. The effect is presumably because it minimises sample orientation differences from sample to sample.

J) Use of a 'Blocker'

In 1985, Messerschmidt [51] described a commercially available diffuse reflectance device named a 'blocker'. This device is a thin metal blade that contacts the surface of the sample perpendicularly, bisecting the sample surface (figure 2.5).

Figure 2.5 : The Blocker.



The effect of this is to eliminate the specular reflectance component from the diffuse reflectance spectra (i.e. any radiation reflected without penetration into the sample). Although this is the case, radiation throughput is greatly decreased and the spectra obtained suffer from baseline shifts. This approach does not eliminate the diffuse specular component and as a result reduces, but does not eliminate, specular distortions.

2.1.2.4) Quantification in DRIFTS

If an analytical technique is to be deemed quantitative its whole procedure needs to be reproducible. There are two main problems that make the technique of DRIFTS only semi-quantitative. The first is the difficulty in preparing reproducible samples (both analyte and diluent) that have the same physical characteristics. The second arises from the difficult task of converting the reflectance spectrum to a format in which band intensities vary linearly with concentration over a wide concentration range. This second problem arises because there is always a specular reflected component observed in a diffuse reflectance spectrum and also the scattering changes from sample to sample. It is therefore very difficult to correlate the amount of true diffuse reflectance (i.e. the component that contains the information about the amount of sample) to sample concentration.

2.1.2.4.1) Reproducing the physical characteristics of a sample

Not only do the physical characteristics of a sample need to be reproducible, they also need to be of a form that allows the minimum amount of specular reflectance to be collected. Hence, all the fundamental factors discussed earlier that effect the diffuse reflectance spectrum need to be optimised (i.e. more diffuse reflectance and less specular reflectance needs to be collected).

- Particle size of analyte and diluent needs to be small (approximately $<10\mu\text{m}$) and constant from sample to sample. Ball milling analytes (and diluent/reference powder) for constant times helps to overcome this problem.
- The orientation of sample crystallites need to be the same from sample to sample. Packing the sample under pressure for constant times decreases the variability from sample to sample.
- Samples need to be of 'infinite thickness'
- Samples need to be homogeneous. Good mixing is essential and can be achieved by the use of a ball mill (this also regulates particle size).
- Sample height must be optimised to give more radiation throughput. An optical accessory that allows the sample height to be adjusted is ideal.

- Sample cups engineered to exact specifications help to reduce sample height and sample packing variations.
- Samples should be diluted in a non-absorbing matrix (preferably KCl or KBr), this has a dramatic effect on the reduction of specular reflection and enhancement of diffuse reflectance

Hughes et al. [48] followed a strict sampling preparation procedure for the analysis of sandstones and showed the standard deviation for samples prepared in this manner is 0.01 absorbance units. This method was reproducible when different analysts followed the procedure and is more reproducible than other methods.

Krivacsy and Hlavay [52] have also found DRIFTS to be a reliable quantitative analytical technique. They showed that the precision can be equal to that of the transmission technique if the optimal experimental conditions are used. They proved this by analysing quartz and calcite concentrations in aerosols and clinoptilolite in natural zeolite rocks.

It is found that if the physical characteristics of a sample are reproducible then as the sample concentration increases, so does the amount of specular reflectance and thus a decrease in diffuse reflectance is observed. This is why most DRIFTS calibration plots fall below the linear calibration plot at higher concentrations.

2.1.2.4.2) Quantitative relationship between diffuse reflectance and sample concentration

The most widely accepted theory regarding the relationship between the light absorbed in a diffuse reflectance experiment and the concentration of an absorbing component was developed by Kubelka and Munk [53, 54]. The relationship is described using the Kubelka-Munk (K-M) function, $F(R_\infty)$, which is given by:-

$$F(R_\infty) = (1 - R_\infty)^2 / 2R_\infty = K/S$$

where R_∞ is the diffuse reflectance spectrum of an 'infinitely thick' sample ratioed against that of a non-absorbing reference, K is the absorption coefficient, and S is the scattering coefficient.

As described earlier a sample is often mixed with a diluent and the reference spectrum is usually that of the pure diluent. The dilution matrix should be non-absorbing so

that K is related to the absorption of the sample alone. In this scenario, K, is related to the absorptivity, a, and the concentration, c, by:-

$$K=2.303ac$$

In practice the K-M function is valid only if the amount of specular reflectance is negligibly small and the scattering coefficient remains constant as the concentration is varied. Thus it is only found useful if samples are small absorbers and the concentration range is small. The greater the absorptivity of the band under investigation, the more non-linear the plot tends to be. Although problems may arise when using the K-M function, many quantitative analyses have been performed [55].

Some scientists have modified the K-M function in order to overcome the problems associated with it and have produced improved quantitative results. For example, Christy et al. [56], investigated the effects of particle size on diffuse reflectance spectra and made a modification in the K-M equation to include particle size. It showed that the proposed model could be used for dilute samples in a quantitative manner. Also, Boroumand et al. [57] used an adapted version of the K-M function to quantify non-diluted surface derivatised silica powders.

Alternative formulae that may be applied to diffusely reflecting samples are those of Pitts and Giovanelli [58], and Rozenberg [59]. These were tested and compared to the K-M formula by Hecht [60] on a number of different sample preparation types. No single formula was found to be superior for all sample types, but the K-M function was found to be the best for powdered samples.

Spectral data may also be displayed as:-

$$-\log(R_s/R_o),$$

which is referred to as diffuse absorbance by analogy to normal transmission data, where R_s and R_o are the reflectance of the sample and reference, respectively.

Smyrl et al. [61] chose this alternative presentation for measuring the reaction of water vapour and carbon dioxide within lithium compounds. They found that quantitative analyses were possible with either diffuse absorbance or K-M when adequate standard samples are used. They also noticed that when using the K-M function the strong bands were accentuated and the weaker bands were depressed, resulting in the possibility of important spectral details being lost. This behaviour was not observed when diffuse absorbance was used.

Horr et al. [62] compared the appearance, reproducibility and linearity of K-M and diffuse absorbance spectra for undiluted samples. The samples studied were thin films of polystyrene and long chain alcohols adsorbed on silica powder. They found the appearance of the spectra to be the same as that observed by Smryl et al. [61], i.e. the K-M function depresses all the weakly absorbing bands and accentuates the strongly absorbing bands. They showed that the diffuse absorbance spectra were more reproducible than the K-M spectra because the latter always produced larger relative errors than the former. Relative errors are associated with the small variations seen (as a voltage) on running a FTIR interferogram of a sample over time. These small variations of intensity may be due to fluctuations of light from the source or even variations in the detection efficiency of the detector. Whatever the variations, they result in relative error. The authors demonstrated the difference by using the same single beam spectra of polystyrene to generate the diffuse absorbance and K-M spectra. The band heights from the K-M spectra always gave equal or larger errors than those measured in diffuse absorbance. They also found that band heights measured at high wavenumbers are more in error than those in the lower wavenumber region and suggested that in the high wavenumber region there are more fluctuations in the photon energy from the source or more variations in the detector efficiency (the same trend in errors was also found if band areas were measured). In addition, the relative error in the K-M function due to noise in the reflectance spectrum has been discussed by Kortum [27] and Krivacsy [63] who have shown that it is desirable (less error) to select infrared bands that do not have a reflectance value too low or too high. To determine which transformation gave the best linearity they studied a range of alcohol concentrations adsorbed on silica. They plotted the absorbance band height values against concentration and showed that both the K-M and diffuse absorbance data showed some linearity for low concentrations of adsorbed alcohol on the silica. The K-M values appeared more linear, despite the fact that the error in band height between K-M spectra at any single concentration is greater than the error in band height obtained from the diffuse absorbance spectra.

Improved quantification can be achieved by the use of Multivariate analysis of which there are many different types. In this thesis, factor analysis and regression methods have been applied.

2.1.2.5) Variable Temperature - Diffuse Reflectance Infrared Fourier Transform Spectroscopy (VT-DRIFTS)

Basically, VT-DRIFTS allows diffuse reflectance spectra to be obtained at a range of temperatures and can provide information regarding the changes in the solid sample as it is heated. The information can also be correlated with information obtained by conventional thermal analysis techniques, for example, Thermogravimetric Analysis, Thermomechanical Analysis, Differential Thermal Analysis and Differential Scanning Calorimetry.

Hamadeh et al. [64] were among the first to develop a heatable-evacuatable cell that could interface with DRIFTS optics. This cell was used to study the infrared absorption spectroscopy of alumina-supported rhodium clusters under varying amounts of carbon monoxide. Several other papers describe the use of VT-DRIFTS for solid state structure changes [65 and refs. 1-8 therein, 51].

There are two types of VT-DRIFTS

- 1) Stepped VT-DRIFTS: here samples are heated to selected temperatures and infrared spectra are obtained after equilibration at each temperature. Spectra may be measured while the sample temperature is maintained at each step or the sample can be cooled to a selected temperature before spectral measurements are made [66, 67].
- 2) Ramped VT-DRIFTS: [references 1,2,5-8 in [68]] here samples are heated at a constant rate and each infrared spectrum is collected over a temperature range.

Ramped VT-DRIFTS results are more easily correlated with TGA and DSC measurements than stepped VT-DRIFTS results, but the latter generally yield spectra with fewer baseline distortions. Ramped VT-DRIFTS is a much faster analysis than stepped VT-DRIFTS.

VT-DRIFTS spectra are highly susceptible to baseline artifacts, which can result from instrumental fluctuations (instrumental drift) occurring between collection of reference and sample spectra. This happens because some FT-IR instrument parameters vary with time [69, 70] e.g. source output, interferometer instabilities, and, fluctuations in detector pre-amplification and filter electronics. Depending on the

number of different temperatures at which the sample holder must be equilibrated in stepped VT-DRIFTS and the temperature range and heating rate in ramped VT-DRIFTS, the time delay between sample and reference interferograms measurements can be in the order of many minutes, hours or days.

Also unmodulated infrared radiation emitted from the heated sample may effect the DRIFTS spectrum, especially if a liquid nitrogen cooled MCT detector is employed [71]. Baseline artifacts are typically broad features superimposed on DRIFTS spectra. Heating of the sample results in significant thermal expansion of the sample holder which changes the characteristics of the incident-beam-sample interface and may result in baseline shifts [66].

A simple procedure [70] for eliminating temperature dependent artifacts from VT-DRIFTS spectra consists of measuring sample and reference single beam spectra at the same temperature. This is less of a problem for stepped VT-DRIFTS rather than ramped VT-DRIFTS because the sample and reference temperatures are equilibrated for the former and are more likely to be comparable. A good temperature controller is therefore essential.

Figure 2.6 demonstrates the effect of sample holder temperature on the DRIFTS baseline, (also demonstrated by White [70]):-

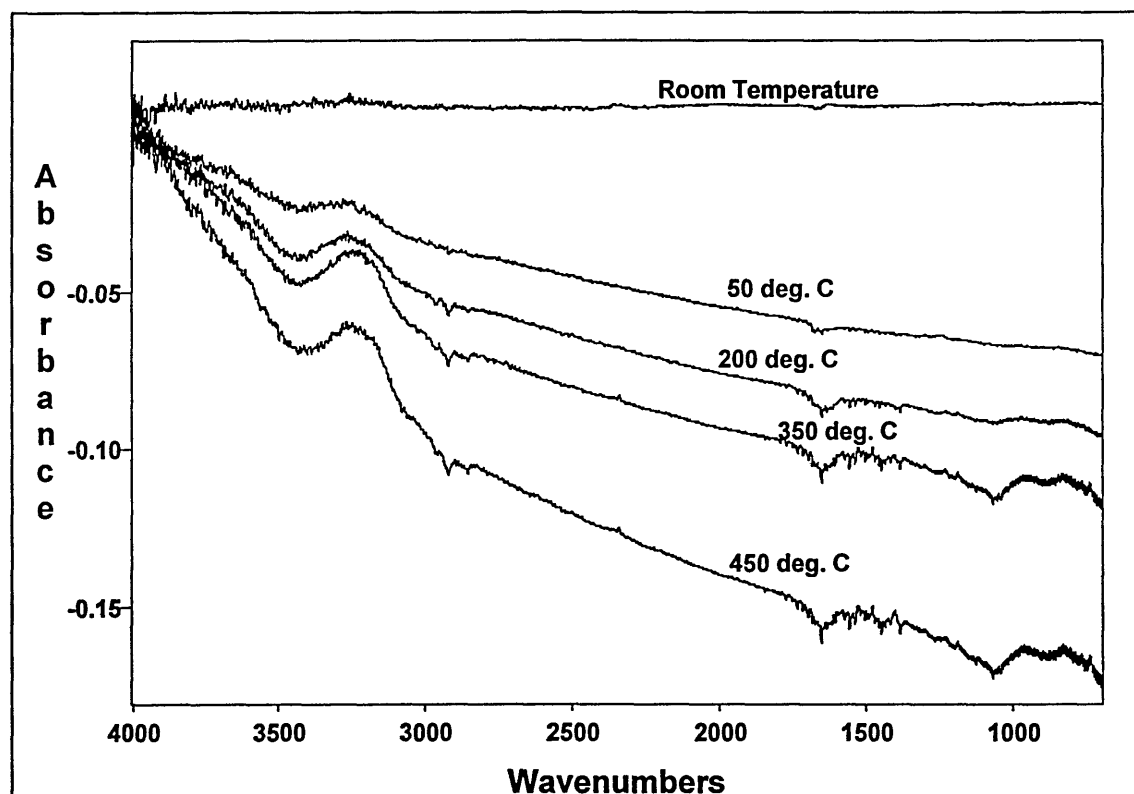
The baselines shown in the figure were obtained by ratioing the sample single beam of KBr at increasing temperatures against the sample single beam of KBr at 25°C. The spectra were then converted to absorbance. The same KBr was used for both the sample and reference spectra and so no changes due to scattering or absorptivity of the KBr will affect the spectra. Sample and reference spectra ratioed at the same temperature do not show this baseline offset, as indicated by the top spectrum, i.e. a flat baseline is observed.

DRIFTS baselines similar to the 'corrected' baseline in figure 2.6 are not always obtained in VT-DRIFTS because sample and reference scattering coefficients differ in actual experiments. Thus, although they can be minimised, they can not be eliminated. White [72] has discussed the possibility of removing baseline artifacts mathematically.

White [73] also found that apparent absorbance ($\log 1/R$) is less sensitive to spectral baseline offsets resulting from sample holder thermal expansion than the K-M format.

Although it was not possible to derive quantitative information regarding sample degradation from apparent absorbance spectra, it was possible to compare temperature dependant absorbance band changes qualitatively. This is because apparent absorbance is not a linear function of concentration.

Figure 2.6 : Effects of temperature on the baselines of VT-DRIFTS spectra.

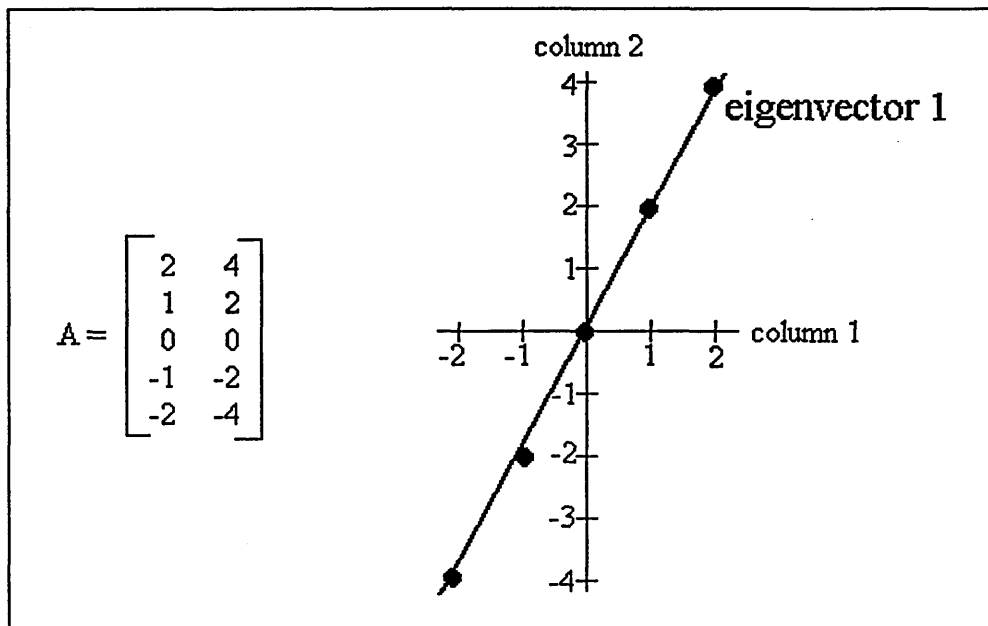


During a VT-DRIFTS experiment, the sample tends not to be compressed. This is so that good gas contact with the entire sample is possible and thus effusion of products from the sample is much faster than it would be for compacted powders. Some cell designs [19] allow gas to be passed through the sample and thus equilibration will be faster.

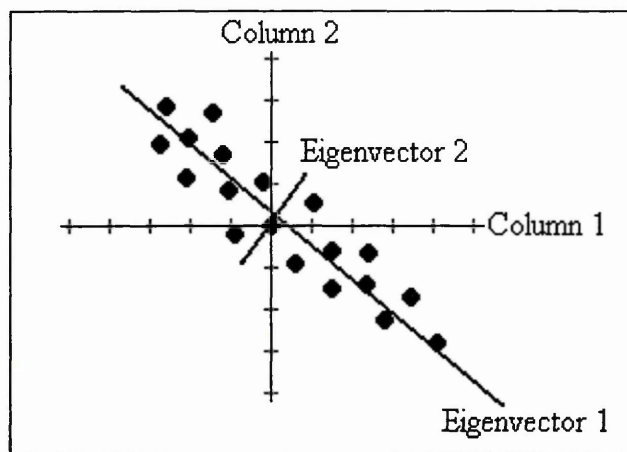
2.2) Multivariate Analysis - Partial Least Squares

Partial Least Squares (PLS) analysis is a statistical approach to quantitative analysis based on the partial least squares algorithm [74-77]. It has been applied in this thesis to infrared spectra of mixtures of minerals in order to determine the quantity of each individual component. The PLS algorithm examines regions of the spectra to determine which areas vary as a function of component concentration.

In PLS analysis a regression model is established between a matrix A, of absorbances at p wavenumbers for m samples and a matrix C, of the concentrations of n components in the same samples. The values for the concentration matrix need to be obtained by independent means. For example, if the mineral components in a sandstone were to be determined by DRIFTS, then XRD analysis could be used to construct C. Prior to modelling the matrices are split into a calibration set and a validation set. The matrices are divided randomly and pairs of data records (i.e. repeat experiments) are always kept together. A PLS model is created using the calibration set and then the matrices in the validation set are used to choose the optimum number of factors required to model each analyte component. A factor is defined as any linear combination of the original variables. Factors can be defined using eigenvectors, these are directions in space that describe the maximum amount of variation or spread in the samples. This can be illustrated in the 5 x 2 matrix A shown below:-



The figure shows the data and the direction of the first eigenvector where the space is defined by A is a plane. In this case all the variation in the data can be described using one eigenvector. The samples all fall on a line in column space, and therefore all the variation lies in one direction. If all the variation is not accounted for by the first eigenvector, a second eigenvector can be found that is perpendicular or orthogonal to the first and describes the maximum amount of residual variation in the data. This is demonstrated in the figure below,



The factors of A are re-expressed in a matrix U and is termed the score matrix. This matrix results from projecting A onto the eigenvector V, as $RV=U$. The score matrix U is composed of the original data points in a new co-ordinate system described by the eigenvectors.

The method of PLS is a modelling procedure that simultaneously estimates underlying factors in both A and C (a modelling procedure that only determines the factors in A is called Principal component regression). This is accomplished by using the columns of the C matrix to estimate the factors for A and at the same time the columns of A are used to estimate the factors for C. The resulting models are:-

$$A = TP + E$$

$$C = UQ + F$$

where the T and U are termed the score matrix of A and C, respectively, and P and Q are called the loadings. The loadings are chosen to maximise the correlation between the scores and the analyte, high loadings correspond to a high correlation whereas

small loadings correspond to a low correlation. The advantage of this is that if a column in the A matrix poorly describes the concentration of a component it can be given a low weighting. The matrices E and F are the residual errors associated with modelling A and C with the PLS model.

In the ideal situation, the sources of variation in A are exactly equal to the sources of variation in C and the factors for A and C are identical. However this is never the case and the factors for the A and C matrices have the following relationship

$$u = bt + \epsilon$$

where b is termed the inner relationship between u and t and is used to calculate subsequent factors if more than one factor is necessary to describe the variation.

Validation matrices are used to choose the optimum number of factors for each component. In order to determine the recommended number of factors to use, the Predicted Error Sum of Squares (PRESS) is calculated. PRESS is a cross validation technique used to determine the number of statistically significant factors. It begins by determining the predictive ability of using only one factor on a set of validation samples. The next step is to determine the predictive ability of the first and second factors. As the true number of significant factors is reached, the prediction should improve and thus the PRESS should decrease. However, as the truly significant number is passed the model includes noise, which results in a poor predictive ability. Thus the PRESS should start to increase again at this point.

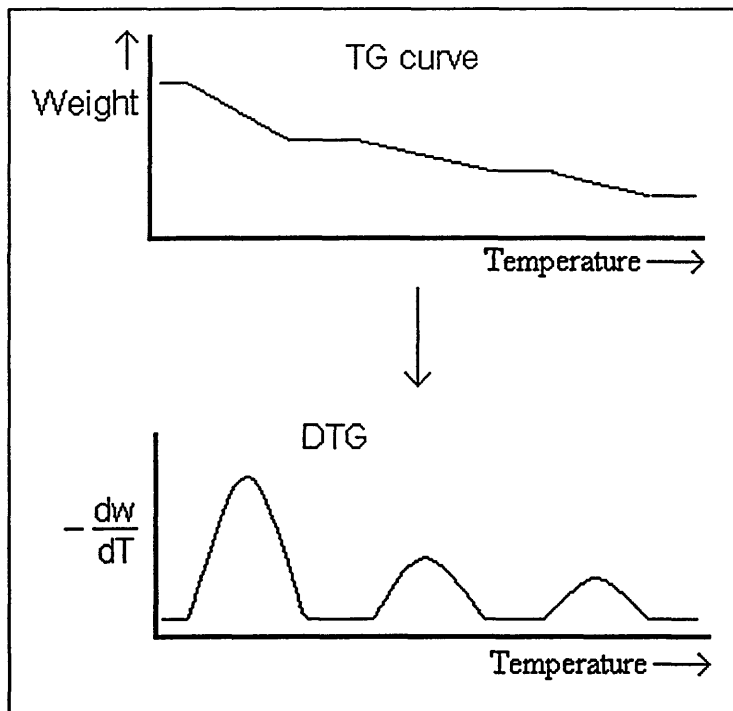
In a PLS model, certain criteria need to be met:-

- 1) The number of calibration standards need to be more than the number of components being measured.
- 2) The standards need to be mixtures that contain all the components present in the samples to be analysed.
- 3) The concentrations of components in the standards must vary independently i.e. a plot of one component against another should show no trends. They also need to cover the expected range.

2.3) Thermogravimetric Analysis (TGA)

This technique involves the measurement of mass loss from a sample under a linear temperature gradient. The sample is contained in a refractory crucible and suspended from a sensitive recording balance. Mass and temperature readings can therefore be made simultaneously. Samples may be heated from room temperature to 1000°C or in some instances up to 1500°C. The data output is in the form of a TG curve which shows a decrease (or increase) in weight as the sample is heated. Alternatively the TG curve may be represented as the negative derivative (DTG), this enables weight losses to be represented as maxima (figure 2.9).

Figure 2.9: Typical data output from TGA.



There are several factors that influence the shape of a TG curve which are related to the sample, the apparatus and experimental conditions. These need to be taken into account in order to achieve reproducibility;

- i) particle size distribution and packing density.
- ii) use of inert atmospheres, for example nitrogen and/or helium which may be used to suppress the oxidation of organic materials in clays.

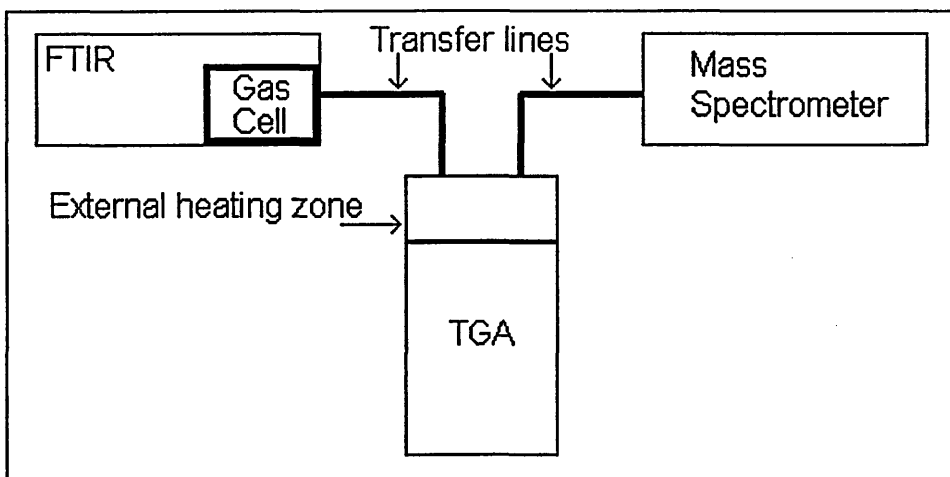
iii) the sample holder which must enable product gases in the immediate vicinity of the sample to be efficiently removed.

iv) the heating rate of 10°C/min has become standard, but only due to historical factors. The resolution of maxima decreases with increasing heating rate and maxima temperatures increase with increasing heating rate. The maxima size also increases with heating rate. It is important that the same heating rate is used for any samples that must be compared.

2.4) Evolved Gas Analysis by Thermogravimetric - Fourier Transform Infrared Spectroscopy (TG-FTIR) and Thermogravimetric- Mass Spectrometry (TG-MS).

TG-FTIR and TG-MS involve recording the weight loss of a sample and analysing the evolved gases by FTIR and/or MS. FTIR uses characteristic vibrations to identify particular functional groups in molecules whilst MS breaks up a molecule and identifies it from the diagnostic pattern. The Evolved Gas Analysis in this thesis has been performed on an Unicam-Cahn Synergic Chemical Analysis System (figure 2.10)

Figure 2.10: Diagrammatic representation of the synergic analysis system.



Mass Spectrometry

The mass spectrometer used in the synergy system is an ATI Unicam Automass System 2 quadrupole mass spectrometer. The MS is operated in the Electron Impact (EI), positive ionisation mode. There are three main sections in the quadrupole mass spectrometer; i) the ion source, ii) quadrupole mass analyser and iii) the detector.

Ion Source: The Ion source is where the sample is introduced into the MS. The sample passes through an electron beam (70eV) and ionisation of the sample occurs (i.e. electron removal leaving a positive ion). The molecular ions may also fragment to form charged and neutral fragments. Only positive charged fragments will be detected. The ions are then accelerated by electric fields towards the quadrupole mass analyser.

Quadrupole Mass Analyser: This is used to select the required mass range of molecular ions to be detected.

Detector: The ions which have travelled through the quadrupole are then sent towards the detector. The ions strike a dynode which emits secondary electrons, these are transformed into photons and then detected by a photo-multiplier. This amplifies the photon signal.

FTIR spectroscopy

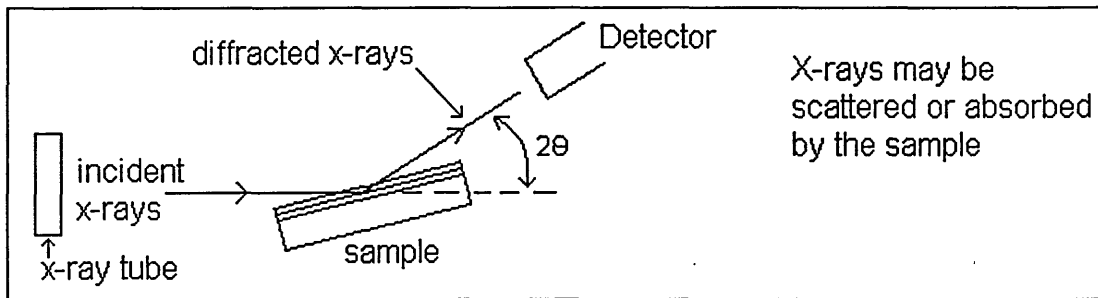
The basic principles of FTIR have already been outlined in section 2.1. When using FTIR in the synergic system the reader should note that the spectra collected will be of the evolved gases. Gas phase spectra will be different to the corresponding liquid phase spectra. Bands are often sharper and positioned at higher frequencies.

The Synergy system can accommodate sample sizes from a few milligrams to 100 grams, although typically in this thesis the sample size was between 25 and 100mg.

2.5) X-ray Diffraction (XRD) and Variable Temperature-X-ray Diffraction (VT-XRD)

XRD is a powerful technique used to identify the crystalline phases present in materials [10, 78, 79]. Figure 2.11 shows the basic features of an XRD experiment.

Figure 2.11:



X-rays are produced when high speed electrons strike the atoms of any substance. A modern x-ray tube consists of a heated filament (source of electrons) and a metal target (e.g. Cu) in an evacuated chamber.

In a typical experiment the diffracted intensity (of the scattered x-rays that obey Bragg's Law) is measured as a function of the diffraction angle (2θ) and the orientation of the sample, which yields the diffraction pattern.

Diffraction will occur if a beam of x-rays falls on a series of atom-bearing planes, each a distance d apart, at an angle θ , if the Bragg Law:

$$n\lambda = 2d \sin \theta$$

(where λ is the wavelength of the rays and n is an integer) is obeyed.

During an experiment the detector and sample are rotated by a goniometer in order to reach the required angle ranges (3-75°).

Samples can be offered as a deposited film or as a powder. Deposited films are obtained by smearing a solution of the clay on a glass slide and allowing the film to dry. The use of powder samples involves compacting a finely ground sample into an aluminium sample holder.

VT-XRD is achieved by placing a glass slide (on which a film has been deposited) on a small heating plate. The heating stage used in this thesis allows samples to be heated up to 300°C.

2.6) Scanning Electron Microscopy (SEM)

During SEM electrons are bombarded on the surface of a sample. The energy of the electrons is deposited in the sample and its dissipation yields a variety of signals for analysis. These include the formation of secondary electrons (SE), back scattered electrons (BSE) and characteristic x-rays.

The detection of secondary electrons provides a topographical/morphological image of the sample which appears three-dimensional, whereas the detection of BSE provides a flatter two-dimensional image. One advantage of using BSE imaging is that the intensity of the signal from different minerals strongly depends on their average atomic number. This allows different mineral phases to be distinguished on the basis of differences in grey level. The quality of data using BSE is dependent on sample preparation, the sample should have a flat smooth surface so that the elemental data is not influenced by topographical irregularities.

The detection of x-rays is termed Energy Dispersive x-ray Analysis (EDX) and provides semi-quantitative elemental spectra of surfaces. Elemental analyses of rock surfaces may therefore be possible which can confirm the mineral-type.

2.7) X-ray Fluorescence (XRF) spectrometry

XRF spectrometry is used to determine the quantity of elemental oxides present in a sample. X-rays are directed towards the elements in the sample, which produces characteristic x-ray fluorescence radiation of specific wavelengths. The amount of fluorescence at a specific wavelength is then related to the concentration of the element in the sample.

2.8) Molecular modelling

A detailed understanding of the theory of molecular modelling has not been acquired. The modelling work performed in this thesis was achieved under the guidance of Edo Boek and Stuart Jenkins (Schlumberger Cambridge Research). The reader is referred to reference [80] for a detailed description of the fundamentals behind molecular modelling.

There are two types of molecular modelling, Monte Carlo (MC) and Molecular dynamics (MD) simulations. MC simulations are based on interaction potentials between atoms whereas MD uses classical equations to describe the movement of molecules (e.g. Newton's equations).

3) Traditional and Current Methods of Characterising Minerals

Although the techniques used to characterise minerals are described individually in this chapter, they are often employed side by side so that they are complimentary to each other. For example, El-Shabiny et al. [81] used thermal, XRD and infrared methods to study Egyptian bentonitic clays, and, Sucha et al. [82] used XRD, infrared and chemical analyses to study different illites obtained from the western carpathians (Slovakia).

3.1) X-ray Diffraction

The most satisfactory single procedure for the identification of minerals is X-ray Diffraction (XRD) [83, 84]. It is one of few procedures presently available that can adequately evaluate complex mixtures of minerals. Quantitative analysis can be performed, but the accuracy depends on the complexity of the mixture and the availability of good standards. This is because a natural clay standard can vary in structural composition and crystallinity, which leads to changes in the intensities and widths of the diffraction peaks. Other difficulties arise because XRD cannot detect non-crystalline materials and the diffraction intensity varies with particle size.

Collection of an XRD trace requires the particle size to be as small as possible (finely crushed) and thoroughly mixed, because if there is not a completely random orientation of a particular component, variations in the diffraction peaks will appear from sample to sample. This type of preparation is ideal for determining the bulk mineralogy, but does not distinguish the surface mineralogy from that of the bulk. Whole rock XRD gives only semi-quantitative estimates of clay mineral abundance, especially for sandstones in which clay mineral contents are fairly low (<5-10%). Other techniques involve analysing only the <5 μ m sized fraction of a rock (i.e. the clay minerals). Quantification of the relative proportions of different clay minerals can therefore be made easier by ignoring reflections due to non-clay minerals

The intercalation of organic molecules into clay minerals present in soils has been used to identify their presence. Lim et al. [85 and references therein] have used the

intercalation of dimethyl sulphoxide into clay minerals (e.g. kaolinites) because their resulting x-ray diffraction peaks could be used to differentiate between them.

Churchman et al. [86] used XRD to determine the presence of halloysite in kaolinite. They achieved this by utilising the difference in time required for formamide to intercalate into the minerals. If each mineral is intercalated with formamide both of their XRD traces show a distinctive peak at 10.4Å. The intercalation process is much faster in halloysite (20-30 minutes) and therefore recording the XRD trace of a mixture before intercalation occurs in kaolinite enables the amount of the former to be determined. The total concentration of kaolinite and halloysite is then determined via TGA, which can be used to determine the amount of kaolinite by simple subtraction. The error involved in their estimates is $\pm 10\%$. XRD traces of the minerals before intercalation could not be relied upon to differentiate between kaolinite and halloysite because their differences are too subtle. Churchman [87] has compared this procedure to other similar intercalation methods using different molecules (DMSO and glycerol). Formamide was found to be the best because the others tended to also intercalate quickly into some crystalline forms of kaolinite.

3.2) Infrared Absorption Spectroscopy

Infrared spectroscopy has been used since the late 1950's to identify mineral species and to derive information concerning the structure and composition of minerals [88-90]. Its value lies in its ability to give a quick preliminary examination of the general nature and purity of a specimen. Advantages of infrared as a technique include:

- i) speed of handling
- ii) applicable to crystalline and amorphous compounds
- iii) direct structural information is provided, leading to immediate recognition of broad classes of compound such as nitrates, carbonates, sulphates, etc.
- iv) a close and precise identification not only of a particular mineral species, but also a placing within a range of composition may be possible.

The value of this technique should not be overestimated because there is the possibility of spectral variations due to particle size and shape, and also changes due to preparatory techniques used.

The technique is best suited to the qualitative identification of minerals rather than quantitative identification, especially when investigating a mixture of minerals. This is because there are many overlapping vibrational bands that result in very few or no independent diagnostic bands. Thus, chemometrics are necessary in order to gain quantitative data. It is also difficult (or impossible) to obtain suitable mineral standards that are either pure or have the same structural composition. Despite these limitations it is possible to quantify minerals. For example Matteson and Herron [91] have shown that it is possible to determine the type and quantity of feldspars present in a mixture of feldspars using FTIR spectral analysis. They have also used similar spectral analysis to determine the abundance of minerals in two carbonate rocks [92]. Koadama and Oinuma [93] used infrared spectroscopy to identify the presence of kaolinite minerals from sedimentary rocks. Their method gave the same detection limit (approximately 4.5%) as that of a XRD method and did not require the severe sample pretreatments used in the XRD method (e.g. treatment with acid to remove clay minerals other than kaolinites).

3.3) Scanning Electron Microscopy

Scanning Electron Microscopy (SEM) is an established method for the characterisation of reservoir rocks [94-97]. Coupled with Energy Dispersive X-ray Analysis (EDX) it can provide pertinent data on the morphology of the samples, the distribution of lining clay minerals present at the rock surface together with elemental analysis. Clay minerals do have distinct morphologies which can be determined by SEM. Although this method is excellent at identifying clay minerals, the problem is that a quantitative analysis of the whole rock is not possible. It is also good at providing an image of the surface, but because the surface has to be disturbed/alterd before analysis, it cannot truly differentiate between blocked and unblocked sections [98].

3.4) Chemical Analysis

Chemical Analysis involves accurately determining the elemental composition of a sample and subsequently comparing the proportion of elements so that the type of minerals present can be determined. The calculations require a number of assumptions, the main one being that the minerals present have already been determined qualitatively by other methods. The calculations can be very involved, requiring the solution of a number of simultaneous equations. Difficulties in relating the proportion of elements in a sample to complex mixtures do arise and therefore makes the technique less than ideal for the analysis of complex mixtures.

There are several methods available to determine the proportion of elements. The 'classical' and most accurate uses only wet chemistry methods [99], but a long time is required for its completion and a high level of skill is required for reliable results. Developments in instrumental technology allows accurate determination of elemental composition and is therefore less time consuming. Techniques such as flame photometry, emission and atomic absorption, colorimetric and XRF are sometimes used [100]. Instrumental methods are replacing classical methods for routine work, but the latter still needs to be used for occasional checking and calibration.

3.5) Thermal Methods

Thermal methods used to characterise minerals include; Thermogravimetric Analysis (TGA), Differential Thermal Analysis (DTA), Differential Scanning Calorimetry (DSC), and more recently Evolved Gas Analysis (EGA).

DTA depends on the detection of the heat given out or absorbed when a substance is heated. EGA involves the analysis of natural gases evolved when a mineral is heated over a linear increasing temperature gradient. The gases can be related to many physical and chemical changes within a mineral including; dehydration, oxidation of organic matter, dehydroxylation, destruction of the crystalline structure, decomposition, sublimation, vaporisation, fusion and solid-state transitions. Examples of evolved gases are; organic vapour, H₂O, CO₂ and SO₂, and less commonly CO, H₂ and O₂. Evolved gasses are usually detected by infrared

spectroscopy (IR) or mass spectrometry (MS), each technique having its own advantages and disadvantages. TGA, DTA and DSC are often combined with EGA so that simultaneous experiments can be performed and accurately related. IR and MS also have the potential to detect very small levels of evolved gas. These hyphenated techniques are, for example, termed TG-FTIR, TG-MS, DTA/FTIR, etc..

DTA has been used [101] to distinguish kaolinite from other members of its group (halloysite, dickite and nacrite) and to detect their degree of disorder. The distinguishing features occur when their structures change to the meta form upon heating, this occurs during dehydroxylation. The temperature at which dehydroxylation occurs is strongly related to the member of the mineral family and its degree of order and thus its history. Warne et al. [102] used variable atmosphere DTA to determine the iron content of carbonates in the dolomite-ferroan and dolomite-ankerite series (here, Mg in dolomite is exchanged for Fe). They have found that flowing CO₂ over carbonates enhances the maxima separation, attenuation and detection limits (0.25%). Whereas in air, maxima resolution is found to deteriorate on dilution of the sample, resulting in coalesced maxima of little diagnostic value. The carbonates studied dissociate in three stages to give three characteristic endothermic maxima which correspond to three weight loss steps on TG curves. One of the maxima is related directly to the amount of Fe present. Lopez et al. [103] used TGA and DTA to determine the major surface silt components in the province of Tucuman (Argentina). Smectite & illite, and, kaolinite & chlorite were identified as the major and minor components, respectively.

Carbonate, sulphate, sulphide and clay minerals are all suitable for examination by EGA, as they produce distinctive patterns of volatile generation related to thermally induced reactions such as decarbonation, oxidation and dehydroxylation. Provided that the stoichiometry of the reaction is known, measurement of the amount of volatile generated gives the concentration of the host mineral phase in the rock.

Morgan et al. [104] reviewed the application of evolved gas analysis in 1988 for the assessment of geological materials. They show that the same evolution profiles from a brick clay can be obtained when using either an IR or MS detector. The advantage

of using these techniques instead of or along-side TGA is that they have the potential to detect very small levels. Indeed, Milodowski and Morgan [105] have identified and quantified amounts of calcite, magnesite and strontianite down to 50 ppm in alumina using an infrared detector.

Bloodworth et al. [106] have used EGA successfully to quantify kaolinite mixed in quartz. This was based on the measurement of water resulting from dehydroxylation by infrared from artificial dilution sequences of kaolinite in quartz. They were able to detect amounts as low as 0.25%. They applied their technique to natural sandstones, believed to contain kaolinite. Problems did occur which were related to differences in dehydroxylation temperatures of differing ordered kaolinites and the presence of other minerals that produce H₂O in the same region as kaolinite.

Cai [107] used EGA to identify trace amounts of pyrite and siderite in dolomite and also establish their thermal degradation mechanism. Moreover, it was possible to perform compositional analysis of a mixture of minerals (siderite, kaolinite, dolomite, calcite and quartz). The EGA analysis system was coupled to a DTA. The gases were collected when a change in the DTA curve occurred and were analysed by Gas Chromatography (GC). In order to analyse the mixture of minerals, both the DTA and GC data are used. For example, the loss of H₂O detected at 540°C by GC is due to the presence of kaolinite and the presence of quartz was detected by a small exothermic effect in the DTA at 580°C when the heated residue was programmed cooled. Calcite and dolomite could be distinguished if the carrier gas flow was CO₂ and air (1:1). The procedure seems complicated but worked well and was reliable for the mixture used. The method was not quantitative and difficulty in interpretation may arise if additional components are added to the mixture.

Holdiness [108] reviewed evolved gas analysis by MS in 1984 and paid particular attention to the instrumentation available at the time along with some selected applications. Gibson and Johnson [109] used TG-quadrupole MS for investigating the decomposition and identification of released volatile components from a meteorite sample. Several gases were released during the heating program which were related to minerals that had previously been identified. These included;

i) H₂O (150-200°C) = limonite (α -FeO₃.H₂O),

- ii) H₂O (300-500°C) = montmorillonite and chlorite
- iii) SO₂ (400-500°C) = epsomite (MgSO₄·7H₂O) and gypsum (CaSO₄·2H₂O), the loss of water was also observed in this region,
- iv) CO₂ (500-600°C) = siderite
- v) CO₂ (600-700°C) = dolomite
- vi) CO (600-700°C) = carbonaceous matter.

This information was of interest because it cast light on the possible conditions that prevailed during formation of the meteorite.

Gibson [110] later applied the TG-quadrupole MS instrument to the analysis of shale and lunar soil samples. TG-analysis of the shale showed two distinct weight losses which coincided with the detection of two evolved gas peaks. The first peak was due to the loss of hydrocarbons and the second was due to CO₂ which derived from the decomposition of the former. The weight loss during the heating of the lunar soil samples to 1000°C was very low (0.35±0.10 weight %) and thus the TG-trace was not very informative. However, the high sensitivity of the mass spectrometer showed that numerous volatile gas species were released during the heating of the samples. These gases were related to; contaminants, solar-wind-derived species, breakdown products of carbon and sulphur containing mineral phases, and, gas phases in vesicles and gas rich inclusions.

Muller-Vonmoos et al. [111] developed a system which allowed for combined use of DTA, TG and EGA with a quadrupole MS. This instrument was applied to the investigation of clay samples of complex mineralogical composition. Prior to clay analysis, calcium oxalate hydrate (CaC₂O₄·H₂O) and sodium hydrogen carbonate (NaHCO₃) were analysed in order to clarify how accurately H₂O, CO and CO₂ could be determined quantitatively by EGA with a mass spectrometer. They stated that as low as 0.005mg of H₂O and CO₂ could be detected accurately (i.e. a straight lined calibration plot was obtained) during the decomposition of the CaC₂O₄·H₂O. Decomposition of NaHCO₃ was used to show that if H₂O and CO₂ are evolved simultaneously during the experiment little effect on the quantitative ability of the MS occurs. Analysis of the clay sample showed the loss of CO₂ and H₂O which were related to; organic matter, dehydroxylation of clay minerals, and, siderite and calcite decomposition. Values relating to their amounts were tabulated (i.e. 2.17, 2.21, 6.55

and 6.75%, respectively) but were not compared to results obtained from other methods of analysis.

A recent publication by Thornley and Primmer [112] has shown how a combination of techniques can make quantitative determination of illite and kaolinite in rocks possible. It describes how routine analysis of clay fractions from a whole rock by XRD can be combined with the detection of evolved water (EWA) by infrared to quantitatively detect the abundance of illite and kaolinite in mixtures of chlorite and quartz. They studied mixtures of mineral standards with compositions similar to sandstones. The lowest amount of kaolinite and illite studied was 2.3 and 1.4%, respectively. The precision of repeat determinations of weight percentage of evolved water by EWA for 20 analyses over a 12 month period was <5%. This technique was also applied in a case study involving real sandstones in order to determine accurately the illite abundance.

4) Literature Survey and Strategy

The main programme of research in this PhD was focused on developing two characterisation methods. The first method employed an infrared technique, Diffuse Reflectance Infrared Fourier Transform Spectroscopy (DRIFTS), which can distinguish the constituents of a rock using differences in their vibrational spectra. This technique has been applied to several rocks which have undergone various sample preparations. The intention is that the spectra obtained can be used to determine and quantify the surface mineralogy.

The second method aims to use organic molecules as ‘chemical probes’ to elucidate the surface mineralogy of the rock. If the chemical probe associates itself with a particular constituent of a sandstone, under certain conditions, then the probe may be used to identify the particular constituent. Research in this thesis has considered a number of techniques for the detection of a chemical probe. These include Thermogravimetric analysis and Evolved Gas Analysis by Fourier Transform Infrared Spectroscopy and Mass Spectrometry.

4.1) Method 1 : Characterisation by DRIFTS

4.1.1) Review of DRIFTS for mineral analysis

With the advent of FTIR spectrometers and improvements in diffuse reflectance accessories, the use of DRIFTS has become widespread. The content of the many papers published on DRIFTS show that the technique is applicable to many types of samples. An up-to-date review on recent applications of diffuse reflectance has been written by McKelvy et al. [113]. Some examples of the applications that DRIFTS has been used for are pharmaceutical tablets (forensics and quality control), coals and minerals, polymer powders and painted surfaces [21 and references therein].

Blitz and Augustine, praised DRIFTS highly for the characterisation of heterogeneous catalysts [114]. Since most catalysts are in a powdered form, DRIFTS is the ideal technique for their analysis. Cloutis et al. [115] used diffuse reflectance spectroscopy in the near infrared region to characterise minerals in oil sands, which are a complex

mixture of clays, bitumen (an array of various hydrocarbons), quartz grains, water and minor accessory minerals. Infrared bands (either overtone or combination) could be attributed to both the major and minor constituents in the samples.

Delgado et al. [116] compared transmission spectroscopy (TS), photoacoustic spectroscopy (PAS) and DRIFTS for the characterisation of construction cement minerals. They stated that the TS technique gave simpler and better defined bands than those obtained by either DRIFTS or PAS. This is unlike other DRIFTS results [117] and is probably due to the very basic sample preparation procedure used. The results of Delgado show that DRIFTS is a good alternative to TS because the latter is very labour-intensive. The PAS technique was found to be the easiest technique of the three since it required minimal sample preparation. However, the bands obtained via this technique were at a lower wavenumber than those of the other two techniques.

Nguyen et al. [117] compared DRIFTS with the pressed halide disc (transmission) method for characterising a range of Australian soils. A number of advantages were found when using the DRIFTS method of which some are listed in section 4.1.2. A secondary aim of the paper was to demonstrate the ability of the DRIFTS technique as a tool for the rapid characterisation of clay mineralogy and organic matter in soil, which proved successful. This paper is of particular interest because it determines the presence of minerals such as; kaolinite, illite, bentonite, quartz, carbonates and gibbsite which are also mineral constituents of sandstones and reservoir rocks.

Methven and Hughes [118] used DRIFTS for qualitative comparisons of the mineralogy within six surface-quarried sandstones. The sandstones were studied as ground powders. This data alongside quantitative data obtained via transmission spectroscopy, and physical property data (i.e. pore size distribution, permeability and porosity) were used to evaluate methods for improving the placement of treatment fluids during oil recovery. The DRIFTS spectra were of excellent quality and were able to describe the mineral composition of each sandstone.

The diverse use of DRIFTS as a technique for analysing solids has been established in the literature and so it has been used to characterise rocks in this thesis.

4.1.2) Advantages over transmission spectroscopy

For many years the pressed halide disc transmission method has been used to successfully characterise pure minerals [88-90, 119] because the spectra are sensitive both to structural and compositional variations in the minerals. However, several publications [117, 120] have compared DRIFTS to the pressed halide disc transmission method for a variety of studies and have shown the former to exhibit several advantages, which include:-

- i) minimal or no sample preparation
- ii) very high sensitivity (down to low ppm levels)
- iii) applicability across a wide range of sample concentrations from ppm to neat
- iv) useful overtone and combination bands are observed.
- v) enhancement in bands at high wavenumbers compared to transmission spectra
- vi) during the preparation of pressed halide pellets, high pressure is required and this can cause; unexpected spectral changes [121], chemical reactions [120] and structural damage to the sample surface [114]. The problem is an important consideration for the analysis of clay minerals because for example, the pressing of kaolinite into halide pellets can change the relative intensities of its hydroxyl peaks [122] due to preferred orientation effects. The magnitude of change depends on the absolute pressure and the pressing time used. Grinding during the preparation of pellets may also change the crystallinity of kaolinite and hence its infrared spectrum [123]. This will be discussed in more detail in section 5.2. DRIFTS does not require sample pressing, eliminating this variable in kaolinite studies. This improves the ability of infrared spectroscopy to distinguish kaolinites according to their hydroxyl group differences. Changes in spectra are not necessarily restricted to kaolinite samples, other clay minerals may change under pressure, for example smectite clay may undergo ion-exchange with the halide matrix. During a DRIFTS experiment, the sample may be dispersed in a non-absorbing matrix such as KBr. Although, this physical dispersion preparation is much milder than that of the halide pellet method, it is not completely immune from artifacts of sample preparation. Iwaka and co-workers [124] have shown that ion-exchange takes place when obtaining a diffuse reflectance spectrum of $\text{CuSO}_4 \cdot 5\text{H}_2\text{O}$ in KCl. Although a reaction occurred for this particular sample, it is

thought that the clay minerals will undergo no such change, because they are far more robust.

DRIFTS also has the ability to analyse irregular surfaces [19, 23-25] and thus should cope well with sandstone grains.

4.1.3) Quantification with DRIFTS

Diffuse reflectance data is usually converted to either diffuse absorbance or Kubelka-Munk units (see section 2.1.2.4.2) in order to produce data that is linear. This is necessary if quantitative analysis is to be performed. These two forms of conversion do not always produce data that is linear and so quantification becomes difficult. The data is not always linear because of the problems associated with collecting DRIFTS spectra (section 2.1.2). Although quantitative analysis using DRIFTS has its problems many publications report quantitative data.

Moudgil et al. [125] analysed a binary mixture of dolomite species, which differed only in their surface chemical groups. Conventional characterisation by x-ray diffraction could not be used because the dolomite species had the same diffraction patterns. A successful quantitative technique employing DRIFTS which used the K-M transformation was therefore devised.

Tsuge et al. [55] used DRIFTS to determine the particle size and concentration of the α -component in silicon nitride powders. The former was achieved by measuring the intensity ratio between two bands and the latter was achieved by comparing the band intensity to that of standard α -silicon nitride. The results obtained by this technique were in good agreement with those obtained by an XRD method.

Babu and Seehra [126] proposed a DRIFTS method for the quantification of silica in mine dust samples. They chose the 1875cm^{-1} band of silica, which does not suffer interference from other minerals usually present in mine dust samples. Incidentally, this band has proven very useful for the quantification of quartz in sandstones (section 5.2). The results obtained were compared with independent results obtained by XRD and a good agreement was found. Pandurangi and Seehra [127] also chose the 1875cm^{-1} band for quantitative analysis of silica in silica-kaolin mixtures. In addition, they

found DRIFTS to be more accurate for silica analysis than photoacoustic spectroscopy.

Sobkowiak and Painter [128] compared the DRIFTS and halide pellet techniques for the quantitative analysis of functional groups in coal. They analysed a large set of pyridine soluble coal extracts by the above techniques in order to obtain the absorption coefficients for the aromatic and aliphatic CH bands so that these could be used in structural studies of the parent coals. They found that the halide pellet technique gave superior results to DRIFTS when compared to an independent NMR method. Unfortunately, the DRIFTS sample preparation procedure used was old and did not incorporate modern sampling procedures that produce superior results.

Quantification of complex mixtures using any infrared technique is restricted by overlapping bands of the constituents. A means of overcoming this problem could be to employ curve-resolving techniques, but this requires a detailed knowledge of the bands arising from each component. Another means of overcoming this problem was demonstrated by Painter et al. [129], who used spectral subtraction techniques in order to determine mineral matter in coal. The multicomponent analysis technique is based on the successive subtraction of the spectra of the individual components from the spectrum of the mixture. This enables the removal of high intensity bands, revealing the characteristic absorption bands of others. Although the authors used spectra obtained via transmission spectroscopy, the subtraction techniques could be applied to DRIFTS spectra. They were able to quantify the presence of some of the common minerals present in coals such as quartz, kaolinite, montmorillonite, gypsum and calcite by using only the mid-infrared region. Unfortunately, the analysis of pyrite had to be achieved in the far-infrared region, which took additional time. The process was found to be time consuming but, with care and experience, quantitative analysis was possible.

An additional means of improving quantification of diffuse reflectance data is to employ multivariate analysis. This involves the use of additional mathematical manipulations after either diffuse absorbance or Kubelka-Munk (K-M) has been

applied in order to improve linearity of the spectral data. There are several different types of multivariate analysis available that can be applied to diffuse reflectance spectra.

Isaksson and Naes [130] used a mathematical transformation in order to remove the scattering effects when studying near-infrared spectra. The method, called multiplicative scatter correction (MSC), was developed by Martens et al. [131] and uses linear regression of spectral variables versus the average spectrum and corrects for scatter effects. This method was used for the prediction of protein, fat, water and carbohydrates in food stuffs before using regression analysis and was found to improve prediction compared to when regression analysis was used alone. The method was further developed [132] and was called "Piece-Wise-MSC". It was used to study near-infrared reflectance spectra for the determination of protein, fat and water content in meat samples and found to give better predictive results than normal MSC. Again this transformation accounts for the differences in scattering from sample to sample.

Fredericks et al. [133, 134] successfully used factor analysis and multiple linear regression on DRIFTS spectra of coal, bauxite and diesel fuel in order to relate them to many of the significant properties of the materials. Porro and Pattacini [135] also used these methods on DRIFTS spectra of neat silanized kaolin clay samples. They obtained excellent quantification with good precision. Measurements were made on eight concentrations (0-1.5%) of three types of silanized kaolin clays.

A useful type of multivariate analysis that can handle interferences, such as scatter correction and over-lapping bands, is Partial Least Squares Regression (PLS). This technique has been successfully applied in spectroscopy, for the quantification of; complex mixtures of effluents from sulphite pulp mills [136], in clinical chemistry [137], in research on the structural determination of pharmaceutical compounds [138], and the quantitative determination of crystalline and amorphous silica [139]. This last investigation required PLS because there is an almost complete spectral overlap in the region where the various forms of silica have their main absorption bands. This method was found to be more robust and more accurate than the commonly used method that combined infrared spectroscopy and XRD. The combination of these two

methods was necessary because amorphous silica cannot be studied using XRD. Although the spectral data was acquired via transmission spectroscopy, the technique could be applied to spectra obtained by DRIFTS.

A recent publication by Hughes et al. [140] has shown that the combination of DRIFTS with multivariate calibration models, allows the composition of unknown cements to be determined quantitatively. Cements are used during the extraction of oil and because of their unpredictable nature during ageing and deterioration, they need to be characterised before use. Their composition needs to be known so that poor performing cements can be discarded. Obviously, a fast and accurate characterisation method would be required and this has been achieved by the authors. The DRIFTS spectra of 156 cements of varied origin were used to construct the multivariate model which were calibrated by reference to accurate elemental analysis (ICP and others). The models were able to describe up to 14 components with adequate accuracy. In addition the models used had the capacity to be extended further in order to improve the predictability of characterisation. The method described by Hughes et al. for obtaining high quality DRIFTS spectra has been modified and applied to the rocks in this thesis.

Moreover, information other than the composition of a cement has been determined from DRIFTS spectra. For example, through the use of artificial neural network and PLS techniques, DRIFTS spectra of cement powders can be used as a measurement for the prediction of; cement physicochemical parameters (e.g. particle size), slurry performance properties (i.e. thickening times) and cement ageing and deterioration [141-143]. The use of FTIR-ATR as a technique for cement hydration has also been investigated [144]. Overall these techniques are very important in a field laboratory, especially because cements which may cause major operational failures in the field can be eliminated.

4.1.4) Application of DRIFTS in this thesis

The DRIFTS technique has a wide sampling range (ppm to neat) which has allowed various preparations of rocks to be investigated within this thesis, with the intention that they may be related to the surface mineralogy.

Before these investigations were undertaken DRIFTS was applied to rocks that had been ball milled since the resulting fine particle size provides better resolution of bands (see section 2.1.2). The fine particle size together with an optimised spectral collection procedure (see section 5.1.1) has provided reproducible spectra which can be directly compared with other spectra. The spectra of the rocks have been compared with those from several mineral standards (Table 4.1) in order to correlate spectral features with particular minerals. In addition, this particular application is suited to the determination of the bulk mineralogy.

The possible rock preparations, for the determination of the surface mineralogy can be summarised into 3 categories:-

- 1) The analysis of whole rocks as a function of particle size
- 2) The analysis of the rock components separated by sedimentation or ultrasonics.
- 3) The direct analysis of cut and fractured surfaces.

Category 1 was performed in order to investigate the effect on the DRIFTS spectra when the size of the rock grains and particles were changed by increasing the harshness of crushing. It has been shown that the separation of clay minerals by sedimentation and ultrasonics maybe been achieved [145]. Category 2 was therefore performed in order to discover whether a change in the spectra would be observed when separation was achieved.

Category 3 was performed in order to minimise the time required for sample preparation and to determine whether representative DRIFTS spectra of the sandstones could be obtained. Also, less disruption to the surface mineralogy would occur.

Initially, the sample preparation procedures were applied to surface quarried sandstones selected from the 'The building sandstones of the British Isles' handbook [146]. A list of the seven sandstones selected and their source, colour and grain size is given in Table 4.2.

Table 4.1 : Mineral Standards used in this study

MINERAL TYPE	CODE	SOURCE	FORMULA
Tectosilicates			
Quartz	Chelford Sand		SiO ₂
	Hpf5 Sand	British Industrial Sand Ltd. (Oakmoor, Staffs.)	SiO ₂
Feldspar	Orthoclase (Potash Feldspar)	BCS No. 376	KAlSi ₃ O ₈
	Albite (Soda Feldspar)	BCS No. 375	NaAlSi ₃ O ₈
Phyllosilicates			
Montmorillonite	SWy-1 (Na)	Source Clay Repository	[(Al,Mg,Fe) ₂ (OH) ₂ Si ₄ O ₁₀ (Ca,Mg,Na,K)] nH ₂ O
	SWy-2 (Na)	Source Clay Repository	variation of above
	SWa-1 (Fe)	Source Clay Repository	variation of above
	SCa-1 (Ca)	Source Clay Repository	variation of above
Kaolinite	KGa-2	Source Clay Repository	Al ₄ Si ₄ O ₁₀ (OH) ₈
Illite	Silver Hills Illite		Al ₄ Si ₄ O ₁₀ (OH) ₂ .K,Al
Illite-Smectite	CMS ISMt-1	Clay Mineral Standard	
Chlorite	CCa-2	Source Clay Repository	(Mg, Fe, Al) ₆ (Al,Si) ₄ O ₁₀ (OH) ₈
Carbonates			
Dolomite		BCS No. 368	CaCO ₃ .MgCO ₃
Magnesite			MgCO ₃
Siderite			FeCO ₃
Calcite			CaCO ₃
Aragonite			CaCO ₃

Table 4.2 : Selected Sandstones used in DRIFTS studies

Sandstone	Source of Sample	Grain Size	Colour
Clashach	Hopeman Moray Firth	fine	buff to fawn
Hollington Red	Staffordshire	medium	pale pink with darker banding
Stancliffe	Derbyshire	fine	buff
Birchover	Derbyshire	medium	pink to buff
York Stone	West Yorkshire	fine	light buff
Berea			
Castlegate			

Hollington Red is a medium grained laminated sandstone. The darker bands are approximately 1cm apart, and vary in thickness between 1-3mm. The bands contain finer grain particles than those between the bands. The remainder of the sandstones are homogeneous with no evidence of banding. A table showing their mineral composition can be found in section 5.2.6 (page 124). Table 4.3 shows the mean-pore diameter, permeability and porosity of the sandstones

Table 4.3: Physical properties of the sandstones used in this study

	Median pore diameter (μm)	Mean KCl permeability (mDarcies)	Mean porosity (%)
Clashach	26.6	644	22.0
Hollington Red	20.04	normal to banding 376 parallel to banding 669	24.7 23.7
Stancliffe	2.8	6.2	13.2
Birchover	2.64	12.5	16.1
York Stone	0.74	6.3	11.5
Berea	unknown	unknown	unknown
Castlegate	unknown	unknown	unknown

The physical properties were determined [118] by:-

- mercury porosimetry (pore size distribution)
- constant pressure core flooding experiments (KCl permeability)
- gravimetric determination following core saturation (Porosity).

The mean results were obtained from experiments performed on several cores from each sandstone (the range of results obtained are exhibited in reference [118]).

These sandstones which are impure due to the presence of clay minerals are representative of the hydrocarbon reservoir rocks. These sandstones are used as standards in studies concerning oil recovery from reservoir rocks and pertinent petrophysical and geological information for these sandstones are available in the literature [3, 147, 148]. Subsequent to these analyses, a selection of reservoir rocks obtained from a range of depths in the North sea were analysed. Table 4.4 presents a physical description of their appearance.

Table 4.4: Physical description of the reservoir rocks used in this thesis

Reservoir Rock (RR)	Description
RR1	Very fine grains, powdery surface. Cores are very soft and light grey in colour. One sample was solvent cleaned and one was oil saturated.
RR2	Medium sized grains. Cores are very hard and dark grey in colour.
RR3	Fine to medium sized grains. Cores are very hard, with dark grey edges and a light grey centre.
RR4	Large grains. Cores are soft and dark grey in colour. Saturated in oil.
RR5	Fine grains. Cores are fairly soft and light grey in colour
RR6	Medium grain size. Cores are hard and light grey in colour with small black regions

In addition to DRIFTS, XRD traces of the mineral standards and rocks have been obtained so that the presence of a mineral can be confirmed.

The feasibility and application of multivariate analysis on the DRIFTS spectra of rock samples has been discussed and performed, respectively in section 5.1.7. Partial Least Squares was chosen as the multivariate technique to be used for the minerals.

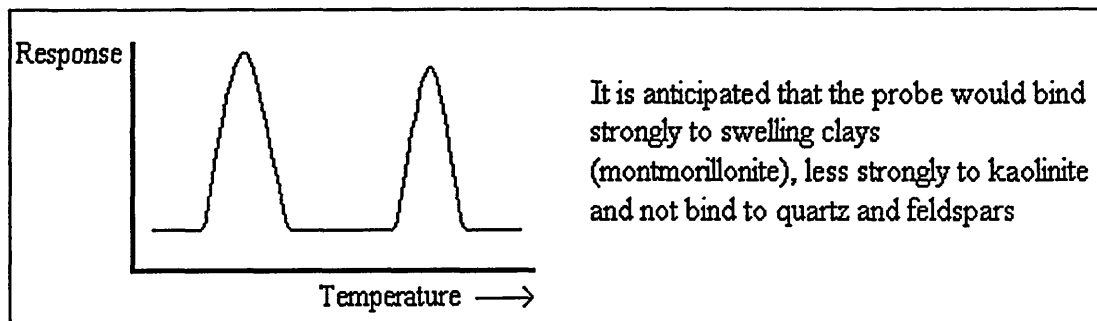
4.2) Method 2 - Characterisation of pore lining minerals using 'Chemical Probes'.

Method 2 has been designed so that minimal disruption or destruction to the internal structure of a rock (i.e. the surface mineralogy) will occur. This is to be achieved by simply analysing an uncrushed fragment of rock. The method therefore attempts to account for the presence of blocked pores within a rock and hence determine whether there is a difference between the surface and bulk mineralogy.

4.2.1) The 'Chemical Probe' strategy

This method aims to use organic molecules as chemical probes to elucidate the surface mineralogy of a rock. If an organic molecule is introduced into a rock, it will to some extent interact with the mineral constituents. The strength and type of interaction of the probe with the various minerals should be different because of their differing structures. If a treated rock is heated the desorption temperatures of the probe from each mineral should also be different. Thus, monitoring the desorption of the chemical probe (as pulses of gas) from a rock as a function of increasing temperature should produce a chromatogram-type trace as shown in figure 4.1.

Figure 4.1: Expected chromatogram-type trace



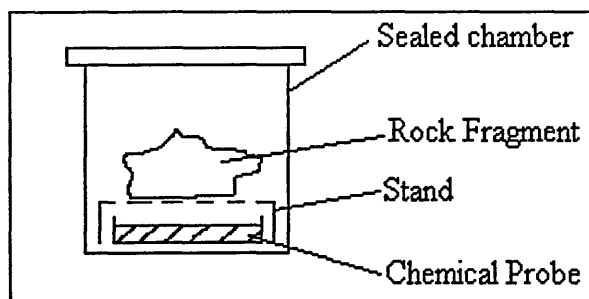
A knowledge of the desorption temperatures associated with individual minerals can then be used to characterise the rock.

4.2.1.1) Chemical probe requirements

The principal objective for using chemical probes is to overcome disruption to the inner core of a rock. A chemical probe therefore needs to penetrate through the pores of a rock core and interact with the pore lining minerals without disrupting them.

Ideally, a rock core should be exposed to a chemical probe via the vapour phase because it is known [2, 32] that changing or introducing a liquid in a pore can move fines. This results in the blocking of pores and hence the true composition will change. It is envisaged that exposure of the rock will be achieved by simply suspending a rock core in a sealed chamber containing an atmosphere saturated with the vapour of the chemical probe (figure 4.2). In order to obtain a saturated environment the chemical probe therefore needs to be sufficiently volatile.

Figure 4.2: Exposure procedure of rocks to chemical probe



A chemical probe needs to be selective towards the different mineral constituents that may be present in a rock. It is necessary that the probe desorbs from each mineral over a unique temperature range.

The chemical probe also needs to be easily detected. For example, if the desorption of the chemical probe was to be detected by infrared spectroscopy then it should contain a group with a high extinction coefficient (e.g. a carbonyl).

4.2.1.2) Instrumental techniques that could be used to detect a chemical probe

The choice of technique depends on the characteristics of the chemical probe. The simplest and cheapest technique to employ would be thermogravimetric analysis

(TGA). This involves measurement of mass loss from a sample under a linear temperature gradient and so it is possible to monitor the desorption of a chemical probe. The greater the loss in mass from a sample within a specific temperature range would indicate the presence of a greater quantity of a particular mineral constituent.

A more sophisticated and sensitive technique to employ would involve monitoring the evolution of a chemical probe from a rock by either infrared spectroscopy or mass spectrometry as a function of increasing temperature. If using infrared analysis the chemical probe under investigation would require a strong characteristic absorbance band and when using mass spectrometry, a unique fragment ion related to the chemical probe would be needed. It is worth noting at this stage that some of the types of rocks under investigation may contain oil residues. The desorption of organics from the oil residues may occur in the same temperature range as the chemical probe and it is therefore essential that the chemical probe can be distinguished. These latter techniques, termed Evolved Gas Analysis (EGA) techniques have an advantage over TGA because they are not only able to determine what actually leaves the rock over a given temperature range, but because these are very sensitive techniques they offer the ability to determine much smaller quantities of mineral constituents. All these techniques have been used in this thesis.

During the development of this strategy, other ideas based on mineral determination using chemical probes came to light (some of which are discussed in section 8). One idea was based on the fact that infrared absorbance bands of organic molecules are known to shift in frequency or change shape when their environment changes. The infrared spectrum of an organic molecule associated with one mineral may be quite different when associated with another mineral. These differences could be exploited as a means for mineral identification. For example, if a rock surface was treated with a chemical probe and the surface of the rock was mapped using infrared spectroscopy, then a characteristic shift or band shape change could be used to characterise the surface. An image similar to that observed under SEM could then be obtained. An obvious advantage would be that expensive and complicated SEM equipment would not be needed.

4.2.2) Review of organo-mineral interactions.

The interactions between minerals and organic molecules have been studied by a great number of people within a great number of industries, for a great number of years [149]. Some of the many industries interested in such interactions include: geological, oil exploration [150], pharmaceutical [151], waste treatment industry [152], plastics, catalyst [149], laundry powders [153], agricultural [154-156], and many more. Most interest is associated with clay minerals because these can be highly reactive. For example, clay minerals in soils play a vital role in the pollution control of hazardous organic molecules. The adsorption of such hazardous materials slow down their migration through soils and may also change the activation energy of their decomposition. Another example involves the addition of smectites, as fillers, to paint and dye suspensions [157]. This can lead to changes in the colour of the dye due to π -interactions between the aromatic compounds and the oxygen plane of the clay, a knowledge of these interactions is therefore vital. The adsorption behaviour of surfactants and polymers on montmorillonite has also been studied [158] because mixtures of polymers, surfactants and clays may be used in treatment fluids for enhancing oil recovery.

The adsorption of pyridine on surfaces has been employed as a probe for acid sites by many people [159] and its interactions have received much interest [160]. Montmorillonite can also be used in catalysis reactions because of its intercalation and retention properties. These properties can be modified so that their catalytic behaviour can be tuned/manipulated [161, 162].

Haderlein and Schwarzenbach [163] have studied the sorption of a large number of nitroaromatic compounds on montmorillonite, illite and kaolinite surfaces in order to predict their movement through soil systems. They studied the effects of environmental factors, such as pH on the sorption processes and found these to be very important. Their experiments gave a fuller understanding to the interactions between nitroaromatic molecules and minerals [164, 165].

Many papers have been published concerning the kinetics and effect of pH on organo-clay interactions. Naidja and Huang [166] studied the adsorption and desorption of aspartic acid intercalated into Ca-montmorillonite. They showed the adsorption in an

aqueous medium was a fast reaction process since 78% of the aspartic acid was retained by the clay surfaces at the end of a 15 minute period. Maximum adsorption reached 84% (56.2 μ mol/g clay) after 2 hours. They studied the adsorption at pH 7 whereas others had used acid conditions. The results showed that it was weakly held at pH 7 and would be expected to be readily transported from soil (at the same pH) to ground and surface waters. Other papers investigating the effects of pH include; Zhang and Sparks (kinetics of phenol and aniline adsorption on hexadecyl trimethyl-ammonium montmorillonite) [167], and Harter and Ahlrichs (effect of pH on the nature of aniline and urea adsorbed by montmorillonite) [168].

Many techniques, which will be discussed later in this section, have been used to characterise organo-clay mineral complexes and properties. The techniques used can determine:-

- i) whether adsorption complexes are formed or the clay and organic are present simply as a mechanical mixture,
- ii) the type and strength of interactions between organic molecules and clay layers,
- iii) the effect of the clay surface on the stability or degradation mechanism of the adsorbed organic.

4.2.2.1) Types of organo-mineral interactions

Each type of clay mineral will interact with an organic molecule differently since each clay surface and its interlayer space have different types and populations of Bronsted and/or Lewis acidic and basic sites. The principal interactions observed between clays and organic molecules are of the acid-base type.

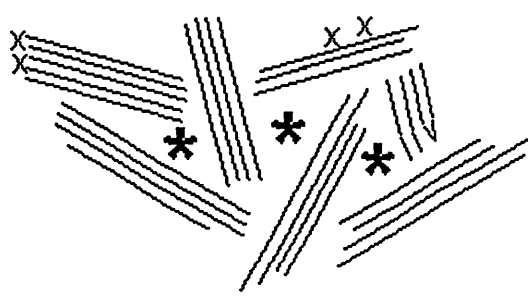
4.2.2.1.1) Typical smectite and organic molecule interactions

The interaction of organic molecules with smectite clays is a complex process. Lacher et al. [169-171] performed a very detailed study on the interactions between different cation-exchanged montmorillonites and benzinine (a pesticide) and showed that numerous types of interactions were formed. Other examples of organo-smectite

complexes include; sulfolane adsorbed on cation substituted montmorillonites [172], the interactions of alachlor (a herbicide) with homoionic montmorillonites [173], and the adsorption of atrazine on smectites [174].

The different types of interaction are summarised in Table 4.5.

Table 4.5: Possible clay-organic interactions

<p>1)</p> $\text{BH}^+ \cdots \text{O} \begin{array}{c} \\ \text{H} \end{array} \text{--- Mn}^{n+}$	<p>Water coordinated to exchangeable metallic cations serves as a proton donor (Bronsted acid). Depending on the polarising power of the metal (M^{n+}) and the basic strength of the organic molecule (B), the organic molecule may be protonated by accepting a proton from a H_2O molecule, thus gaining a positive charge (1)</p>
<p>2)</p> $\text{B} \cdots \text{H} \text{---} \text{O} \begin{array}{c} \\ \text{H} \end{array} \text{--- Mn}^{n+}$	<p>The organic molecule may form a H-bond with the polar water molecule (2), i.e. the water acts as a bridging molecule.</p>
<p>3)</p> $\text{B} \cdots \text{Mn}^{n+}$	<p>After thermal dehydration or at room temperature the exchangeable cations may serve as Lewis acids and adsorbed bases become co-ordinated directly to the cations. If M is an alkali metal cation, then the bond between it and B is mainly electrostatic, ion-dipole attraction.</p>
<p>4)</p> $\text{B} \cdots \text{B} \cdots \text{H} \text{---} \text{O} \begin{array}{c} \\ \text{H} \end{array} \text{--- Mn}^{n+}$	<p>Organic molecules may also be associated to molecules of type 2. The presence of these depends greatly on the size of the molecule</p>
<p>5) Organic molecules may also be associated with broken edges, external clay surfaces with substitutions in the tetrahedral layer or clusters between stacks of clay layers.</p> <div style="text-align: center;">  </div> <div style="margin-left: 400px;"> <p>* - clusters</p> <p>x - individual organic molecules</p> </div>	

In addition to the five main types of interactions described in table 4.5, it is possible for positively charged organic molecules to exchange with interlamellar cations [175]. However, the number and variety of organic compounds which can acquire a positive charge is limited. Many such compounds (e.g. alkylammonium ions) contain nitrogen, of which the amines form perhaps the largest class. The benefit of such cation-exchanges is that a fixed internal porosity is achieved since the pore size and shape depend on the alkylammonium ion. Harper and Purnell [176] used this fact to create a novel adsorbent system for organic vapour sampling which would overcome problems encountered by other adsorbent systems (e.g. active carbons). Incidentally, Barrer [177], has reviewed his own studies, lasting 40 years, on the behaviour of clay minerals (in particular smectites) and their derivatives as sorbents.

Cation-exchange with organic molecules may also occur indirectly. Ruiz-Conde et al. [178] studied the interaction of aqueous solutions of formamide, acetamide and propionamide with vermiculite. Vermiculite is similar in structure to montmorillonite but has a higher exchange capacity. They showed that the amides hydrolysed to liberate NH_4^+ to form NH_4^+ -vermiculite-Mg-vermiculite (mixed layer) and then NH_4^+ vermiculite phases.

There are a number of factors that govern the adsorption of organic molecules to smectites. Dashman and Stotzky [179] examined the effect of molecular weight and basicity on the adsorption and binding ability of amino acids to homoionic montmorillonites. It was found that these factors were not as important as the type of exchangeable cations in their adsorption.

4.2.2.1.2) Typical kaolinite and organic molecule interactions

Although fewer molecules intercalate into kaolinites than smectites a range of compounds are known to do so, which include:-

- i) inorganic salts such as potassium acetate [180],
- ii) organic salts [175, 181],
- iii) long chain fatty acids [182], and

iv) small and large highly polar organic molecules such as; urea, formamide, glycerol, benzidine and n-octylamine [175, 180, 183]

It is more difficult for polar organic molecules to intercalate into kaolinites than smectites because strong hydrogen-bonding between the kaolinite layers needs to be overcome. Some molecules are able to intercalate directly into kaolinites from either the liquid or concentrated aqueous solution, but others can only enter by means of an entraining agent, or by displacement of a previously intercalated compound [184].

The interactions of organic molecules and kaolinites are not as varied as those of smectites. In general, the bonding from the clay to the organic molecules, involve the inner-surface-hydroxyls and sometimes the basal oxygens of the adjacent kaolinite surface. Some molecules that are known to intercalate and bond to both surfaces are N-Methylformamide, N, N-Dimethylformamide and Formamide.

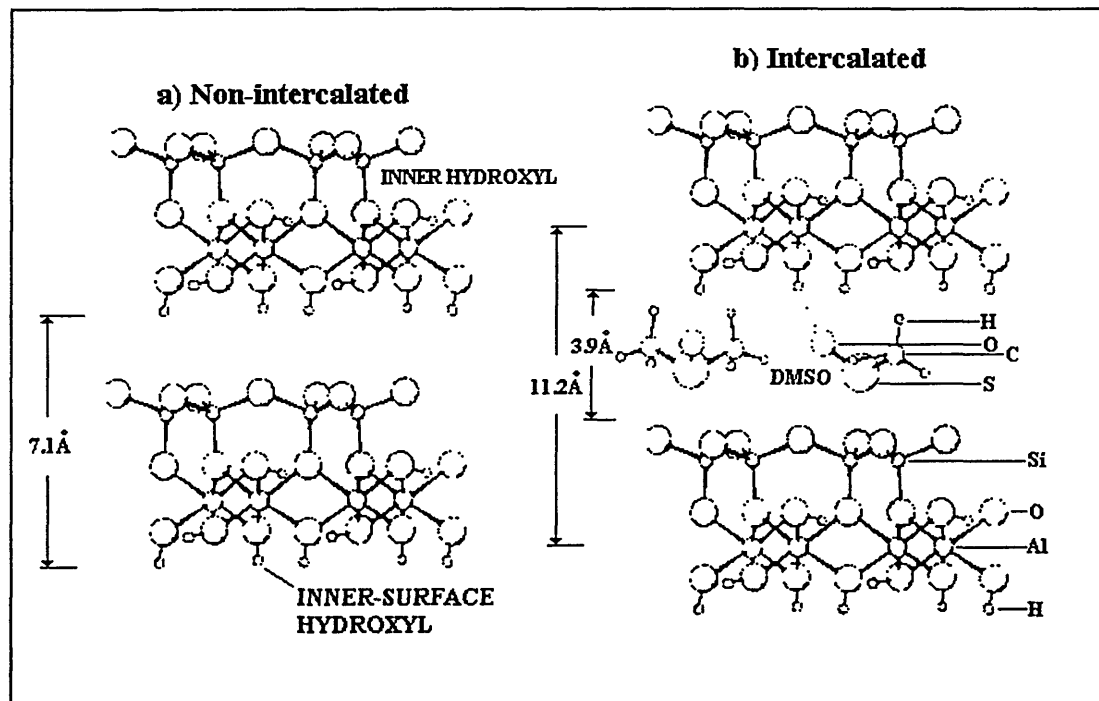
The intercalation of Dimethyl sulphoxide (DMSO) into kaolinite has received considerable attention. This is because i) it can be used to prepare complexes with other compounds via the displacement method [175], ii) it is used as an intermediate in the synthesis of hydrated kaolinites, and iii) sulphur compounds are among the most common atmospheric pollutants and DMSO is present in the effluents of various industrial processes, thus kaolinite has been used in its control. The intercalation of DMSO into kaolinite has been represented diagrammatically by Johnson [185] and this shows that the interlayer distance increases as the DMSO is intercalated (figure 4.3). It also shows that the DMSO molecules are oriented within the layers so that the oxygen of the DMSO molecule hydrogen bonds to the inner-surface hydroxyls of the kaolinite.

Most interactions between kaolinite and organic molecules occur in the interlamellar region, that is if the organic molecule is capable of penetrating into the H-bonded network. Whereas montmorillonite may intercalate up to 3 layers of organic molecules, never more than a single layer of molecules is taken up by kaolinite or halloysite. Other interaction sites may involve broken edges, external clay surfaces or clusters between stacks of kaolinite layers.

Other studies of organo-kaolinite interactions include; trimethyl phosphate induced decomposition of kaolinite [186], ethylene glycol intercalates [187], and, N, N-Dimethylacetamide and pyridine interactions with homoionic kaolinites [188].

A unique fact that differentiates the intercalation of organic molecules into smectites and kaolinites is that the molecules are specifically aligned when in the interlamellar space of the latter.

Figure 4.3: Diagram taken from Johnson [185] showing the intercalation of DMSO into kaolinite.



4.2.2.1.3) Other organo-mineral interactions

Illite is a non-expanding 2:1 layer silicate and adsorption of organic molecules is confined to external crystal edges. Since this is the case its adsorption capacity is less than that of montmorillonite [189]. Pinck et al. [190] have studied the adsorption of a number of antibiotics (e.g. streptomycin) on several clay types and found that adsorption decreased in the order montmorillonite>illite>kaolinite. Frissel and Bolt [191] compared the capacity of different clays to take up non-ionic herbicides and found adsorption to decrease in the same order. Grim et al. [192] has shown that illite reacts with organic ions up to its exchange capacity. The ions were thought to be limited to the exterior surface of the illite particles, i.e. they did not replace the K ions between the silicate layers.

The adsorption of organic molecules to chlorite has not been investigated in much detail simply because its adsorption capacity is very small. It is believed that if adsorption does occur then it will be limited to external crystal edges [175].

Very little literature is available relating to the adsorption of organic molecules to carbonates. However, Ince et al. [193] have studied the adsorption of oleic acid and oleate on surfaces of apatite (a phosphate rock) and dolomite. This was investigated because separation of the two minerals by froth flotation using oleic acid or oleate is difficult due to their similar surface properties. Improvement in the flotation of dolomite relative to that of apatite was achieved by the addition of Na ions and maintaining the solution at pH 4. This occurred because oleic acid preferred to adsorb onto dolomite in these conditions which was supported by FTIR spectroscopy studies. Literature relating to the adsorption of organic molecules to quartz and feldspar samples is sparse [194] because they are relatively un-reactive compared to clay minerals. However, several papers discuss the interaction of organic molecules on silica and alumina samples, which behave similarly. Sokoll et al. [195] studied the thermal desorption of n-butylamine from SiO₂ and Al₂O₃ surfaces by infrared spectroscopy. Their results showed that butylamine formed only weak H-bonds with the surface hydroxyl groups of SiO₂, whereas it formed stronger bonds between the nitrogen atom and the Al³⁺ cations of Al₂O₃. The formation of H-bonds between butylamine molecules and surface hydroxyl groups of Al₂O₃ also occurred. This paper highlights the fact that adsorption of molecules to silica and alumina surfaces occurs. The samples studied showed a large sharp O-H stretching band indicating the presence of a large number of hydroxyls. Quartz samples rarely possess such a large number of hydroxyls to bind with and thus interaction would be less likely and more difficult to observe.

Titova and Kosheleva [196 and references therein] have studied the interaction between triethylamine (TEA) and silica by IR spectroscopy. This was performed because TEA is widely used as a probe for acidic sites on silica. They showed that TEA can bind strongly or weakly to silica surfaces. This is due to the formation of different types of bonds ranging from H-bonding to complete proton transfer from SiOH to TEA, yielding a thermostable, salt-like (Et₃HN)⁺(Si-O)⁻ species. This species is stable under vacuum to over 500°C [197].

By analogy with silica and alumina samples the types of interactions expected between quartz, feldspar and organic molecules are likely to be simple H-bonding or maybe proton transfer to both undamaged and broken surfaces. Although the surface chemistry of alumina has been used as a guide to the surface chemistry of feldspars it has been suggested by Korentsky et al. [198] that it may not be a reliable correlation. They performed a very detailed VT-DRIFTS study on the hydroxyl species of synthetic and natural; quartz, feldspar, alumina and silica samples. The study showed that isolated SiOH surface species analogous to those present on quartz and silica do occur on feldspar species while AlOH groups analogous to those on alumina do not. The total surface area of quartz and feldspars in a rock will be a lot smaller than those of the clay minerals and thus very little interaction will occur which will be difficult to detect using even the most sensitive of techniques.

4.2.2.1.4) Factors affecting the adsorption of organic molecules onto minerals

Some properties of minerals and organic compounds which influence the adsorption of organic compounds by minerals have been commented upon already. A more comprehensive list of the properties of minerals and organic compounds that effect the adsorption process is shown below:-

Properties of surface

- Extent (total surface area)
- Accessibility (size of interlamellar spaces)
- Chemical nature of atoms forming surface (O or OH)
- Exchangeable ions on surface
- Configuration of surface
- Particle size and crystallinity [199, 200]

Properties of organic compound

- Charge
- Size
- Polarity

- Polarisability
- Shape
- Flexibility

Reaction conditions

- Raising the temperature disrupts the structure of the interacting liquid due to greater thermal motion, this increases the relative number of free molecules and the rate of intercalation.
- Addition of water to the intercalating liquid, this effects the extensive associated structure of the pure liquid into smaller aggregates of molecules, which in turn increases the rate of intercalation. Too much water results in the solvation of the intercalating molecules which results in relatively few unsolvated molecules to intercalate, this decreases the intercalation rate.
- Reaction medium. For example the selectivity of adsorption of organic ammonium ions to smectite clays can change depending on whether water or other solvents are used [201]. Batouti et al. [202] showed that the rate of exchange of Cu^{2+} on a Na-montmorillonite clay was faster in acetonitrile than dimethylformamide.

There are no well defined trends to determine whether an organic molecule will intercalate or how fast it will do so. For example, a large dipole moment will favour the formation of a complex, but a large dipole moment may cause extensive association in the liquid state and this will decrease the rate of intercalation.

4.2.2.2) Methods used to analyse organo-mineral interactions

4.2.2.2.1) Thermal Methods (TGA, DTA, DSC and EGA)

Thermal methods such as TGA and DTA have been used for studying organo-mineral interactions [203]. TGA curves can show the desorption of an organic molecule from a clay mineral as weight loss and DTA curves show both exothermic and endothermic maxima, which can be associated with; adsorption, desorption, combustion, decomposition, dehydration, sublimation, vaporisation, fusion and solid-state transitions [204]. When DTA or TGA is carried out in an air atmosphere the adsorbed organic material undergoes oxidation although some pyrolysis usually occurs also. In an inert atmosphere (e.g. N₂ or He), pyrolysis and liberation of the organic material occurs.

If TGA and DTA are used as individual techniques it is not possible to determine whether a weight loss or maxima, respectively, is actually due to desorption of the organic molecule and/or clay structure. In addition the weight loss or maxima does not give information related to the type of interaction occurring between the clay and organic molecule.

For example Yariv [205] used DTA to study the adsorption/desorption of aliphatic and aromatic amines by montmorillonite. He was able to determine that some amines adsorb more strongly than others, but could not correlate between the behaviour of non-adsorbed, either free or associated amine and, adsorbed amine.

Sidheswaran et al. [206] used DTA, TGA and DSC to study the thermal behaviour of intercalated kaolinites. They noticed that the decomposition temperature of potassium salts of acetic, malic, malonic and other acids lowered when intercalated into kaolinite compared to the salt alone, indicating a catalytic contribution from the clay.

Many additional techniques are used to support the information gained from TGA and DTA. Evolved Gas Analysis (EGA), is one technique that is becoming more popular in the characterisation of organo-clay interactions. This technique can be split into several categories depending on the type of detector used to monitor the evolved gases. Infrared (IR) and mass spectrometry (MS) detectors are two commonly used

systems applied with EGA. The advantages of EGA compared to TGA and DTA have already been outlined in section 3.5. More often than not TGA and/or DTA are combined with EGA so that both experiments can be performed simultaneously. These are often termed Thermogravimetric-infrared (TG-IR (or FTIR)) and Thermogravimetric-mass spectrometry (TG-MS).

Morillo et al. [207] used EGA for the study of pesticide adsorption by clay minerals in relation to pollution control, a knowledge of the stability of pesticide-clay complexes being of special interest. They studied the thermal behaviour of montmorillonite treated with the pesticide aminotriazole (AMT) by DTA, TG and EGA-MS. The results showed that montmorillonite 'protects' adsorbed AMT, delaying its first decomposition step, and catalyses the final decomposition step of AMT at lower temperatures. They also showed that AMT can i) be exchanged for the interlamellar cations, ii) remain around interlamellar cations as polarised molecules, or iii) be coordinated to the interlamellar cations through water bridges.

Inglethorpe and Morgan [208] have used EGA-IR to detect ammonia evolved when heating natural NH_4 -bearing minerals. This study was of interest because NH_4 -bearing minerals can be associated with:-

- i) host rocks of precious and base metal mineralisation
- ii) coal and oil shale deposits
- iii) indication of organic maturation and hydrocarbon generation.

NH_4^+ arises in minerals because it can substitute K^+ in silicate and sulphate minerals; some examples include NH_4 -feldspar (buddingtonite), NH_4 -jarosite, NH_4 -illite and NH_4 -alunite. They used IR to detect the evolution of NH_3 to discover if the NH_3 evolution maxima are diagnostic for specific ammonium host minerals. Their investigation demonstrated that several NH_4 minerals (the above examples) could be distinguished from each other. The method was not fully quantitative because the evolved NH_3 partially oxidised to N_2 and H_2O . However, the amounts of NH_3 evolved did show a moderate positive linear correlation with NH_4 content determined independently by a modified Kjeldahl method.

Rodriguez and Bugay [151] have used TG-IR to identify the volatile content of pharmaceutical solids. They used VT-XRD and DSC to determine whether the

evolved gases were due to a solvent incorporated into the crystal lattice or physically adsorbed onto the solid. Three examples of its application are given.

4.2.2.2.2) X-ray Diffraction

Interlamellar adsorption of organic molecules by clay minerals can be observed by XRD methods very easily. The X-ray observations establish that intercalation has occurred and provide information regarding the orientation of the adsorbed molecule or number of adsorbed layers. The latter two are derived from a knowledge of known molecular dimensions of the adsorbed molecules and the determined interlamellar separation distance. Direct evidence relating to the mechanism of adsorption cannot be provided by X-ray diffraction.

4.2.2.2.3) Infrared Spectroscopy (direct analysis of clay/organic complex)

Many groups [209-212] have used infrared to study directly the interactions between organic molecules and minerals. Infrared enables the identification of bands which are formed between functional organic groups and active sites in the clay surfaces. Bond formation and its strength can be estimated from the perturbation of characteristic infrared absorption bands of both the active organic and mineral groups. Presumably, the greater the change in the infrared bands upon intercalation, the stronger the bonding between organic molecules and the clay.

Lercher et al. [213] have reviewed the use of infrared spectroscopy of adsorbed molecules, of which many are organic, as a means of studying the surface acidity of oxides and zeolites and hence their catalytic ability. They show that infrared spectroscopy is an excellent technique because it is able to determine that one molecule can associate to a surface via different sites. Although it only reviews zeolites and simple oxides, these have similar structures to clay minerals and thus it can be applied to the minerals of interest herein. The organic molecules reviewed include; ammonia, aliphatic amines (e.g. n-butylamine), pyridine, nitriles and benzene. Typical absorbance band shifts for these molecules include the N-H

deformation band of ammonia (which appears at 1450 and 3300 cm^{-1} when it is the ammonium ion and 1250, 1630 and 3330 cm^{-1} when it is coordinated) and changes in the $\text{C}\equiv\text{N}$ band of nitriles.

Johnston et al. [214] have used infrared spectroscopy to study the vapour phase sorption of p-xylene on Co and Cu-exchanged montmorillonite. They used a cell that incorporated TG and FTIR analysis to determine the amount of water and p-xylene sorbed by the clays. Whereas most systems monitor the evolved gases produced when heating a sample, this system monitored the infrared changes in the sample. This is similar to VT-DRIFTS but in addition the sample is weighed. The sample is studied in the form of a self-supporting film and the infrared sampling beam passes through this which is contained between two windows. Perturbations of the infrared absorbance bands of p-xylene were noted when in the presence of Cu-montmorillonite, but not Co-montmorillonite and therefore showed chemisorption occurred for the former but not the latter.

Knözinger [215] has reviewed the application of infrared spectroscopy for the study of acidic sites on oxides and zeolites using probe molecules.

Infrared absorption spectra can be obtained via several methods including; self-supporting films, alkali-halide discs, films sedimented on infrared-transparent windows, or from oil mulls. In this thesis, DRIFTS and VT-DRIFTS has been chosen to study the interactions between the chemical probes and the clay minerals.

Parker and Frost [216] have used DRIFTS to study both the molecular reactions and concentrations of volatile organic chemicals adsorbed on montmorillonite. They studied the adsorption and desorption of volatile organic chemicals from montmorillonites as a means of slow release odour generation, for the application in attracting pest animals, in particular wild dogs. DRIFTS was able to show evidence of interaction of organics with the clay with both physi- and chemisorption determination. Multicomponent analysis of the DRIFTS spectra using a least square curve fitting technique provided an effective means of measuring low concentrations ($\approx 10\text{mg.g}^{-1}$). The organic molecules studied included; dimethyl sulfide, dimethyl disulphide, propanoic acid and trimethylamine.

Leyden and Proctor [217] used VT-DRIFTS to obtain qualitative and quantitative information regarding the acidity of surface sites on silica. They used pyridine as a

probe to determine the acidic nature of the surface, a technique [159, 160] known for many years, to demonstrate the ease and speed of use of VT-DRIFTS.

Other examples that use DRIFTS to study organo-mineral interactions include; Lee et al. (polyacrylate adsorption on alumina) [218], Davies et al. (fuel hydrazines adsorbed on silica, alumina and ferric oxide surfaces [219], Davydov & Budneva (paraffins adsorbed on simple oxides) [220], and Horr et al. (adsorption and oxidation of alcohols on silica) [221].

4.2.2.2.4) Other Techniques

Other techniques have been used to study organo-clay interactions. Breen and Rock [222], and, Cenens and Schoonheydt [223] have used UV-VIS spectrophotometry to study the kinetics of the interactions of methylene blue and neutral red (dyes) on montmorillonite and hectorite. Absorption bands were assigned to specific dye-clay complexes. Akyuz et al. [224] used Raman spectroscopy to study organo-clay complexes. Tennakoon et al. [225] used ^{13}C , ^{27}Al and ^1H Nuclear Magnetic Resonance (NMR) with XRD to characterise clay-organic systems as a means to explore the catalytic activity of natural clays. Particular attention was directed at comparing catalytically-active clays (e.g. Al-exchanged) to those generally less effective (Na-exchanged). ^{13}C NMR was used to identify products formed within the interlayer region. NMR has also been used to study water in kaolinite [226] and hallosite [227], and, DMSO, NMF and formamide/kaolinite complexes [228].

Electron paramagnetic resonance spectroscopy has been used to study subtle changes in the structure of kaolinite layers. Most work has mainly been performed in order to compare different kaolinites, but it has also been used to study kaolinite/organic complexes [228, 229].

Raman Spectroscopy has also been used to verify observations found by infrared and X-ray data on the bonding of DMSO and kaolinites after intercalation [185].

During the investigation of organo-mineral interactions the techniques discussed above are often used side by side so that their results are complimentary. For example, Gabor et al. [230] used DTA-EGA, XRD and FTIR methods to investigate

the thermal behaviour and decomposition of kaolinite intercalated with hydrazine and potassium acetate. Breen et al. [231] used TGA, infrared and XRD to determine the acidity of cation-exchanged montmorillonites by studying the desorption of pyridine and n-butylamine.

The use of molecular modelling has become a popular technique for the study of the interactions between liquids and solids. In recent years particular attention has been focused on the interactions between liquids and clay minerals. Keldson et al. [232] has presented simulations of the adsorption of hydrocarbons on the surfaces of clay minerals. This was performed in order to gain information about the factors used in different modelling techniques. This paper was part of on going research in to determining the ideal parameters to employ for such simulations.

A number of Monte Carlo (MC) and Molecular dynamic simulations on clay-water-cation systems have also been published [233-237]. Boek et al. [238] have used MC simulations to study the sorption of water in a stepwise fashion (from 0 to 300mg/g of clay) into the interlayer of Li, Na and K montmorillonites. This was performed in order to determine why Na and Li smectites swell macroscopically (unlimited adsorption of water) but why K clays do not. They found that comparison between computer results and experimental results were remarkable. They showed that K ions lie close to the clay surface and are reluctant to hydrate and thus reduces the tendency of K-saturated clays to expand.

4.2.3) Application of Chemical probes in this thesis

Although the method using chemical probes is still in its development stage, great progress has been achieved.

The potential chemical probes studied so far are shown in Table 4.6. All of these probes are liquid at room temperature and are sufficiently volatile to interact with minerals via their vapour phase. These chemical probes were chosen progressively throughout the development of the method, i.e. when an initially chosen probe proved to be limiting (for example a long exposure time was required for interaction with a mineral), then another chemical probe was chosen to try and overcome the limiting factor.

The first two chemical probes to be studied were N-Methylformamide (NMF) and Dimethylsulfoxide (DMSO). These were selected because they are known to intercalate between the strongly held 1:1 sheets of kaolinite and it was thought that they would not between the 2:1 sheets of chlorite. Thus, the chemical probes were known to be selective to these two minerals. DMSO and NMF are also known to intercalate into smectites [175, 239].

Table 4.6: Organic molecules used as potential chemical probes

Chemical Probe (molecular formula)	Molecular Structure	Relevant information	Abbreviation used throughout thesis
N-Methylformamide C_2H_5ON		RMM = 59.07 bp. = 180-185°C	NMF
N,N-Dimethylformamide C_3H_7ON		RMM = 73.10 bp. = 153°C	DMF
Cyclohexylamine $C_6H_{13}N$		RMM = 99.18 bp. = 134°C	CY
Acetone C_3H_6O		RMM = 58.08 bp. = 56°C	Acetone
Dimethylsulfoxide C_2H_6SO		RMM = 78.13 bp. = 189°C	DMSO
RMM = Relative Molecular Mass, bp. = boiling point			

Ultimately, the use of chemical probes will be applied to real rock fragments obtained from working reservoirs, but before this can be done a more basic understanding of their interactions with pure mineral standards needs to be established. To date no rock fragments have been studied in this thesis. Only the interaction with pure powdered

mineral standards and mixtures of mineral standards have been examined. Preliminary studies have also been performed on powdered sandstones.

The interaction process of the chemical probes has been studied using the mineral standards, montmorillonite, kaolinite, illite, feldspar, chlorite, quartz and dolomite. In a reservoir, montmorillonite can undergo cation exchange with the cations present in the reservoir fluids, and so it is important to know whether the type of cation can have an effect on the intercalation process. In order to explore whether there was an effect due to the cation present, the montmorillonite was cation-exchanged to produce homoionic samples and then individually exposed to the chemical probe. It is expected that cations will have an effect on the strength of interaction since several papers have already shown this [169-171] with other molecules. Indeed, Haderlein and Schwarzenbach [163] suggest that the availability and the type of cations associated with clay mineral surfaces need to be quantified as important environmental factors for predicting the retardation of pollutants in soil and sediments. Whether the desorption temperatures of a chemical probe from each cation-exchanged clay differs when studied by TGA needs to be determined.

The interactions of the chemical probes with the individual minerals was first studied by TGA. Each mineral was exposed to each chemical probe separately and their respective derivative thermogram (DTG) was collected. The results showed that some of the chemical probes were more suited to the requirements than others. Intercalation of the chemical probes into some of the clay minerals was found to occur. This was known due to supporting XRD data.

The results also showed that a progressive interaction of NMF occurred with montmorillonite and kaolinite over time, i.e. a progressive build up of NMF associated itself with each clay. Since this was the case, both of these clay minerals were exposed directly to the NMF liquid. This was performed so that maximum intercalation/interaction could be achieved and a comparison made.

TGA alone was unable to determine whether the DTG maxima were due to the presence of the probe or residual water within the clay, or indeed a mixture of both (this is more so the case for montmorillonite, as it is nearly always hydrated in nature). After the individual minerals were studied, physical mixtures of the mineral standards resembling typical rocks were examined using the probes. As expected, the TGA

technique was unable to detect the low levels of the chemical probe being desorbed from the mixtures.

In order to overcome these last two problems TG-FTIR and TG-MS was performed on the individual minerals, mixtures of mineral standards and the quarry rocks so that:-

- i) determination of what was being desorbed at each maxima could be achieved.
- ii) whether TG-FTIR and/or TG-MS could be used to mimic the traces observed for TGA.
- iii) lower quantities of the mineral could be detected than those for TGA alone.

Most of the TG-FTIR and TG-MS experiments involve the use of NMF and DMF as chemical probes because these were found to be the most appropriate probes from the original five.

Whilst developing this strategy, VT-DRIFTS and VT-XRD were employed so that a greater understanding of the types of interactions occurring could be achieved. For example, some of the minerals show the possibility of two or more types of sites via which a probe can interact with a clay mineral. VT-DRIFTS was used to monitor the changes in the infrared spectra of the mineral and chemical probe as it was heated. Whereas TG-FTIR only monitored the evolved gases as a treated mineral is heated, VT-DRIFTS is able to monitor the changes in infrared spectra of the mineral and associated chemical probe as it is heated. Hopefully, these results can show how a particular probe is oriented, for example, does the NMF bind via its carbonyl group. VT-XRD was used to monitor the changes in the $d_{(001)}$ -spacing of the clays as it was heated. This allowed the amount of clay that had been intercalated to be determined. The majority of the VT-DRIFTS and VT-XRD is discussed in chapter 7.

Molecular modelling was also employed in order to 'visualise' the orientation of the NMF molecules within a montmorillonite clay. The modelling results were compared with the experimental results collected during the study (section 7.2.6).

Infrared spectra were obtained via transmission and VT-DRIFTS of the chemical probes and individual minerals. These were compared to see whether characteristic shifts and band changes could be observed. The results of the comparisons were discussed to determine whether characteristic changes could be used to map the surface of a rock and hence produce an SEM-type image (see section 7.3).

5) The characterisation of sandstones and reservoir rocks by Diffuse Reflectance Infrared Fourier Transform Spectroscopy (DRIFTS) and Scanning Electron Microscopy (SEM)

5.1) Experimental

5.1.1) Equipment

FTIR spectrometer and Diffuse Reflectance Accessory

The characterisation of sandstones and reservoir rocks by DRIFTS was developed using a Nicolet 5DX system FTIR spectrometer equipped with a pyroelectric triglycine sulphate (TGS) detector. All the spectra except those of the mixtures used for partial least squares (PLS) analysis were collected using a 600 Series Workstation with Nicolet operating system (NICOS) software and DXFTIR application program. The spectra of the mixtures for PLS analysis were collected using OMNIC (version 3) software. PLS analysis was performed using 'turboquant' software which is part of the OMNIC package. The FTIR system used a CollectorTM DRIFTS accessory manufactured by Spectrotech Inc., which has been modified to allow the sample cup to rotate during a measurement. It should be noted that the standard BLOCKER device supplied by Spectratech Inc. for the accessory was not used. The resulting spectra therefore contains both diffuse and specular reflectance components.

Retsch MM2 ball mill grinder

The Retsch MM2 ball mill grinder uses two tungsten carbide grinding pots (internal volume of 10ml) and two tungsten carbide grinding balls (diameter of 12mm) for each pot. The grinding frequency was set at 45Hz and the grinding time can be altered. The grinding frequency is regularly checked using a xenon stroboscope. If a sandstone, reservoir rock or mineral standard was ball milled, then 5g of the sample would be placed into a grinding pot and shaken between 5-20 minutes.

Centrifuge

The centrifugation of all suspensions was performed on a Sorvall RC5C instrument with a SA-600 rotor capable of a maximum speed of 17000rpm.

X-ray Diffraction

X-ray Diffraction patterns were obtained using a Philips PW1830 Diffractometer, operating at 35kV and 45mA with a copper target. Data was collected in the form of a powder diffraction pattern from 5 to 65 [$^{\circ}2\theta$] collected at 2 [$^{\circ}2\theta$] per minute.

5.1.2) Mineral Standards preparation

Most of the mineral standards came from the Clay Minerals Repository or British Chemical Standards (see table 4.1). If the standard was a fine powder, for example kaolinite, then no sample preparation was performed. If the standard was a rock or coarse powder then it was ball milled until a fine powder was obtained (5 to 20 minutes). This was performed because a small particle size aids in the collection of diffuse reflectance.

5.1.3) Sample preparation

Several sandstones have been investigated (table 4.2) but Berea, Birchover and Clashach have been studied in the most detail.

Analysis of whole rock as a function of particle size

The different particle sizes were obtained by increasing the level of crushing applied to the sandstone samples. To create a coarse particle size the sandstones were lightly crushed using a pestle and mortar. Here the aim was to separate the single quartz grains within the sandstone but not to crush them. This technique produced a wide particle size distribution, i.e. large quartz grains and the smaller clay mineral crystals.

To create a medium particle size the sandstones were heavily crushed using a pestle and mortar. This crushed the quartz grains and therefore increased the surface area of the quartz. To create a fine particle size the sandstones were ball milled for 20 minutes. This produced a very fine powder because the quartz grains and clay particles were thoroughly crushed. The DRIFT spectrum of each particle size was collected via the spectral procedure described in section 5.1.4 (spectral collection).

The ball milled sandstone samples were also used to collect XRD patterns, so that the presence of a particular clay mineral could be confirmed.

In addition to crushing the sandstones, mixtures of kaolinite with various particle sizes of Chelford sand (quartz) were prepared. This was performed in an attempt to mimic the effects observed in the DRIFT spectra of the crushed sandstone samples. Firstly the DRIFTS spectra of various particle sizes of Chelford sand were collected. The particle sizes studied were coarse, medium and fine. The coarse particle size was represented by the neat, uncrushed sand. The medium particle size was obtained by heavily crushing the sand with a pestle and mortar and a fine particle size was obtained by ball milling for twenty minutes. Secondly the various particle sizes of the Chelford sand were then mixed thoroughly with kaolinite at a 90:10 ratio, respectively, and the DRIFTS spectra collected.

Minerals released from deconsolidated rocks (sedimentation)

The separation of the rock components was achieved by sedimentation. The objective of this was to lightly crush a sandstone so that the minerals could be coaxed off the quartz grains. A light grinding was employed to deconsolidate the sandstone and prevent the smearing of the clay onto the quartz grains. Next fractionation of the minerals was achieved by sedimentation yielding fraction sizes, x , of:-

- i) $x < 2\mu\text{m}$,
- ii) $2\mu\text{m} < x < 8\mu\text{m}$,
- iii) particles left in suspension,
- iv) large grains.

The resulting fractions from sedimentation were centrifuged down and the supernatant was disposed of, therefore the samples did not contain any soluble minerals. The

whole procedure was repeated except that the fractions were prepared by driving the water off in an oven, thus retaining any soluble minerals present in the sandstone.

Samples derived from ultrasonication of whole rocks

This involved sonicating fragments of sandstones using a Telsonic (TEL-40) Ultrasonic bath. The fragments were obtained by chipping at a sandstone core with a hammer and chisel. The aim of the sonication was to displace particles from the surface of the quartz grains. The particles in suspension resulting from the sonication were collected at 3, 12 and 51 minutes and 2, 4, 9.5 and 16 hours. The solids in the suspension were then centrifuged down and the supernatant which contained any soluble minerals was discarded.

The DRIFT spectrum of each sedimented fraction and ultrasonicated suspension was collected via the spectral procedure described in section 5.1.4

Direct analysis of cut and fractured surfaces

A cut surface was obtained by simply cutting a disc (≈ 1.5 cm diameter) from a core with a saw mill which had the option of using water as a lubricant. A fractured surface was obtained by hitting a core with a hammer and chisel until a flat disc was obtained. Scoring the edges of the core helped to create a flatter surface.

Mixtures used for partial least squares modelling

The seven components and their percentage concentrations used in the 21 mixtures for modelling are listed in table 5.1. Each mixture was ball milled for 20 minutes before collection of spectra.

Table 5.1: Weight percentage concentrations of the components in the 21 mixtures.

	Quartz	Mont.	Kaolinite	Illite	Chlorite	Dolomite	Feldspar
1	55	10	4	4	8	12	4
2	75	10	0	7	0	8	0
3	85	0	0	8	1	1	5
4	65	9	10	0	3	10	3
5	50	6	3	10	9	5	17
6	80	0	6	0	2	6	6
7	75	0	10	2	0	12	1
8	55	8	5	1	0	25	6
9	60	6	3	5	6	12	8
10	60	4	8	4	4	20	0
11	90	5	0	2	3	0	0
12	50	10	5	0	0	30	5
13	85	2	7	3	1	1	1
14	70	0	0	0	9	8	13
15	60	0	5	6	0	27	2
16	70	2	6	4	10	4	4
17	90	0	0	1	2	6	1
18	80	0	3	0	5	2	10
19	55	5	3	5	2	28	2
20	50	9	10	6	7	10	8
21	65	0	0	3	3	20	9

5.1.4) Collection of Spectra

Instrumental parameters

Prior to collecting any spectral data the diffuse reflectance accessory was optimised. This involved adjusting the height of a prepared background cup (see later) so that the maximum throughput of radiation could reach the detector. The instrumental parameters used during the collection were:-

Number of scans = 176

Detector gain = 1

Mirror velocity = 30

Apodisation function = Happ-Genzel

Resolution = 4.0cm^{-1}

Before a spectrum was collected, the background or sample was purged, in the sample chamber, for three minutes with dry, CO₂ free air. Every sample spectrum was ratioed against a pre-recorded background.

Collection of the background spectra

Before the KBr (Aldrich >99%) was used to prepare any background (or mineral) samples it was ball milled for 5 minutes, since a well controlled and reproducible particle size ensures that the depth of penetration of radiation in both the background and sample preparations is constant. 0.4500g of the ball milled KBr was transferred to a diffuse reflectance cup situated within a specially built compaction cell. The KBr was then compacted under a 20kg load for 1 minute, this was performed for every background sample because it resulted in a reproducible packing. The excess KBr was removed by scraping a razor blade over the surface so that it was level with the sides of the cup. The background spectrum was then collected using the above instrumental parameters.

Collection of the mineral standards spectra

0.0450g of each mineral standard was thoroughly blended using a pestle and mortar with 0.4050g of the ball milled KBr creating a 10% dispersion in KBr. The 10% dispersion was then transferred to a diffuse reflectance cup and the compaction procedure described for the KBr background was performed. The spectrum was then collected.

Collection of sample spectra

The DRIFTS spectra of sandstones that had undergone grinding and mixing were also collected as a 10% dispersion in the ball milled KBr (the standard compaction procedure was used).

The DRIFTS spectra of the sandstones that had undergone sedimentation and ultrasonication were also collected as a 10% dispersion in KBr apart from when there

was not enough sample. A lesser percentage dispersion was therefore used (i.e. the sample and KBr always weighed 0.4500g).

The DRIFT spectra of the cut and fractured discs involved no KBr. The background was a flat mirrored disc which was optimised for maximum radiation throughput before each spectrum was collected. This was achieved by changing the height of the cup. The sandstone discs were not the same height as the mirrored cup, so optimisation was also necessary before the spectrum of each disc was collected.

5.1.5) SEM-Experimental

The characterisation of the samples was conducted on a Philips XL40 SEM equipped with an Oxford Instruments LINK Energy Dispersive X-ray Analyser (EDX). The samples studied (Berea, Birchover and Clashach) were prepared by two different methods. The first method involved cutting a disc from a core using a dry saw mill. The second method involved fracturing a core with a hammer and chisel to produce small discs of rock which provided a fresh flat surface for analysis. Caution was exercised during this preparation procedure because damage may occur to the delicate structures and change the original character of the mineral. Samples were coated with a very thin, uniform conductive layer of either carbon, gold or platinum. This was achieved using a sputter coater.

5.2) Interpretation of DRIFTS spectra obtained from ball-milled sandstones, reservoir rocks and limestones.

The fine particle size of the ball-milled samples and the spectral collection procedure has enabled reproducible diffuse reflectance spectra to be collected. Figure 5.1 shows two overlaid spectra of Berea sandstone which clearly demonstrates the high reproducibility of the technique. The figure also shows that excellent band shapes spanning the whole mid-infrared region can be obtained. This enables the spectra to be used to interpret, qualitatively, the major mineral components in the sandstones and reservoir rocks.

5.2.1) Berea sandstone

If the diffuse reflectance spectrum of Chelford sand (figure 5.2) is taken as representative of quartz then Berea (figure 5.1) contains a high proportion of quartz. The main bands associated with quartz are:-

i) 2000-1200 cm^{-1} range,

These bands are due to overtone and combination bands, and are considerably more enhanced in DRIFTS spectra when compared to spectra obtained from the pressed halide disc transmission method [117]. The bands at higher wavenumber in this group are in a window of the spectrum free from bands due to other mineral constituents in sandstones and are thus very important for its characterisation (see later).

ii) 1200-1050 cm^{-1} range

These are due mainly to the antisymmetric Si-O-Si stretching vibrations. In natural quartz specimens, Al can replace Si and hence, Si-O-Al stretching vibrations could be present in this region. XRF data of Chelford sand shows that there is 2.6% Al present and therefore Si-O-Al bands may be present.

These bands are not very useful for the characterisation of quartz in sandstones because they overlap the bands due to other mineral constituents (see later).

Figure 5.1 - Two reproducible DRIFTS spectra of Berea

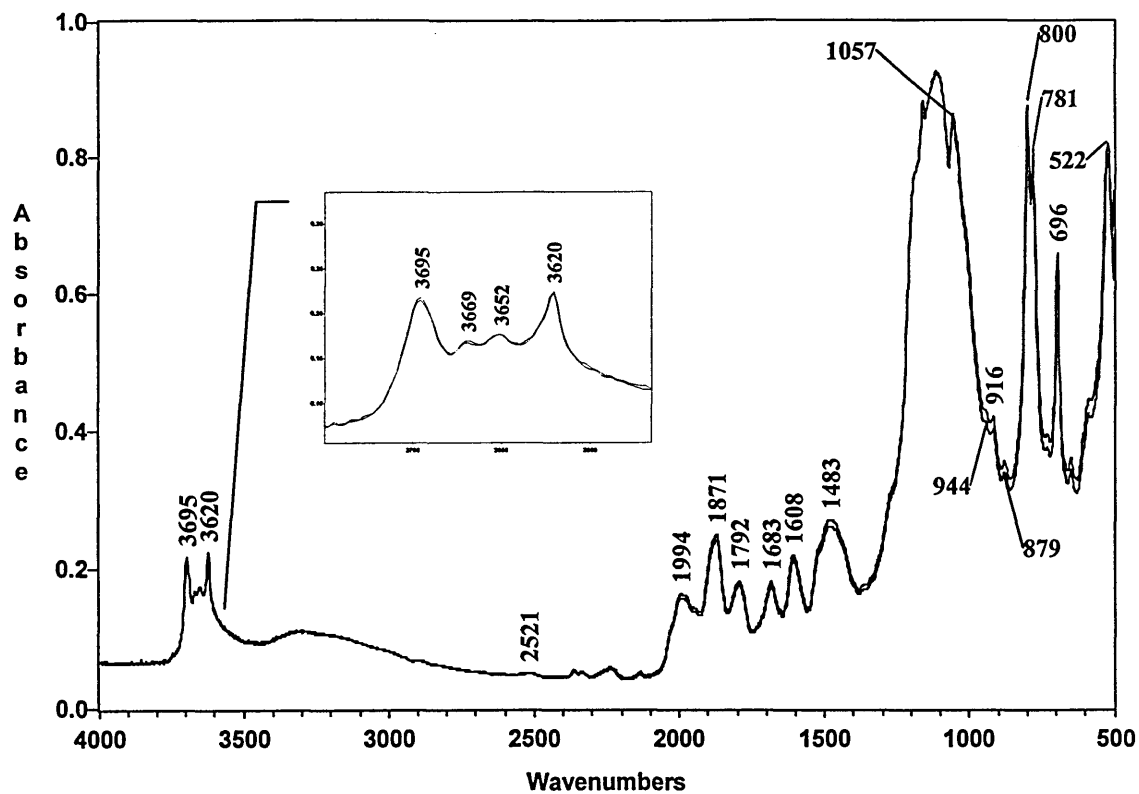
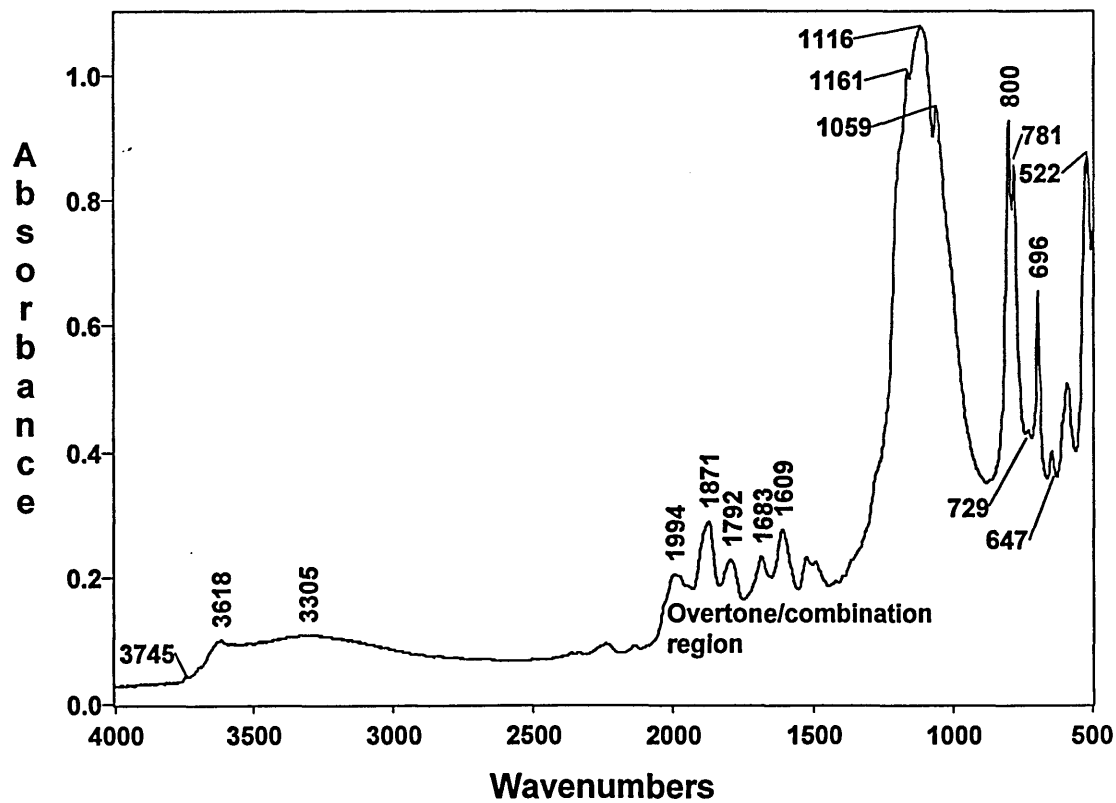


Figure 5.2 - DRIFTS spectrum of ball milled Chelford sand



The transmission spectra of quartz obtained from different sources [90] tend to show the most intense band in this region at around 1082cm^{-1} . As this is not the case for Chelford sand it indicates that the sand may contain impurities (e.g. feldspar).

iii) 800 and 781cm^{-1} bands

These are assigned to the symmetric Si-O-Si stretching vibrations and are quite useful for the identification of quartz.

iv) 696 and 522cm^{-1} bands

These are due to the O-Si-O bending vibrations and may be used for additional characterisation of quartz in sandstones.

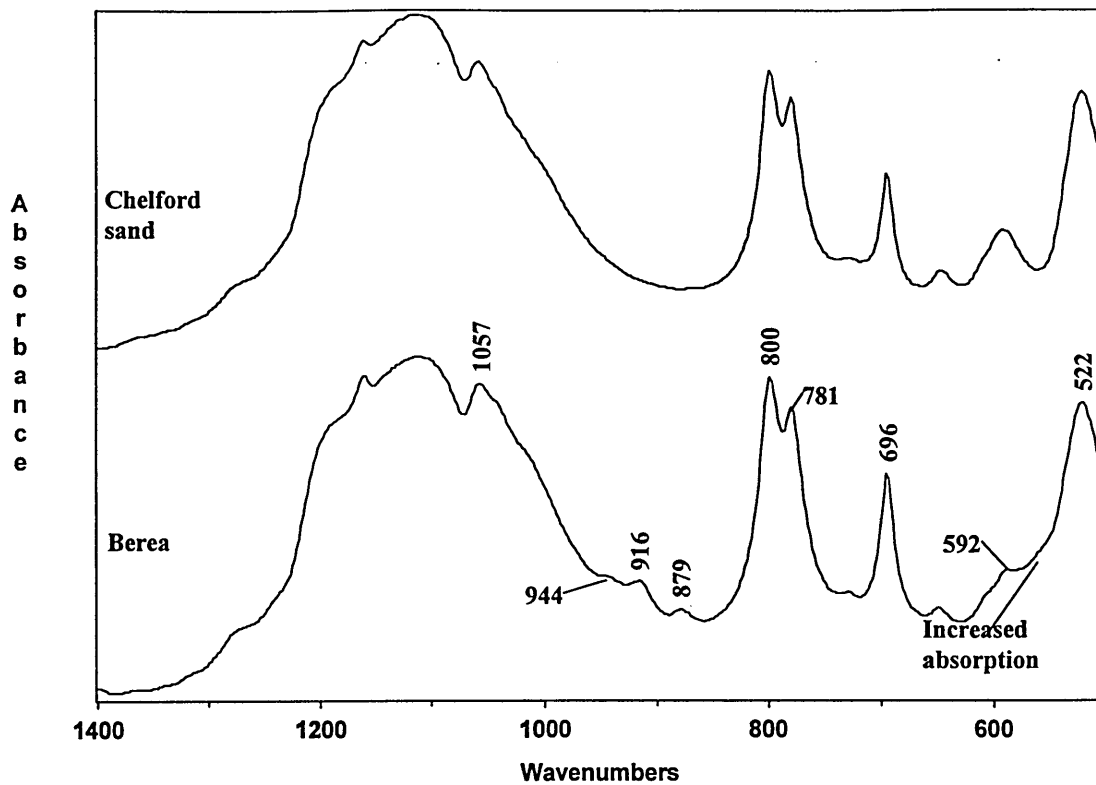
v) $3200-3800\text{cm}^{-1}$ region

In Chelford sand (figure 5.2), there are two broad bands present in this region at 3618 and 3305cm^{-1} . Koretsky et al. [198] studied the assignment of these bands and showed that after heating (i.e. the removal of physisorbed water) a band at 3745cm^{-1} becomes more apparent. They assign this band to SiOH (O-H stretching) which may be a combination of vicinal (i.e. neighbouring) surface groups or H-bonded geminal ($\text{Si}(\text{OH})_2$) groups. The 3745cm^{-1} band is apparent in the Chelford sand spectrum. There are also bands between $3500-3300\text{cm}^{-1}$ present after heating and may be due to internal OH groups associated with Li, Na and other impurity ions in the quartz lattice [240, which is referenced in 198].

Bands present in the Berea spectrum but absent in the Chelford sand spectrum are:-

- i) the 4 bands present in the region $3700-3600\text{cm}^{-1}$,
- ii) a broad band at 1483cm^{-1} ,
- iii) the increased absorption between the 522 and 592cm^{-1} bands (Figure 5.3),
- iv) the 3 bands at 944 , 916 and 879cm^{-1} (Figure 5.3)

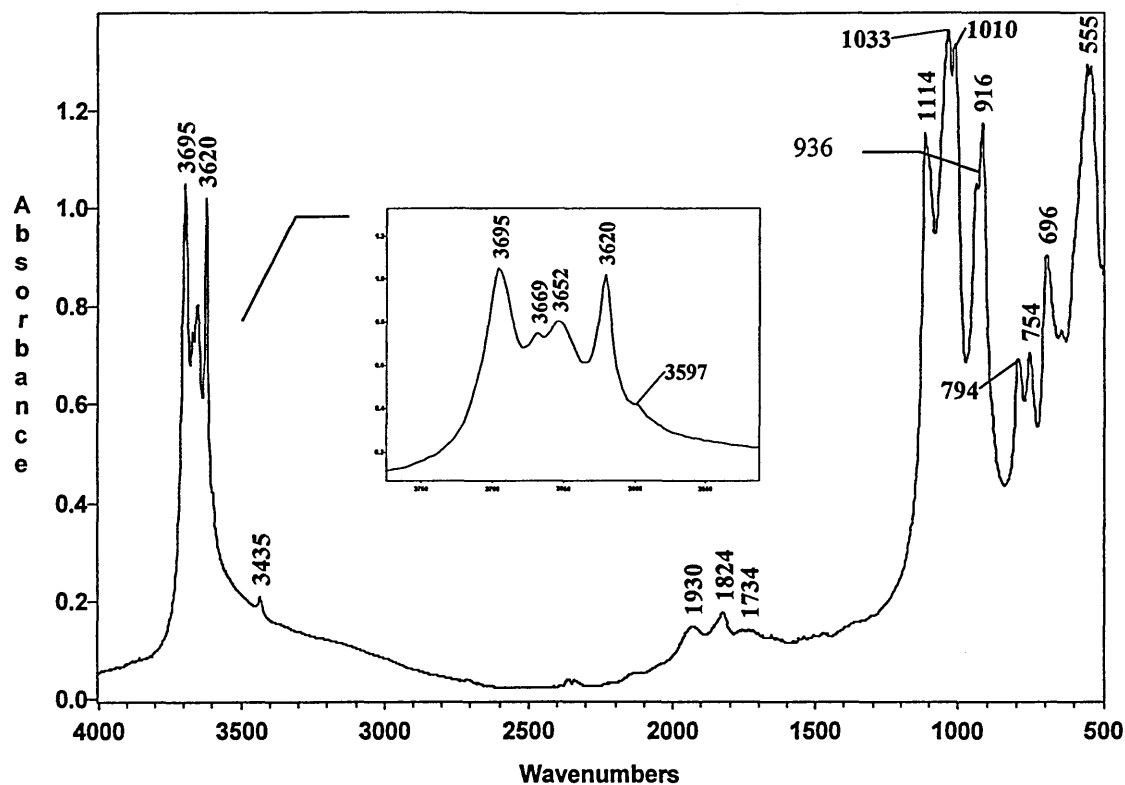
Figure 5.3 - DRIFTS spectra of Berea and Chelford sand



The infrared spectra of kaolinites have been studied extensively in the literature [89, 90, 119 and references therein].

The 4 bands in the region $3700\text{-}3600\text{cm}^{-1}$ indicate that Berea sandstone contains kaolinite (compare the DRIFTS spectra of Berea (figure 5.1) and pure kaolinite (figure 5.4)). In the Berea spectrum the bands at 944 and 916cm^{-1} also indicate the presence of kaolinite. However, the band at 944cm^{-1} is at a higher wavenumber than that of the kaolinite standard (936cm^{-1}); the shift to higher wavenumber could be due to absorption bands from other minerals. Furthermore, the increased absorption between the bands 522 and 592cm^{-1} in the Berea spectrum could be due to the presence of kaolinite. This is supported by the spectrum of a physical mixture of kaolinite and Chelford sand which also shows an increased absorption between the bands 522 and 592cm^{-1} (figure 5.29).

Figure 5.4 - DRIFTS spectrum of kaolinite (KGa-2)



The distinct and characteristic OH stretching region in kaolinite (figure 5.4, 3700-3600 cm^{-1}) reflects the extent of order/disorder within the clay [28, 241]. When disorder is present, the 3669 and 3652 cm^{-1} bands are replaced by a broad band at 3653 cm^{-1} . This effect is not seen in the spectrum of Berea and suggests the kaolinite present is relatively well ordered. The presence of dickite can also result in a broad band at 3653 cm^{-1} . Dickite is a rare polymorph of kaolinite, it has the same structural formula and differs from kaolinite in the way the basic structural unit (the aluminosilicate layer) is stacked. It is well recognised that grinding and pressure treatments to kaolinite change not only the size and shape of the particles but also decrease the crystallinity. It also causes structural changes such as polymorphic transformations or even structural disorder [89]. Therefore when studying the DRIFTS spectra of kaolinite the effect of grinding and pressure treatments must be considered.

The shoulder at 3597 cm^{-1} (see inset, figure 5.4) has been assigned by Delineau et al. [241] to OH stretching associated with Fe^{3+} environments in the kaolinite structure. Trivalent Fe is the main impurity in all natural kaolinites and influences the degree of

disorder. The authors analysed a wide range of kaolinites from different origins (sedimentary, primary ores and soil kaolinites) of varying degrees of disorder and stated that there is a quantitative relation between the relative intensity of the band and Fe^{3+} content.

To the right of the OH bands in the kaolinite standard is a band at 3435cm^{-1} . It has been observed in natural kaolinites [referenced in [241]] and synthetic kaolinites [242]. It disappears after heating at 300°C and its assignment is unknown.

The bands at 936 and 916cm^{-1} in kaolinite are assigned to the in-plane bending vibrations of surface and inner hydroxyl groups, respectively [243]. These bands are also present in Berea and thus support the presence of kaolinite in it. Incidentally, these bands are susceptible to change by grinding but not pressure [123].

The three bands at 1010 , 1033 and 1114cm^{-1} (Si-O-Si in plane deformation) do not assist in the identification of kaolinite in Berea because they are overlapped by the quartz bands.

A number of weak and broad bands at 1930 , 1824 and 1734cm^{-1} are observed in the DRIFTS spectrum of kaolinite, which are also present in other kaolinite spectra [117] obtained from different sources. These bands would overlap some of the overtone/combination bands due to quartz, rendering the useful quartz bands ineffective in their unique characterisation role. However, the highest band in quartz at 1994cm^{-1} should be unaffected.

The bands at 794 and 754cm^{-1} in the kaolinite spectrum can be used to distinguish between well-crystallised kaolinite and halloysite (a polymorph of kaolinite). The bands are of equal intensity for kaolinite, whereas for halloysite the 794cm^{-1} band is reduced considerably. Incidentally, a disordered kaolinite will have an intermediate value [89, 90, 119].

The change in the ratio of the 4 kaolinite bands in the OH stretching region (3700 - 3600cm^{-1}) suggests the presence of illite in Berea. In 'pure' kaolinite (figure 5.4) the 3695cm^{-1} band is the most intense whereas in Berea it is the 3620cm^{-1} band. The increased intensity at 3620cm^{-1} could be due to the presence of illite or smectite since these minerals have a strong absorption band at this wavelength (figures 5.5 and 5.6, respectively). Since a band at 1628cm^{-1} would be expected for smectite, and no such

band is present in the spectrum of Berea, illite is most likely to be the mineral causing the enhanced absorption at 3620cm^{-1} .

The DRIFTS technique offers an improved representation of the OH-stretching mode band shapes (centred at 3620 & 3624 and 3359 & 3393cm^{-1}) in both illite and montmorillonite, respectively, and thus result in an improved characterisation of these minerals. The former are associated with cations within the complex lattice of the clay and the latter are due to water present within the clay layers and broken edges [90, 244 and references therein]. The 3620cm^{-1} band of montmorillonite can shift to near 3558cm^{-1} if a high Fe content is present. Madejova et al. [244] have studied the complex nature of this broad band using decomposition and curve-fitting techniques and were able to relate the components of the band to hydroxyls associated with cations within the complex lattice of the clay.

The dominant bands of montmorillonite and illite at 1030 - 1020cm^{-1} (O-Si-O stretching) would be overlapped by the bands of other mineral constituents in sandstones or reservoir rocks (e.g. quartz) and would result in their presence difficult to identify. The spectra of illite and montmorillonite are very similar due to their similarity in crystal structure and thus differentiation of the two within a rock may be difficult.

The broad band at 1483cm^{-1} in the spectrum of Berea is indicative of a carbonate mineral constituent. This can be shown by comparison with a typical carbonate e.g. dolomite, $\text{CaCO}_3 \cdot \text{MgCO}_3$, (figure 5.7). Most carbonates exhibit a strong absorption band around 879cm^{-1} which can be seen in the spectrum of Berea. Also a weak, broad band at 2521cm^{-1} supports the presence of a carbonate.

Figure 5.5: DRIFTS spectrum of Silver Hills Illite

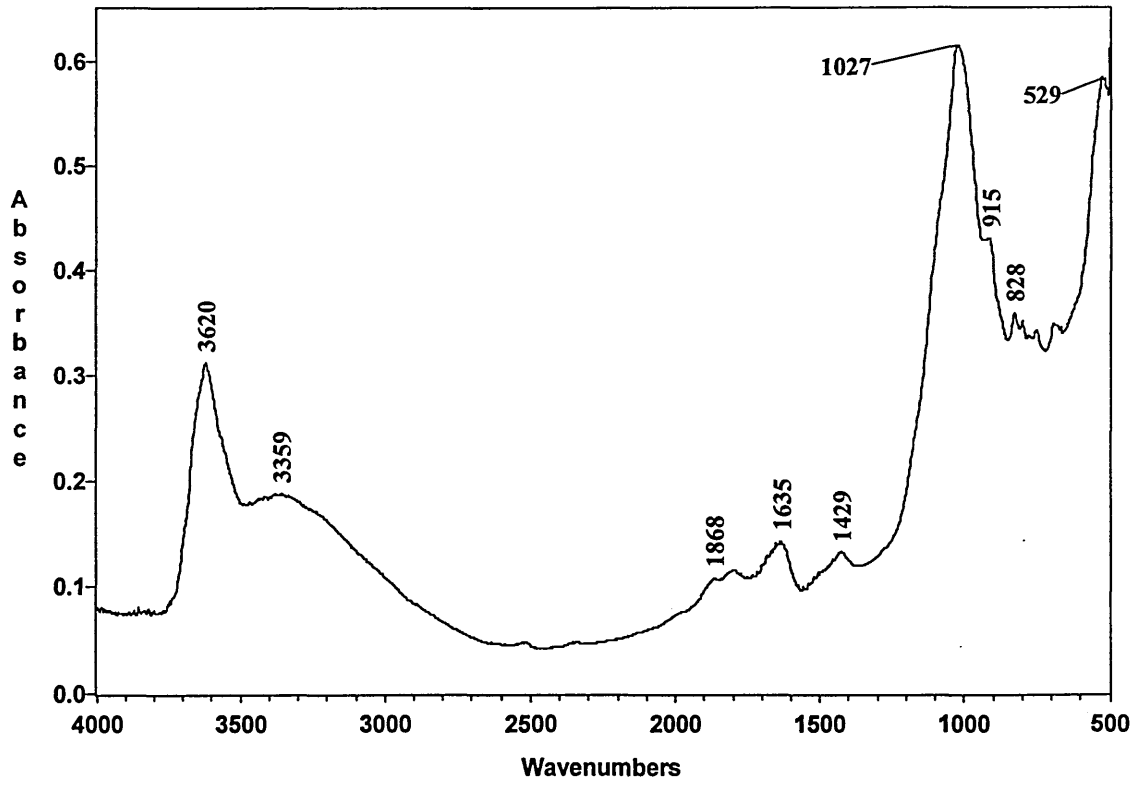


Figure 5.6 - DRIFTS spectrum of montmorillonite (SWy-2)

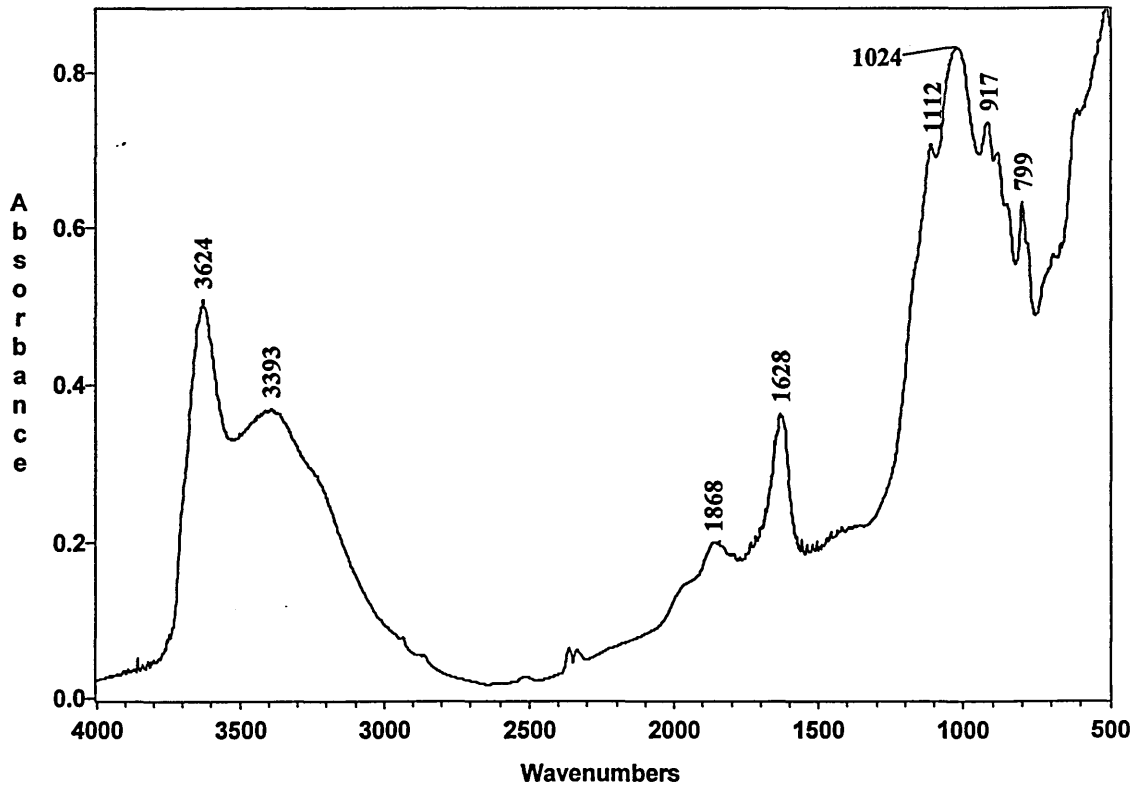
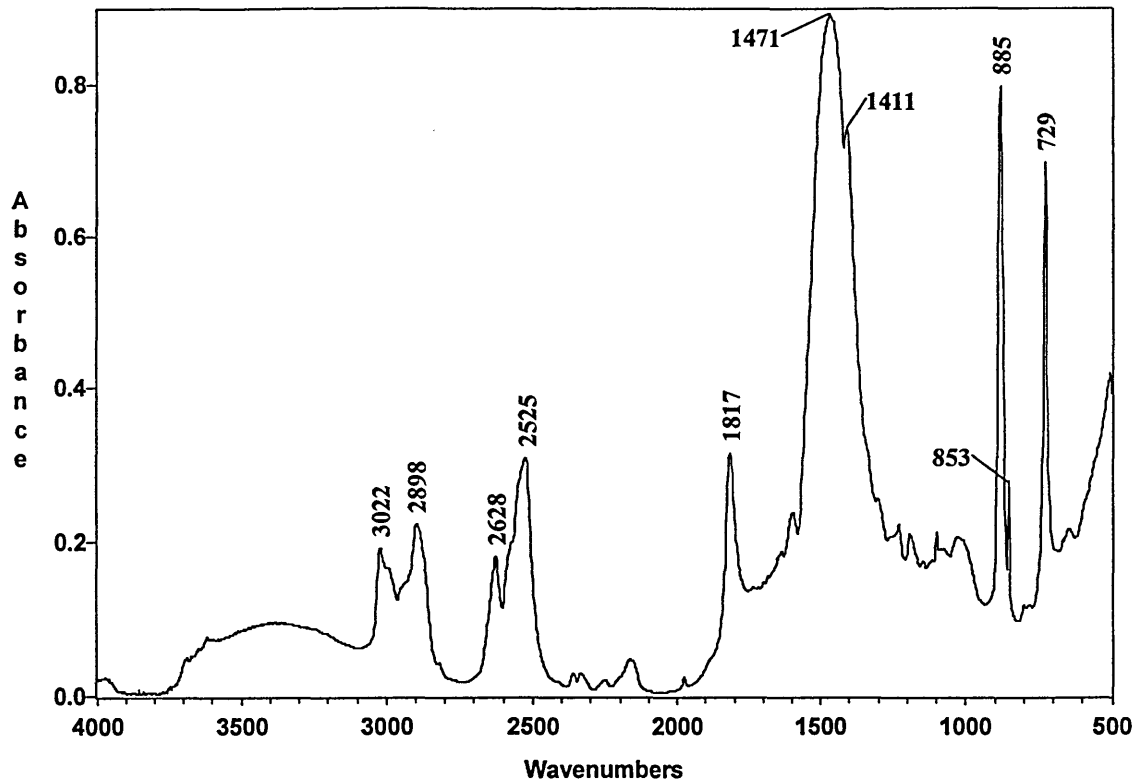


Figure 5.7 - DRIFTS spectrum of Dolomite



The carbonate present in Berea is not necessarily dolomite, it could be a number of others for example calcite (CaCO_3 , figure 5.8), aragonite (CaCO_3 , figure 5.9), magnesite (MgCO_3 , figure 5.10), siderite (FeCO_3 , figure 5.11) or perhaps a mixture.

The aim of this study is not necessarily to determine the exact type of carbonate present within a sandstone or rock. To determine whether carbonate is present will suffice. Carbonate-type can be determined using infrared spectroscopy by the distinctive bands in regions of the spectrum other than around 1483cm^{-1} and will be discussed in more detail later in this section.

The spectra of all the minerals likely to be present in Berea exhibit a broad band in the region $3000\text{-}3500\text{cm}^{-1}$. Therefore the broad band in Berea will result from various contributions, and hence is very difficult to interpret.

Figure 5.8 - DRIFTS spectrum of Calcite

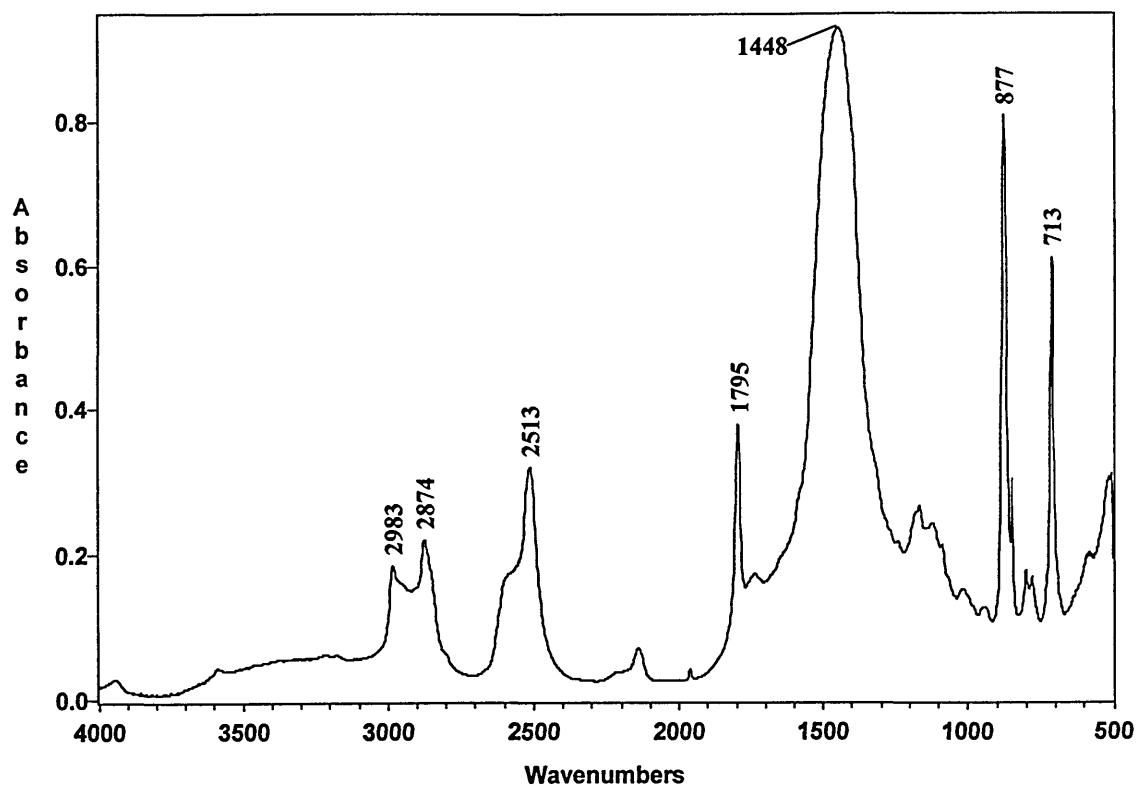


Figure 5.9 - DRIFTS spectrum of Aragonite

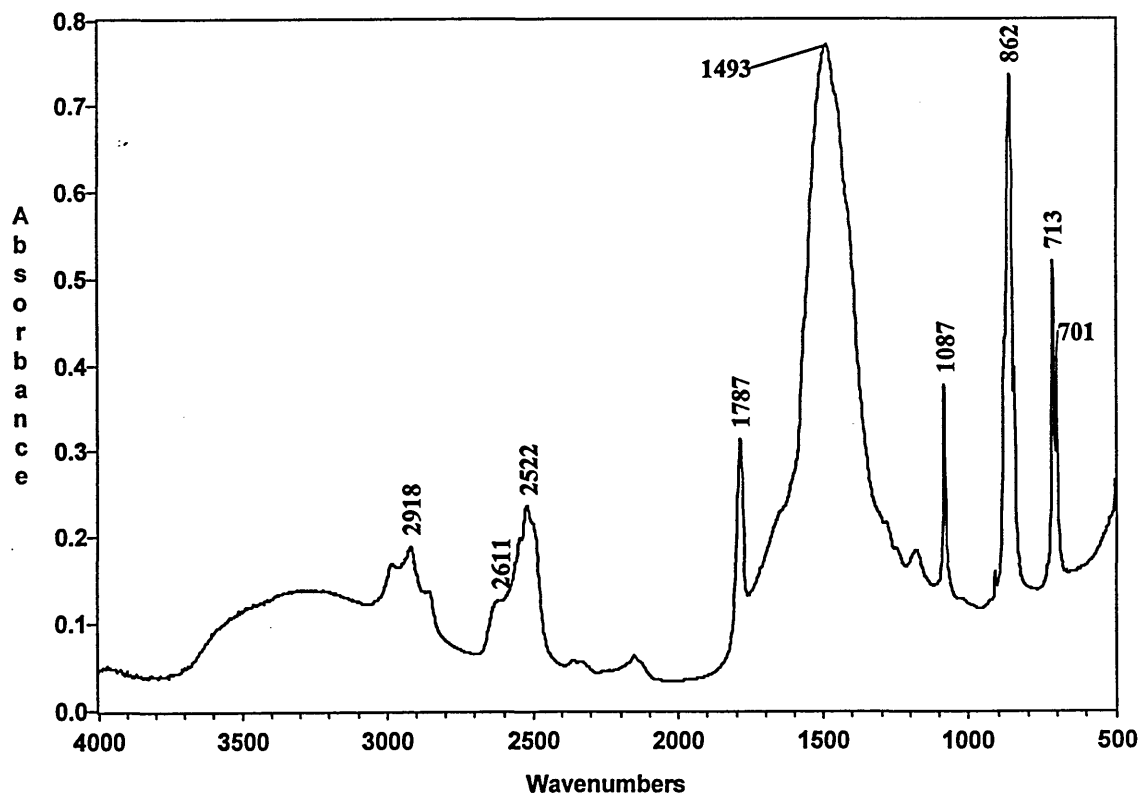


Figure 5.10 - DRIFTS spectrum of Magnesite

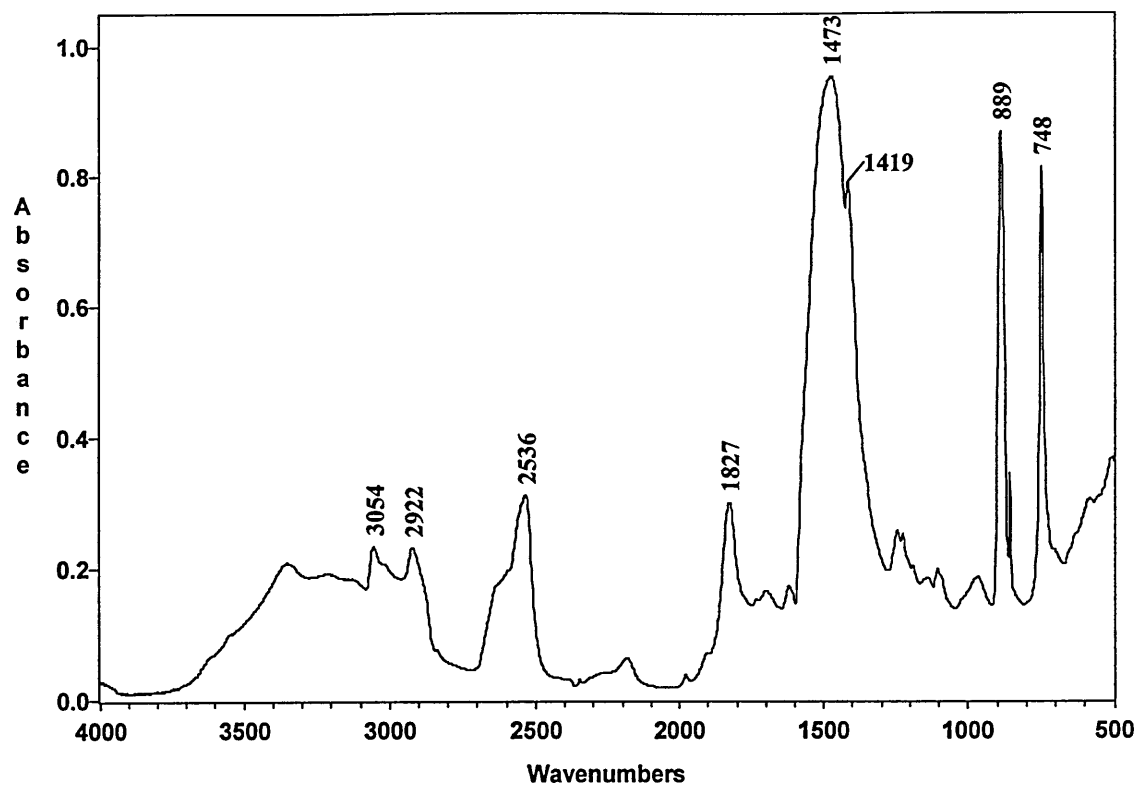
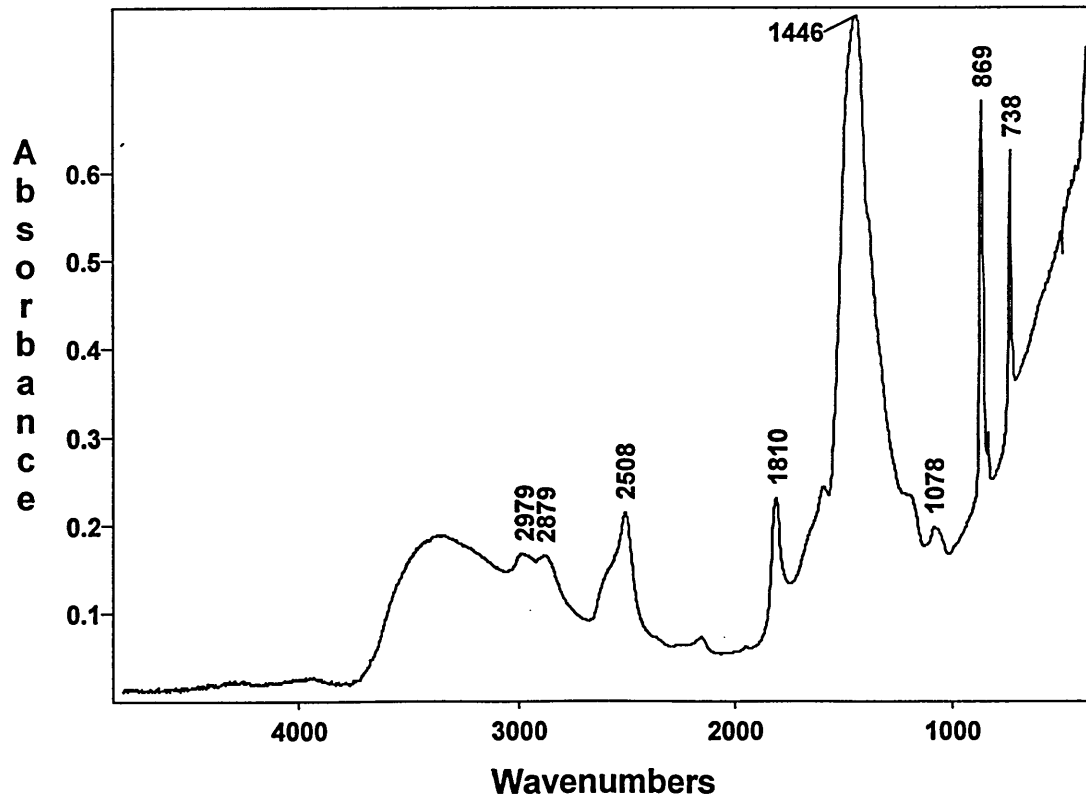


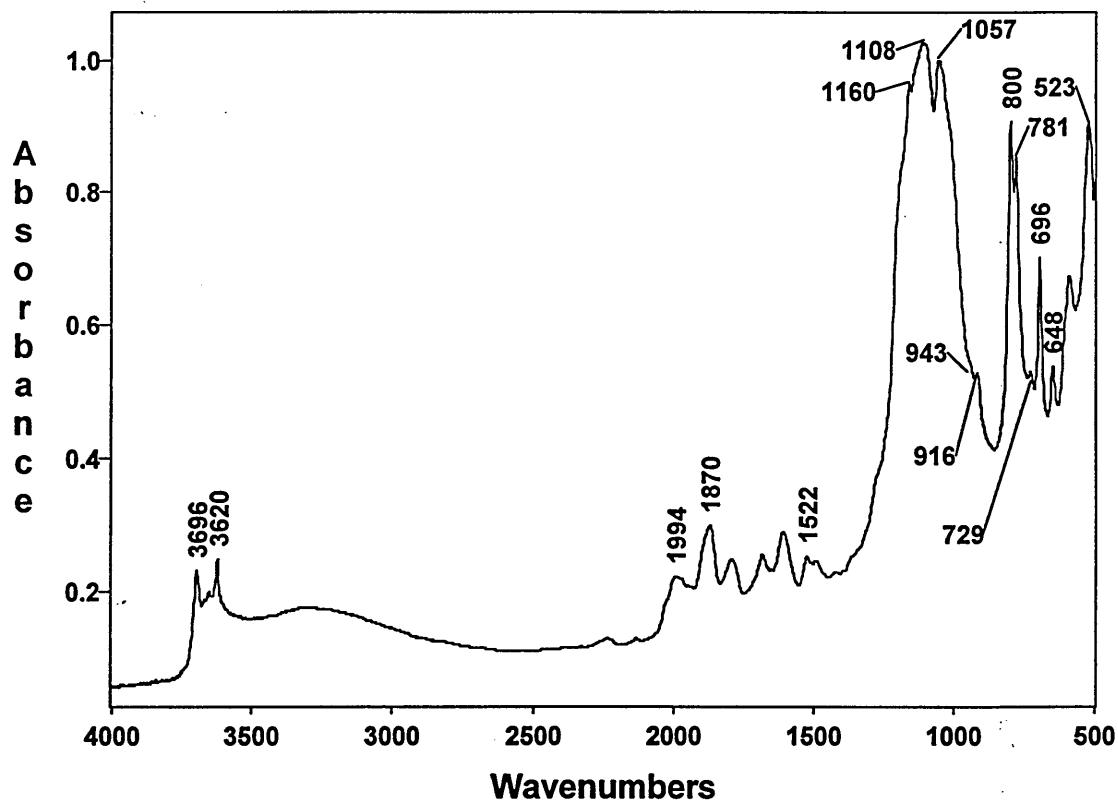
Figure 5.11: DRIFTS spectrum of Siderite



5.2.2) Birchover sandstone

As with Berea the interpretation of the Birchover spectrum (figure 5.12) indicates a high content of quartz and the presence of kaolinite. The presence of illite is also suggested by the enhanced absorption at 3620cm^{-1} (and the absence of absorption at 1625cm^{-1} due to smectite). The bands at 1483 and 879cm^{-1} which indicated the presence of carbonate in Berea, are not observed in the spectrum for Birchover.

Figure 5.12: DRIFTS spectrum of ball milled Birchover



An additional feature in the Birchover spectrum is observed when studying the intensity ratio of the bands in the $1200\text{-}1050\text{cm}^{-1}$ range. Birchover exhibits a stronger 1055cm^{-1} band than Chelford sand. This may result from the presence of the feldspars, albite and orthoclase (Figures 5.13 and 5.14 respectively) both of which absorb strongly in this region. This interpretation fits in with the mineral analysis [147] performed by SDR and SCR in which they state Birchover contains quartz, albite, orthoclase, kaolinite and illite.

Figure 5.13 - DRIFTS spectrum of Albite

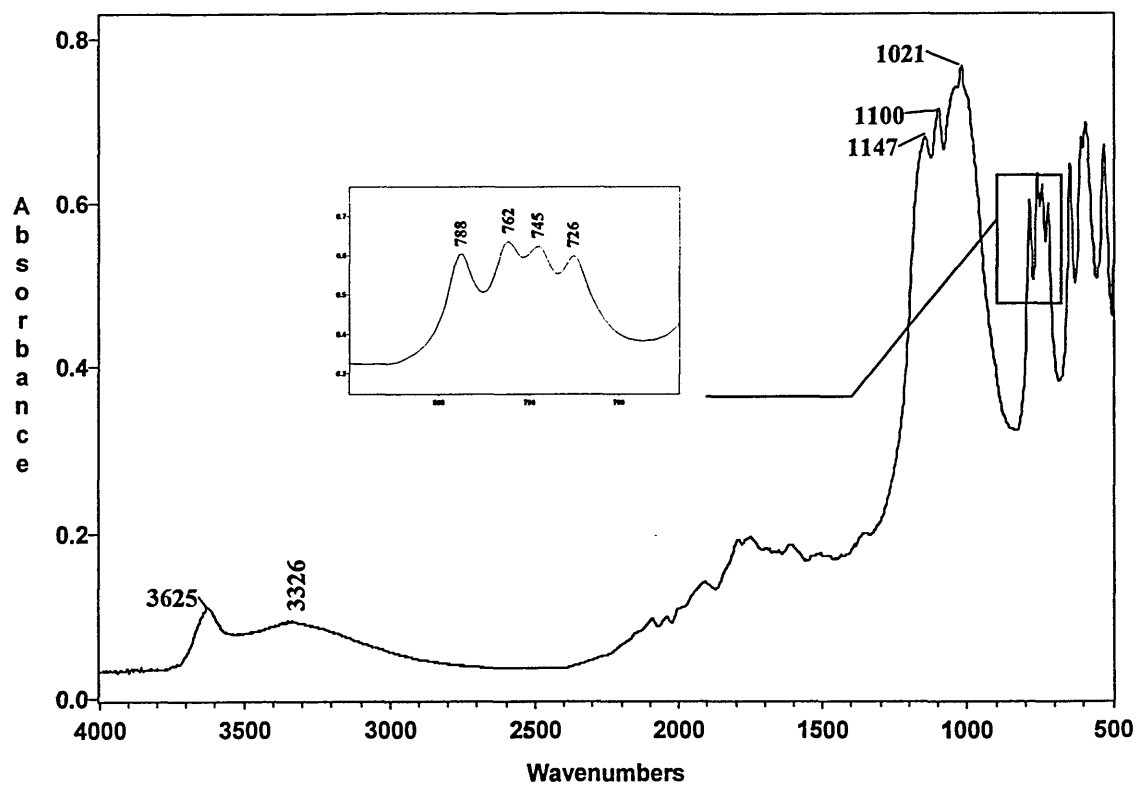
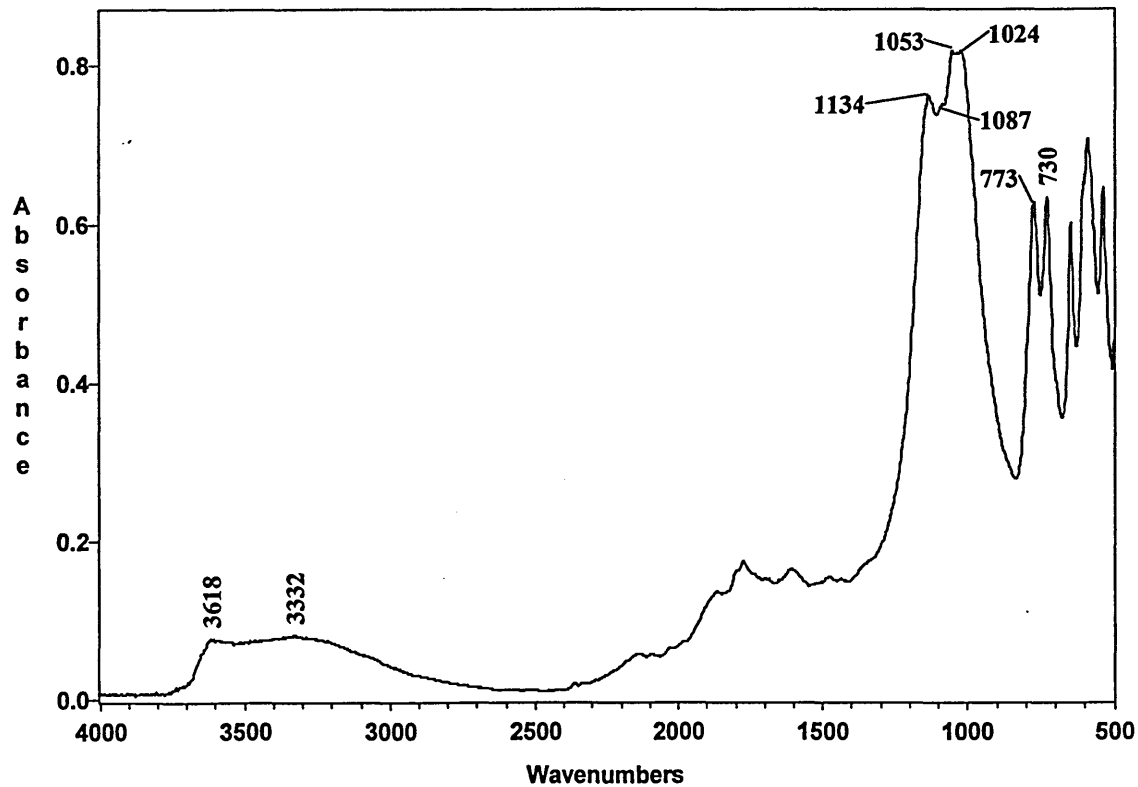


Figure 5.14 - DRIFTS spectrum of Orthoclase



Two other bands that are associated with albite and orthoclase occur at 729 and 648 cm^{-1} . These bands are present in the Birchover and Chelford sand spectra. This suggests that the Chelford sand may contain orthoclase and/or albite and therefore is not 100% representative of quartz. This interpretation is supported by other evidence:-

- 1) The spectrum of Hpf5 (Figure 5.15), another sample representative of quartz does not show bands at 729 and 648 cm^{-1} .
- 2) The XRD data of Chelford sand (figure 5.16) exhibits peaks (marked F for feldspar) at angles that are representative of orthoclase.

In summary, by relying on the XRD interpretation, Chelford sand only contains orthoclase in addition to quartz. The spectrum of Birchover does not indicate clearly whether orthoclase and/or albite is present but the XRD data and mineral analysis suggest both are present with the quartz (Note, however that XRD only detects crystalline phases).

Figure 6.15 - DRIFTS spectrum of ball milled Hpf5 sand

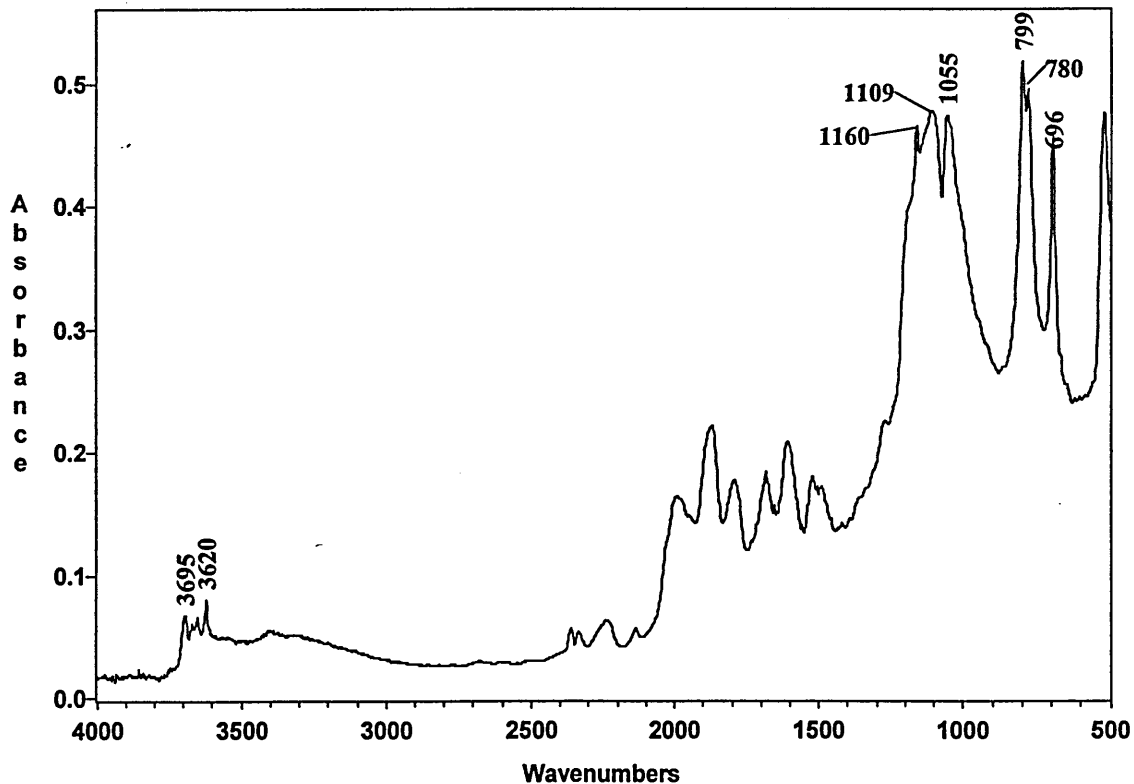
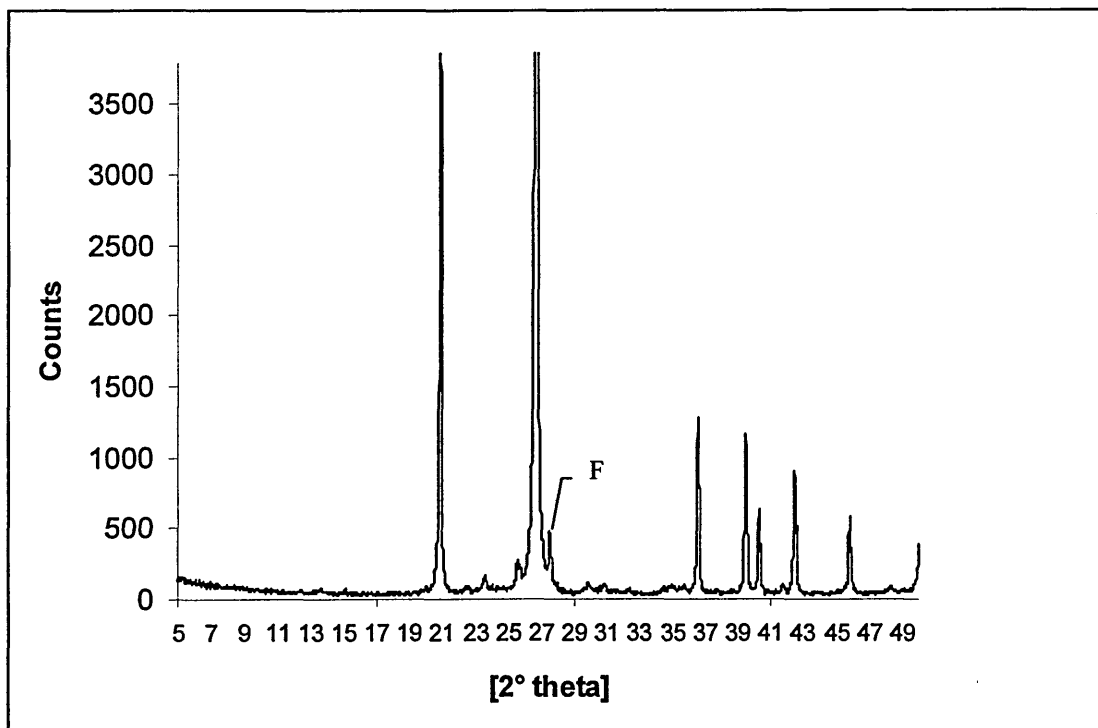


Figure 5.16: XRD trace of Chelford sand (F = Feldspar).



The transmission spectra of the alkali and plagioclase feldspar series have been studied by many spectroscopists [89, 90, 119]. Matteson and Herron [91] have shown that the vibrational modes of the alkali feldspars are fairly insensitive to variations of Na and K content. Whereas, the plagioclase feldspars exhibit absorbance band shifts as a function of Na composition. The absorbance bands of both series are affected by the degree of order/disorder; highly ordered feldspars exhibit a larger number of sharp bands. For example, the Si-O stretching region ($1000\text{-}1150\text{cm}^{-1}$) in the spectra of albite and orthoclase used in this study are split into 4-5 components. This indicates these feldspars are of high order. Although these bands are highly characteristic for individual feldspars, they will be overlapped by bands due to the other mineral constituents in a sandstone or rock.

Koretsky et al. [198] has studied the hydroxyl region of feldspars. The results show the presence of isolated Si-OH groups indicated by a band at approximately 3645cm^{-1} which becomes more apparent during heating as physisorbed water is removed. Although Al-OH groups are to be expected, no direct evidence was found. The results were related to similar infrared studies performed on alumina-silica catalysts and Al_2O_3 .

5.2.3) Clashach sandstone

The spectrum of Clashach (Figure 5.17) shows a high quartz content and perhaps the presence of albite/orthoclase. This sandstone is different to the other three in that the absence of the sharp, characteristic bands in the 3700-3600 cm^{-1} region suggest that it contains no kaolinite. The broad bands at 3700-3000 cm^{-1} are probably due to the presence of illite. The Clashach spectrum shows no indication of any carbonate.

5.2.4) Stancliffe, Yorkstone and Castlegate sandstones

The DRIFTS spectra of these sandstones (figures 5.18, 5.19 and 5.20, respectively) can also be used to qualitatively interpret their mineral composition. This can be achieved by using the same principles as those applied to the interpretation of the DRIFTS spectra of Berea, Birchover and Clashach (see table 5.2 in summary).

Figure 5.17 - DRIFTS spectrum of ball milled Clashach

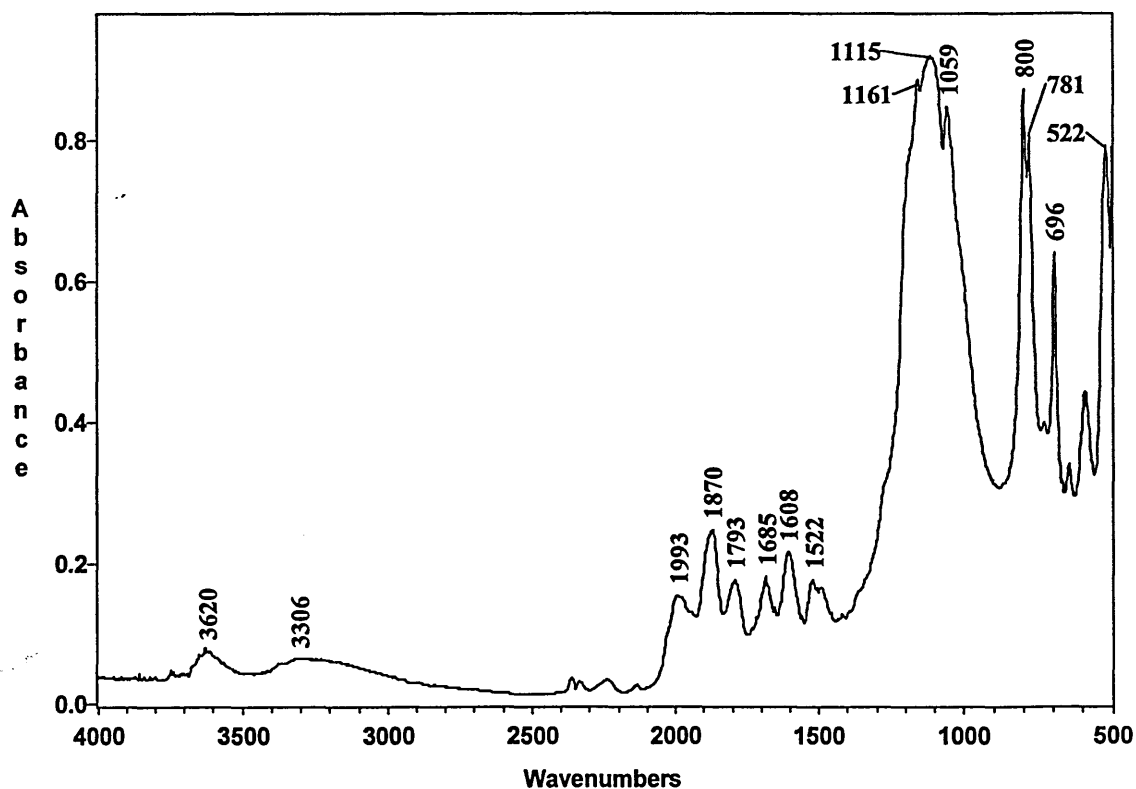


Figure 5.18 - DRIFTS spectrum of ball milled Stancliffe

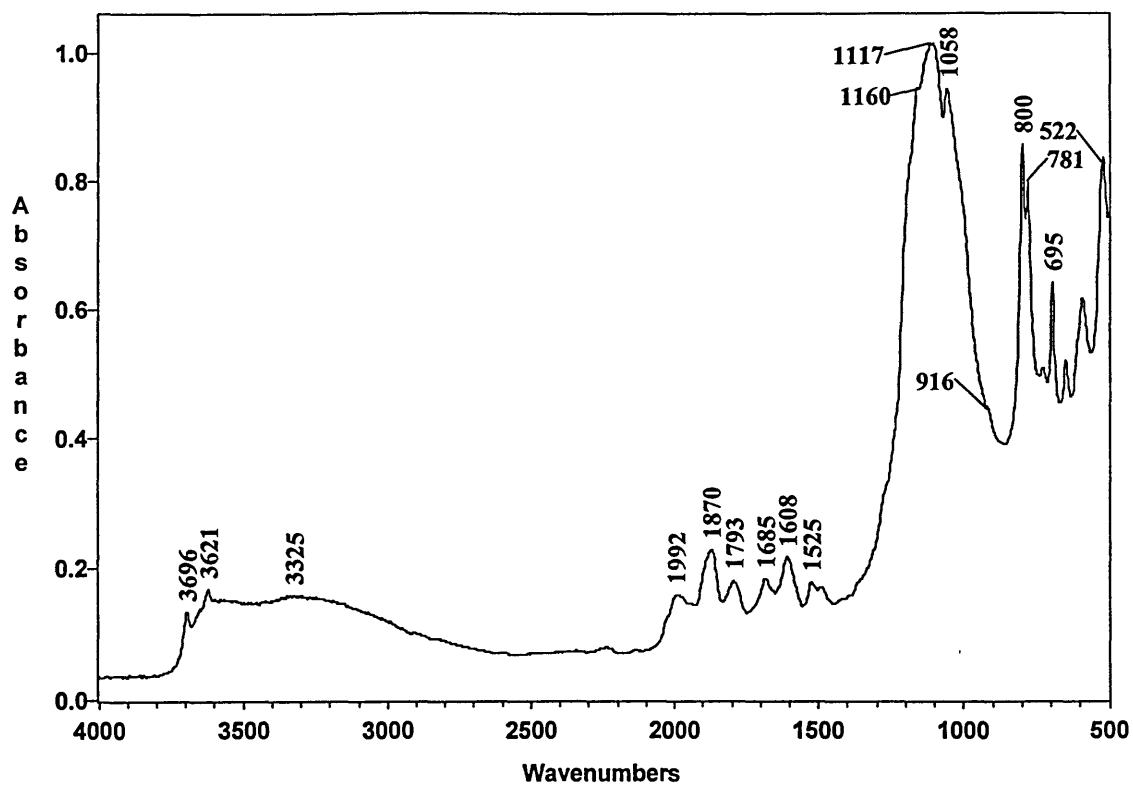


Figure 5.19 - DRIFTS spectrum of ball milled York Stone

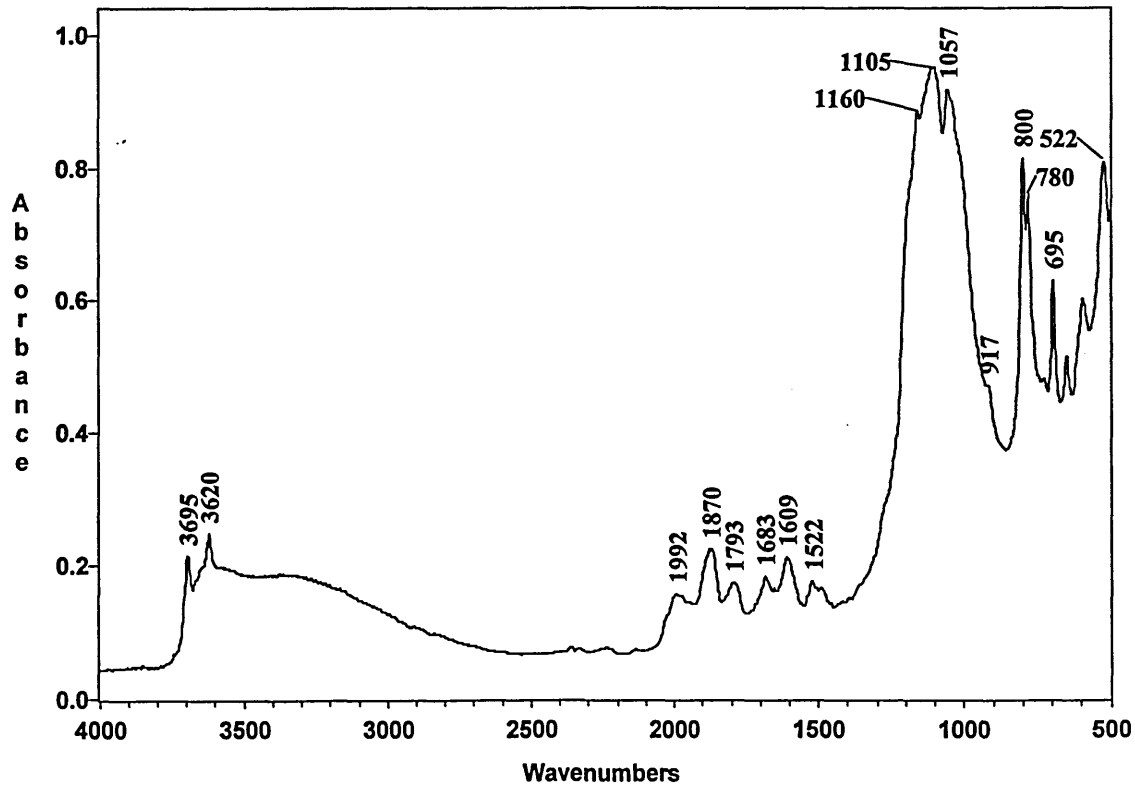
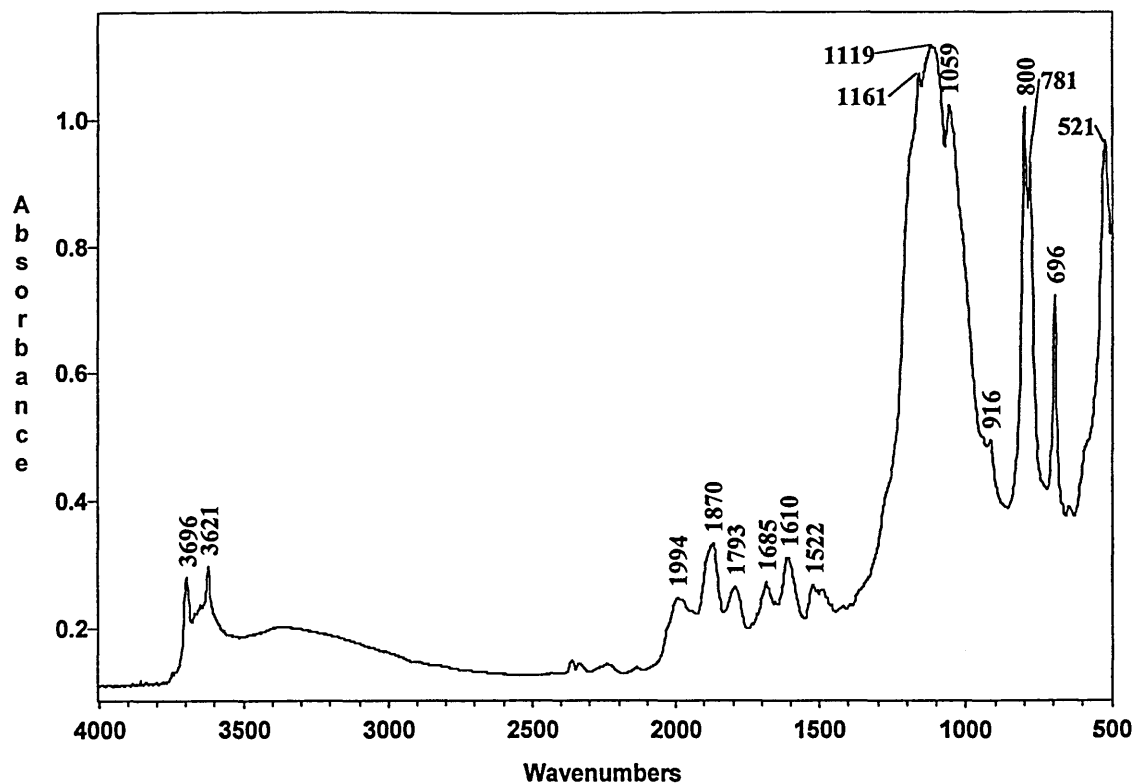


Figure 5.20 - DRIFTS spectrum of ball milled Castlegate



5.2.5) Hollington Red sandstone

The DRIFTS spectrum shown in figure 5.21 describes the bulk mineralogy of Hollington Red (i.e. both the banded area and the area between the bands was sampled). Individual analysis of the two areas was not possible because separation of the two areas was difficult using the cores available at the time. Nonetheless, the spectrum obtained can still be described in terms of its mineral components. A high content of quartz is present, along with a higher illite and lower kaolinite content relative to those of Berea and Birchover.

Figure 5.21 - DRIFTS spectrum of bulk, ball milled Hollington Red

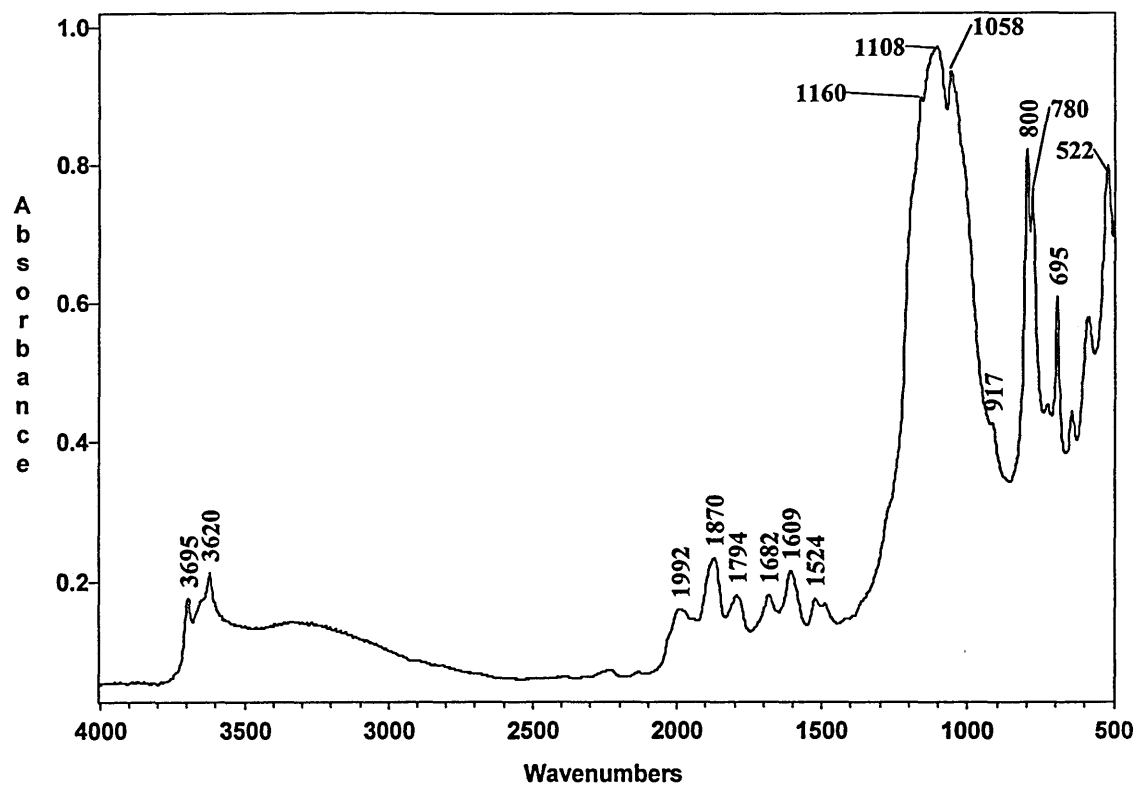
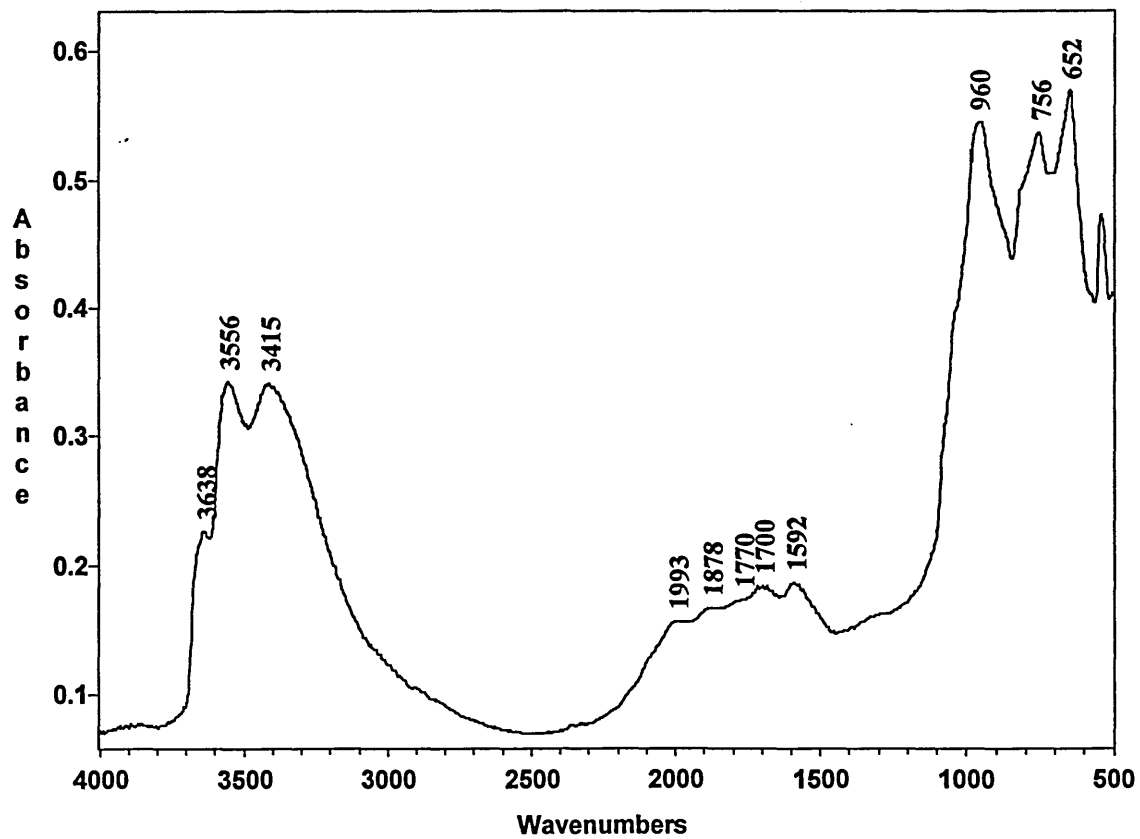


Figure 5.22 - DRIFTS spectrum of Chlorite (CCa-2)



5.2.6) Summary of the components found in Sandstones by DRIFTS

A table showing the main characteristic bands for individual minerals in DRIFTS spectra of sandstones is presented in table 5.2.

The qualitative interpretation of DRIFTS spectra (table 5.3) is in good agreement with the analysis performed by external means (table 5.4). The quantitative mineral analysis of York Stone, Birchover and Stancliffe and the samples of the bands and between-band regions of Hollington Red were completed by Matteson and Herron (SDR) [245], procedural details of their FTIR transmission analyses are given in the reference.

Table 5.2 : Characteristic bands of minerals in sandstone spectra

MINERAL	MAIN CHARACTERISTIC BANDS
Quartz	Overtone/combination region (2000-1400 cm^{-1}). The 800, 781 and 695 cm^{-1} bands.
Kaolinite	The four hydroxyl bands between 3696-3620 cm^{-1} . The 916 cm^{-1} band.
Smectite and Illite	Band at 3620 cm^{-1} or the enhancement of the 3620 cm^{-1} within the four hydroxyl bands of kaolinite. Can distinguish smectite from illite by the presence of the 1628 cm^{-1} band (OH bending, water).
Feldspar	Very difficult to distinguish. Enhanced absorption around 1055 cm^{-1} , but could be due to other minerals. Bands at 729 and 648 cm^{-1} .
Carbonate	Broad band at 1483 cm^{-1} and a sharp band at \approx 879 cm^{-1} .
Chlorite	Enhanced absorption at 3556 and 3415 cm^{-1} (hydroxyl bands).

Table 5.3: Mineral compositions of the quarry rocks.

Quarry Rocks	Quartz	Feldspar	Illite	Kaolinite	Carbonate	Chlorite
Berea	✓	✓ (small)	✓	✓	✓	
Birchover	✓	✓	✓	✓		
Clashach	✓	✓ (small)	✓ (small)			
Stancliffe	✓	✓	✓	✓ (small)		
Yorkstone	✓	✓	✓	✓		
Castlegate	✓	✓	✓	✓		
Hollington Red	✓	✓	✓ (large)	✓		

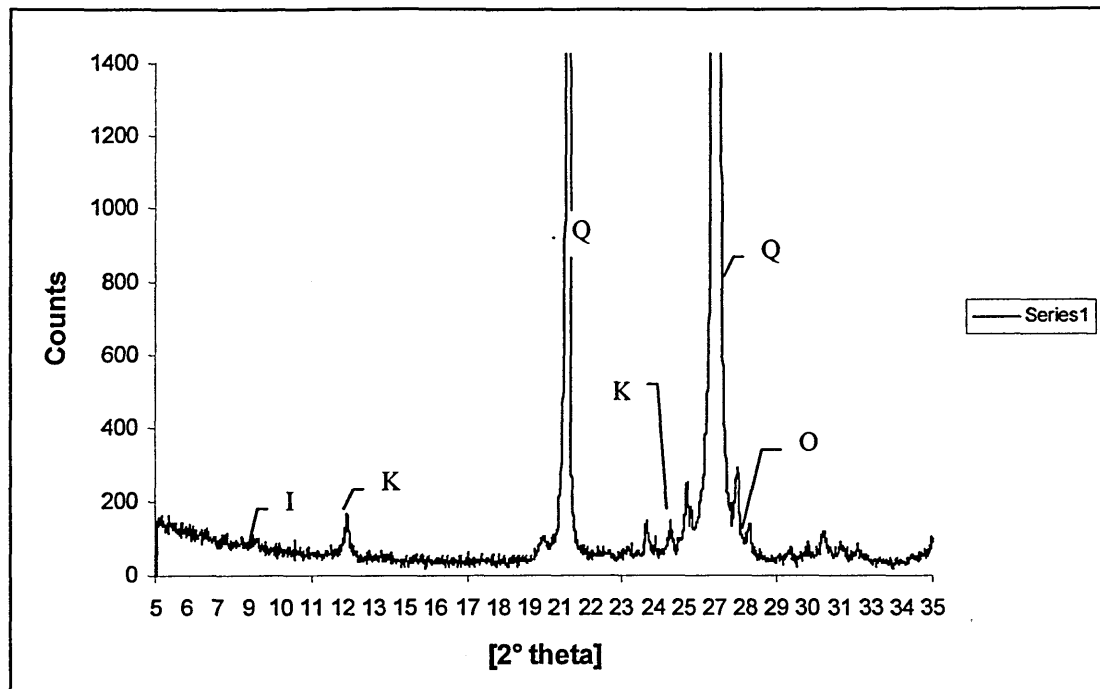
The analysis of Clashach by XRD shows that it has a very low clay content (<5%). The analysis of Berea has been reported in reference [3]. Table 5.4 states that the bands in a core of Hollington Red contains 3% chlorite. The DRIFTS spectrum of chlorite (figure 5.22) shows that its main characteristic bands are at 3415, 3556 and 3638cm⁻¹. These bands are not prominent in the spectrum of Hollington Red and therefore do not clearly suggests its presence. Since the Hollington Red core used for this analysis contained little of the banded area and more of the rock between bands, then perhaps the infrared bands due to chlorite will not be observed.

Table 5.4 : Mineral Analysis of the Sandstones (these values were obtained from reference [147])

Sample	Berea	Birchover	York stone	Stancliffe	Hollington Red between bands	Hollington Red bands
Mineral (wt%)						
Quartz	84	75	72	72	74	72
Albite	0	8	11	11	3	<1
Orthoclase	3	8	3	8	12	7
Anorthite	0	0	0	<1	0	0
Total Feldspar	3	16	14	19	15	7
Mica	0	0	1	1	<1	0
Calcite	1	0	<1	0	0	0
Dolomite	1	<1	0	<1	0	0
Magnesite	0	0	0	0	0	<1
Siderite	1	0	0	0	0	0
Total Carbonate	3	<1	<1	<1	0	<1
Total Sulphate	0	<1	1	0	2	4
Kaolinite	7.6	5	5	3	<1	3
Illite	2	4	7	5	6	10
Smectite	<1	0	0	0	3	<1
Chlorite	0.4	0	0	0	0	3
Total clays	13.6	9	12	8	9	17
Total	100	100	100	100	100	100

The data obtained using XRD also suggests the same general picture. For example, figure 5.23 shows the XRD trace of Berea where the labelled peaks indicate the presence of quartz, illite, kaolinite and orthoclase.

Figure 5.23: XRD trace of ball milled Berea (Q = Quartz, K = Kaolinite, O = Orthoclase and I = Illite)



5.2.7) Reservoir Rocks

Figures 5.24 and 5.25 show the DRIFTS spectra of the reservoir rocks, RR1 and RR2, respectively. The spectrum of RR1 is very similar to that of Berea in that similar bands are present but at different intensities. The presence of kaolinite is indicated by the four characteristic hydroxyl bands, a high quartz content is indicated by the overtone/combination bands ($1500\text{-}2000\text{cm}^{-1}$) and illite is present due to the enhanced absorption at 3620cm^{-1} . A small amount of carbonate is present (band at 1486cm^{-1}) and also a high amount of feldspar (enhancement at 1050cm^{-1} and a band at 729cm^{-1}). The spectrum of RR2 shows that it contains no kaolinite, carbonate or feldspar and the clay mineral that is present within the quartz grains is illite. Table 5.5 shows the mineral compositions (determined by XRD) of reservoir rocks (RR1 to RR6), quantitative mineral percentages are not shown since these were not available at the time of publishing. The DRIFTS spectra of the reservoir rocks, RR3 to RR6, are shown in appendix 1.

Figure 5.24 - DRIFTS spectrum of ball milled reservoir rock RR1.

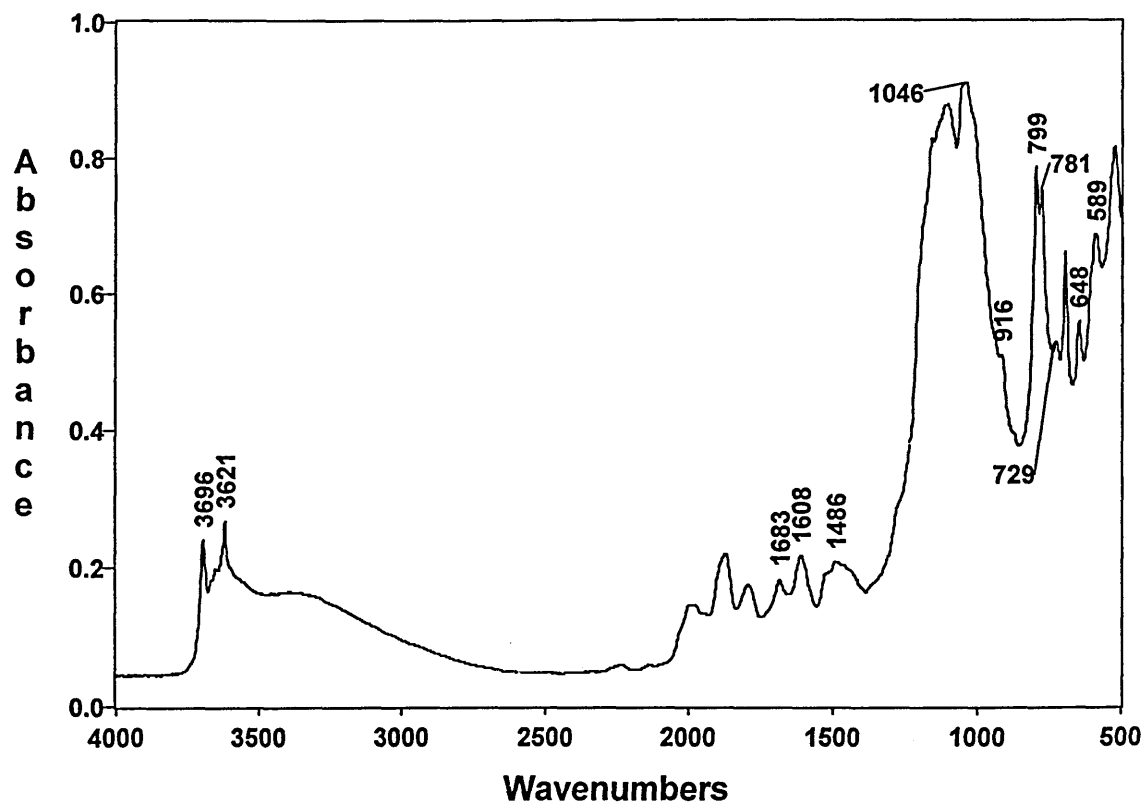


Figure 5.25 - DRIFTS spectrum of ball milled reservoir rock RR2

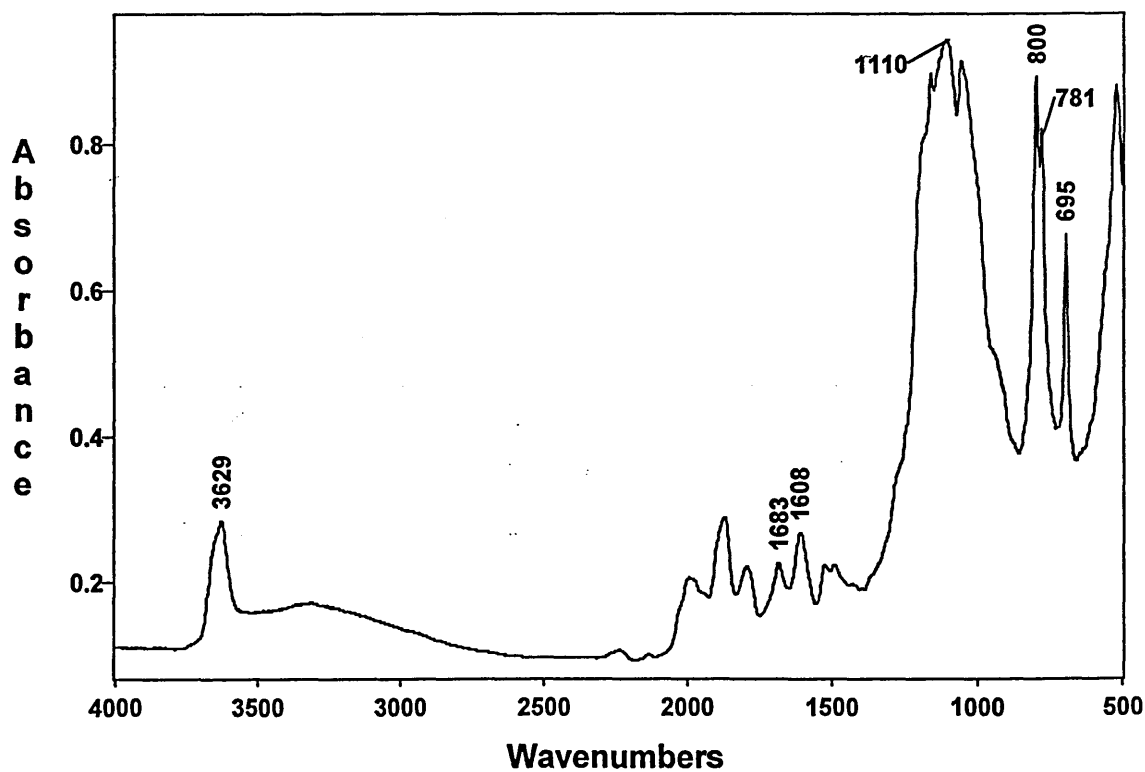


Table 5.5: Mineral compositions of the reservoir rocks (RR1 to RR6)

Reservoir Rock	Quartz	Feldspar	Illite	Kaolinite	Carbonate	Chlorite
RR1	✓	✓	✓ (small)	✓ (small)	✓ (v. small)	✓ (small)
RR2	✓		✓			
RR3	✓	✓	✓ (v. small)			
RR4	✓			✓		
RR5	✓ (relatively small)	✓	✓ (v. small)	✓ (large)	✓	✓ (v. small)
RR6	✓	✓		✓		

5.2.8) Limestones

Within this study two limestones have been studied, namely; Ketton and BCS-Limestone (No. 393). Figure 5.26 shows the DRIFTS spectrum of ball milled Ketton limestone. Of particular interest are the enhanced absorption bands above 2000cm^{-1} . These bands are considerably pronounced when compared to the infrared spectra of carbonates obtained via the halide pellet transmission technique [89, 119]. If the spectrum of Ketton (figure 5.26) is compared with the spectra of dolomite (figure 5.7), calcite (figure 5.8), aragonite (figure 5.9), magnesite (figure 5.10), and siderite (figure 5.11) it is clear that Ketton limestone is mainly composed of carbonate minerals, but to identify each constituent carbonate mineral requires a more detailed examination. Figure 5.27 shows the DRIFTS spectrum of BCS-Limestone. There are many broad similarities in the spectra of Ketton and BCS limestone. However a detailed examination is required to identify the constituent carbonate minerals.

Theoretically, there are six modes of vibration possible for the free moving carbonate CO_3^{2-} group. Two are non-degenerate (ν_1 and ν_2) and two of them are doubly degenerate (ν_3 and ν_4). Their assignments are listed below:-

ν_1 = symmetric stretching

- ν_2 = out of plane bending
- ν_3 = asymmetric stretching
- ν_4 = planar bending

Figure 5.26: DRIFTS spectrum of ball milled Ketton limestone

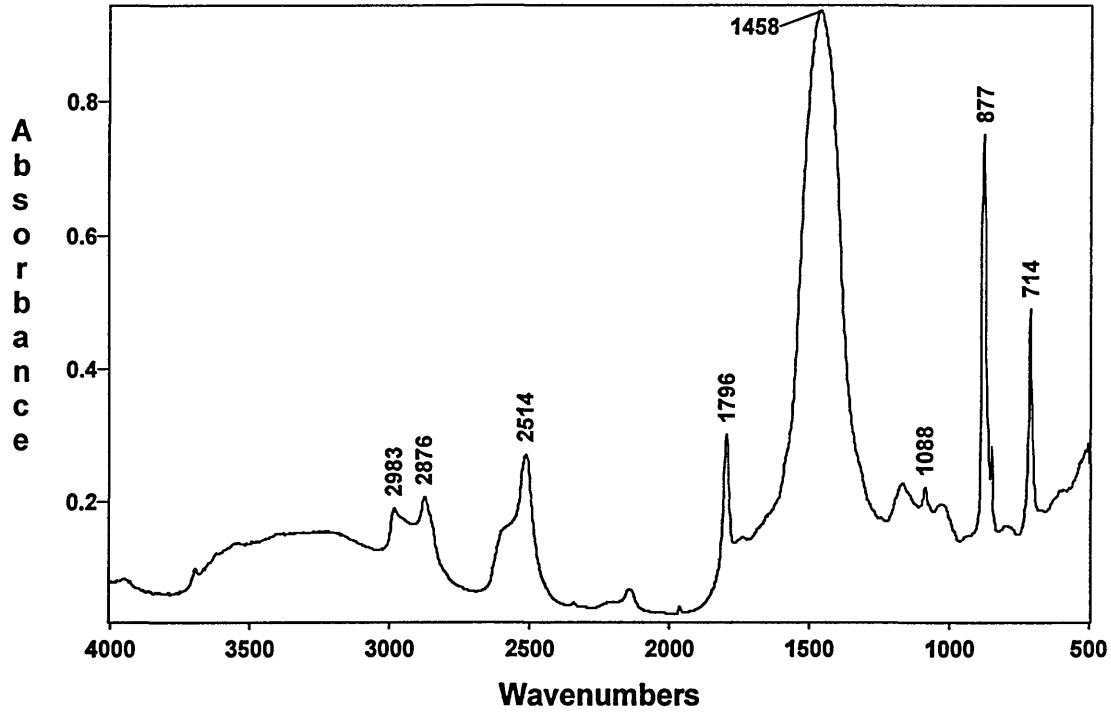
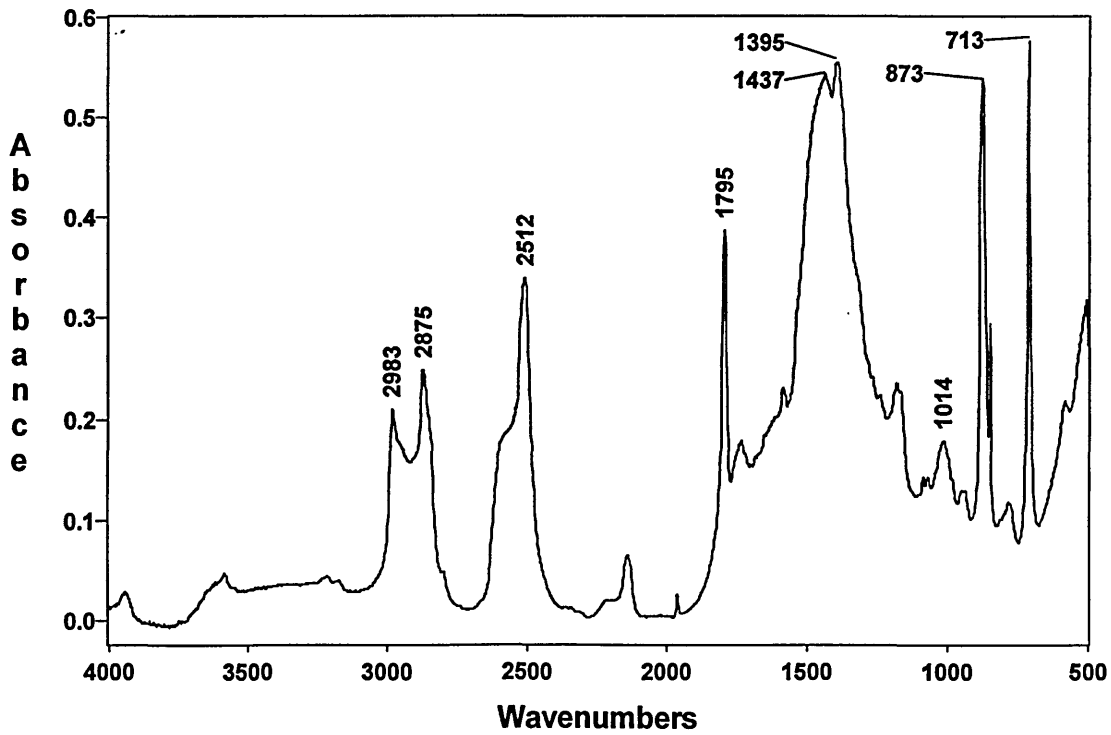


Figure 5.27: DRIFTS spectrum of BCS-Limestone (No. 393)



The $\nu_1 - \nu_4$ notation is based on the practice of Herzberg [referenced in [90]]. The exact frequencies of these fundamental modes are dependent on the identity of the carbonate mineral. Table 5.5 shows the exact frequencies of the carbonate-mineral standards and limestones. Included in the table are band frequencies obtained from other references.

The first observation to notice from the results is that only some of the carbonates show a ν_1 band (1068-1087 cm^{-1}). This is because it is mainly Raman active and hence only a weak band is observed. However, aragonite possess an intense ν_1 band, at 1084 cm^{-1} , which is unique and characteristic to this carbonate.

The second observation to consider is the variability of the ν_3 band position. The position of this band does not only vary from carbonate-type to carbonate-type (e.g. calcite = 1448 cm^{-1} and magnesite = 1473 cm^{-1}) but it also varies within each carbonate-type, probably due to natural variance within its structure. For example, the ν_3 band position for calcite varies from 1422-1448 cm^{-1} . Since this is the case, it is very difficult to determine the character of a limestone using this band alone.

The ν_2 and ν_4 bands vary only slightly within each carbonate-type and vary with a high enough resolution from carbonate-type to carbonate-type to enable characterisation via these bands. The ν_2 and ν_4 bands of Ketton and BCS-Limestone are at; 877 & 714 cm^{-1} , and, 873 & 713 cm^{-1} , respectively. These bands could be due to the presence of calcite or aragonite (table 5.4). The ν_2 band of BCS-Limestone is at a slightly lower wavenumber than that of calcite. The reason for this could be due to combined presence of calcite and aragonite. Another factor to support this assumption is that the ν_3 band is much broader and of lower intensity, indicating a wider spread of environments and hence the presence of multiple carbonates.

Chemical analysis data states there is 55.4% CaO present after loss on ignition (43.3%) and insignificant amounts of other elements. This therefore suggests, aragonite is also present since like calcite it is composed of CaCO_3 . Since no strong ν_1 band (representative of aragonite) is present in the spectra the major component in the limestones is probably calcite.

Table 5.5: Position of bands observed in the carbonate spectra

MINERAL	V ₁		V ₂		V ₃		V ₄	
	DRIFTS assignment	referenced assignment	DRIFTS assignment	referenced assignment	DRIFTS assignment	referenced assignment	DRIFTS assignment	referenced assignment
Ketton	1086 (weak)		877		1458		714	
BCS-Limestone			873		1437 1395		713	
Calcite	1087 (weak)		877	878* 877+	1448	1452sh* 1428* 1422+	713	714* 712+
Aragonite	1084 (strong)	1082* 1085* (strong)	862	857* 858+ 875, 870*	1493	1473* 1472+ 1490*	713	714* 712+ 712, 699*
Dolomite			885	882* 882+	1471 1412	1443* 1430+	729	729* 728+
Magnesite			889	886+	1473 1419	1485sh+ 1445+	748	748+
Siderite	1068 (weak)		869	867+	1446	1417+	738	737+

* - bands referenced from [119] / + - bands referenced from [89] / * - bands referenced from [90] (Spectra were obtained via the transmission method)

The bands in the $1700\text{-}3000\text{cm}^{-1}$ region are greatly enhanced in DRIFTS and it is this area that is of interest when studying sandstones because the characteristic bands (i.e. ν_2 and ν_4) are usually masked by overlapping bands due to the other mineral components. It has already been established that the ν_3 band can be used to determine carbonate is present but not which type. There are three other areas of interest in the $3000\text{-}1700\text{cm}^{-1}$ region, namely; the single band around 1800cm^{-1} , the bands between $3000\text{-}2800\text{cm}^{-1}$ and the bands between $2600\text{-}2400\text{cm}^{-1}$. The two groups of bands are enhanced more so than the single band.

The band around 1800cm^{-1} is due to the combination of the ν_4 and ν_1 modes. This band can be used in addition to the ν_2 and ν_4 bands for the characterisation of carbonates because it is at a characteristic wavenumber for each type. However, it is not useful for the identification of carbonate-type within sandstones because it overlaps either the 1792 or 1871cm^{-1} quartz overtone bands.

The group of bands near 2900cm^{-1} are probably due to the ν_2 ($\approx 1450\text{cm}^{-1}$) overtone. These groups of bands are characteristic for each carbonate-type and could be used in addition to the other bands as a form of characterisation of limestones. If these bands were intense in the spectrum of a sandstone containing carbonate, then they could be used as a means of identifying the carbonate-type. Although these bands are well resolved from absorption bands of other mineral constituents, they may be overlapped with aliphatic CH stretching bands of oil saturated rocks, which will hinder its characterisation.

The group of bands between $2600\text{-}2400\text{cm}^{-1}$ are due to a combination of the ν_2 ($\approx 1450\text{cm}^{-1}$) and the Raman active ν_1 (1085cm^{-1}) bands. For the same reasons above, these bands could be used to characterise limestones. These bands are ideal for the characterisation of carbonate matter in sandstones because they are completely resolved from bands of the other mineral constituents. Although the spectra of carbonates shown in this thesis are individually characteristic, the natural variance within each carbonate-type has not been accounted for, i.e. the variance may complicate the characteristic bands. Preliminary experiments comparing the spectra of dolomite and magnesite, each from two different sources show that the bands in this region are almost identical. Additional experiments are required to determine whether the same correlation occurs over a wider range of sources for each carbonate.

5.3) Analysis of whole rock as a function of particle size

The effect of grinding and mixing on the DRIFTS spectra have been studied in three ways.

- A) Particle size fractions of Chelford sand.
- B) The mixing of various sizes of Chelford sand with kaolinite.
- C) Particle size fractions of Berea.
- D) Particle size fractions of reservoir rocks

Note: all samples in this section were diluted in KBr (i.e. a 10% dispersion in KBr) before spectral collection.

5.3.1) Influence of particle size on the DRIFTS spectrum of Chelford sand

The distinctions in the particle sizes used were coarse, medium and fine. Figure 5.28 shows the differences in the spectra of the three size fractions. The spectra of the coarse and medium grain sizes exhibit bands of poor quality (i.e. poor band shape and weak in intensity) in the region below 2000cm^{-1} whereas the spectrum of the fine grain size exhibits bands of good intensities and widths. The spectrum obtained from the coarse sized sand exhibits band distortions (centred at 1159cm^{-1}) between 1000 and 1250cm^{-1} . In addition the bands between 900 and 500cm^{-1} are no longer present and the overtone/combination region is less defined. In effect a lot of information relating to the absence of bands is apparent.

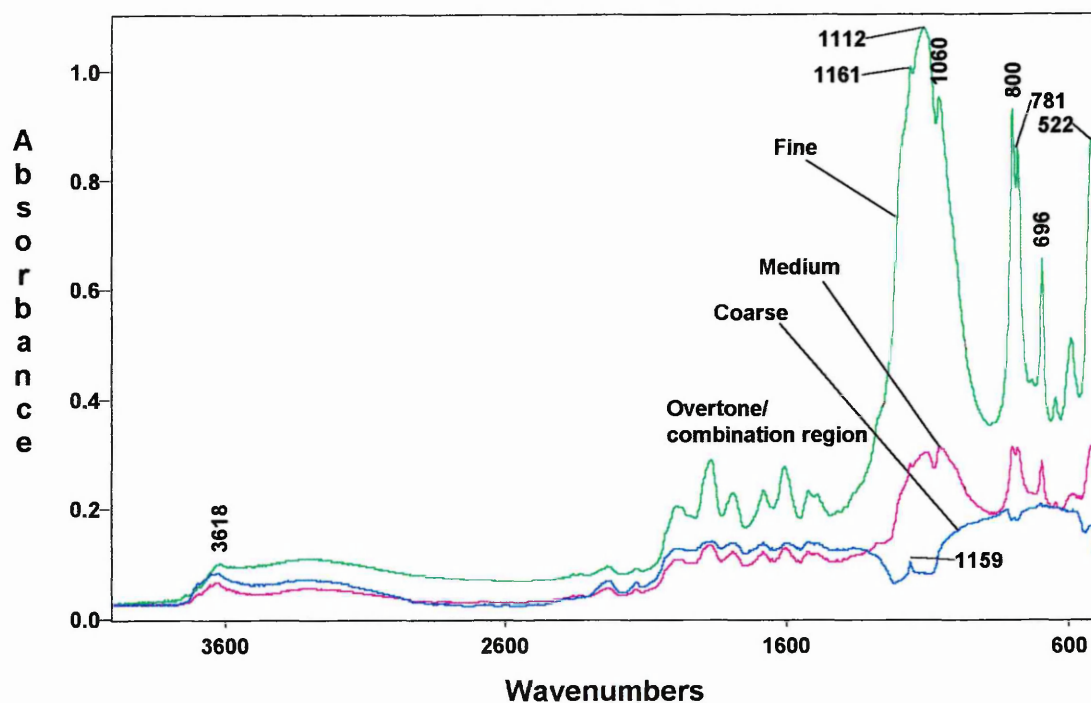
The spectrum obtained from the medium sized sand still exhibits bands in the region below 2000cm^{-1} . These bands are less distinct than those of the fine grained sand. In addition the ratios of the bands have changed.

Although the shape of the bands between 3700 - 2900cm^{-1} have changed only slightly as the particle size was varied, the intensity has changed considerably.

All this data is in good agreement with similar studies performed on Ottawa sand [21, 23].

Spectra from the coarse and medium grain sizes exhibited poor reproducibility whereas those obtained for the fine size were very reproducible.

Figure 5.28 - Particle size variation of Chelford sand



5.3.2) DRIFTS spectra of Chelford sand and kaolinite mixtures

The three particle sizes of Chelford sand were each mixed with kaolinite as a 90:10 ratio as a 10% mixture with KBr. Figure 5.29 shows the differences in the spectra of the three mixtures. The bands representing quartz (1162, 1112, 800, 781 and 696cm⁻¹) can only be distinguished in the spectrum of the sample containing fine grained quartz. Also the overtone/combination bands are only clearly defined for the fine grained quartz.

The loss of the quartz bands in the spectra of the medium (pestle and mortar sand) and coarse (neat sand) grained sand reveals the characteristic kaolinite bands at 1106, 1036, 1010, 937 and 916cm⁻¹. The height of these bands and the hydroxyl bands between 3695-3620cm⁻¹ increase as the sand grain size decreases. This occurs more so in the low wavenumber region (1200-1050cm⁻¹) than in the high wavenumber region (3700-3600cm⁻¹).

Figure 5.29 - Chelford sand and kaolinite mixtures

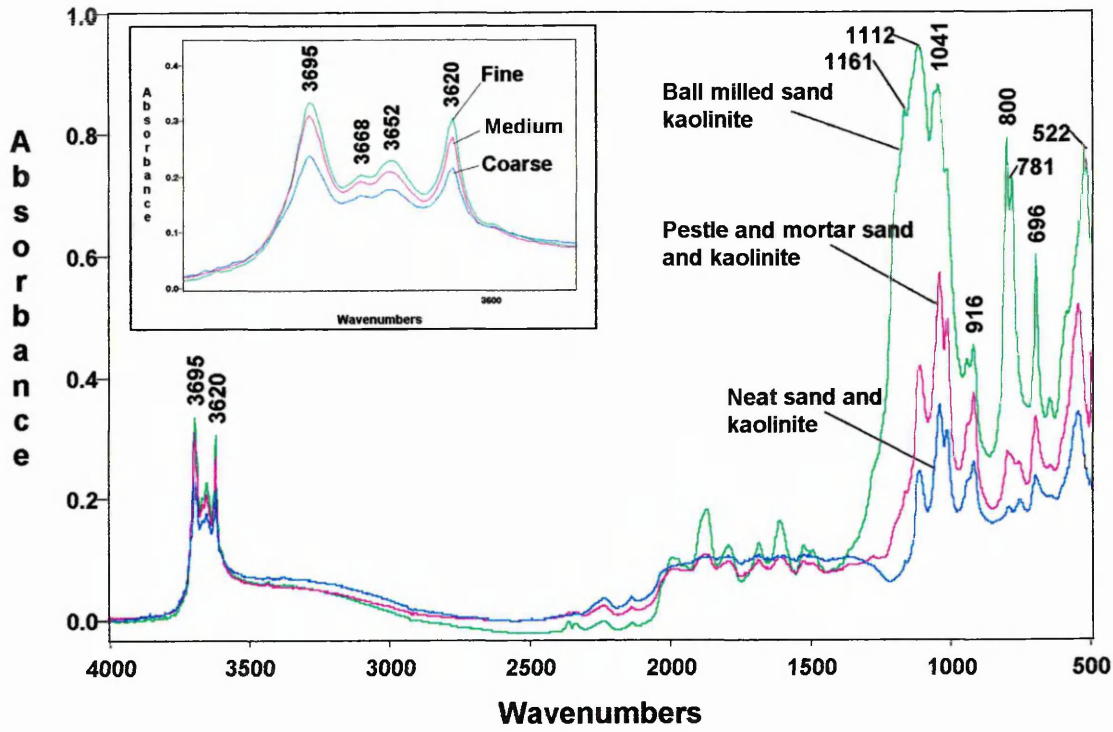
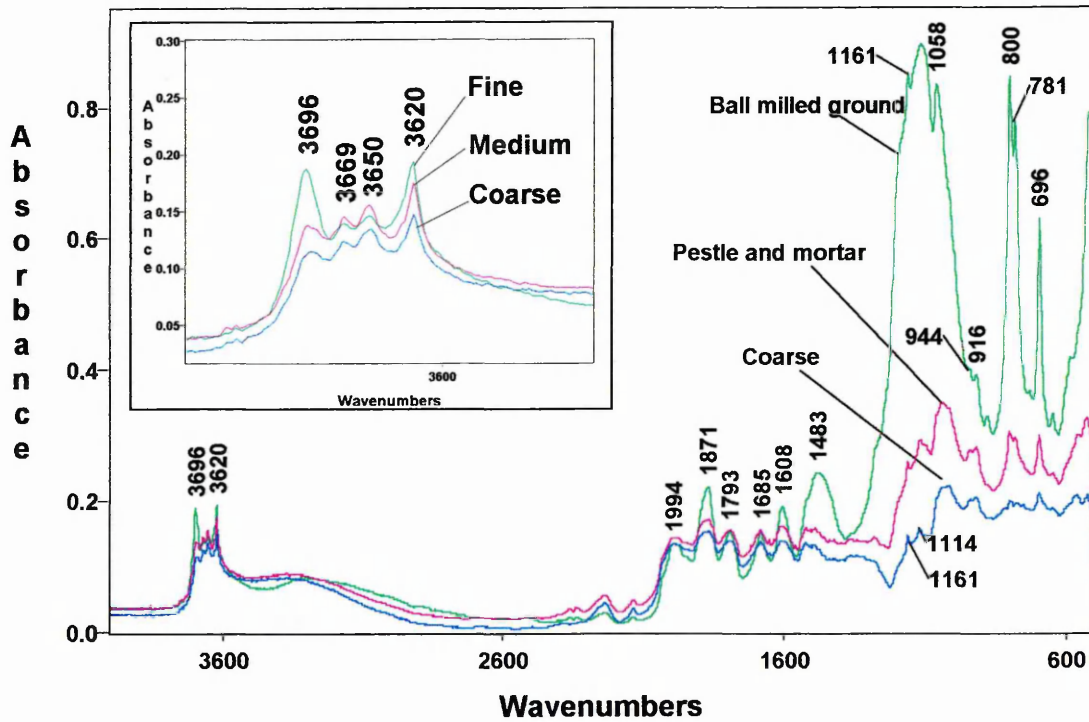


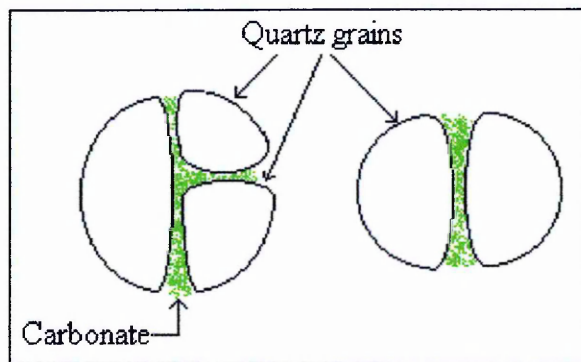
Figure 5.30 - Particle size variation of Berea



5.3.3) Influence of particle size on the DRIFTS spectrum of Berea.

The distinctions in particle sizes were again coarse, medium and fine. Figure 5.30 shows the differences in the spectra of the three different sized fractions. Similarities to the physical mixtures are observed although the band shape is poorer in the range $1200\text{-}1050\text{cm}^{-1}$. The reasons for the poorer band shapes could be due to less kaolinite and more illite being present. It should be noted that the carbonate band at 1483cm^{-1} is only present in the fine grained Berea. This suggests the carbonate is acting as a cement holding small grains of quartz together as shown in figure 5.31. The carbonate only becomes exposed to the infrared beam after it is severely crushed (i.e. ball milled).

Figure 5.31: Possible distribution of carbonate in Berea



The height of the 3696cm^{-1} band increases relatively to the 3620cm^{-1} as the particle size of Berea decreases. This could be due to several factors, for example

- i) there is more illite being sampled in the coarse grained Berea and hence increased absorption at 3620cm^{-1}
- ii) ball milling changes the crystallinity of kaolinite and thus changes the OH bands which are sensitive to changes in crystallinity.

5.3.4) Influence of particle size on the DRIFTS spectra of reservoir rocks

Only two particle sizes were analysed for each of the reservoir rocks, these were fine (ball milled) and coarse (deconsolidated). The results for all the reservoir rocks

followed the same trend as that observed for the various particle sizes of Berea. That is, the DRIFTS spectra of the fine sized particles exhibited a higher contribution from quartz when compared to the DRIFTS spectra of the coarse sized particles.

Summary

These experiments have shown DRIFTS is a surface weighted technique.

Initially, the analysis of the whole rock as a function of particle size has confirmed the need to obtain a fine particle size in order to produce a spectrum with bands of high intensity and good band shape. It has also showed that the technique is more sensitive to particle size effects in the low wavenumber region.

The mixtures of kaolinite and Chelford sand have shown that it is possible to obtain a spectrum of the fine clay particles whilst large grains of quartz are present although the quality of the spectrum is slightly reduced. There is less contribution to the spectrum from quartz mainly because i) the larger particle size increases the amount of specular and reduces the amount of diffuse reflectance, and ii) less quartz surface area is exposed to the incident radiation.

These results suggest that if a core of rock is coarsely ground, dispersed in KBr and a DRIFTS spectrum is collected, then the spectrum will exhibit more data from the smaller particle fractions (clay minerals) compared to the larger particle fractions (quartz grains). Since the clay minerals constitute the majority of the surface mineralogy, then it is reasonable to assume that this technique provides information representative of the surface mineralogy.

In addition, the spectra of the mixtures have allowed the interpretation of some of the bands to be confirmed. For example, the bands at 944 , 916cm^{-1} and the increased absorption between the 522 and 592cm^{-1} bands can be assigned to kaolinite.

5.4) DRIFTS spectra of the minerals released from deconsolidated rocks

Deconsolidation of rocks is simply a process in which the connected matrix of grains and particles of a rock are 'released' from each other. A simple method of achieving this is to lightly crush a rock using a pestle and mortar. The aim of this section is to sediment a deconsolidated rock into its individual mineral constituents and then determine whether the DRIFTS spectra of each sedimented fraction can reveal additional information regarding the separated mineral constituents within it. In addition confirmation of the presence of a mineral may be possible if the bands of a major constituent (e.g. quartz) is removed.

The calculations that were used [145] to determine the different sedimentation times of the clay minerals in this method assumed that all the particles are spherical. Unfortunately the clay particles are not spherical and therefore accurate fall times will be difficult to obtain. Moreover, this method also assumes that when the sandstones are lightly crushed the clay minerals are separated from the quartz grains. This is unlikely because clay minerals have planes of facile cleavage and thus will probably smear over the quartz grains. If the clay minerals were to be separated from the quartz grains there is still the possibility that the clay will not necessarily break up into single particles. For example grains, tactoids or particles may be present.

Firstly, the spectra obtained from samples of deconsolidated Berea that have undergone sedimentation and centrifugation will be discussed. These spectra will therefore contain no evidence of any soluble components because the water used for the sedimentation and centrifugation was disposed of.

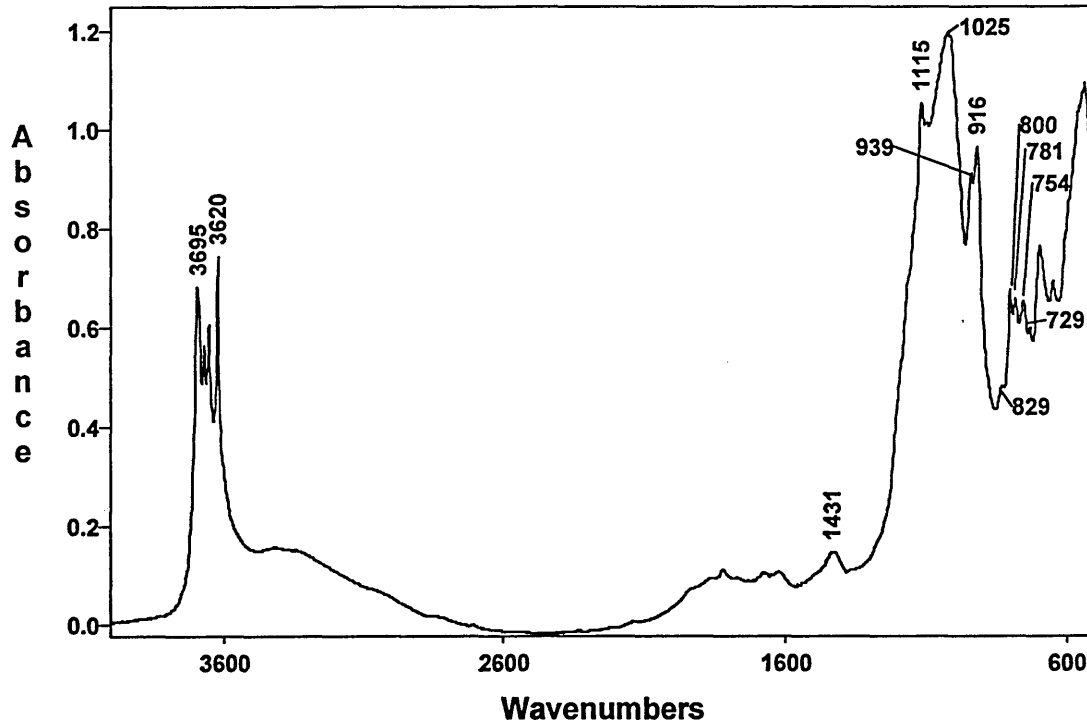
<2 μ m fraction

Figure 5.32 shows the spectrum of the less than 2 μ m fraction. The major difference in the spectrum when compared to the whole Berea spectrum (fine grain sized, figure 5.1) is the dramatic increase in the ratio of the kaolinite bands at 3693-3620 cm^{-1} to the

bands in the $1200\text{-}1050\text{cm}^{-1}$ region. The spectrum shows that little or no quartz is present because:-

- i) the clearly defined overtone/combination bands are largely absent,
- ii) there is a considerable decrease in the intensity of the 800 and 781cm^{-1} bands.
- iii) the main bands of quartz in the $1200\text{-}1050\text{cm}^{-1}$ region are absent,

Figure 5.32 - Berea (Insolubles) $\times < 2$ microns



Two new bands (829 and 754cm^{-1}) are present that are not observed in the whole Berea spectrum. There are several minerals that could give rise to such bands (e.g. illite, kaolinite, feldspar or smectite) so the assignment is not currently resolved. It is likely to be due to a combination of the illite and kaolinite.

The ratio of the 3620 and 3695cm^{-1} bands compared to those of pure kaolinite suggest that illite is also present in this fraction.

The bands in the $1115\text{-}916\text{cm}^{-1}$ region of this fraction are similar to the bands observed in the pure kaolinite spectrum, except that the former has an increased absorption at 1025cm^{-1} . Both illite (figure 5.5) and feldspars (figures 5.13 and 5.14) have a band in this region and could account for the enhanced absorption. It is likely to be due to illite for several reasons:-

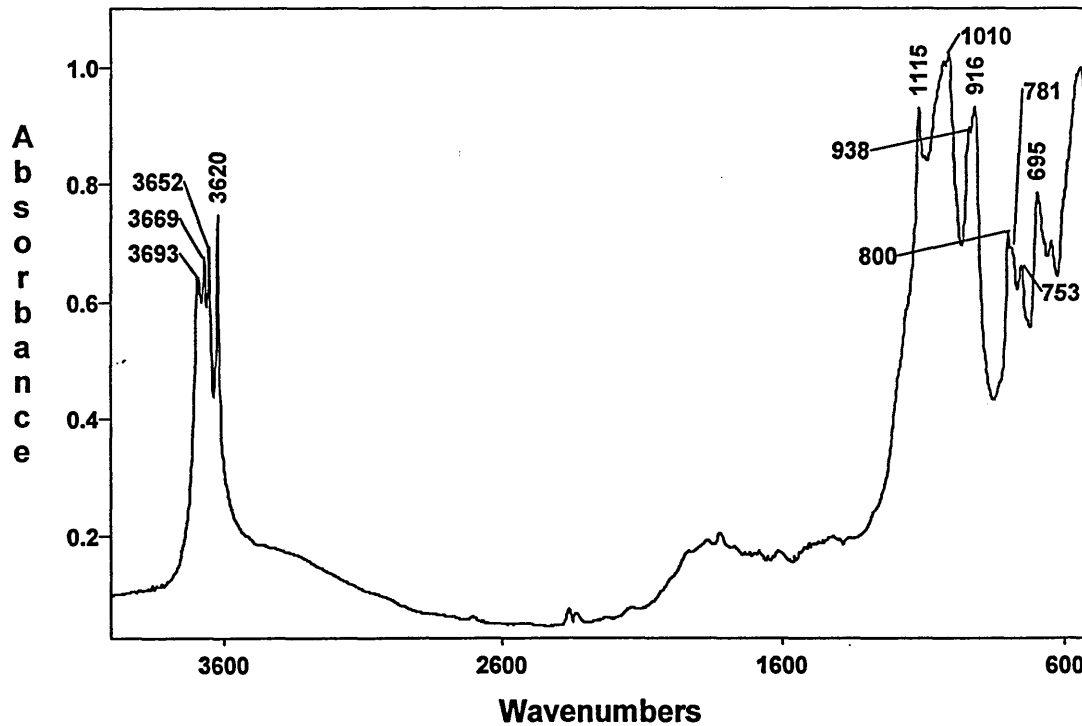
- i) the enhanced 3620cm^{-1} band is associated with illite,
- ii) the feldspars are large grains and are not expected in this fraction,
- iii) illite has a band at 1429cm^{-1} which may account for the absorbed band observed at 1431cm^{-1} .

The carbonate bands at 879 and 1483cm^{-1} that are present in the whole Berea spectrum are not present in the spectrum of the $<2\mu\text{m}$ fraction, and thus indicates it is absent.

Other fractions

The spectrum of the $2\mu\text{m} < x < 8\mu\text{m}$ fraction is shown in figure 5.33.

Figure 5.33: Berea (Insolubles) $2 < x < 8$ microns



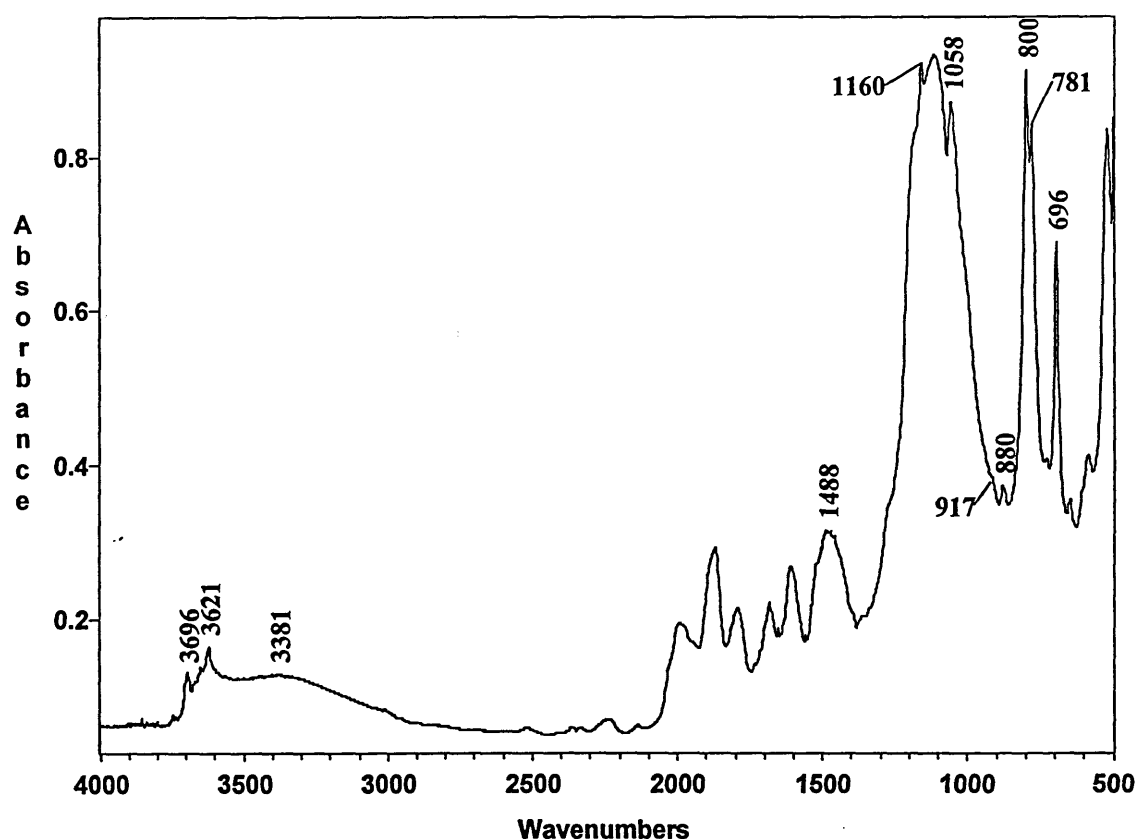
The number of bands and their positions are the same as those observed in the spectrum of the $<2\mu\text{m}$ fraction. The only significant difference is that the intensity ratios of the bands within the spectrum have changed. For example, the bands at 800 and 781cm^{-1} have increased in intensity and could therefore indicate an increase in the

quantity of quartz in the fraction. An increase in the intensity of the band at 3620 cm^{-1} would suggest an increase in the amount of illite in this fraction.

The fraction containing the particles left in suspension ($>8\mu\text{m}$) yielded a similar spectrum to those of the smaller size fraction. The significant difference was that the overtone bands were more clearly defined.

The fraction containing the large grains produced a spectrum exhibiting a considerable amount of specular reflectance and so the fraction was ball milled. The spectrum of the ball milled sample was collected and is shown in figure 5.34.

Figure 5.34 - Berea (large grains)



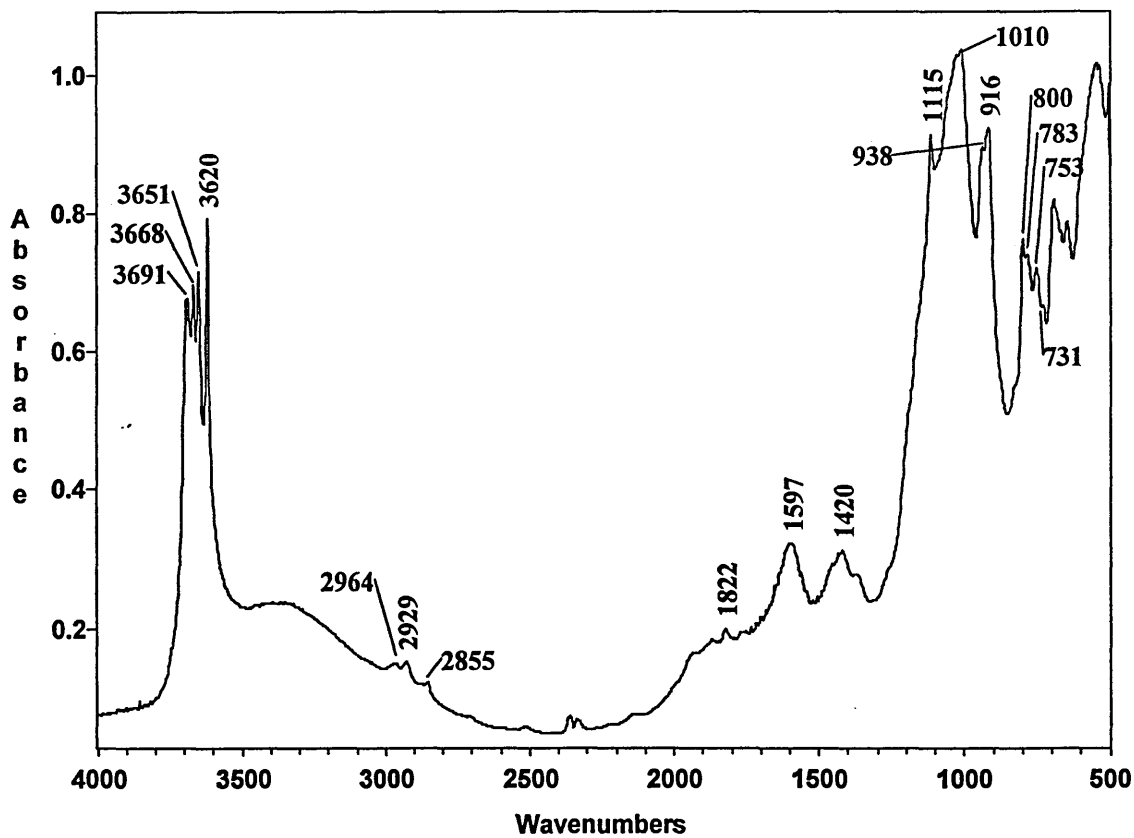
This spectrum is very similar to the spectrum of the whole Berea in that the number of bands and their positions are the same. The only significant difference is that the ratio of the bands have changed. For example, the bands due to kaolinite have decreased dramatically, this was expected because the kaolinite is present in greater amounts in the smaller fractions. The carbonate bands at 1483 and 879cm^{-1} in this large grain fraction are present, whereas for the smaller fractions they are not. This suggests that

the carbonates present in the sandstones are not soluble under the conditions used for sedimentation and were still intimately associated with the quartz grains. This agrees with the view that carbonate acts as a cement between quartz grains (figure 5.31). Alternatively, there may be large grained carbonates present within the rock but is unlikely.

Secondly, the spectra of Berea that has undergone sedimentation followed by the water being driven off by heating will be discussed. These spectra will therefore contain spectral evidence of any soluble components present in the Berea.

To date only the $<8\mu\text{m}$ fraction has been studied (figure 5.35).

Figure 5.35 - Berea (solubles) $x < 8$ microns



If this spectrum is compared to the spectrum of the $2\mu\text{m} < x < 8\mu\text{m}$ fraction from the insolubles (figure 5.33) then the bands are very similar apart from the region between $3000-1300\text{cm}^{-1}$. The bands (not in the $3000-1300\text{cm}^{-1}$ region) are similar in that they have approximately the same ratios as each other (there is very little quartz and there

is a large amount of kaolinite). The carbonate bands present at 1483 and 879 cm^{-1} in the whole Berea spectrum are no longer present in this fraction, but new bands have arisen, for example at 1419, 1597 and 2962-2876 cm^{-1} . Bands of this nature in the region 3000-2800 cm^{-1} arise from C-H stretching and therefore indicates the presence of an organic. The possibility of contamination whilst the fraction was being dried could be responsible for these extra bands. This could be likely because the clay minerals in the sample can easily adsorb organics.

Summary

Considering the number of assumptions involved in the sedimentation of the minerals, this appears to be a relatively successful technique for separating the clay minerals (i.e. the main constituent of the surface mineralogy) from the quartz. The procedure almost managed to obtain a fraction that contained only clay minerals and a separate fraction that contained a high proportion of quartz. This method has also revealed extra bands via the removal of the large quartz bands from the spectra. Unfortunately, the additional bands have not yet been assigned.

5.5) DRIFTS spectra of samples derived from ultrasonication of whole rocks

Fragments of Berea sandstone were treated ultrasonically for three minutes and the DRIFTS spectrum of the solids (fines) collected from the resulting suspension was obtained. (Note: any suspensions collected did not contain any large quartz grains that fell to the bottom during ultrasonication). This spectrum (figure 5.36) is very similar to the 2 μm <x<8 μm fraction of Berea/solubles (figure 5.35) in that it indicates it contains very little quartz and a high proportion of kaolinite. All the other spectra of the suspensions collected are very similar to the three minute fraction apart from the residual fragments remaining after 16 hours of ultrasonication. The residual fragments were ball milled before the DRIFTS spectrum was collected, (figure 5.37). The definite presence of quartz and a smaller amount of the clay minerals was

recorded. Again it can be noted that no carbonate is observed in the spectrum of the fines but is in the spectrum of the residual fragments.

Figure 5.36 - Berea, Ultrasonics - 3 minutes

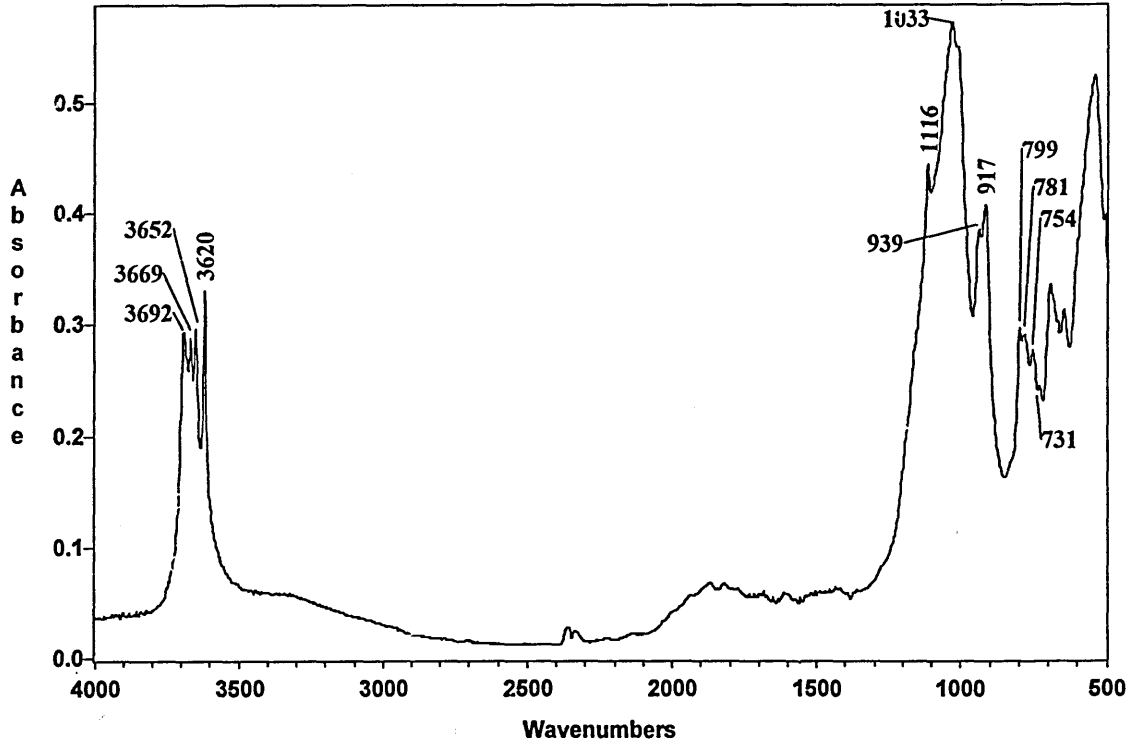
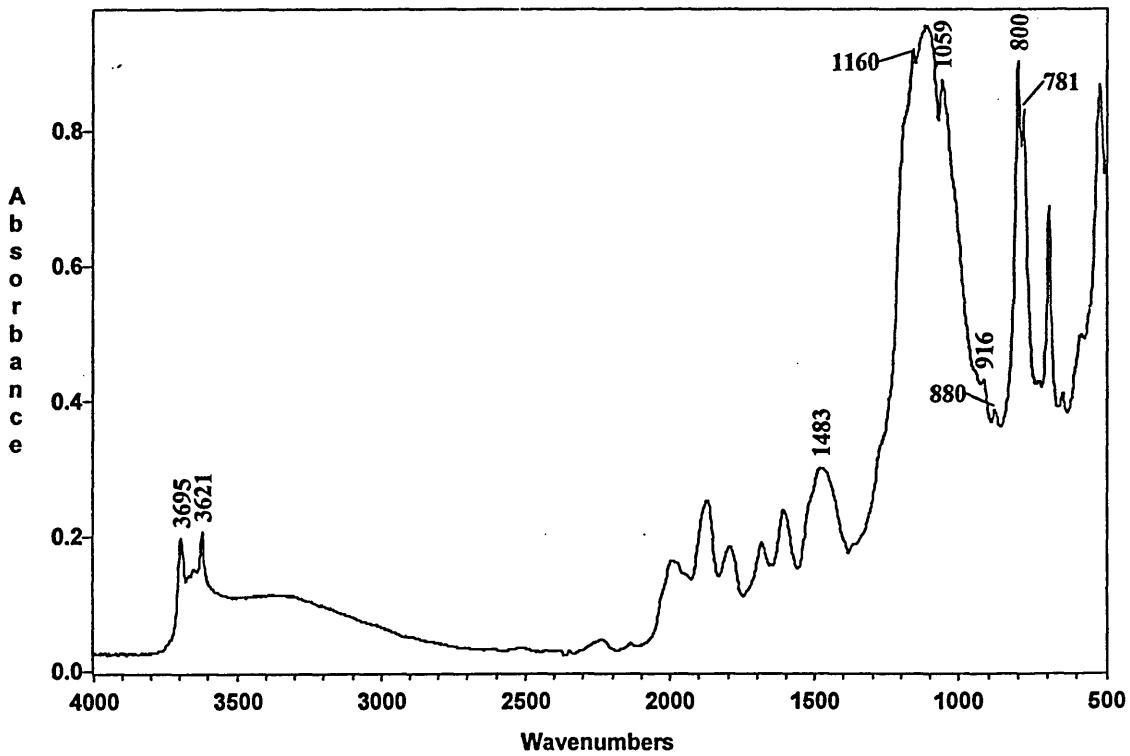


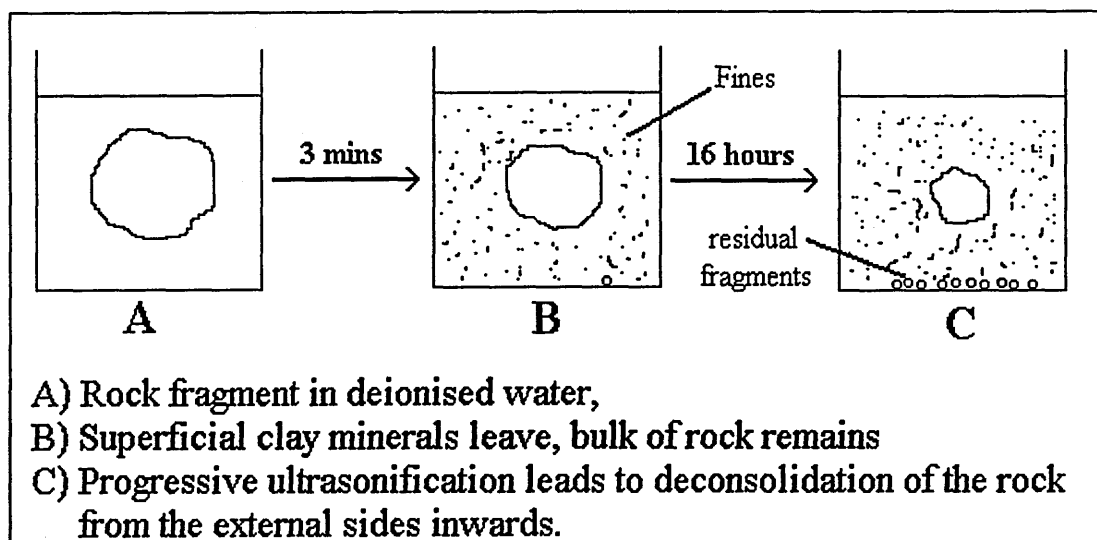
Figure 5.37 - Berea, fragments remaining after 16 hours of Ultrasonication



Summary

This ultrasonic technique was successful at separating the clay minerals from the quartz grains. It is less time-consuming than the sedimentation method because a similar spectrum of the clay minerals (i.e. the smallest fraction) can be obtained after just three minutes of ultrasonication. The process is shown diagrammatically in figure 5.38.

Figure 5.38: Diagram showing the ultrasonication process.

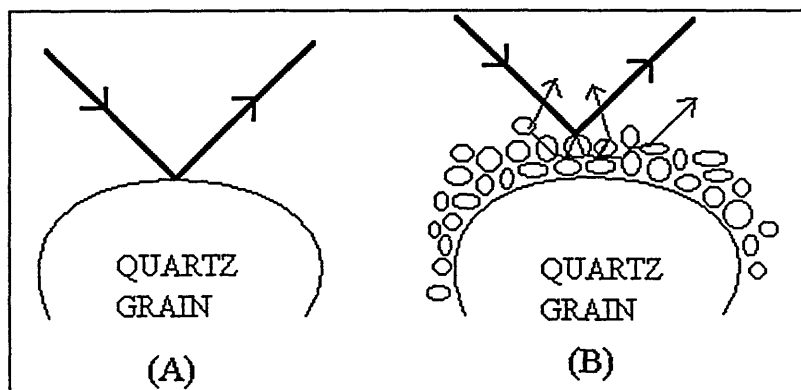


Although, both the sedimentation and ultrasonication techniques are disruptive to the surface mineralogy and none of the spectra obtained truly represent the bulk mineralogy, they are techniques that have great potential for determining clay mineralogy within rocks.

5.6) Direct DRIFTS analysis of rocks (cut/fractured discs)

Direct DRIFTS analysis of both the sandstones and reservoir rocks has been performed. Hopefully the spectra obtained should be weighted to the clay if present.

This is shown diagrammatically in the figure below:-

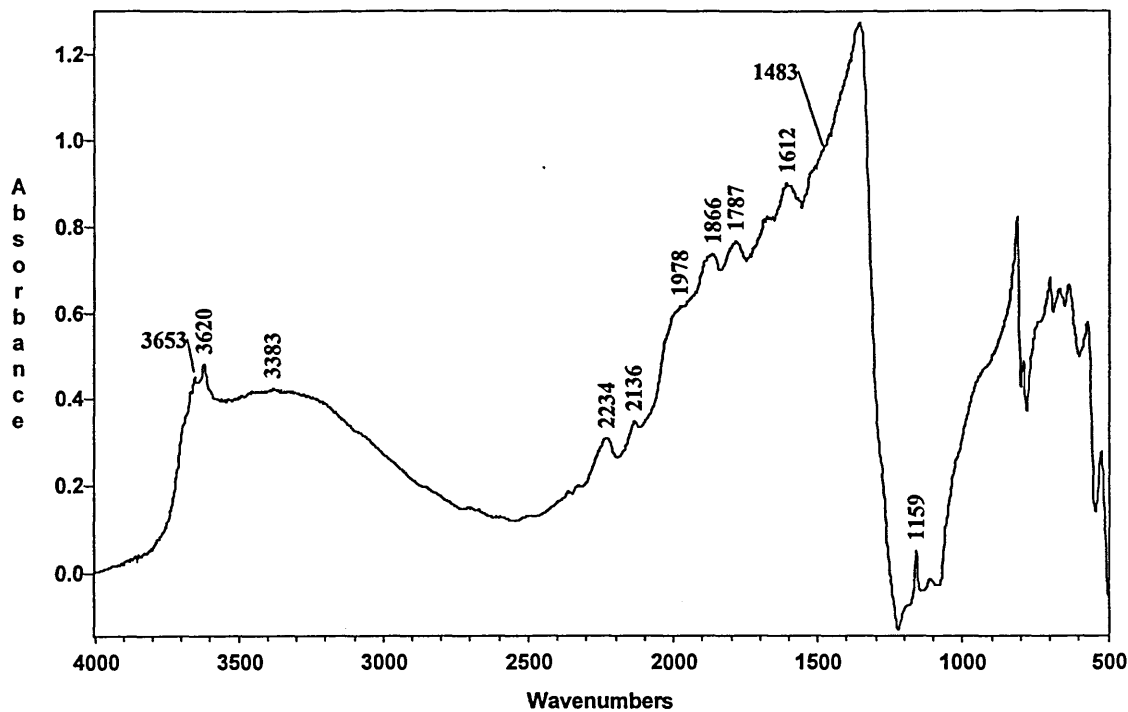


If no clay is present (A), a higher contribution from the quartz will be collected, whereas if clay is present (B) then a higher signal from the clay will be observed. Since the quartz grains will not be broken up and the surface area will be less, the signal from quartz should be reduced. Cut and fractured surfaces have been compared because a fractured surface is more likely to represent the surface mineralogy since it has undergone less disruption, and, a cut surface is more likely to help obtain a more reproducible spectrum since its topography will be easier to reproduce.

5.6.1) Cut rock surfaces

Generally all the spectra of the cut rock surfaces are severely affected by specular reflectance. An example of the specular effect can be seen in the spectrum of the cut surface of Berea (figure 5.39). Prolific distortions in the band shapes are apparent in the 1500-500 cm^{-1} region. The distortion is so great in the 1000-1250 cm^{-1} region that a reststrahlen band has appeared. In the 4000-2500 cm^{-1} region, band broadening has occurred accompanied with an increase in intensity for all the bands present. No band distortions have occurred in this region. Enhancement of the overtone/combination bands has also occurred.

Figure 5.39 - Berea (cut rock surface)



Note that a cut surface spectrum is very similar to that of a neat powder (not diluted in KBr) spectrum (figure 2.4) and thus its appearance is not necessarily a product of cutting.

The spectra of the cut surfaces of Clashach and Birchover are shown in figures 5.40 and 5.41, respectively. These spectra are similar to the Berea spectrum in that high specular reflectance is evident. Although the spectra show similar trends small differences are apparent which distinguish one spectrum from another. For example, the spectrum obtained from Birchover shows the four characteristic kaolinite (which are distorted but still noticeable) bands between 3693 and 3620 cm^{-1} , whereas the spectrum of Clashach does not.

Two bands that are prominent in the spectra obtained from cut surfaces are those positioned at approximately 2238 and 2316 cm^{-1} . These are due to overtone or combination bands of quartz.

Surprisingly, the reproducibility of the spectra taken from different areas of the cut surface is very good over the whole mid-infrared range. If any variance is observed it is usually in the 1500-500 cm^{-1} region (i.e. the region expected to be susceptible to such

Figure 5.40 - Clashach (cut rock surface)

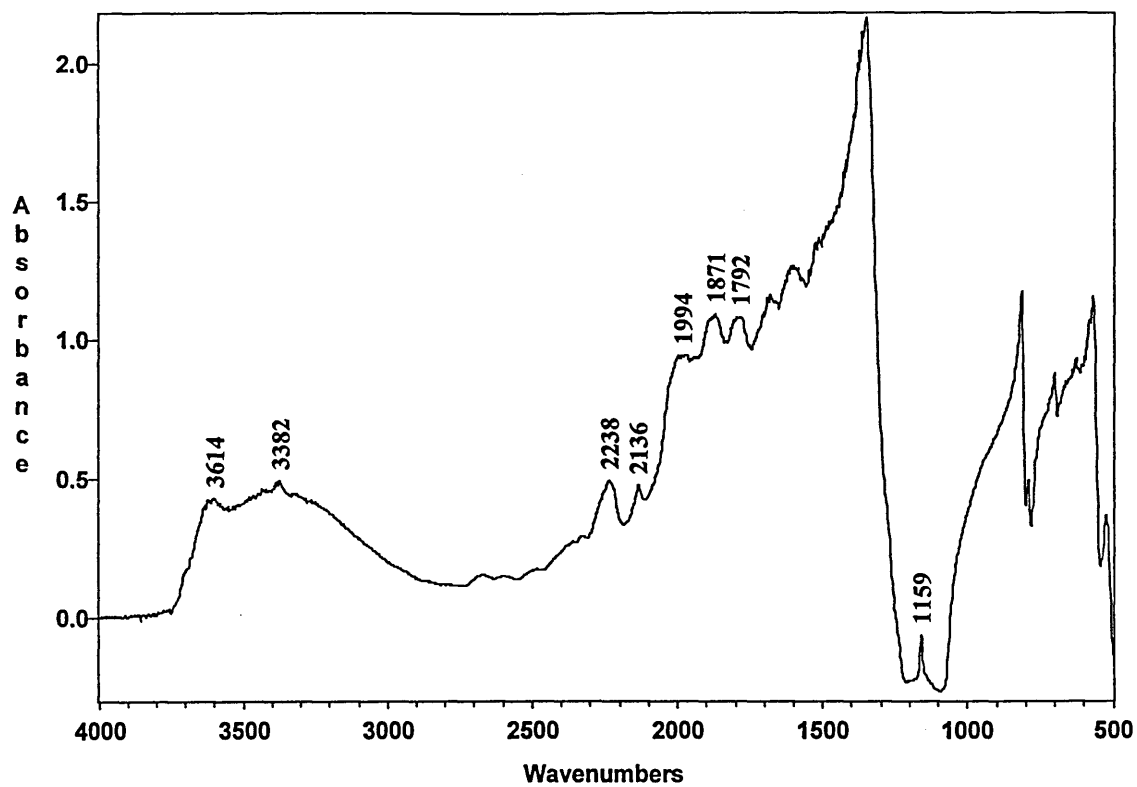


Figure 5.41 - Birchover (cut rock surface)

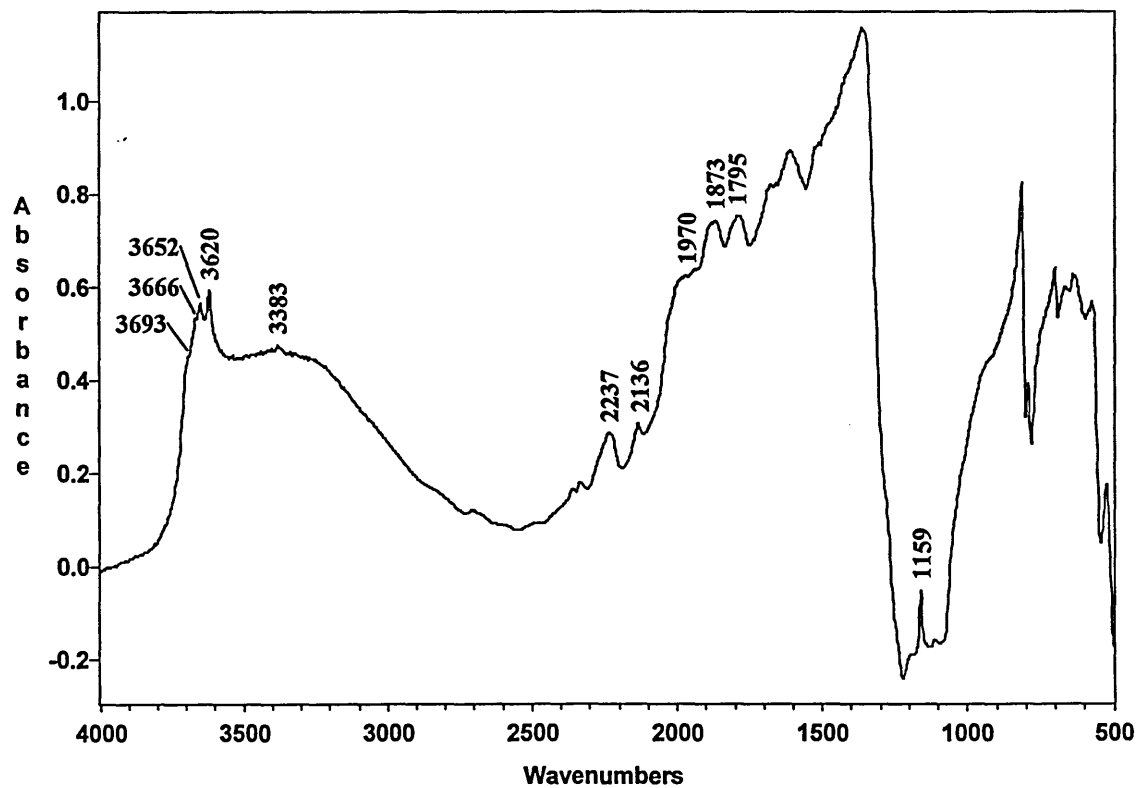
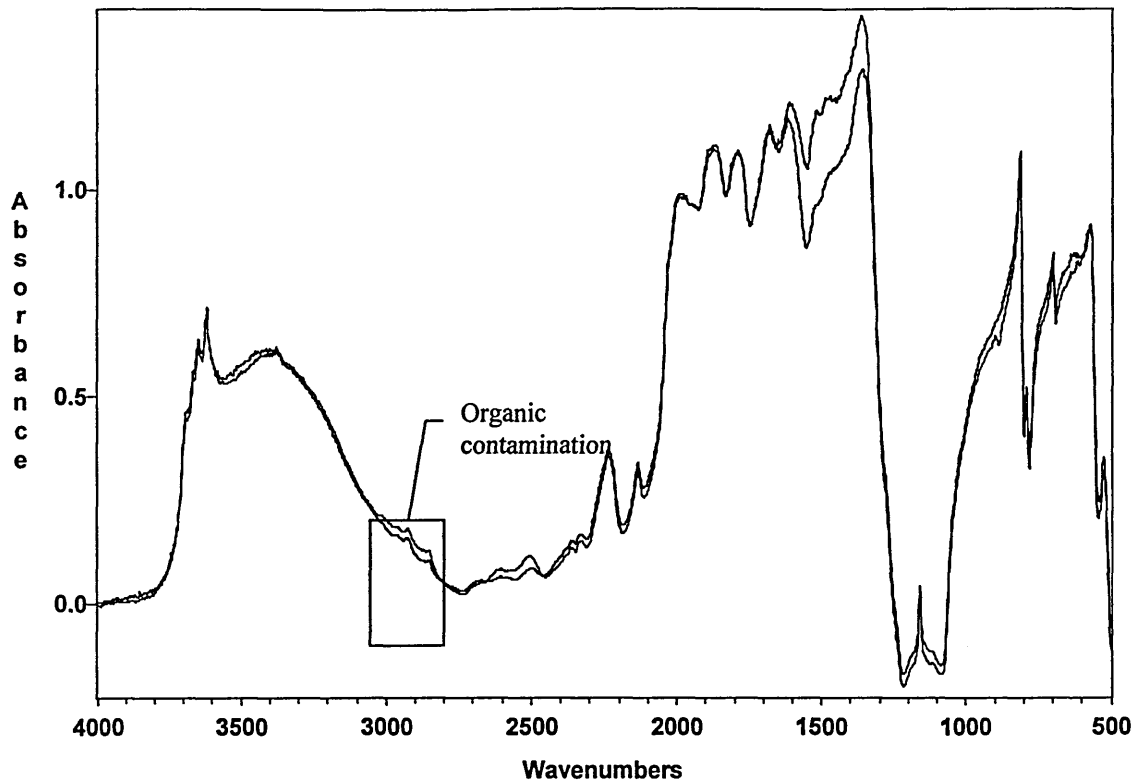


Figure 5.42 - Reproducibility of cut surfaces from Berea



variance). This is because this region is more sensitive to particle size, which was demonstrated in section 5.3. Spectra obtained from both sides of a disc cut from a Berea core are presented in figure 5.42 and show good reproducibility. The disc used to collect these spectra was cut using water as a lubricant and subsequently dried in an oven. New bands are present in these spectra and indicate the presence of organics. Contamination whilst the discs were being dried could be their source. This problem highlights the need for cores to be cut with a dry saw.

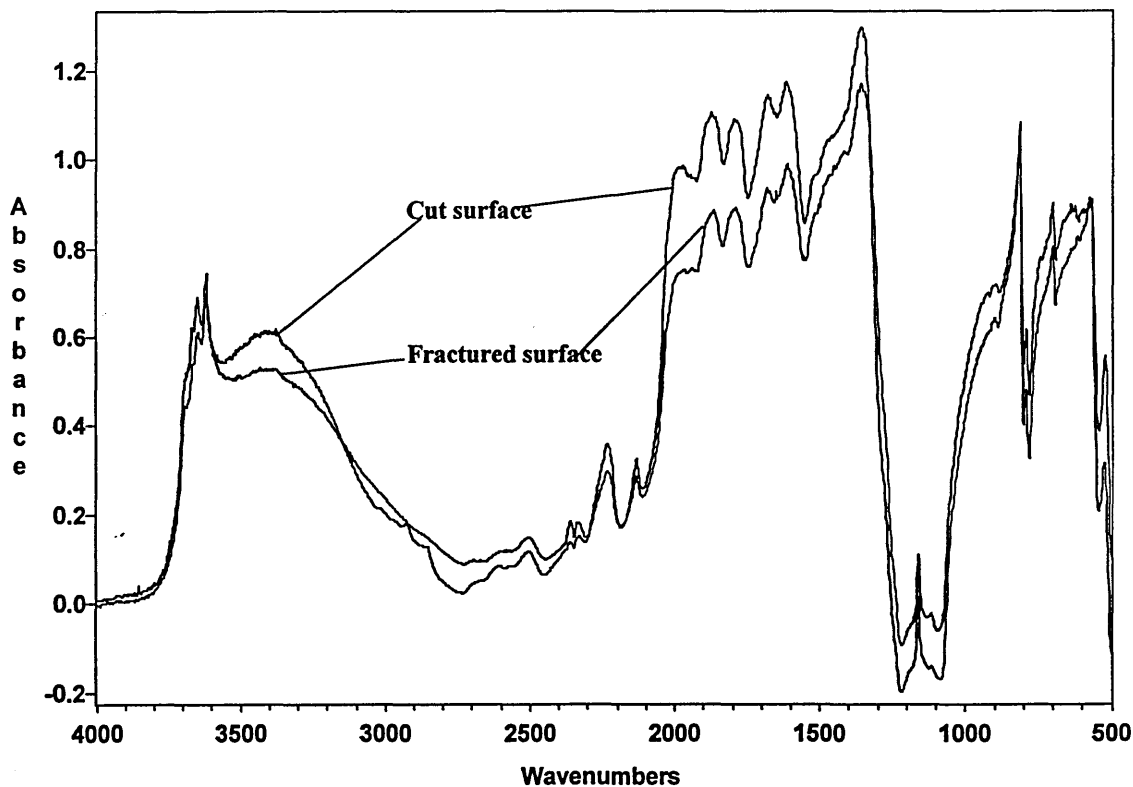
Summary

Although the qualitative interpretation of the spectra obtained from cut surfaces is much more difficult than the spectra obtained from ball milled samples due to the distorted region, differences in the bands can still be observed and the possibility of using these differences to distinguish and identify the mineral components (especially clay minerals) may be possible (see later). The unexpected reproducibility of the spectra is also of great importance in a quantitative method.

5.6.2) Fractured rock surfaces

The appearance of the spectra obtained from fractured rock surfaces are very similar to the spectra obtained from cut surfaces. Figure 5.43 compares the spectra of Berea obtained from the two types of surfaces and shows that the same distortions are obtained. These observations are also noted when studying the other sandstones and reservoir rocks. Figures 5.44 and 5.45 show the spectra obtained from the fractured surface of Birchover and Clashach, respectively.

Figure 5.43 - Spectra of cut and fractured surfaces from Berea



The spectra obtained from fractured surfaces are less reproducible than the spectra obtained from cut surfaces, more so in the 1500-500 cm^{-1} region than the 4000-2500 cm^{-1} region. The reproducibility in the latter region is reasonable, but sometimes rotation (a sloping baseline) in the spectra is observed. Rotation in spectra occurs due to a mismatch in height between the background and the non-level surface of the fractured disc. The effect of a non-level surface on spectra is very similar to the effect observed when a sample with flat surface is raised or lowered with respect to the

Figure 5.44 - DRIFTS spectrum of fractured surface from Birchover

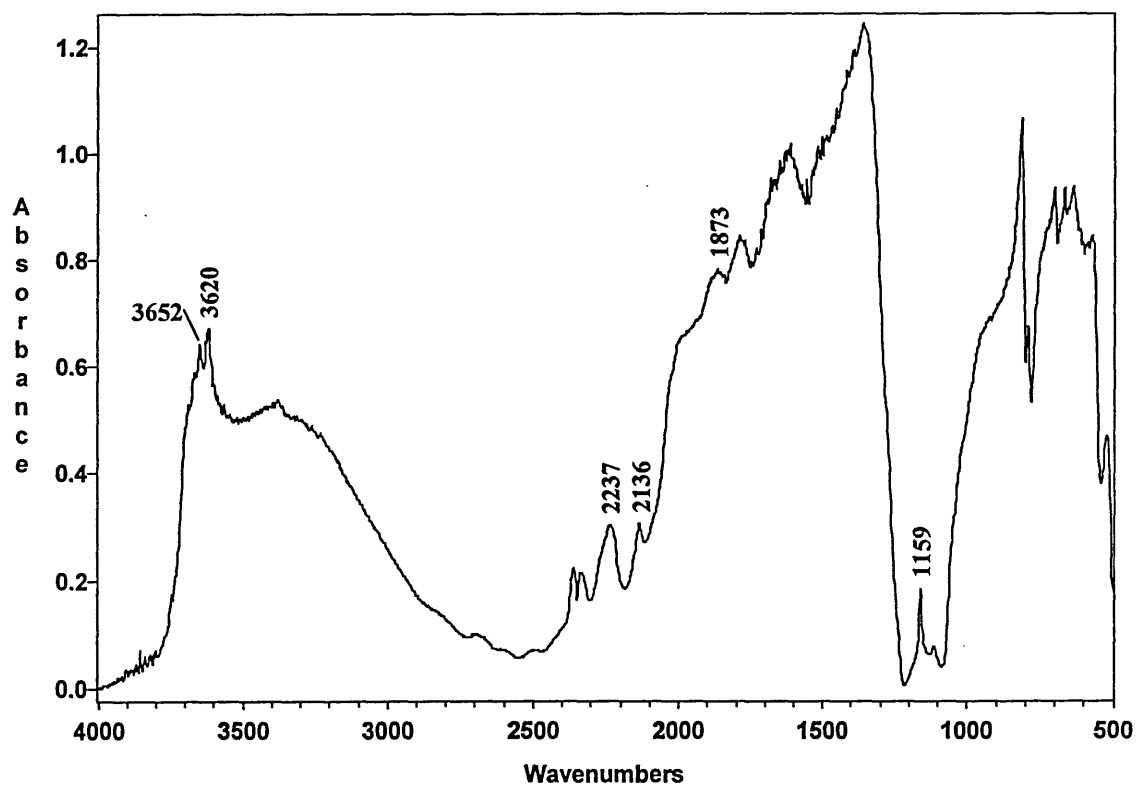
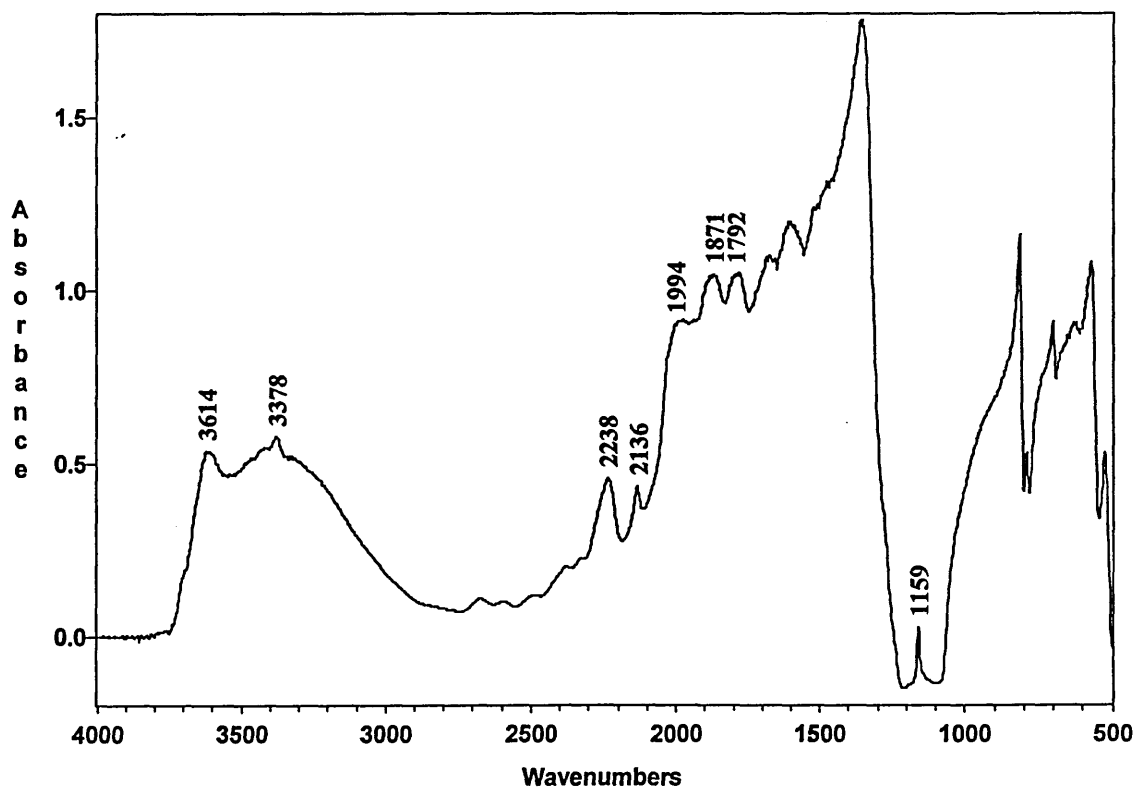


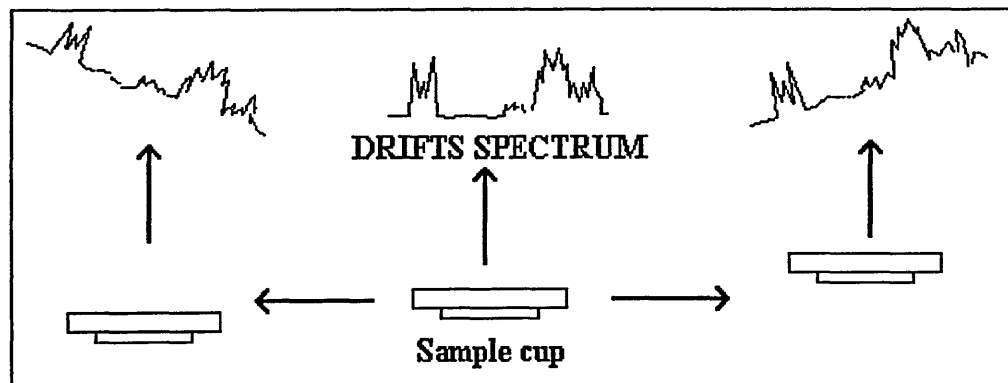
Figure 5.45 - DRIFTS spectrum of fractured surface from Clashach



background sample, i.e. a change in the sample height results in a corresponding rotation in the spectra (see figure 5.46). A level, fractured surface is very difficult (if not impossible) to obtain and so these spectra will always be less reproducible.

Barnes et al. [246] used a mathematical transformation to account for sloping baselines. However, sloping baselines are not always linear so this needs to be taken into consideration.

Figure 5.46: The effect of sample surface height on a DRIFTS spectrum.



Although the appearance of the fractured and cut surfaces are clearly different, the DRIFTS spectra obtained from each are very similar. In order to determine in more detail what the mineral orientation is at the surface of each type of disc, SEM was employed. It was anticipated that this investigation should determine whether the incident beam was sampling the bulk or the very top surface of the disc. It was expected that the bulk mineralogy was being sampled because the appearance of each surface was visibly different. Although since the absorptivity of the minerals is high, the penetration depth should be low.

5.6.3) Scanning Electron Microscopy

SEM micrographs (EM) of fractured and cut surfaces from both Clashach and Birchover were collected. These two sandstones were chosen because they differ in the fact Clashach is a 'clean' rock and Birchover contains a high amount of clay.

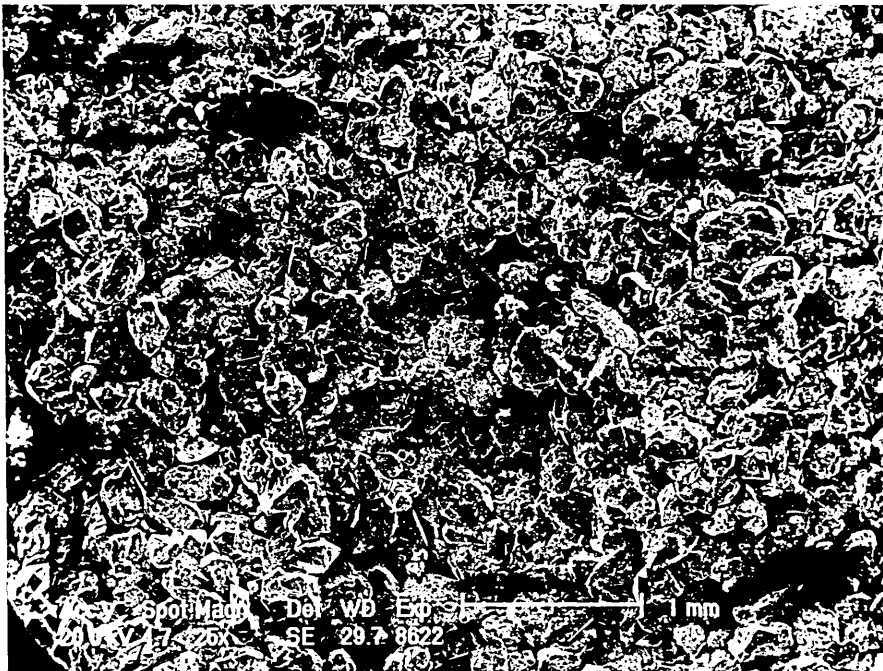
Clashach

Fractured surface : here the quartz grains are still intact and very little clay is present (EM 1).

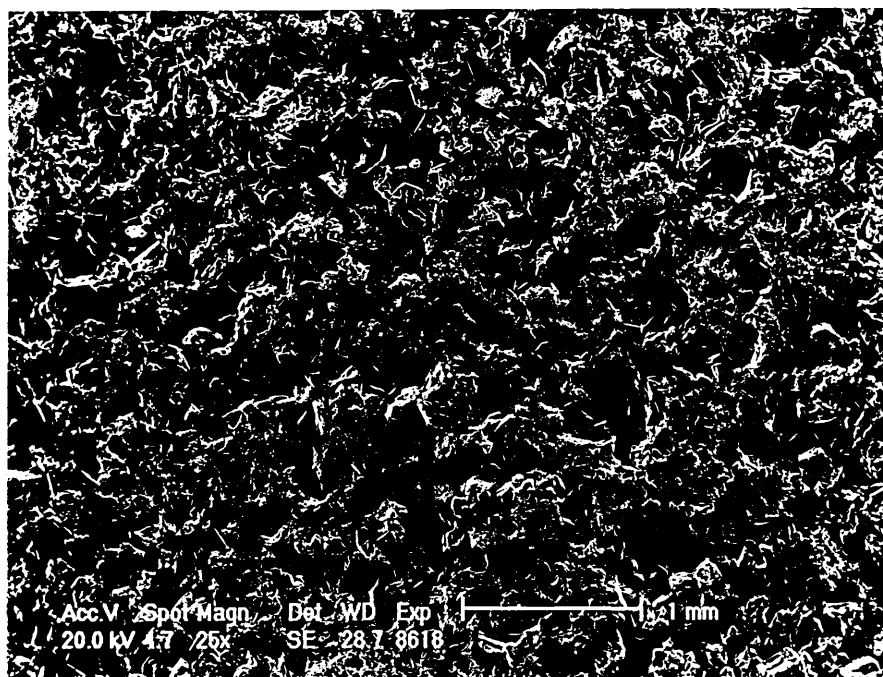
Cut surface : here the quartz grains are still clearly visible, but the top grains have been damaged by the saw (EM 2A and B).

Although the surface topology is different between the two discs, the general appearance is similar. It is therefore expected that the spectra of each surface will be similar.

Electronmicrograph 1A: Fractured surface obtained from Clashach (x25).



Electronmicrograph 2A: Cut surface obtained from Clashach (x25).



Electronmicrograph 2B: Cut surface obtained from Clashach (x100).



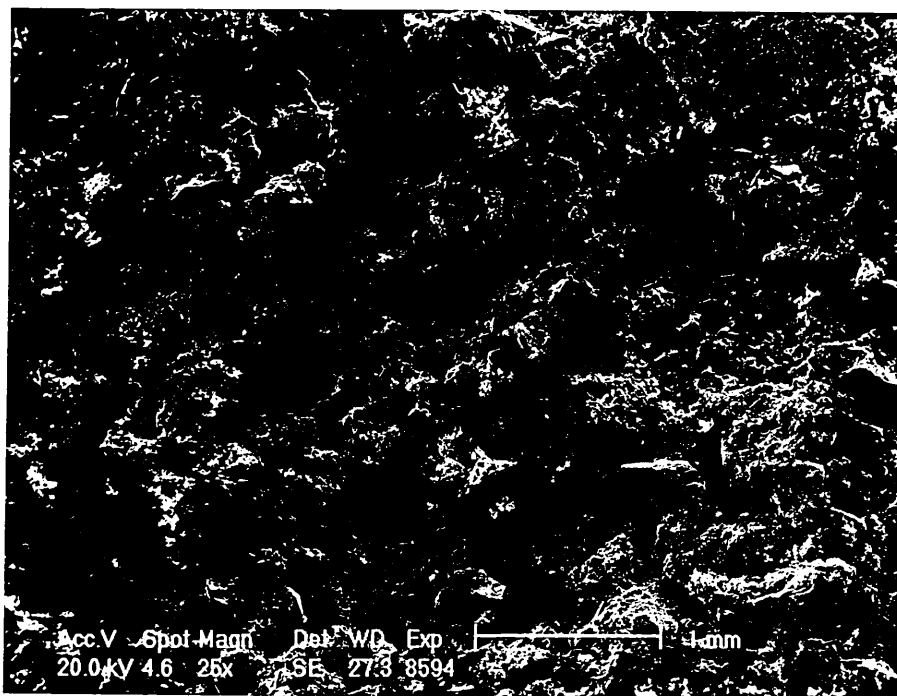
Birchover

Fractured surface : here the quartz grains are still visible. The clay present is covering the quartz grains and lining the pore throats (EM 3A and B).

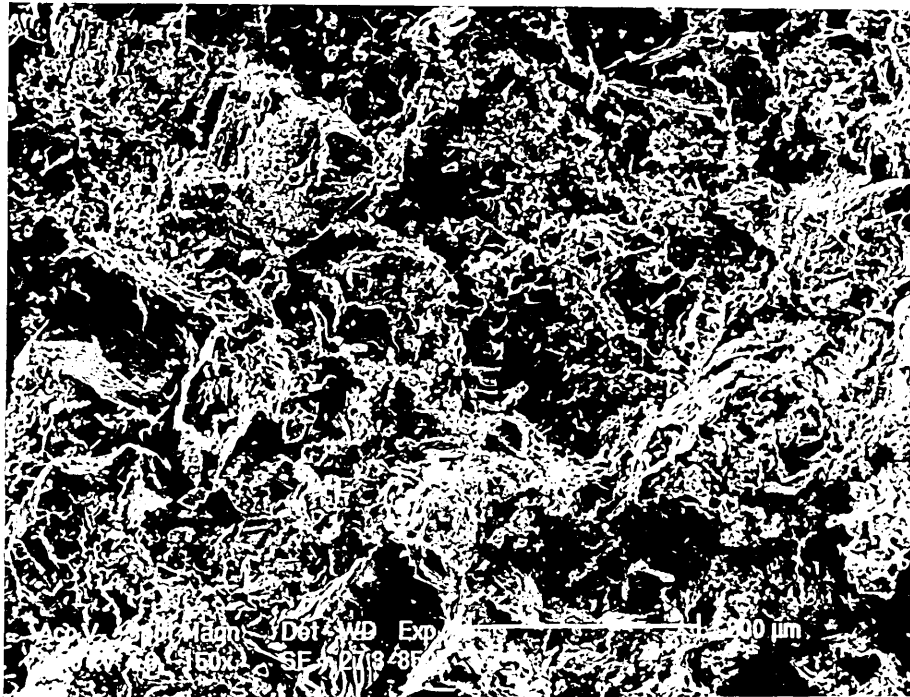
Cut surface : here the surface is much flatter than the fractured surface (EM 4A and B). The quartz grains are not visibly present and a sheet-like appearance is observed. There is very little clay existing in its original morphological state on the bulk of the surface, but some is present in the few pore throats that remain. Some broken quartz grains may also be present in the pore throats.

It appears that either i) the clay present in the sandstone has been smeared over the surface of the disc or ii) the quartz grains have amalgamated to form a sheet. Although EDX analysis of the surface has not been carried out to confirm this, the former scenario is more likely.

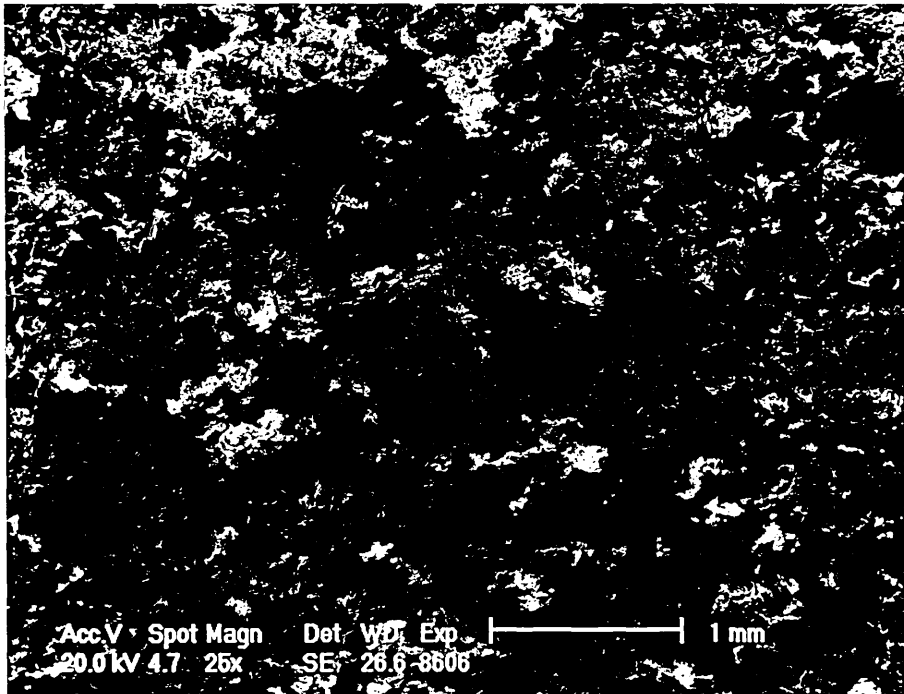
Electronmicrograph 3A: Fractured surface from Birchover (x25)

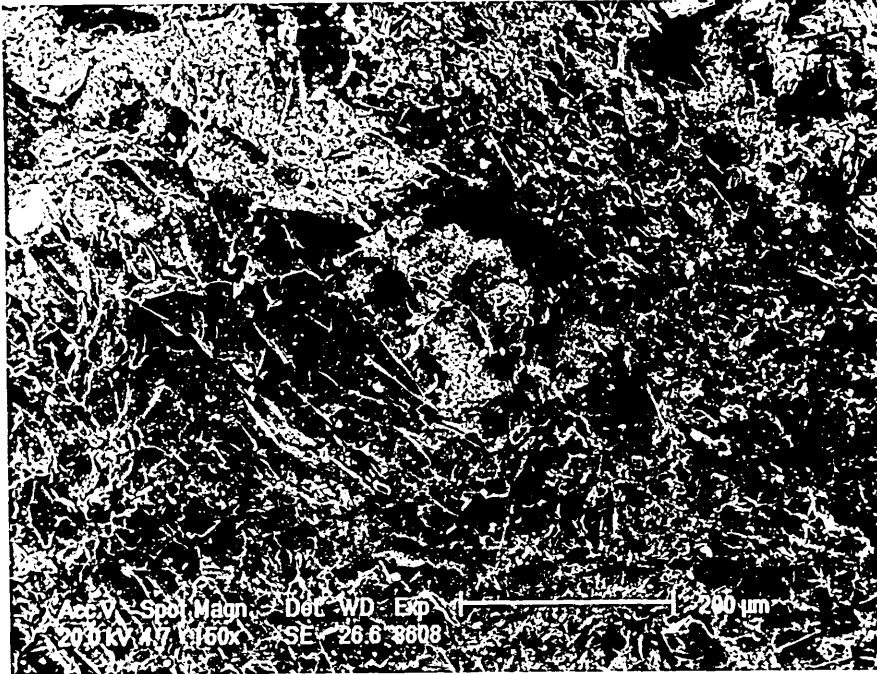


Electronmicrograph 3B: Fractured surface from Birchover (x150)



Electronmicrograph 4A: Cut surface from Birchover (x25)



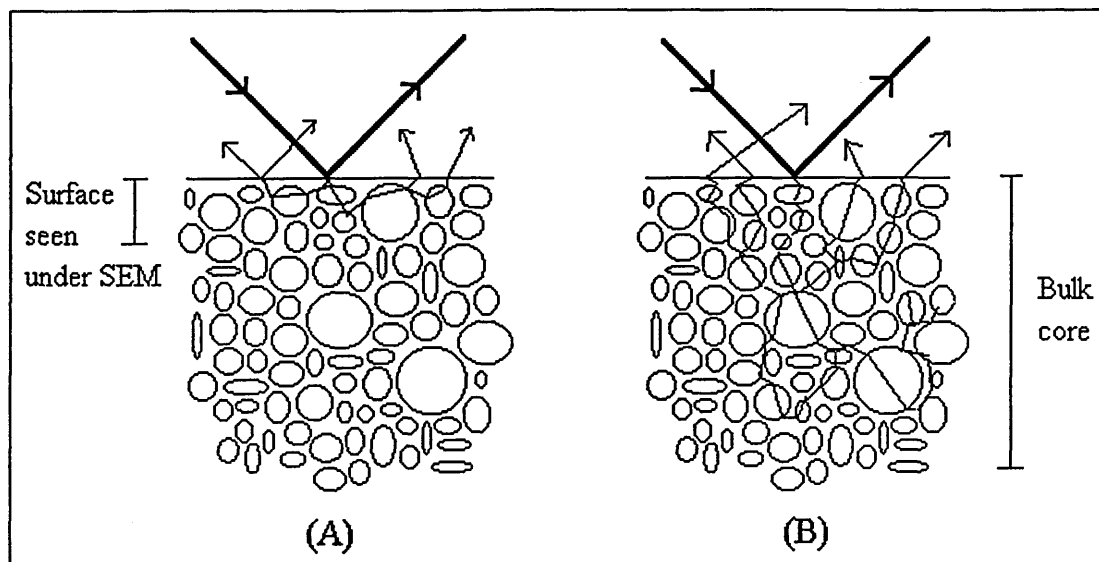


By studying the electronmicrographs, it can be observed that the surfaces from the cut and fractured discs of Birchover are different, unlike the case for Clashach.

The depth of penetration of the incoming beam will vary from sandstone to sandstone since they contain different particle and grain sizes. The depth also depends on the absorptivity of the sample. Since minerals have a high absorptivity, the depth should be very small. Although this may be so, radiation can easily pass through pore throats and hence allow a greater depth to be sampled.

Whether the spectrum obtained is representative of the surface seen under the SEM (figure 5.47A) or the surface of the bulk core (5.47B) is difficult to determine. Since the spectra of the cut and fractured discs are very similar but the SEM micrographs show the surface to be different may suggest the spectra is largely obtained from the bulk of the core.

Figure 5.47: Proposed sampling regions of the infrared beam in cut and fractured surfaces.



The distortions observed in the spectra are due to the collection of an increased amount of specular reflectance. If the specular reflectance can be minimised, a more ideal spectrum may be obtained. Thus, various methods that are capable of decreasing specular reflectance were investigated.

5.6.4) Methods to remove distortions in spectra

A) KBr Overlayers

It has been shown by McKenzie et al. [247] that by placing a layer of KBr over the surface of a sample the amount of specular reflectance is reduced and the amount of diffuse reflectance increases. They wanted to obtain the spectrum of a coupling agent on the surface of glass fibres by subtracting a spectrum of the fibres alone from that of the treated fibres. The subtraction did not work as a result of the specular reflection (i.e. non-Kubelka-Munk behaviour). In order to overcome this, they used a relatively thin layer of KBr on top of the sample. This scrambled the incident radiation and removed specular reflectance contribution. Good subtractions were then possible.

The added KBr reduced the spectral intensities of all bands, but the reduction factor was greater for the fibre than the coupling agent. They postulated that the KBr overlayer method makes the incident and reflected radiation isotropic, which removes the orientation dependence, and increases the average angle of incidence of the radiation to the fibres, which causes greater reflection at the fibre surface and less penetration into the fibre itself. This effect has also been used to depth profile polymer films [248]. A thin layer of KBr dispersed over a sample limits the penetration of the incident beam into the sample and so as the layer of KBr increases, the depth of penetration decreases and thus contribution from the surface material increases.

This method was crudely applied to the fractured surface of Clashach. Instead of a uniform layer of KBr over the surface, KBr was sprinkled over it in increasing amounts.

After a small amount of KBr was sprinkled over the surface, all the bands reduced in intensity (middle spectrum - figures 5.48A & B). The 2000-500 cm^{-1} region became flatter but the bands were still highly distorted. An interesting observation is that although the bands between 3700-3900 cm^{-1} reduced in intensity, their characteristic shape remained.

Additional KBr decreased the intensity further, but did not remove the distorted bands. Too much KBr removed the spectrum completely (figures 5.48A & B). These preliminary experiments show little reduction of specular distortions and indicate that the problem could arise from the difficulty in achieving a uniform layer of KBr on the surface. It has been shown [249] that the penetration depth of the beam through pressed ball milled KBr is 0.2mm (i.e. pressing technique used for ball milled samples). If a layer this thick can be uniformly placed on the surface of a rock then the removal of specular reflectance and the enhancement of diffuse reflectance may be optimised. This would be more difficult for a fractured surface rather than a cut surface, since a uniform depth of 2mm over the non-level surface of a fractured disc will be difficult to achieve (figure 5.49).

Figure 5.48A - Sprinkling of KBr on Clashach

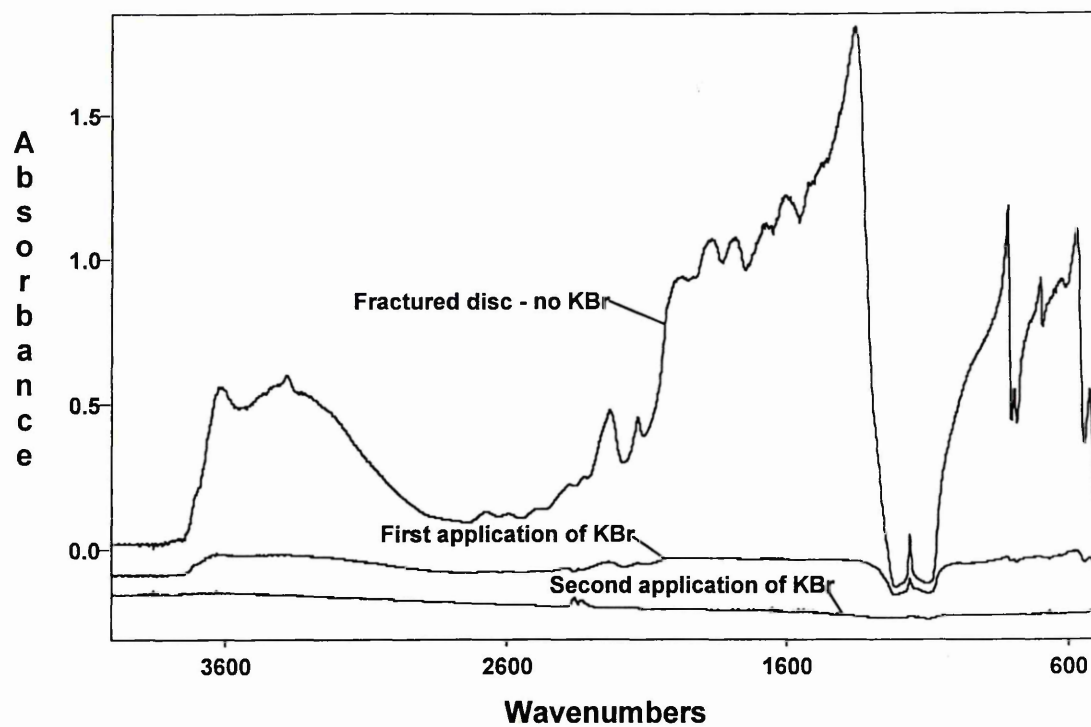


Figure 5.48B - Sprinkling of KBr on Clashach

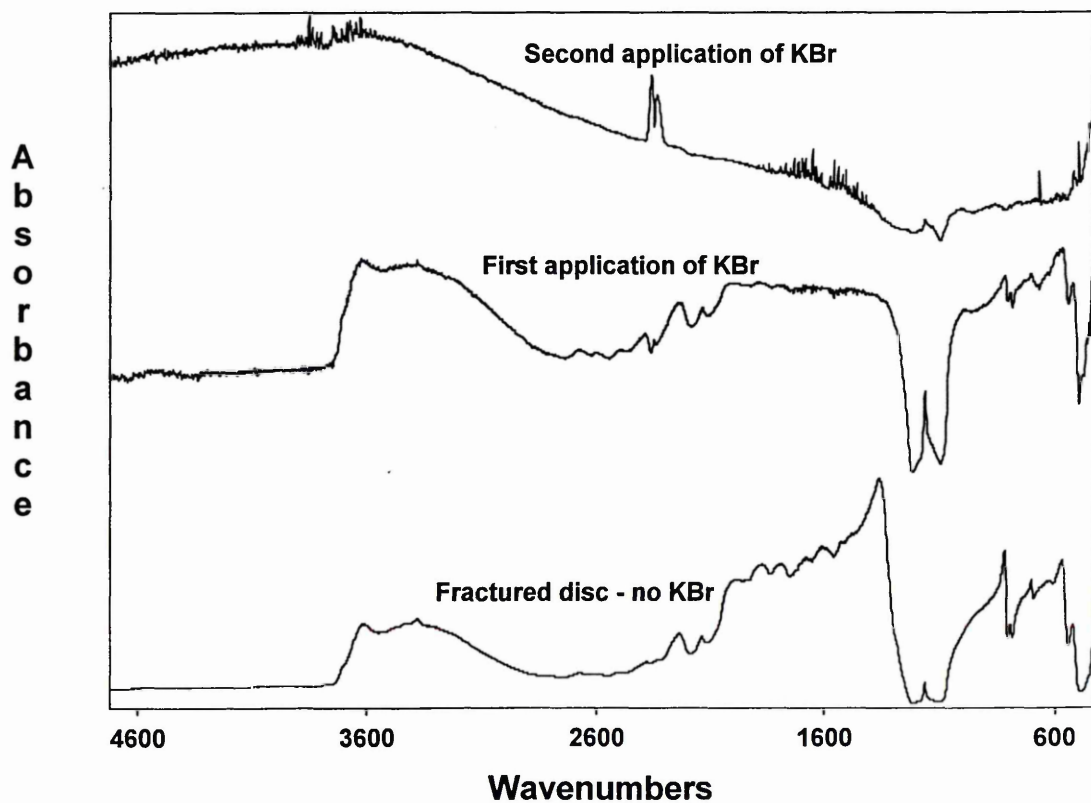
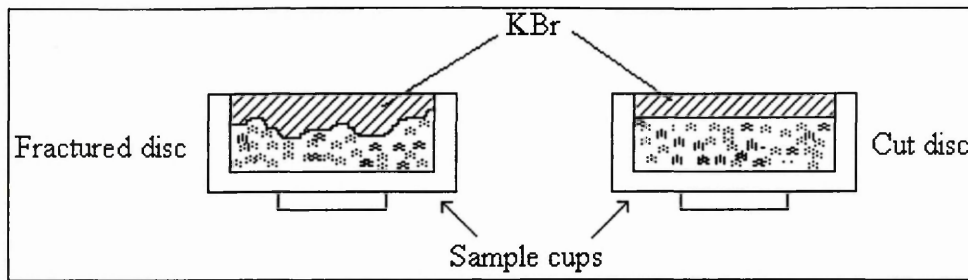


Figure 5.49: KBr overlays on fractured and cut sandstone surfaces



B) Blocker

The use of a 'Blocker' (see section 2.1.2.3) could be used to remove specular reflectance from the spectrum. In order for the Blocker to work efficiently a very flat surface would be required, again this would be more applicable to a cut rather than a fractured surface. Both KBr and the Blocker could be used in conjunction with each other to minimise specular reflectance.

C) Angle variance of both the incoming beam and the reflected light collected

The contribution of specular reflectance is very dependant on the optical geometry (see section 2.1.2.2). Although the effect can be reduced it is never completely removed, this is because diffuse specular reflectance occurs in all directions.

D) Polarisers

Specular reflectance can be reduced by placing polarisers before and after reflection, but as above the effect is never completely removed.

It should be noted that all of the above methods result in a loss of signal intensity.

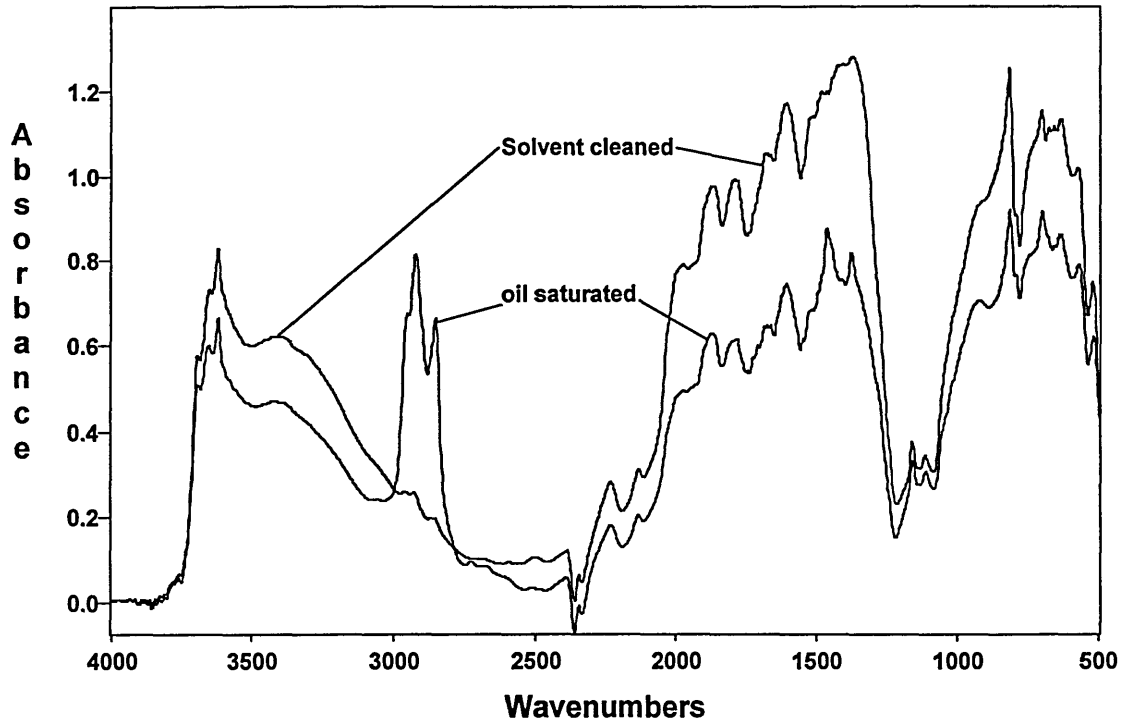
E) Kramers-Kronig transformation

Distortions can to some extent be overcome by using the Kramers-Kronig (K-K) transformation. This is a mathematical operation that removes the specular component by separation of the real and imaginary components and can often be used to correct spectra that are dominated by the refractive index contribution. Through the use of the K-K transformation a spectrum displaying absorption information can be calculated from a spectrum which consists of primarily specular reflectance information [250].

5.6.5) Effect of oil on the spectra of cut and fractured rock surfaces.

Figure 5.50 shows the DRIFTS spectra of the cut surfaces of oil saturated RR1 and solvent cleaned RR1. The spectrum of the oil saturated rock exhibits additional bands between $3000\text{-}2800\text{cm}^{-1}$, these are due to the C-H stretching bands of the hydrocarbons. The spectra show that the presence of oil reduces the overall reflectance and bands depths, but does not completely suppress mineral adsorption bands, i.e. absorption bands attributable to both the major and minor constituent minerals such as quartz, clays and feldspars can be recognised in both oil containing and oil free samples. The effect of oil obviously changes the spectra and this fact needs to be considered if quantification of mineral components in reservoir rocks is to be achieved.

Figure 5.50: DRIFTS spectra from the cut surfaces of oil saturated and solvent cleaned RR1.



5.7) Partial Least Squares Modelling

Section 2:2 describes the basic principles of PLS modelling

5.7.1) Feasibility of PLS modelling

The motive for applying PLS modelling to the DRIFTS spectra is to facilitate the quantification of either the bulk or surface mineralogy of a sandstone/reservoir rock. PLS modelling can help the quantification by overcoming problems such as overlapping bands and scattering effects, which occur in the DRIFTS spectra of sandstones/reservoir rocks. PLS is also, to some extent, capable of modelling non-linear response-concentration relationships. Since this is the case the spectra were studied in a diffuse absorbance format rather than a K-M format. Although the latter format produces linear data over a larger concentration range, it also unfortunately

suppresses the high wavenumber bands leading to possible loss of information (see section 2.1.2.4).

PLS modelling requires calibration standards that are able to explain the spectral and compositional variance of real samples. The calibration standards may be the samples under investigation of a known composition that has been determined by external means. The variations that are expected to arise whilst studying sandstones/reservoir rocks are;

- i) the wide variation of mineral components e.g. kaolinite, illite, quartz etc., and,
- ii) the wide variation of mineral component concentrations.

In addition, the DRIFTS spectra of one type of clay mineral (e.g. kaolinite) can vary depending on its source. This variation is mainly due to how it was formed and hence its crystallinity. Thus, in order for the model to determine the concentration of kaolinite in a sandstone it needs to account for these changes in the spectra. To account for all the variations, a lot of calibration samples (>150) would be required. Unfortunately, only a few sandstones/reservoir rocks have been studied with the DRIFTS technique, this is insufficient to build a working PLS model.

The whole process of building a complete model would take a long time because:-

- i) a suite of rocks needs to be collected,
- ii) these rocks have to cover the expected range of mineral components and their expected concentrations in a rock,
- iii) their composition will need to be determined (via external means), and,
- iv) the DRIFTS spectra of each will need to be collected.

Ultimately, the model may not be able to perform its purpose and so firstly, the feasibility of using PLS on A) balled milled samples and B) cut/fractured surfaces to determine the bulk mineralogy and surface mineralogy, respectively, has been discussed. Secondly, five simple model examples have been studied using mixtures of mineral standards in order to confirm the feasibility of applying PLS to the above analyses. The simple models studied will be explained after the feasibility has been discussed.

A) Ball milled samples - BULK COMPOSITION

It is expected that the application of PLS to the DRIFTS spectra of ball milled samples will be feasible, since a similar problem was solved by Hughes et al. [140] involving cement samples (see section 4.1.3).

The feasibility of bulk analysis using ball milled samples is also anticipated because the DRIFTS spectra are highly reproducible (which is essential) and a lot of information describing the components of the rock is available from the entire mid-infrared region.

B) Cut/fractured surfaces - SURFACE COMPOSITION

Quantifying the surface mineralogy from sandstones/reservoir rocks is a non-trivial matter. For this discussion, the assumption that the DRIFTS spectra represent the surface mineralogy will be made.

The main problem that arises when studying the DRIFTS spectra obtained via this method is the distorted region of poor reproducibility between $1500\text{-}500\text{cm}^{-1}$. The loss of spectral information describing the mineral components in this region would make PLS modelling more difficult. The possibility of removing these distortions has been discussed (section 5.6.4), but the application of such methods introduces extra problems. An alternative solution would be to use calibration standards that can mimic these distortions in the DRIFTS spectra. As stated earlier, the calibration standards may be real samples (i.e. cut/fractured surfaces) of known composition. Unfortunately, the quantitative surface mineralogy of such samples would be difficult to obtain by external means. If standards with known composition could be prepared so as to mimic the cut/fractured surfaces of sandstones/reservoir rocks, then in turn the distortions will be mimicked.

Possible synthetic preparations could include:

i) Synthetic alumino-silicate cores and sprinkled minerals : synthetic cores can be purchased, which physically resemble 'a sandstone core that contains no minerals apart from the quartz grains'. These cores may be used in permeability experiments

[251]. Since the core used has a similar elemental structure to quartz, a similar DRIFTS spectra will be obtained. In addition, the grain sizes of these cores are graded and so the effect of grain size can be introduced into the model. This will help to describe the variation observed in the spectra due to particle size.

Known weights of additional minerals (clays, feldspars, etc.) can then be sprinkled on the surface, which will provide calibration standards of known composition. One problem with this approach, is that the mixture of quartz and other minerals will not be homogeneous and since the area being sampled during a DRIFTS experiment is not known, the true composition of the standard is not known.

ii) Mixing of sand grains with other representative minerals standards : this procedure is simple and could be effective (Note: no dilution of KBr will be employed so that spectra mimic cut/fractured surfaces). The only physical difference between a mixture of minerals and a cut/fractured surface is that the latter are physically joined together. This does not appear to have an effect, since similar distortions are observed in the DRIFTS spectra obtained from each type. To confirm this observation, additional degrees of pressure could be applied to the mixtures, to determine whether changes in the spectra would occur.

Like the synthetic core scenario, the effect of grain size could be introduced into the model, simply by using mineral standards of known size. Equally, the variation of a mineral-type (e.g. kaolinite) could be introduced into the model, simply by using minerals from different sources. An advantage of this method over the previous case is that the samples will be homogeneous and thus the need to know what area of a sample is being observed becomes less relevant.

If it is not possible to obtain a reproducible spectrum in the $1500\text{-}500\text{cm}^{-1}$ region, only the $4000\text{-}1900\text{cm}^{-1}$ region could be used. The obvious drawback from this is that a lot of spectral information will be lost. However all the minerals are still represented in this region of the spectrum.

5.7.2) Application of PLS analysis

PLS analysis has been applied to five simple models in order to determine whether:-

- i) bulk analysis of sandstones is possible using the ball milled sample preparation technique,
- ii) the reduced mid-infrared region ($3900-1900\text{cm}^{-1}$) can be used to describe all the expected mineral components in a sandstone,
- iii) quantification is possible when distortions are present in the DRIFTS spectra (i.e. when samples are not dispersed in KBr and the spectra are effected from specular reflection).

5.7.3) PLS models

Models ① to ③

The first three models were applied to the DRIFTS spectra of 21 mixtures of 7 mineral standards (table 5.1, page 101), that had been collected after ball milling. This is a high enough number of mixtures for a PLS model to successfully describe 7 components. Only seven mineral standards were chosen (quartz, Na-feldspar, kaolinite, illite, chlorite, montmorillonite and dolomite) because this is the least number of components that could describe a rock. Dolomite was used to represent the carbonate content, only one end member (Na) was used to represent the feldspar group and each mineral was only represented by one crystallinity (e.g. the kaolinite sample was KGa-2, which is poorly crystalline).

The DRIFTS spectra of all the 21 mixtures were collected. Five of the mixtures were repeated in order to add noise variation into the model, and thus 26 standards were created in total. Nineteen of these were used as calibration standards (including the five repeats) and the remaining seven were used as validation standards.

Model ① utilised the data from the whole mid-infrared region of the DRIFTS spectra ($3900-450\text{cm}^{-1}$). The results showed that montmorillonite and illite were poorly predicted (see later) since they have very similar spectra.

Model ② also used the whole mid-infrared region, but combined montmorillonite and illite to represent one component.

Model ③ only used the data from the reduced region ($3900\text{-}1900\text{cm}^{-1}$) and combined montmorillonite and illite to represent one component.

Models ④ and ⑤

Models ④ and ⑤ were applied to the DRIFTS spectra of 20 mixtures of 7 mineral standards. Model ④ used the full region of the spectrum and model ⑤ used only the $3900\text{-}1900\text{cm}^{-1}$ region. The DRIFTS spectra were taken directly from the surface of the neat powders (i.e. no KBr was used) after they had been ball milled. Of the 20 mixtures none were repeated, 13 were used as calibration standards and seven were used as validation standards. The samples were ball milled so that a reproducible particle size was observed for all the standards. This alleviated the effects of particle size on the spectra.

The predictive ability of the models is calculated as described in the theory. The figures of interest are the validation correlation coefficients and the number of factors used. A validation correlation coefficient value close to one indicates good predictability for the mineral component and a value close to zero indicates poor predictability (An excellent value is 0.99, the ability to predict is poor if the value is less than 0.85).

If the number of factors used is too high, a poor prediction of external samples will result and if it is too low all variation in the data will not be accounted for.

The calculated correlation coefficients and the number of factors used for the five models are shown in Table 5.6.

Model ① was unable to successfully predict the concentrations of montmorillonite and illite, this is indicated by the low correlation coefficient values. This was expected because the DRIFTS spectra of these minerals are very similar (figures 5.5 and 5.6).

Table 5.6A : Correlation coefficients and number of factors used for models ①-③.

	MODEL ①		MODEL ②		MODEL ③	
	Correlation Coefficient	No. of Factors	Correlation Coefficient	No. of Factors	Correlation Coefficient	No. of Factors
Quartz	0.99643	7	0.99399	5	0.94549	4
Mont. & Illite	0.75938	7				
	0.71760	8	0.92470	5	0.94042	7
Kaolinite	0.98629	8	0.98629	8	0.97553	5
Chlorite	0.98995	9	0.99257	7	0.97940	5
Dolomite	0.99581	9	0.99603	8	0.99593	6
Feldspar	0.98000	8	0.98854	10	0.48337	3

Table 5.6B : Correlation Coefficients and number of factors used for models ④ and ⑤.

	MODEL ④		MODEL ⑤	
	Correlation Coefficient	No. of Factors	Correlation Coefficient	No. of Factors
Quartz	0.99231	7	0.97664	7
Montmorillonite & Illite	0.85065	9	0.92950	9
Kaolinite	0.92273	7	0.96383	7
Chlorite	0.94192	5	0.97688	5
Dolomite	0.99719	9	0.97120	9
Feldspar	0.85820	8	0.50146	8

Model ② was able to successfully predict the concentration of combined montmorillonite and illite. The high correlation coefficient indicates this.

Model ③ gave a good prediction for all the mineral components apart from feldspar. This implies that feldspar does not have any clearly representative bands in the 3900-1900cm⁻¹ region. Feldspars do have broad bands at approximately 3625 and 3377 cm⁻¹

¹ as indicated by their DRIFTS spectra (figures 5.13 and 5.14). Unfortunately, the clay minerals show stronger absorption bands in this region and therefore may inhibit the prediction of feldspar.

Model ④ gave good prediction values for quartz, kaolinite, chlorite and dolomite, but gave poor prediction values for feldspar and the combined montmorillonite and illite

Model ⑤ gave worse prediction values for feldspar than model ④. This was expected since model ③ was also unable to describe feldspar. Surprisingly, the use of the cut down region improved the prediction for the combined montmorillonite and illite.

In general models ④ and ⑤ gave poorer prediction values than models ①, ② and ③.

An indication of how well a model describes a component is to compare the DRIFTS spectra of the mineral standards with the 'pure component spectra' calculated by the model. Each pure component spectrum is composed of the spectral information that correlates with the concentration information for a given component in all of the standards. Figures 5.51-5.56 compare these spectra for the mineral components. The lower spectrum in each figure is the pure component spectrum. The regions where good similarities are observed are usually the regions used to describe the component.

The DRIFTS spectrum and the 'pure component spectrum' of quartz (figure 5.51) are very similar. Quartz is the only mineral that exhibits overtone/combination bands in the 2000-1500 cm^{-1} region. It has been shown [127, 252] that these bands (especially the 1875 cm^{-1}) are relatively unaffected by particle size when compared to the other bands of quartz. It is these bands (i.e. those above 1900 cm^{-1}) that allow good prediction of quartz when only data from the reduced region (the non-distorted region) is used.

Figure 5.52 shows the DRIFTS spectra of montmorillonite and illite and their combined pure component spectrum. Good similarities occur for the band at 3624 cm^{-1} and the OH stretching region at 3380 cm^{-1} .

Figure 5.51 - 'Pure component spectrum' of Quartz

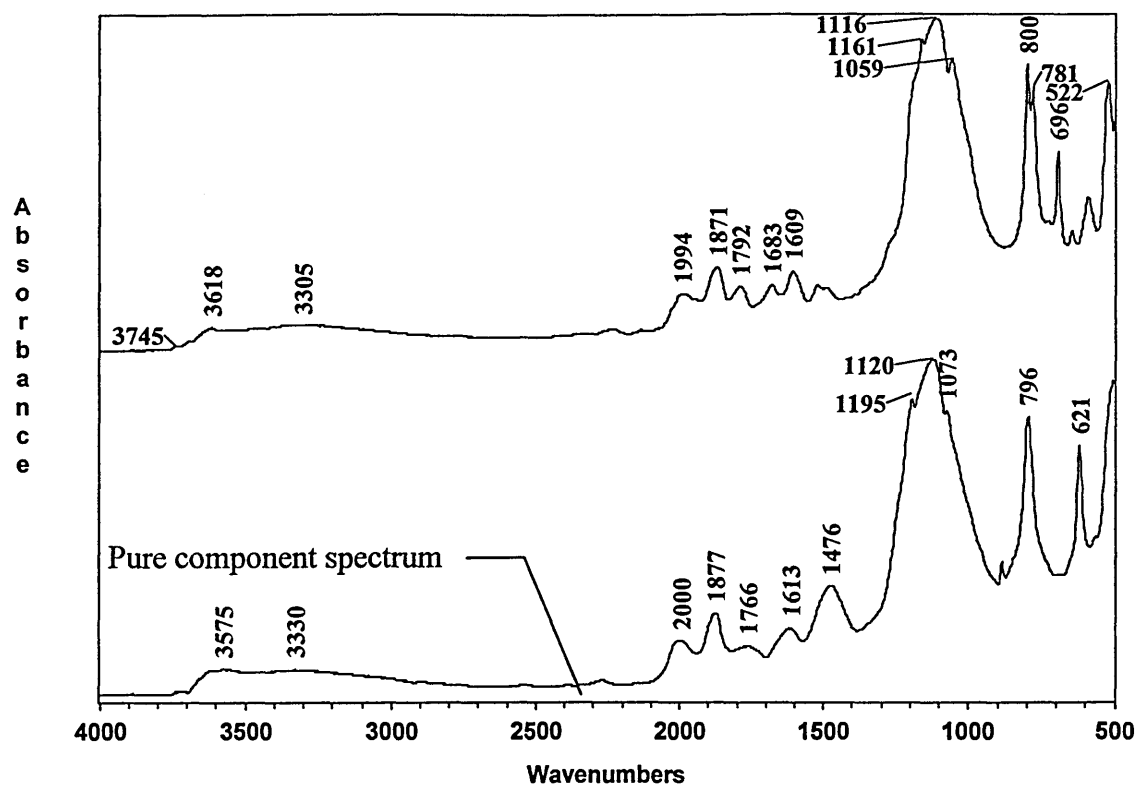


Figure 5.52 - 'Pure component spectrum' of montmorillonite and illite

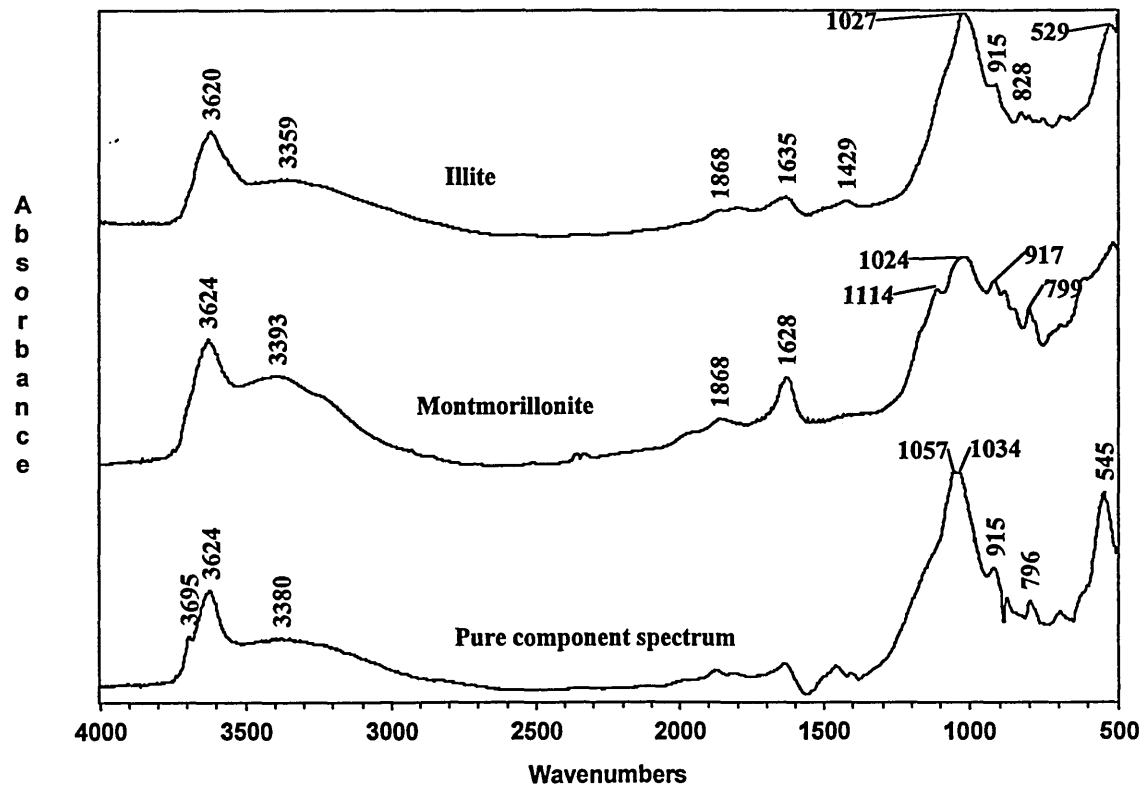


Figure 5.53 - 'Pure component spectrum' of Kaolinite

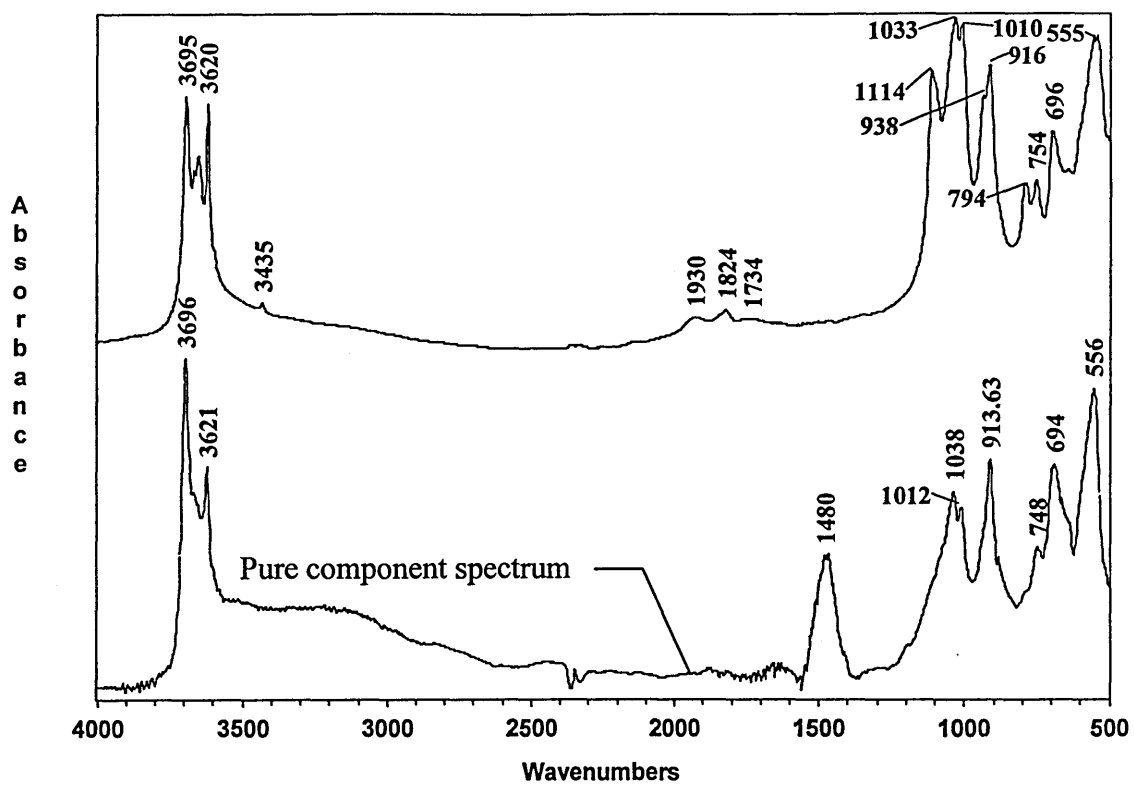


Figure 5.54 - 'Pure component spectrum' of Chlorite

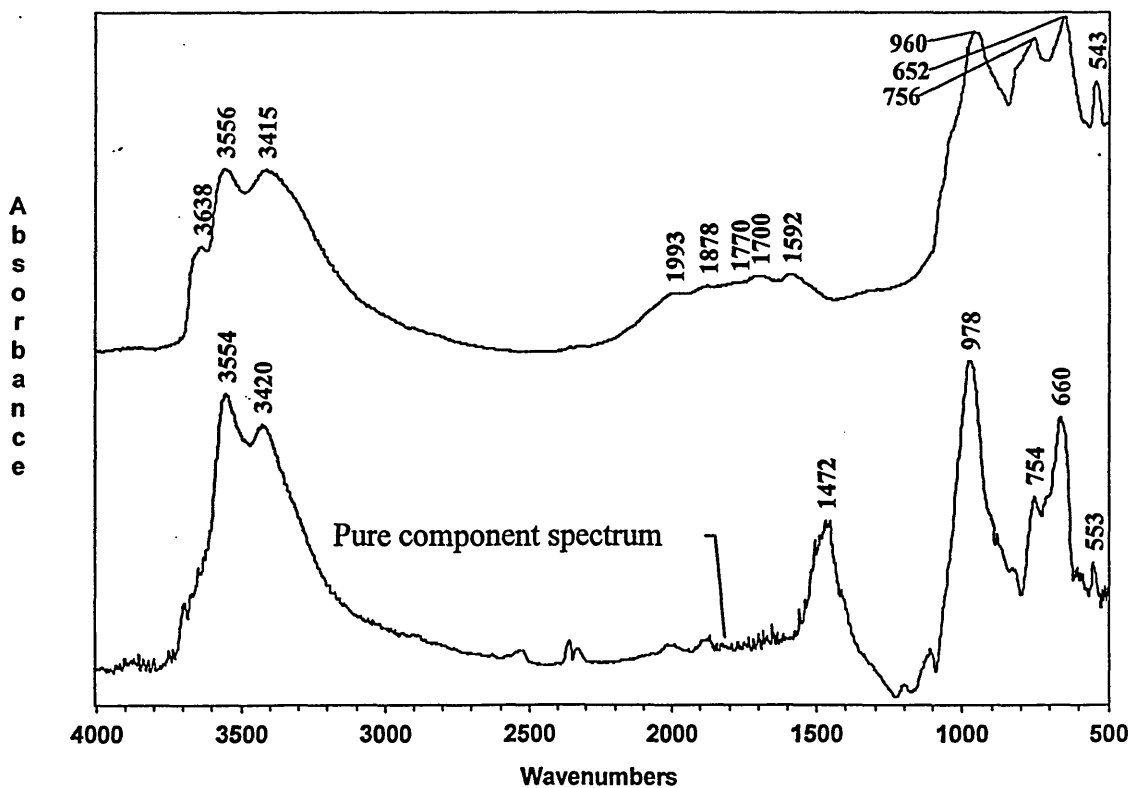


Figure 5.55 - 'Pure component spectrum' of Dolomite

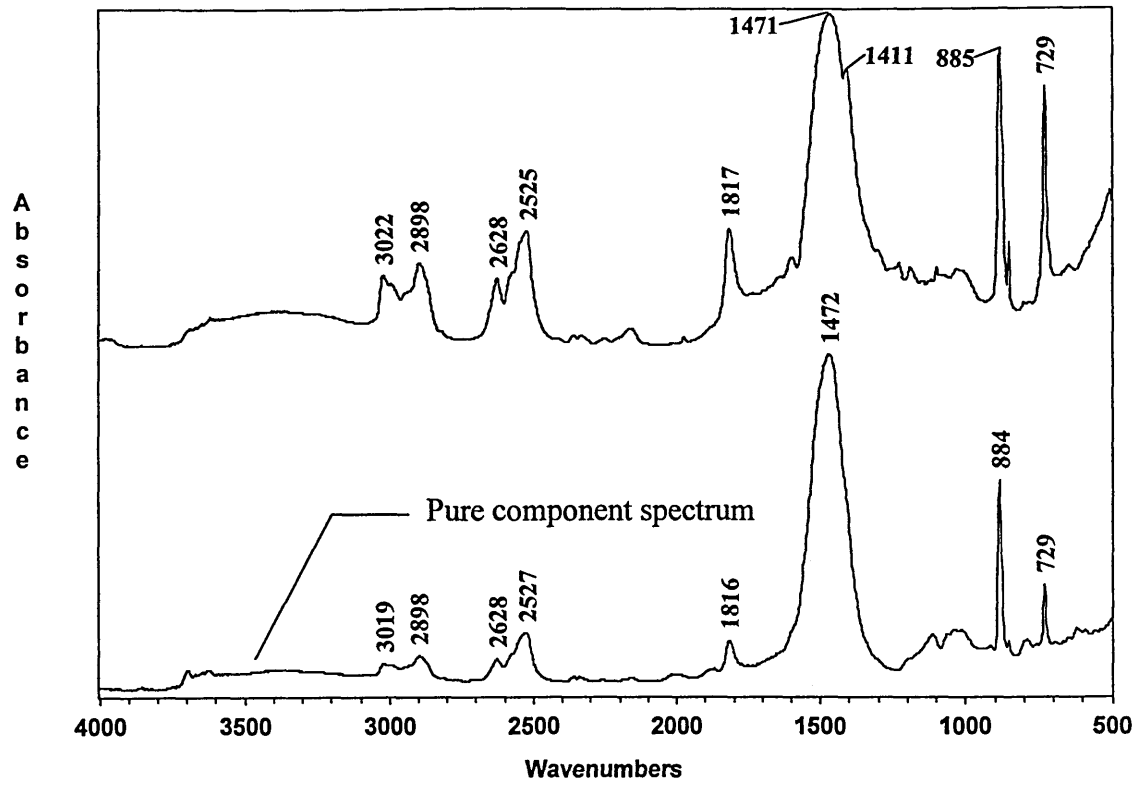


Figure 5.56 - 'Pure component spectrum' of Feldspar

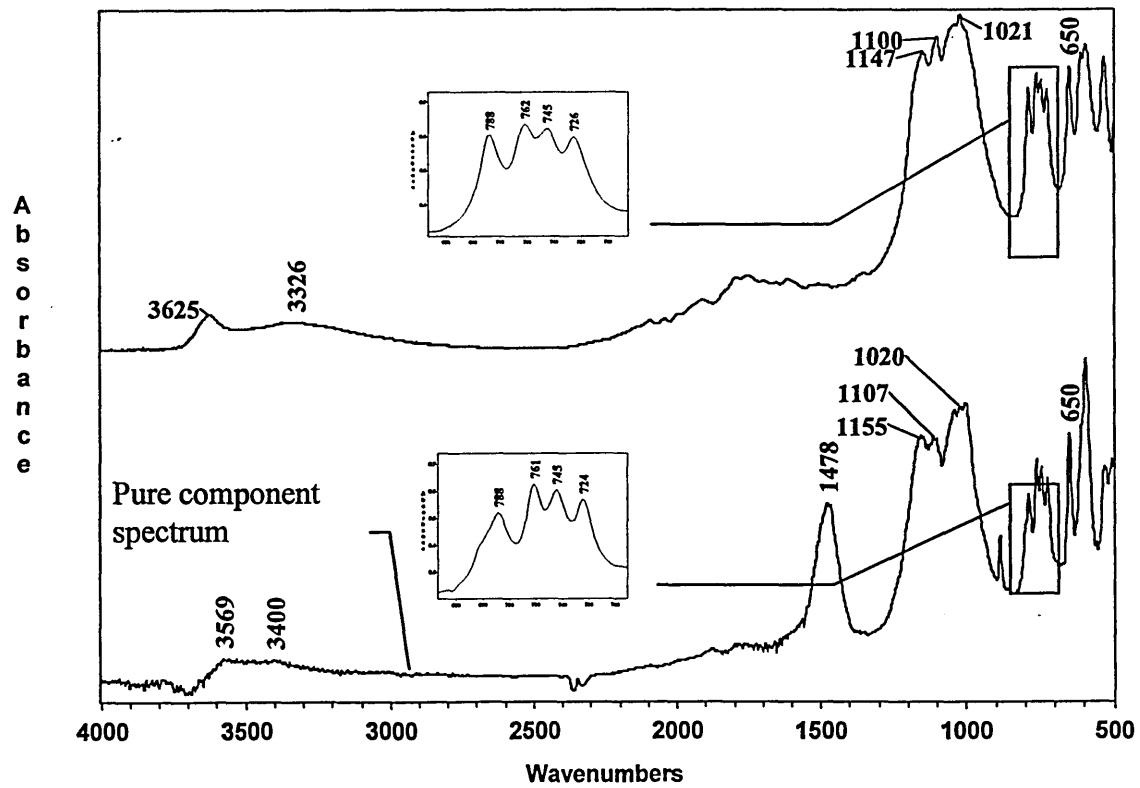


Figure 5.53 shows the DRIFTS spectrum of kaolinite (top) and its calculated 'pure component spectrum' (bottom). Here, it is possible to observe the similarities between the spectra, especially the four characteristic hydroxyl bands between 3695 and 3620 cm^{-1} . Good similarities occur at 3354 and 3420 cm^{-1} for the DRIFTS spectrum of chlorite and its pure component spectrum (figure 5.54).

Figure 5.55 shows the two spectra of dolomite, an excellent comparison is observed not only for the band positions, but also their ratios.

The similarities for feldspar (figure 5.56) occur in the region below 1400 cm^{-1} . An excellent correlation occurs for the four bands between 788 and 724 cm^{-1} . There are no clearly related bands in the reduced region (3900-1900 cm^{-1}) used for models ③ and ⑤. This is the reason why poor prediction of feldspar occurs in these models.

All of the pure component spectra show a band around 1475 cm^{-1} . This band may be associated with the ν_3 stretching band of dolomite. Whilst ball milling the mineral mixtures, dolomite preferentially coated the sides of the ball mill holders and insufficient cleaning between samples could have lead to extra or lower amounts of dolomite in each mixture. Alternatively, the presence of this band could be due to a deconvolution problem within the algorithm at this particular wavenumber region.

In order to demonstrate the predictive ability of the best model (i.e. model ②) a plot of actual concentration against predicted concentration for the validation samples are shown for each mineral component in figure 5.57. This figure allows a judgement of how the correlation coefficient is related to prediction accuracy. A correlation coefficient near to one would produce a plot of the actual versus predicted concentrations on a line at 45°. The figure shows that the points on the feldspar, and, combined montmorillonite and illite graphs deviate more so from the 'ideal' 45° line than the other components. This is expected since these components are difficult to distinguish in a DRIFTS spectrum containing such minerals.

Figure 5.58 shows the plot of the actual concentrations against predicted concentrations, calculated by model ⑤, for each component in the validation samples. The graphs show that there is more general scatter in the points than those predicted

using model ②. This is especially the case for the feldspar, and, combined montmorillonite and illite graphs.

The results show that model ② yielded the best predictions for the mineral components, therefore it was applied to the sandstones in order to test the model. Table 5.7A and B shows the predicted and actual concentrations of the quarry rocks. A poor prediction can be noted and is probably due mainly to the variance in spectra of mineral types (i.e. those of different crystallinities). Although this is the case, general trends are observed in the results. For example; i) Clashach and Berea are predicted to contain the highest amount of quartz, they do, ii) Berea is predicted to contain the lowest amount of feldspar, they do, and, iii) Clashach is predicted to contain very little clay, it does.

Figure 5.57: A plot of actual concentration against predicted concentration, calculated using model ②, for each mineral component in the validation samples.

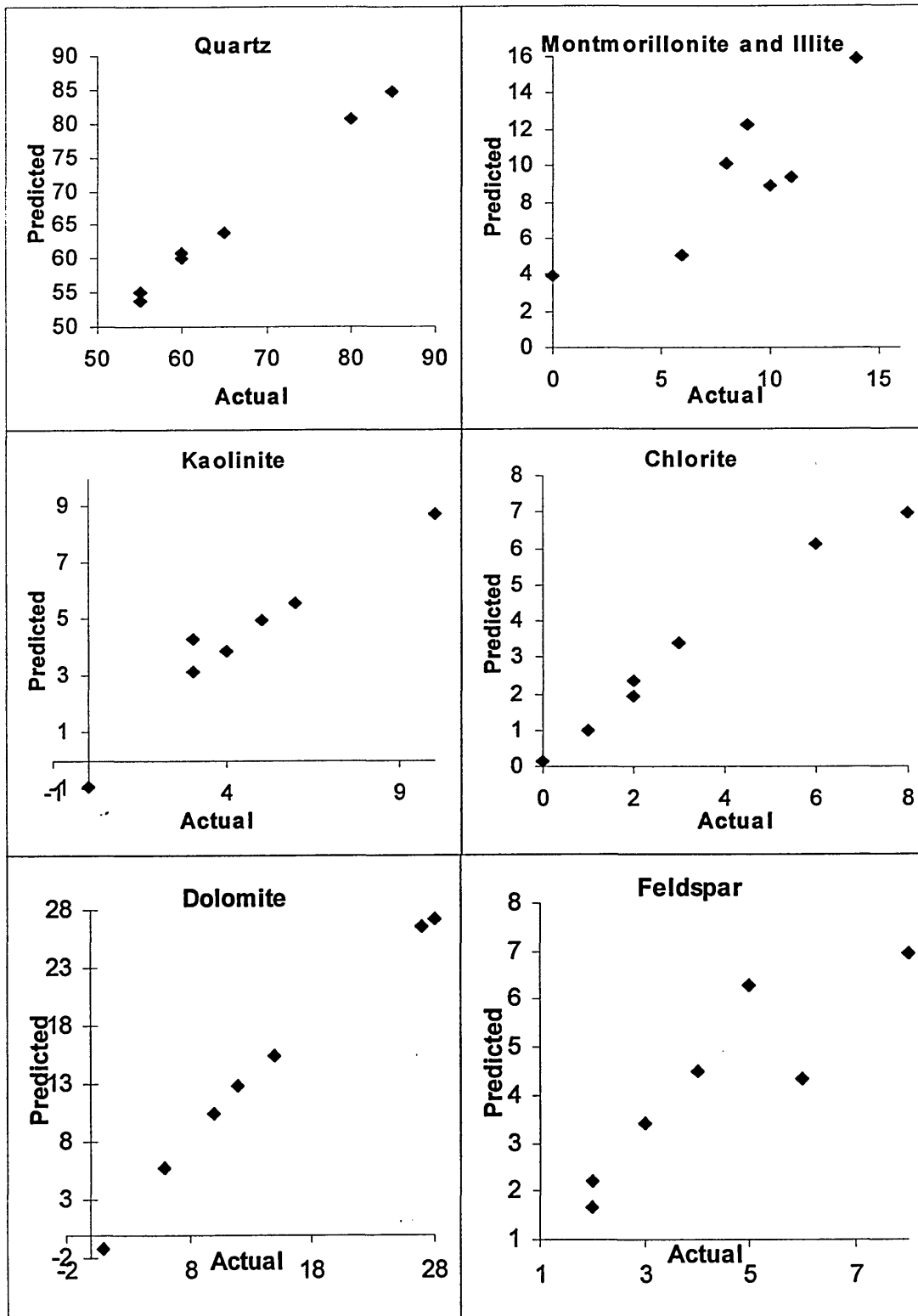


Figure 5.58: A plot of actual concentration against predicted concentration, calculated using model ⑤, for each mineral component in the validation samples.

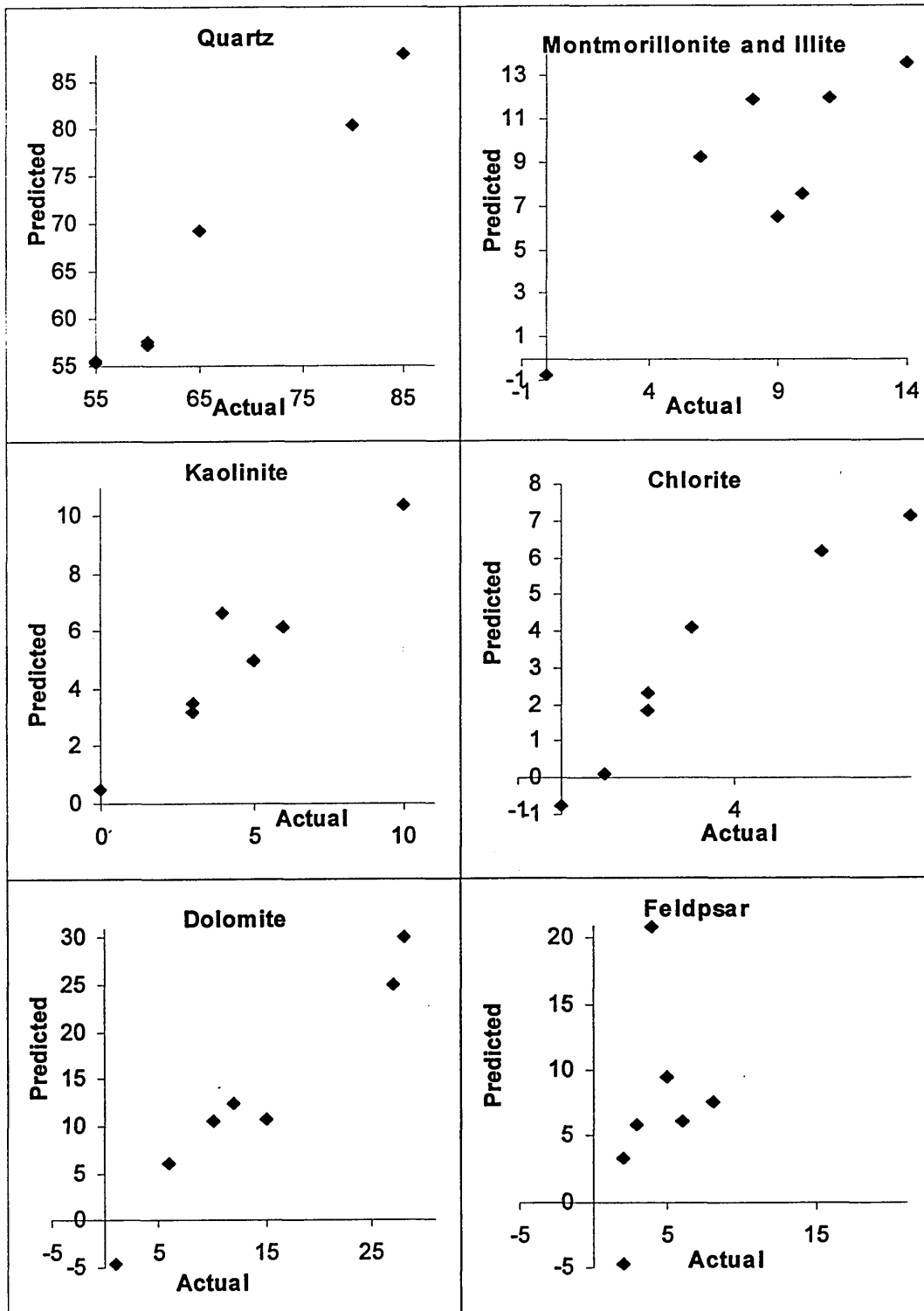


Table 5.7A - Predicted concentrations of sandstones.

	Stancliffe	York Stone	Hollington Red (Clay band)	Hollington Red (Between bands)	Clashach	Berea	Birch-over
Quartz	61.8	58.0	61.0	62.1	81.7	79.7	61.7
Mont. & Illite	5.8	8.2	7.3	9.6	0.89	2.7	10.1
Kaolinite	1.98	4.8	4.2	3.6	0.09	6.96	1.9
Chlorite	2.5	5.1	1.0	2.4	0.82	1.24	0.3
Dolomite	3.6	2.8	0.8	5.6	0.6	2.5	1.3
Feldspar	28.6	24.5	28.1	5.7	17.8	4.2	31.7

Table 5.7B - Actual concentration for sandstones

	Stancliffe	York Stone	Hollington Red (Clay bands)	Hollington Red (between bands)	Berea	Birchover
Quartz	72	72	72	74	84	75
Montmorillonite	0	0	<1	3	0	0
Illite	5	7	10	6	2	4
Kaolinite	3	5	3	<1	7.6	5
Chlorite	0	0	3	0	0.4	0
Dolomite	<1	<1	0	0	3	<1
Feldspar	19	14	15	15	3	16
Others			2 (pyrite)	4 (hematite)		
Bulk Analysis for Clashach is not available, but is believed to contain less than 5% clay						

5.7.4) Summary

The results have shown that the application of PLS to ball milled samples dispersed in KBr (10%) could be used to determine the bulk mineralogy of sandstones and reservoir rocks. High correlation coefficients and 'low number of factors used' was achieved for each mineral component in model ②. This was especially the case for the mineral components; quartz, kaolinite, feldspar, dolomite and chlorite which is ideal for a good predictive model. It was found necessary to combine illite and montmorillonite to represent one component since model ① was unable to differentiate their similar DRIFTS spectra. The amount of feldspar could not be determined accurately using only the high wavenumber region ($3900-1900\text{cm}^{-1}$). If only the cut-down region was to be used in the spectra obtained from cut/fractured surfaces then it may be possible to combine quartz and feldspar to represent one component. This may be successful since they have similar spectra.

The application of PLS to neat ball milled samples (not dispersed in KBr) has shown that by using the full spectral region (model ④) it was able to quantify the presence of quartz, kaolinite, dolomite and chlorite successfully. This model was less successful at quantifying the presence of feldspar, and, the combined montmorillonite and illite component than model ②. If only the cut down region was used (model ⑤) it was found that it was better at predicting the combined quantity of montmorillonite and illite. The application of PLS to neat ball milled samples has therefore shown that the presence of distortions in the spectra does have some detrimental effect on its predictive ability.

In order to improve predictions further either i) a larger number of standards can be employed, or ii) data from the near and/or far infrared regions could be incorporated into the models. There are several published papers [253-255] that describe the spectra of minerals in these regions. Many bands in the near infrared region are overtone/combination bands and are not distorted by the high collection of specular reflection. Major NIR spectral features of silicate minerals are located in the $4000-5500\text{cm}^{-1}$ and $6500-7500\text{cm}^{-1}$ domains.

As with all analytical techniques, the small analyte studied needs to be representative of the bulk sample. As for example the amount of clay in a sandstone will vary from

core to core. Since the sampling area of the infrared beam is only 7mm^2 , a single spectrum obtained will not be representative of a massive block of sandstone. Regulated sampling procedures will therefore be required. A successful technique could map the variance of a clay within a reservoir.

6) Results - Characterisation of pore lining minerals using chemical probes

6.1) Experimental

6.1.1) Chemical probes, mineral standards and sandstones studied

Chemical probes: The chemical probes studied (figure 4.6) were obtained from Aldrich (>99% pure).

Mineral standards: Most of the mineral standards came from the Clay Minerals Repository or British Chemical Standards (see table 4.1).

Preparation of a homoionic clay

Montmorillonite containing sodium, calcium, potassium and magnesium-exchange cations have been prepared.

i) Na-exchanged SWy-2

Na-SWy-2 was prepared by dispersing SWy-2 in deionised water and stirring for two hours before adding sufficient NaOH to provide 10 times the necessary amount of Na⁺ (i.e. 10 times the CEC). EDTA was added to aid the removal of divalent ions from the exchange sites. The SWy-2/NaOH/EDTA dispersion was stirred overnight and repeatedly washed and centrifuged until the conductivity of the supernatant was less than 50 μ S.

ii) Ca, Mg and K-exchanged clays

The cation-exchange of the clay with these cations used the same procedure as for the Na-exchanged clay. In this case no EDTA was used and extra mixing with the cation was performed (a total of 3 contacts). The source of all the cations was the chloride salt (Analytical grade).

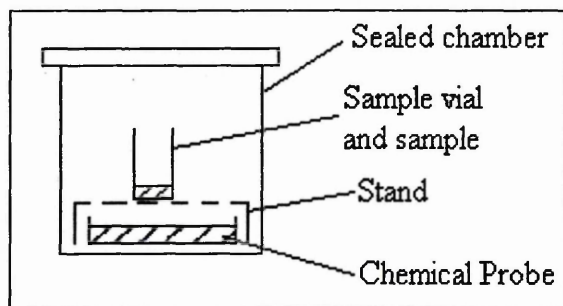
In order to check if the clays were successfully exchanged, X-ray fluorescence (XRF) analysis was performed. Samples for XRF analysis were prepared using the Li₂B₄O₇ fusion method and the data was collected using a Philips PW2400 XRF spectrometer.

Sandstones studied: The sandstones studied in most detail include Berea, Birchover and Clashach (table 4.2). These were ball milled before exposing to any chemical probe.

6.1.2) Exposure/Intercalation procedures

Exposure of a sample to a chemical probe was achieved via two methods. The first method involved exposing the clay to the probe vapour and the second involved directly mixing the liquid probe and sample together.

i) Intercalation via the vapour phase: 50mg of the sample, ball milled or ground using a pestle and mortar, was weighed into a small sample vial and transferred to a sealed gas jar which contained 5ml of the chemical probe for fixed periods of time (see below).



ii) Intercalation via direct contact: 2 grams of the sample (either ball milled or ground) was immersed in 10ml of the chemical probe. If NMF was the chemical probe then NMF was diluted in water to produce a NMF:H₂O ratio of 90:10. The mixture was placed in a water or oil bath at the required temperature (25, 70 or 140°C) for a specific time period (24 or 48 hours). The solution was shaken occasionally. The solid sample was then centrifuged down and the supernatant decanted off. The complex was then left to dry at room temperature on a petri dish and then stored in a sealed sample vial.

6.1.3) Instrumental Techniques

Thermogravimetric Analysis

The desorption of a chemical probe from an exposed sample was measured using a Mettler TA3000 Thermogravimetric Analyser. The sample (6-12mg) was transferred directly out of the vapour into an alumina crucible and placed directly in the thermobalance. The sample was preconditioned in a nitrogen gas flow (20cm³/minute) for 15 minutes at 35°C. The sample was then heated to 800°C using a temperature gradient of 20°C/minute.

The measurement was recorded as weight loss and then converted into the negative of the first derivative (i.e. -dw/dT).

X-ray Diffraction

XRD patterns were collected for the intercalated and non-intercalated samples via the procedure described in 5.1.1. Samples were either in a powdered form or prepared on glass slides. The confirmation and extent of intercalation was noted by measuring the intensities and positions of their respective $d_{(001)}$ peaks.

Evolved Gas Analysis (EGA-FTIR and EGA-MS)

EGA was performed on a Unicam-Cahn Synergic chemical analysis system (see section 2.4). This incorporates a Matteson Galaxy FTIR spectrometer (with gas cell accessory) and an ATI Unicam Automass System 2 quadrupole mass spectrometer.

Sample weights for EGA were between 25-100mg. The experimental parameters will be discussed in the results section (6.4).

6.2) Thermogravimetric Analysis of untreated minerals

In this section the Derivative Thermogram (DTG) traces of minerals not treated with chemical probes will be discussed. Weight losses will be assigned with reference to published papers. The samples studied were initially purged at 35°C for 15 minutes and then heated from 35-800°C at 20°C/minute. It should be noted that between these two events (i.e. after 15 minutes) a negative minimum followed by a small positive maximum occurs. This is most noticeable on the DTG trace of clinochlore (figure 6.2). The cause of this is not known but could be due to either i) a change in pressure of the carrier gas as the temperature is increased or ii) an electrical interference from the instrument. Whatever the reason, it is not due to a change in the sample since it occurs when a control is performed i.e. no sample present in the furnace.

Figure 6.1 shows the DTG traces of Ca, Mg, Na and K-exchanged montmorillonites (X-SWy-2). Maxima denoted -H₂O and -OH are due to the loss of physisorbed water and dehydroxylation of the clay structure, respectively. The numbers in brackets denote the percentage weight loss from the clay. The percentage weight loss of the dehydroxylation (-OH) maximum centred at approximately 700°C should always remain constant and can be used as a qualitative internal reference to the size of other maxima present. Ca and Mg-SWy-2 show the loss of physisorbed water in two stages (i.e. two maxima) whereas loss of water from Na and K-SWy-2 occurs in one stage. This is due to the fact that Mg and Ca hold more strongly on to water than Na or K. The extent of dehydration depends on the exchangeable cation, temperature and moisture in its atmosphere. These results are typical of those presented in other papers [81, 100]. The TG curves of the X-SWy-2 clays also shows a weight loss during the first 15 minutes and is due to the loss of weakly adsorbed water. This region of the TG curve is not important for the development of the chemical probe method and will not be discussed further.

Figure 6.2 shows the DTG traces of illite, kaolinite and three types of chlorite. Maxima are denoted as in figure 6.1. Illite differs from montmorillonite because the

Figure 6.1: DTG traces of Ca, Mg, Na and K-exchanged montmorillonites (X-SWy-2)

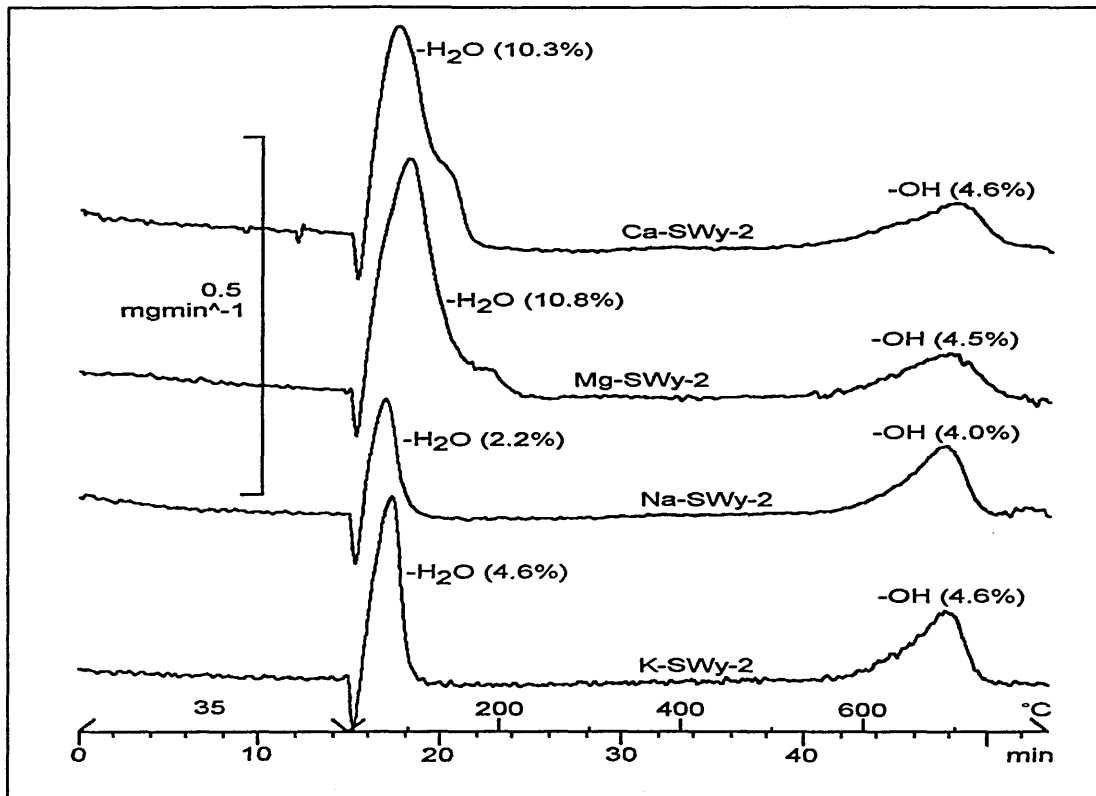
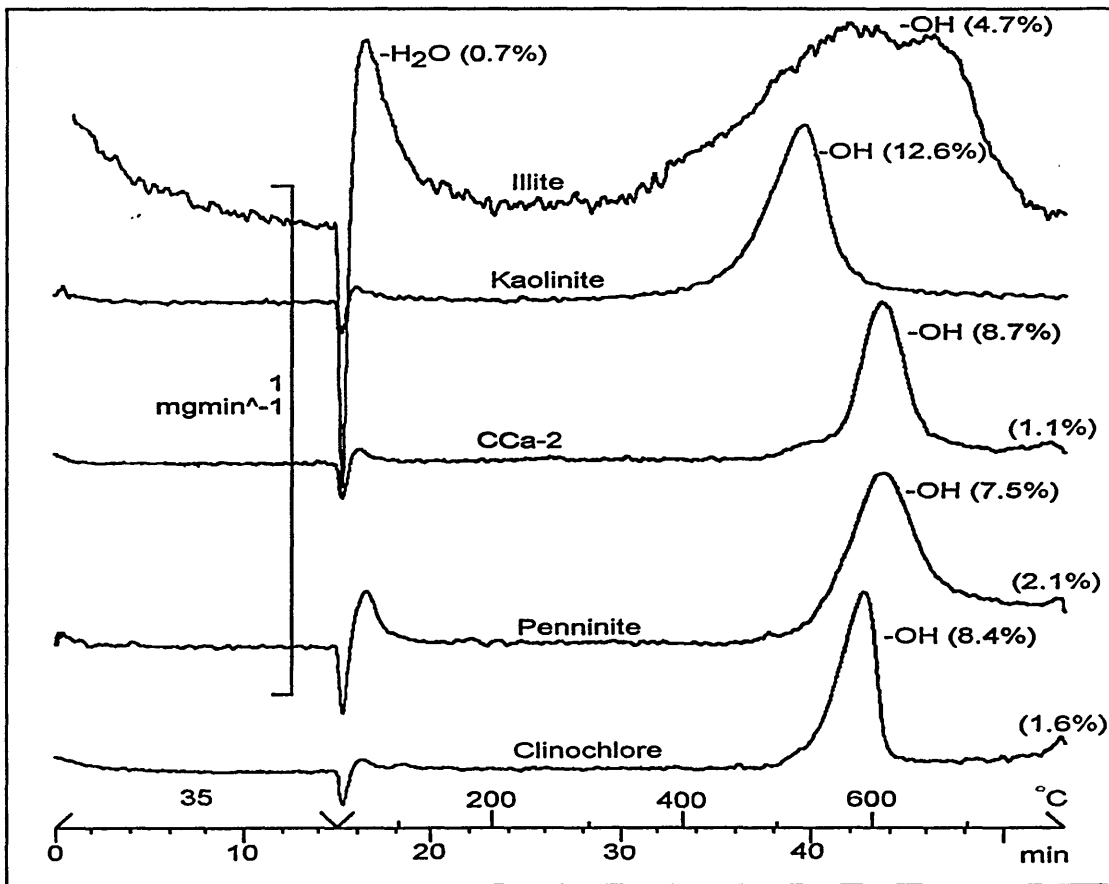


Figure 6.2: DTG traces of illite, kaolinite and three types of chlorite.



dehydroxylation is much broader and less physisorbed water is lost. Kaolinite and chlorite differ because very little or no physisorbed water is lost and the weight loss upon dehydroxylation is almost triple.

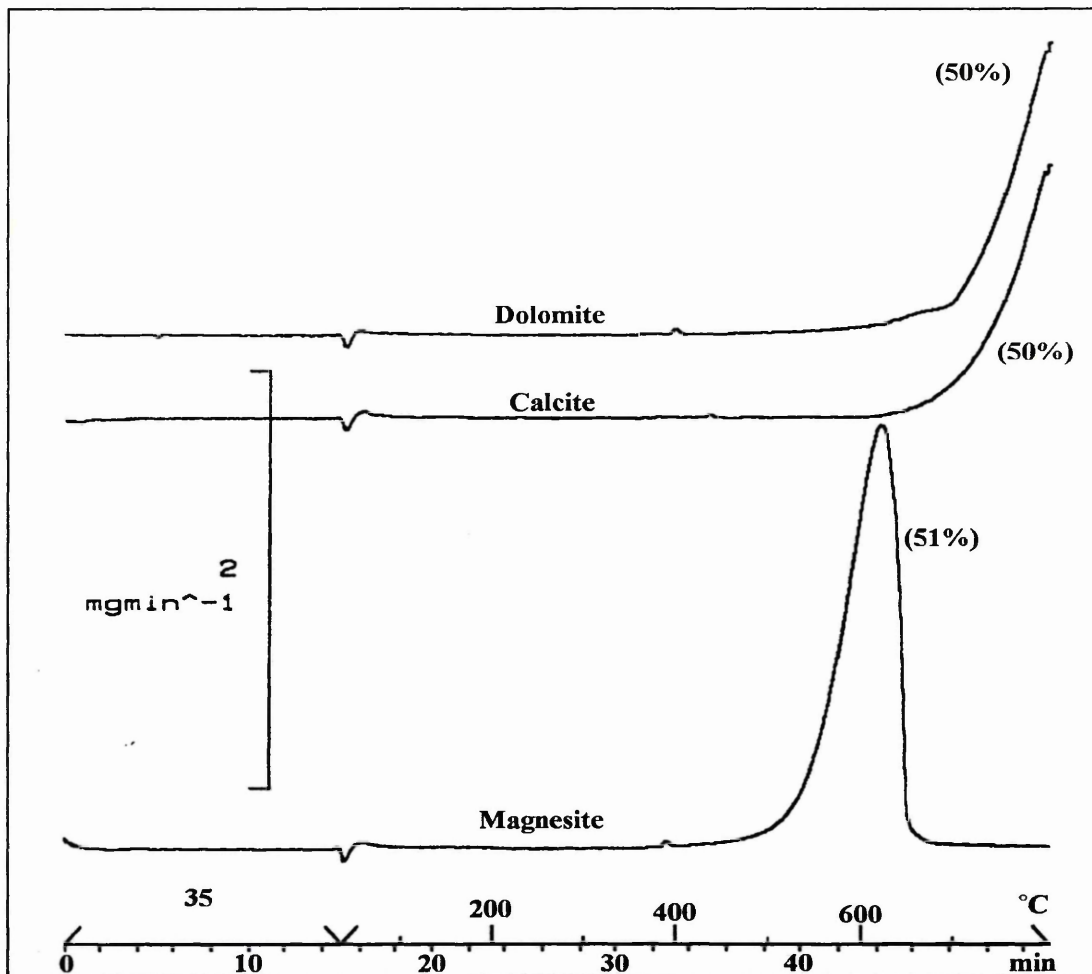
Van der Goost et al. [101] proposed that dehydroxylation of kaolinite occurs in two steps. The first involves the hydroxyls of the upper un-shared plane in the octahedral sheet followed by the hydroxyls of the inner shared plane in the octahedral sheet (see figure 4.3). The temperature at which these occur are linked to both degree of ordering and crystal size. Most kaolinites lose their hydroxyls between 450-600°C, but it is known for some well ordered kaolinites to give dehydroxylation temperatures as high as 690°C (e.g. kaolinite from Keokuk, Iowa [256]). The amount of structural water expected from kaolinite, derived from its formula $(\text{OH})_8\text{Si}_4\text{Al}_4\text{O}_{10}$ amounts to 13.96%. Again this can change depending on its ordering. After dehydroxylation metakaolinite is produced and at higher temperatures (>1010°C) a characteristic reaction occurs which presumably results in mullite crystallisation [257].

The DTG traces of the different chlorites (CCa-2, Penninite and Clinocllore) demonstrate that not all chlorites behave in the same manner. This is the case for all mineral groups, although some are effected more (e.g. kaolinites) than others (e.g. smectites). Chlorite undergoes a distinctive two stage dehydroxylation behaviour [257]. A low temperature event at approximately 600°C is associated with dehydroxylation of the brucite sheet, which is followed by separate dehydroxylation of the talc sheet at approximately 800°C. Significantly more hydroxyl water is evolved during the first event which is also demonstrated in the samples studied here (e.g. 8.7 vs. 1.1%, respectively, figure 6.2). The dehydroxylation of clay minerals has been studied by several techniques [258 and references therein]. The dehydroxylation is believed to result from the interaction of two hydroxyls groups in a two step process to form a water molecule. The first step is deprotonation of a hydroxyl, which leaves a chemically bonded oxygen as a superoxide anion in the lattice. The proton then diffuses (proton hopping) to another hydroxyl resulting in the formation of water.

The DTG traces of dolomite, calcite and magnesite are shown in figure 6.3. The majority of carbonates decompose around 850°C. Unfortunately, the full decomposition of dolomite and calcite is not observed in figure 6.3 as the samples were only heated to 800°C. Some carbonates can decompose at lower temperatures,

for example, magnesite at 610°C (figure 6.3) and ferrous carbonates at 350°C [100]. The thermal decomposition of dolomite has been studied by Milodowski et al. [259] and show that two degradation steps occur. Both of these result in the formation of carbon dioxide. The ferroan (Fe) and ankerite (Mg)-dolomite series are shown to breakdown in three stages, of which all of the three steps result in the formation of carbon dioxide.

Figure 6.3: DTG traces of dolomite, calcite and magnesite.



The DTG traces of silica (representative of quartz) and feldspars are not shown because no maxima were observed. Although this was the case, a gradual decrease in weight was observed for both as they were heated from 35-800°C. The percentage weight loss from quartz and feldspar (Na) were 0.5% and 1.7%, respectively.

Table 6.1 summarises the characteristic maxima observed in the DTG traces of the minerals studied in this thesis.

The above results already show that characteristic DTG maxima (e.g. maximum at 500°C indicates presence of kaolinite) could be used to identify a mineral type within a geological sample. Indeed, many people have tried to do this [101-103]. Unfortunately problems occur, of which the most significant is that the maxima are liable to shift due to the ordering of the minerals. Thus, overlapping and shifting maxima makes their assignment difficult. The use of EGA could alleviate some problems, for example, overlapping maxima due to chlorite and carbonate could be overcome by detecting H₂O for chlorite and CO₂ for carbonates. Unfortunately, EGA would not be able to distinguish overlapping maxima due to, for example, kaolinite and chlorite. The use of chemical probes should be able to overcome some of these problems.

Table 6.1: Summary of the Characteristic maxima observed in the DTG traces of minerals

Mineral	Characteristic DTG maxima, °C (% wt. loss)
X-SWy-2	90 & 130°C (2-11%) <---700°C (≈5%)--->
Illite	70°C (0.7%) <-----570 & 650°C (4.7%)----->
Kaolinite	<-530°C (13-14%)----->
Chlorite (CCa-2)	<--600°C (8.7%) & 780°C (1.1%)-->
Dolomite	<-800°C (≈50%)>
Magnesite	<-600°C (≈50%)-->
Calcite	<-800°C (≈50%)>
Quartz, Feldspar	No characteristic maxima

6.3) Thermogravimetric analysis of powdered mineral standards treated with prospective chemical probes

This section will show and discuss the TGA results obtained from the individual mineral standards (X-SWy-2, kaolinite, illite, chlorite, feldspar, carbonates and quartz) treated with the chemical probes NMF and DMF. Of the five main chemical probes studied these two were discovered to produce the most unique DTG traces for each mineral standard.

6.3.1) TGA of N-Methylformamide/mineral complexes

6.3.1.1) Ca, Mg, Na and K-exchanged montmorillonites (X-SWy-2)

Initially, each exchanged-montmorillonite was exposed to NMF vapour for 3 days. Subsequently, they were exposed for a longer periods of time and it was noticed that a progressive build-up of NMF on each X-SWy-2 was occurring.

Figure 6.4 shows the progressive build-up of NMF on Ca-SWy-2. The dehydroxylation region represents approximately 5% weight loss from the clay and can be used as an internal reference to the size of the other maxima. Table 6.2 shows the percentage weight (% wt.) losses of the observed maxima. The % wt. loss is derived using the weight of the clay before dehydroxylation. The following observations derived from the results should be noted:-

- After 30 hours exposure, a maximum at 320°C, similar in size to the dehydroxylation region has appeared and the dehydration maximum (i.e. loss of physisorbed water (90°C)) has dramatically decreased.
- After 3 days exposure the maximum at 320°C has increased and the dehydration maximum has decreased further.
- After 8 days exposure the maximum at 320°C no longer increases in height, an additional maximum at 180°C has appeared and the dehydration maximum, which is no longer distinctive has decreased.

Figure 6.4: DTG traces of Ca-SWy-2 after exposure to NMF vapour for 0, 30 hours, 3, 8, 15 and 31 days

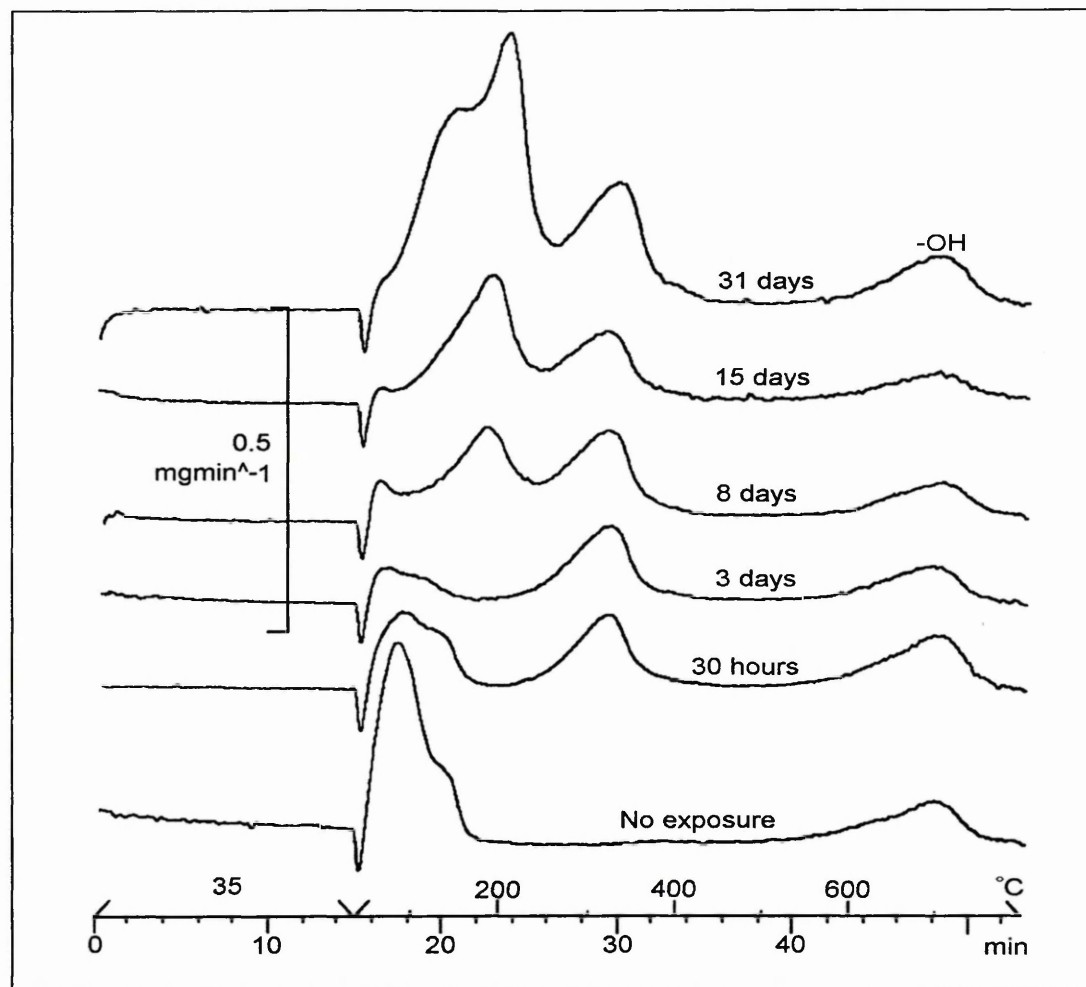


Table 6.2: Percentage weight losses of maxima observed in the DTG traces of Ca-SWy-2/NMF complexes.

Exposure times	Temperatures (°C) and (% wt. losses)				
	≈90°C (-H ₂ O)	≈110°C	≈180°C	320°C	700°C (-OH)
No exposure	90 & 130 (10.3%)	-----	-----	-----	(4.6%)
30 hours	90 (4.0%)	-----	160-260 (0.9%)	(4.0%)	(4.2%)
3 days	90 (2.7%)	-----	160-260 (1.2%)	(6.4%)	(4.6%)
8 days	-----	80-160 (3.2%)	180 (6.0%)	(7.3%)	(4.8%)
15 days	-----	80-160 (4.1%)	190 (10.1%)	(7.8%)	(5.4%)
31 days	-----	140 (7.7%)	200 (13.0%)	(8.3%)	(4.5%)
3 months	-----	120 (13.3%)	190 (12.6%)	(8.3%)	(5.8%)
1 year	-----	120 (15%)	190 (12.8%)	(8.0%)	(5.6%)

- After 15 days exposure the maximum at 180°C has almost doubled in size. This maximum is asymmetric on the low temperature side.
- After 31 days exposure, the low temperature asymmetry observed after 15 days is now prominent and has a maximum at 110°C. This maximum continues to grow very slowly upon additional exposure to NMF vapour until the intensity is greater than the maximum at 180°C. After 3 months and 1 year exposure, the percentage weight losses of the maximum at 110°C are 13.3 and 15.0%, respectively.

Figure 6.5 shows the progressive build-up of NMF on Mg-SWy-2. Table 6.3 shows the percentage weight losses of the observed maxima.

- After 3 days exposure a small maximum at 350°C has appeared and the dehydration maximum has decreased
- After 8 days an additional maximum at 400°C has appeared, whilst the dehydration maximum has decreased further.
- After 15 days a new maximum at 180°C has appeared and the maximum at 400°C no longer increases in height.
- After 30 days exposure another maximum at 110°C is present which continues to slightly increase upon further exposure.

The behaviour of Mg-SWy-2 is very similar to that of Ca-SWy-2 except that the highest temperature maximum is at 400°C for the former and 320°C for the latter. The progressive build up of NMF is slower for Mg-SWy-2 than Ca-SWy-2.

Figure 6.6 shows the progressive build-up of NMF on Na-SWy-2. Table 6.4 shows the % wt. losses of the maxima observed.

- After 30 hours exposure all the physisorbed water originally present in the untreated clay has been removed. A small maximum at 190°C has appeared.
- The maximum at 190°C increases no further in height after 8 days and is accompanied by an additional maximum at 130°C.
- After 15 days exposure the maximum at 130°C no longer increases in height. Additional exposure results in little change to the DTG trace apart from a small shoulder to the left of the maximum at 130°C.

Figure 6.7 shows the progressive build-up of NMF on K-SWy-2. Table 6.5 shows the % wt. losses of the maxima observed.

- After 30 hours exposure the clay has almost completely dehydrated and a small maximum at 310°C is present.
- After 3 days the maximum at 310°C has increased slightly in height and an additional maximum at 180°C has appeared.
- Additional exposure (8, 15 and 30 days) leads to a broadening of the maximum at 180°C. This maximum gradually broadens on the low temperature side so that by 30 days the centre of the maximum is at 150°C.

Figure 6.5: DTG traces of Mg-SWy-2 after exposure to NMF vapour for 0, 3, 8, 15 and 30 days

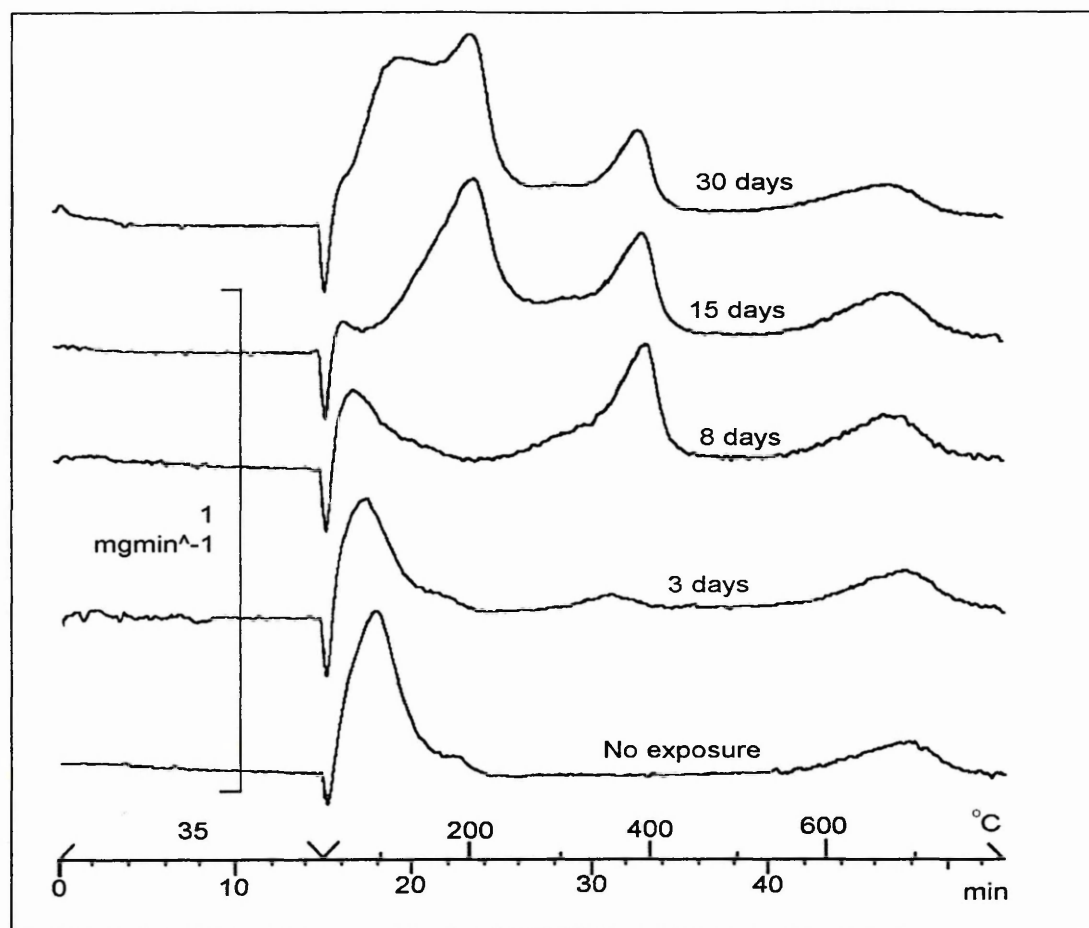


Table 6.3: Percentage weight losses of maxima observed in the DTG traces of Mg-SWy-2/NMF complexes

Exposure times	Temperatures (°C) and (% wt. losses)					
	≈90°C (-H ₂ O)	≈110°C	≈180°C	260-340°C	≈400°C	≈700°C (-OH)
No exposure	99 & 170 (10.7%)	-----	-----	-----	-----	690 (4.5%)
3 days	80 & 160 (6.3%)	-----	-----	(0.8%)	340-440 (3.0%)	690 (4.7%)
8 days	80 & 160 (2.9%)	-----	170-260 (0.9%)	(1.6%)	400 (4.8%)	680 (4.8%)
15 days	-----	80-170 (2.5%)	220 (5.8%)	(2.3%)	400 (3.9%)	680 (3.9%)
30 days	-----	130 (12.4%)	200 (8.9%)	(5.0%)	390 (5.6%)	670 (5.4%)
85 days	-----	120 (13.6%)	220 (11.3%)	(3.1%)	400 (5.0%)	680 (4.7%)

Figure 6.6: DTG traces of Na-SWy-2 after exposure to NMF vapour for 0, 30 hours, 3, 8, 15, and 30 days.

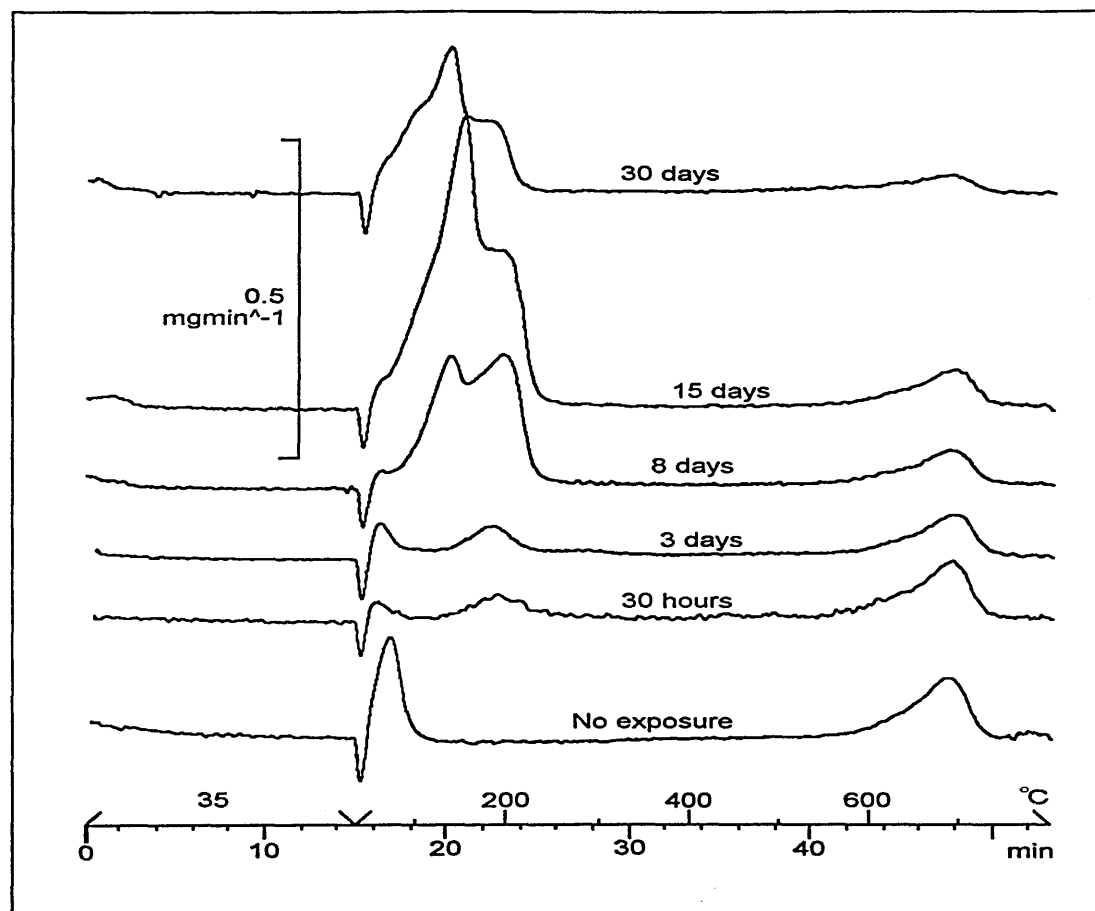


Table 6.4: Percentage weight losses of maxima observed in the DTG traces of Na-SWy-2/NMF

Exposure times	Temperatures (°C) and (% wt. losses)			
	80°C (-H ₂ O)	≈160°C	≈200°C	≈690 (-OH)
No exposure	80 (2.17%)	-----	-----	690°C (4.0%)
30 hours	-----	80-170 (1.3%)	190 (1.5%)	700 (5.2%)
3 days	-----	80-170 (1.3%)	190 (1.6%)	690 (4.5%)
8 days	-----	100 (10.8%)	200 (7.1%)	690 (5.1%)
15 days	-----	160 (21.8%)	200 (8.0%)	690 (5.1%)
30 days	-----	150 (26.2%)	190 (7.6%)	690 (7.3%)

Figure 6.7: DTG traces of K-SWy-2 after exposure to NMF for 0, 30 hours, 3, 8, 15, and 30 days.

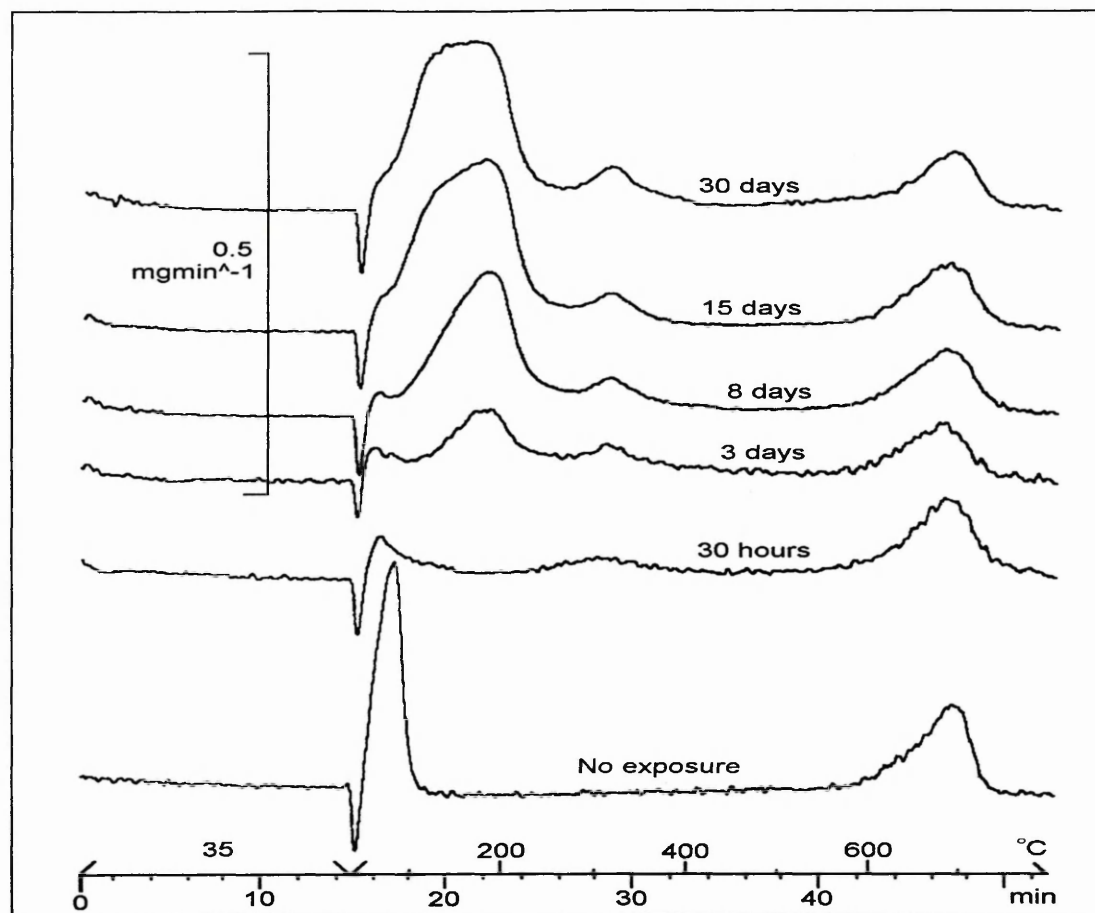


Table 6.5: Percentage weight losses of maxima observed in the DTG traces of K-SWy-2/NMF

Exposure times	Temperatures (°C) and (% wt. losses)				
	≈90°C (-H ₂ O)	70-120°C	≈180°C	310°C	690°C (-OH)
No exposure	90 (2.1%)	-----	-----	-----	(4.5%)
30 hours	50-180 (0.8%)	-----	180-260 (0.6%)	(1.3%)	(4.5%)
3 days	-----	(1.0%)	180 (4.7%)	(2.5%)	(4.3%)
8 days	-----	(1.7%)	190 (7.3%)	(2.2%)	(5.5%)
15 days	-----	(3.6%)	180 (9.4%)	(2.2%)	(4.6%)
30 days	-----	(4.9%)	130-260 (13.2%)	(3.4%)	(6.1%)

In order to determine the maximum extent of interaction, each X-SWy-2 was directly mixed with liquid NMF. This is a more severe treatment and so maximum intercalation/interaction should be achieved. Unfortunately, after treatment the clays took several days to dry and it was difficult to determine between when the clay actually became dry and when physisorbed NMF left the clay. The DTG traces of the clays exposed to NMF liquid always showed less build-up than the clay exposed to vapour for 30 days and so it was not possible to determine the maximum amount of interaction.

It is clearly evident from the results that each cation-exchanged montmorillonite interacts differently with NMF. Associated with each X-SWy-2 are characteristic sites or environments for NMF, where each site or environment is represented by a maximum on the DTG trace. Mg-SWy-2 exhibits the strongest association (i.e. the maximum at 400°C) followed by Ca-SWy-2 (320°C), Na-SWy-2 (190°C) and K-SWy-2 (180°C), respectively.

The speed at which each site appears on each X-SWy-2 is different. The appearance of the highest temperature maximum on Mg-SWy-2 is much slower (8 days) than that on Ca-SWy-2 (3 days), which in turn is slower than the first sites to appear on Na and K-SWy-2. The high temperature site observed at 310°C on the K-SWy-2 may be due to residual Ca^{2+} cations in the interlamellar region which were not successfully exchanged for K^+ cations. The XRF data (table 6.6) supports this hypothesis and thus the maximum at 310°C can be assigned to NMF associated with Ca^{2+} ions. A possible reason for the differences in speed of build-up may be due to the polarisability of each cation. Mg is more polar than Ca and thus the hydration water around a Mg cation within the clay will be more tightly held. It would therefore be more difficult for the NMF to interact with the Mg cation because it has to displace the tightly held water. The same principal can be applied to Na and K-SWy-2, i.e. Ca and Mg cations are more polarising than Na and K cations and thus the build-up of NMF on the latter is quicker. This observation is also reflected in the speed at which the maximum associated with adsorbed water is removed from each clay. The water on Mg-SWy-2 is retained for longer than on the Ca-SWy-2 and in turn longer than the Na and K-SWy-2.

The slower NMF uptake by Mg and Ca could also be attributed to competition from water for active sorption sites. Mg and Ca-SWy-2 contains more naturally held water than Na and K-SWy-2, which leads to NMF being able to sorb onto the latter two more easily.

Table 6.6: XRF results of the original and Ca, Mg, Na and K exchanged SWy-2

Percentage Oxide	Original	Ca-SWy-2	Mg-SWy-2	Na-SWy-2	K-SWy-2
Al ₂ O ₃	20.16	20.77	21.12.	20.84	20.61
SiO ₂	68.47	68.43	69.09	68.75	68.28
Na ₂ O	1.70	0.27	0.12	3.06	0.15
MgO	2.77	2.48	4.29	2.46	2.27
CaO	1.77	3.05	0.3	0.05	<u>0.75</u>
K ₂ O	0.69	0.50	0.43	0.36	3.39
TiO ₂	0.16	0.13	0.14	0.13	0.14
FeO ₃	4.13	4.22	4.38	4.23	4.27
Others	0.15	0.15	0.13	0.12	0.14

When performing the experiments described above each sample was contained in a saturation chamber for the appropriate length of time. It was discovered that if the chamber was opened half-way through the appropriate length of time then NMF sorption would increase. For example, if Ca-SWy-2 had been exposed to NMF for 8 days, the maximum at 180°C would be smaller than the maximum at 180°C for Ca-SWy-2 which had been exposed to NMF for the same length of time but had been disturbed on day 4. The chamber would only need to be open for approximately 30 seconds for an effect to be noticed. The reason for this behaviour is not known, but two possible reasons could be:-

- i) water vapour from the lab enters the chamber once open and is involved in complexing with the clay, or,
- ii) water vapour removed from the clay saturates the chamber, less NMF molecules are thus available to interact with the clay and thus a slower build-up is observed.

From the TGA data it is not possible to determine whether each maximum is associated with NMF, H₂O or both. In order to determine this TG-FTIR and TG-MS have been employed and will be discussed later (see section 6.4).

The X-SWy-2/NMF complexes were quite stable. An exposed clay could be left in a sealed vial for up to 5 days and no change is observed in the DTG trace.

Corresponding XRD data for the Ca-SWy-2/NMF complexes show that maximum interlayer expansion occurred after 3 days in vapour, which correlates with the establishment of the high temperature maximum (320°C). Figure 6.8 shows the XRD traces of Ca-SWy-2 after exposure to NMF for 0, 3, 8 and 15 days. A similar observation is noted for the Na and Mg-SWy-2/NMF complexes (table 6.7) but not the K-SWy-2/NMF complexes. Figure 6.9 shows the XRD traces for K-SWy-2 after exposure to NMF for 0, 3, 8, and 15 days. No sudden intercalation step was noted, it occurs in stages. Also it is nearly 2Å bigger than the Ca and Mg complexes and 1Å greater than the Na complex. Olejnik et al. [239] have also studied the intercalation of NMF into Ca and Mg-exchanged montmorillonite and found the $d_{(001)}$ -spacings to be 17.5 and 17.7Å, respectively.

Figure 6.8: XRD traces of Ca-SWy-2 after exposure to NMF for 0, 3, 8 and 15 days

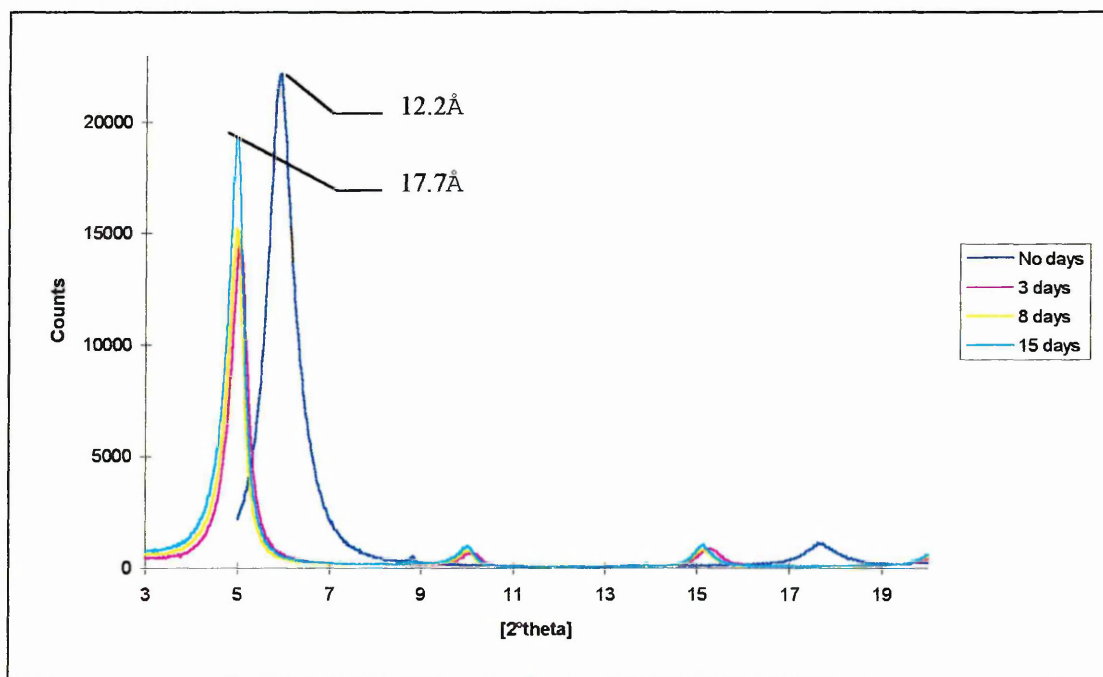
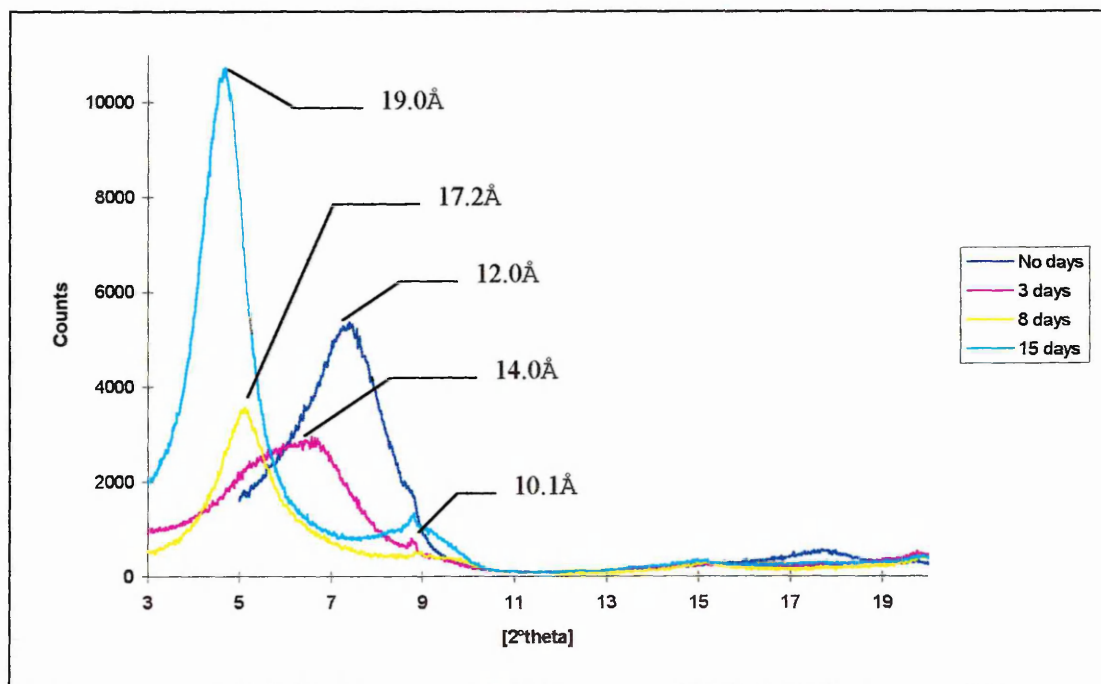


Table 6.7: Summary of the $d_{(001)}$ -spacings of X-SWy-2 upon progressive exposure to NMF

Cation-exchanged Montmorillonite	Before Exposure (hydrated state)	Exposure to NMF
Ca-SWy-2	12.2Å	17.7Å after 3 days and remains constant
Mg-SWy-2	15.1Å	17.7Å after 3 days and remains constant
Na-SWy-2	12.5Å	18.2Å after 3 days and remains constant
K-SWy-2	12.0Å (broad)	3 days: 14.0Å (becomes broader) 8 days: 17.2 & 10.1Å (still broad) 15 days: 19.0Å (tall) & 10.1Å (short)

Figure 6.9: XRD traces of K-SWy-2 after exposure to NMF for 0, 3, 8 and 15 days



The overall results do show that different exchangeable cations do have an affect on the strength of interaction between NMF and clay. These differences could be used to determine the type of exchangeable cation present in a montmorillonite clay. For example, after 8 days exposure the maxima at 400, 320, 190 and 180°C could be used to determine the presence of Mg, Ca, Na and K, respectively. Obviously, 8 days is a long period of time and therefore a quicker interaction procedure is required. The different NMF sites will be discussed in more detail in section 7.

6.3.1.2) TGA of kaolinite/NMF complexes

Kaolinite (KGa-2) has been treated with NMF via the vapour and the liquid. The effect of temperature on intercalation whilst in the liquid medium has been studied. The following four treatments have been performed.

- A) Progressive exposure to the vapour of NMF (0, 5, 17 and 20 days)
- B) Direct contact with NMF for 48 hours at room temperature ($\approx 25^{\circ}\text{C}$)
- C) Direct contact with NMF for 48 hours at 70°C
- D) Direct contact with NMF for 48 hours at 140°C

A)

Figure 6.10 shows the DTG traces of kaolinite after exposure to NMF vapour for 0, 5, 17 and 20 days. The numbers without and within brackets represent the temperature at peak maximum and % wt. losses, respectively. The build up of NMF via the vapour phase on to kaolinite is very slow in comparison with the cation-exchanged montmorillonites. After 20 days there is only a small % wt. loss of 3.2% at 115°C .

Figure 6.10: DTG traces of kaolinite after exposure to NMF vapour for 0, 5, 17 and 20 days.

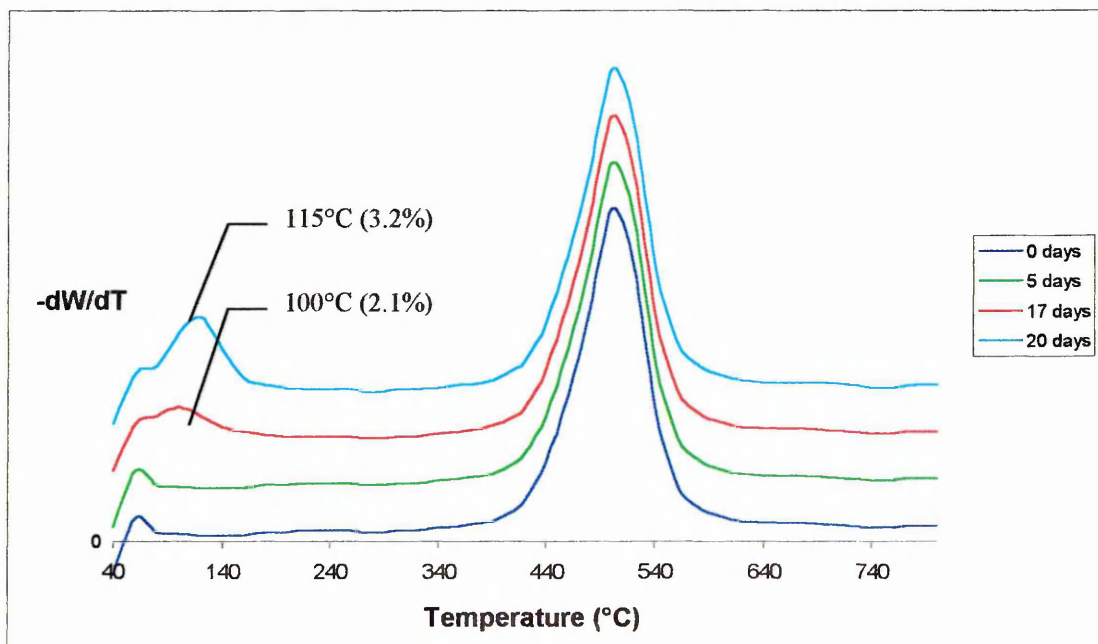
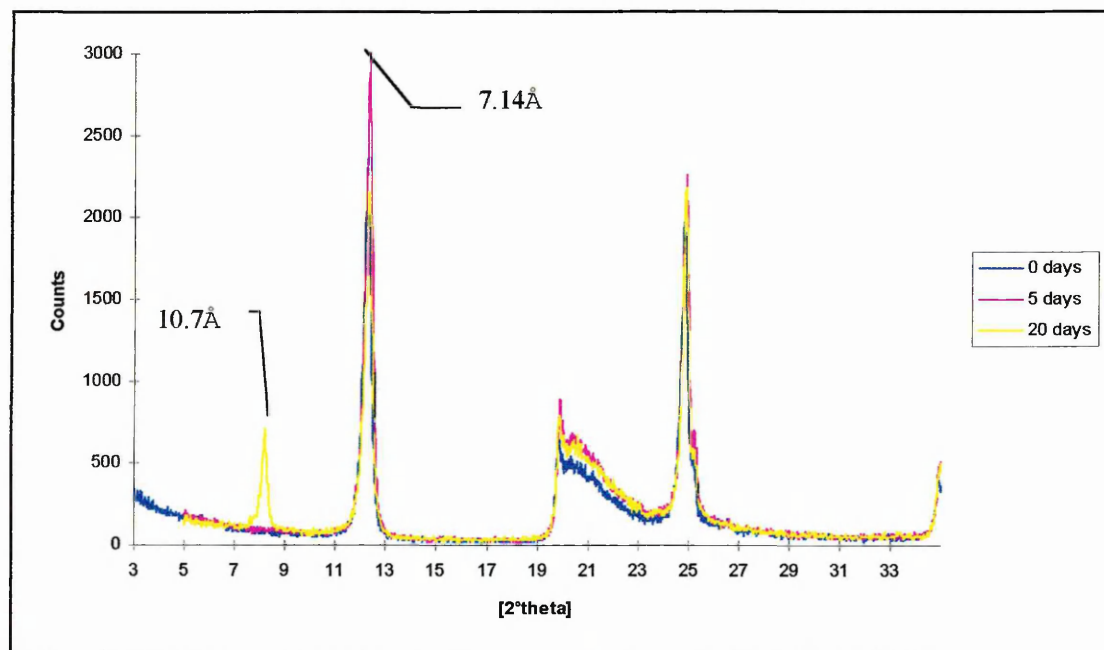


Figure 6.11 shows the XRD traces of kaolinite exposed to vapour for 5 and 20 days. The extent of intercalation of NMF into kaolinite can be determined by the XRD traces [175]. Since the ratio of the intensity, I , of the (001) peak of the complex to the sum of the intensity of the (001) peaks due to the complex and the unexpanded mineral i.e.

$$\frac{I_{(001) \text{ complex}}}{I_{(001) \text{ complex}} + I_{(001) \text{ kaolinite}}}$$

gives the proportion of expanded layers within a single crystal. The intercalation ratio therefore serves as a useful and readily measurable index of the intercalation rate. The $d_{(001)}$ of kaolinite and the kaolinite/NMF complex is observed at 7.17 and 10.7Å, respectively.

Figure 6.11: XRD traces of kaolinite exposed to NMF vapour for 0, 5 and 20 days.



The intercalation ratios for the kaolinite exposed to vapour for 20 days is 0.13. Considering the maximum ratio observed in the literature for KGa-2 [260] is 0.70, then only little interaction has occurred (18.5% of maximum) over 20 days via the vapour phase.

B-D)

Figure 6.12 shows the DTG traces of kaolinite directly exposed to NMF liquid at 25, 70 and 140°C (for 48 hours). Table 6.8 shows the % wt. losses of; the dehydroxylation maximum, the total NMF and each of the two NMF maxima. The DTG traces of the KGa-2/NMF complexes formed at 25 and 70°C are similar, whereas the DTG of the complexed formed at 140°C is different. Two maxima are observed for the KGa-2/NMF complex formed at 140°C. Of these the second maximum (150°C) is smaller than the related maximum present at the same temperature in the complexes formed at 25 and 70°C. If the KGa-2/NMF complex formed at 140°C is stored in a chamber saturated with NMF vapour the first maximum reduces in size.

Figure 6.13 shows the XRD traces of the KGa-2/NMF complexes formed at 70 and 140°C. Their intercalation ratios are 0.59 and 0.62, respectively. The XRD trace for the complex formed at room temperature is the same as the XRD trace for the complex formed at 70°C. The extents of intercalation are almost the same for all the KGa-2/NMF complexes. These are not intercalated to their maximum extent since Unwins [260] has achieved intercalation ratios of 0.7. Unwins achieved intercalation via the displacement method and this could be the reason for a lower yield in the samples studied in this thesis (need to note also that obviously a different clay batch was used which could be the reason for the difference).

The second maximum for the complex formed at 140°C may be due to the high temperature used to form the complex which could cause damage to crystal edges and surfaces creating more places for NMF to bind to. This could be the case since damage has occurred to the kaolinite crystals. This is known because the % wt. loss during dehydroxylation has decreased significantly.

Figure 6.12: DTG traces of KGa-2 after exposure to NMF liquid at 25, 70 and 140°C (each for 48 hours).

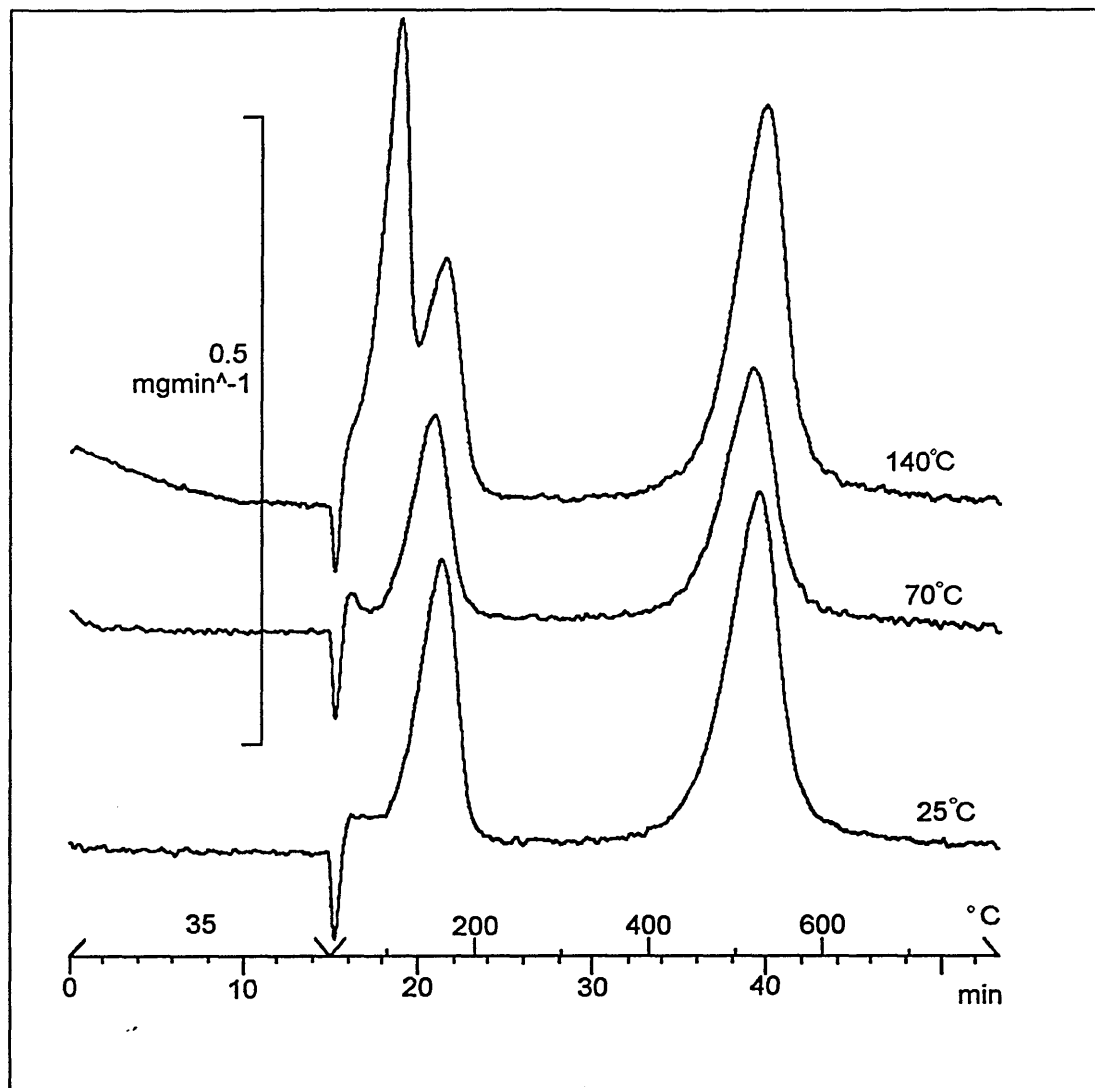
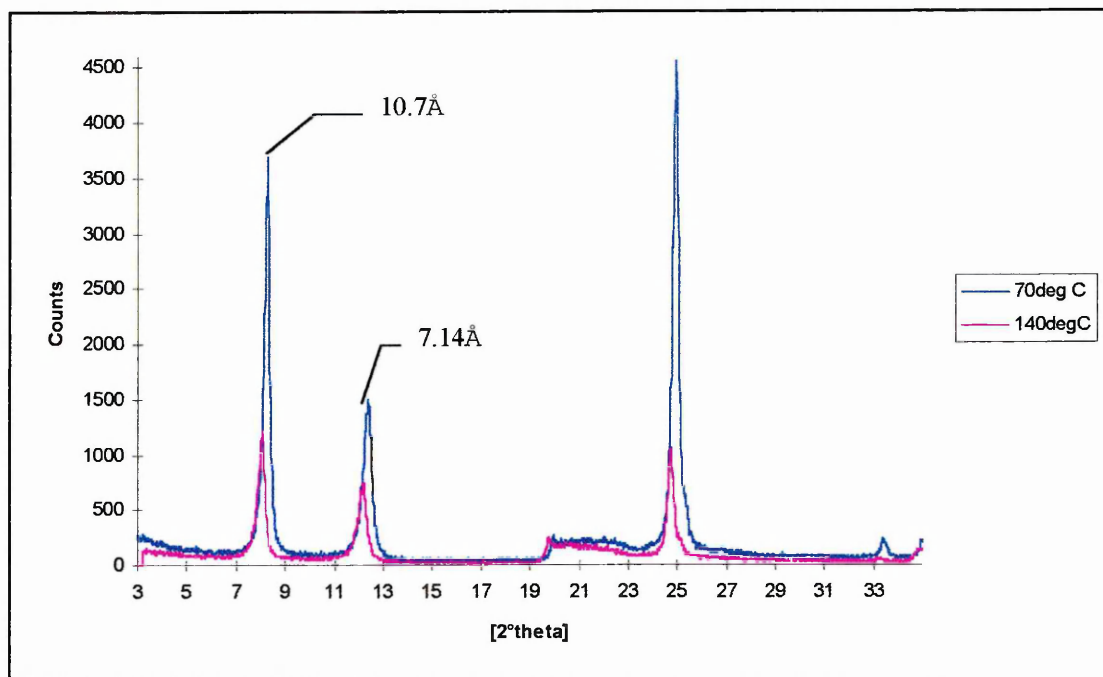


Table 6.8: Percentage weight losses of; the dehydroxylation maximum, the total NMF and each of the two NMF maxima observed in the DTG traces of the KGa-2/NMF complexes formed at 25, 70 and 140°C.

% wt losses	KGa-2/NMF complexes		
	25°C	70°C	140°C
Dehydroxylation	13.1%	12.9%	10.2%
Total NMF	7.7%	7.4%	11.9%
First NMF maximum (35-130°C)	-----	-----	4.1%
Second NMF maximum (130-220°C)	2.2%	1.7%	7.8%

Figure 6.13: XRD traces of the KGa-2/NMF complexes formed at 70 and 140°C



Unwin's et al. [260] have studied the variability of intercalation yield for the NMF-kaolinite reaction for nine different kaolinites with various microstructural and morphological properties. They used the Hinckley Index (HI) [261] to estimate the crystallinity (order) of each kaolinite and compared the effect of this on intercalation yield. Their results showed that there is a general relationship between order and intercalation yield, i.e. a well ordered (e.g. KGa-1) and poor ordered (KGa-2) kaolinite gives a high (>90%) and low (70%) intercalation yield, respectively. However, this relationship did not always hold true.

Subsequent to these investigations using bulk kaolinites Unwins et al. [260] investigated the effect of particle size fractions on the intercalation yield. They found that particle size effects the intercalation yield in that kaolinites < 0.4µm did not show high intercalation yields whereas greater sized fractions (0.5-0.6µm and >2.0µm) did. This relationship was not well defined and, in this paper other effects such as specific defect types (discussed in reference [262]) and the relative number of different defect types in a given size fraction were described.

Unwin's study highlights the fact that the extent of intercalation for NMF is different for kaolinites of differing origin, since their crystallinity, particle size and defect-types are not the same. This fact means that the amount of chemical probe bound to a pure

kaolinite sample will differ between kaolinite types. Thus, correlation between amount of chemical probe desorbed and % kaolinite in a mineral will be subject to error. A potential benefit of this phenomena could be that the chemical probe will be specific to the amount of 'reactive' kaolinite in a rock rather than the total amount of kaolinite. However, a suitable chemical probe needs to be able to intercalate to the same extent in every kaolinite-type, a 100% intercalation yield in every kaolinite would be preferable provided it doesn't mask or superimpose upon another desorption maxima.

6.3.1.3) TGA of illite/NMF complexes

Figure 6.14 shows the DTG traces of illite after exposure to NMF vapour for 0 & 19 hours, and, 3 & 31 days. Table 6.9 shows the % wt. losses of the maxima observed in the DTG traces.

After 19 hours exposure additional maxima have appeared between 100-400°C. There is one broad maximum at 100°C and a spread of maxima between 240-400°C. The maximum observed at 100°C could be due to the loss of water and/or NMF. After 3 days exposure, the maximum observed at 100°C is now masked by the presence of several unresolved maxima between 40-200°C, resulting in a maximum at 120°C. Exposure for longer periods of time results in no further increase in the maximum at 120°C and thus the complex is in an equilibrium state.

The XRD traces of illite show no change ($d_{(001)}$ -spacing remains at 10.2Å) upon exposure to NMF and thus suggests that intercalation does not occur. This is expected because illite has strong electrostatic attractions between its layers [175].

These results show that illite has only one characteristic maximum at 120°C. In a mixture of minerals, this maximum could be masked by the characteristic maximum of K-SWy-2 and thus a distinction between the two could not be made.

The DTG traces of illite/NMF complexes are dissimilar to those of kaolinite and montmorillonite/NMF complexes in that the latter two exhibit distinct and clear maxima whereas the former exhibits a broad, envelope of unresolved maxima.

NMF molecules are expected to be associated by strong bonds to K^+ ions at frayed and splayed edges of illite.

Figure 6.14: DTG traces of illite after exposure to NMF vapour for 0, 19 hours, 3, 31 days

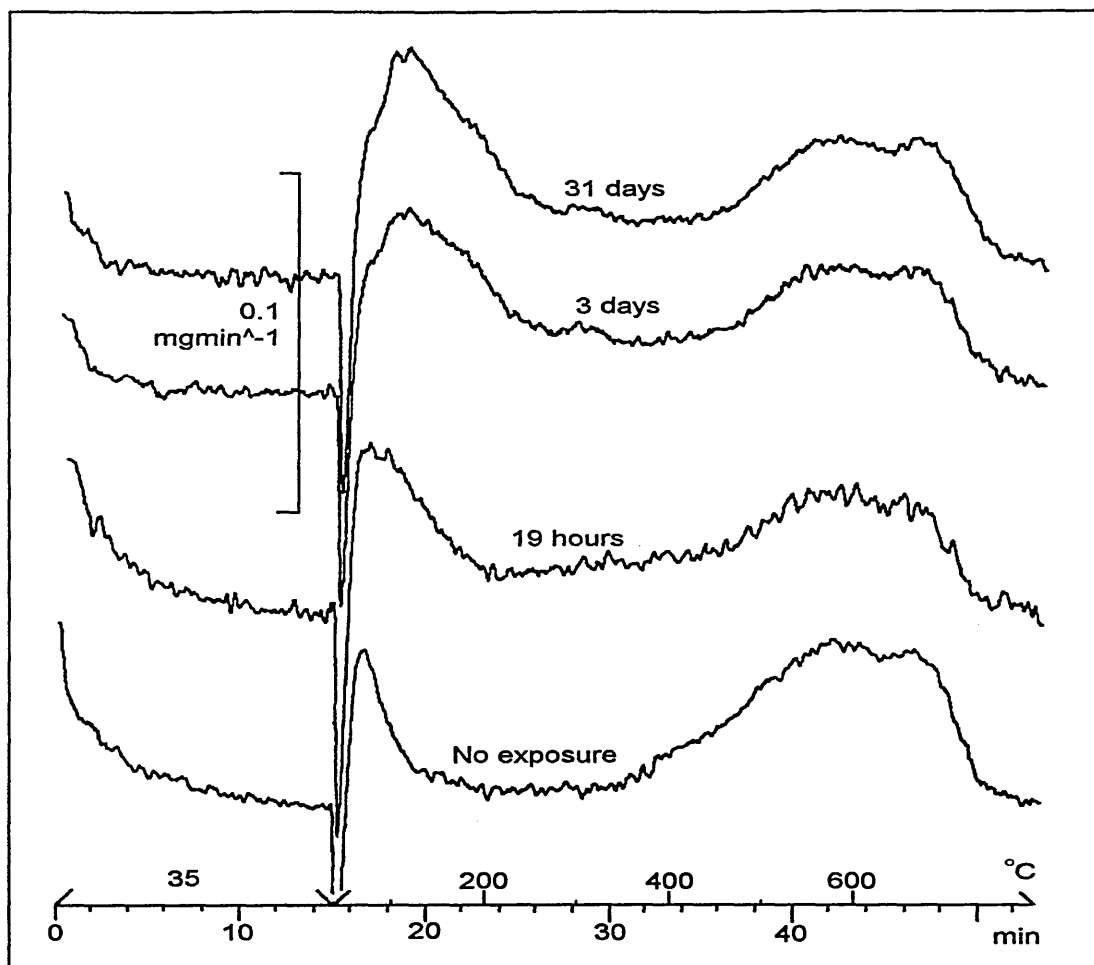


Table 6.9: Percentage weight losses from maxima observed in the DTG traces of illite/NMF complexes.

Exposure times	Temperatures and (% wt. losses).			
	60°C (-H ₂ O)	80-270°C	270-440°C	440-760°C (-OH)
0 days	(0.7%)	140→440°C (1.6%)		(4.7%)
19 hours	-----	100 (2.2%)	(1.8%)	(4.6%)
3 days	-----	120 (3.8%)	(1.7%)	(4.7%)
8 days	-----	120 (3.7%)	(1.8%)	(4.7%)
15 days	-----	120 (3.8%)	(1.6%)	(4.9%)
31 days	-----	120 (3.7%)	(1.5%)	(4.8%)

6.3.1.4) TGA of chlorite (CCa-2), quartz, feldspar and carbonates exposed to NMF vapour.

The DTG traces of CCa-2, Seesand (quartz), feldspar (Na), dolomite, calcite and magnesite after exposure to NMF by the vapour phase show no changes compared to their respective unexposed state. Thus, no significant interactions between the minerals and NMF can be detected by TGA.

Summary of TGA of NMF/Mineral complexes

The results so far show that:-

- i) NMF is selective towards minerals, it interacts with montmorillonite, illite and kaolinite, but not quartz, feldspar, carbonates or chlorite.
- ii) The minerals it selects are the most important i.e. these are more likely to effect treatment fluids in the exploration of oil and can also be used to describe the history of a rock.
- iii) NMF selectively interacts with different cation-exchanged clays. Distinction can be made after 8 days exposure to NMF vapour. Mg and Ca can be clearly distinguished, whereas Na and K show similar but distinctive maxima.
- iv) Interaction of NMF with KGa-2 is very slow, it prefers to intercalate via the liquid phase at elevated temperatures, which is not wanted.
- v) the time scale for interactions are too slow, having to wait 8 days for a sample to equilibrate is much too long.
- vi) It would be difficult to distinguish between a mixture of illite and K-SWy-2. Although the detection of the combination of the two would still be useful.

6.3.2) TGA of Dimethylformamide/mineral complexes

6.3.2.1) TGA of Ca, Mg, Na and K-SWy-2/DMF complexes

The behaviour of X-SWy-2 with DMF is similar to that observed with X-SWy-2 and NMF in that a progressive build up of DMF on each X-SWy-2 occurs. Figure 6.15 shows the progressive adsorption of DMF on Ca-SWy-2. Table 6.10 shows the % wt. losses of the maxima observed. The following details derived from the results should be noted:-

- The maxima appear in the order 330, 140 then 80°C. The maxima at 330 and 140°C no longer increase in height after 24 and 41 hours, respectively.
- Ca-SWy-2 is almost fully loaded by 41 hours. Additional build-up of DMF occurs in the temperature range 60-100°C between 41 hours and 16 days.
- The highest temperature maximum is at 330°C, which is 10°C higher than the highest maximum in the DTG trace of Ca-SWy-2/NMF. 2-3% more weight loss is also observed in the NMF complex.
- The second highest temperature maximum (140°C) in the Ca-SWy-2/DMF complex is more resolved, more intense (i.e. greater % wt. loss) and at a lower temperature than the second highest temperature maximum (180°C) in the Ca-SWy-2/NMF complex.

Figure 6.16 shows the progressive build-up of DMF on Mg-SWy-2. Table 6.11 shows the % wt. losses of the maxima observed.

- After 5 hours exposure a maximum at 410°C appears and the dehydration maximum decreases by approximately 50%.
- After 24 hours exposure the maximum associated with adsorbed water is no longer present and has been replaced by a maximum at 140°C.
- The clay is almost fully loaded after 41 hours exposure, the maximum present at approximately 90°C increases slowly between 3-30 days exposure.

Figure 6.15: DTG traces of Ca-SWy-2 after exposure to DMF vapour for 0, 5, 24, 41 hours and 16 days.

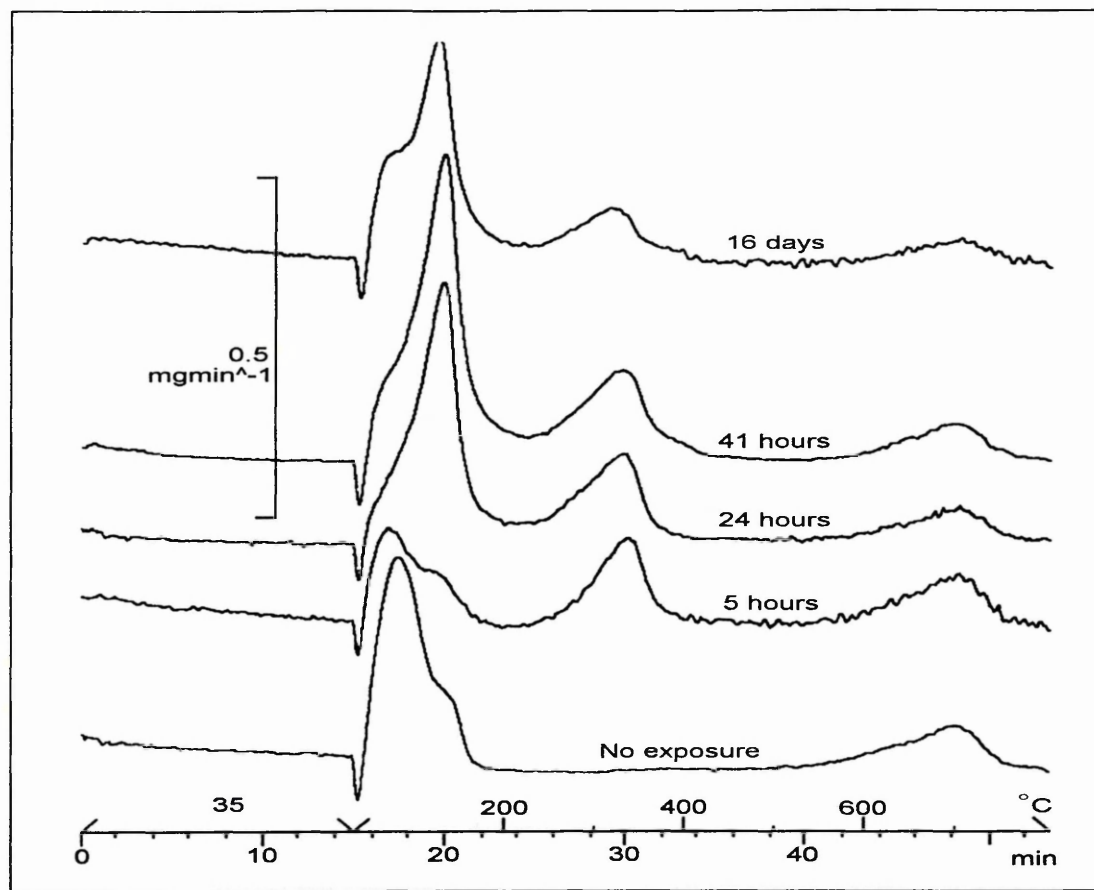


Table 6.10: Percentage weight losses of the maxima observed in the DTG traces of Ca-SWy-2/DMF complexes.

Exposure Times	Temperatures and (% wt. losses)				
	90 & 130°C (-H ₂ O)	≈60-100°C	≈140°C	≈330°C (200-420°C)	700°C (-OH)
0 days	(10.3%)	-----	-----	-----	(4.6%)
5 hours	(5.2%)	-----	-----	330 (5.1%)	(4.7%)
24 hours	-----	60-100 (3.75%)	130 (14.0%)	330 (9.8%)	(4.8%)
41 hours	-----	60-100 (3.9%)	130 (15.5%)	330 (11.1%)	(4.2%)
3 days	-----	60-100 (5.3%)	140 (15.6%)	320 (10.2%)	(5.0%)
16 days	-----	80 (6.65%)	140 (17.2%)	330 (10.0%)	(5.3%)

Figure 6.16: DTG traces of Mg-SWy-2 after exposure to DMF vapour for 0, 5, 24, 41 hours, 3 and 30 days.

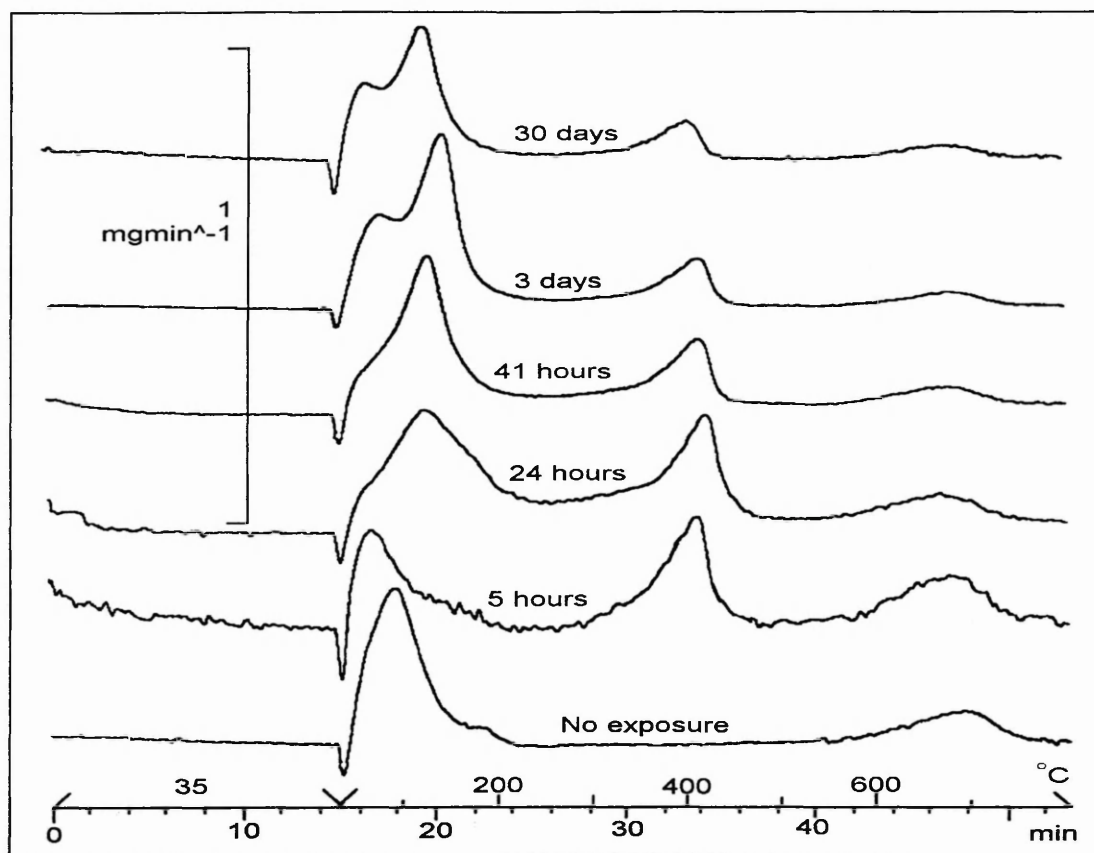


Table 6.11: Percentage weight losses of the maxima observed in the DTG traces of Mg-SWy-2/DMF complexes.

Exposure times	Temperatures and (% wt. losses)					
	(-H ₂ O)	≈ 80°C	≈ 120°C	220-320°C	≈ 400°C	≈ 690°C (-OH)
0 days	100 & 170 (10.7%)	-----	-----	-----	-----	690 (4.5%)
5 hours	80 & 160 (5.5%)	-----	-----	(0.8%)	410 (6.1%)	690 (5.3%)
24 hours	-----	60-100 (2.4%)	140 (10.0%)	(3.1%)	430 (8.6%)	670 (4.5%)
41 hours	-----	60-100 (3.3%)	140 (13.4%)	(2.8%)	420 (7.5%)	670 (4.2%)
3 days	-----	90 (6.0%)	155 (20.5%)	(3.4%)	420 (7.1%)	680 (4.3%)
16 days	-----	85 (7.2%)	150 (19.7%)	(2.4%)	420 (6.4%)	680 (4.6%)
30 days	-----	70 (7.3%)	140 (18.8%)	(2.8%)	410 (7.3%)	680 (5.0%)

- The highest temperature maximum (420°C) is at a higher temperature than the highest temperature maximum (400°C) observed in Mg-SWy-2/NMF. 2% more weight loss is also observed in this region for the DMF complex.
- The second highest temperature maximum (150°C) in the Mg-SWy-2/DMF complex is more resolved and at a lower temperature than the second highest maximum (180°C) in the Mg-SWy-2/NMF complex.
- The temperature of the second highest temperature maximum for Mg-SWy-2/DMF is 10°C higher than the second highest temperature maximum in Ca-SWy-2/DMF.

Figure 6.17 shows the progressive build-up of DMF on Na-SWy-2. Table 6.12 shows the % wt. losses of the maxima observed.

- After 24 hours exposure two maxima at 100 and 220°C are observed.
- After longer exposure times, the maximum at 220°C remains constant while the maximum at 100°C increases in size. The clay becomes almost fully loaded after 3 days in vapour.
- Comparison of Na-SWy-2/DMF and Na-SWy-2/NMF complexes when almost fully loaded, shows that:-
 - i) three maxima are observed for the NMF complex whereas only two are observed for the DMF complex. This could be due to the coalescence of two maxima in the DMF complex, i.e. the site producing the third maximum is lost at the same temperature as the site producing the second maximum
 - ii) the two maxima in the DMF complex are more resolved than the two highest temperature maxima in the NMF complex.

Figure 6.18 shows the progressive adsorption of DMF on K-SWy-2. Table 6.13 shows the % wt. losses of the maxima observed.

- The DTG traces of K-SWy-2/DMF are more complex than those of the Ca, Mg and Na-SWy-2/DMF complexes because four maxima are observed in the former whereas three or two maxima are observed in the latter three. These maxima are positioned at 120°C, 150°C, the shoulder to the high temperature side of the maximum at 150°C, and 330°C.

The complexity of the DTG traces could be due to the presence of residual Ca-exchangeable cations in the clay (which is confirmed in the XRF results, figure 6.6). This means that the maxima at 330, 80 and 140°C observed in the Ca-SWy-2/DMF complex are also present in the K-SWy-2/DMF clay. Hence, the characteristic maxima due to K-SWy-2 would be positioned at $\approx 180^\circ\text{C}$, i.e. the shoulder to the high temperature side of the maximum at 150°C, and the maximum at 120°C, which would be the low temperature maximum.

Summary

A comparison of the DTG traces of the X-SWy-2/DMF and X-SWy-2/NMF complexes shows that DMF adsorbs at a much faster rate than NMF. The main reason why this occurs is presumably due to the hydrogen-bonding network of NMF. NMF molecules associate to each other by hydrogen-bonding whereas DMF molecules do not, this leads to DMF being a more volatile liquid which in turn allows the DMF to vaporise more quickly and interact with the X-SWy-2. It is difficult to determine which X-SWy-2 undergoes the fastest interaction with DMF because the exposure times used do not allow it.

The DTG traces of the Mg and Ca-SWy-2/DMF complexes show that there are three different DMF sites or environments present, each represented by a separate maximum. The DTG traces of the same cation-exchanged clays when exposed to NMF also showed three sites, which could be of the same nature as the three DMF sites. This could be possible because DMF and NMF are similar in structure.

Assuming that the highest temperature maximum in the DTG trace of the Ca-SWy-2/DMF is of the same nature as the highest maximum in the DTG trace of the Ca-SWy-2/NMF, it could be stated that the strength of bonding to this particular site is much stronger in the DMF complex than the NMF complex. This is indicated by the fact the maximum in the latter complex is at a lower temperature. This observation associated with the highest temperature maximum is also the same for the other X-SWy-2 clays. The second highest temperature maximum in each of the X-SWy-2/DMF complexes behave differently to the first highest temperature maximum in the X-SWy-2/DMF complexes when compared to the X-SWy-2/NMF complexes in that

Figure 6.17: DTG traces of Na-SWy-2 after exposure to DMF vapour for 0, 24, 41 hours, 3 and 16 days.

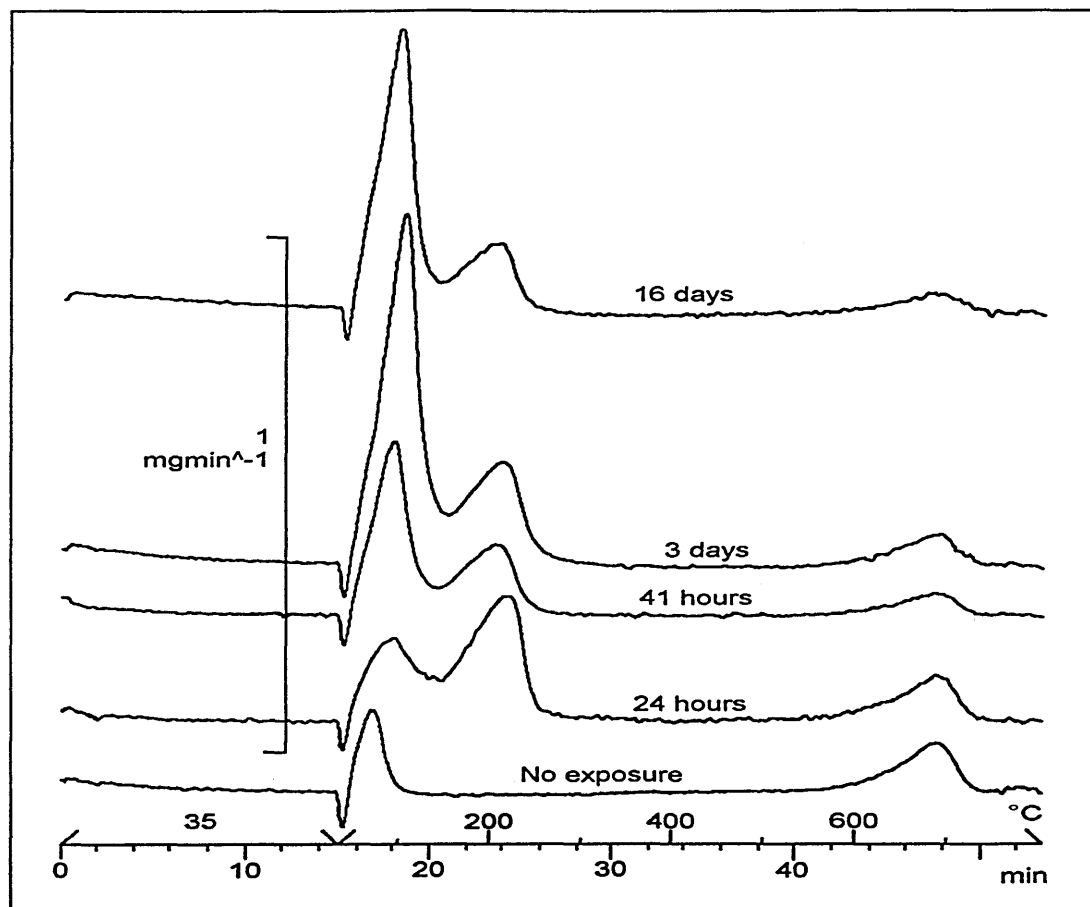


Table 6.12: Percentage weight losses of the maxima observed in the DTG traces of Na-SWy-2/DMF complexes.

Exposure times	Temperatures and (% wt. losses)			
	80°C (-H ₂ O)	≈100°C	≈220°C	≈690°C (-OH)
0 days	(2.2%)	-----	-----	690 (4.0%)
24 hours	-----	100 (6.0%)	220 (11.5%)	690 (5.3%)
41 hours	-----	100 (13.0%)	210 (9.2%)	680 (4.6%)
3 days	-----	105 (18.3%)	210 (10.0%)	690 (4.3%)
11 days	-----	110 (16.5%)	220 (9.3%)	690 (3.8%)
16 days	-----	105 (22.7%)	205 (10.2%)	690 (5.0%)

Figure 6.18: DTG traces of K-SWy-2 after exposure to DMF vapour for 0, 24, 41 hours, 3 and 16 days.

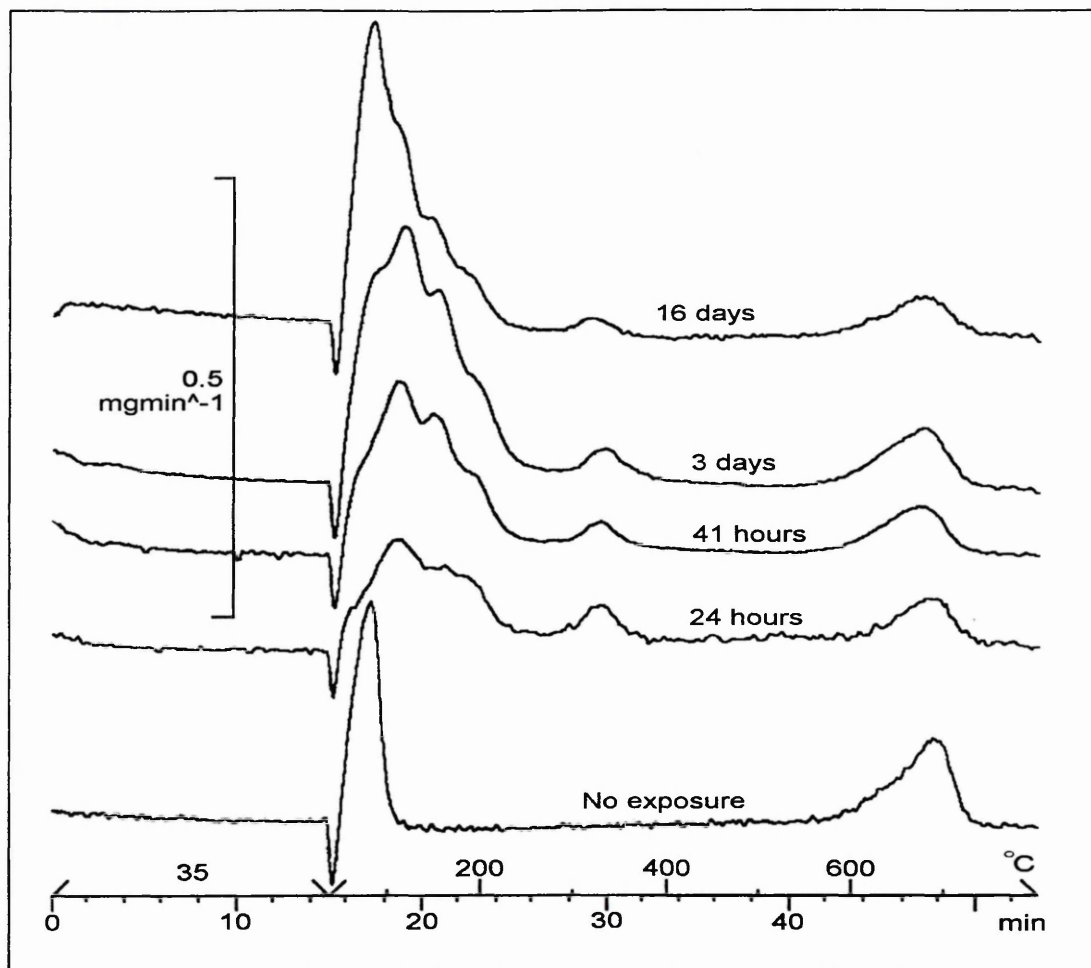


Table 6.13: Percentage weight losses of the maxima observed in the DTG traces of K-SWy-2/DMF complexes.

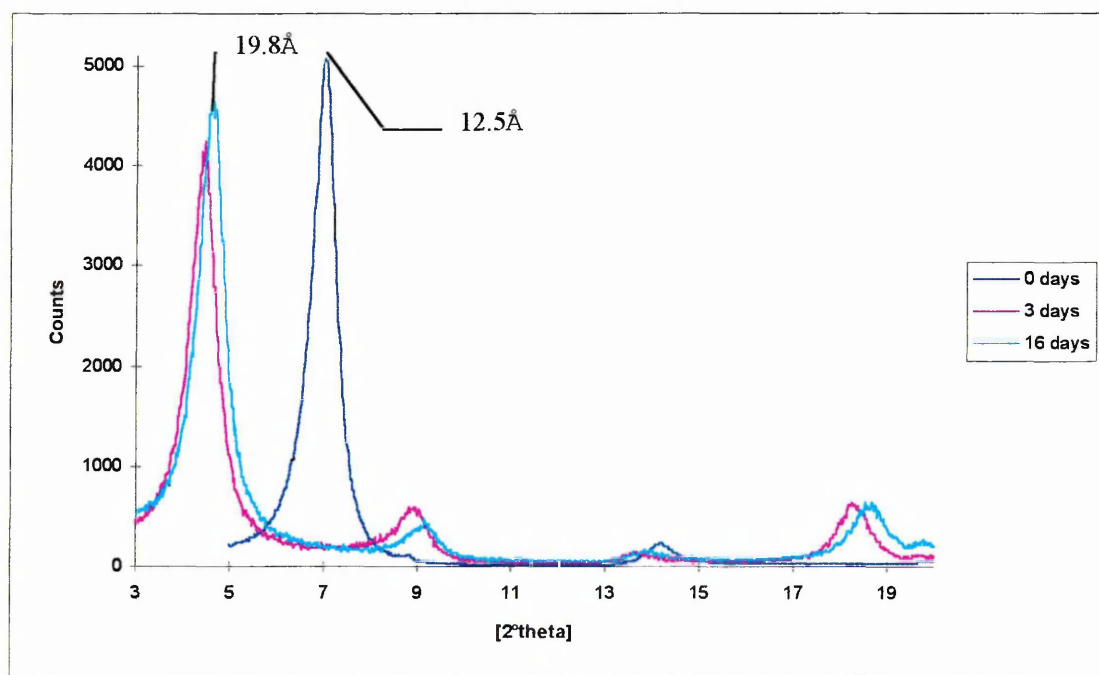
Exposure times	Temperatures and (% wt. losses)					
	(-H ₂ O)	60-145°C	145-180°C	180-280°C	≈300°C	≈690°C (-OH)
0 days	-----	-----	-----	-----	-----	-----
24 hours	-----	110 (6.6%)	(2.7%)	(3.3%)	330 (3.0%)	690 (5.6%)
41 hours	-----	120 (8.6%)	150 (4.0%)	(3.1%)	330 (2.3%)	670 (4.4%)
3 days	-----	120 (11.6%)	160 (4.2%)	(3.4%)	330 (2.5%)	680 (4.7%)
16 days	-----	90 & 110 (19.0%)	150 (3.8%)	(3.6%)	320 (1.4%)	680 (5.4%)

it is less strongly held. The reasons for the differences in strengths of bonding is probably due to the hydrogen bonding ability of the free N-H group in NMF and will be discussed in more detail in chapter 7.

The differences in temperature between the first and second highest temperature maxima in the X-SWy-2/DMF complexes (discussed above) allows the lowest temperature maximum to be more distinctive if it was to be used as a means of identifying the type of cation present in a montmorillonite. Thus, DMF is more suited to being a chemical probe than NMF is.

The XRD traces of Na-SWy-2 after exposure to DMF for 0, 3, and 16 days are shown in figure 6.19. These results show that the clay is intercalated after 3 days in vapour. Although no XRD data is present for exposure times less than 3 days, it is assumed that intercalation occurs when the first maximum (220°C) in the DTG trace is formed. No further increase in $d_{(001)}$ -spacing occurs for Na-SWy-2 when exposed for longer periods.

Figure 6.19: XRD traces of Na-SWy-2 after exposure to DMF for 0, 3, and 16 days



The XRD traces for Mg and Ca-SWy-2 exposed to DMF vapour for 11 days show that intercalation has occurred. No data is available to indicate that intercalation occurs

when the first maximum in the DTG trace appears, but it is assumed so. Table 6.14 shows the d-spacings of X-SWy-2 after exposure to DMF vapour. Olejnik et al. [239] have also studied the intercalation of DMF into Ca, Mg and Na-exchanged montmorillonites and found their $d_{(001)}$ -spacings to be the same for the latter two and slightly larger for the Ca-montmorillonite (19.1Å).

Table 6.14: $d_{(001)}$ -spacings of X-SWy-2 after exposure to DMF vapour.

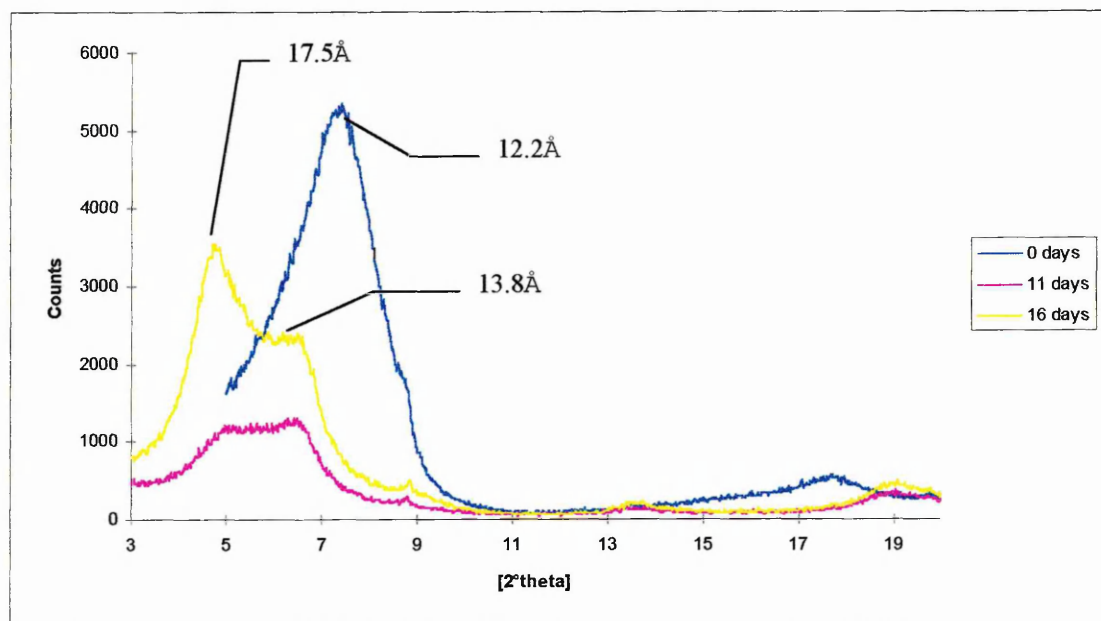
X-SWy-2	Before Exposure (hydrated state)	Exposure to DMF vapour
Ca-SWy-2	12.2Å	18.7Å after 11 days
Mg-SWy-2	15.1Å	19.2Å after 11 days
Na-SWy-2	12.5Å	19.8Å after 3 days
K-SWy-2	12.2Å	13.8 & 17.5Å after 11 days 17.5Å peak increases in intensity after 16 days

Figure 6.20 shows the XRD traces of K-SWy-2 after exposure to DMF for 0, 11 and 16 days in vapour. These results are similar to those of K-SWy-2/NMF in that intercalation occurs in steps. After 11 days exposure to DMF, the $d_{(001)}$ -spacing for K-SWy-2 increases from 12.2Å, to two peaks of the same intensity at 13.8 and 17.5Å. After 16 days exposure, the peak at 17.5Å has increased in relative intensity to the peak at 13.8Å and has shifted to 18.7Å.

The reason for this is unknown, but could be due to:-

- i) competition between Ca and K cations present in the interlayer
- ii) the fact that K cations change the nature of the clay considerably. This is due to their size and the resulting strong electrostatic forces between the clay layers and K cation. K cations tend to lie on the surface of the clay layers whereas Ca, Mg and Na lie in the middle when hydrated.

Figure 6.20: XRD traces of K-SWy-2 after exposure to DMF for 0, 11 and 16 days in vapour.



6.3.2.2) TGA of KGa-2/DMF complexes

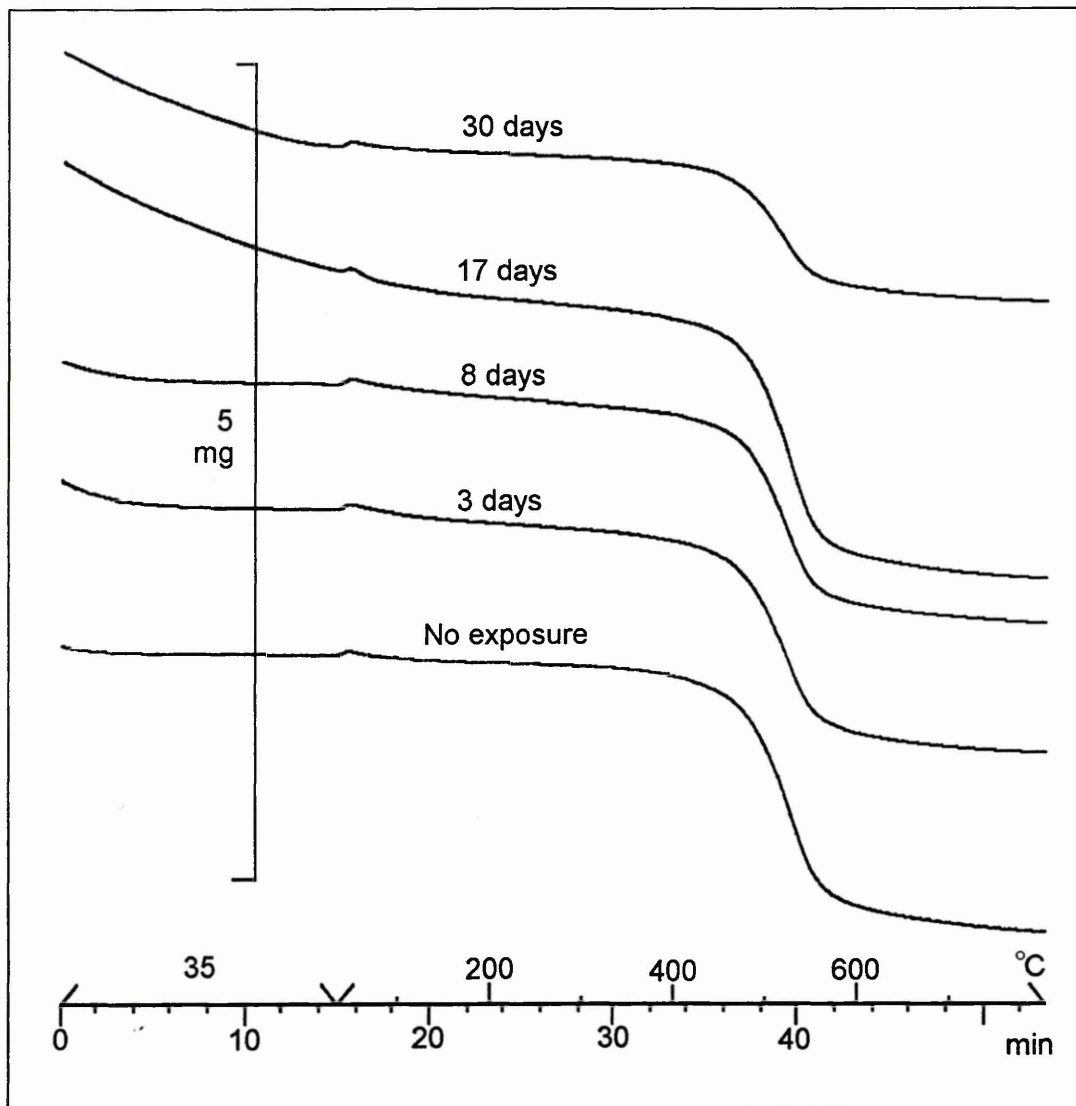
KGa-2 has been treated with DMF via a vapour and liquid medium. The following three treatments have been performed.

- A) Progressive treatment via the vapour phase (0, 3, 8, 17 and 30 days)
- B) Direct contact with liquid for 2, 5, 12 days at room temperature
- C) Direct contact with liquid for 2 days at 80°C.

The DTG traces of KGa-2 after exposure to DMF for 3, 8, 17 and 30 days show no additional maxima and therefore no distinct interactions have occurred. However, the thermogravimetric (TG) traces (figure 6.21) do show an increasing weight loss during the first 15 minutes (isothermal run at start) as the exposure time is increased. The remainder of the TG-curve is the same as that of unexposed KGa-2.

The XRD data of KGa-2 exposed to DMF shows that no intercalation occurs since the $d_{(001)}$ -spacing remains at 7.2 Å.

Figure 6.21: TG traces of KGa-2 after exposure to DMF vapour for 0, 3, 8, 17 and 30 days.



All the DTG traces of KGa-2 exposed directly to DMF liquid also show no maxima. Their % wt. losses for the first 15 minutes, together with those for the samples exposed to vapour are shown in table 6.15. The % wt. losses are less for the kaolinite exposed to liquid rather than vapour. This is due to the drying procedure since it is difficult to determine between when the clay is dry and when the physisorbed, unstable DMF leaves the clay surface.

Table 6.15: Percentage weight losses during the isothermal stage (0-15 minutes) of the TG experiment.

Exposure criteria	% wt. loss (0-15 minutes)
None	0.4%
3 days in vapour	1.8%
8 days in vapour	1.5%
17 days in vapour	5.8%
30 days in vapour	9.6%
2 days in liquid (25°C)	0.2%
5 days in liquid (25°C)	0.4%
12 days in liquid (25°C)	0.2%
2 days in liquid (80°C)	1.5%

Summary

- No distinct and characteristic maxima are observed for KGa-2/DMF complexes, although very weakly bound DMF is associated with the clay, i.e. the DMF loss during the first 15 minute period. This is expected since similar work involving DMF and kaolinite has been performed. Olejnik et al. [184] have shown that intercalation is very slow and only a small proportion of the kaolinite expands to 12.2Å. They showed that after 42 days in liquid the intercalation ratio was only 0.05 and the addition of H₂O or heating at 60°C caused no apparent increase in the intercalation ratio of DMF into kaolinite. It reacts very weakly with kaolinite because it cannot enter the hydrogen bonding network.
- DMF is already selective in that it interacts strongly with montmorillonite and only very weakly with kaolinite.

6.3.2.3) Illite/DMF complexes

The DTG traces of illite after exposure to DMF vapour for 0 and 17 hours, and, 3 and 30 days are shown in figure 6.22. The % wt. losses for the maxima observed are shown in table 6.16. After 17 hours in vapour the illite has reached maximum interaction with DMF as no further weight losses are observed upon longer exposure times. The original dehydration maximum observed for illite has been replaced by a broader and more intense maximum at 80°C. Whether the water has been replaced by

Figure 6.22: DTG traces of illite after exposure to DMF for 0, 17 hours, 3 and 30 days

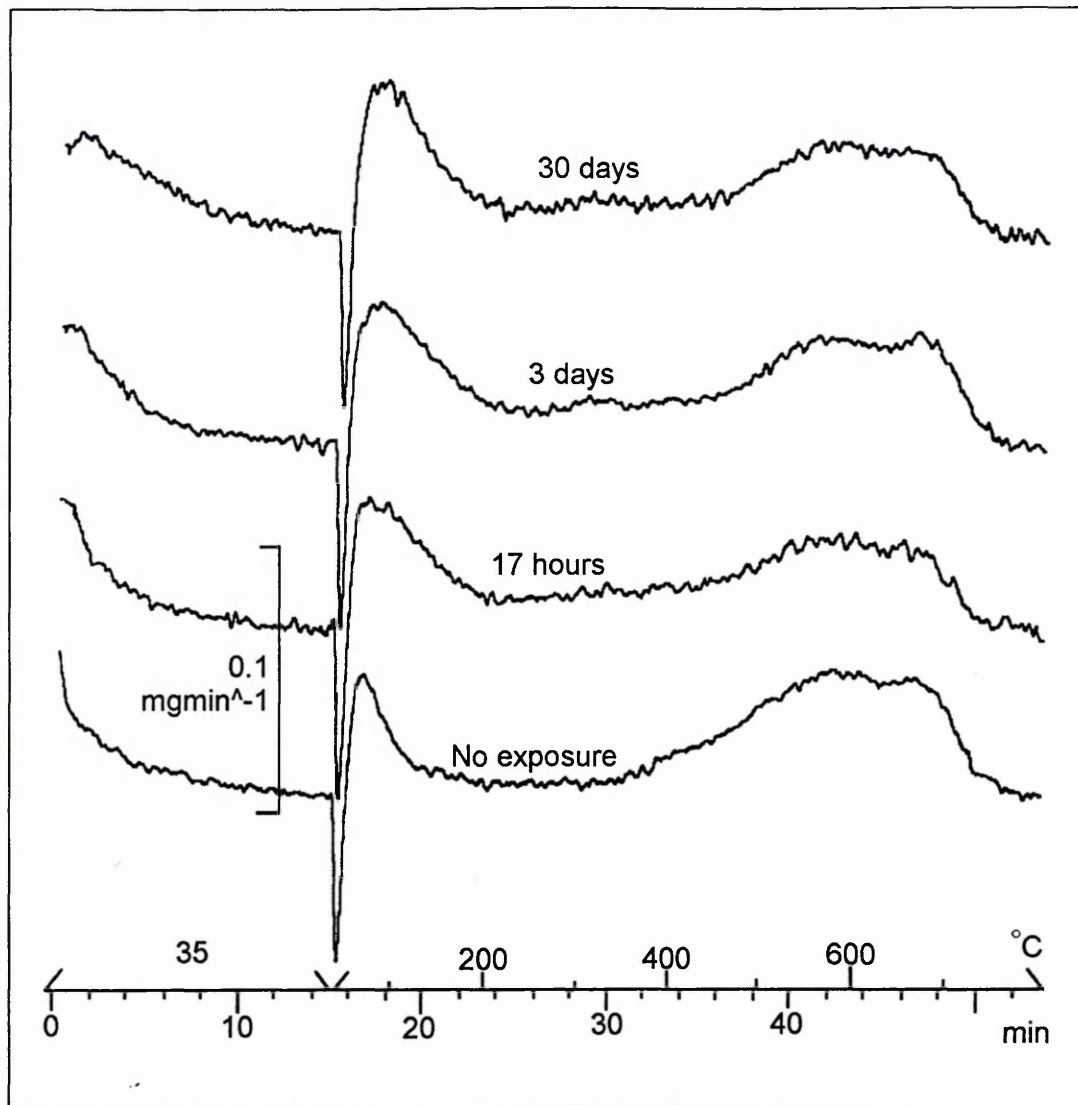


Table 6.16: Percentage weight losses of the maxima observed in the DTG traces of illite/DMF complexes.

Exposure times	Temperatures and (% wt. losses)			
	60°C (-H ₂ O)	80°C	220-440°C	440-760°C (-H ₂ O)
0 days	(0.7%)	140→440°C (1.6%)		(4.7%)
17 hours	-----	(2.3%)	(3.25)	(3.8%)
3 days	-----	(2.3%)	(2.0%)	(4.8%)
8 days	-----	(2.6%)	(1.9%)	(4.7%)
17 days	-----	(2.9%)	(1.9%)	(4.4%)
20 days	-----	(3.1%)	(1.7%)	(4.8%)
30 days	-----	(2.7%)	(1.9%)	(4.4%)

DMF or is still present is not discernible by TGA alone. A small increase in weight loss also occurs between 220-440°C upon exposure to DMF.

The XRD traces of illite exposed to DMF show that no intercalation has occurred since the $d_{(001)}$ -spacing remains at 10.1Å.

Summary

The behaviour of DMF interacting with illite is very similar to that of NMF and illite, although the maximum observed in the former is less broad. This indicates that there are fewer interacting DMF molecules than NMF molecules per gram of clay.

6.3.2.4) TGA of chlorite (CCa-2), quartz, feldspar, and carbonates exposed to DMF vapour.

The DTG traces of CCa-2, Seesand (quartz), feldspar, dolomite, calcite and magnesite after exposure to DMF by the vapour phase show no changes compared to their respective unexposed state. Thus, no significant interaction between the minerals and DMF can be detected by TGA.

Summary of Mineral/DMF interactions

- DMF only interacts strongly with montmorillonite and illite. Montmorillonite becomes intercalated by DMF whereas illite does not. DMF is therefore selective, it could be used to detect the presence of illite and smectite in the presence of the other minerals used in this study.
- DMF has a much faster adsorption/intercalation rate than NMF. The distinctive maxima in their DTG traces for montmorillonite and illite can be seen after only 5 and 17 hours exposure, respectively (probably less for illite, but experiments not yet done). This is considerably less than the 8 days needed for NMF to show distinctive maxima.

- Maxima in X-SWy-2/DMF complexes at lower temperatures are more resolved, due to the temperature of the second highest maximum being lower
- No maxima are observed in the DTG traces of kaolinite/DMF and thus its characterisation would not be directly possible using DMF as a chemical probe.

6.3.3) TGA of other chemical probe/mineral interactions

The DTG traces of the other chemical probe (CY, acetone and DMSO)/minerals proved not to be as unique or distinct as those of the DMF/mineral complexes and are not shown in this thesis.

CY was chosen because it is more volatile than DMF and should therefore interact faster with the minerals. In addition its interaction with montmorillonite clays has already been studied. Breen et al. has investigated the desorption of CY from Ni, Co [263], Na and acid treated montmorillonites [264] by TGA and found that sharp desorption maxima occur. This characteristic is ideal for a chemical probe, since the resolution of maxima will be improved. The results did show that CY adsorbed onto X-SWy-2 much faster than that of NMF and DMF, which was expected. However, sharp characteristic maxima in the DTG traces of the Ca and K-SWy-2/CY complexes were not present. Broad maxima that covered the whole desorption range were apparent. The large range of sites (or environments) of CY in each cation-exchanged montmorillonite has also been observed by Yariv [211, 212] and Ballantine [265]. Types of sites that have been observed are i) protonated CY, ii) chemisorped species such as coordinated CY in which the N atom is coordinated directly to an exchangeable cation, via a water bridge on a hydrated cation, or to the proton of a cyclohexylammonium species via a hydrogen bond. A problem that arose from using CY as a chemical probe is that if CY was to be detected by EGA-FTIR then the low extinction coefficient of the infrared bands in CY are relatively small and thus it will be more difficult to detect.

Acetone did prove to be a good chemical probe in that it is highly volatile, but unfortunately the complexes formed were relatively unstable (compared to NMF and

DMF complexes). Also the DTG traces were not as characteristic as the NMF and DMF/mineral DTG traces.

DMSO did not prove to be a successful chemical probe since the DTG traces of the X-SWy-2/DMSO complexes were not as characteristic as the X-SWy-2/DMF complexes.

Summary of Mineral/Chemical Probe Interactions

The most ideal chemical probe studied so far is DMF since it interacts rapidly and distinct characteristic maxima are observed for each cation-exchanged montmorillonite. The initial objective of the 'chemical probe method' was not to determine the different types of cation-exchanged montmorillonites present but to determine the total amount of montmorillonite present. However these results show that differentiation may be possible. The detection of illite is also possible by DMF, but differentiation between illite and Na and K-exchanged montmorillonites may be difficult because desorption of DMF occurs in the same temperature region. Although this may be the case a knowledge of the total amount of these clays will still be useful. The other four organic molecules studied (DMSO, NMF, CY and acetone) all produced too many maxima and hence distinction between different cation-exchanged montmorillonites was difficult. The interaction of CY and acetone was very fast, whereas that of NMF and DMSO was very slow.

None of the molecules could intercalate kaolinite via the vapour phase at a fast enough rate (although DMSO and kaolinite interactions were not investigated it is assumed a slow process would occur). Thus, the detection of kaolinite is not possible.

In order to detect kaolinite several solutions are proposed:-

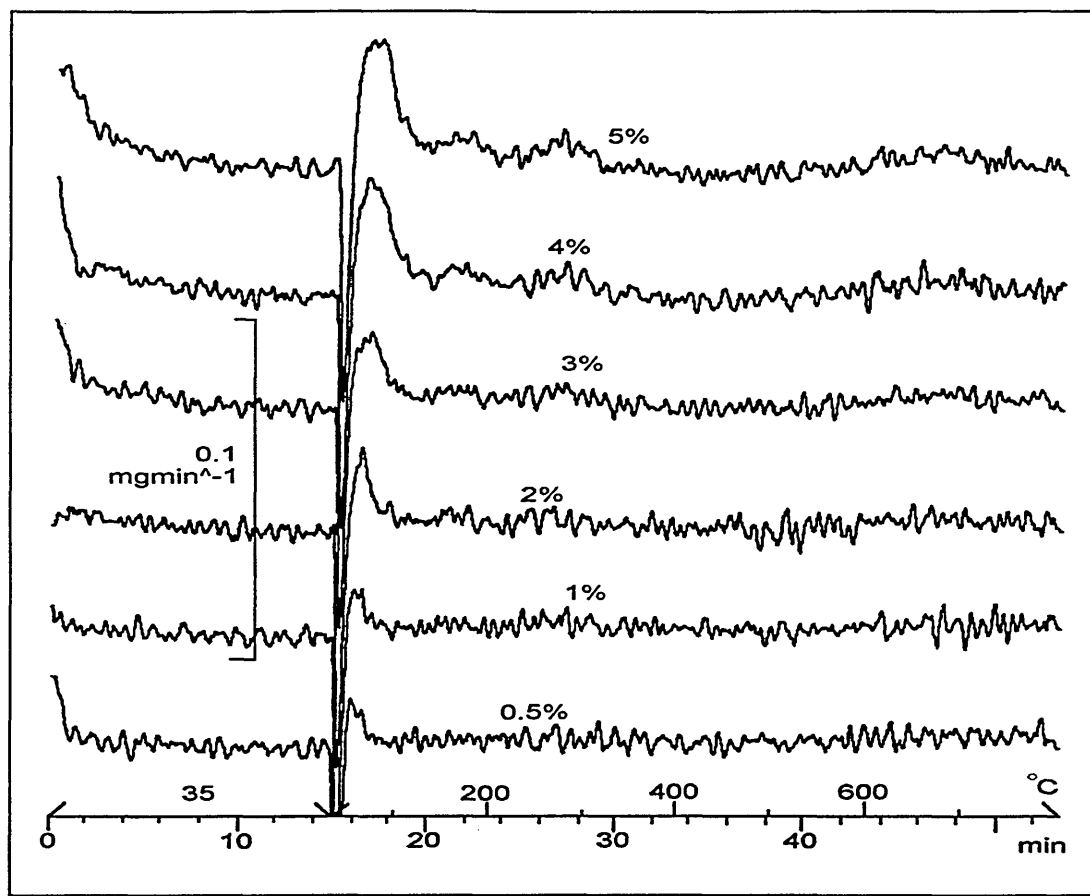
- i) find a chemical probe that can intercalate fast via the vapour phase and produce a characteristic desorption maximum.
- ii) heat the saturation chamber, so that the chemical probe interacts faster
- iii) use the dehydroxylation maximum of kaolinite to detect its presence. Problems will occur using this solution due to shifting maxima caused by different degrees of order of kaolinite.

The minerals quartz, feldspar, chlorite and carbonates could not be detected using organic molecules. This is due to the non-reactive nature of the minerals. A solution to this may be to use a very strong base molecule that will interact with them. However, a stronger base molecule may lead to additional adsorption on the reactive clay minerals leading to the observation of many overlapping maxima.

So far only the major minerals found in rocks have been considered. Kaolinite is sometimes non-reactive to some organic molecules but related minerals to kaolinite, sometimes found in rocks, e.g. halloysite, (which can be considered a kaolinite:H₂O intercalate) is significantly more reactive with respect to intercalation than kaolinite [266, 267]. Costanzo and Giese [267] list 29 organic molecules of which only five intercalate into kaolinite but 19 intercalate into a synthetic kaolinite:H₂O complex, which behaves similarly to halloysite. Churchman and Theng [268] have shown that NMF and DMF intercalate into halloysite to give $d_{(001)}$ -spacings of 10.9 and 12.2Å, respectively. The extent of intercalation of DMF into halloysite is not published and so cannot be compared to the low intercalation ratio of DMF into KGa-2 observed in the results of this thesis.

The samples discussed so far have not been diluted and therefore do not represent the typical concentrations of minerals expected to be found in real sandstones or reservoir rocks. In order to check the sensitivity of TGA seven samples of varying concentrations of SWy-2 (0-5 % wt.) in Seesand were mixed. Their DTG traces were then collected after 3 days exposure to DMF vapour (figure 6.23). The loss of physisorbed DMF between 35-100°C from SWy-2 can only just be detected at the 3% level. The loss of co-ordinated DMF between 100-300°C can only be distinguished at the 5% level (i.e. the maxima at 180 and 230°C). These results show that TGA is not a sensitive enough technique and hence the use of EGA-IR or EGA-MS needs to be employed. The following section goes onto discuss the application of such techniques.

Figure 6.23: DTG traces of SWy-2 (0-5%) mixed with Seesand after exposure to DMF for 3 days.



6.4) Evolved Gas Analysis (EGA) by Infrared and Mass Spectrometry

There are several reasons why EGA must be used in the ultimate characterisation method. The first and main reason is that TGA alone is not sensitive enough to detect low mineral concentrations, whilst the second is that TGA alone cannot determine whether a maximum is due to H₂O or the chemical probe. The basic principles of the synergic analysis system have been outlined in section 2.4.

In this thesis, DMF and NMF-clay mineral interactions have been discussed. DMF has been chosen because it is the most suitable chemical probe investigated to-date and NMF was chosen because it is similar in structure to DMF and the experimental results obtained help to interpret how DMF molecules sorb onto clay minerals.

Whilst studying the desorption of DMF from the clay minerals by EGA there was a suggestion that some of the DMF molecules may be breaking down before reaching the detectors. In order to fully understand the adsorption/desorption mechanisms of DMF on/off clay minerals, the position at which the DMF breaks down needs to be determined. Breakdown of DMF could occur on the clay itself, as it immediately leaves the clay or as it travels along the transfer lines in the synergy system. A factor that needs to be considered whilst determining the breakdown mechanism of DMF is that the synergic analysis equipment is not 100% hermetic, so although inert carrier gases were (N₂ and He) used, oxidation could possibly occur. Water is often a breakdown product of oxidation and thus it would not be possible to determine whether the water observed in an experiment was due to water originally present in the clay or water resulting from oxidation of the chemical probe. However breakdown by pyrolysis could occur, as an alternative to oxidation.

6.4.1) EGA-FTIR/MS analysis of DMF alone

In order to determine the fate of DMF during EGA, two dynamic thermal experiments were performed. One involved keeping the transfer lines, TGA cell, etc. at the usual temperatures (high temperature experiment, table 6.17) whilst the other involved keeping the temperatures below the boiling point of DMF (low temperature

experiment). The DMF was then heated in the crucible from 35-800°C at 20°C/minute after an initial 15 minutes at 35°C. The transfer lines are usually maintained at high temperatures during EGA because this minimises the adsorption of evolved gases which may result in the broadening of maxima in the resulting chromatographs. In effect, during the low temperature experiment the DMF did not encounter a temperature higher than its boiling point until 20.9 minutes into the experiment (i.e. 5.9 minutes after the temperature of the crucible had started to increase). The apparatus in the low temperature experiment was kept at a temperature below the boiling point of DMF because DMF was less likely to breakdown.

Table 6.17: Temperatures of apparatus during the low and high temperature experiments.

	Low Temperature Experiment	High Temperature Experiment
External Heat Zone	145°C	235°C
Transfer line (FTIR)	145°C	240°C
TGA cell (FTIR)	145°C	250°C
Transfer line (MS)	145°C	250°C

TG-Results

The TG data for both experiments were found to be the same. Figure 6.24 shows the TG-curve and the DTG trace for the low temperature experiment. The figure shows that DMF vaporises slowly during the first 15 minutes whilst the crucible was maintained at 35°C. After 15.45 minutes (50°C) the DMF begins to rapidly evaporate and after 35 minutes (240°C) was completely removed. The DTG trace shows a maximum at 25 minutes (135°C).

EGA-FTIR Results

Figure 6.25A, B and C show the infrared spectra of DMF vapour, water vapour and CO₂, respectively. The spectrum of DMF vapour is similar to that of DMF liquid except some bands have shifted and are narrower. Bands of interest in this section of

Figure 6.24: TGA of pure liquid DMF

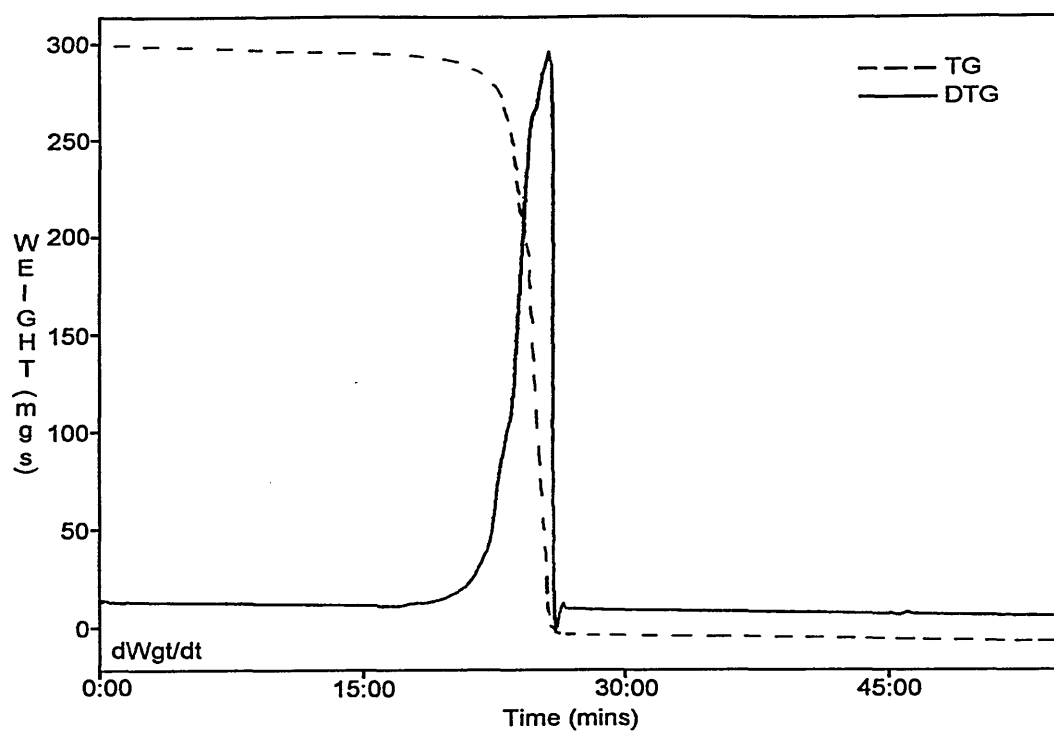


Figure 6.25A: Infrared spectrum of DMF vapour

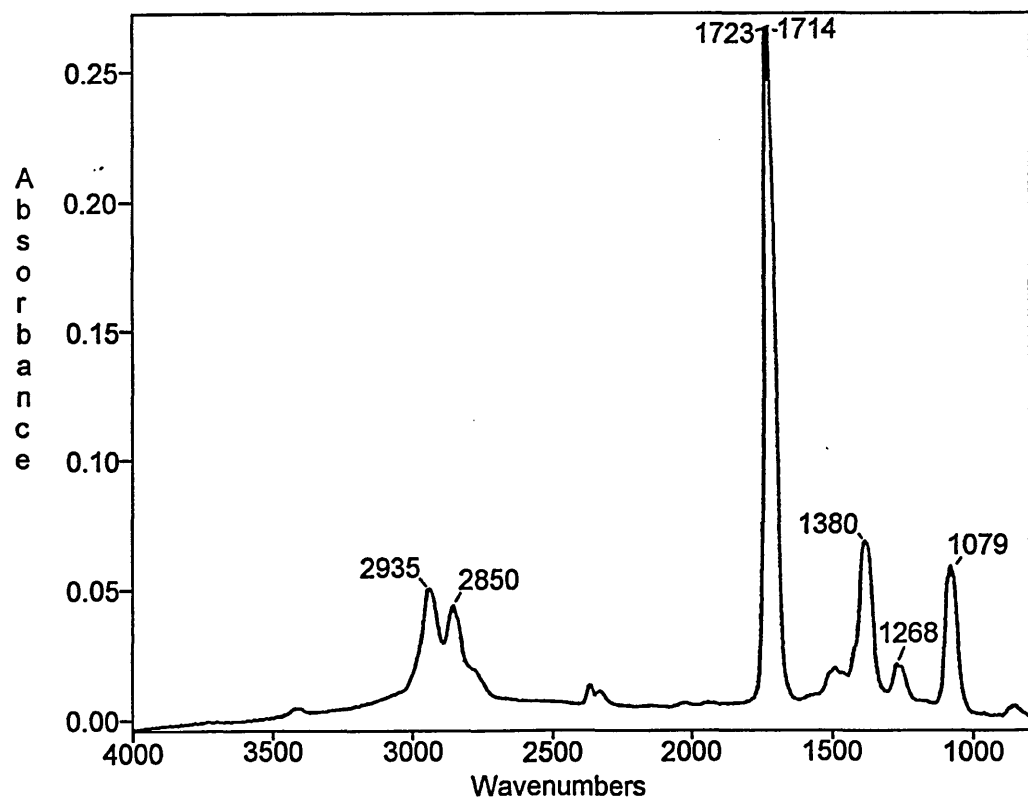


Figure 6.25B: Infrared spectrum of water vapour

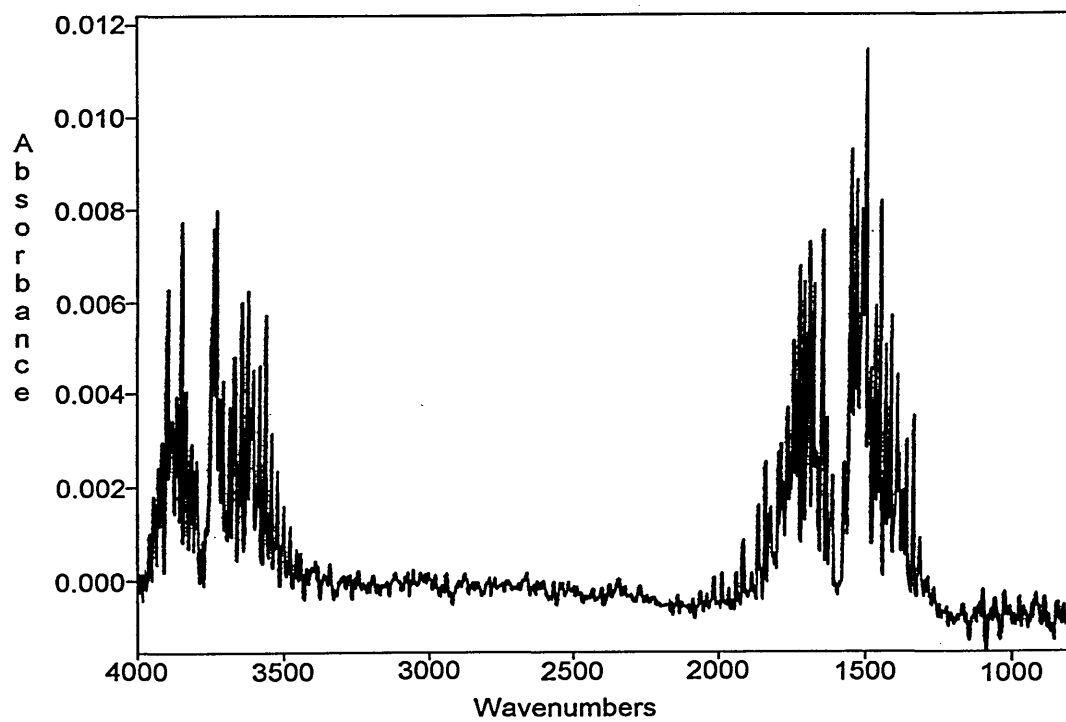
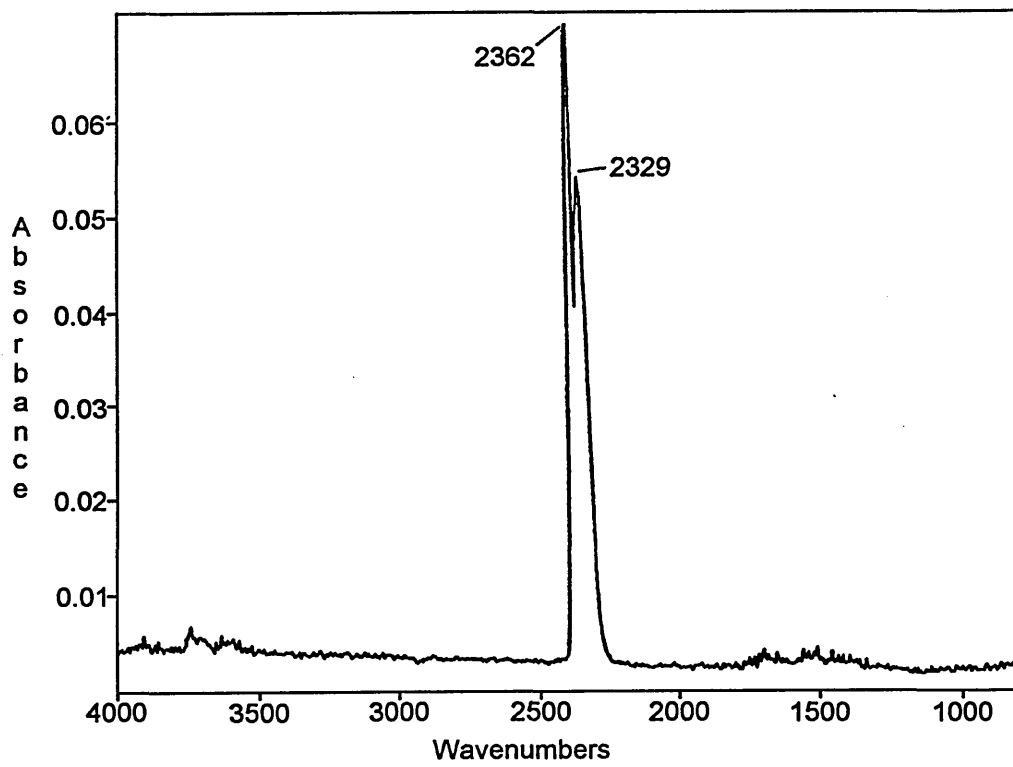


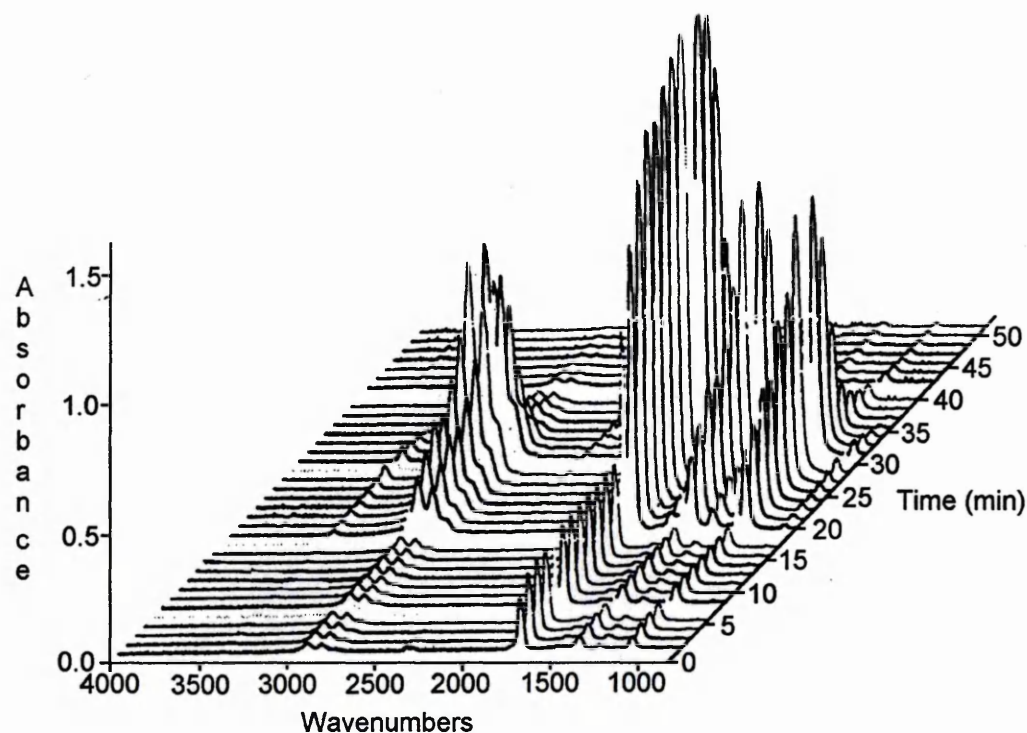
Figure 6.25C: Infrared spectrum of CO₂.



the thesis are the aliphatic ($\nu_s(\text{C-H})$) stretching bands ($3000\text{-}2800\text{cm}^{-1}$) and the carbonyl ($\nu_s(\text{C=O})$) stretching bands ($\approx 1714\text{cm}^{-1}$). The spectrum of water exhibits the expected vibrational/rotational fine structure, whilst the spectrum of CO_2 shows two bands at 2362 and 2329cm^{-1} .

A 3-dimensional (3D) plot of the infrared spectra collected during the low temperature experiment is shown in figure 6.26. This is almost identical to the respective 3D-plot of the high temperature experiment (figure not shown). If the intensity of the $\nu_s(\text{C-H})$ and $\nu_s(\text{C=O})$ bands (which are representative of DMF) are noted during the experiment, it can be stated that i) the amount of DMF detected during the first 15 minutes is constant and ii) as the temperature is increased the amount of DMF detected increases until approximately 32 minutes (375°C). These observations are as expected.

Figure 6.26: EGA-FTIR of liquid DMF obtained from the low temperature experiment



Although the $2400\text{-}2200\text{cm}^{-1}$ region at high temperatures (>35 minutes) in the 3D-plot is hidden by the large, intense $\nu_s(\text{C=O})$ band (due to the 3-dimensional perspective) it can be shown that some bands do appear in this region after approximately 22 minutes

(175°C), which gradually increase in intensity as the time (temperature) increases. These bands can be observed more clearly in the upper two individual spectra shown in figure 6.27. The bands positioned at 2362 and 2329 cm^{-1} are due to carbon dioxide and the bands at 2185 and 2104 cm^{-1} are due to carbon monoxide. A detailed comparison of the four individual spectra suggests that DMF breaks down as it is exposed to higher temperatures. This is noted by comparing the intensity (height) ratios of the $\nu_s(\text{C-H})$ and $\nu_s(\text{C=O})$ bands (table 6.18).

Figure 6.27: Individual infrared spectra collected during the EGA of DMF liquid (low temperature experiment).

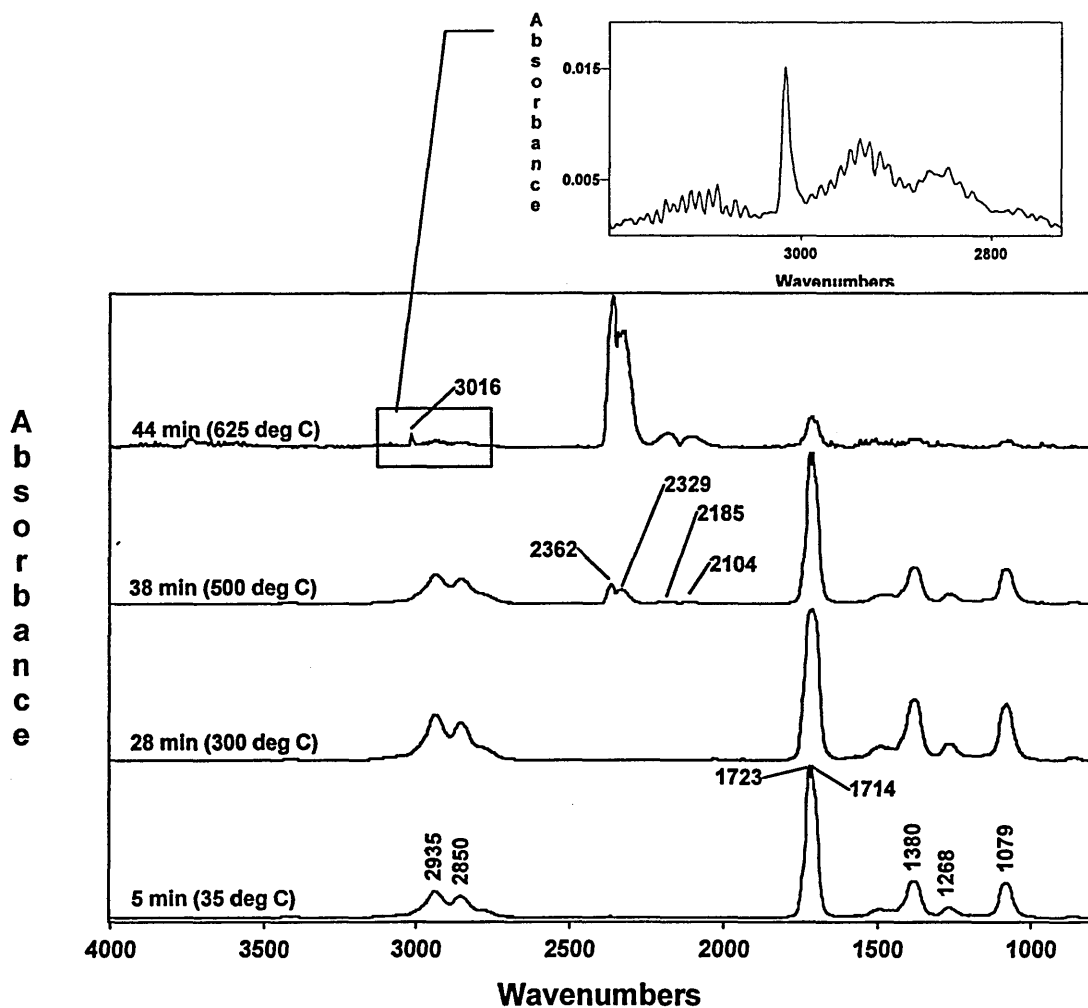


Table 6.18: Intensity ratios of the $\nu_s(\text{C-H})$ and $\nu_s(\text{C=O})$ carbonyl bands observed in the low temperature experiment.

Time (Crucible Temperature (°C))	C-H : C=O
5 minutes (35°C)	1:5.6
28 minutes (300°C)	1:3.4
38 minutes (500°C)	1:5
44 minutes (625°C)	1:4

The table shows that the intensity of the $\nu_s(\text{C=O})$ band decreases relative to the $\nu_s(\text{C-H})$ bands after 28 minutes (300°C). This observation is not completely due to a breakdown of DMF but also reflects the fact the detector is saturated because of the high amount of DMF present (note: the maximum absorbance level is approximately 1.5 in the 3-D plot). At 38 minutes (500°C) the detector is not saturated and the ratio shows that the intensity of the $\nu_s(\text{C=O})$ band has decreased relative to the $\nu_s(\text{C-H})$ bands (also bands due to CO_2 are present). This may be due to the breakdown (or oxidation) of the carbonyl group of the DMF molecules to produce CO_2 .

Although the TG data shows that all the DMF has left the crucible after approximately 25 minutes (235°C), some DMF must linger within the heating zone and transfer lines since DMF is still detected at the end of the experiment. The DMF that remains in the apparatus longer (> 40 minutes) breaks down even further as shown by the intensity ratios of the $\nu_s(\text{C=O})$ and $\nu_s(\text{C-H})$ bands. In addition bands due to carbon monoxide and methane are observed at 2185 and 2104 cm^{-1} , and, 3016 cm^{-1} , respectively.

The changes in intensity of the bands throughout an experiment can be observed more clearly if the intensity at a specific wavenumber or region is plotted against increasing time (or temperature). These are termed reconstructed chromatograms. A selection (H_2O , CO_2 , $\nu_s(\text{C=O})$ and $\nu_s(\text{C-H})$ regions) are shown in figures 6.28A and B, which were obtained from the low and high temperature experiments, respectively. These reconstructed chromatograms show the only major difference between the low and high temperature experiments (i.e. the bulk of the DMF is detected in a narrower time/temperature range in the latter experiment).

In both experiments, DMF is detected in two main stages, as indicated by two broad maxima in the $\nu_s(\text{C-H})$ and $\nu_s(\text{C=O})$ chromatograms. The first stage is the same for both, in that an increase after 17 minutes (75°C) is observed followed by a decrease

after 25 minutes (235°C). This stage corresponds to the removal of the majority of DMF from the crucible. The second stage is different for each experiment. For the high temperature experiment the second stage reaches a maximum after 28 minutes (295°C) and ends after 33 minutes (395°C). This is much narrower than the second stage of the low temperature experiment which reaches a maximum after 31 minutes (355°C) and ends after 37 minutes (475°C). This effect is expected since adsorption/desorption of DMF along the transfer lines, which is continually occurring, is effected by the temperature. At lower temperatures the adsorption process will be relatively more favoured and thus slow the movement of DMF. This effect is known as diffusional broadening.

Figure 6.28A: Reconstructed chromatograms obtained from the low temperature experiment.

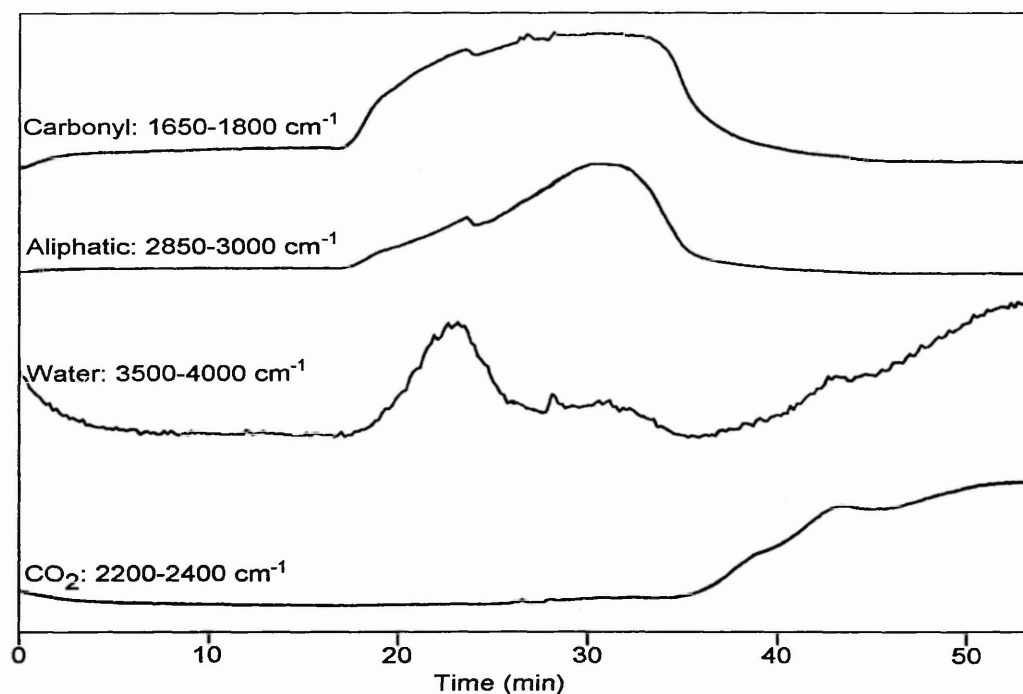
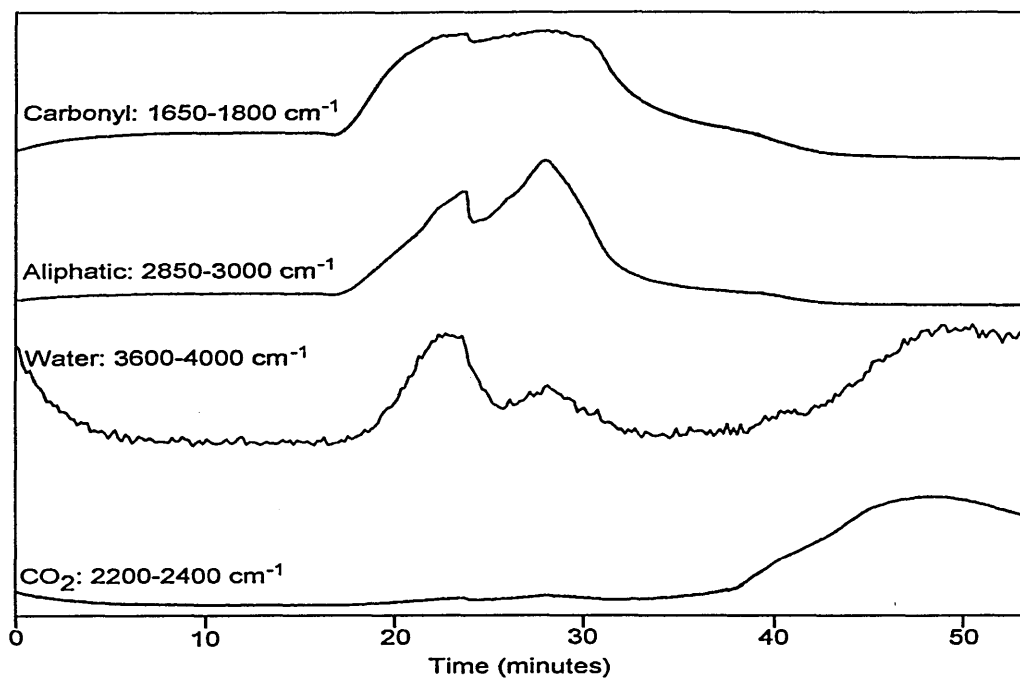


Figure 6.28B: Reconstructed chromatograms obtained from the high temperature experiment.



The reconstructed chromatograms demonstrated that CO₂ was formed after the majority of DMF had passed through the detector. However, some is detected at lower temperatures (i.e. after 22 minutes).

The reconstructed chromatogram formed from the region 3600-4000cm⁻¹ is representative of water. In both the high and low temperature experiments they show that water is detected between; 15-25 minutes (35-235°C), 25-33 minutes (235-395°C) and >35 minutes (435°C). The actual amount of water detected is very small as indicated by the poor signal to noise ratio. The small amount of water may be due to the breakdown of DMF into water or water contamination.

EGA-MS Results

Figure 6.29 shows the mass spectroscopic fragmentation pattern of DMF and table 6.19 shows the expected fragment ions and their relative percentage intensities. The mass spectrum was obtained from the library on the synergy database and is the same as those obtained experimentally by GC-MS. A change in column and injection temperature during GC-MS did not effect the intensity ratios.

In order to monitor the fate of DMF via MS, ion-chromatograms (IC) have been constructed. These are a plot of the intensity of one ion, for example {73}, against increasing time (or temperature). Alternatively a total ion chromatogram (TIC) can be constructed which is simply the sum of all ions against increasing time (or temperature). Figures 6.30 and 6.31 show the TIC and individual ion chromatograms obtained from the high and low temperature DMF experiments, respectively.

The TIC of both the low and high temperature experiments show the detection of ions over a wide time (temperature) range. The detection of ions occurs over a wider time (temperature) range in the low temperature experiment. The TICs show that the ions are detected in two stages, which is more distinct in the low temperature experiment and corresponds with the EGA-FTIR data. The maximum of the second stage occurs after a longer time in the low temperature experiment (i.e. 33 rather than 28 minutes). This is due to diffusional broadening.

Table 6.19: Relative intensities of the fragment ions of DMF and their possible molecular structure.

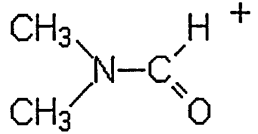
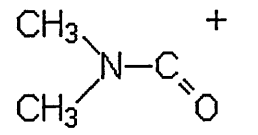
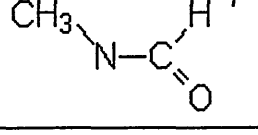
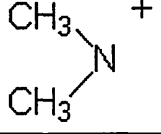
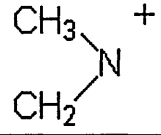
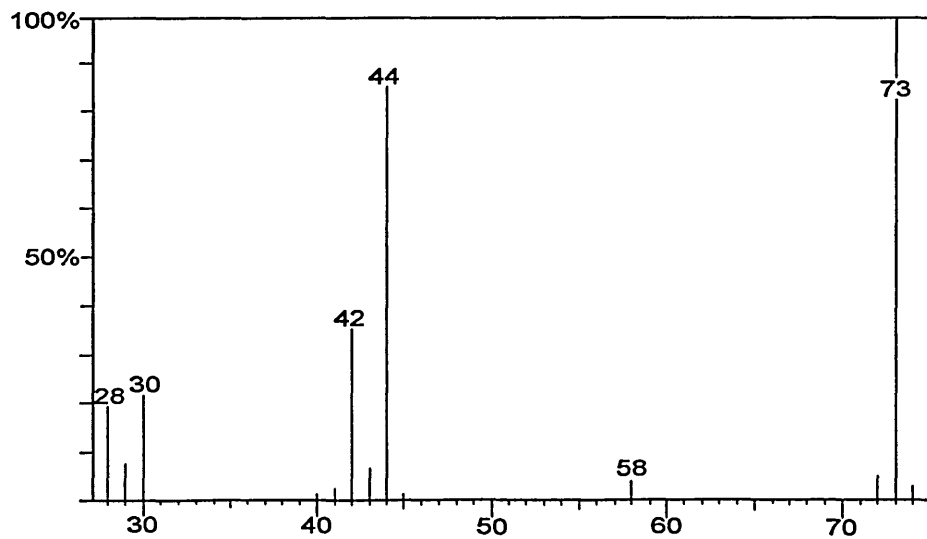
Ion mass	Possible fragment ions	Relative % intensity
73		100%
72		6%
58		4.8%
44		86%
43		7.2%
42	$\text{CH}\equiv\text{N}-\text{CH}_3^+$	36%
30	currently unknown	22%
29	CH_3-N^+ $\text{H}-\text{C}=\text{O}^+$	8%
28	CO^+	20%
15	CH_3^+	no data

Figure 6.29: Mass spectrum of DMF



A comparison of the individual ICs shows that differences are apparent. The numbers in the top right hand corner of each IC represents the intensity of the highest maximum within the IC.

High temperature experiment

The first point to note in the 18-34 minutes (95-205°C) region of the ICs in the high temperature experiment is that two stages are observed. All the ICs apart from the {58}-IC are similar in shape to the TIC. The {58}-IC is different in that its first stage is of similar intensity to its second stage. This means that relatively more of the fragment of mass 58 (CH_3NCHO) is detected in the first phase.

The intensity of the three most intense ion chromatograms observed at 28 minutes (295°C) decrease in the order {44}, {41} and {29}. Also the intensity of the {58} and {73}-ICs are relatively very low. If these are compared to the mass spectrum obtained by GC-MS (figure 6.29) then it is obvious that the ratios are different. In the mass spectrum of DMF obtained by GC-MS the ion of mass 58 is 4.8% the size of the ion of mass 78. In the mass spectrum of the high temperature experiment collected at 28 minutes (295°C) the ion of mass 58 is approximately twice the size of the ion of mass 78, whereas in the low temperature experiment it is approximately the same size. This suggests that the DMF is breaking down before it reaches the detector.

The relative increase in intensity of the {44}-IC could be due to an increased amount of CO_2^+ or the fragment $\text{CH}_3\text{-N-CH}_3^+$. It is unlikely to be CO_2^+ since the infrared spectra shows CO_2 is only observed at times greater than 38 minutes (>495°C). The {29}-IC is also very high compared to the mass chromatogram obtained by GC-MS and could possibly be due to the formation of CH_3N^+ and/or HC=O^+ . A high amount of HC=O^+ would correspond with a high amount of $\text{CH}_3\text{-N-CH}_3^+$ since it simply involves the cleavage of one bond in the DMF molecule.

The {41}-IC is also very high and is not observed in the mass chromatogram obtained by GC-MS. Its assignment is somewhat indistinct, but it may be due to the formation of $\text{C}\equiv\text{N-CH}_3^+$.

Figure 6.30: TIC and ICs obtained from the high temperature experiment

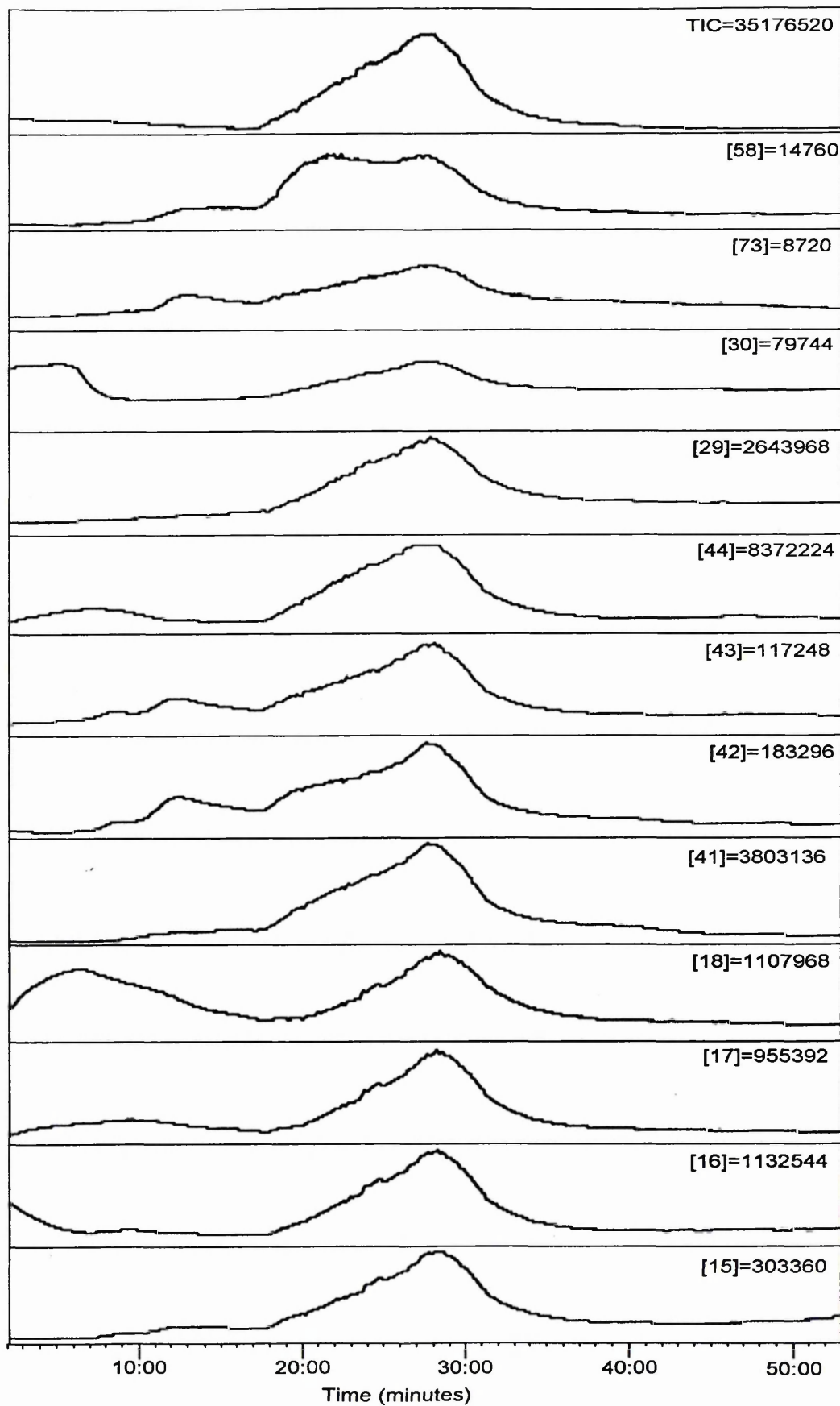
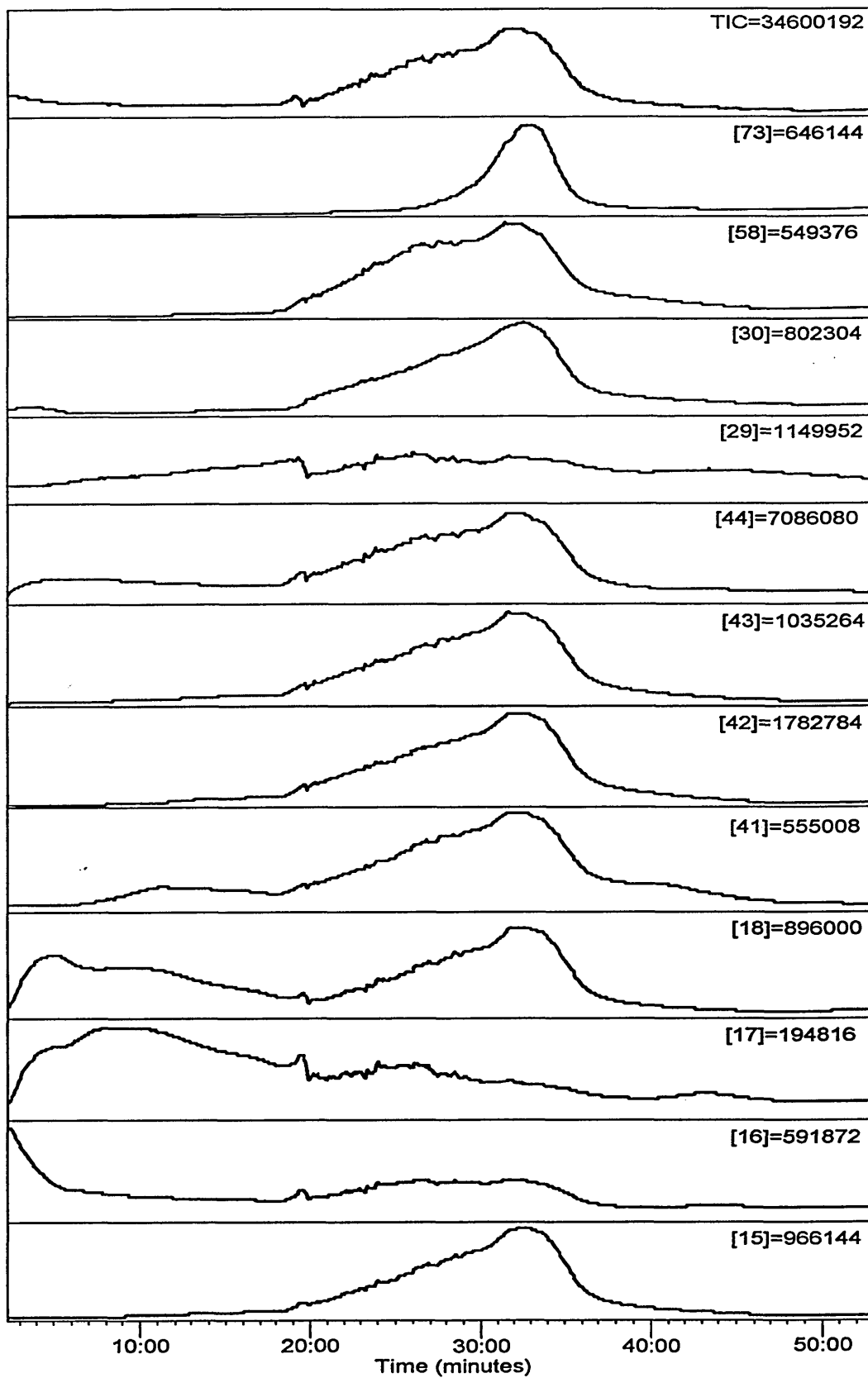


Figure 6.31: TIC and ICs obtained from the low temperature experiment



The {18} and {17}-ICs are similar in shape to the other ICs. It was originally thought that these were due to the presence of water, but the intensity ratio of {18}:{17} is 100:86. Since the intensity ratio of pure water is 100:20 this indicates another product is formed. A possible product could be ammonia (molecular weight =17) which also has a fragment ion of 16. The {16}-IC is also the same shape as the {17}-IC and thus supports this assignment. Unfortunately, the intensity ratio of the {17}:{16}-ICs in pure ammonia is 100:80 but in the ICs of the high temperature experiment it is 84:100. Either the temperature of the transfer lines causes the ammonia to degrade to NH_2 (which is not likely) or it is not due to ammonia. The EGA-FTIR does not indicate the presence of ammonia.

Low temperature

The individual ICs (except for the {73} and {58}-ICs) of the low temperature experiment are similar in shape to the TIC. The {73}-IC is more prominent in its second stage whereas the {58}-IC is more prominent in its first stage. This indicates that a higher proportion of DMF is observed in the second stage and there is a higher proportion of the ion of mass 58 in the first stage.

If the intensity ratios of the ICs at 33 minutes in the low temperature experiment are compared to those in the high temperature experiment then it can be noted that the {73} and {58}-ICs are much more intense relative to the {44}-IC in the former. This indicates that there are relatively more DMF molecules and CH_3NCHO^+ fragments, respectively, reaching the detector in the low temperature experiment. This infers that the DMF molecules do breakdown in the transfer line and more so at higher temperatures.

Summary

The results show that breakdown of DMF does occur along the transfer lines, although it is not clear how. Breakdown of DMF whilst on the clay is unlikely (see VT-DRIFTS results later, section 7) but may occur as it immediately leaves the clay. The complexity of the MS results means that although DMF is not an ideal chemical probe

to be studied by EGA-MS it does establish that the strategy is potentially very useful. One problem is that the main fragment ion has a mass of 44 which is the same as CO_2^+ and thus a distinction between the two would not be possible. CO_2^+ could therefore not be used to detect the presence of carbonate.

Nonetheless some clay mineral/DMF interactions have been studied by EGA-FTIR and EGA-MS, in order to demonstrate the sensitivity of these techniques.

During the research for this thesis many experiments have been performed on the mineral/DMF complexes using the same parameters as the low and high temperature experiments. However, the majority of the results discussed in this thesis were obtained using the same parameters as the high temperature experiment unless otherwise stated.

The reason why two stages are observed in the data obtained from the liquid DMF is probably due to the large amounts of DMF used in the experiments. The amounts of DMF desorbed from the minerals in the following experiments are only a fraction of the amount used in the liquid DMF experiments and thus the DMF is not detected in stages.

6.4.2) EGA of individual clay minerals and clay mineral/DMF complexes.

Primarily undiluted, pure powdered clay minerals before and after exposure to DMF were studied by EGA. This was performed in order to determine whether similar desorption traces to those obtained via TGA could be achieved. In addition, the identity of the products under each desorption maximum could be ascertained.

6.4.2.1) Na, Ca-SWy-2 and Mg-SWy-2/DMF

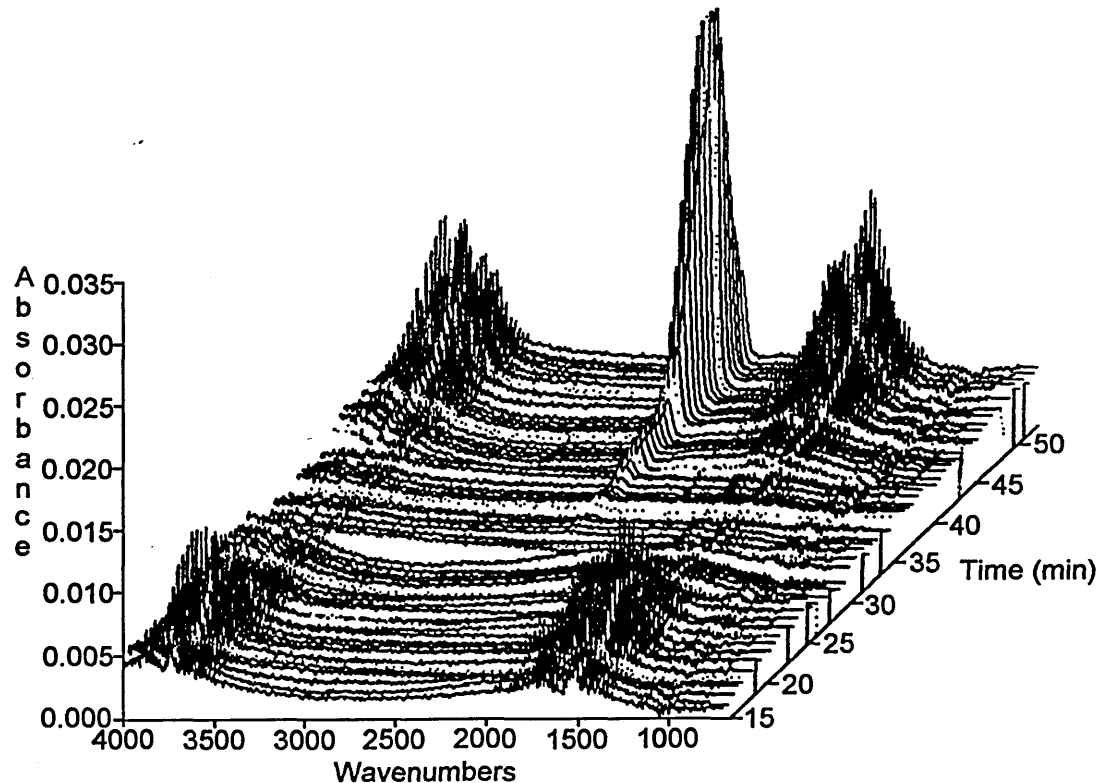
The DTG traces obtained from the Mettler TGA and the Synergic Analysis system of all samples are almost identical. Thus the DTG traces shown in sections 6.1 and 6.2

(obtained via the Mettler system) can be directly compared to the EGA-FTIR and EGA-MS data.

Na, Ca-SWy-2

Figure 6.32 shows a 3D-plot of the infrared spectra obtained from the evolved gases of Na, Ca-SWy-2 (without any pretreatment) as it was heated from 35-800°C at 20°C/minute (the initial 15 minutes are not plotted). The plot clearly shows that water is detected at the start and end, which relate to the removal of physisorbed water and dehydroxylation of the clay structure, respectively. Some CO₂ is also observed at high temperatures. Although the intensity of the CO₂ bands are higher than those of H₂O, very little CO₂ is actually present because the extinction coefficient of H₂O is much lower than that of CO₂ (this fact needs to be considered in all of the following figures). Its occurrence could be due to the presence of carbonate impurity or more likely trapped CO₂ within the Na, Ca-SWy-2 sample.

Figure 6.32: EGA-FTIR of Na, Ca-SWy-2 (sample weight 27 mg)



Dehydroxylation of the clay is detected by EGA-FTIR between 40 (535°C) and greater than 53 minutes (795°C) and rises to a maximum at 51 minutes (755°C) (see reconstructed chromatograms in figure 6.33).

Figure 6.33: Reconstructed chromatograms of water and CO₂ obtained from Na, Ca-SWy-2

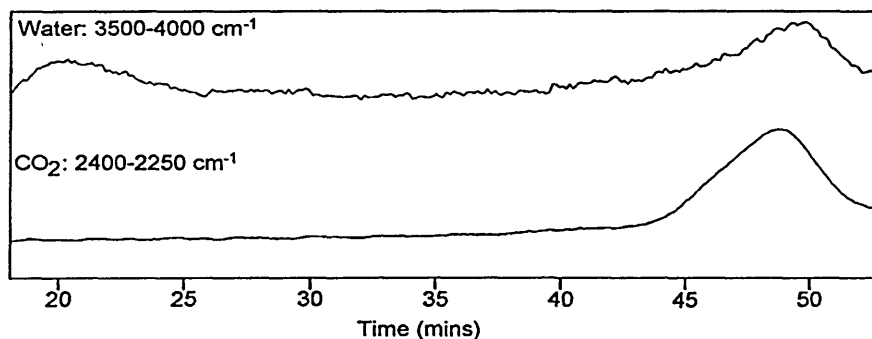


Figure 6.34: DTG trace of Na, Ca-SWy-2 (obtained from the Synergic system)

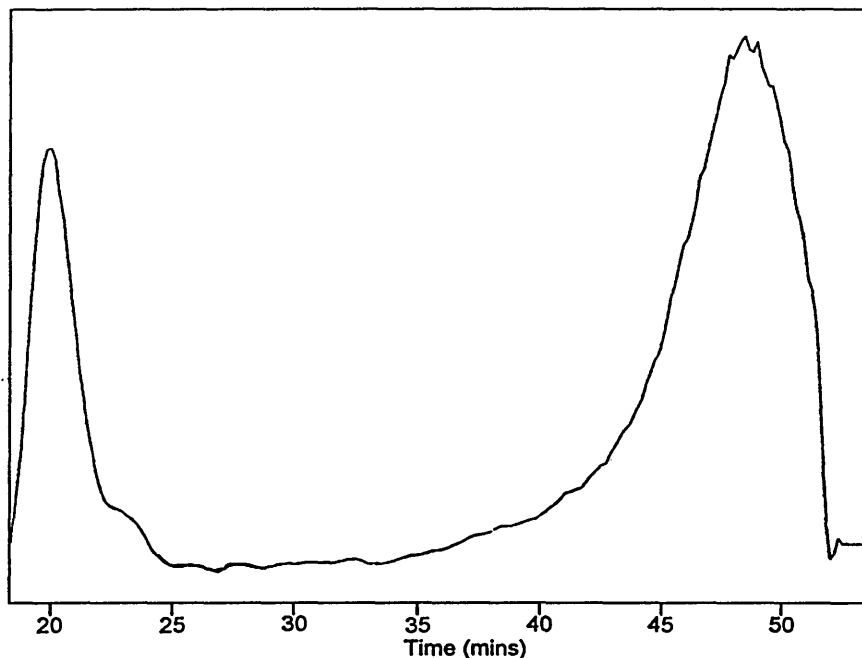
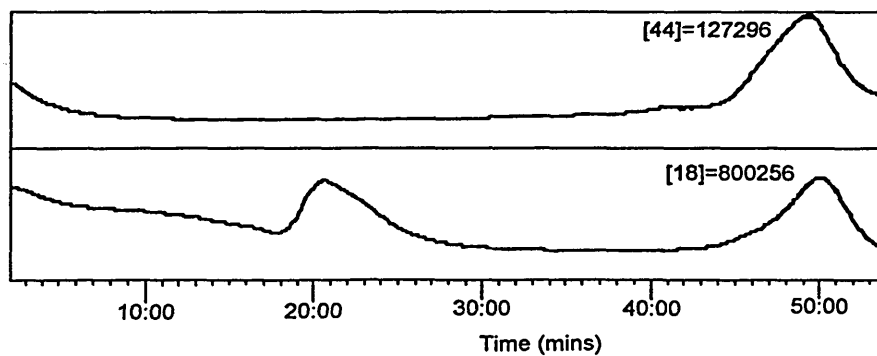


Figure 6.35: ICs obtained from Na, Ca-SWy-2



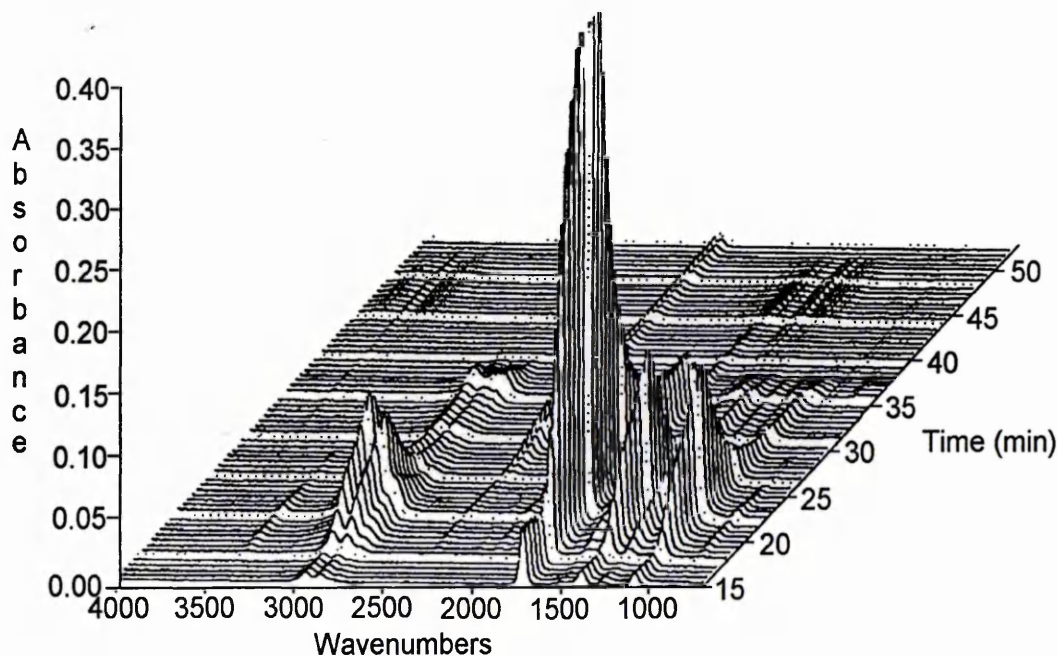
The corresponding maximum in the DTG trace (figure 6.34) occurs between 38-53 minutes (495-795°C) and reaches maximum intensity after 48 minutes (695°C). This indicates that it takes approximately 2-3 minutes to travel from the crucible to the infrared detector and some diffusional broadening occurs. The analysis of the evolved gases by MS also reveal the detection of water and CO₂. The {18} and {17}-ICs (representing water) exhibit the same pattern as the IR-chromatograms of water and is therefore also liable to diffusional broadening (figure 6.35).

Mg-SWy-2/DMF

EGA-IR results

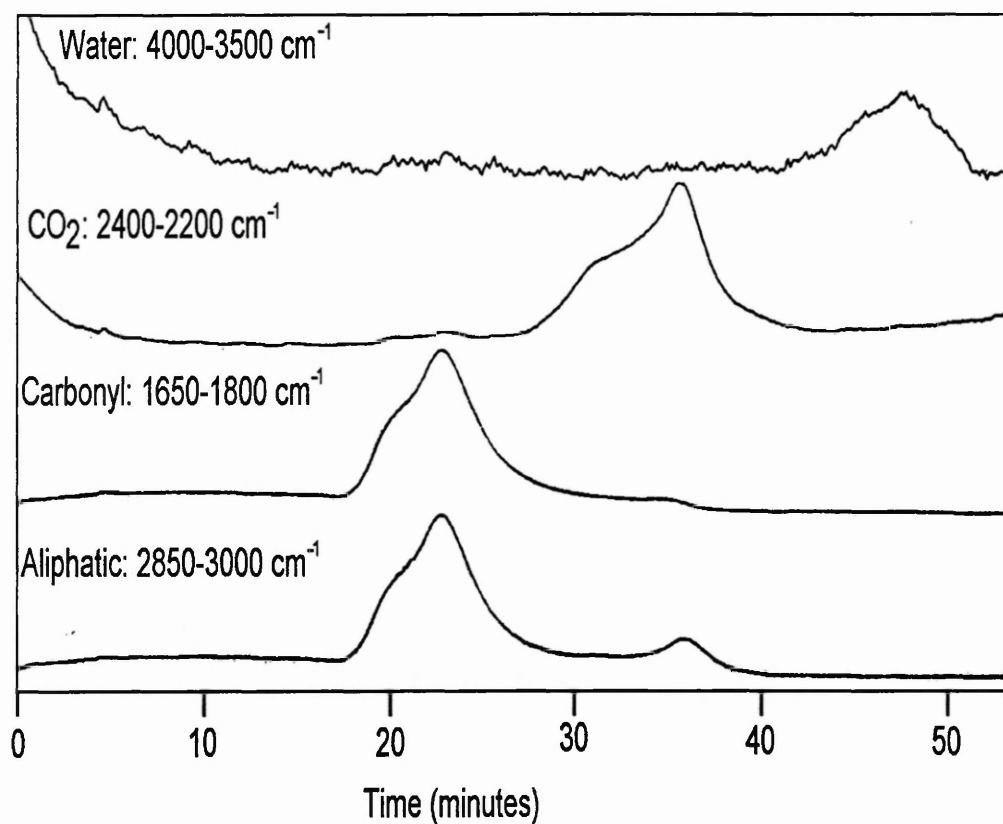
Figure 6.36 shows the 3D-plot of the infrared spectra obtained from the evolved gasses of Mg-SWy-2 after treatment with DMF vapour for 30 days (the initial 15 minutes are not plotted).

Figure 6.36: EGA-FTIR of Mg-SWy-2 after exposure to DMF vapour for 30 days (sample weight=38mg).



The plot shows that infrared bands due to DMF are observed as the temperature begins to increase and are followed by the infrared bands of water. Bands between $2400\text{-}2000\text{cm}^{-1}$ are also observed throughout the run. The reconstructed chromatograms of the regions $4000\text{-}3500\text{cm}^{-1}$ (water), $2850\text{-}3000\text{cm}^{-1}$ ($\nu_s(\text{C-H})$), $1650\text{-}1800\text{cm}^{-1}$ ($\nu_s(\text{C=O})$) and $2400\text{-}2200\text{cm}^{-1}$ (CO_2) are shown in figure 6.37.

Figure 6.37: Reconstructed chromatogram obtained from the EGA-FTIR of Mg-SWy-2/DMF.



The reconstructed chromatogram of water shows a decrease at the start of the run (0-10 minutes, 35°C) and a maximum at 47 minutes (675°C). The water at the start is present because when the sample is placed into the crucible atmospheric water vapour is introduced into the instrument, which travels along the transfer lines to the detector. The removal of the atmospheric water vapour takes approximately 10 minutes. The maximum at 47 minutes (675°C) is due to dehydroxylation of the clay. Note that no water is observed during the desorption of DMF, and this indicates that only DMF is

coordinated to the clay. Note also that the extinction coefficients of DMF are much higher than those of water.

The $\nu_s(\text{C}=\text{O})$ and $\nu_s(\text{C}-\text{H})$ reconstructed chromatograms monitor the desorption of DMF. Their traces are similar but the latter exhibits a more distinct maximum at 36 minutes (455°C). This maximum corresponds to the characteristic maximum observed in the respective DTG trace at 400°C (figure 6.16). The reasons why these traces are not as resolved as the DTG traces could be 3-fold:-

- i) diffusional broadening occurs along the transfer lines,
- ii) DMF is desorbed from the clay between 22 and 33 minutes (180 and 400°C) but is not represented in the DTG trace because it is lost at a constant rate. However, the EGA-FTIR does represent the loss and thus the distinction is not as clear
- iii) breakdown of DMF occurs at higher temperatures. This is indicated by comparing the CO_2 and $\nu_s(\text{C}=\text{O})$ chromatograms. The CO_2 chromatogram shows that CO_2 is detected at the same time as the maximum at approximately 34 minutes (400°C). CO_2 will derive from the carbonyl group of DMF upon breakdown and thus a decrease in the $\nu_s(\text{C}=\text{O})$ chromatogram at 400°C is noted.

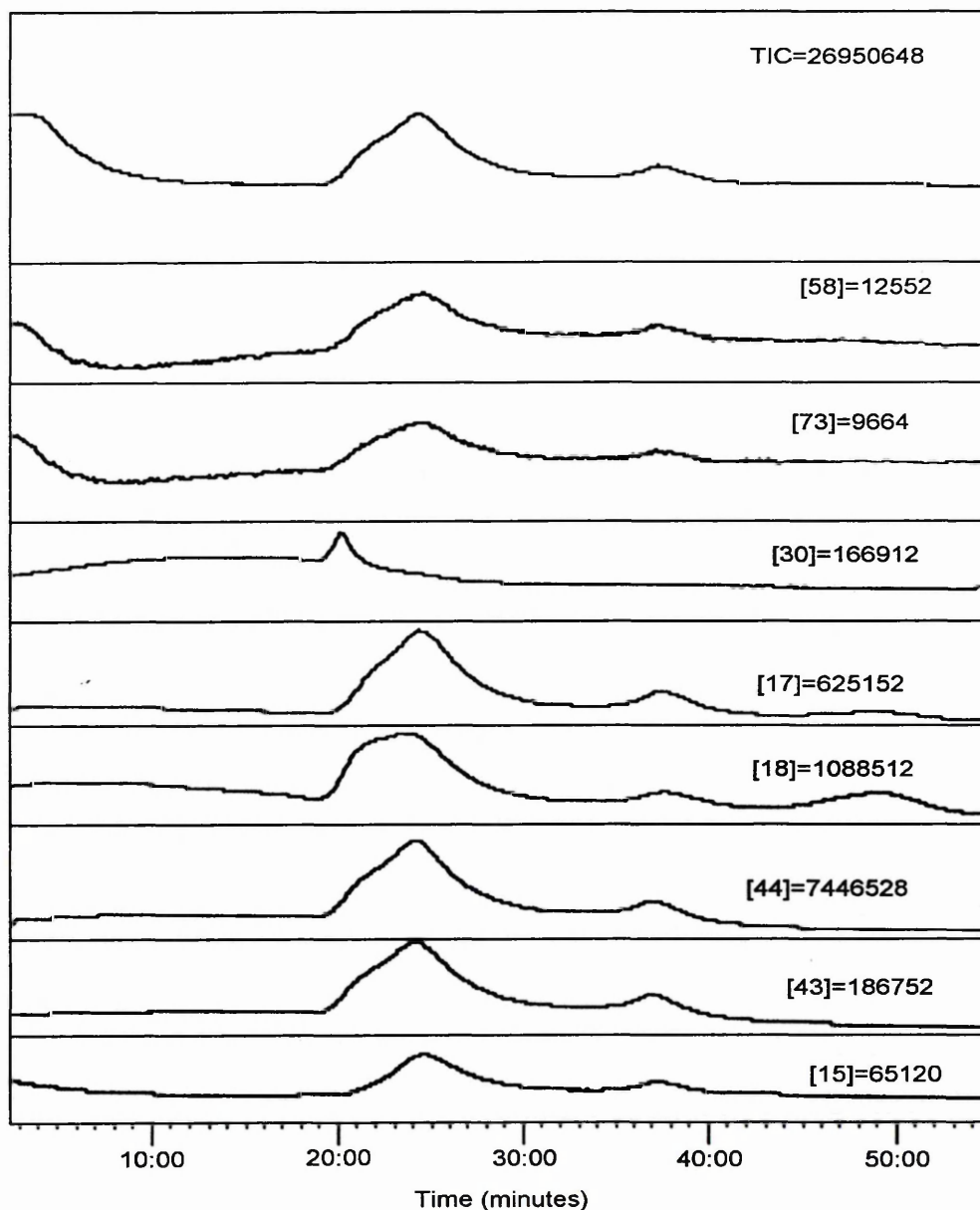
These results show that the desorption of DMF from Mg-SWy-2 can be monitored by EGA-FTIR so that a similar trace to that of its DTG can be obtained. The $\nu_s(\text{C}=\text{O})$ chromatogram does not resemble the DTG trace as well as the $\nu_s(\text{C}-\text{H})$ chromatogram. This is unfortunate because the carbonyl stretching band has a higher extinction coefficient than the $\nu_s(\text{C}-\text{H})$ bands. Detection at low concentrations would therefore be more difficult using the $\nu_s(\text{C}-\text{H})$ chromatogram rather than the $\nu_s(\text{C}=\text{O})$ chromatogram.

EGA-MS results

Figure 6.38 shows the TIC and some individual ICs obtained from the DMF treated Mg-SWy-2. The shape of the TIC is similar to the DTG trace in that maxima are present at 24 and 37 minutes (180 and 400°C, respectively). In addition a shoulder to the left of the maximum at 24 minutes (215°C) is observed. The TIC does not clearly show a maximum at 49 minutes due to the dehydroxylation of the clay but is observed

in the individual ICs representing water. The TIC is more similar to the DTG trace than the IR-chromatograms in that the maximum at approximately 400°C is more resolved. The decrease in intensity in the TIC at the very start of the run (0-10 minutes) is due to atmospheric air entering the instrument whilst the sample is placed in the crucible.

Figure 6.38: TIC and ICs obtained from Mg-SWy-2 after exposure to DMF vapour for 30 days (high temperature experiment).



Not all the individual ion chromatograms show the same distinct trends as the TIC. The {73} and {58}-ICs are quite weak, which is expected since the experiments

involving only liquid DMF using the same temperature parameters for the transfer lines, etc. showed similar results. This indicates that very few intact DMF molecules are reaching the MS detector. The {30}-IC behaves differently in that only a maximum at approximately 24 minutes is observed. The {15}-IC follows the same pattern as the TIC.

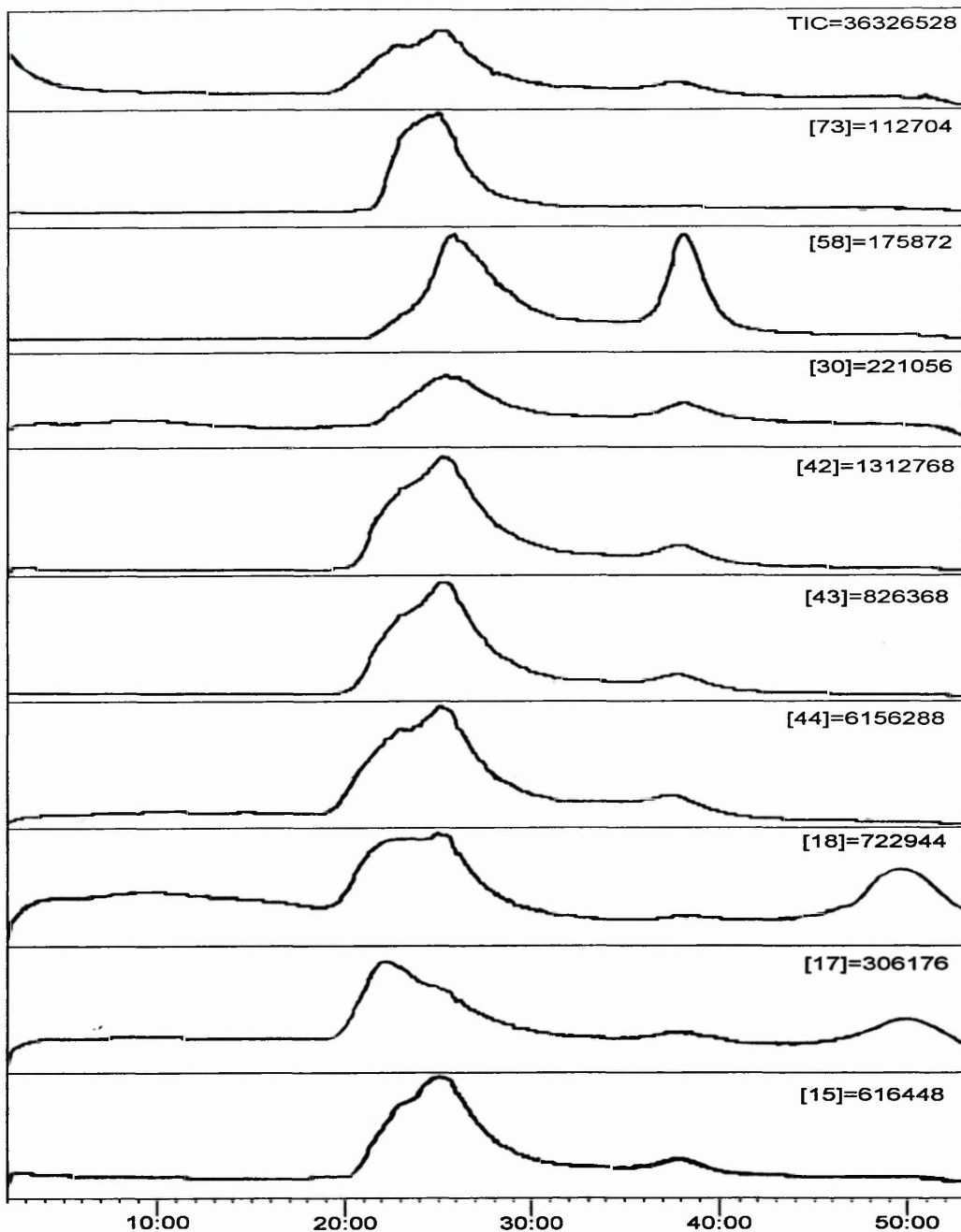
The {18} and {17}-ICs show three peaks at 24, 37 and 48 minutes (215, 475 and 695°C). The last maximum is due to dehydroxylation of the clay and is confirmed as being water because their ratios are 100:20 ({18}:{17}, respectively). The first two maxima are not due to water (their ratios are 100:58) and must therefore be due a breakdown product or fragment of a breakdown product. The EGA-FTIR data confirms that water was not present in the first two maxima but was in the third.

The most abundant ion detected throughout this experiment has a mass of 44. Its IC and also the {43}-IC are very similar in shape (in the 19-43 minute region) to that of the DTG trace. A molecule/fragment that could produce a mass of 44 is $\text{CH}_3\text{-N-CH}_3^+$ or CO_2^+ . The majority of the IC is likely to be due to $\text{CH}_3\text{-N-CH}_3^+$ and not CO_2^+ because significant quantities of CO_2 in the infrared data were only observed between 30-40 minutes (335-535°C).

An interesting observation noted in the experiments of the EGA-MS of Mg-SWy-2 exposed to DMF performed using the same parameters as the low temperature experiment is that the {58}-IC provides a very distinct pattern (figure 6.39). Since a higher proportion of the ion of mass 58 is present at higher temperatures the characteristic maximum at 400°C is much more prominent and easily distinguishable. This behaviour could be exploited in order to detect the presence of montmorillonite within a mixture.

Summary

It has already been shown that DMF breaks down as it travels through the transfer lines to the detector. Even less DMF travels to the detector from the crucible when it is associated with Mg-SWy-2 than when it is in its liquid state. This is indicated by a Figure 6.39: TIC and ICs obtained from Mg-SWy-2 after exposure to DMF vapour for 30 days (low temperature experiment).



higher proportion of ions (of mass 73) detected in the latter.

These results therefore suggest that DMF does not only breakdown as it travels through the transfer lines but it also breaks down as it leaves the clay. Whether it is present as DMF when complexed to the clay cannot be ascertained via these results. However, VT-DRIFTS results which will be discussed in chapter 7 show that DMF is complexed on the clay and thus breakdown occurs as it leaves the clay.

Although the breakdown and fragmentation of DMF is unknown, ion chromatograms (e.g. {44}, {18} & {17}-ICs) can be obtained from the Mg-SWy-2/DMF complex that are similar in shape to those of the DTG traces. Unfortunately, there is a breakdown product/fragment of DMF that has a molecular weight the same as H₂O and thus distinction between the two cannot be achieved.

6.4.2.2) Illite and illite/DMF

Illite

A 3D-plot of the infrared spectra collected during EGA of illite alone is shown in figure 6.40. Three events occur:-

- i) H₂O is evolved between 15-25 minutes (35-235°C), which is due to the loss of physisorbed water,
- ii) H₂O is evolved between 35-48 minutes (435-695°C), which is due to dehydroxylation of the clay,
- iii) CO₂ increases gradually from 30-45 minutes (335-635°C) and then rises to a maximum after approximately 50 minutes (735°C). This could be due to trapped CO₂ within the clay structure, carbonate impurity in the illite, or organic contaminants adsorbed on the illite.

The reconstructed chromatograms for CO₂ and water are shown in figure 6.41. The DTG trace (figure 6.21) of illite showed two broad maxima between 35-53 minutes (435-795°C) which were both originally attributed to dehydroxylation. The reconstructed chromatograms indicate that dehydroxylation of the illite does not occur over such a wide temperature range since water is not detected over the whole region. The EGA-MS data (figure 6.42) supports this observation. Water represented by the {17} and {18}-ICs shows two maxima, the first is due to the loss of physisorbed water and the second is due to dehydroxylation of the clay. CO₂ is represented by the {44}-IC and shows the maximum in the DTG trace at approximately 52 minutes (645°C) is not due to dehydroxylation, but is more likely to be due to carbonate impurity.

Figure 6.40: EGA-FTIR of illite (sample weight = 46mg)

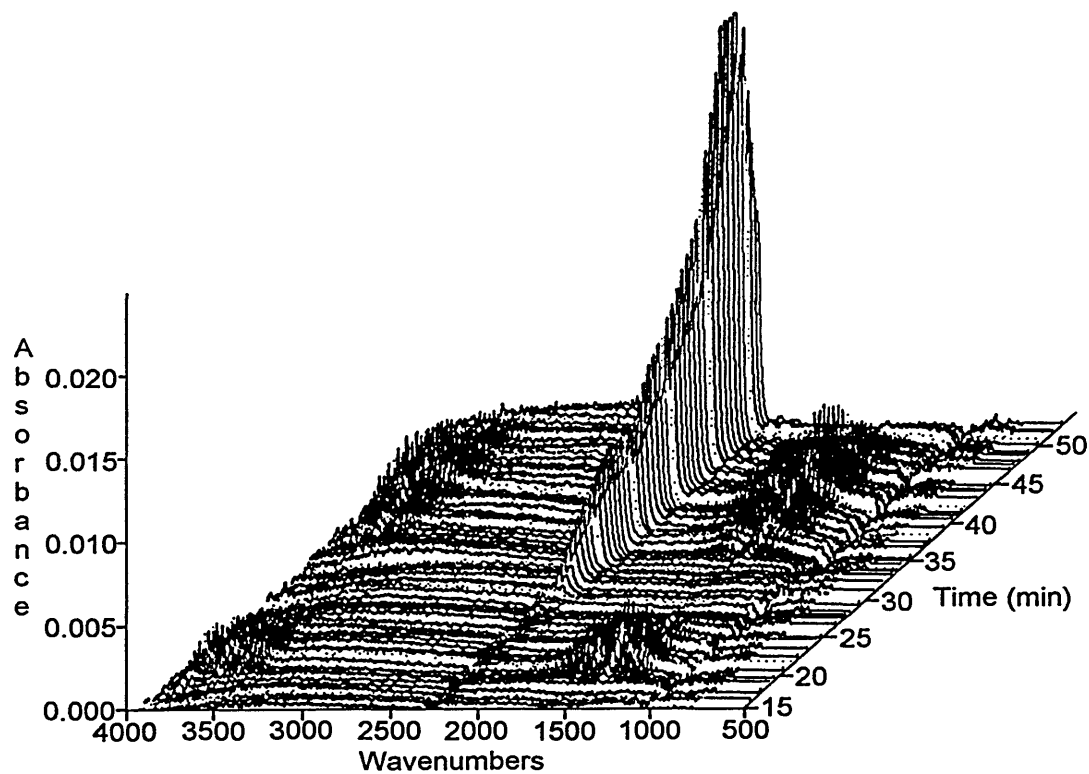


Figure 6.41: Reconstructed chromatograms for water and CO₂ obtained from illite

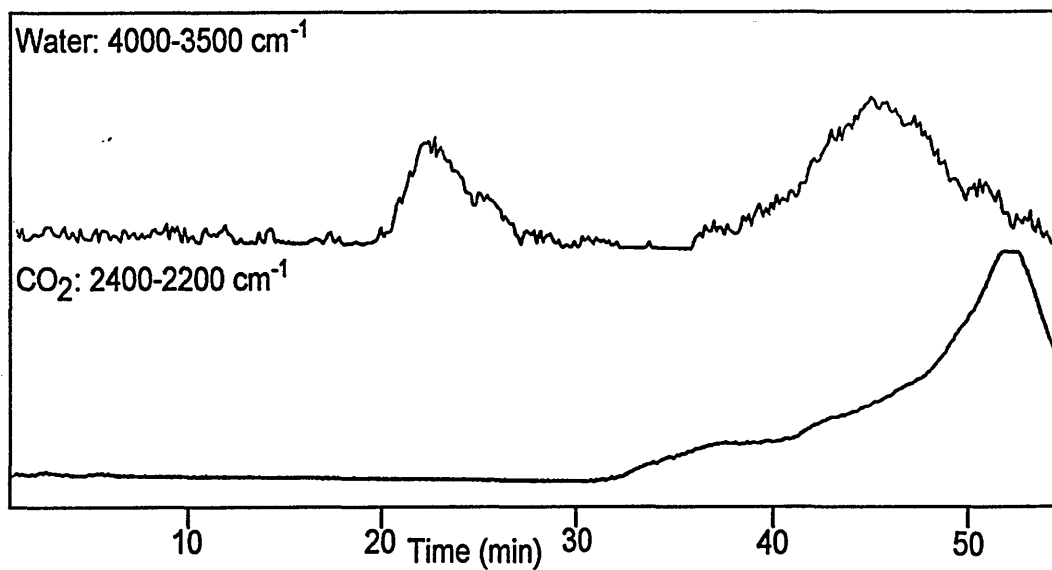
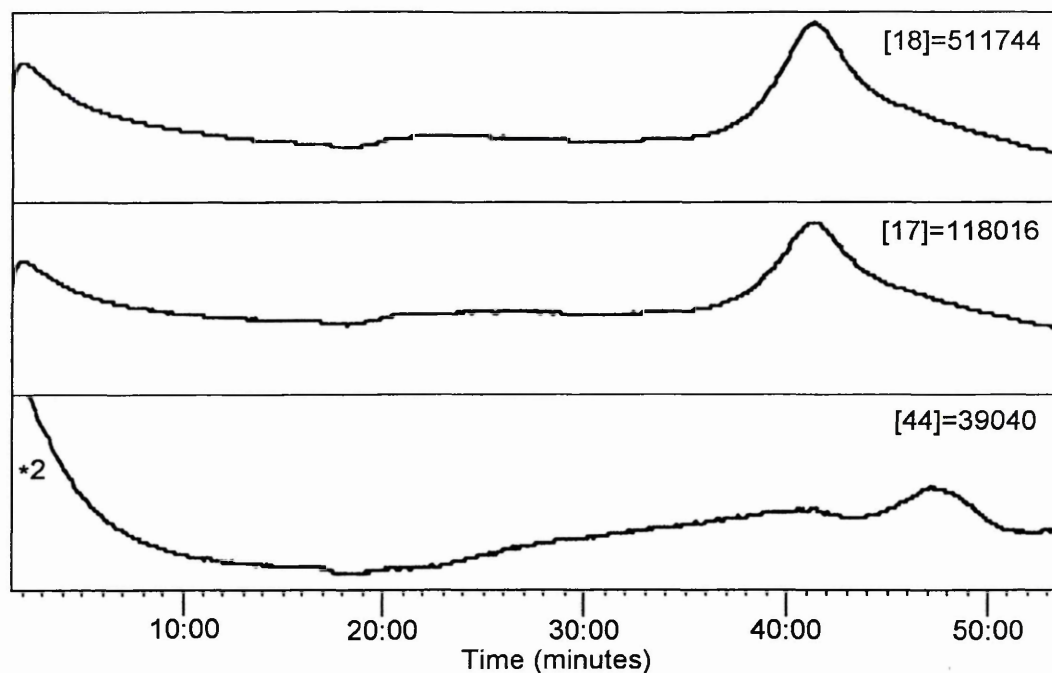


Figure 6.42: Ion chromatograms obtained from illite



Illite/DMF

Figure 6.43 shows a 3D plot of the infrared spectra collected during the EGA of illite which has been exposed to DMF vapour for 22 days. The reconstructed chromatograms for CO_2 , $\nu_s(\text{C-H})$, water and the $\nu_s(\text{C=O})$ bands are shown in figure 6.44.

The figures show that water is detected between 35-48 minutes ($435\text{-}695^\circ\text{C}$), which is due to dehydroxylation of the clay. They also show that the loss of water in the 15-25 minute ($35\text{-}235^\circ\text{C}$) region observed in the unexposed mixture is no longer present. This is because the water has been replaced by DMF. The DMF bands reach a maximum after approximately 20 minutes (135°C) and are removed by approximately 32 minutes (375°C).

A comparison of the CO_2 reconstructed chromatograms for the unexposed and exposed illite samples shows that there is an increase in the bands after approximately 32 minutes (375°C) in the latter. This is possibly due to the breakdown of DMF producing CO_2 . This behaviour is similar to that observed in the Mg-SWy-2/DMF complex. The remainder of the CO_2 chromatogram is similar to that observed in the

unexposed illite. The ICs obtained from the complex also show the detection of DMF between 19-33 minutes (115-395°C)(figure 6.45).

Figure 6.43: EGA-FTIR of illite after exposure to DMF vapour for 22 days (sample weight=50mg)

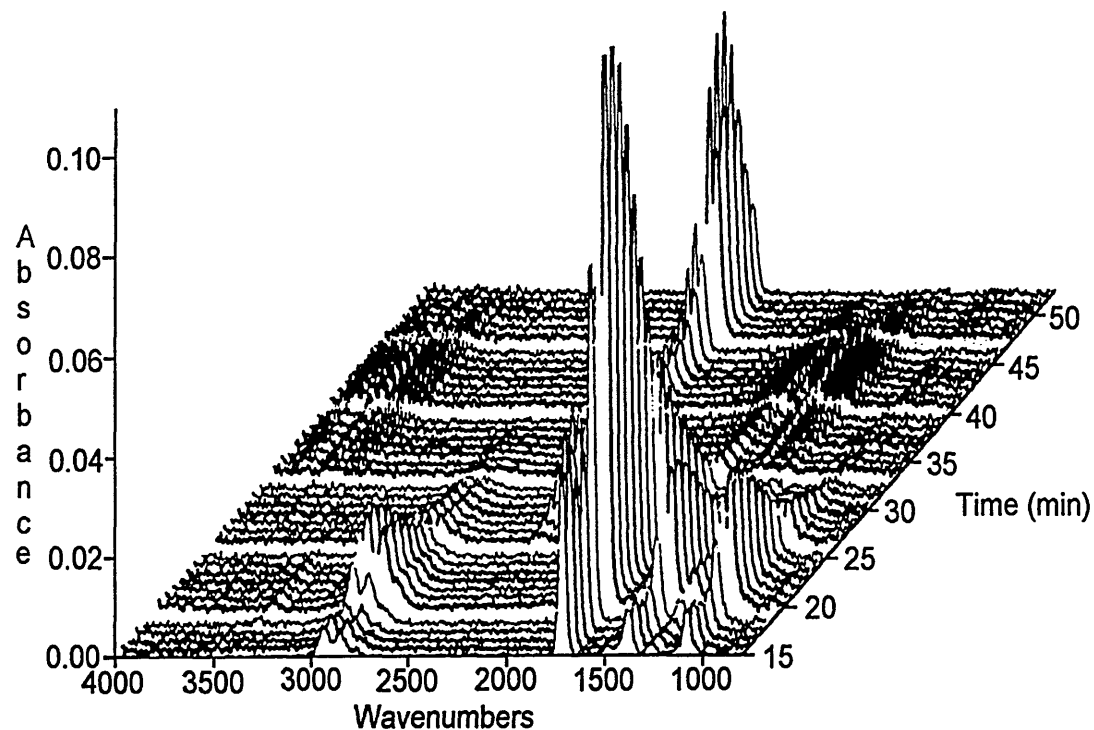


Figure 6.44: Reconstructed chromatograms obtained from the EGA-FTIR of the illite/DMF complex.

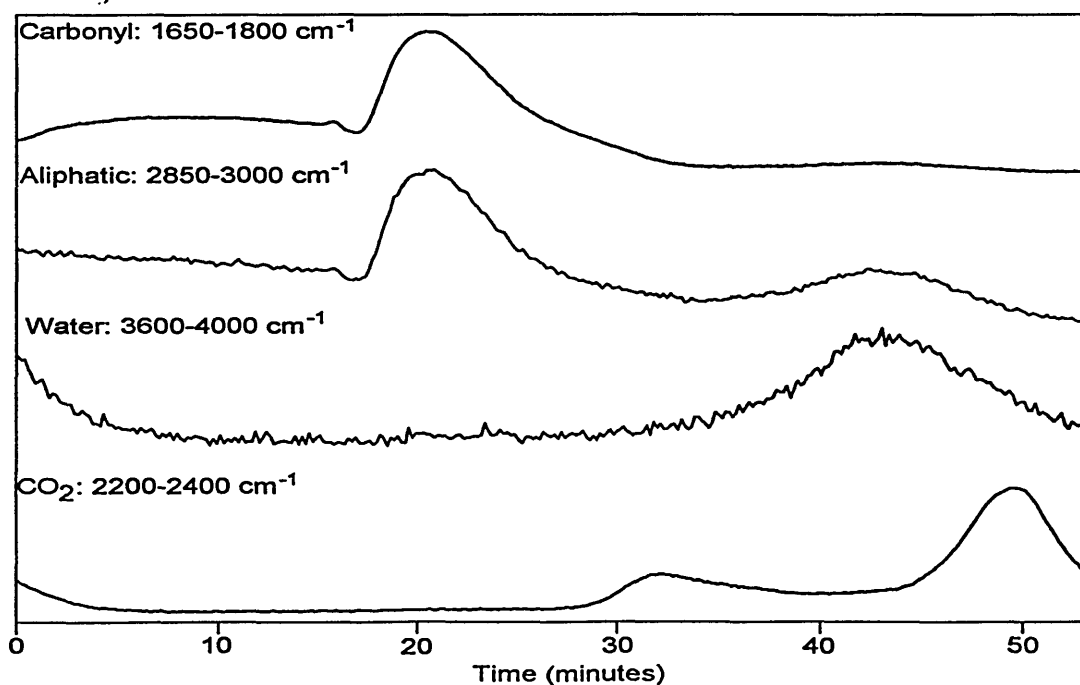
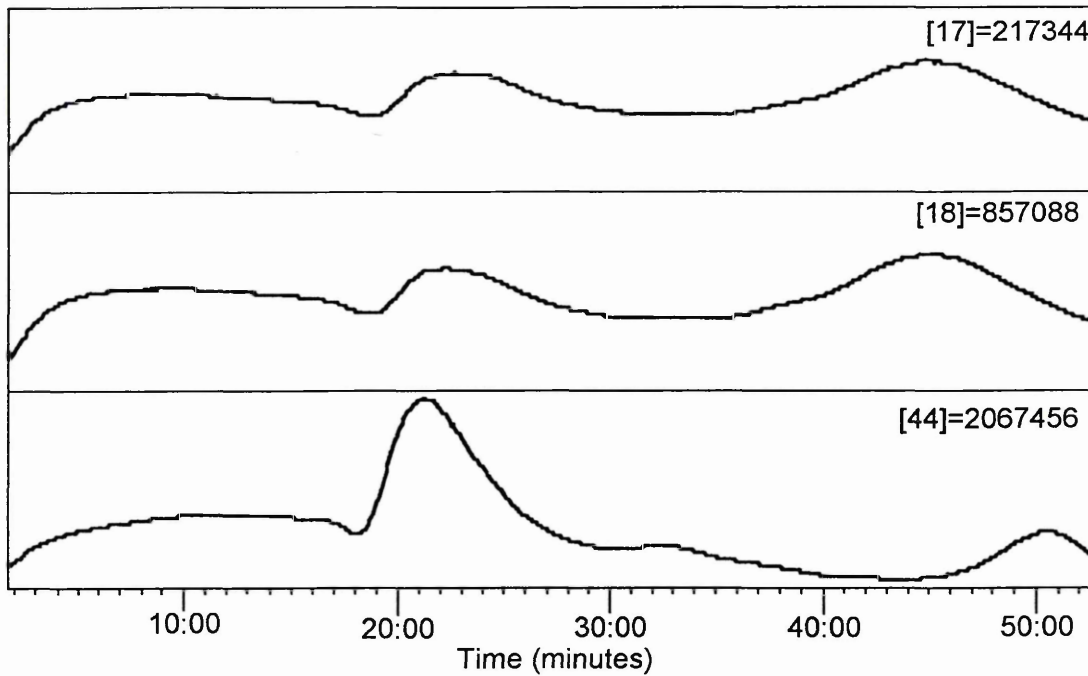


Figure 6.45: Ion chromatograms obtained from illite exposed to DMF vapour.



6.4.3) Mixtures of minerals

This section aims to determine whether the presence of illite and Mg-SWy-2 within a mixture of other minerals can be detected using DMF as a chemical probe. The mixtures analysed in this thesis are shown in table 6.20.

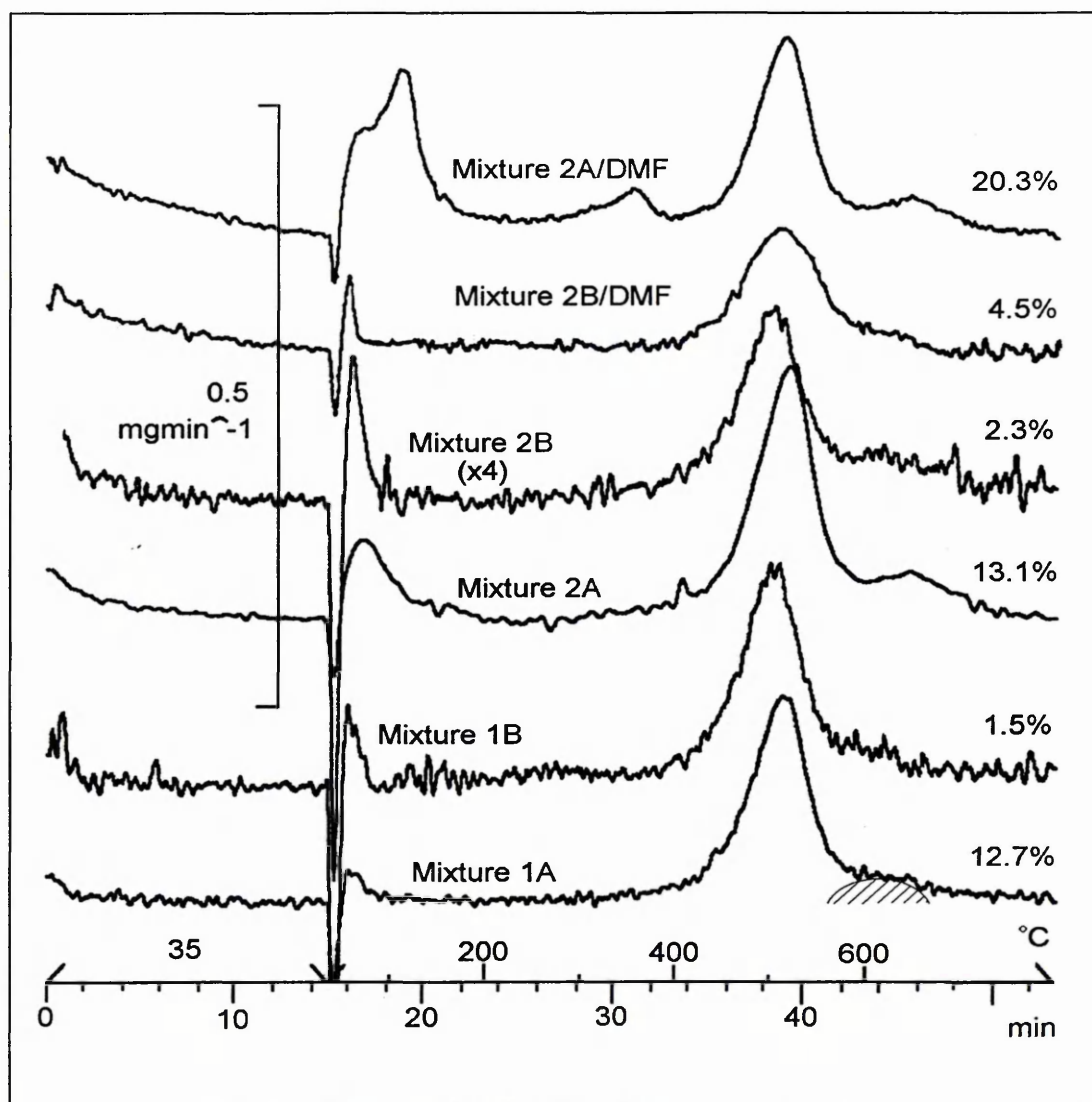
These investigations will also demonstrate how sensitive EGA-MS and EGA-FTIR are compared to TGA. The composition of the mixtures diluted with Seesand (1B and 2B) are representative of sandstones and reservoir rocks found in nature. These are not the same as any real rock but mixture 1B is based on berea.

Some DTG traces of the 4 mixtures before and after exposure to DMF are shown in figure 6.46. With reference to the DTG traces of the individual minerals the maxima in the DTG traces of the mixtures can be assigned to the mineral which gives rise to them. The only noticeable feature on the DTG trace of sample 1A is the large maximum at 500°C which is attributable to the dehydroxylation of kaolinite. To the right of this a small almost unnoticeable maximum (shaded area) can be seen between 550-700°C, which is due to a combination of the dehydroxylation of the chlorite and illite. These features are even less noticeable in the diluted mixture (1B).

Table 6.20: Composition of mixtures used in the analysis of illite and Mg-SWy-2 using DMF as a chemical probe.

Mineral	Mixture (weight)			
	1A	1B	2A	2B
Seesand	-----	90	-----	90
Kaolinite	76	7.6	56	5.6
Illite	20	2	20	2
Chlorite	4	0.4	4	0.4
Mg-SWy-2	-----	-----	20	2

Figure 6.46: DTG traces of physical mixtures of standard minerals (percentages denote the total weight lost between 15-23 minutes).



Note also the noisier baseline in the DTG trace of the diluted mixture due to the poor signal to noise ratio. The exposure of mixtures 1A and 1B to DMF vapour does not

change their subsequent DTG traces. Hence TGA alone is unable to detect this small change even though DMF is expected to interact with illite.

The DTG trace of mixture 2A shows 3 features of interest, which are:-

i) a maximum between 35-200°C, which is due to the removal of physisorbed water from montmorillonite and illite. The main contribution must be loss of water from Mg-SWy-2, since the DTG trace of mixtures 1A and 1B were unable to show the contribution from illite in this region.

ii) a maximum at 500°C, which is due mainly to the dehydroxylation of kaolinite.

iii) a maximum between 580-800°C. This is due to a combination of the dehydroxylation of illite, chlorite and Mg-SWy-2.

From the DTG trace it is not possible to positively identify any of the minerals except kaolinite. This becomes even more difficult when the clay minerals are diluted in Seesand because the signal-to-noise ratio decreases (2B).

If mixtures 2A and 2B are exposed to DMF their respective DTG traces show two changes. The first is an increase in intensity between 35-200°C and the second is an extra maximum at approximately 380°C. This change is due to the interaction of DMF with Mg-SWy-2 and illite. Note also that in the DTG trace of the diluted mixture (i.e. that containing Seesand) the baseline is noisier and it is more difficult to distinguish the characteristic features.

EGA of Mixture 1B

EGA-FTIR

A 3D plot of the infrared spectra collected during the EGA of mixture 1B before exposure to DMF is shown in figure 6.47. The reconstructed chromatograms for CO₂ and water are shown in figure 6.48. These figures show only two features, namely, the detection of water between 34-44 minutes (415-615°C) and CO₂ between both 25-44 minutes (235-615°C, gradual increase) and 44-54 minutes (615-800°C, rapid increase). Both these features are due to the combination of the minerals present. The water maximum at 39 minutes (500°C) is due mainly to kaolinite. It should be noted

that physisorbed water from illite is not detected between 15-25 minutes (35-235°C). However, physisorbed water is detected in the EGA-IR data of mixture 1A (figures not shown).

Figure 6.47: EGA-FTIR of mixture 1B before exposure to DMF (sample weight = 35mg).

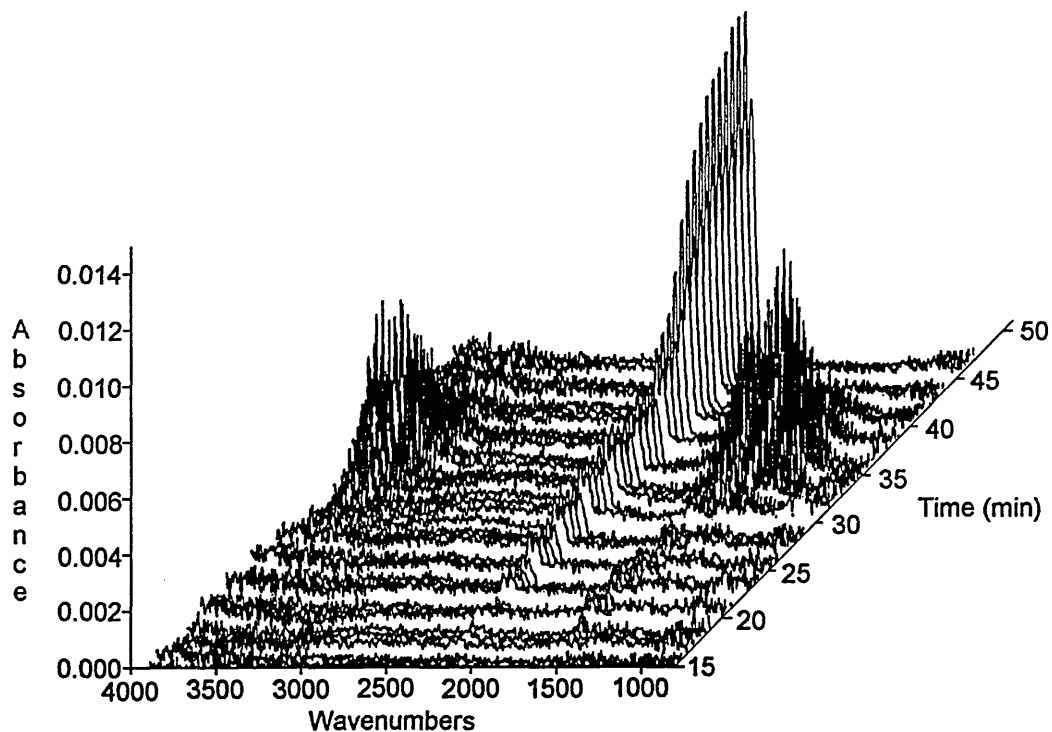
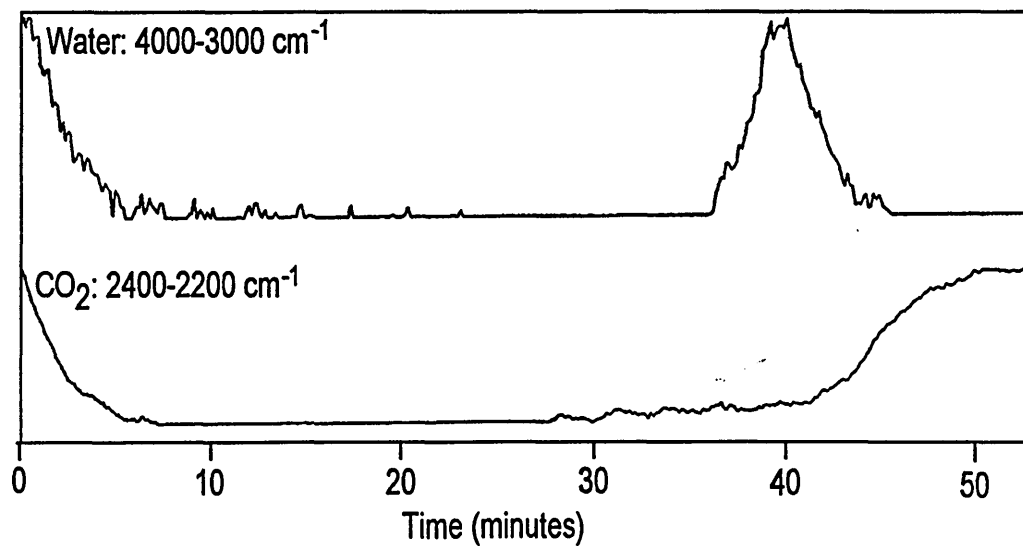


Figure 6.48: Reconstructed chromatograms for water and CO₂ obtained from mixture 1B



The 3D plot of mixture 1B after exposure to DMF vapour is shown in figure 6.49. The corresponding reconstructed chromatograms for $\nu_s(\text{C}=\text{O})$, water and CO_2 are shown in figure 6.50. The 3D plot is the same as the 3D plot of the unexposed mixture except the $\nu_s(\text{C}=\text{O})$ band of DMF is observed between 15-28 minutes (35-295°C). The intensity of the water bands are not as intense as the previous plot simply because a smaller weight of sample was used (35mg rather than 50mg). The reconstructed chromatograms for the $\nu_s(\text{C}=\text{O})$ band shows two regions of desorption between 17-30 minutes (75-335°C) and 35-43 minutes (435-595°C). The latter region is not due to the desorption of DMF, but is due to the desorption of water which has infrared bands in the same wavenumber region.

Figure 6.49: EGA-FTIR of mixture 1B after exposure to DMF vapour (sample weight = 35 mg).

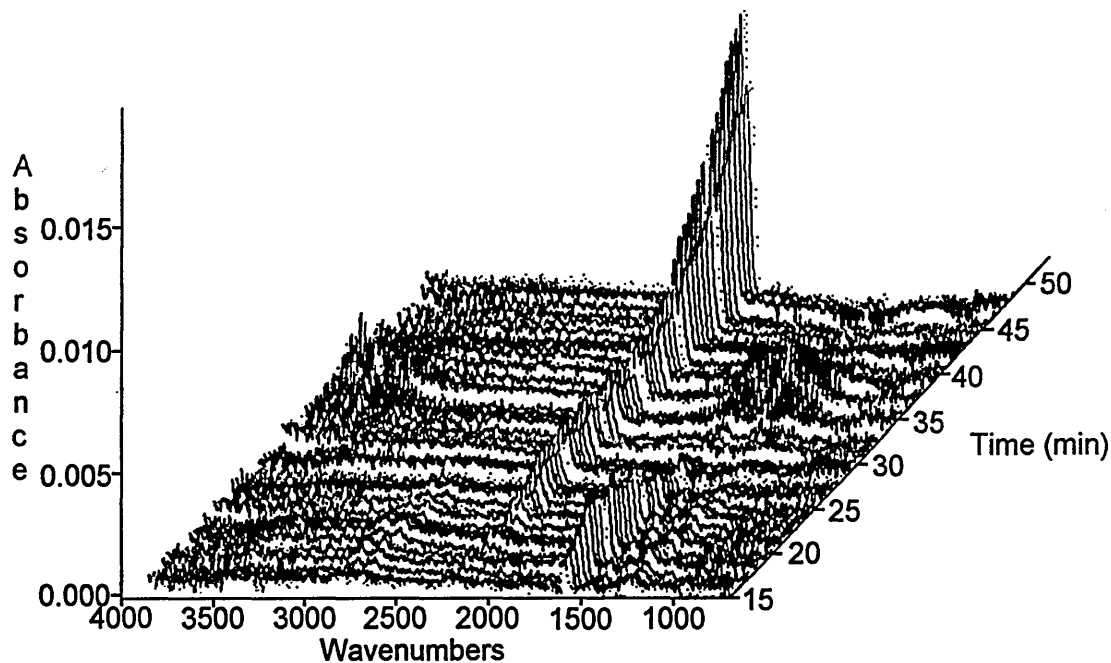
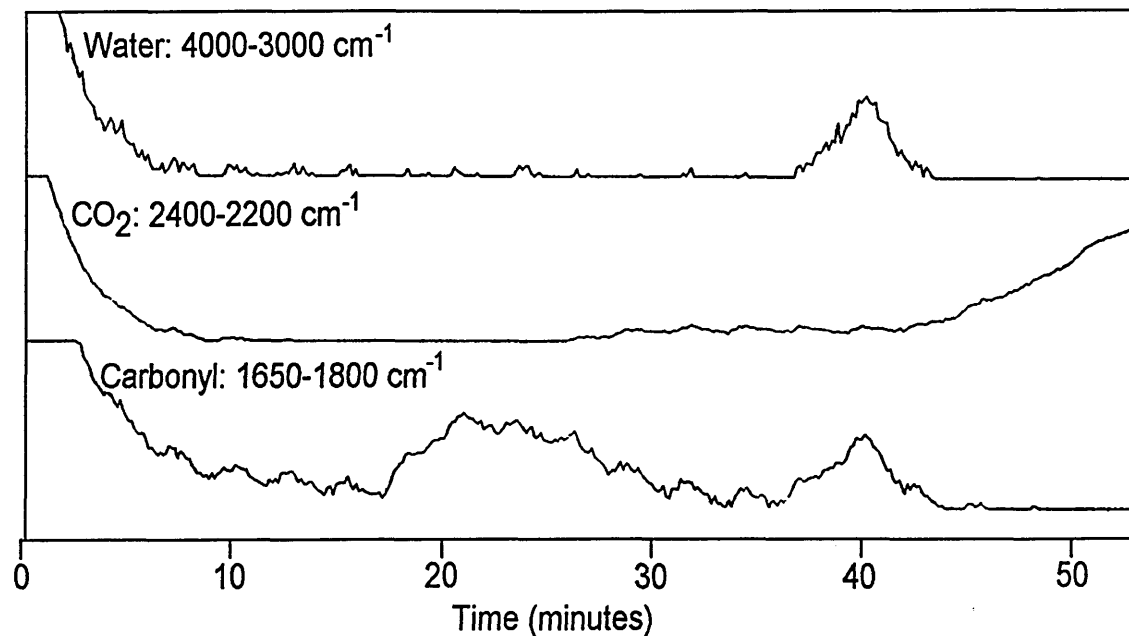


Figure 6.50: Reconstructed chromatograms obtained from mixture 1B after exposure to DMF vapour.

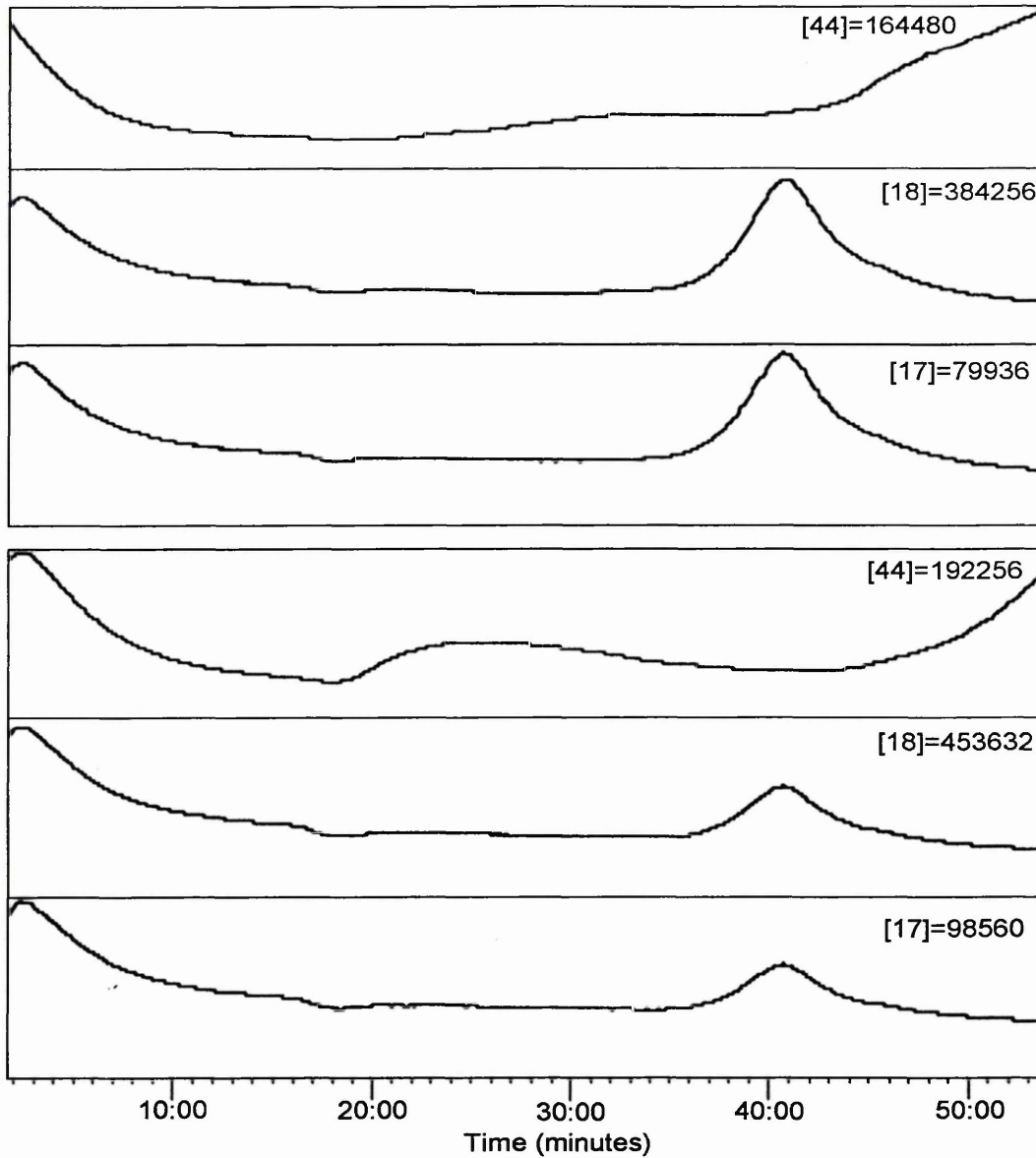


EGA-MS

The {18}, {17} and {44}-ICs for mixture 1B before and after exposure to DMF are shown in figure 6.51. The ICs due to water show the same pattern before and after exposure to DMF. Physisorbed water from illite in mixture 1B cannot be detected using MS, but is possible in mixture 1A (figures for 1A are not shown).

The shape of the {44}-IC changes after the mixture (1B) has been exposed to DMF, a broad hump is observed between 15-28 minutes (35-295°C). This is due to the interaction of DMF with illite. The increase at the end of the IC is due to the presence of CO₂. Unfortunately, in this experiment the {73}-IC could not be used since DMF breaks down along the transfer lines as previously discussed. Thus, no maxima in the {73}-IC is observed.

Figure 6.51: Ion chromatograms from mixture 1B both before (top three) and after exposure (bottom three) to DMF vapour.



Summary

Using TGA alone it was not possible to detect the presence of illite in mixture 1B because i) TGA was not sensitive enough to detect the loss of physisorbed water and ii) its broad characteristic dehydroxylation maximum was masked by the dehydroxylation of kaolinite and chlorite. EGA-FTIR and EGA-MS was able to obtain chromatograms of the diluted mixture (1B) similar to the DTG traces. When

DMF was used as a chemical probe on the diluted mixture, it was able to enhance and distinguish the presence of illite within the mixture.

Mixture 2B

EGA-FTIR

A 3D plot of the infrared spectra collected during the EGA of mixture 2B before exposure to DMF is shown in figure 6.52. The reconstructed chromatograms for CO₂ and water are shown in figure 6.53. The figures show the detection of water between 38-45 minutes (495-635°C), which is due to the combination of illite, Mg-SWy-2, chlorite and kaolinite dehydroxylation. The reconstructed chromatograms show that only the presence of kaolinite can be clearly distinguished. Physisorbed water from illite and montmorillonite cannot be detected at this low level (2% and 2%, respectively) when a low sample weight is used (50mg).

Bands in the 2400-2200cm⁻¹ region are noted after 30 minutes (>335°C) in two stages, this is due to CO₂ and is derived from trapped CO₂ or carbonate impurity.

Figure 6.52: EGA-FTIR of mixture 2B before exposure to DMF vapour (sample weight=50mg).

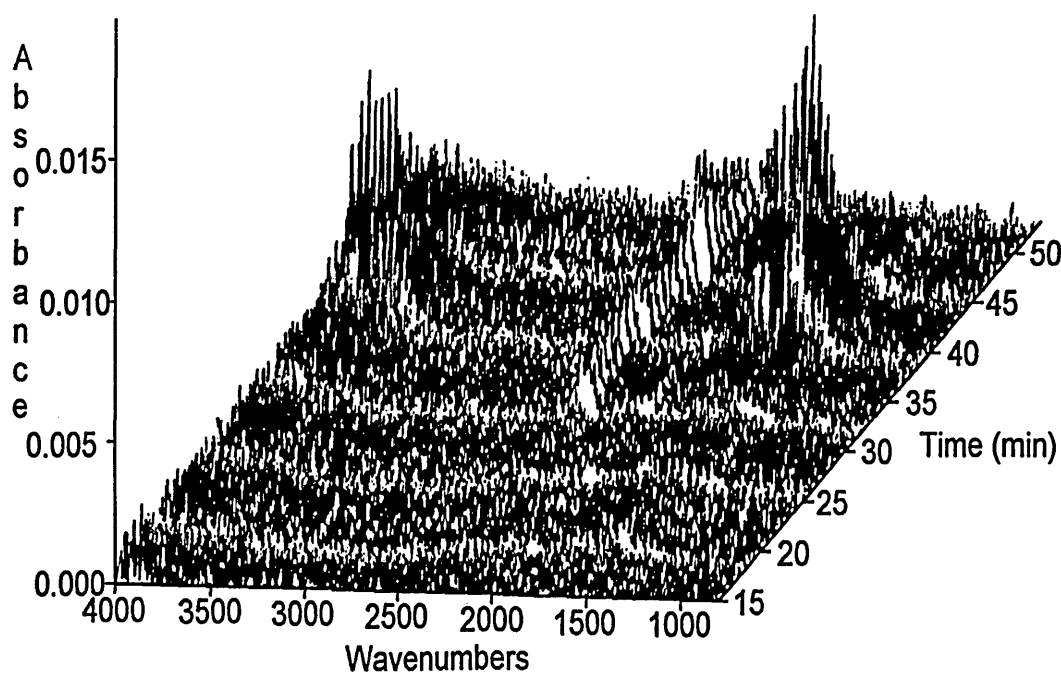
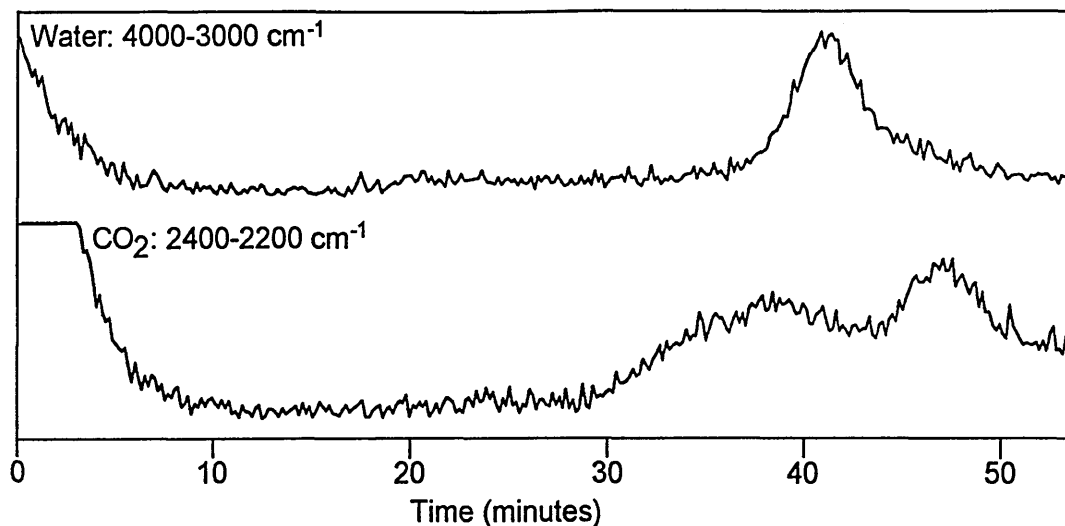


Figure 6.53: Reconstructed chromatograms for water and CO₂ obtained from mixture 2B.



The 3D plot of the infrared spectra collected during the EGA of the mixture after exposure to DMF is shown in figure 6.54. The reconstructed chromatograms of the $\nu_s(\text{C}=\text{O})$, $\nu_s(\text{C}-\text{H})$, water and CO₂ bands are shown in figure 6.55.

Figure 6.54: EGA-FTIR of mixture 2B after exposure to DMF vapour (sample weight = 93 mg).

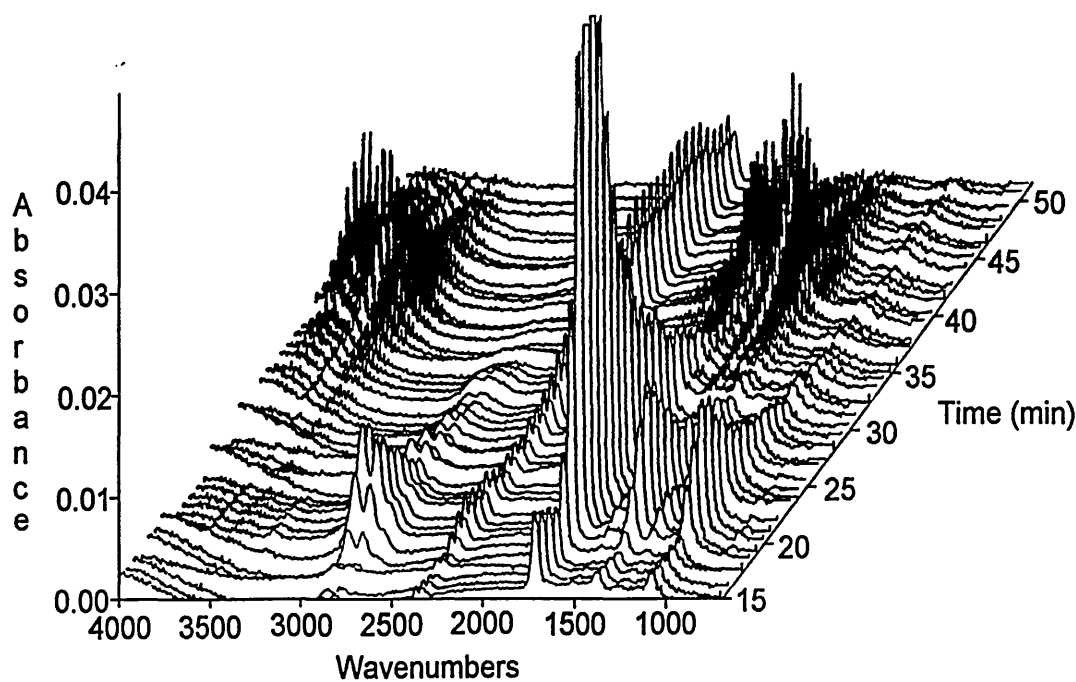
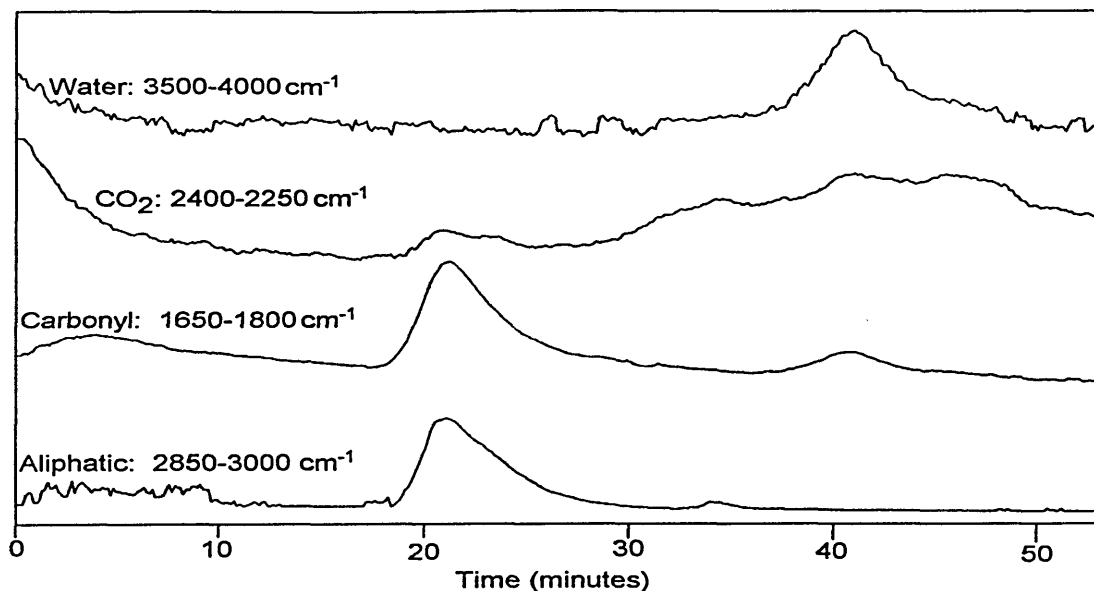


Figure 6.55: Reconstructed chromatograms from Mixture 2B after exposure to DMF.



The figures show the detection of water between 35-45 minutes (435-635°C). A large maximum at approximately 41 minutes (555°C) is clearly present and is due to the dehydroxylation of kaolinite. The detection of water after this large maximum is due to the dehydroxylation of Mg-SWy-2, illite and chlorite.

The reconstructed chromatogram of the $\nu_s(\text{C}=\text{O})$ band shows three features; a maximum at 21 minutes (155°C), a shoulder to the right of this maximum, and, a maximum at 41 minutes (555°C). The maximum at 41 minutes (555°C) is not due to the desorption of DMF, but is due to water absorbance bands which are in the same wavenumber region.

The DTG trace of Mg-SWy-2 after exposure to DMF exhibits a maximum at approximately 400°C (equivalent to approximately 35 minutes in figure 6.55). This is not observed in the reconstructed $\nu_s(\text{C}=\text{O})$ chromatogram, but is evident in the $\nu_s(\text{C}-\text{H})$ chromatogram. This is attributable to breakdown of DMF as discussed previously. In addition DMF interacts with illite present in the mixture and desorbs in the region between the large desorption maximum of Mg-SWy-2 at 180°C and the high temperature maximum at 400°C. Thus, the characteristic maximum is not as clearly observed.

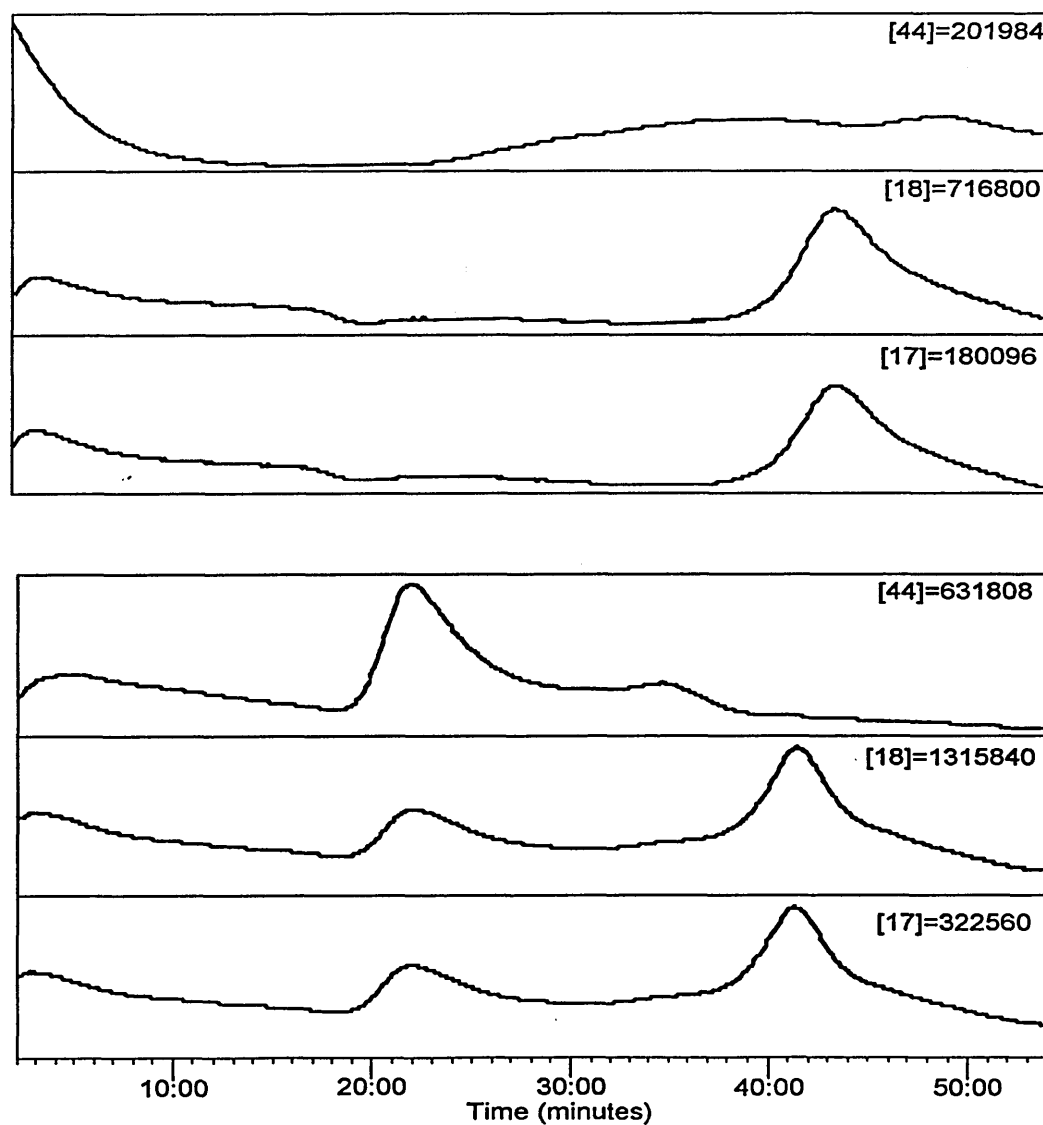
Comparison of the CO_2 chromatogram before (figure 6.53) and after (figure 6.55) exposure to DMF shows that the latter exhibits additional detection of CO_2 between 20-25 minutes (135-235°C). This is due to the breakdown of DMF.

EGA-MS

The {18}, {17} and {44}-ICs for mixture 2B before and after exposure to DMF vapour are shown in figure 6.56.

The ICs of the non-exposed mixture show the presence of water and CO₂ in the expected regions, that is water is noted between 38 and 45 minutes ((495-635°C) which is due to the dehydroxylation of the clay minerals, especially kaolinite) and CO₂⁺ is detected over a broad range (30-50 minutes (335-735°C)).

Figure 6.56: Ion chromatograms obtained from mixture 2B both before (upper three) and after exposure (bottom three) to DMF vapour.



The {44}-IC obtained from the mixture exposed to DMF shows two maxima at 22 and 35 minutes (175 and 435°C, respectively), which are due to the desorption of DMF from Mg-SWy-2. The higher temperature maximum is not as resolved as expected from the lower temperature maximum (as observed in figure 6.38) because DMF is desorbed from illite in between them. However, the maximum at 35 minutes (435°C) is more resolved than in the infrared chromatogram.

The {17} and {18}-ICs obtained from the exposed mixture shows a maximum after 22 minutes (175°C). This is probably not due to water, but is due to a breakdown product or fragment of a breakdown product of DMF. This assignment is supported by the fact no H₂O is observed in the IR data.

Summary

These results show:-

- Ion chromatograms and reconstructed infrared chromatograms similar in shape to those of the DTG traces can be obtained.
- DMF can be used as a chemical probe and be detected by EGA-FTIR/MS to determine the presence of illite and Mg-SWy-2 in a powdered mixture typical of a sandstone or reservoir rock.
- DMF is a good chemical probe to be detected by EGA-FTIR since the $\nu_s(\text{C}=\text{O})$ band has a high extinction coefficient. The presence of illite in mixture 1B would not have been detected by any other absorbance band of DMF apart from the $\nu_s(\text{C}=\text{O})$ band. However a small sample weight was used and an increase may enhance the intensity of the other bands.
- Some diffusional broadening was observed in the infrared data. This may be overcome by shortening, or increasing the temperature of, the transfer line. Care needs to be taken when increasing the transfer line temperature because this may aid the breakdown of the chemical probe.
- It is interesting to note that only very small samples were analysed (50 or 100mg) and yet the detection of illite and Mg-SWy-2 at the 2% level presented no problem. Sample sizes could easily be increased in order to enhance sensitivity.

- Although the results discussed so far are very promising, DMF is not the ideal chemical probe. The main reason for this is that DMF tends to breakdown as it leaves the clay and travels down the transfer line. This can be overcome to some extent by reducing transfer line lengths and temperatures. However, diffusional broadening results from a decrease in temperature and thus poorer resolution of the maxima in the chromatograms were observed. DMF also has fragment ions or breakdown products with the same mass as water and CO₂. This therefore does not allow the distinction between these and DMF by MS.
- Kaolin (KGa-2) can be detected via its dehydroxylation maximum at 500°C but chlorite (CCa-2) cannot be detected at the levels used in the mixtures.
- The reader should note that none of the results have been compared to relevant data published in the literature. This is simply because no such data involving the detection of evolved organics from minerals has been found. However, mineral/organic complexes have been studied by other techniques (e.g. XRD has been employed to detect the intercalation of DMSO into kaolinite and halloysite in order to distinguish their presence) which have been discussed in chapter 3.

7) Chapter 7 - Characterisation of the chemical probe-mineral complexes

VT-DRIFTS and VT-XRD has been employed on selected chemical probe-clay mineral complexes in order to determine the site distributions and modes of interaction of the chemical probes when sorbed onto clay minerals. This chapter will discuss the site distributions and modes of interaction of NMF and DMF on cation-exchanged montmorillonite

The heating parameters for a TGA experiment involve heating the sample from 35 to 800°C at a rate of 20°C/minute, whereas during a VT-DRIFTS experiment the sample is heated in steps, i.e. the sample is heated to a predetermined temperature, left to equilibrate for 15 minutes, then the infrared spectrum is collected at that temperature before the procedure is repeated at a higher temperature. Since this is the case a completely accurate comparison cannot be achieved. However, the results obtained from VT-DRIFTS and TGA do show a good deal of correlation.

7.1) Experimental

7.1.1) Variable Temperature-DRIFTS

The use of VT-DRIFTS to study the desorption of a chemical probe from an exposed sample was achieved using a Matteson Polaris FTIR spectrometer. Winfirst and First software was used to collect and analyse the spectra. To collect the diffuse reflectance the system used a SelectorTM DRIFTS accessory and an environmental chamber controlled by an automatic temperature controller (temperature range 20-500°C). Both these were manufactured by Graseby Specac. Before any spectral data was collected the accessory needed to be optimised to allow maximum throughput of radiation to reach the detector. The spectra were collected using the following parameters:-

Resolution = 4.0cm⁻¹

Detector gain = 1

Mirror Velocity = 40

Apodisation function = triangle

Number of scans = 276

Iris = 95%

The compartments of the spectrometer were purged continuously with nitrogen throughout the experiments.

All the samples were prepared by mixing the sample with finely ground KBr as a 10% mixture. Approximately 0.25mg of the mixture was then transferred to the diffuse reflectance cup positioned in the heating chamber and the surface levelled. Unlike the DRIFTS spectra obtained in section 5.1.1.5 for the characterisation of sandstones no ball milling of KBr or compaction of the mixtures was performed. A DRIFTS spectrum of the prepared samples was collected prior to any heating or purging treatment at 25°C. The sample was then purged with nitrogen (20cm³/min) gas for 15 minutes and another spectrum collected. The sample was then heated to the required temperature, allowed to equilibrate for 15 minutes and then another spectrum was collected (the instrument was purged continuously with nitrogen gas). This process was repeated until the chemical probe was completely desorbed. Background spectra were collected using only KBr powder via the same procedure and used to ratio against the respective sample spectra.

7.1.2) Variable Temperature-XRD

Samples for VT-XRD were coated on a glass slide, exposed to the chemical probe and then the XRD pattern was collected. A simple heating apparatus was constructed in order to heat the samples whilst placed in the diffractometer. This allowed diffractograms to be recorded at a specific temperature after a 15 minute equilibration period. The maximum temperature of the heating stage was 300°C. Any further heat treatment (i.e. above 300°C) to the sample was achieved in a solvent-free oven, the sample was then immediately replaced on the heating stage (at 300°C) and the XRD pattern collected. The temperature readings were accurate to approximately ±8°C. All VT-XRD was performed on a PW1830 Diffractometer. No nitrogen purging over the sample was employed.

7.1.3) Fourier-self Deconvolution

Deconvolution of the relevant spectral regions was achieved using the following parameters:-

$$\text{Width} = 28.5\text{cm}^{-1}$$

$$\text{Enhancement factor} = 1.7$$

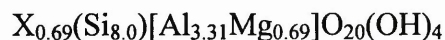
$$\text{Lorentzian fraction} = 0.8.$$

7.1.4) Molecular modelling

Computer simulations were performed using Cerius 2 software. A brief description of the modelling procedures is given below.

Firstly, a Monte Carlo (MC) simulation was performed in order to simulate the sorption of NMF into Na and Mg-exchanged montmorillonites.

The cell formula for the clay in the model is,



where X is the exchange cation (i.e. Na or Mg). Periodic boundary conditions were applied in three-dimensions, and thus the model simulates an infinite stack of clay platelets, infinitely wide. This is similar to the real clay minerals, but broken bonds at crystal edges are not represented.

The MC simulation was performed within a grand canonical ensemble (i.e. constant μVT). This means that during the run, the volume (V), the temperature (T) and chemical potential (μ) of the system was fixed. The volume was fixed so that the $d_{(001)}$ -spacing of the clay layers was set to a value in excess of the anticipated equilibrium, i.e. 1Å greater than the $d_{(001)}$ -spacing obtained from the experimental results. The cations were fixed in a plane between the clay layers, approximately 7Å apart for the Na-exchanged clay and 14Å for the Mg-exchanged clay.

250,000 MC cycles were used in the simulation and equilibrium had been reached at the end. The cations were then allowed to move and the energy in the NMF/clay system was minimised. Subsequently a molecular dynamic simulation was performed using a (NpT) ensemble. This means that during the run the number of NMF molecules, the pressure and the temperature of the system was fixed. During the

simulation the $d_{(001)}$ -spacing, the NMF molecules and the cations were allowed to move and a total of 20,000 steps were performed.

7.2) VT-DRIFTS and VT-XRD of the X-SWy-2/NMF and X-SWy-2/DMF complexes

It has been shown previously by XRD that NMF and DMF are able to intercalate between the layers of various cation-exchanged montmorillonites. TGA and TG-FTIR has shown that NMF is associated with each cation-exchanged montmorillonite via a number of different sites. This is also the case for DMF and X-SWy-2.

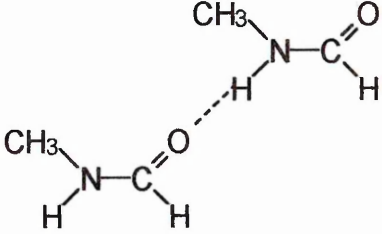
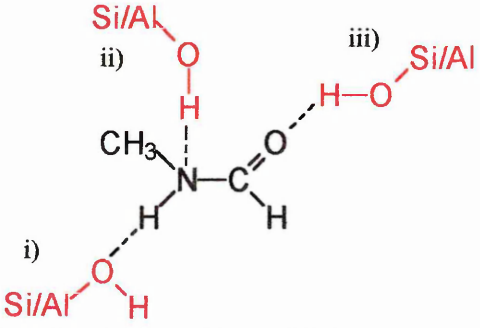
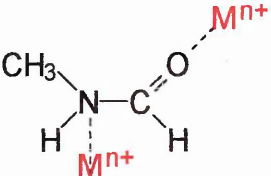
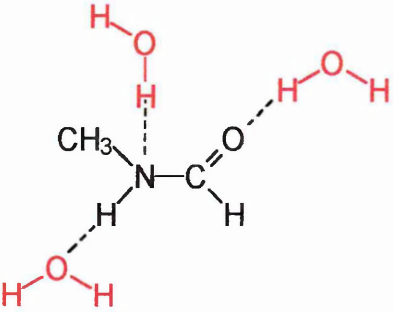
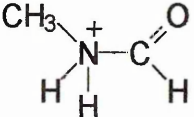
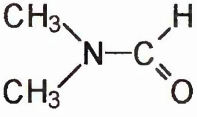
VT-DRIFTS has been used in order to try and determine whether infrared spectroscopy is able to distinguish the different sites occupied by the NMF and DMF molecules when they are associated with the cation-exchanged clays. Since NMF (and DMF) is associated with sites on the clay with different affinities, the vibrational frequencies of the NMF bands associated with each site should be different. This should in turn lead to shifts in the infrared bands and thus result in a means of identifying the type of sites present.

VT-XRD has been used in order to determine the $d_{(001)}$ -spacing of the cation-exchanged clay/NMF complexes as they are heated.

It is worth recapping at this point that the molecules in pure liquid NMF are self associated by very strong intermolecular hydrogen-bonding (this occurs between the carbonyl and N-H groups), whereas the molecules in DMF are not self hydrogen bonded (this is due to the absence of a N-H group).

Table 7.1 shows some of the possible ways in which NMF and DMF could interact with the cation exchanged clays.

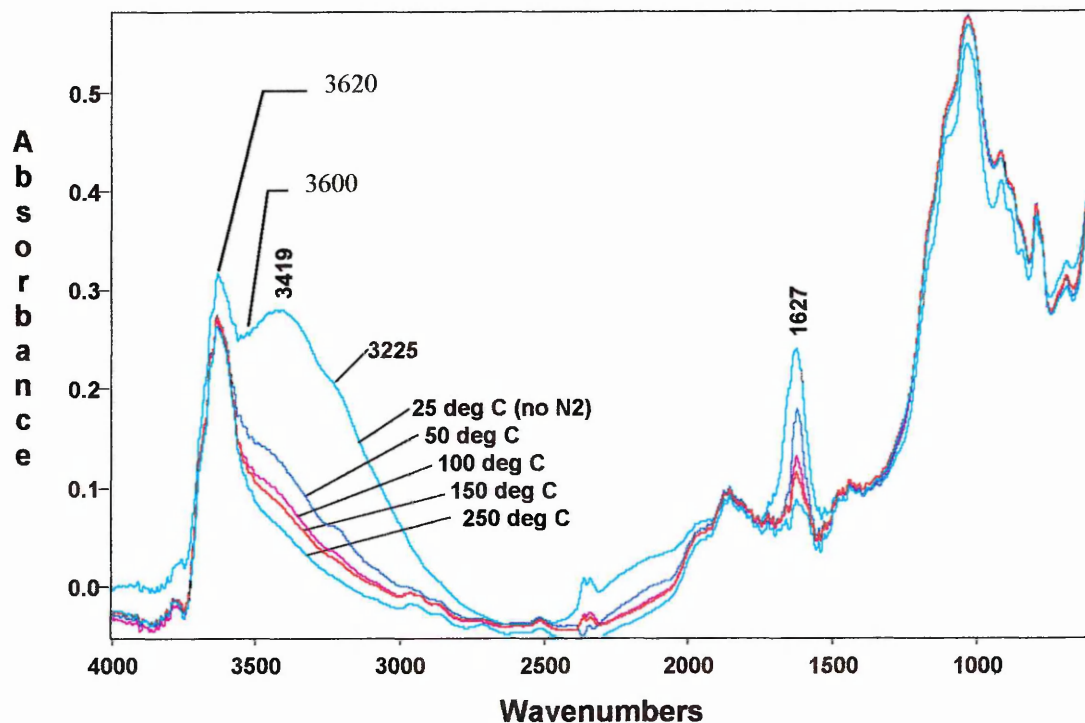
Table 7.1: Possible interactions between NMF and DMF and cation exchanged clays.

<p>NMF A)</p> 	<p>Intermolecular hydrogen-bonded NMF molecules</p>
<p>B)</p> 	<p>i) hydrogen bonding of NH to oxygen on clay surface. ii) H-bonded via the lone pair of electrons on the nitrogen to hydroxyl of clay structure. iii) H-bonded via the carbonyl group to hydroxyl of clay structure (note: very few of these sites are accessible in a smectite clay)</p>
<p>C)</p> 	<p>Coordination to exchangeable cations (M^{n+}) via i) carbonyl or ii) nitrogen. Cations could be positioned in the interlayer or on external surfaces.</p>
<p>D)</p> 	<p>H-bonded to water via:- i) carbonyl ii) lone pair of electrons on N iii) H on N atom. (note: the water molecules could be bridges to the exchange cation)</p>
<p>E)</p> 	<p>Protonated species. Hydrogen could come from water either present in the interlayer or from dehydroxylation of the clay structure</p>
<p>DMF</p> 	<p>DMF could interact via:- B ii) and iii) C i) and ii) D i) and ii) E</p>

7.2.1) VT-DRIFTS analysis of Ca-SWy-2/NMF complexes

Figure 7.1 shows the VT-DRIFTS spectra of Ca-SWy-2 before exposure to NMF. The spectra were recorded at 25°C (prior to purging with nitrogen), 50, 100, 150 and 250°C.

Figure 7.1: VT-DRIFTS spectra of Ca-SWy-2 (25-250°C)



The spectra show that as the clay is heated, the bands between 3600-3000 cm^{-1} and the band at 1627 cm^{-1} decrease in intensity. These bands are due to water and therefore the spectra clearly shows the removal of water from the clay as it is heated. According to Bishop et al. [269] these bands have been assigned as:

3600 cm^{-1} = antisymmetric stretching (H-O-H)

3419 cm^{-1} = symmetric stretching (H-O-H)

3225 cm^{-1} = bending overtone

1627 cm^{-1} = H-O-H bending

The other bands are due to the clay structure skeletal modes [89-90]. The removal of water from smectite clays has been studied extensively by infrared spectroscopy in film and slurry form [88, 270-273] and it has been shown that there are two distinct environments of adsorbed water present:-

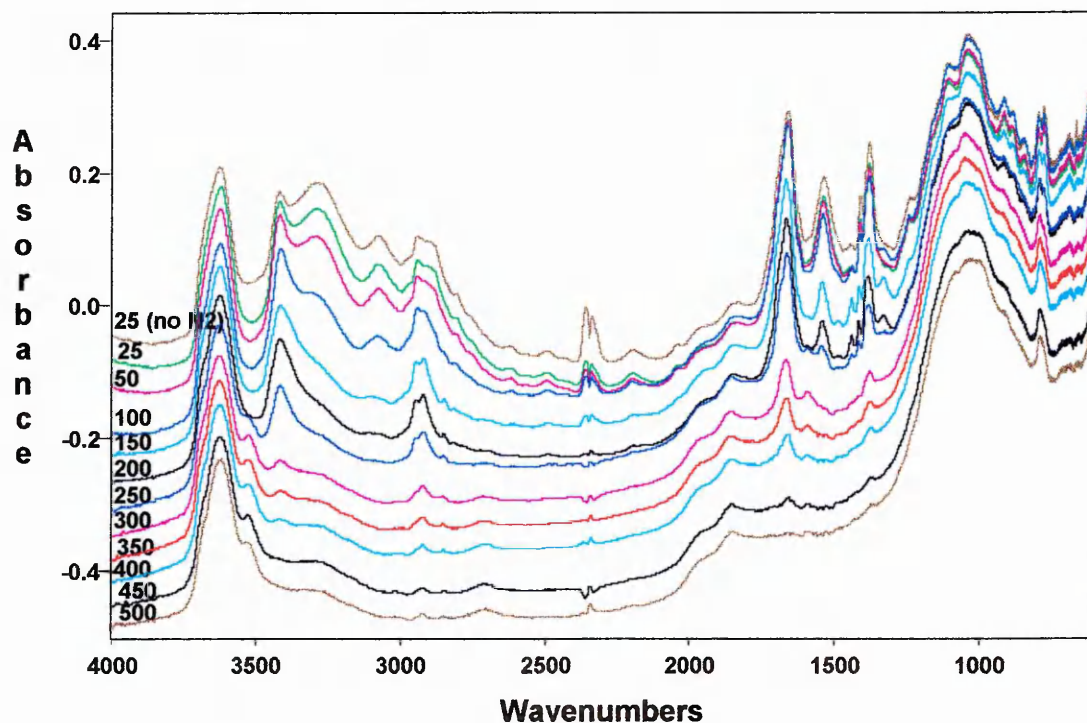
- 1) firmly bound water molecules directly coordinated to exchangeable cations
- 2) weakly bound physisorbed water molecules occupying interlamellar spaces between saturated exchangeable cations and on polar sites on external surfaces.

The position and intensity of the bands depends on the environment of the water molecules and the type of exchangeable cation present. For example, it has been shown [273] that the frequency of the H-O-H bending vibration decreases and the molar absorptivity increases upon removal of water from the clay mineral. This paper also showed smaller decreases when Na^+ and K^+ were the exchangeable cations than when Co^{2+} or Cu^{2+} were present (this is due to polarisation effects).

The DTG trace (figure 6.1) of Ca-SWy-2 does not show the loss of physisorbed or chemisorbed water above 250°C (i.e. no maximum is present), although the spectrum collected at 250°C shows that there is still some residual water remaining on the clay, which is indicated by the water band at 1627cm^{-1} . However, the TG trace does show a slow constant weight loss between 250°C and the dehydroxylation temperature, which does not produce a maximum in the DTG trace. This weight loss is due to tightly held water.

Figure 7.2 shows the VT-DRIFTS spectra ($4000\text{-}600\text{cm}^{-1}$) of Ca-SWy-2 after exposure to NMF vapour for 31 days. The first spectrum was recorded at 25°C prior to purging with nitrogen. Subsequent spectra were recorded whilst purging with nitrogen at 25°C , 50°C and at 50°C increments until a maximum temperature of 500°C . The spectra are stacked and progressively ordered so that the spectrum collected at the lowest temperature is at the top. If the clay/NMF spectra are compared to those collected from the water clay (figure 7.1), additional bands are observed for the former. Although these bands decrease in intensity as the temperature of the sample is increased they do not all decrease at the same rate. These bands may be due to the presence of either NMF and water or NMF alone on the clay.

Figure 7.2: VT-DRIFTS spectra of Ca-SWy-2 after exposure to NMF vapour for 31 days (4000-600 cm^{-1})



The position of the bands observed in the infrared spectrum of liquid NMF (figure 7.3) are listed in table 7.2. These assignments were taken from Olejnik et al. [274 and references therein], and agree with those of De Graaf and Sutherland [275], and, Fogarasi and Balazs [276]. These will be used to aid the interpretation of the spectra obtained from the Ca-SWy-2/NMF complex. The interpretation will then in turn be used to determine the types of sites present in the complex (i.e. the sites represented by maxima in the respective DTG trace, figure 7.4). The reader should note that the shoulder on the high wavenumber side of the band at 3300cm^{-1} is due to the presence of water contamination in the liquid NMF. The DTG traces to be discussed in this section have been re-plotted in figure 7.4.

Figure 7.3: Infrared Spectrum (transmission) of Liquid NMF

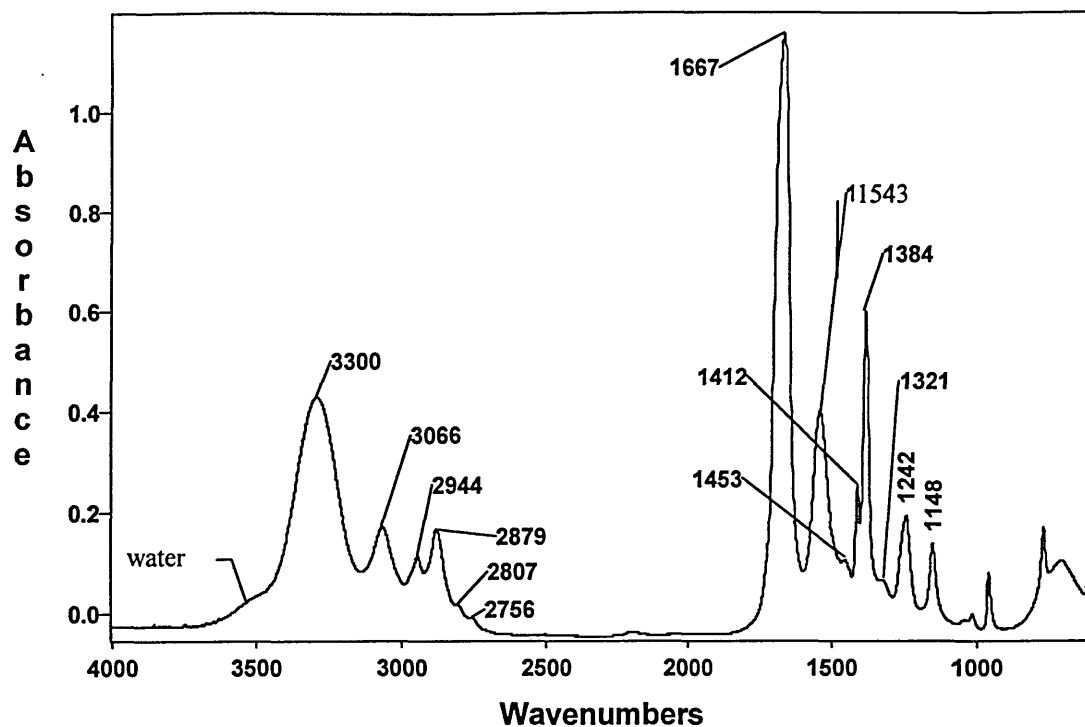
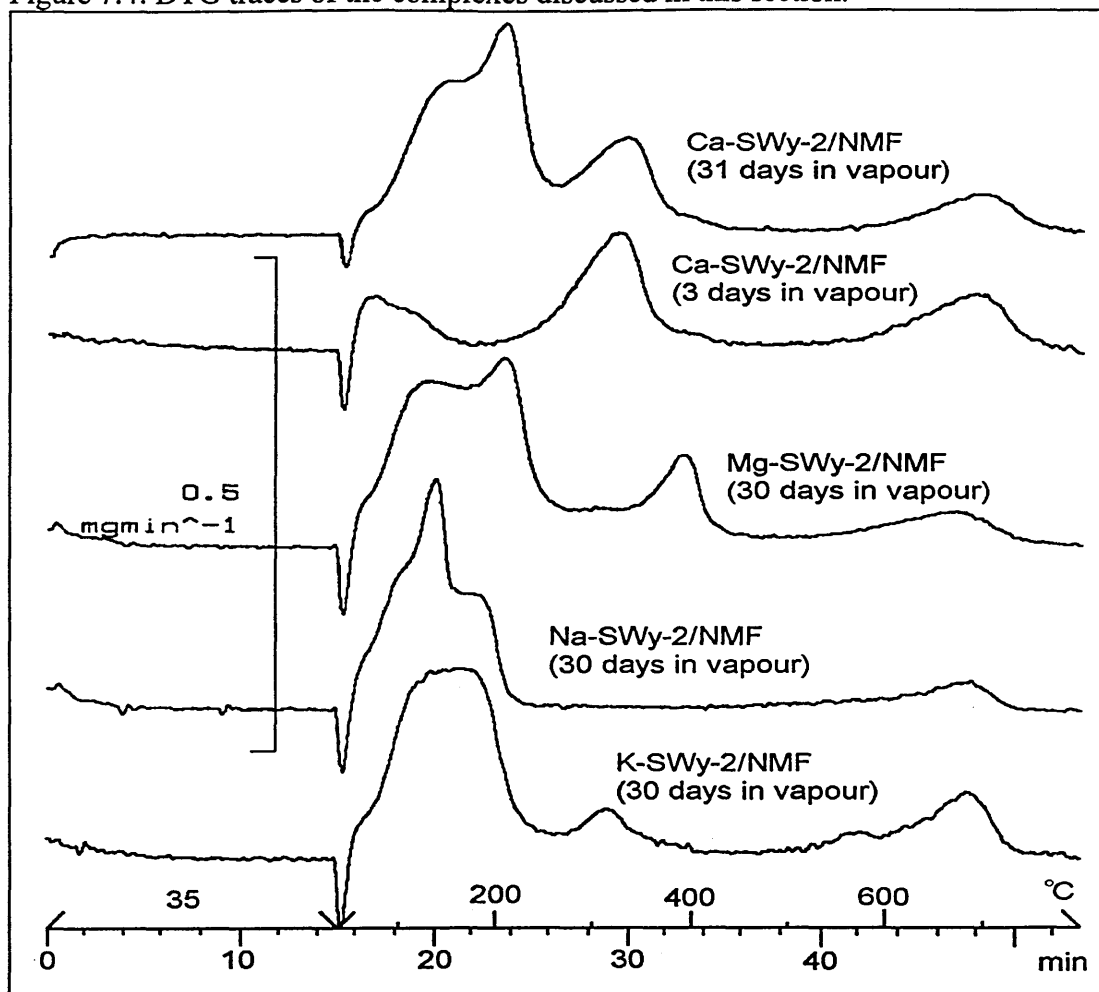


Table 7.2: Assignment of the bands observed in the infrared spectrum of pure liquid NMF.

Band position (cm ⁻¹)	Assignment
3300	ν_{NH}
3066	Fermi Resonance band
2944	$\nu_{\text{as}}(\text{CH}_3)$
2879	$\nu_{\text{s}}(\text{C-H})$
2807(shoulder) 2756(shoulder)	$\nu_{\text{s}}(\text{CH}_3)$
1667	Amide I, (mostly $\nu_{\text{C=O}}$)
1543	Amide II ($\delta_{\text{NH}} + \nu_{\text{CN}}$)
1453	$\delta_{\text{as}}(\text{CH}_3)$
1412	$\delta_{\text{s}}(\text{CH}_3)$
1384	$\delta(\text{CH})$
1321 (shoulder)	
1242	Amide III, ($\nu_{\text{CN}} + \delta_{\text{NH}}$)
1148	CH_3 rocking

Figure 7.4: DTG traces of the complexes discussed in this section.



Firstly, the infrared bands observed in the $3800\text{-}2500\text{cm}^{-1}$ region of the Ca-SWy-2/NMF complex will be discussed (figure 7.5) followed by the $2000\text{-}1000\text{cm}^{-1}$ region (figure 7.8). These spectra have been offset so that the spectra are at zero absorbance units at 4000 and 1800cm^{-1} , respectively.

$3800\text{-}2500\text{cm}^{-1}$

The spectra show that by 150°C , the bands positioned at 3300 and 3075cm^{-1} were removed, thus revealing the low wavenumber asymmetry of the band at 3420cm^{-1} and a broad band at 3105cm^{-1} of lower intensity. The intensities of the bands at 3300 and 3075cm^{-1} as a function of temperature are plotted in figure 7.7. This plot clearly shows that the majority of absorbance occurring at these wavenumbers has decreased by 150°C . These bands are assigned to the N-H stretching and Fermi resonance bands of NMF, respectively (table 7.2). The frequencies of these bands are similar to those

Figure 7.5: VT-DRIFTS spectra of Ca-SWy-2 after exposure to NMF vapour for 31 days (3800-2500 cm^{-1})

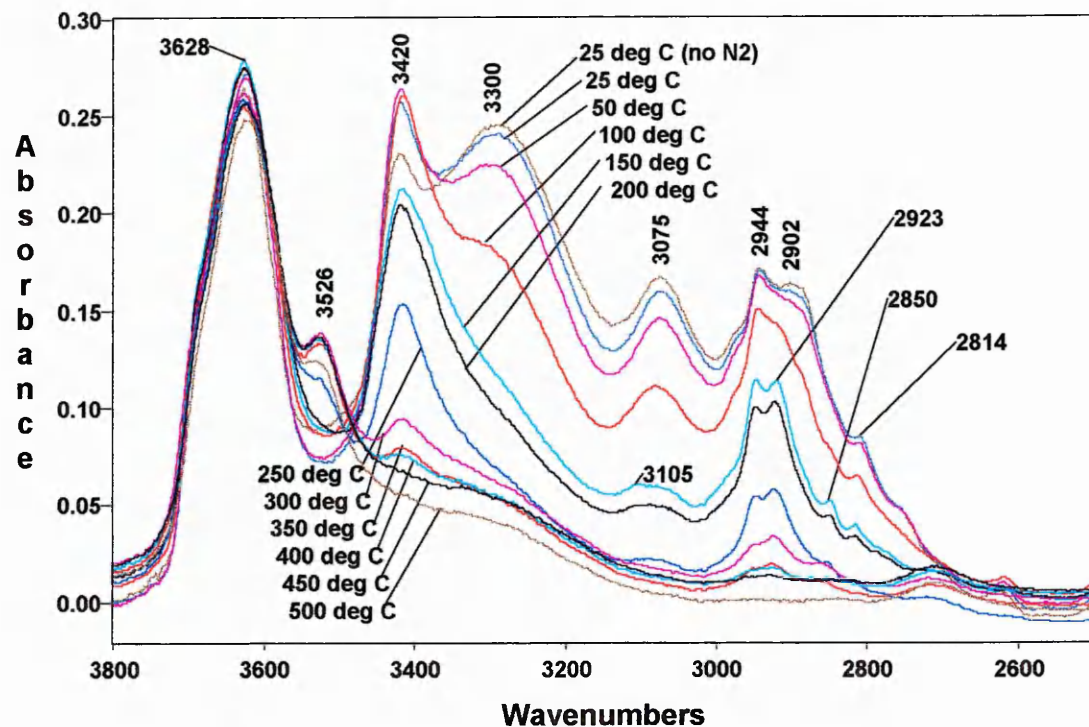
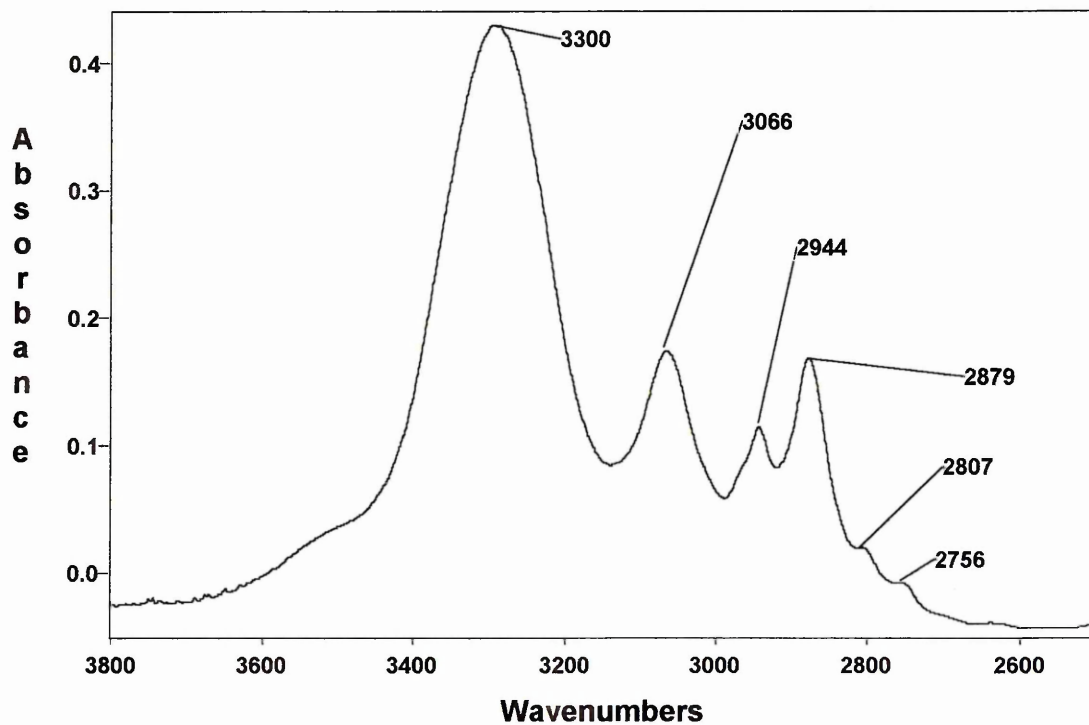


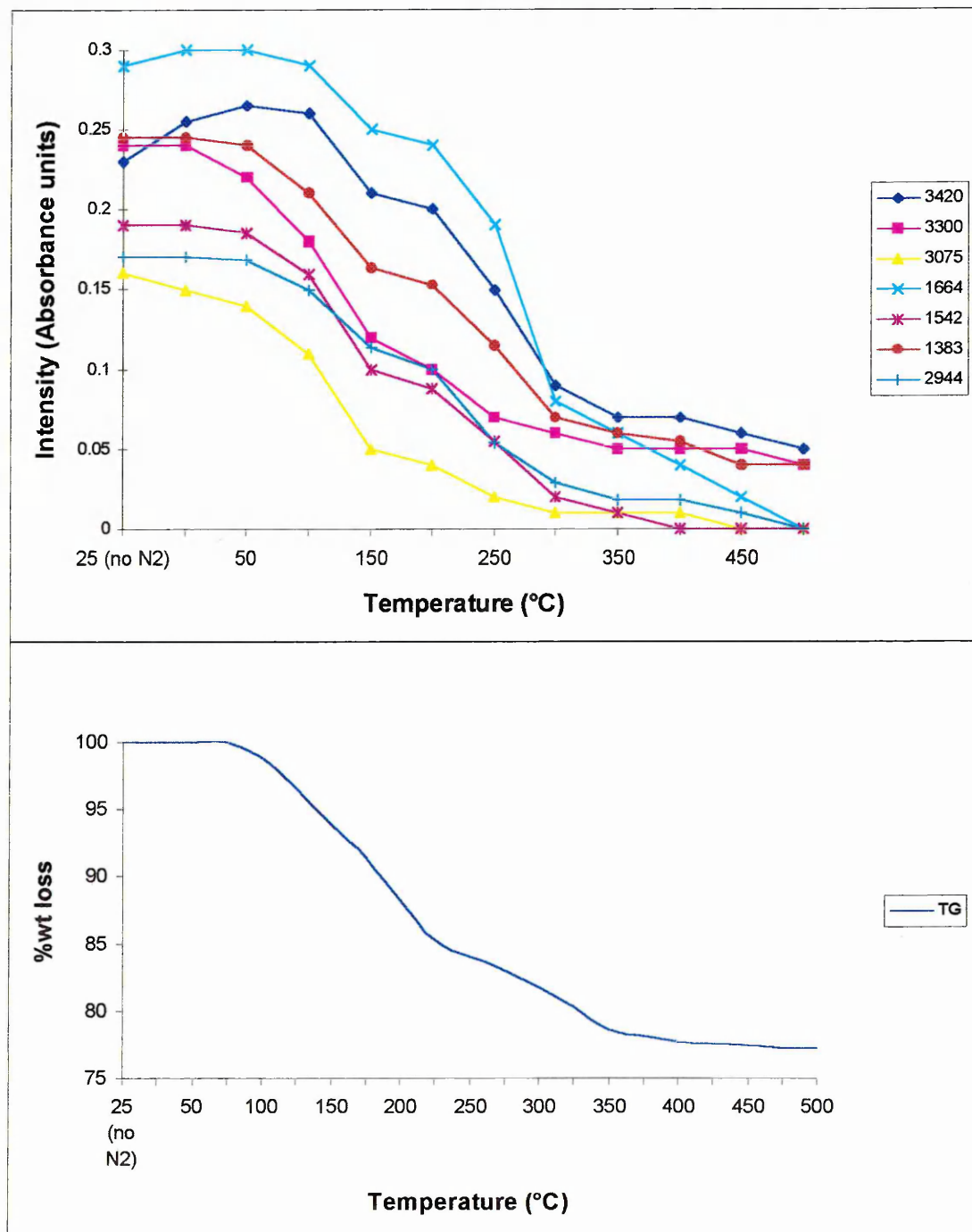
Figure 7.6: Infrared spectrum (transmission) of NMF (3800-2500 cm^{-1}).



of NMF when it is in its liquid state (figure 7.6). These bands, which relate to the low temperature maximum in the DTG trace (120°C), suggest that the NMF present up to

150°C in the complex is in a form similar to that of the liquid state (i.e. self associated with a strong H-bonding network).

Figure 7.7: A plot of intensity of selected bands in the VT-DRIFTS spectra of the Ca-SWy-2/NMF complex (30 days in vapour). Its TG curve is also plotted.



When NMF molecules change from a pure liquid state to a diluted solution (e.g. in CCl_4) and then to a vapour, they move further apart and the hydrogen-bonding

network becomes weaker. As a result the N-H stretching band progressively shifts to a higher wavenumber. This fact suggests that the band at 3420cm^{-1} is assigned to the N-H stretching bond of NMF molecules that are not hydrogen bonded to other NMF molecules. This band is unlikely to be due to water since the TG-FTIR data shows the majority of water has been replaced by NMF. The infrared spectrum of NMF molecules that have been diluted in CCl_4 (so that little or no H-bonding occurs), shows two N-H stretching bands at 3466 and 3429cm^{-1} , and no Fermi resonance band [274]. The position of these bands are at a higher wavenumber than that in the complex (3420cm^{-1}) and therefore suggest that the N-H bonds are not totally free but are still experiencing some form of interaction. It is therefore possible that the N-H bonds in the NMF molecules giving rise to this infrared band are forming a relatively weak interaction with the clay structure.

The band at 3420cm^{-1} increases in intensity after the sample is purged with nitrogen for 15 minutes. This band then slightly decreases in intensity between $100\text{-}200^\circ\text{C}$ and decreases significantly between $200\text{-}350^\circ\text{C}$. The intensity of this band is plotted as a function of temperature in figure 7.7. This plot clearly shows that the majority of the 3420cm^{-1} band is lost between $200\text{-}350^\circ\text{C}$, which relates to the high temperature maximum (300°C) observed in the DTG trace of the complex. Thus, the N-H bonds in the NMF molecules occupying this high temperature site are undergoing relatively weak interactions (i.e. not hydrogen-bonded to other NMF molecules). The plot also shows that the band decreases in intensity between $100\text{-}200^\circ\text{C}$, which relates to the two low temperature maxima observed in the DTG trace. This indicates that the N-H bonds in some of the NMF molecules occupying these sites are also undergoing relatively weak interactions.

When the sample is heated from $150\text{-}250^\circ\text{C}$, the asymmetry on the low wavenumber side of the band at 3420cm^{-1} band is reduced. The asymmetry of this band is presumably due to a range of N-H bonds that exhibit an intermediate range of strengths of interactions. These bands relate to the second highest temperature maximum (180°C) in the DTG trace.

It is interesting to note that after purging the sample with nitrogen for 15 minutes (at 25°C) the number of NMF molecules that have N-H bonds experiencing relatively weak interactions (which is indicated by the 3420cm^{-1} band) increases. This could be

due to liquid-like NMF clusters being removed leaving non-intermolecular hydrogen-bonded NMF molecules on clay surfaces. It could also be due to the removal of water which may be hydrogen-bonded to the N-H group of NMF molecules.

The behaviour of the N-H stretching bands observed in the infrared spectra of the Ca-SWy-2/NMF complex is characteristic of other amide-smectite complexes. Tahoun and Mortland [277] studied the interaction of N-ethylacetamide with Na and Ca-montmorillonite by infrared spectroscopy. They found that the spectra of the complexes exhibited two N-H stretching bands at 3450 and 3320 cm^{-1} which were assigned to free N-H bonds and intermolecular-hydrogen-bonded N-H bonds, respectively. The infrared spectrum of the pure liquid showed the N-H stretching band to be at 3320 cm^{-1} .

The assignment of the band at 3105 cm^{-1} observed in the Ca-SWy-2/NMF complex at 150°C is unclear, although three possibilities exist;

i) it could be assigned to the Fermi resonance band of the NMF molecules that produce the low wavenumber asymmetry of the band at 3420 cm^{-1} . The N-H band being at higher frequency could correspond with the Fermi resonance band also being at higher frequency. This assignment may not be correct since as the hydrogen bonding network in NMF 'breaks up' as it is diluted in CCl_4 , the frequency of the N-H stretching band increases and the Fermi resonance band becomes weaker in intensity and almost disappears. The Fermi resonance band results from the fundamental N-H stretching band being of similar frequency to the first overtone band of the $\delta(\text{NH})$ band. As the fundamental N-H stretching band of the NMF molecules not self-hydrogen-bonded shifts to higher frequency the similarity in the frequency between this and the overtone band becomes less and the Fermi resonance effect decreases. Hence, this assignment may be unlikely

ii) it could be assigned to the N-H stretching band of the cis form of the NMF molecules. This suggestion arises from an infrared investigation into the interaction of N-ethylacetamide with Ca and Na-exchanged montmorillonite [277]. The authors assigned a band at 3120 cm^{-1} to the N-H stretching vibration of the less stable cis isomer. It was suggested that the small percentage ($\approx 5\%$) of cis isomer in the liquid was selectively chosen in order to accommodate some steric considerations when intercalated in the clay. It is known that the N-H stretching band of secondary amides

in the trans configuration is near 3300cm^{-1} whereas the band in the cis configuration is near 3200cm^{-1} [278]. Several controversial papers have discussed whether the cis isomer of NMF is present in either the liquid or vapour phase [279, and references therein]. It is generally assumed that a certain amount is present in the vapour phase. Balaza [279] has calculated that there is approximately 3.7% cis form in the vapour phase at room temperature. Only one paper discussing the N-H stretching band in the infrared spectrum of the cis form of NMF has been found in the literature [280]. The authors used matrix isolation spectroscopy and the high temperature nozzle technique to obtain the infrared spectrum of the cis form. This involves analysing NMF in the gas phase and the N-H stretching frequencies of the trans and cis forms were found to be at 3490 and 3452cm^{-1} , respectively. Although these wavenumbers are at a high frequency, due to the removal of the hydrogen-bonding network, the cis form is found at a lower wavenumber than the trans form. The band at 3105cm^{-1} could therefore be due to the N-H stretching band of the cis form which is at a lower frequency than the trans form (3420cm^{-1}). This assignment is unlikely because there is such a large difference (315cm^{-1}) between the N-H bands of the cis and trans form. However, the orientation of the cis form could be different which may account for the large difference.

iii) it could be due to the overtone of the $\delta(\text{NH})$ band.

When the complex reaches 500°C all the bands assigned to the N-H stretching bond are removed, a broad band remains which is due to structural hydroxyl groups. This is known because an unexposed clay heated to 500°C exhibits the same bands.

The intensity of the C-H stretching bands between $3000\text{-}2600\text{cm}^{-1}$ decrease in intensity as the temperature of the sample is increased. In the infrared spectrum of pure NMF, the band at 2879cm^{-1} , which is due to $\nu_s(\text{C-H})$ is more intense than the band at 2944cm^{-1} , which is due to $\nu_{as}(\text{CH}_3)$. In the VT-DRIFTS spectrum collected at 25°C (prior to purging with nitrogen) the $\nu_s(\text{C-H})$ band is of similar intensity to that of the $\nu_{as}(\text{CH}_3)$ band. The relative decrease in intensity of the $\nu_s(\text{C-H})$ band (and slight increase to higher frequency) indicates that the environment of the C-H bond has changed when compared to that in the liquid. When the liquid-like NMF has been removed from the complex (as indicated by the absence of the bands at 3300 and

3076cm⁻¹) at 150°C, the $\nu_s(\text{C-H})$ band of the NMF molecules remaining appears and is at an even higher frequency (2923cm⁻¹). Such a large change ($\approx 44\text{cm}^{-1}$) is very uncommon for a C-H stretching band and this indicates that the C-H bond is orientated in a unique position.

The band positioned at 2944cm⁻¹ does not shift as the temperature is raised and its decrease in intensity is similar to that of the TG curve (figure 7.7). This indicates that the CH₃ group is not significantly involved in the interaction of the NMF molecules with the complex.

When the complex is heated to 250°C a band appears at 3526cm⁻¹, which remains upon further increases in temperature. This band does not appear when the pure clay (not exposed to NMF) is heated, but does so if the clay has been treated with DMF (see later) or acetone (own experiments and not referenced). This band does not occur when the other cation-exchanged clays that have been exposed to NMF are heated. It may be that some form of Ca-hydroxide is created, which may be induced by NMF/DMF.

2000-1000cm⁻¹

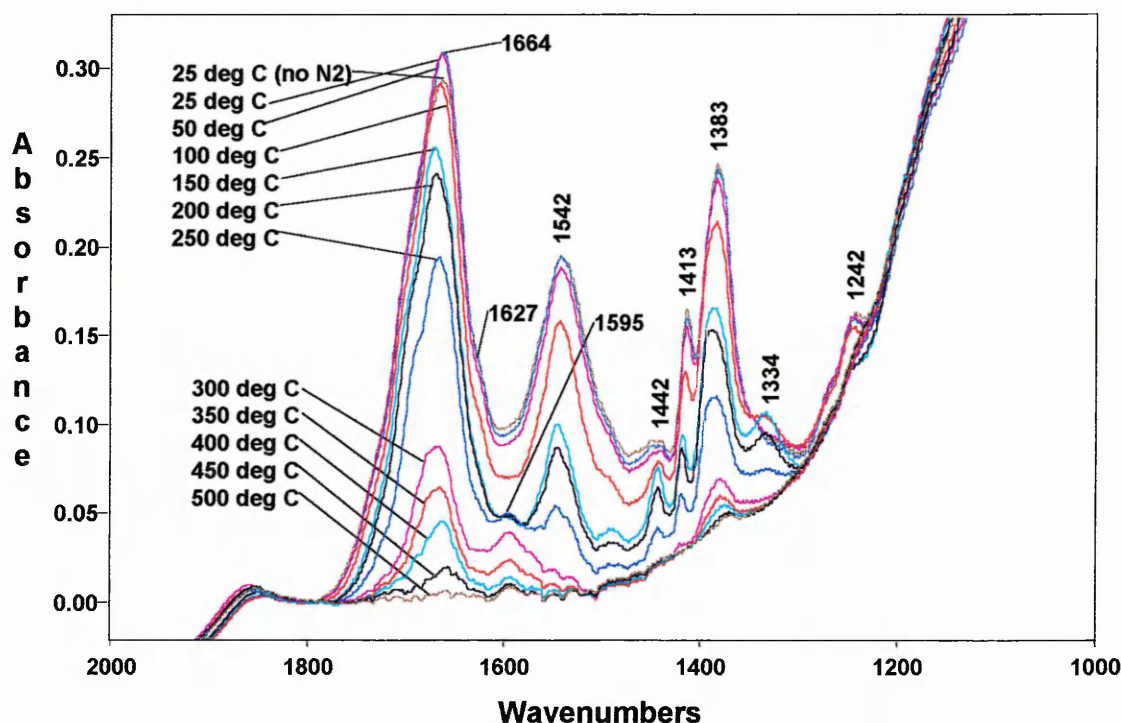
The infrared bands observed in the 2000-1000cm⁻¹ region of the complex are shown in figure 7.8.

Note that the band at 1627cm⁻¹ in the VT-DRIFTS spectra of Ca-SWy-2 not exposed to NMF (figure 7.1) is largely absent in the spectra of the Ca-SWy-2/NMF complex. This is due to the substitution of water by NMF. A small shoulder is observed at 1627cm⁻¹ indicating the presence of a small amount of water, however this is very weakly held and is removed by 100°C.

The band positioned at 1664cm⁻¹ is assigned to the amide I band, which is due mostly ($\approx 80\%$) to the stretching vibration of the carbonyl band. The intensity of this band is plotted as a function of temperature in figure 7.7. The intensity of this band decreases less between 25-250°C than between 250-350°C. This is not expected since a greater percentage weight loss occurs on the TG curve (figure 7.7) between 25-250°C rather than 250-350°C. The reason for this could be that the NMF molecules relating to the high temperature maximum (250-350°C) in the DTG trace have a higher extinction

coefficient than those relating to the two low temperature maxima. This suggestion is supported by the fact the bands at 1542 and 1383 cm^{-1} (also due to NMF) decrease in intensity proportionally to the loss in weight of the complex (figure 7.7). It is expected that a large decrease in the carbonyl band would be observed during the removal of liquid-like NMF (35-150 $^{\circ}\text{C}$) since its extinction coefficient is very large. This does not occur and could be due to a combination of loss of liquid-like NMF and an increase in the extinction coefficient of the coordinated NMF molecules remaining.

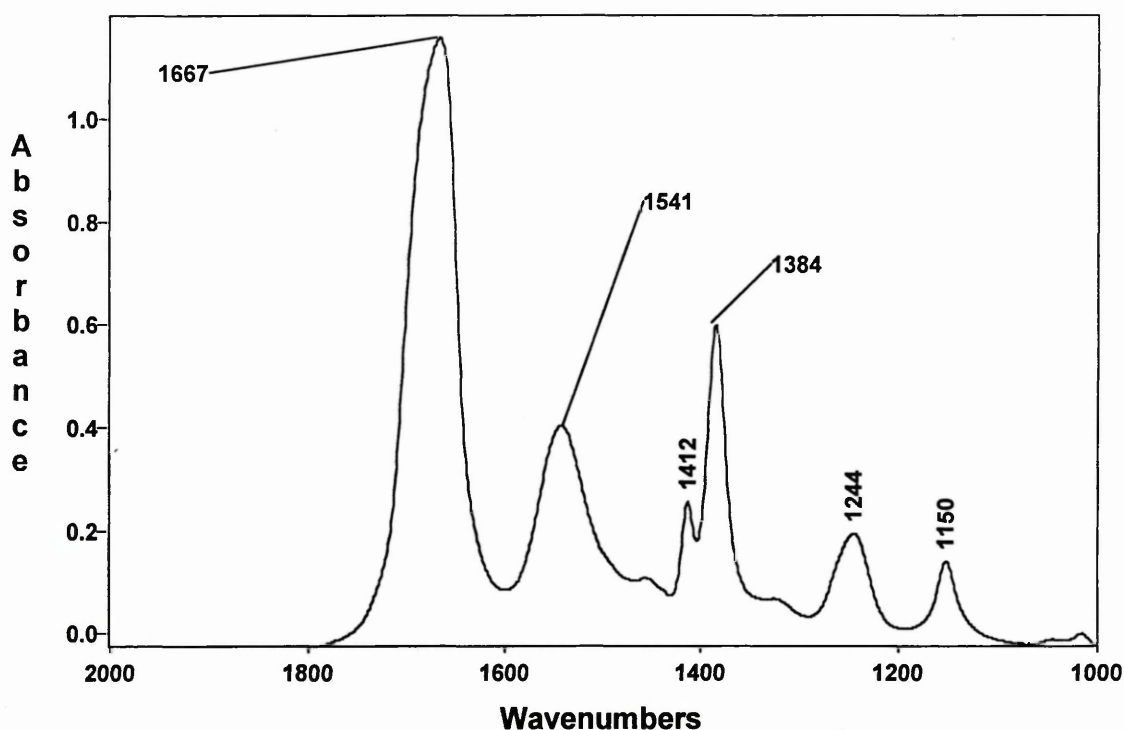
Figure 7.8: VT-DRIFTS spectra of Ca-SWy-2 after exposure to NMF vapour for 31 days (2000-1000 cm^{-1})



There are subtle changes in the carbonyl band shape as the temperature is increased. These will be discussed in comparison with the carbonyl bands of the other cation-exchanged clay/NMF complexes later (section 7.2.3). The point to note at this stage is that the NMF molecules that are not hydrogen-bonded to other NMF molecules bind to the clay via their carbonyl group. This can be shown by observing the band positions in the spectrum collected at 250 $^{\circ}\text{C}$. The position of the carbonyl band in NMF molecules that are not interacting through their carbonyl group (i.e. in a dilute solution of CCl_4) is at 1698 cm^{-1} . In the spectrum collected at 250 $^{\circ}\text{C}$ in the Ca-SWy-

2/NMF complex the carbonyl band is positioned at 1667cm^{-1} , which is the same as that in liquid NMF (figure 7.9). This indicates a strongly interacting carbonyl group, whilst the corresponding N-H stretching band is positioned at a higher wavenumber indicating a free N-H bond (a shift of the C=O band to a higher wavenumber corresponding with the N-H stretching band remaining constant may indicate the reverse). Although amides can donate electrons from either the oxygen atom of the carbonyl group or from the N atom of the amino group, interaction is expected to be more likely through the oxygen atom. Theoretical and experimental evidence has shown this to be more sterically and energetically favourable [281 and references therein].

Figure 7.9: Infrared spectrum (transmission) of NMF ($2000\text{-}1000\text{cm}^{-1}$).



The bands at 1542 , 1413 and 1383cm^{-1} in the VT-DRIFTS spectra of the complex at 25°C (no nitrogen) are at the same position as those in the NMF liquid (figure 7.9). The band at 1542cm^{-1} is assigned to the amide II band which is due to almost pure N-H deformation ($\approx 80\%$). If this band shifts to higher frequency it indicates that the N-H bond is experiencing a higher degree of interaction because more energy is required to overcome the constrained hydrogen atom. Since the position of this band slightly

increases in frequency ($\approx 5\text{cm}^{-1}$) as the temperature increases from 25-250°C, it indicates that the N-H band is progressively interacting more strongly. The spectrum collected at 300°C, and at higher temperatures, shows the appearance of a band at 1595cm^{-1} . The assignment of this band is unclear, although there could be three possibilities:-

i) a shift of the 1542cm^{-1} band to higher frequency, since the 1542cm^{-1} band is not present in the spectrum collected at 300°C. This shift would indicate that the N-H bond will be experiencing an even higher degree of interaction. This could be the case because at 300°C the clay layers (see VT-XRD data later, section 7.2.4) have collapsed and hence the N-H bond of trapped NMF molecules will be in close proximity to the clay layers. The N-H bond could therefore be interacting with the negatively charged oxygen atoms on the clay surface or placed within a hexagonal cavity. However, a 70cm^{-1} shift may be considered to be unlikely.

ii) The band at 1595cm^{-1} could to be due to the carbonyl bonds of NMF molecules that are very strongly coordinated. The NMF molecules retained at high temperatures are likely to be interacting very strongly with the clay (probably through the exchangeable cation), which may result in a shift to lower frequency. However such large shifts are unlikely for amides.

iii) The band could be due to the $\delta(\text{N-H})$ of a protonated NMF molecule. No spectra are available of protonated NMF molecules in the literature and so confirmation of this species is not possible. However, this species is unlikely to be present since no corresponding N-H stretching bands are observed in the $3450\text{-}3000\text{cm}^{-1}$ region.

The band at 1413cm^{-1} is due to $\delta_s(\text{CH}_3)$ and seems to be unaffected upon increasing the temperature and therefore indicates it is not greatly involved in the interaction of the NMF molecules with the clay as suggested by the 2944cm^{-1} band.

The band at 1383cm^{-1} is assigned to the amide III band and is due to almost pure C-N stretching. This also seems to be unaffected when the temperature is increased. However, a band at 1334cm^{-1} appears between 100-250°C and could be a result of a shift of the 1383cm^{-1} band to lower frequency. This shift indicates that the bond order has decreased (i.e. more of a single bond character). The presence of this band relates to the second highest temperature maximum (180°C) in the DTG trace and shows that

some of the NMF molecules at this stage lose some of their double bond character as they are interacting with the clay.

In order to support the above interpretations a sample of Ca-SWy-2 exposed to NMF vapour for only 3 days was studied by VT-DRIFTS. The DTG trace showed two maxima in addition to the dehydroxylation maximum (figure 7.4). The first maximum is small and positioned at approximately 90°C (percentage weight loss = 2.7%) and the second maximum is positioned at 320°C (percentage weight loss = 6.4%). It was assumed that the maxima were due to the removal of physisorbed water and chemisorbed NMF (directly bound to the cation), respectively. The VT-DRIFTS spectra will be able to prove this. In addition it will be possible to determine whether the presence of extra NMF molecules (i.e. those creating the two low temperature maxima in the DTG trace of the complex exposed for 31 days) affects the infrared bands of the NMF molecules creating the high temperature maximum (320°C).

Figure 7.10 and 7.11 show the VT-DRIFTS spectra of Ca-SWy-2 after exposure to NMF vapour for 3 days in the regions 3800-2500cm⁻¹ and 2000-1000cm⁻¹, respectively. The spectra are offset so that the baselines are at zero and 0.1 at 4000 and 1850cm⁻¹, respectively. The small sharp bands observed intermittently between 1800 and 1400cm⁻¹ are due to water vapour.

3800-2500cm⁻¹

The spectra show that as the temperature increases a decrease in the intensity of the bands occurs. The first point to note in the spectrum collected at 25°C (prior to purging with nitrogen) when compared to those obtained after 31 days exposure to NMF vapour (figure 7.5) is that there is no prominent band at 3300cm⁻¹. Instead a very broad band with a maximum at 3392cm⁻¹ is observed. This broad band is due to the O-H stretching bands of water and the underlying NMF bands. This is supported by the presence of a band at 1627cm⁻¹ (figure 7.11), which is due to the H-O-H bending of water. Both these bands are partially removed, and the absorption intensity between 3628 and 3420cm⁻¹ decreases when the sample is heated to 100°C. This

Figure 7.10: VT-DRIFTS spectra of Ca-SWy-2 after exposure to NMF vapour for 3 days (3800-2500 cm^{-1})

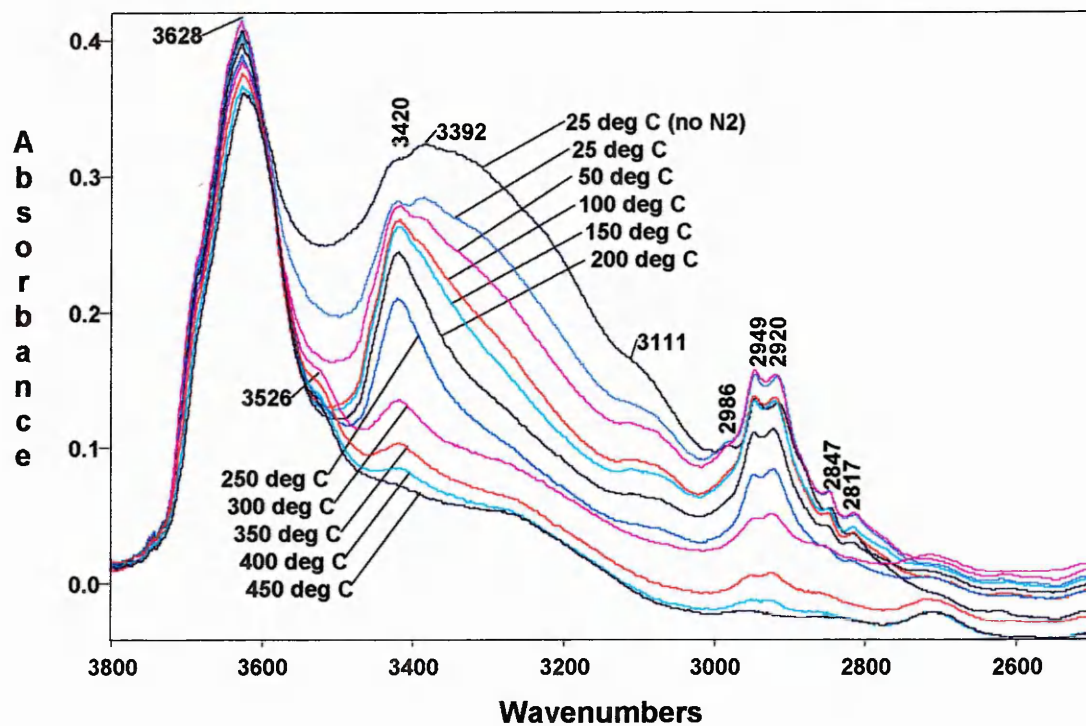
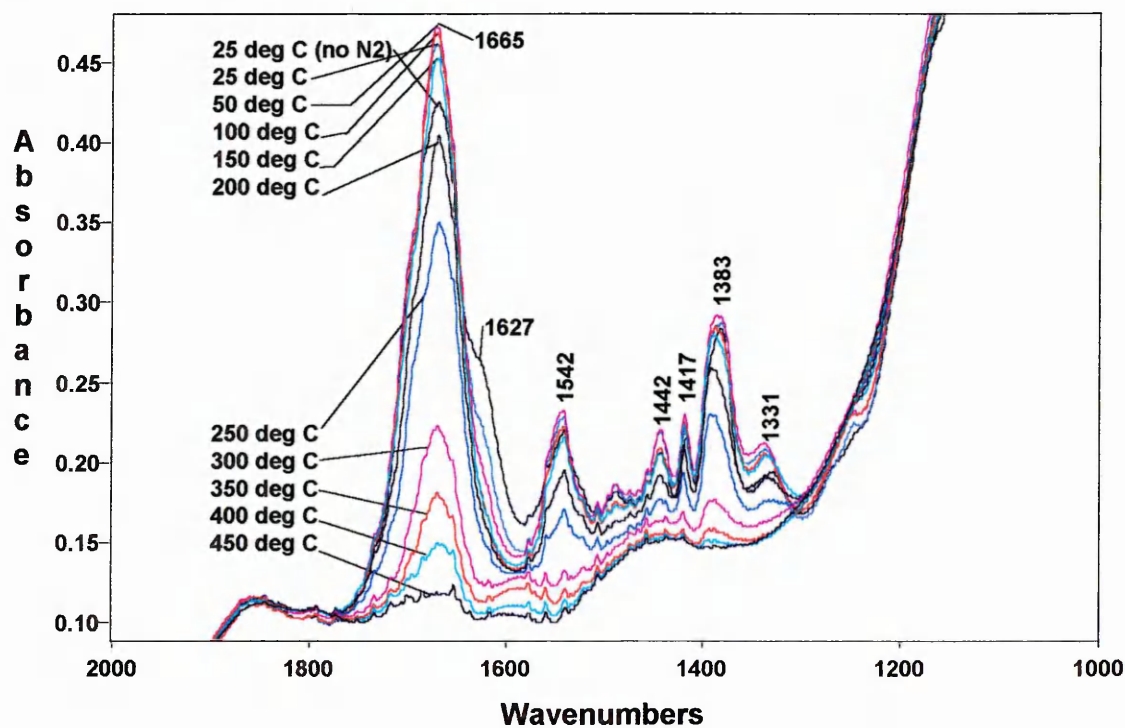


Figure 7.11: VT-DRIFTS spectra of Ca-SWy-2 after exposure to NMF vapour for 3 days (2000-1000 cm^{-1})



observation relates to the first maximum observed in the DTG trace at approximately 90°C and is clearly due to the loss of physisorbed water.

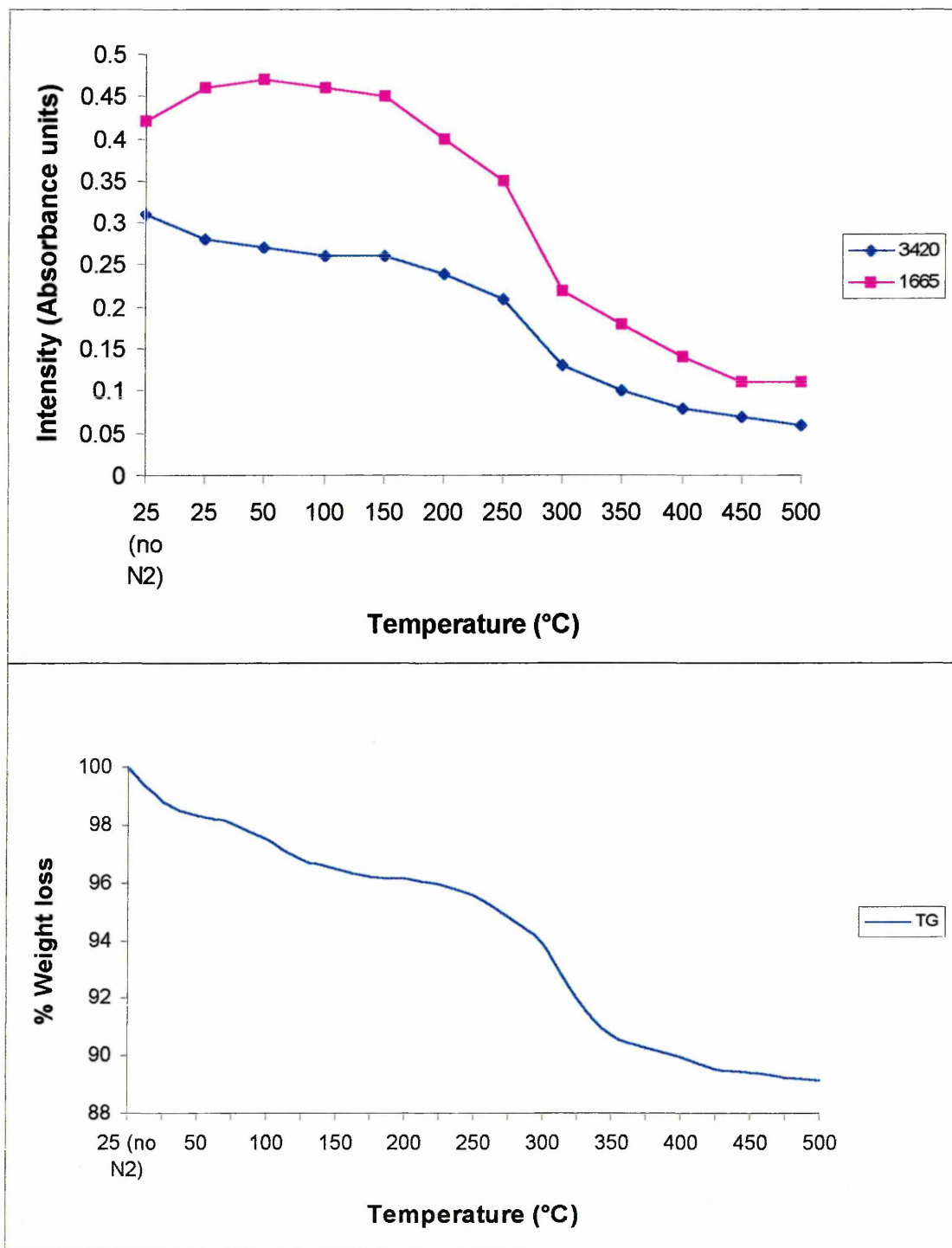
The absence of bands at 3300 and 3075cm⁻¹ indicates that there are no intermolecular hydrogen-bonded NMF molecules similar to those in NMF liquid present.

The spectra collected at 200°C from the complexes formed after 3 and 31 days are almost identical. An asymmetric band at 3420cm⁻¹ is observed in both which indicates the presence of NMF molecules with N-H bonds that are interacting less strongly than those in liquid NMF. The intensity of this band for the complex formed after 3 days is plotted as a function of temperature in figure 7.12. The figure shows that the greatest decrease in intensity occurs between 250-350°C. This loss relates to the high temperature maximum (320°C) in the DTG trace of the complex (see TG curve shown in figure 7.12). The decrease in intensity observed in the plot of the 3420cm⁻¹ band between 25-100°C is due to the removal of the O-H stretching band of water which contributes to the absorbance in the same region.

The band positioned at 3105cm⁻¹ in the spectrum collected after 31 days exposure is not as prominent and appears at a higher wavenumber (3111cm⁻¹) in the spectrum collected after 3 days exposure. The change in position is probably due to the absence of intermolecular hydrogen-bonded NMF molecules which have a Fermi resonance band at 3075cm⁻¹. The absence of this band accentuates the band at 3111cm⁻¹. It is thought that this band may be due to; the N-H stretching band of the cis form, the Fermi resonance band of NMF molecules which possess N-H bonds that are interacting less strongly than those in liquid NMF, or, the overtone of the $\delta(\text{NH})$ band. These spectra do not distinguish between these possibilities.

The intensity of the carbonyl band for the complex formed after 3 days is also plotted as a function of temperature in figure 7.12. This plot shows that the intensity increases slightly between 25-50°C and decreases greatly between 250-350°C. The increase may be due to an increase in the extinction coefficient of the band as NMF binds more strongly to the clay. The decrease is due to the removal of NMF molecules from the complex.

Figure 7.12: A plot of intensity of selected bands in the VT-DRIFTS spectra of the Ca-SWy-2/NMF complex (3 days in vapour). Its TG curve is also plotted.



It is interesting to note that in the spectra obtained after 3 days exposure to NMF the intensity of the band appearing at 3526cm^{-1} after heating the sample to 250°C is not as intense as the corresponding band which appears in the complex formed after 31 days exposure. The data suggests that the formation of this species depends on the amount

of NMF. It is uncertain what this species is, but it may be due to the formation of calcium hydroxide.

Comparison of the infrared bands in the $2000\text{-}1000\text{cm}^{-1}$ region of the Ca-SWy-2/NMF complexes formed after 3 (figure 7.11) and 31 days (figure 7.8) shows that they are in similar positions but their relative intensities are very different. The band at 1627cm^{-1} is more intense relative to the carbonyl band in the former complex. The 1627cm^{-1} band is due to the H-O-H bending of water and therefore indicates that there is a higher proportion of water to NMF in the complex formed after 3 days exposure.

The 1665cm^{-1} band in the spectrum collected at 25°C of the complex formed after 3 days exposure is very intense and almost identical to the corresponding band in the spectrum collected at 25°C of the complex formed after 31 days exposure, whereas the bands at 1542 and 1383cm^{-1} in the spectrum collected at 25°C of the 3 day exposed sample are more like the corresponding bands in the spectrum collected at 250°C of the complex formed after 31 days. This suggests that the extinction coefficient of the carbonyl band of the NMF molecules creating the high temperature maximum in the DTG trace is larger when NMF molecules in other sites are not present (i.e. those that create the two low temperature maxima in the DTG trace).

The band positioned at 1595cm^{-1} formed at 250°C in the Ca-SWy-2/NMF complex formed after 31 days does not appear as prominently in the spectra of the complex formed after 3 days. The reason why this band occurs is not clear as discussed previously, but shows that its formation is dependent on the amount of NMF present.

In these VT-DRIFTS spectra there is an absence of bands in the spectra due to liquid-like NMF. Spectra are thus obtained that represent the sites relating to the maximum at 320°C in the DTG trace. This applies in particular to the C-H stretching region ($3000\text{-}2800\text{cm}^{-1}$).

7.2.2) VT-DRIFTS analysis of Mg, Na and K-SWy-2/NMF complexes

The VT-DRIFTS spectra of the other cation-exchanged montmorillonite/NMF complexes exhibit similar trends. The major differences are the temperatures at which the bands characteristic of intermolecular hydrogen-bonded and non-intermolecular hydrogen-bonded NMF molecules are removed. The differences are attributed to the different polarising strengths of the exchangeable cations selected.

Mg-SWy-2

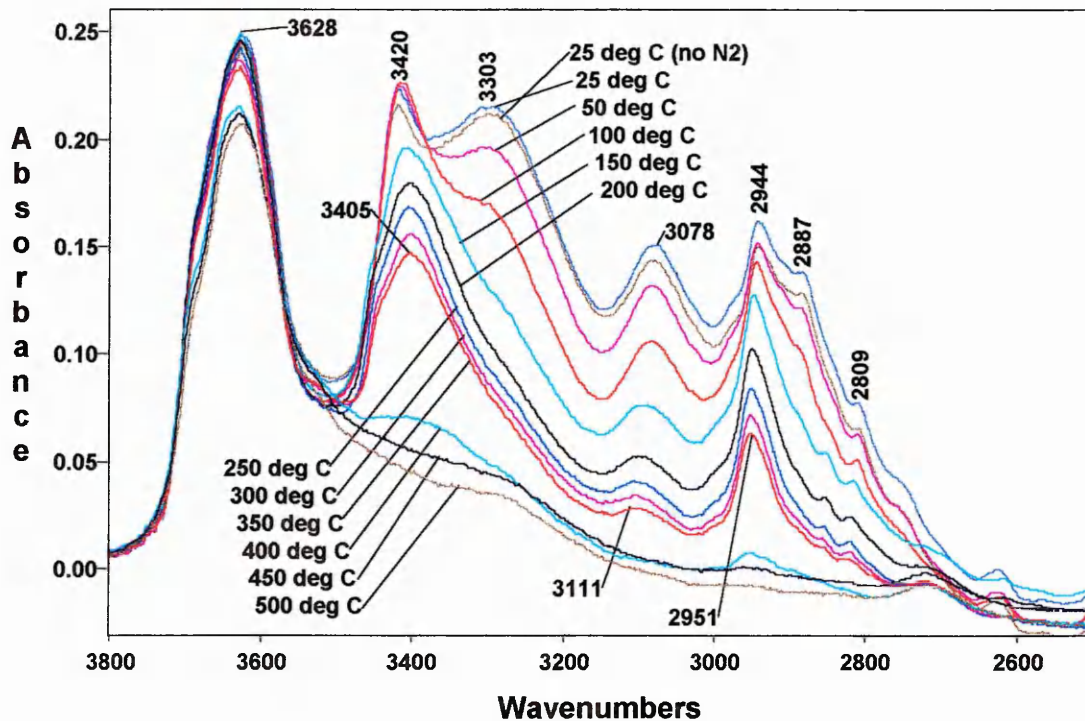
Figure 7.13 shows the $3800\text{-}2500\text{cm}^{-1}$ region of the VT-DRIFTS spectra of Mg-SWy-2 after exposure to NMF vapour for 30 days. These spectra have been offset so that the baseline reads zero absorbance units at 4000cm^{-1} . These results will be discussed in relation to the DTG trace of the complex (figure 7.4).

If these spectra are compared to those of the Ca-SWy-2/NMF complex (31 days in vapour, figure 7.5) several similarities and differences are observed.

One of the similarities is that the intensity of the bands at 3303 and 3078cm^{-1} are reduced dramatically between $25\text{-}150^\circ\text{C}$ (see figure 7.14, which shows a plot of the intensity as a function of temperature). This relates to the first maximum in the DTG trace of the Mg-complex and is due to liquid-like NMF molecules.

The spectra show the band at 3420cm^{-1} increases slightly after purging with nitrogen (at 25°C). This is probably due to the removal of intermolecular hydrogen-bonded NMF molecules leaving single molecules coordinated to the surface via its carbonyl group and hence with N-H bonds that are interacting less strongly. The band then gradually decreases in intensity (figure 7.14) between $150\text{-}350^\circ\text{C}$. As this occurs the band position progressively shifts to lower wavenumbers so that by 350°C the band is at 3405cm^{-1} . These band changes relate to the maximum at 200°C and the valley between $260\text{-}340^\circ\text{C}$ in the DTG trace and indicate that the N-H bonds in the non-intermolecular hydrogen-bonded NMF molecules are interacting with their environment more strongly as the temperature increases. This is related to a decrease in the interlayer space (see VT-XRD data later, section 7.2.4).

Figure 7.13: VT-DRIFTS spectra of Mg-SWy-2 after exposure to NMF vapour for 30 days ($3800\text{-}2500\text{cm}^{-1}$)



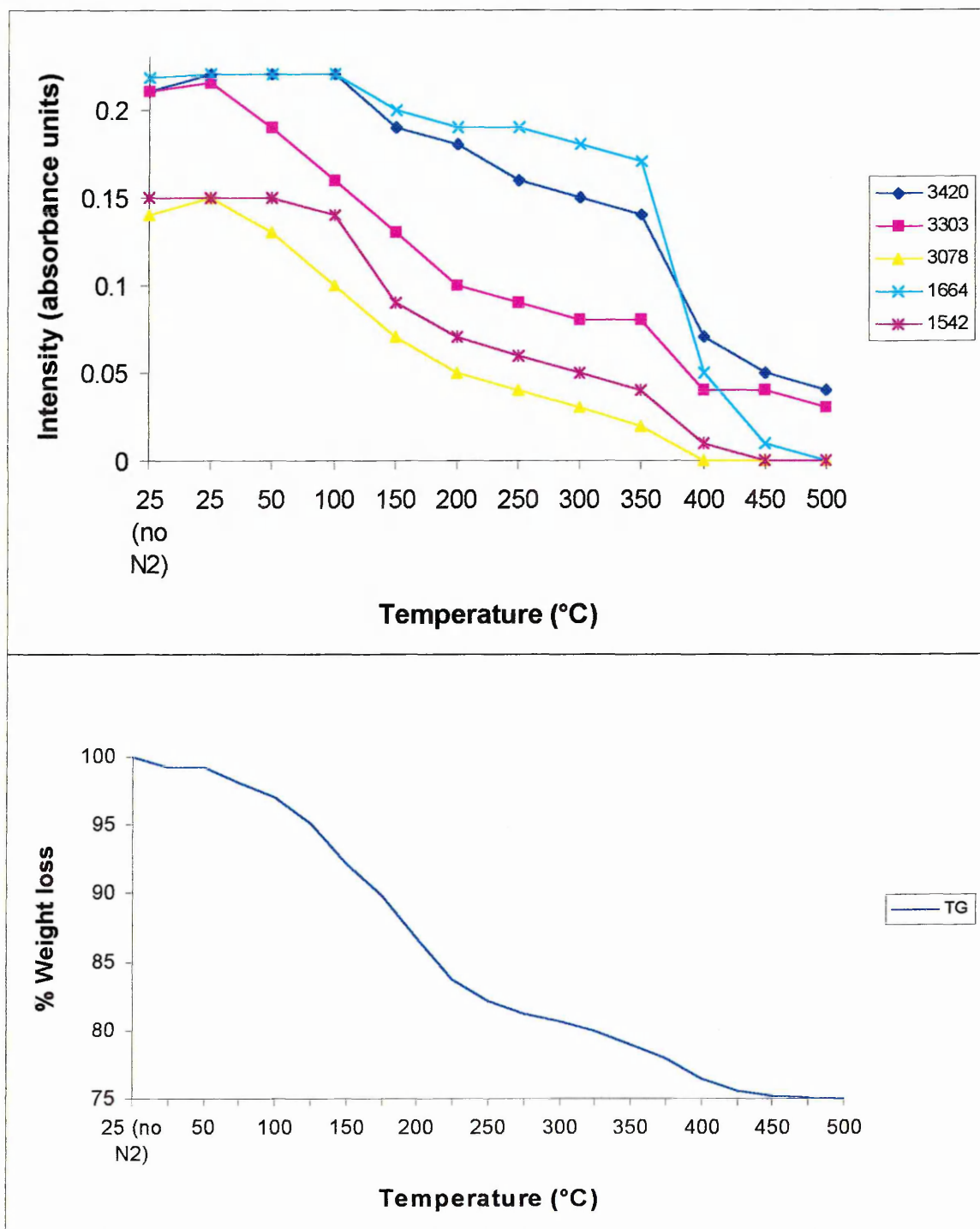
The sudden decrease in the band at 3405cm^{-1} between $350\text{-}400^\circ\text{C}$ relates to the maximum observed in the DTG trace at 400°C and is due to NMF molecules that are coordinated to the cation but not hydrogen-bonded to other NMF molecules.

The spectrum collected at 200°C from the Mg-SWy-2/NMF complex shows a more prominent band at 3105cm^{-1} than that in the Ca-complex. The band also progressively shifts to higher wavenumbers as the temperature of the sample is increased (i.e. 3111cm^{-1} at 350°C).

The spectra collected between $400\text{-}500^\circ\text{C}$ shows that the 3628cm^{-1} band decreases more obviously in the Mg-complex than the Ca-complex, which may indicate a higher amount of dehydroxylation is occurring from the surface of the clay. This may be due to the fact NMF is retained by the clay at higher temperatures and at these higher temperatures NMF catalyses the dehydroxylation. Alternatively, perturbation of the

Figure 7.14: A plot of intensity versus temperature of a selection of bands in the VT-DRIFTS spectra of the Mg-SWy-2/NMF complex (30 days exposure to vapour).

Its TG curve is also shown.



O-H stretching vibration may occur from the Mg cation, because at such high temperatures the cation is able to enter into the hexagonal cavities of the silica sheet.

Although a slight increase in intensity occurs at 3526cm^{-1} , no distinct band is observed as was the case for the Ca-SWy-2/NMF complex and supports the formation of a Ca-hydroxide species.

The C-H stretching bands decrease in intensity as the temperature increases. The C-H stretching region of this complex is different to that of the Ca-SWy-2/NMF complex in that after the $\nu_s(\text{C-H})$ band due to intermolecular hydrogen-bonded NMF molecules is removed (2887cm^{-1}), the $\nu_s(\text{C-H})$ band appears closer to the $\nu_{\text{as}}(\text{CH}_3)$ band (2944cm^{-1}). The $\nu_s(\text{C-H})$ band contributes to the low wavenumber asymmetry side of the band at 2944cm^{-1} . As a result the intensity of the band at 2944cm^{-1} relative to the band at 2809cm^{-1} is larger than the corresponding bands in the Ca-SWy-2/NMF complex (i.e. the bands at 2944 and 2814cm^{-1}). This further increase in frequency of the band indicates that the C-H bond in the NMF molecules retained at higher temperatures is in a more restricted environment. This is probably due to the close proximity of the molecules to the clay layers.

Figure 7.15 shows the VT-DRIFTS spectra of the Mg-SWy-2/NMF complex in the region $2000\text{-}1000\text{cm}^{-1}$. These spectra have been offset so that the baseline reads zero absorbance units at 1800cm^{-1} . If these spectra are compared with those obtained from the Ca-SWy-2/NMF complex several similarities and differences are apparent.

One similarity is the absence of a strong band at 1627cm^{-1} indicating that removal of water from the clay has occurred. A small shoulder is observed at this wavenumber which indicates the presence of a small amount of water, this is removed by 100°C .

The spectra show that the intensity of the carbonyl band (1664cm^{-1}) decreases in four phases;

I) $100\text{-}150^\circ\text{C}$

II) $150\text{-}350^\circ\text{C}$

III) $350\text{-}400^\circ\text{C}$

IV) $400\text{-}500^\circ\text{C}$

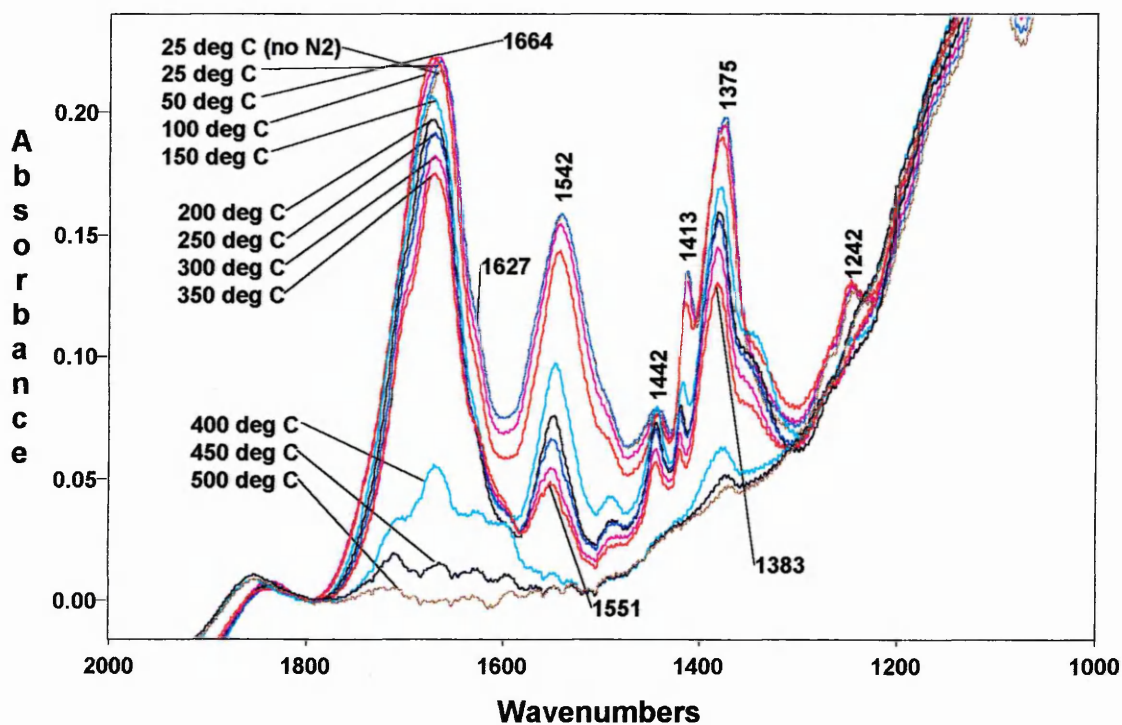
Phase I corresponds to the loss of the first maximum in the DTG trace, whilst phase II corresponds to the loss of the second maximum and the valley between $260\text{-}340^\circ\text{C}$.

Phase III corresponds to the loss of the maximum at 400°C in the DTG trace.

Although the percentage weight loss in the TG-curve (figure 7.14) of the complex

shows that more NMF is lost between 100-350°C than 350-400°C the decrease in intensity of the band does not show this, i.e. a greater decrease is observed in the band intensity between 350-400°C (figure 7.14). The carbonyl band in the NMF molecules creating the high temperature maximum (400°C) in the DTG trace may therefore have a higher extinction coefficient. This is supported by the fact the 1542cm^{-1} behaves as expected, i.e. the decrease in intensity is greater between 100-350°C than 350-400°C. This behaviour is similar to that of the Ca-SWy-2/NMF complex.

Figure 7.15: VT-DRIFTS spectra of Mg-SWy-2 after exposure to NMF vapour for 30 days ($2000\text{-}1000\text{cm}^{-1}$)

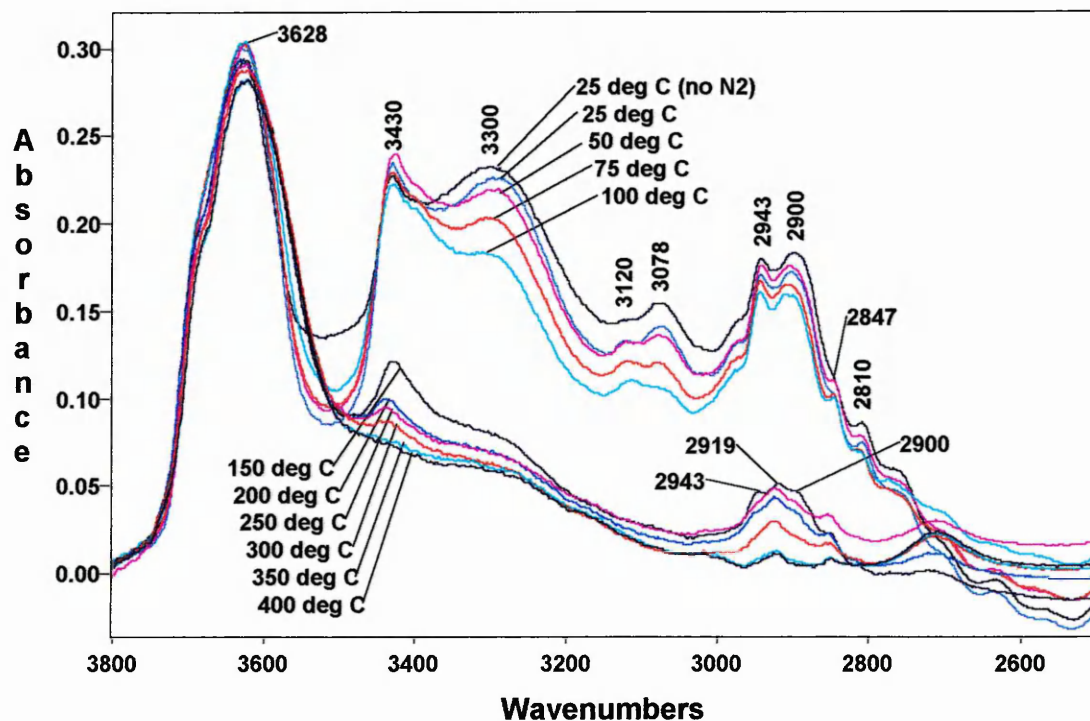


A band at 1595cm^{-1} appears in the spectrum collected at 400°C. A band also appeared in the Ca-SWy-2/NMF complex but at a lower temperature (250°C). The assignment of this band is not clear, as discussed previously.

Na-SWy-2

Figure 7.16 shows the 3800-2500 cm^{-1} region of the VT-DRIFTS spectra of Na-SWy-2 after exposure to NMF vapour for 30 days. Note that an additional spectrum was collected at 75°C.

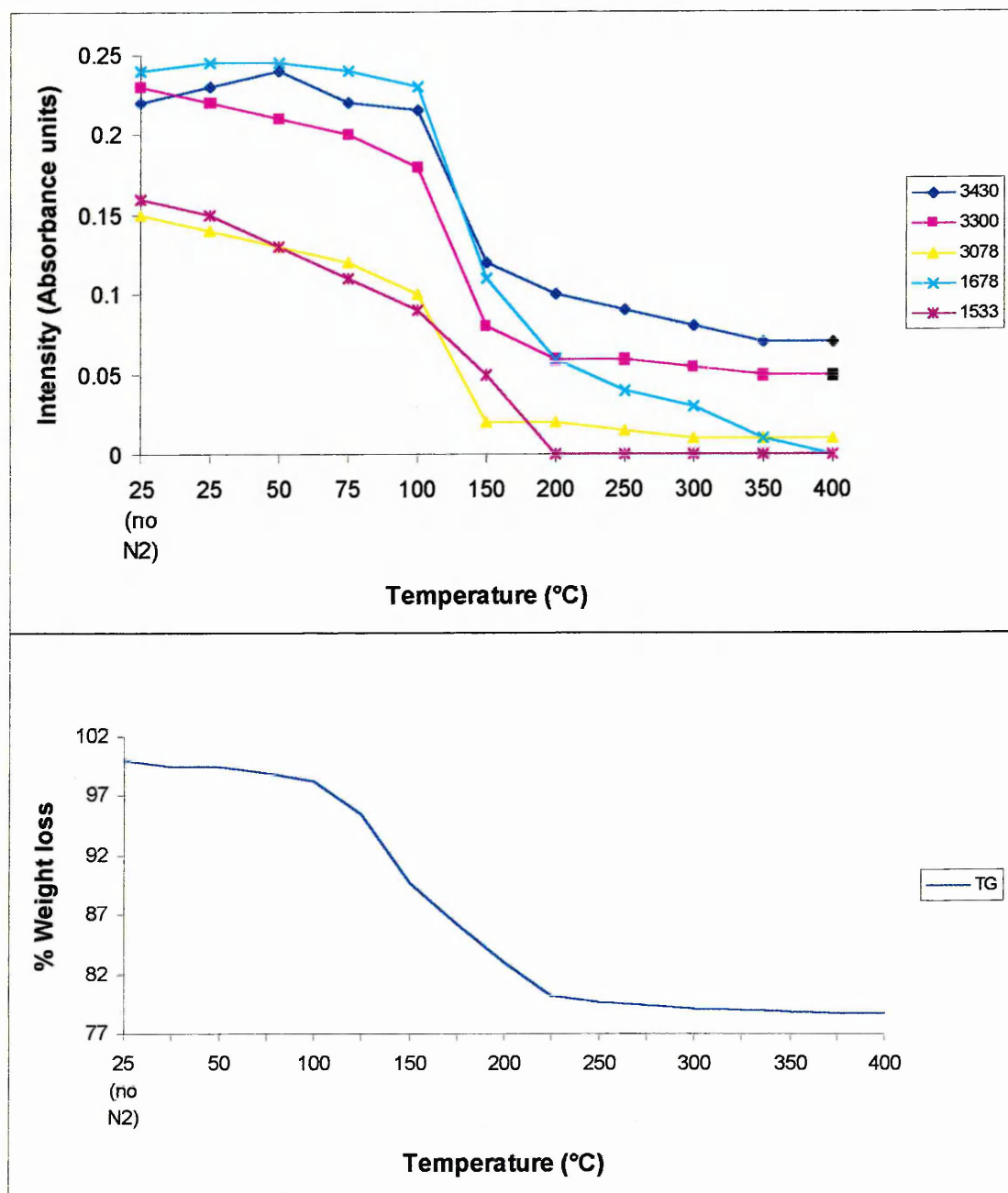
Figure 7.16: VT-DRIFTS spectra of Na-SWy-2 after exposure to NMF vapour for 30 days (3800-2500 cm^{-1})



The spectra show that the bands at 3300 and 3078 cm^{-1} decrease in intensity between 25-100°C, whilst the band at 3430 cm^{-1} remains constant (see figure 7.17 also). This indicates that the low temperature maximum (150°C) in the DTG trace is created by intermolecular hydrogen bonded NMF molecules. A comparison of the spectra collected at 100 and 150°C shows that a large decrease in intensity has occurred in the band at 3430 cm^{-1} . This indicates that the low temperature maximum in the DTG trace is also created by NMF molecules that have N-H bonds which are interacting less strongly (i.e. not liquid-like). The spectra collected at 150°C represents the NMF molecules creating the high temperature maximum (190°C) in the DTG trace. This indicates that they are not self hydrogen-bonded due to the band being positioned at 3430 cm^{-1} .

Figure 7.17: A plot of intensity versus temperature of a selection of bands in the VT-DRIFTS spectra of the Na-SWy-2/NMF complex (30 days exposure to vapour).

Its TG curve is also shown.



It is expected that this band would be greater in intensity, since only half the total weight lost from the complex occurs at 150°C. The reason for this is due to the different heating processes used for the TGA and VT-DRIFTS experiments. The heating process in the VT-DRIFTS experiment is not dynamic since the sample is retained at 150°C for 15 minutes. During this period some of the NMF species

creating the maximum in the DTG trace at 190°C are removed. This effect is not as noticeable in the Ca and Mg-SWy-2/NMF complexes because their high temperature maxima are further apart from their respective second highest temperature maxima.

The band assigned to non-intermolecular hydrogen-bonded NMF molecules is at 10cm⁻¹ higher in the Na-SWy-2/NMF complex, than the Ca and Mg-SWy-2/NMF complexes (3430cm⁻¹). This indicates that the N-H bond is undergoing a weaker interaction in the former complex.

The band at 3120cm⁻¹ is also more prominent, but these spectra do not confirm its assignment as the Fermi resonance of the 3430cm⁻¹ band, the N-H stretching band of the cis isomer, or, the overtone of the δ(N-H) band.

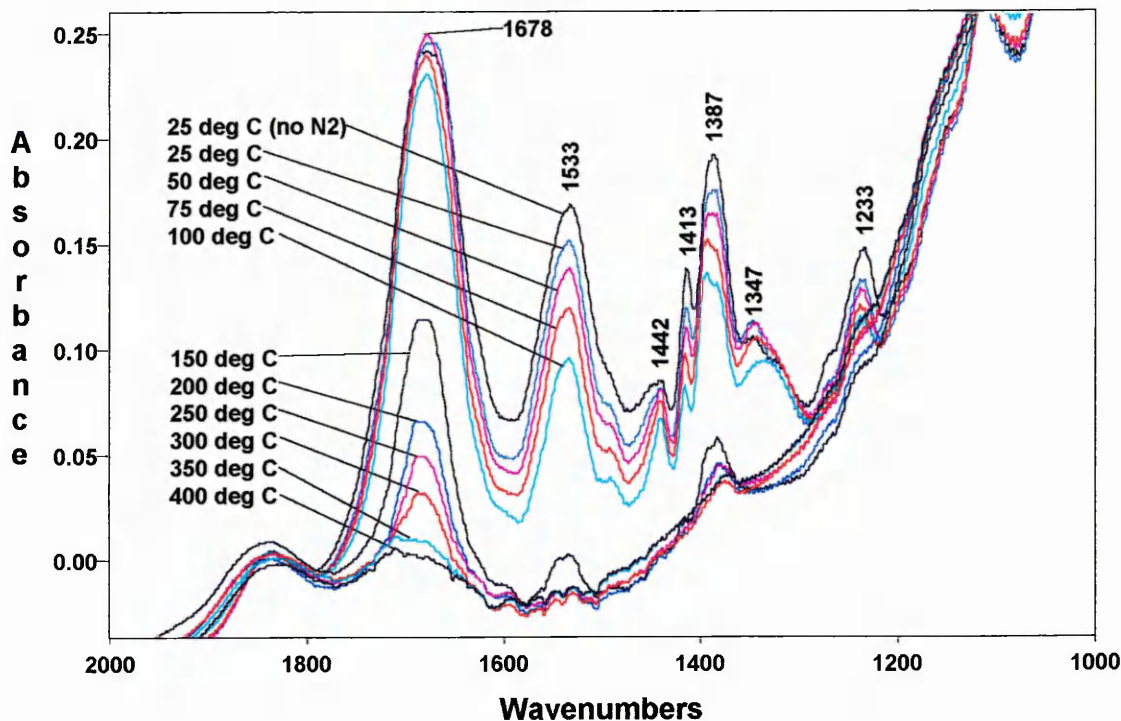
The position of the ν_s(C-H) band of the NMF molecules retained at higher temperatures (i.e. after liquid-like NMF is removed) is difficult to ascertain because of the difference in temperature at which both types are removed is small. However, the VT-DRIFTS spectrum collected at 150°C shows two bands at 2919 and 2900cm⁻¹. The presence of the two bands could be due to the presence of two sites. It is possible that the vibration of the band is restricted due to its closer proximity to the clay layers. It is closer because at this stage the clay layers have collapsed (see VT-XRD data later, section 7.2.4).

Figure 7.18 shows the 2000-1000cm⁻¹ region of the VT-DRIFTS spectra obtained from the Na-SWy-2/NMF complex. The first point to note is that the band observed at 1664cm⁻¹ in the Ca and Mg-SWy-2/NMF complexes has shifted to 1678cm⁻¹. This indicates the NMF molecules are interacting through the carbonyl group less strongly in the Na-SWy-2/NMF complex than either the Ca or Mg-SWy-2/NMF complexes. This is expected due to the stronger polarising nature of the Ca and Mg cations. This band will be discussed in more detail later (see section 7.2.3).

It can be seen in the spectra that the bands at 1533 and 1387cm⁻¹ decrease in intensity between 25-100°C, whereas the 1678cm⁻¹ does not (see figure 7.17 also). This is due to changes in the extinction coefficient of the carbonyl group as it changes its environment.

In these spectra no 1595cm⁻¹ band is formed.

Figure 7.18: VT-DRIFTS spectra of Na-SWy-2 after exposure to NMF vapour for 30 days (2000-1000 cm^{-1})



K-SWy-2

Figures 7.19 and 7.20 show the VT-DRIFTS spectra of K-SWy-2 after exposure to NMF vapour for 30 days in the regions 3800-2500 and 2000-1000 cm^{-1} , respectively. Figure 7.21 shows the plot of intensity against temperature of the bands discussed below. Similarities and differences are apparent in the spectra when compared to those of the Ca, Mg and Na-SWy-2/NMF complexes.

A decrease in intensity in the bands at 3300 and 3076 cm^{-1} occurs between 25-150°C, which indicates that intermolecular hydrogen-bonded NMF molecules create the first half of the broad low temperature maximum (100-260°C) in the DTG trace (figure 7.4). A decrease in intensity also occurs for the band at 3426 cm^{-1} between 25-150°C, indicating the loss of NMF molecules that are not hydrogen-bonded to other NMF molecules during the first half of the broad low temperature maximum in the DTG trace. It is expected that the intermolecular hydrogen-bonded NMF molecules would be removed first before those that are not. However, this is not discernible from the spectra, probably because the differences in temperature at which each species is

Figure 7.19: VT-DRIFTS spectra of K-SWy-2 after exposure to NMF vapour for 30 days (3800-2500cm⁻¹).

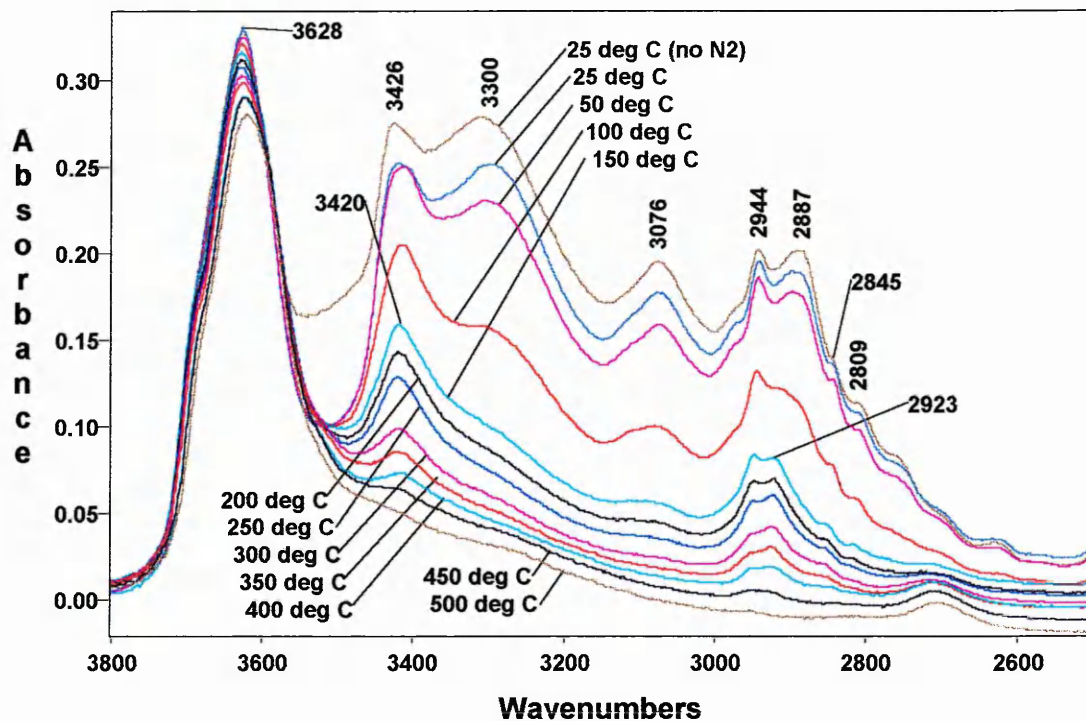
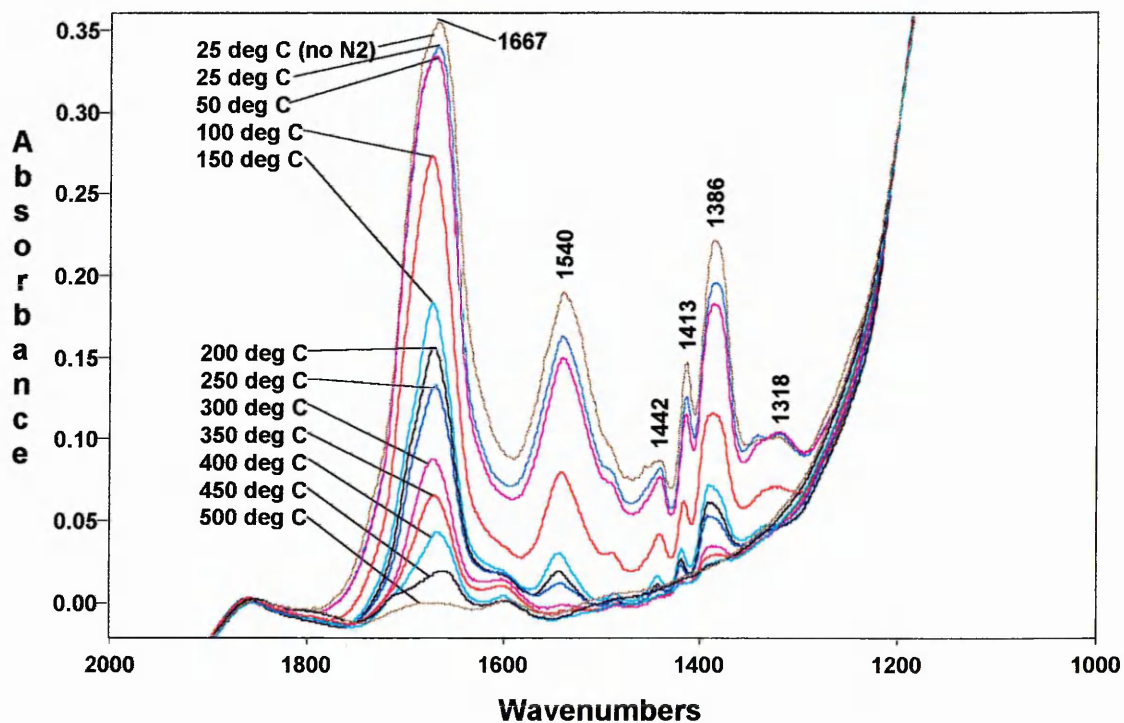


Figure 7.20: VT-DRIFTS spectra of K-SWy-2 after exposure to NMF vapour for 30 days (2000-1000cm⁻¹).

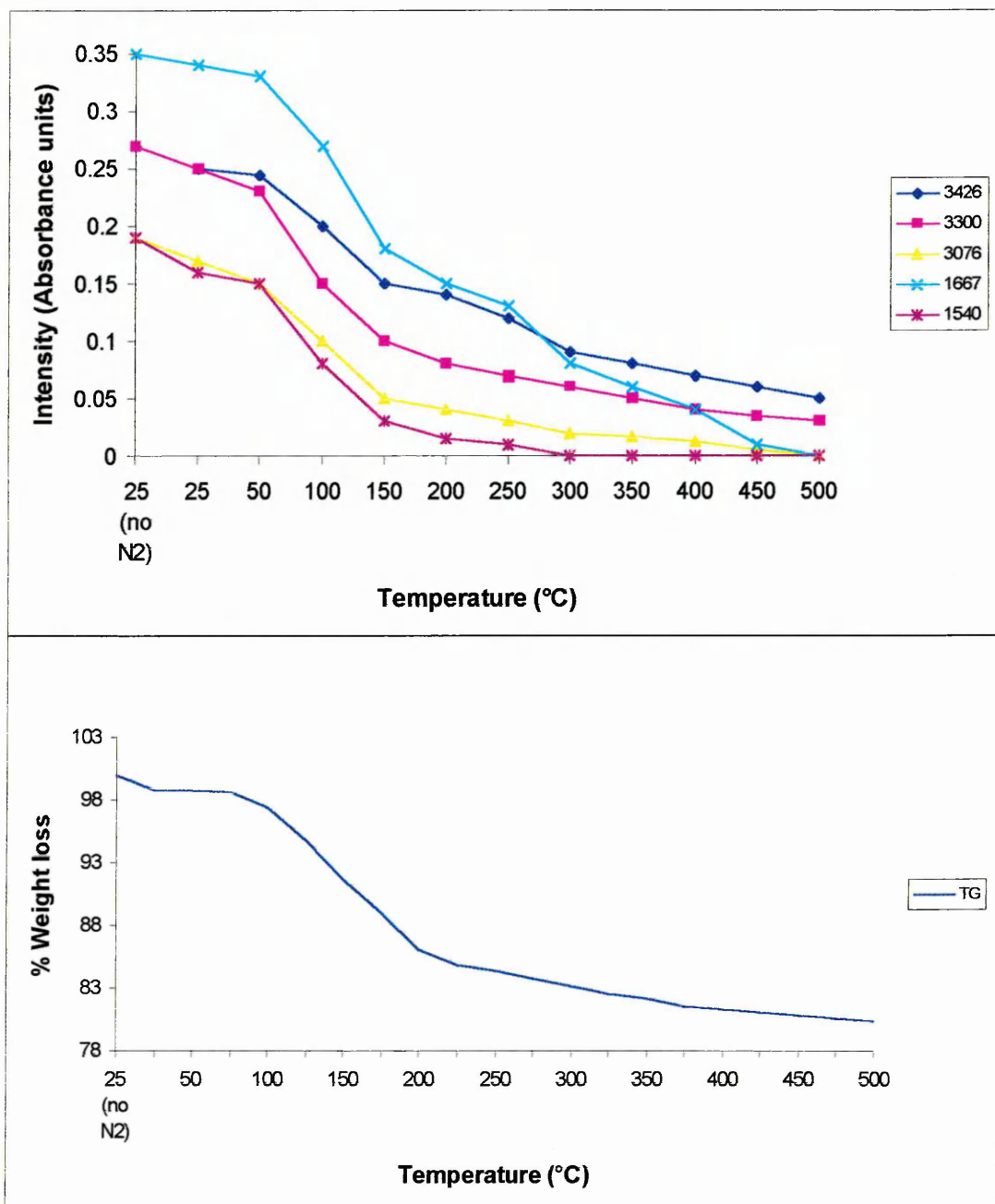


removed is too close for the heating parameters used. A gradual decrease in intensity for the carbonyl band between 25-150°C implies that NMF molecules not hydrogen bonded to other NMF molecules are present at the low temperature side of the maximum in the DTG trace also.

The bands remaining after 200°C are due to the maximum at 300°C in the DTG trace. It was thought that this maximum was NMF associated to residual Ca^{2+} ions that were unsuccessfully exchanged for K^{+} ions. The fact that the bands in the K-SWy-2/NMF complex are the same shape and in the same position as the Ca-SWy-2/NMF complex supports this suggestion.

Figure 7.21: A plot of intensity versus temperature of a selection of bands in the VT-DRIFTS spectra of the K-SWy-2/NMF complex (30 days exposure to vapour).

Its TG curve is also shown.



7.2.3) Carbonyl stretching region of the X-SWy-2/NMF complexes

It was originally thought that the position of the infrared band due to the carbonyl group of the NMF molecules would change dramatically when the NMF molecules were in different sites within the clay structure. For example, a large shift in the carbonyl band would be expected for a NMF molecule that is directly coordinated to a cation when compared to that of liquid NMF, whereas a lesser shift would be observed in the carbonyl band of NMF molecules found in clusters between stacks of clay layers.

Indeed, large shifts in the carbonyl bands of other amides have been observed. Tahoun and Mortland [277] observed shifts in the carbonyl band of acetamide and N-ethylacetamide when they were complexed with Ca, Na and Cu-exchanged montmorillonites. The carbonyl band of the acetamide shifted from 1681cm^{-1} to 1659 , 1667 and 1661cm^{-1} , when complexed with the cation exchanged clays, respectively. Whilst the carbonyl band of the N-ethylacetamide shifted from 1650cm^{-1} to 1637 , 1635 and 1621cm^{-1} , respectively. A preliminary examination of the carbonyl band observed in the clay-NMF complexes studied in this thesis showed that only very small shifts were apparent.

In order to discuss the subtle changes observed in the carbonyl band of the X-SWy-2/NMF complexes, several points need to be noted:-

i) Dilution of pure NMF in CCl_4 results in the carbonyl stretching band shifting from 1665 to $\approx 1700\text{cm}^{-1}$ [274]. This is because the carbonyl groups will be interacting less strongly with the N-H groups of other NMF molecules due to the removal of intermolecular hydrogen-bonding.

ii) The carbonyl band of NMF is very complex and has several component bands. The component bands are related to different chain lengths of NMF molecules involved in a range of interaction strengths. The carbonyl band of pure NMF is asymmetric to the high wavenumber side and indicates that a proportion of the NMF molecules are interacting less strongly via their carbonyl groups.

iii) The effect on the carbonyl band of adding cations to pure liquid NMF has not been greatly discussed in the literature. Only one (old) paper has been identified in the literature and studies both the infrared and Raman spectra of NMF/cation solutions

[282]. The authors stated that the addition of salts to pure liquid NMF causes the carbonyl band to shift to higher frequency. Some examples of the shifts observed are listed in the table below:-

	Infrared	Raman
pure NMF	1665	1655, 1690(shoulder)
NMF + NaI	1671	-----
NMF + LiI	1667	-----
NMF + LiCl	1667	1671, 1700(shoulder)
NMF + NaPF ₆	1675	1670, 1700(shoulder)

They assumed that the increase in frequency was due to the disruption of the strong hydrogen-bonding network between the NMF molecules. It seems unlikely that the carbonyl band shifts to higher frequency because it would be expected that the carbonyl group would interact at least as strongly with a cation as with the N-H bond of another NMF molecule. This is the case for other amide molecules, for example, the table below shows that when fully deuterated DMF (²H₇DMF) or N,N-Dimethylacetamide (DMA) interacts with cations the carbonyl band shifts to lower frequency [283].

M(ClO ₄) _n	DMA	[² H ₇]DMF
pure liquid	1650, 1746	1650, 1700(shoulder)
Li	1640	1642, 1648(shoulder)
Mg	1630	1644
Ca	-----	1640
Al	-----	1644, 1650(shoulder)
Pb	1596	1618, 1612(shoulder)

Note that these are propanol solutions containing 0.5mol dm⁻³ of amide and 0.5mol dm⁻³ of M(ClO₄)_n

These results show the opposite behaviour to those of Bonner and Jordan [282] and so it may not be possible to rely on their infrared results. If their results can be relied

upon then it suggests that the formation of a hydrogen bond between NMF molecules is stronger than the bond formed between the carbonyl group of NMF and a cation.

The results of Bonner and Jordan also show that the anion has an affect on the position of the carbonyl band.

Figure 7.22A shows the carbonyl band in the VT-DRIFTS spectra of the Ca-SWy-2/NMF complex (31 days in vapour). Here, subtle changes are apparent that were not evident in the previous spectra. Figure 7.22B shows the spectra after deconvolution (deconvolution parameters are $K = 1.7$, band width = 28.5cm^{-1} and Lorentzian fraction = 0.8). These spectra are presented so that the band shapes in the original spectra are accentuated. They have been stacked so as to alleviate problems due to overlapping bands. Both the original and the deconvoluted spectra are very complex. The reader should note that temperature has an affect on the position and shape of infrared bands. This should be considered when comparing spectra at different temperatures. The aim of this section is to determine trends within the spectra which can be related to the site distribution of the NMF molecules in the clays, and not to explain all the changes in band positions and intensities in detail.

The position of the carbonyl bands collected between 25 (prior to purging with nitrogen) to 50°C are at 1664cm^{-1} , which is 3cm^{-1} lower than in pure liquid NMF. This suggests that the carbonyl group of the NMF molecules in the complex are interacting more strongly than in pure liquid NMF. The bands are also asymmetrical to the high wavenumber side, more so than the band in pure NMF. This indicates that there are a proportion of NMF molecules interacting through the carbonyl bond less strongly. The band producing the asymmetric shape is more clearly observed in the deconvoluted spectra.

The position of the carbonyl band collected at 150°C is at 1671cm^{-1} . The shift in the band from 1664 to 1671cm^{-1} indicates that the proportion of NMF molecules that are interacting through their carbonyl group more strongly are being removed.

At 150°C the high wavenumber asymmetry is more resolved (see deconvoluted spectra also). As the temperature is increased from 150 - 250°C the bands decrease in intensity and shift to lower wavenumbers. The decrease in intensity indicates that

Figure 7.22A: VT-DRIFTS spectra of the Ca-SWy-2/NMF complex formed after 31 days in vapour (1800-1500 cm^{-1}).

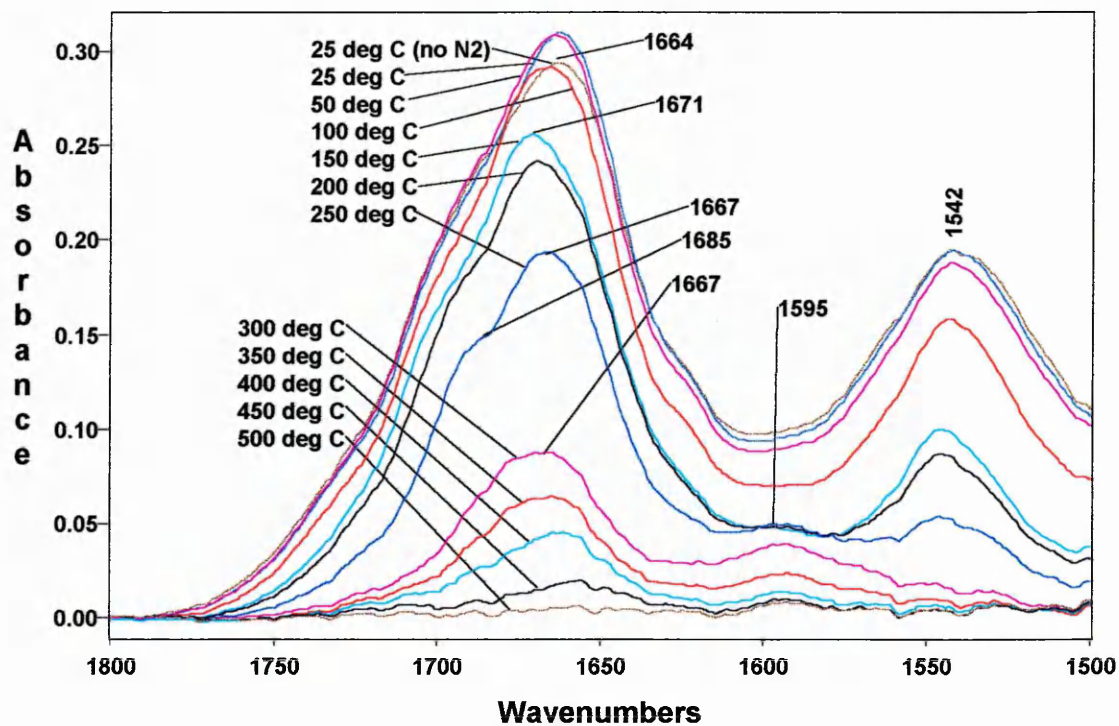
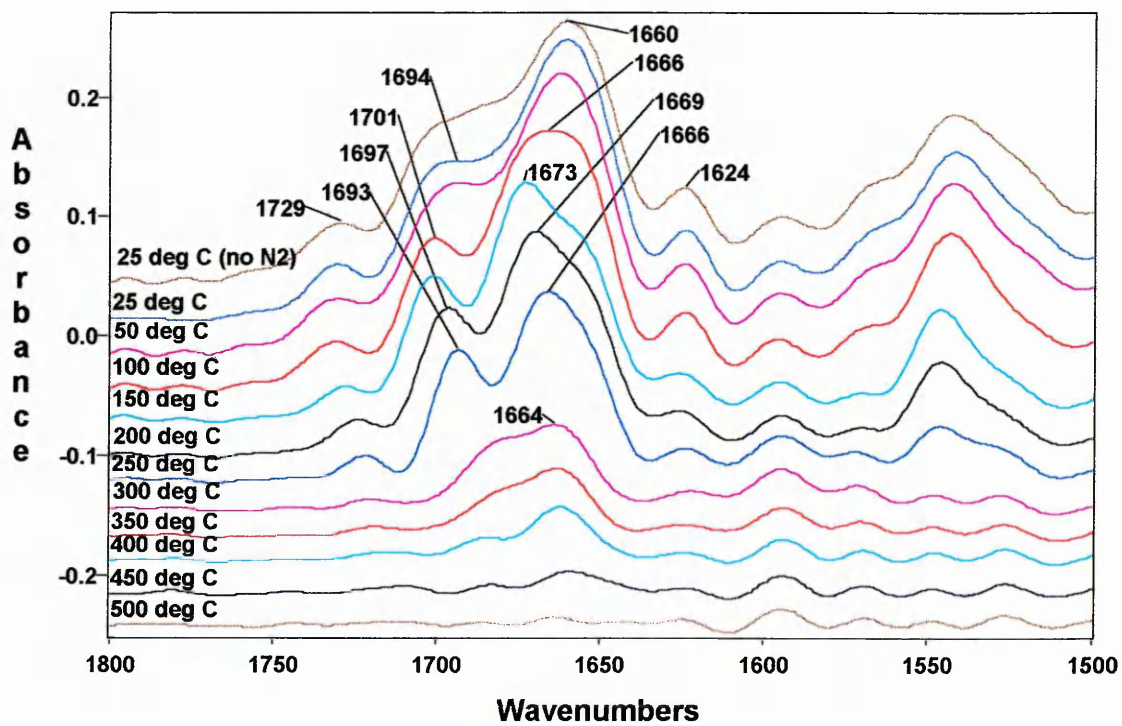


Figure 7.22B: Deconvoluted VT-DRIFTS spectra of the Ca-SWy-2/NMF complex formed after 31 days in vapour (1800-1500 cm^{-1}).



NMF molecules are being desorbed from the complex, and the shift to lower wavenumbers indicates that the remaining NMF molecules are gradually interacting via their carbonyl groups more strongly. This could be due to the fact the removal of some of the NMF molecules from around the cation leaves the coordination requirements of the cation not completely satisfied and hence a stronger interaction occurs with the remaining NMF molecules. The bands also become sharper which indicates a reduction in the number of environments the NMF molecules are in. A further shift to lower wavenumbers of the carbonyl bands between 300-500°C shows that the interaction between the cation and the NMF is becoming even stronger.

The deconvoluted spectra show a band at 1624cm^{-1} , which is the position where the H-O-H bending mode of water is expected. The intensity of this band has decreased greatly by 150°C but is still present at 250°C. This suggests that water may be retained at temperatures greater than those originally thought.

Figure 7.23A shows the carbonyl band in the VT-DRIFTS spectra of the Mg-SWy-2/NMF complex (30 days in vapour). Figure 7.23B shows the spectra after deconvolution. Similar trends are observed in these spectra when compared to the spectra obtained from the Ca-SWy-2/NMF complex.

The position of the carbonyl bands collected between 25 (prior to purging with nitrogen) to 50°C are at 1664cm^{-1} , which is 3cm^{-1} lower than in pure liquid NMF. This suggests that the carbonyl group of the NMF molecules in the complex are interacting more strongly than in pure liquid NMF.

The carbonyl band shifts from 1664 to 1676cm^{-1} between 50-150°C, which is 5cm^{-1} greater than the corresponding bands in the Ca-SWy-2/NMF complex and is 9cm^{-1} greater than that in pure liquid NMF.

As the temperature is increased from 150-350°C, the position of the bands shift to lower wavenumbers ($1676\text{-}1670\text{cm}^{-1}$), this is observed more clearly in the deconvoluted spectra and suggests the carbonyl bond is interacting more strongly. The fact that all these bands are higher than those in pure liquid NMF suggests that the carbonyl bond is interacting with the clay (either to the clay structure or the Mg exchangeable cations) less strongly than it does in the pure liquid state. This may be because of steric restrictions in the clay interlayers. This assumption is reflected in

Figure 7.23A: VT-DRIFTS spectra of the Mg-SWy-2/NMF complex formed after 30 days in vapour (1800-1500 cm^{-1}).

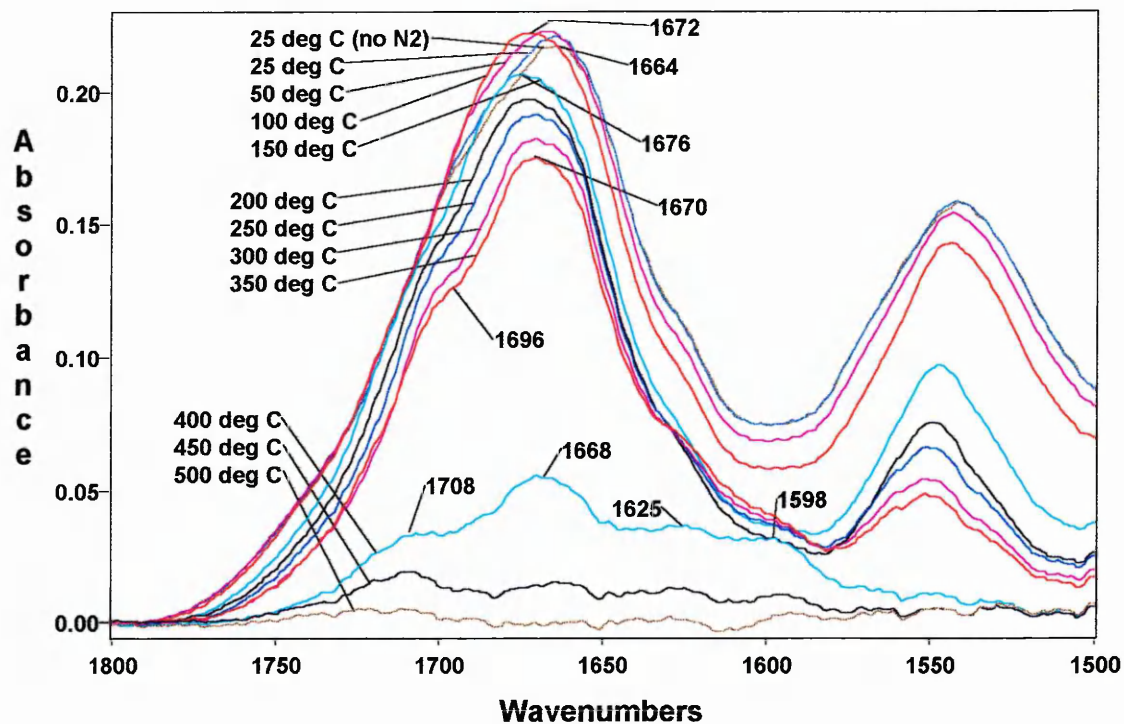
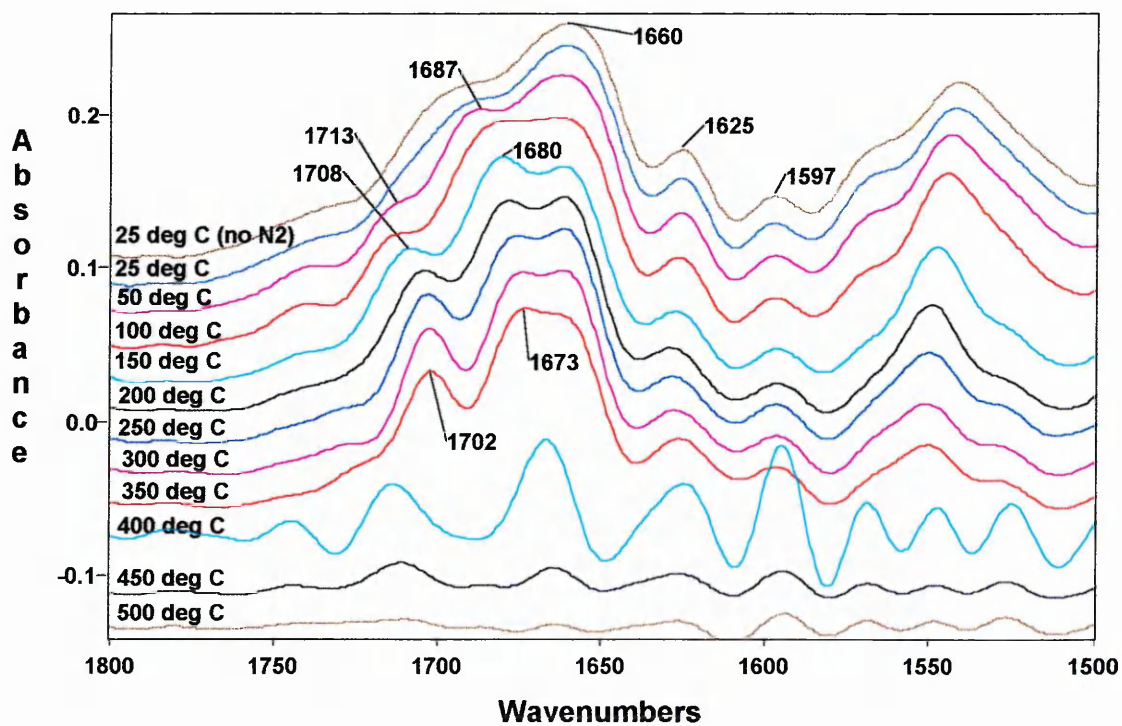


Figure 7.23B: Deconvoluted VT-DRIFTS spectra of the Mg-SWy-2/NMF complex formed after 30 days in vapour (1800-1500 cm^{-1}).



the VT-XRD results and shows that the layers have collapsed. The fact that the carbonyl band is positioned at 1664cm^{-1} at room temperature, which is lower (3cm^{-1}) than that in pure liquid NMF suggests that the NMF molecules are interacting more strongly. At this stage the $d_{(001)}$ -spacing (see VT-XRD later) is large and thus steric restrictions are not as likely.

Figure 7.24A shows the carbonyl band in the VT-DRIFTS spectra of the Na-SWy-2/NMF complex. Figure 7.24B shows the spectra after deconvolution. The first difference to note between the Na-SWy-2/NMF complex and the Ca and Mg-SWy-2/NMF complexes is that the carbonyl band in the spectra of the former is at a higher frequency. This indicates that the NMF molecules in the Na-SWy-2/NMF complex are interacting less strongly than those in the Ca- and Mg-SWy-2/NMF complexes.

The position of the carbonyl band in the Na-SWy-2/NMF complex at 25°C (1678cm^{-1}) is 11cm^{-1} higher than that in pure liquid NMF which suggests that the carbonyl bond interacts less strongly with the cation in the clay than to other NMF molecules in the pure liquid. This behaviour is the opposite to that observed in the Ca and Mg-SWy-2/NMF complexes.

The infrared spectrum collected at 150°C shows that the carbonyl band is asymmetrical to the higher wavenumber side. When the complex is heated further (200 and 250°C) the higher wavenumber side becomes relatively more intense. This suggests that as the complex is heated, the proportion of weaker interacting NMF molecules increases. The band maximum (approximately 1684cm^{-1}) at these temperatures (150 - 250°C) is at a higher frequency than those at lower temperatures and suggests that the NMF molecules are interacting less strongly. As the temperature is increased the proportion of weakly interacting NMF molecules increases. This may be due to steric restrictions as the clay layers collapse (see VT-XRD data later).

Figures 7.25A and 7.25B show the carbonyl band in the VT-DRIFTS spectra of the K-SWy-2/NMF complex before and after deconvolution, respectively. Again similar trends are observed.

Figure 7.24A: VT-DRIFTS spectra of the Na-SWy-2/NMF complex formed after 30 days in vapour (1800-1500 cm^{-1}).

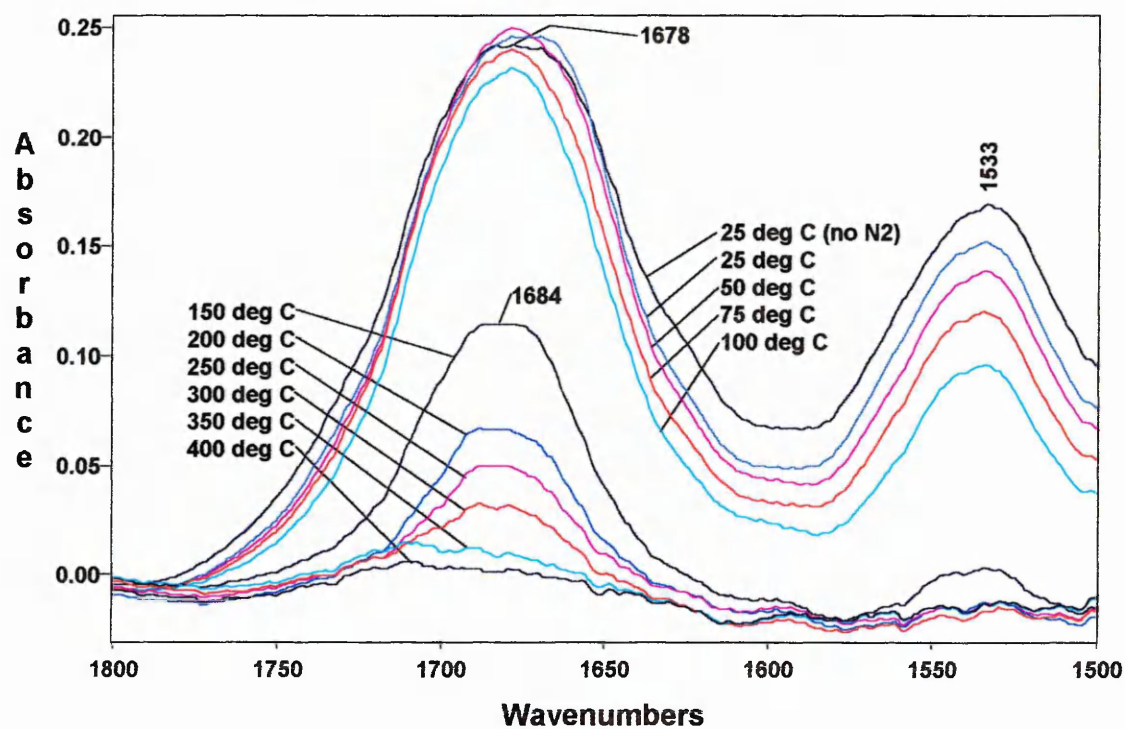


Figure 7.24B: Deconvoluted VT-DRIFTS spectra of the Na-SWy-2/NMF complex formed after 30 days in vapour (1800-1500 cm^{-1}).

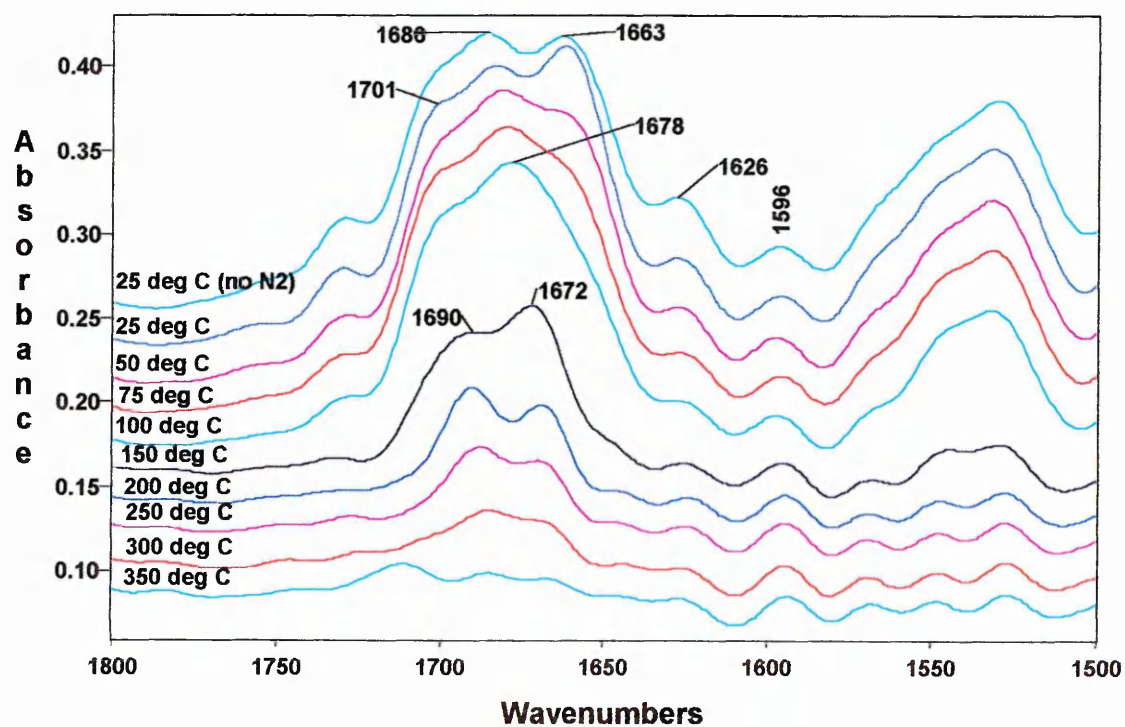


Figure 7.25A: VT-DRIFTS spectra of the K-SWy-2/NMF complex formed after 30 days in vapour (1800-1500 cm^{-1}).

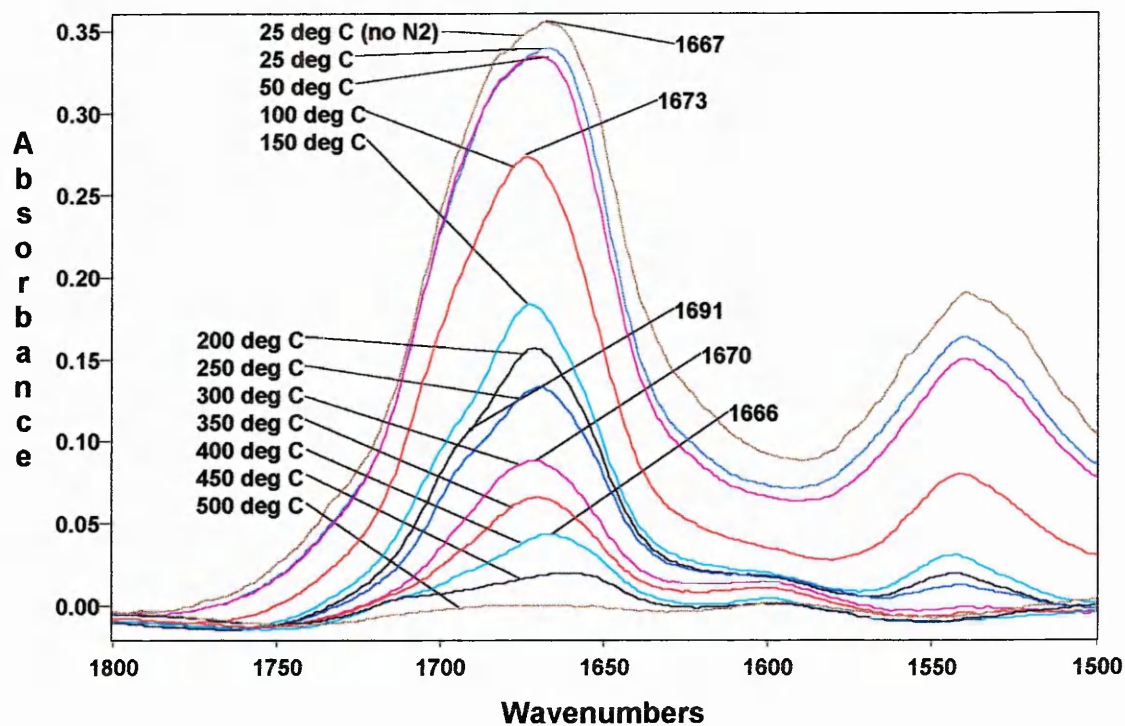
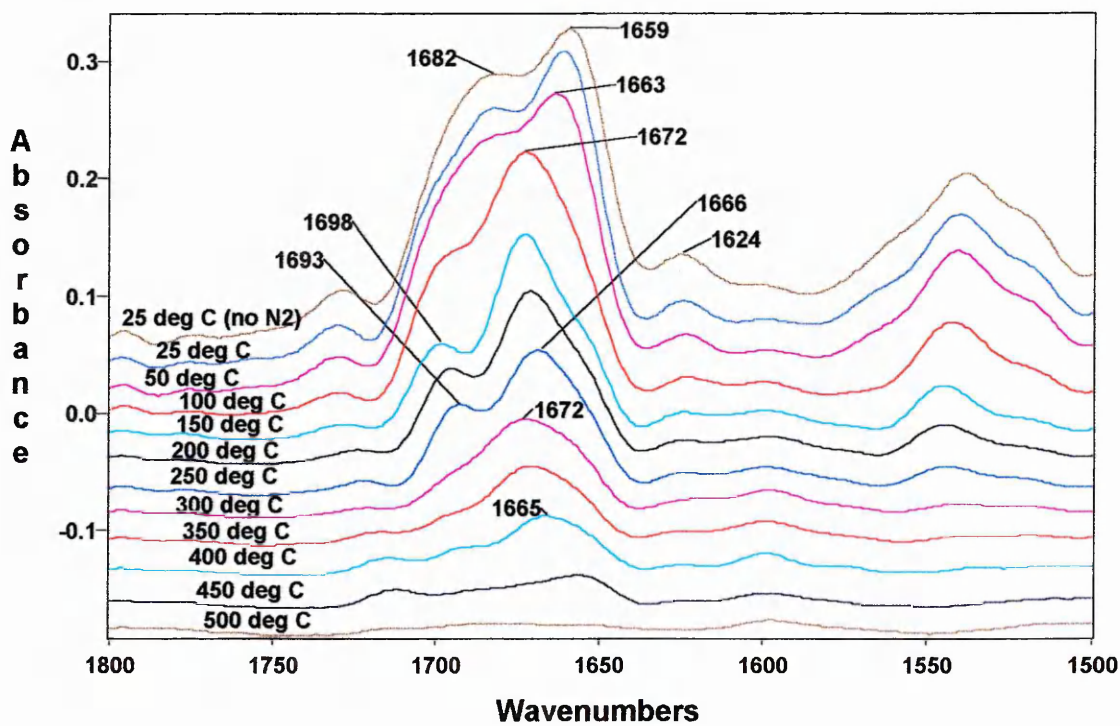


Figure 7.25B: Deconvoluted VT-DRIFTS spectra of the K-SWy-2/NMF complex formed after 30 days in vapour (1800-1500 cm^{-1}).



It is interesting to note that the carbonyl band of NMF when complexed to Ca, Mg, Na or K-SWy-2 shifts to a higher wavenumber, whereas the general trend of amides is that the band shifts to lower wavenumbers. For example, Affrossman et al. [284] studied the adsorption of N-ethylacetamide and 2-pyrrolidone on alumina by DRIFTS. They observed the carbonyl band to shift from 1715 to 1634 cm^{-1} for the former and from 1681 to 1668 cm^{-1} for the latter. Diorio et al. [285] also observed a similar finding with N-methyl propionamide and anhydrous lithium perchlorate, they noted that the carbonyl band moved from a single band at 1645 cm^{-1} to a doublet at 1645 and 1620 cm^{-1} .

The position of the carbonyl bands in the infrared spectra of the complexes at 150°C are shown in table 7.3

Table 7.3: Band positions of the high wavenumber component.

	Band position (cm^{-1})			
	Ca-SWy-2	Mg-SWy-2	Na-SWy-2	K-SWy-2
At 150°C	1671	1676	1684	1673
Prior to the loss of the high temperature maximum	1667 (250°C)	1670 (350°C)	1684 (150°C)	1673 (150°C)

At this temperature, it is believed that intermolecular hydrogen-bonded NMF molecules are removed and thus band shifts due to the influence of the cation are being observed. It is expected that the Mg cation would have a stronger influence on the carbonyl bond of directly coordinated NMF molecules and hence interact to a stronger degree. This would result in a shift to a lower wavenumber relative to a less polarising cation. This is not the case since the carbonyl band of the NMF molecules coordinated to Ca cations is at a lower wavenumber than that of the Mg cation. This observation also occurs when comparing the band position of the Na and K complexes. However, Na and K are less polarising than Mg and Ca, respectively, and do exhibit carbonyl bands at lower wavenumbers. It is interesting to note that the

expected relationship between band shifts and polarisibility of cations does not correlate in the paper discussed previously (Tahoun and Mortland [277]).

The spectra studied in this section have shown that the interactions of the carbonyl group with the clay is very complex. A much greater amount of detail needs to be considered which may be achieved by curve-fitting techniques. Relative intensities of the component bands could then be used to aid their assignments.

7.2.4) VT-XRD analysis of X-SWy-2/NMF complexes

It should be noted that the heating parameters used in VT-XRD are different to those used in VT-DRIFTS, which are in turn different to those used in TGA. During a VT-XRD experiment the sample is heated to the required temperature, allowed to equilibrate for 10 minutes and then the XRD trace is collected. The time taken to collect the XRD trace is approximately 25 minutes. This procedure is then repeated at the next (higher) temperature. In addition the samples are not purged with nitrogen and thus are exposed to air. Since the heating parameters in each technique are not the same a direct comparison cannot be made between the respective results, however, the results do show some correlation.

Figure 7.26 shows the VT-XRD traces of Mg-SWy-2 after exposure to NMF vapour for 30 days. These traces show that the $d_{(001)}$ -spacing of the complex decreases significantly in three steps as the temperature is increased. The first step occurs when the complex is heated from room temperature to 170°C, here a decrease of 4.9Å is observed. The second step occurs between 220-350°C were a decrease of 1.2Å occurs. The third and final step occurs when the complex is heated from 350-400°C and a decrease of 1.7Å is observed. These steps relate to the 3 maxima observed in the DTG trace at 400, 180 and 110°C, respectively.

This data shows that the complex at 25°C has two layers of NMF molecules. This assumption is made on the basis of the size of the NMF molecules, the $d_{(001)}$ -spacing and the general trend of other organo-clay complexes (this assumption will later prevail to be correct).

The point to note at this stage is that before the high temperature maximum (400°C) in the DTG is removed the $d_{(001)}$ -spacing is at 12.0Å (i.e. at 350°C), which then decreases when the maximum is removed (i.e. the $d_{(001)}$ -spacing is at 10.3Å at 400°C). This relates to the fact the NMF molecules creating the high temperature maximum are in the interlayer region. Another point to note is that the XRD trace collected at 170°C exhibits a shoulder to the high spacing side. This indicates that some of the layers are at a greater spacing than the others.

Figure 7.26: VT-XRD traces of the Mg-SWy-2/NMF complex (30 days in vapour).

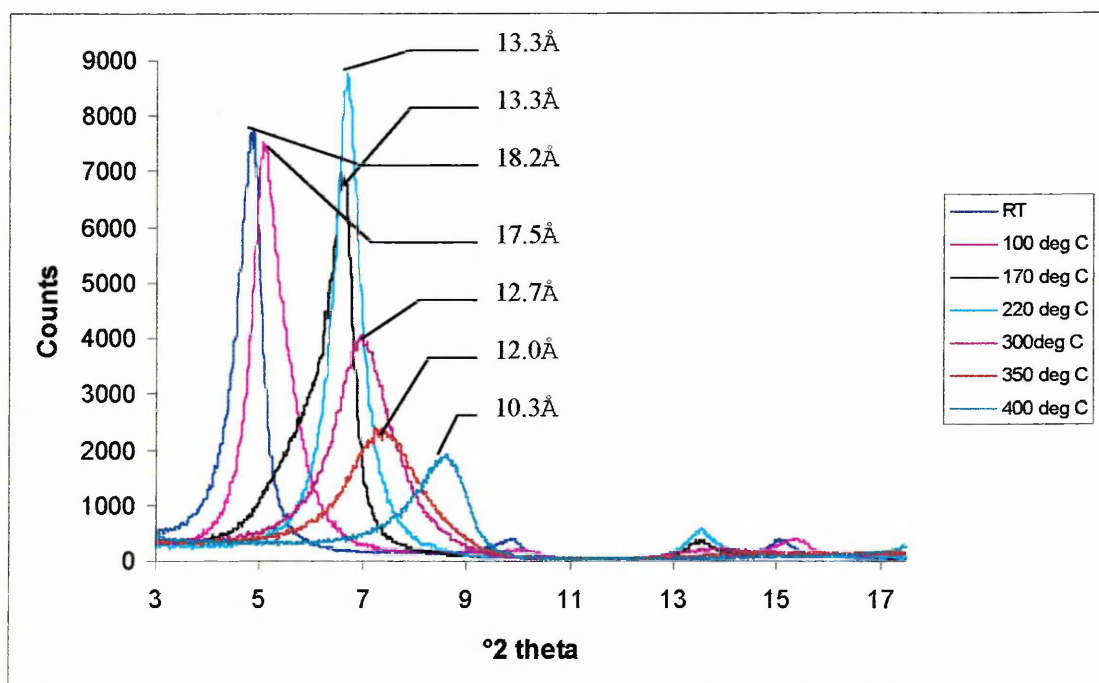


Figure 7.27 shows the VT-XRD traces of Ca-SWy-2 after exposure to NMF vapour for 31 days. The traces show that the $d_{(001)}$ -spacings of the complex decreases significantly in two steps as the temperature is raised. The first step, which shows a decrease of 3.9Å, occurs when the complex is heated to 170°C, and, the second step which shows a decrease of 3Å, occurs when it is heated to 300°C. Each step represents the removal of molecules from within the interlayer region of the complex and indicates that the complex has two layers of NMF molecules at 25°C, which decreases to one layer upon heating to 170°C.

At 350°C the $d_{(001)}$ -spacing is at 10.2Å and remains constant at higher temperatures. At this stage the clay layers have collapsed indicating the removal of all intercalated

species, however, some molecules may be trapped in the collapsed structure. This suggestion is supported by the fact the peak at 10.2Å is much broader, especially at higher spacings (to the left) than a clay that has not been exposed to NMF.

The trace collected at 300°C shows a peak at 10.2Å which is broad and is higher in intensity between 6-8 (°2θ) than the peak in the traces collected at higher temperature.

This indicates that not all but the majority of the layers have collapsed.

At 220°C the d(001)-spacing of the clay is 13.2Å. This suggests that the NMF molecules creating the high temperature maximum are in the interlayer region.

Figure 7.27: VT-XRD traces of the Ca-SWy-2/NMF complex (31 days in vapour).

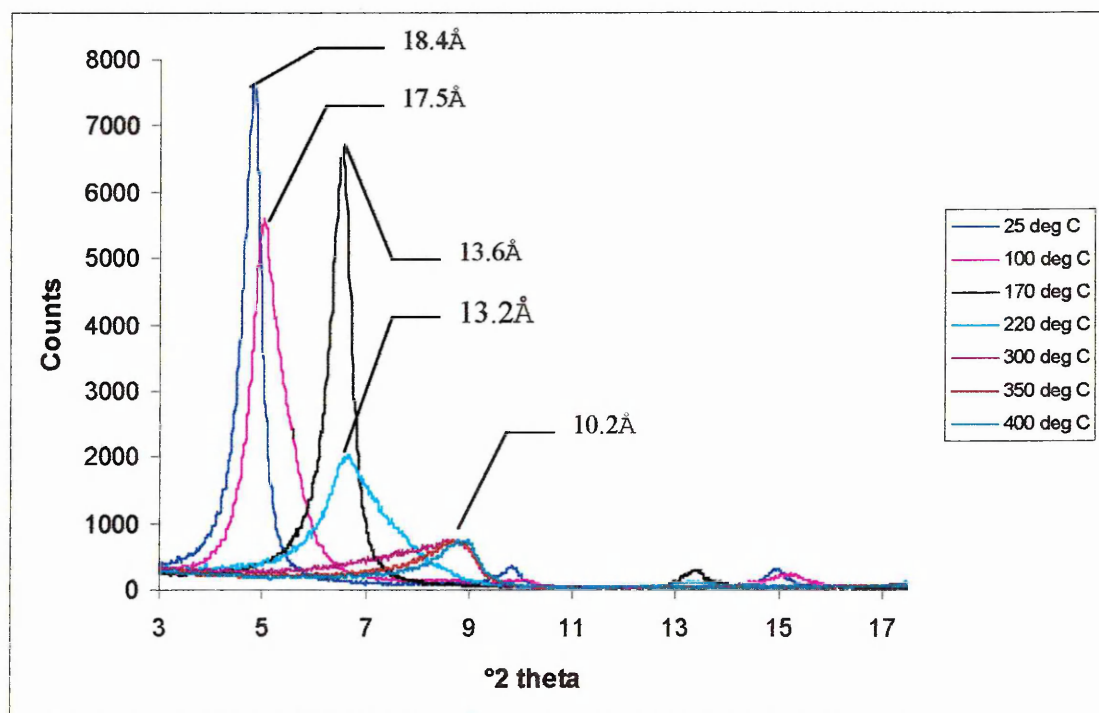


Figure 7.28 shows the VT-XRD traces of Na-SWy-2 after exposure to NMF vapour for 30 days. A comparison between the DTG trace and the VT-XRD traces shows:-

- i) the loss of the shoulder (low temperature side) of the low temperature maximum (130°C) in the DTG trace corresponds with a decrease in the $d_{(001)}$ -spacing from 21.8-17.7Å,
- ii) the loss of the low temperature maximum in the DTG trace corresponds with a decrease in the $d_{(001)}$ -spacing from 17.7-13.6Å, and,

iii) the loss of the high temperature maximum (190°C) in the DTG trace corresponds with a decrease in the $d_{(001)}$ -spacing from 13.6-9.9Å.

The $d_{(001)}$ -spacing of the complex at 25°C is 3.5Å greater than that of the other complexes. This indicates that either there is an extra layer in the interlayer (total of 3) or the NMF molecules are arranged differently. The peak positioned at 10.7Å is the $d_{(002)}$ -spacing of the complex formed at 25°C.

Figure 7.28: VT-XRD traces of the Na-SWy-2/NMF complex (30 days in vapour).

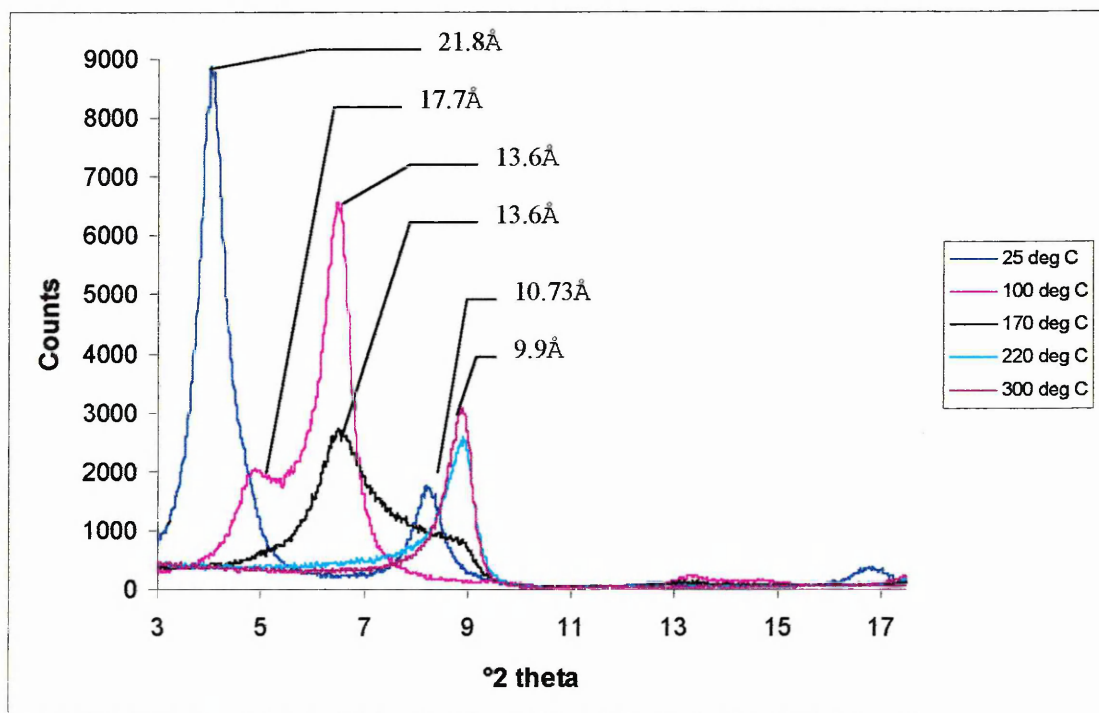
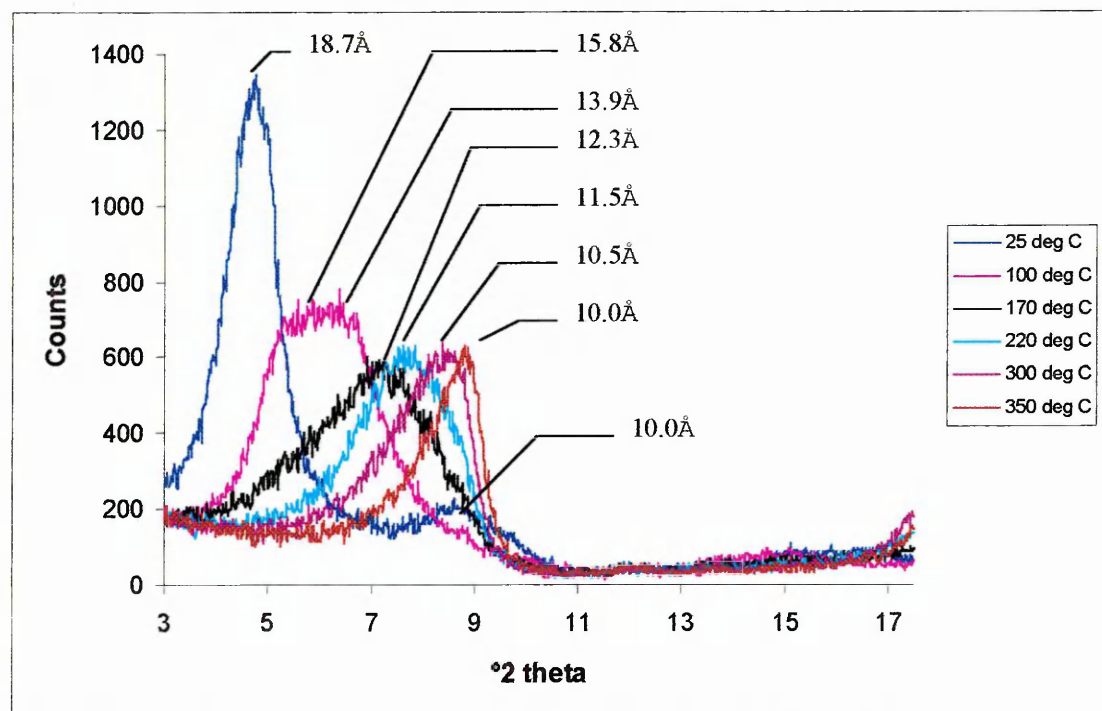


Figure 7.29 shows the VT-XRD traces of K-SWy-2 after exposure to NMF vapour for 30 days. These traces are different to the other complexes in that they are much broader and less well defined. The peaks show that the $d_{(001)}$ -spacing of the complex gradually decreases as the temperature is increased. The total decrease observed is 8.7Å and it is believed that two layers are present. It should be noted that the K ions may lie near the surface of the clay layers when the clay is intercalated, whereas the Ca, Na and Mg ions are situated in the middle. This difference may account for the differences observed in the traces of the K-SWy-2 complex.

Figure 7.29: VT-XRD traces of the K-SWy-2/NMF complex (30 days in vapour).



7.2.5) Summary of the X-SWy-2/NMF complexes

This section aims to describe the distribution of the NMF molecules whilst adsorbed on the cation-exchanged montmorillonites. It will describe the expected sites that the molecules are in with respect to the experimental data. The loss of NMF from each site as the temperature of the complex is increased will be discussed in relation to the maxima observed in the DTG traces. Each cation-exchanged montmorillonite/NMF complex will be discussed individually after certain features of the montmorillonite structure have been presented.

Montmorillonite structure

It is known that in montmorillonites approximately 80% of the total cation-exchange-capacity (CEC) is found on cleavage surfaces, i.e. the interlayer region. When there is more than one layer of water or intercalate present in the interlayer region then the cations are held mid-way between the surfaces. This is the case for exchangeable cations such as Na, Ca and Mg. An exception to this rule occurs when K ions are the exchangeable cation, these are held close to the surfaces. K-exchanged clays are therefore expected to behave differently. When only one layer of water or intercalate is present then small cations such as Na and Mg may be placed preferentially towards the hexagonal cavity of one of the clay surfaces.

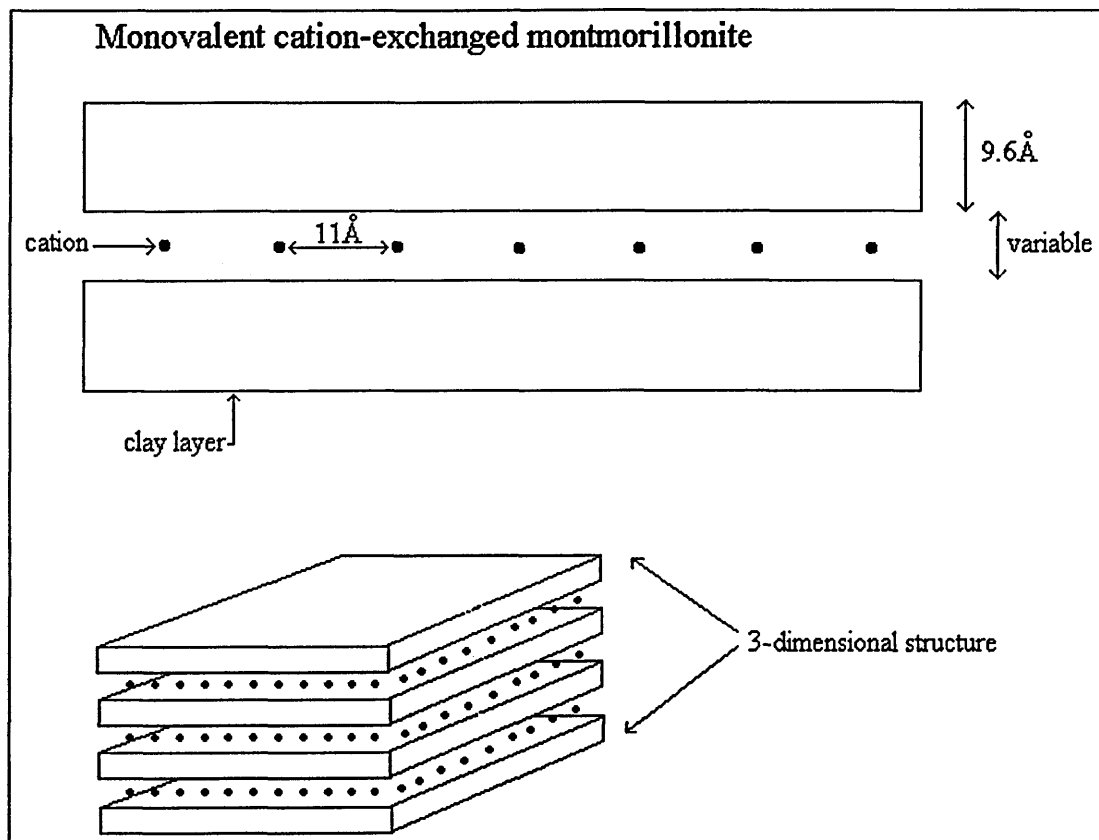
The remaining 20% of the total CEC are associated with broken bonds found at external clay layers and edges.

Monovalent cations are placed approximately 11Å apart whereas divalent cations are placed approximately 22Å apart (figure 7.30). The clay layers are 9.6Å thick and the interlayer space is variable depending on the intercalating species. Whilst discussing the following X-SWy-2/NMF complexes it is necessary to remember that these are 3-dimensional matrices and the average diameter of a clay layer is 1µm.

Although the differences in size of the Ca, Mg, Na and K cations are insignificant for the following diagrams their respective sizes are 1.17, 0.89, 0.98 and 1.33Å. In order to determine the dimensions of an NMF molecule a plastic stick and ball model was built. It was found that the length of the molecule was approximately 6Å and the

width of the molecule was about 3Å. This was also found to be the case using molecular modelling (see later).

Figure 7.30: Diagrammatic representation of a montmorillonite structure.



Ca-SWy-2/NMF

The dimensions of the fully-loaded complex (i.e. Ca-SWy-2 exposed to NMF vapour for 31 days) will be discussed primarily followed by the other fully-loaded cation-exchanged complexes.

The state of the Ca-SWy-2/NMF complex before the loss of the high temperature maximum shown in the DTG trace will be discussed first. The $d_{(001)}$ -spacing at this point is 13.2Å (figure 7.31A).

Assuming that the NMF molecules creating the high temperature maximum are coordinated to exchangeable cations, the number of these can be calculated from the

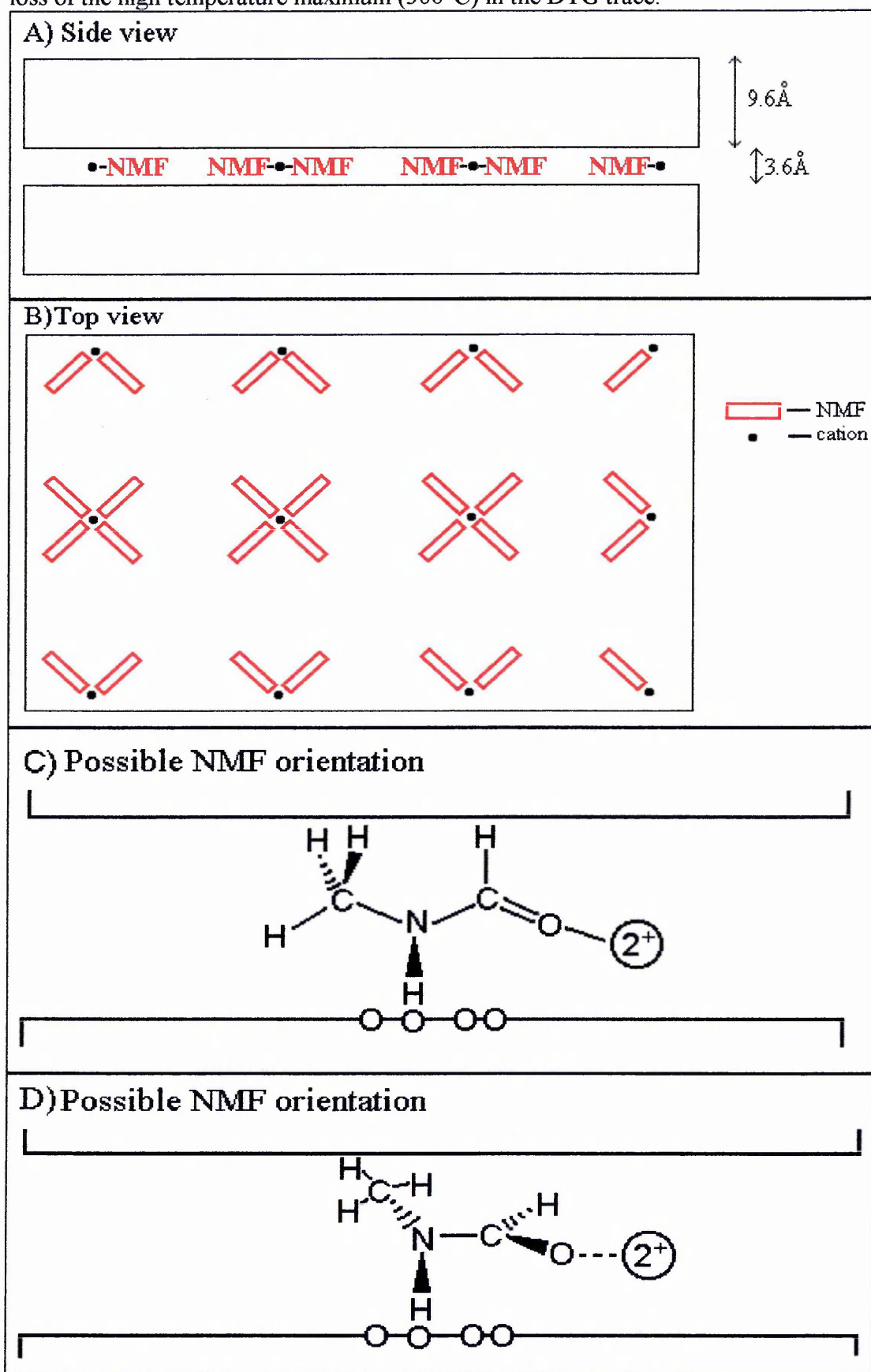
TGA data. It has been calculated that four molecules are coordinated to each interlayer cation. These would be coordinated via their carbonyl group and orientated so that there would be the least amount of steric hindrance between them. Since an NMF molecule is approximately 3Å wide and the spacing between the clay layers is less than 3.6Å, then the NMF molecules must be lying horizontally to the clay layers figure (7.31C). Note that the N-C-O bond would be in the same plane due to its partial double bond character. Figure 7.31C shows that the N-H bond is in very close proximity to the clay layers and indicates that it may be interacting with the negatively charged oxygen atoms on the surface of the clay layer. The VT-DRIFTS results support this indication because the position of the N-H band (3420cm^{-1}) in the spectrum collected at 250°C suggests that the bond is not completely unassociated as in diluted NMF and neither is it strongly associated to another NMF molecule. The negative charge on the oxygen atoms resulting from isomorphous substitution is spread over ten surface oxygen atoms and is relatively weak for each oxygen atom. Thus, an interaction between the N-H bond and the clay layer could produce a band at 3420cm^{-1} .

Figure 7.31C also shows that the C-H stretching band attached to the carbonyl group is in close proximity to the clay layer. The VT-DRIFTS spectra of this complex shows that the C-H bond is at a very high frequency indicating a unique position. This is presumably due to the effect of the negatively charged clay layer on the stretching frequency of the bond. It is possible that the hydrogen atom is positioned in one of the hexagonal cavities of the clay layer.

The combination of both the carbonyl to cation and the N-H to clay bonds results in a strongly interacting species. This is why the NMF molecules are only removed at temperatures in excess of 250°C .

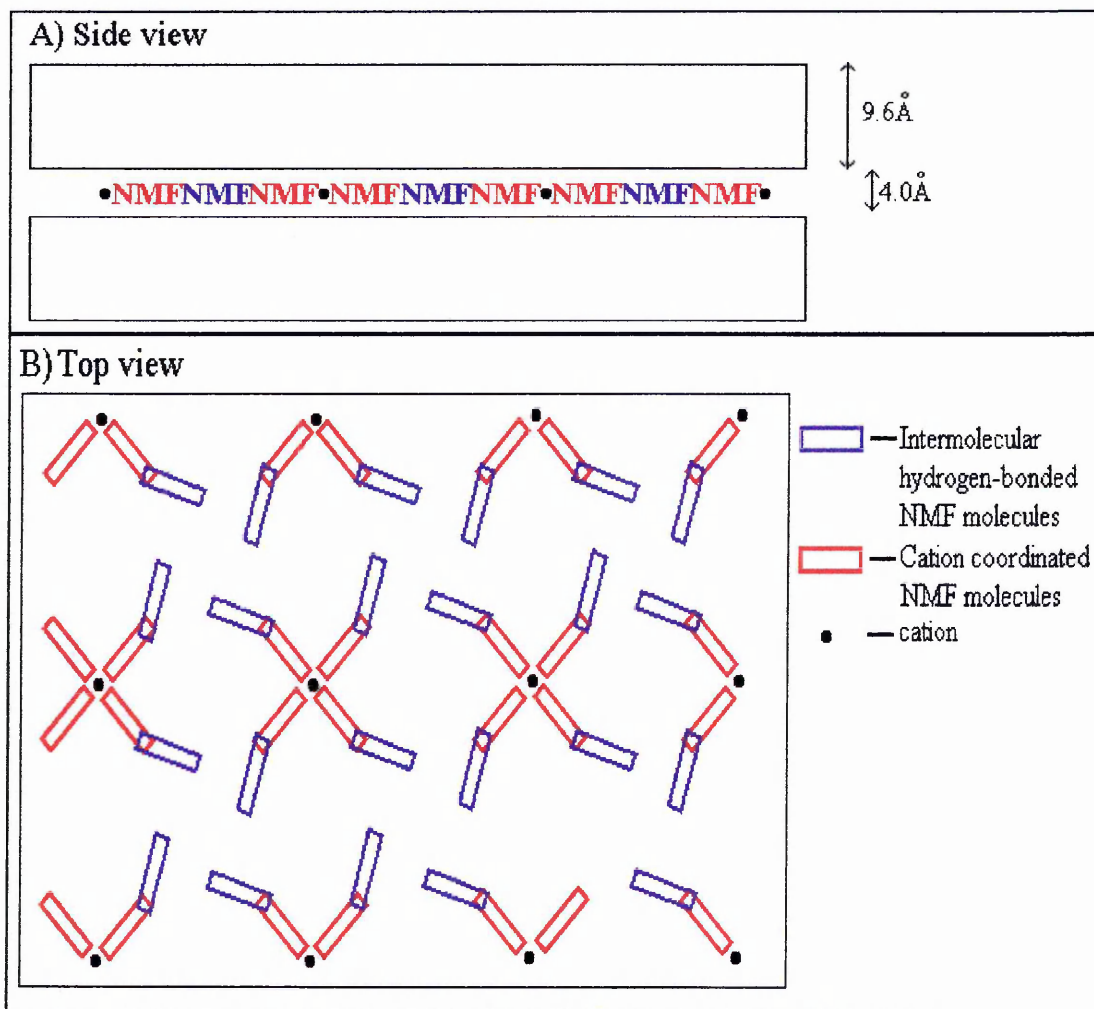
Figure 7.31C shows the plane of the N-C-O bonds to be perpendicular to the plane of the clay layer. Alternatively the plane of the N-C-O bonds could be parallel to the plane of the clay layers. This is shown in figure 7.31D and shows that the methyl group will be controlling the $d_{(001)}$ -spacing.

Figure 7.31: Diagrammatic representation of the Ca-SWy-2/NMF complex prior to loss of the high temperature maximum (300°C) in the DTG trace.



The $d_{(001)}$ -spacing of the complex prior to the loss of the maximum at 180°C in the DTG trace is at 13.6Å. This spacing is only 0.4Å greater than the complex formed prior to the loss of the highest temperature maximum. The reason why the $d_{(001)}$ -spacing is slightly larger could be due to the presence of additional NMF molecules within the interlayer. If this is the case then they will probably be associated to the coordinated NMF molecules that are present at higher temperatures (figure 7.32A and B).

Figure 7.32: Diagrammatic representation of the Ca-SWy-2/NMF complex prior to loss of the second highest maximum (180°C) in the DTG trace.



The VT-DRIFTS data shows that the N-H bond in the NMF molecules creating this site are interacting more strongly than those creating the high temperature maximum in the DTG trace. This is indicated by the asymmetry on the low wavenumber side of

the band at 3420cm^{-1} . It is possible that the NMF molecules hydrogen bonded to the NMF molecules that are coordinated to the cation (blue - figure 7.32A and B) create the band at 3420cm^{-1} and the NMF molecules coordinated to the cations (red - figure 7.32A and B) create the asymmetry side since the N-H bond in the latter is interacting more strongly than the former.

It is probable that not every NMF molecule coordinated to a cation will be associated to another NMF molecule. The additional NMF molecules that create the second highest maximum in the DTG trace may therefore be due to NMF molecules coordinated to external cations that are compensating the charges due to broken bonds. These NMF molecules will possess free N-H bonds and this is why a decrease in the band at 3420cm^{-1} is observed. These molecules are unlikely to be retained at higher temperatures like those coordinated to interlayer cations, because they will not have the additional interaction between the N-H bond and the clay layers, which would make them less thermally stable.

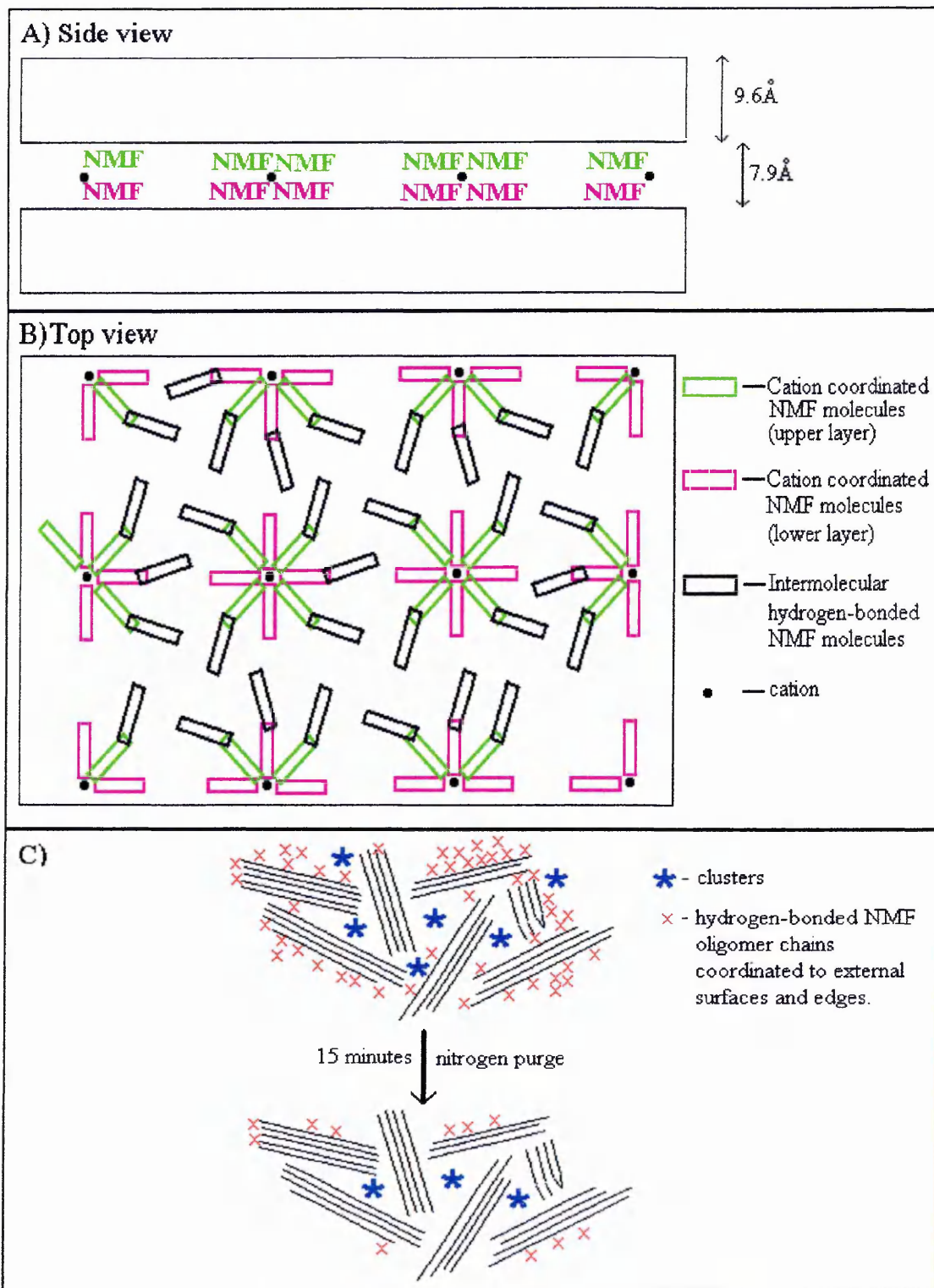
The $d_{(001)}$ -spacing of the complex prior to the loss of the low temperature maximum in the DTG trace is 17.5\AA . The space between the layers is therefore 7.9\AA , which is almost double that of the previously discussed complex. This additional space allows more room for extra NMF molecules to interact with the cation and form a double-layer complex. If for example eight NMF molecules were to orientate themselves around one cation, four molecules would create the upper layer (green) whilst four would create the lower layer (purple), see figures 7.33A and B.

The VT-DRIFTS spectra shows that liquid-like NMF is removed during the low temperature maximum in the DTG trace. This is indicated by loss of the bands at 3300 and 3076cm^{-1} . These NMF molecules are probably associated in clusters between clay stacks and clusters associated to the external surfaces and edges of clay stacks, see figure 7.33C. These will be expected because of the strong hydrogen bonding network exhibited between NMF molecules.

The extra space in the interlayer could create room for more NMF molecules to associate to the cation-coordinated NMF molecules. It could also be possible for small clusters of intermolecular hydrogen-bonded NMF molecules to form in voids between saturated cations. However this would be unlikely due to the limited space.

NMF molecules (black - figure 7.33B) would also prefer to hydrogen bond to the NMF molecules already coordinated to the cations.

Figure 7.33: Diagrammatic representation of the Ca-SWy-2/NMF complex prior to loss of the low temperature maximum (110°C) in the DTG trace.

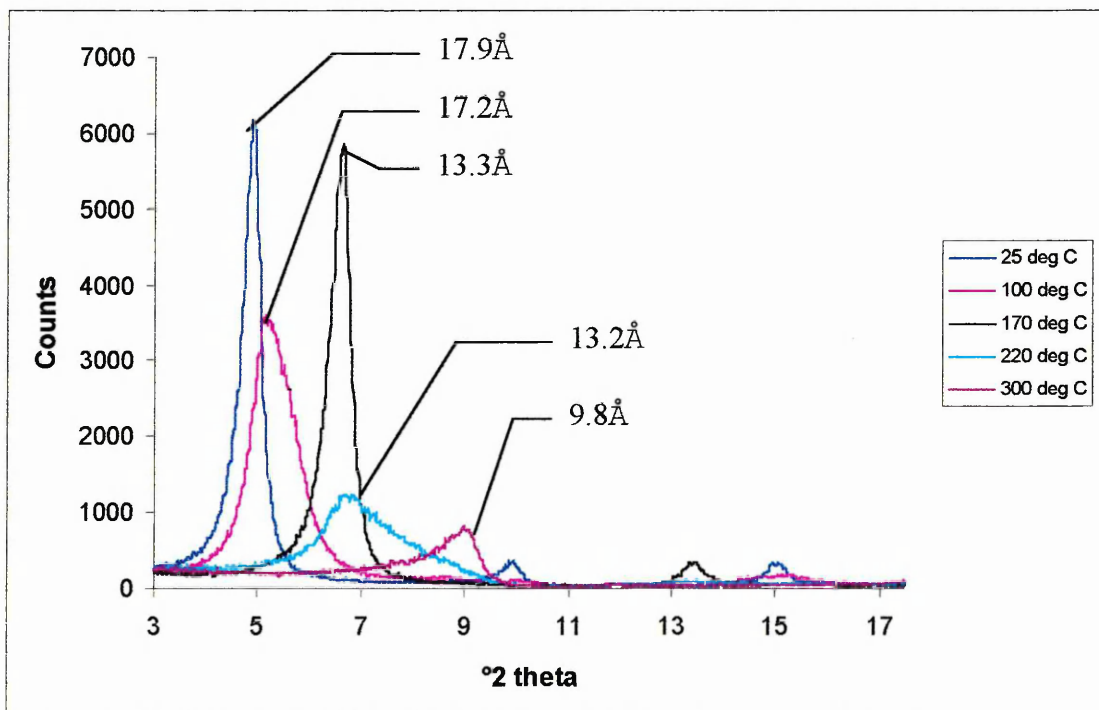


Some of the NMF molecules within the two layers of the complex must also have similar bond strengths to those of liquid-NMF. This is because as the sample is heated between 50-100°C a drop in the $d_{(001)}$ -spacing occurs and the VT-DRIFTS spectra only shows the loss of liquid-like NMF (i.e. no decrease in the band at 3420cm^{-1} is observed). Presumably the NMF molecules at the end of chains of NMF molecules coordinated to cations produce the band at 3420cm^{-1} (black), while those in the middle produce a band at 3300cm^{-1} (green and purple).

The VT-XRD traces of Ca-SWy-2 after exposure to NMF vapour for 3 days (figure 7.34) are almost identical to those exposed for 31 days (figure 7.27). The VT-DRIFTS data show that the majority of water has been removed from the complex when it is heated to 100°C and the only NMF present is that which produces the high temperature maximum in the DTG trace.

The XRD trace of the complex at room temperature shows the d-spacing to be at 17.9\AA . This suggests that the NMF molecules creating the high temperature maxima in the DTG trace controls the spacing and not those packed around them.

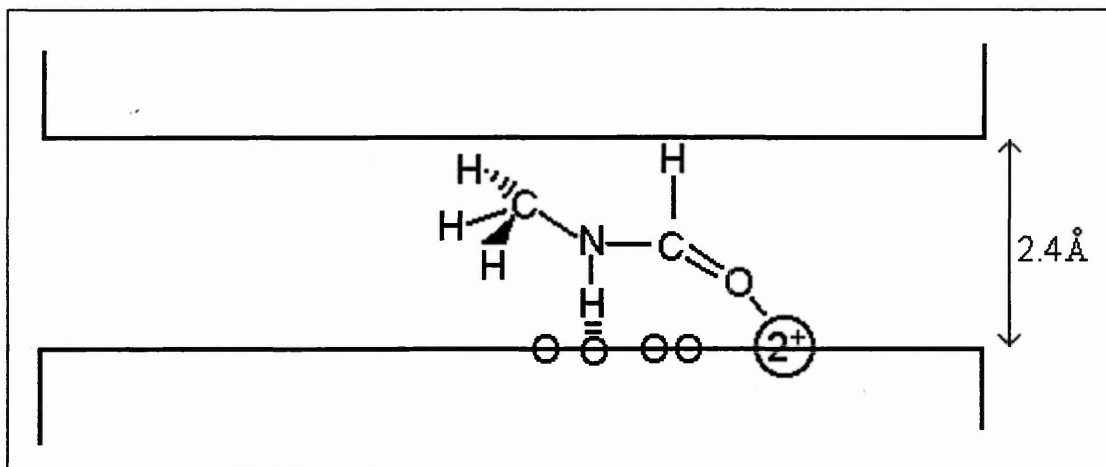
Figure 7.34: VT-XRD traces of Ca-SWy-2/NMF (3 days in NMF vapour).



Mg-SWy-2/NMF

The $d_{(001)}$ -spacing of the Mg-SWy-2/NMF complex prior to the loss of the high temperature maximum in the DTG trace is at 12.0\AA . This spacing is 1.2\AA smaller than the corresponding spacing observed in the Ca-SWy-2/NMF complex (i.e. the complex prior to the loss of its high temperature maximum in its DTG trace). The space available between the layers is only 2.4\AA , which means that the NMF molecules are severely restricted. Mg is a small cation and can position itself within the hexagonal cavity of the tetrahedral sheets at high temperatures [175] (Note that the Mg cation does not fit fully into the cavity but rests very closely in it). This may be one of the contributing factors why such a small $d_{(001)}$ -spacing is observed (figure 7.35). Another factor could be that the plane of the N-C-O bonds are parallel to the plane of the clay layers, which would result in a small $d_{(001)}$ -spacing.

Figure 7.35: Diagrammatic representation of the NMF molecules in the Mg-SWy-2/NMF complex prior to removal of the high temperature maximum in the DTG trace. Note that the plane of the N-C-O bonds could be either parallel or perpendicular to the clay layers as shown in figures 7.31C & D.



It has been calculated that at least three NMF molecules are associated with each interlayer cation, which is one less than the corresponding Ca-complex. The position of the Mg cation in the hexagonal cavity and the higher temperature could be the reason why only three NMF molecules are present.

The VT-DRIFTS spectra of the complex show that the N-H bonds in these NMF molecules are interacting more strongly than those in the corresponding Ca-complex. This is known because the N-H stretching band is positioned at a lower frequency (3405cm^{-1}). This could be due to a closer proximity of the N-H bond to the negatively charged tetrahedral sheet.

The C-H bond will also be in much closer proximity to the clay layer than that in the Ca-complex. This is reflected in the VT-DRIFTS spectra which shows a shift of the C-H bond to an even higher frequency.

The $d_{(001)}$ -spacing of the complex prior to the loss of the maximum at 220°C in the DTG trace is at 13.3\AA . This spacing is 1.3\AA larger than the complex formed prior to the loss of the highest temperature maximum (a total interlayer space of 4.7\AA). This suggests that only one layer of NMF molecules is present. Assuming that all the NMF molecules creating the two high temperature maxima are associated to exchangeable cations it can be calculated (from TGA) that there are approximately 9.8 NMF molecules per interlayer cation. It is expected that the additional NMF molecules creating the site will be associated to the cation-coordinated NMF molecules present at higher temperatures. At this temperature the Mg cation may no longer be positioned in the hexagonal cavity, but rather in the centre of the interlayer.

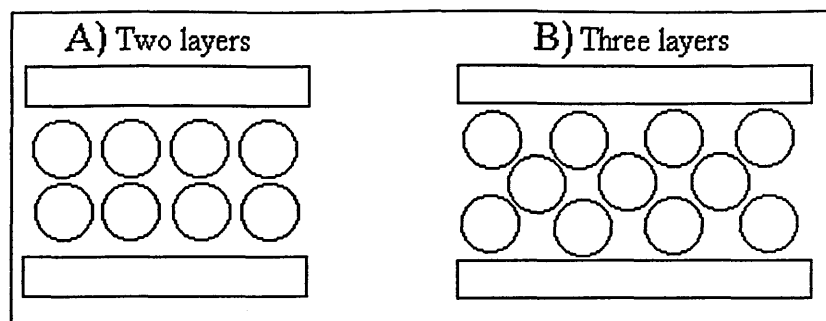
The $d_{(001)}$ -spacing of the complex prior to the loss of the low temperature maximum is at 17.5\AA . This is the same as that of the Ca-complex and the orientation of NMF molecules in the Mg-complex are likely to be similar.

Na-SWy-2/NMF

The majority of the $d_{(001)}$ -spacings (at 170°C) of the Na-SWy-2/NMF complex prior to the loss of the high temperature maximum (220°C) in the DTG trace are at 13.6\AA . This is 0.4\AA greater than the corresponding spacing observed in the Ca-SWy-2/NMF complex. It has been calculated (from TGA data) that only 2 NMF molecules per cation are present.

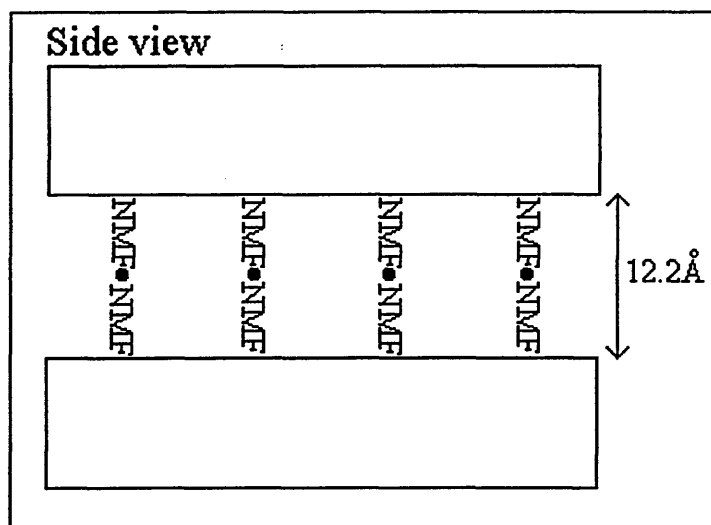
The XRD trace also shows that some of the layers are collapsed or of an intermediate spacing between 13.6 and 9.9\AA . This is indicated by asymmetry on the high angle side

Figure 7.37:



At room temperature (25°C) the complex is different to the other complexes in that the $d_{(001)}$ -spacing is a massive 21.8Å, this is an extra 3.2Å larger than the others (12.2Å interlayer space in total). It is probable that at this stage there is either a three or four layered complex or that at least two of the NMF molecules are coordinated to the cation perpendicular to the clay layers (see figure 7.38). This could be possible because it will allow more NMF molecules to coordinate to the cations.

Figure 7.38: Diagram of the Na-SWy-2/NMF complex at 25°C



K-SWy-2/NMF

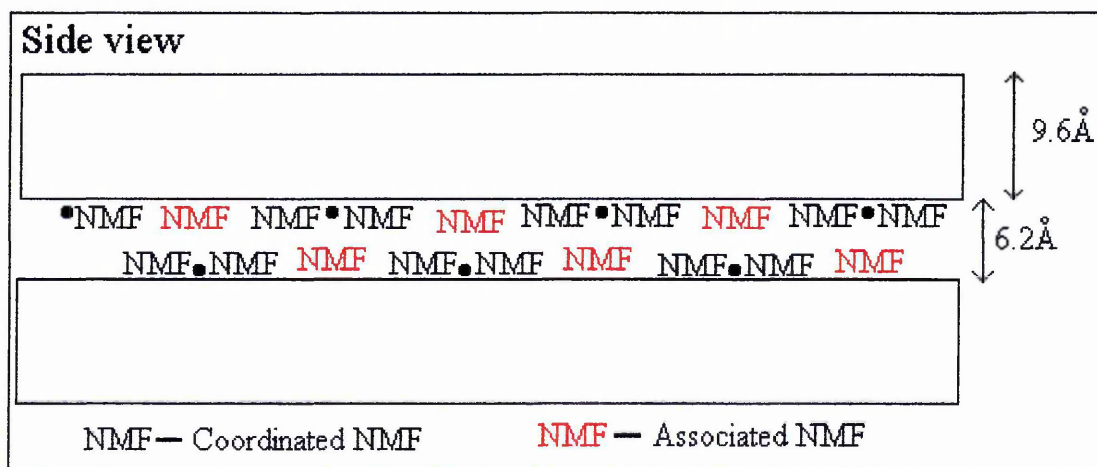
The XRD trace collected at 300°C exhibits a broad band and shows that a range of $d_{(001)}$ -spacings (10-11.5Å) occur in the complex at this temperature. The interlayer space is therefore between 0.4 -0.9Å and indicates the majority of the layers have collapsed.

When the complex is heated to 170°C the $d_{(001)}$ -spacing is 13.9 and 12.3Å which allows enough space for one layer of NMF molecules to be present in the interlayer.

At 100°C the XRD trace shows a broad envelope which is possibly the combination of two spacings at 15.8 and 13.9Å. This suggests that some of the clay layers contain two layers of NMF molecules whilst some only contain one layer.

The two layered species will be different to the other complexes in that the cations will be close to the clay layers (figure 7.39).

Figure 7.39: Diagram of the K-SWy-2/NMF complex at 50°C

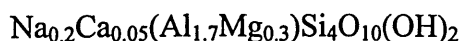


7.2.6) Molecular Modelling of Na and Mg-montmorillonite/NMF complexes

Molecular modelling has been performed in order to try and simulate the model suggested by the experimental results. This will enable a more visual picture of the complex to be observed. The unit cell formula used in the simulations is:



where X is the exchangeable cation. This formula is similar to an 'Otay-type' montmorillonite. The unit cell formula of SWy-2 montmorillonite (Wyoming-type) is:



which shows that there are slightly more exchangeable cations per unit cell in the simulated structure. The average distance between monovalent cations in the simulated structure is approximately 7.4Å, whereas that of SWy-2 is about 11.0Å. Although there is a difference in the structures, similar trends are likely to occur. Simulations involving the sorption of NMF into the interlayer space of Na and Mg-exchanged montmorillonites were performed.

Figure 7.40 shows the structure of the NMF molecule. The distance from end-to-end (oxygen-to-hydrogen atom on the methyl group) is approximately 6.Å, whereas the width of the molecule is approximately 3Å. As previously mentioned, the dimensions are similar to those of the plastic stick and ball construction.

Figure 7.41 shows the results of the simulations of the sorption of NMF into the Na-exchanged clay. The NMF molecules are represented by cylindrical tubes, the cations are represented by spheres and the clay structure (just shown on one side) is represented by the interconnected stick structure. This diagram clearly shows that a two layered complex is formed.

Figure 7.42 shows a corner section of the simulated Na-exchanged/NMF complex. All the atoms are presented as spheres and are colour coded. The diagram clearly shows that the oxygen atoms are directed towards the Na ion and supports that the NMF molecules are in close proximity to the clay layers. Of particular interest is the closeness of the N-H bonds (marked X) to the surface, which was suggested in the VT-DRIFTS spectra. The simulated results showed that the $d_{(001)}$ -spacing was 17.6Å, whereas the experimental results showed it to be 18.2Å. This is not exactly the same and differences could be due to a higher number of exchangeable cations per unit cell in the simulated clay structure.

Similar results were obtained in the simulated results of the sorption of NMF into the interlayer of the Mg-exchanged montmorillonite. These results show that; the NMF molecules coordinate to the cations via the carbonyl group, the complex is bilayered, and, the N-H bonds are in close proximity to the clay surface. The simulated results showed the $d_{(001)}$ -spacing to be 16.0Å, whereas the experimental results showed it to

be 17.7Å. This is a large difference and may be due to the differences in the number of cations per unit cell.

The number of NMF molecules per Na cation was found to be 6.83, whereas that of the Mg-complexes was 11.8. Although all the NMF molecules were oriented around the Na cation, not all were associated around the Mg cation. Some of the NMF molecules in the Mg-exchanged clay were in spaces between NMF saturated cations.

Figure 7.40: Simulated NMF structure. Code; grey=carbon, red=oxygen, blue=nitrogen, and, white=hydrogen.

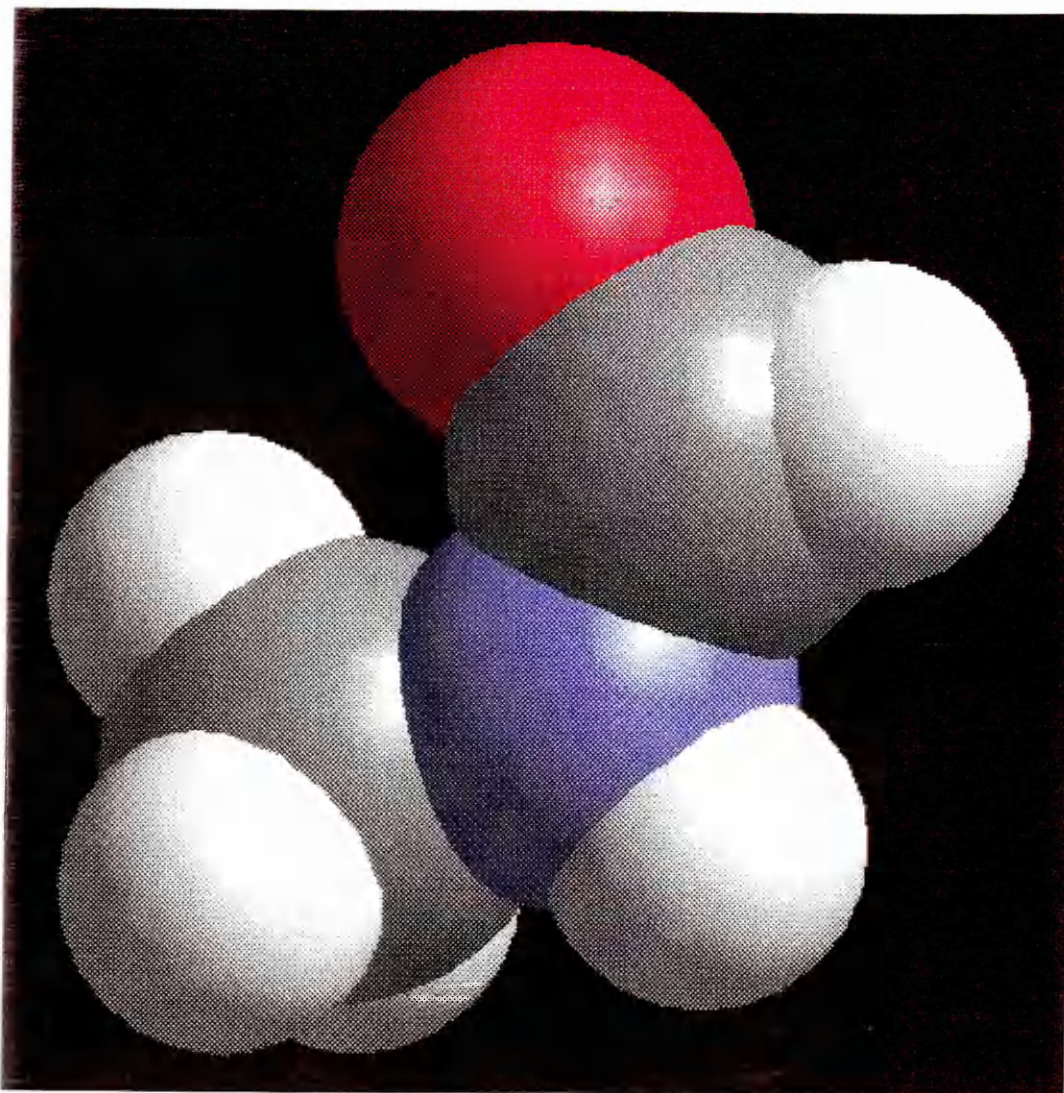


Figure 7.41: Simulated sorption of NMF into Na-montmorillonite. Code; pink spheres=Na ion, grey=carbon, red=oxygen, blue=nitrogen, and, white=hydrogen.

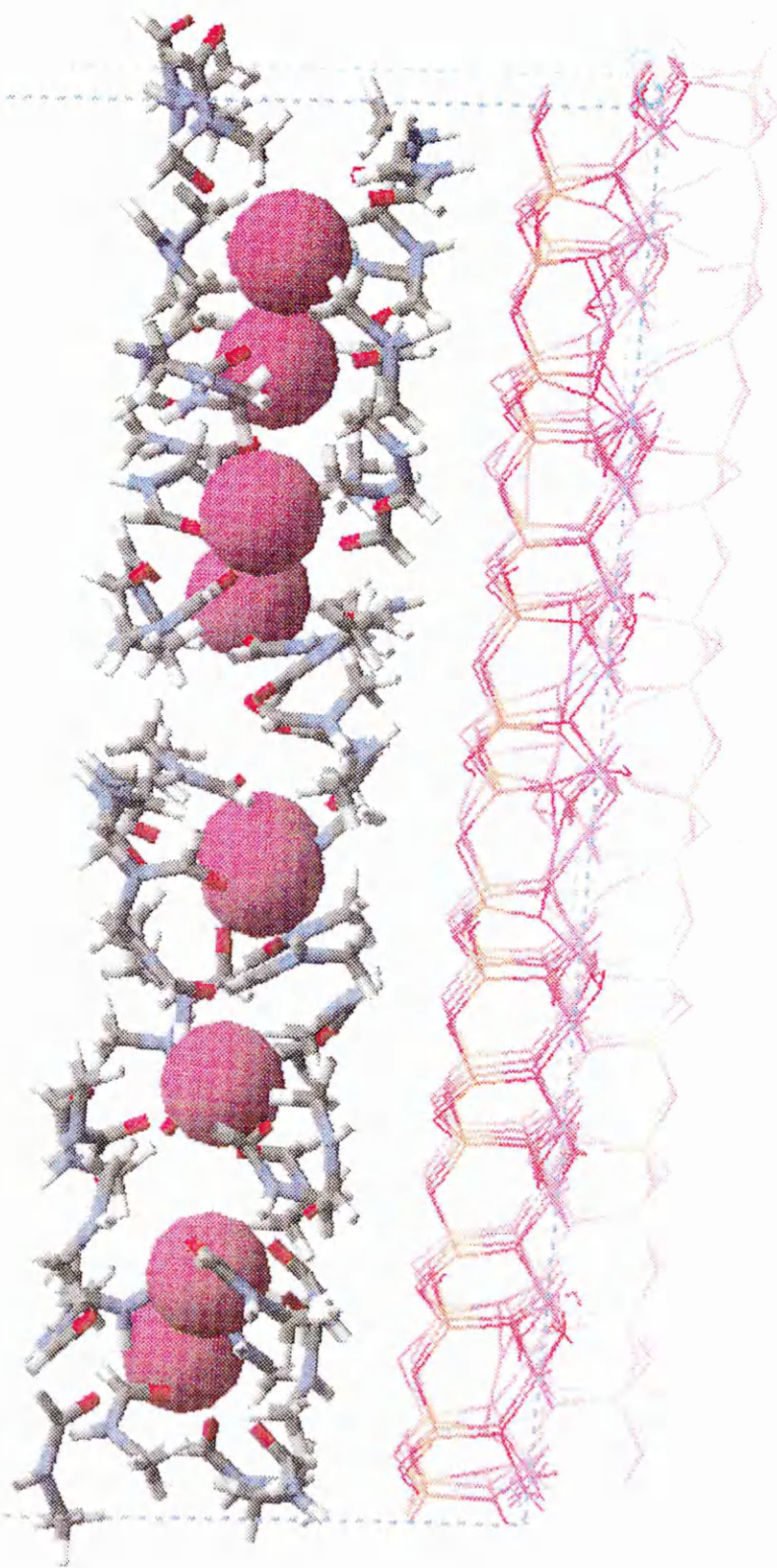
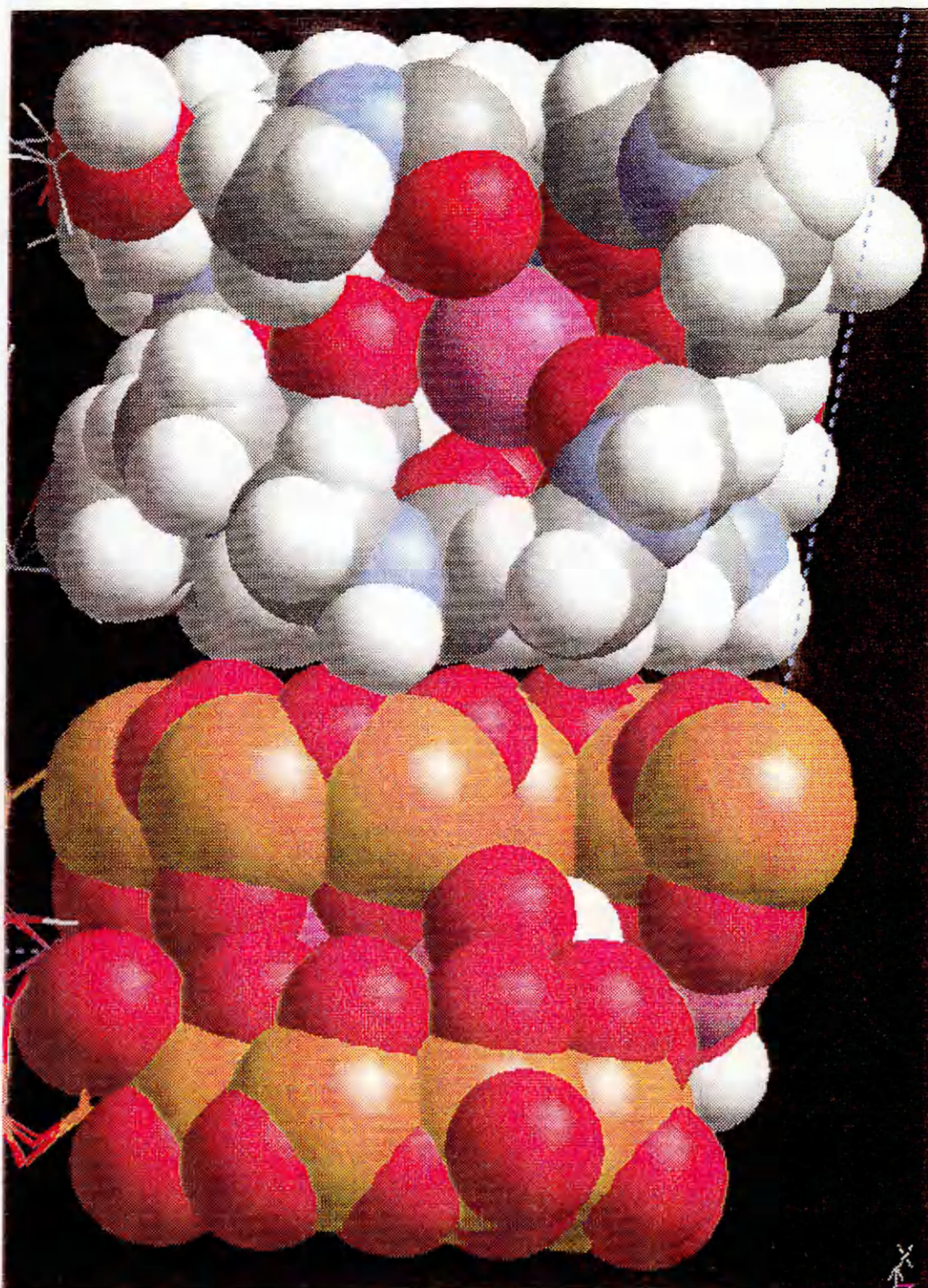


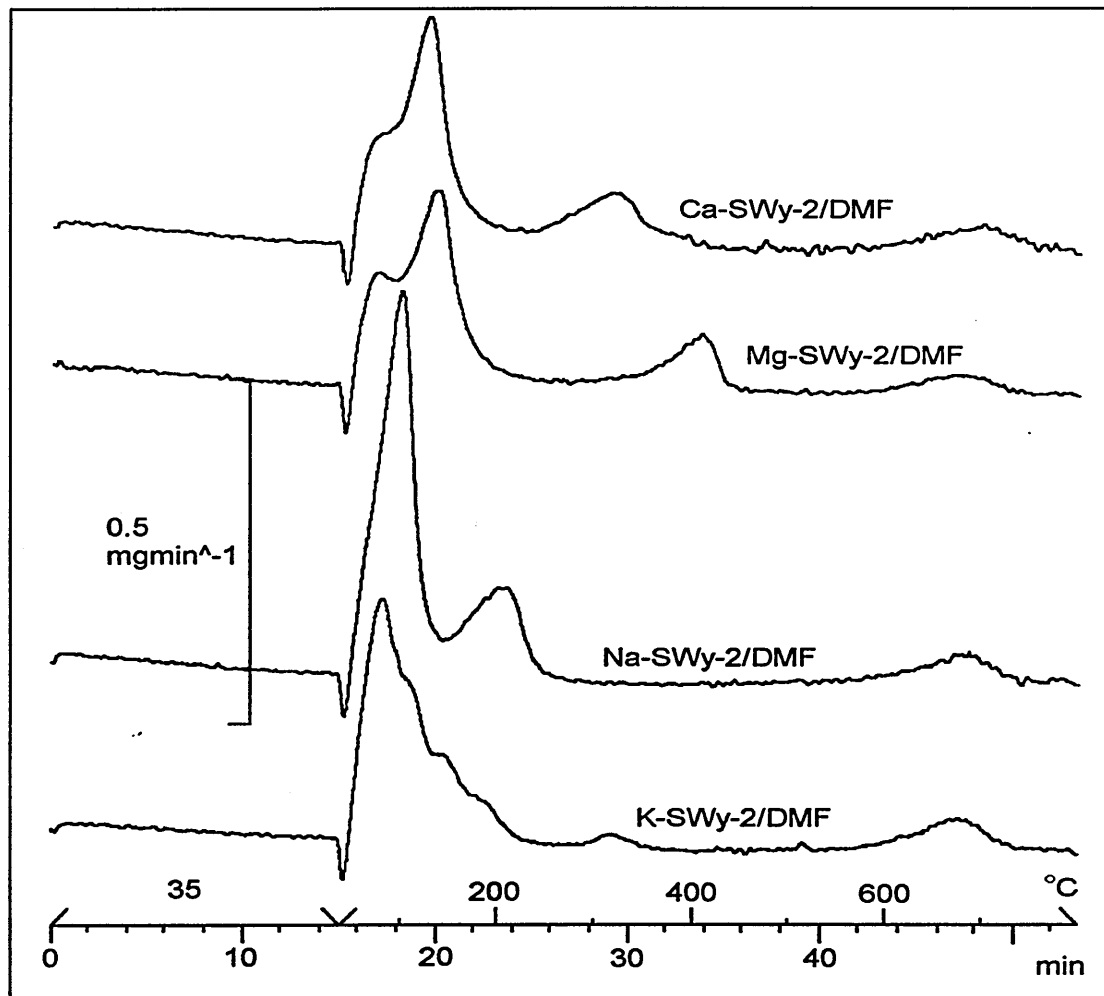
Figure 7.42: Simulated sorption of NMF into Na-montmorillonite. Code; pink spheres=Na ion, grey=carbon, red=oxygen, blue=mitrogen, white=hydrogen, and, orange=silicon



7.2.7) VT-DRIFTS analysis of the Ca, Mg, Na and K-SWy-2/DMF complexes

In this section the VT-DRIFTS spectra of the above complexes will be discussed in relation to their DTG traces. Figure 7.43 shows the DTG traces of the complexes that will be discussed here.

Figure 7.43: DTG traces of the X-SWy-2/DMF complexes discussed in this section.



The infrared spectrum of liquid DMF (figure 7.44) is superficially very similar to that of NMF except that it does not possess any N-H stretching bands in the region 3400-3538cm⁻¹. Although this is the case the two liquids behave very differently. The spectra does exhibit a broad band at 3538cm⁻¹ and is due to water contamination present in the liquid DMF. The assignments of the bands are listed in table 7.4, these were taken from Olejnik et al. [274, and references therein]. These assignments agree with those of Jao et al. [286].

Figure 7.44: Infrared spectrum (transmission) of DMF (4000-600 cm^{-1}).

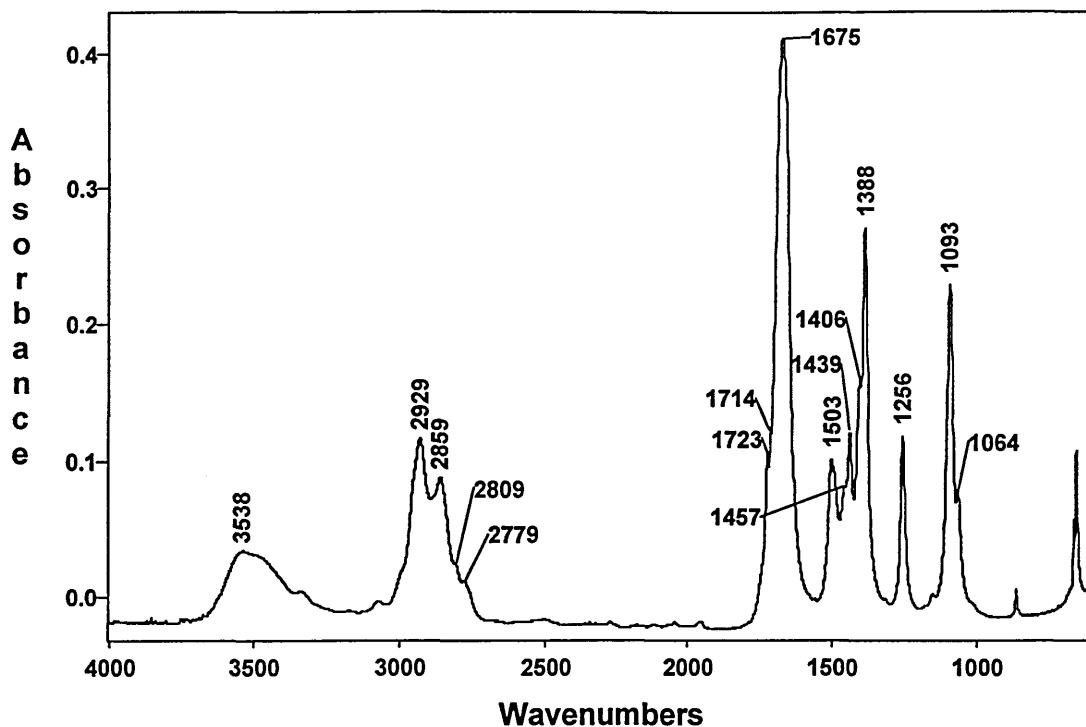


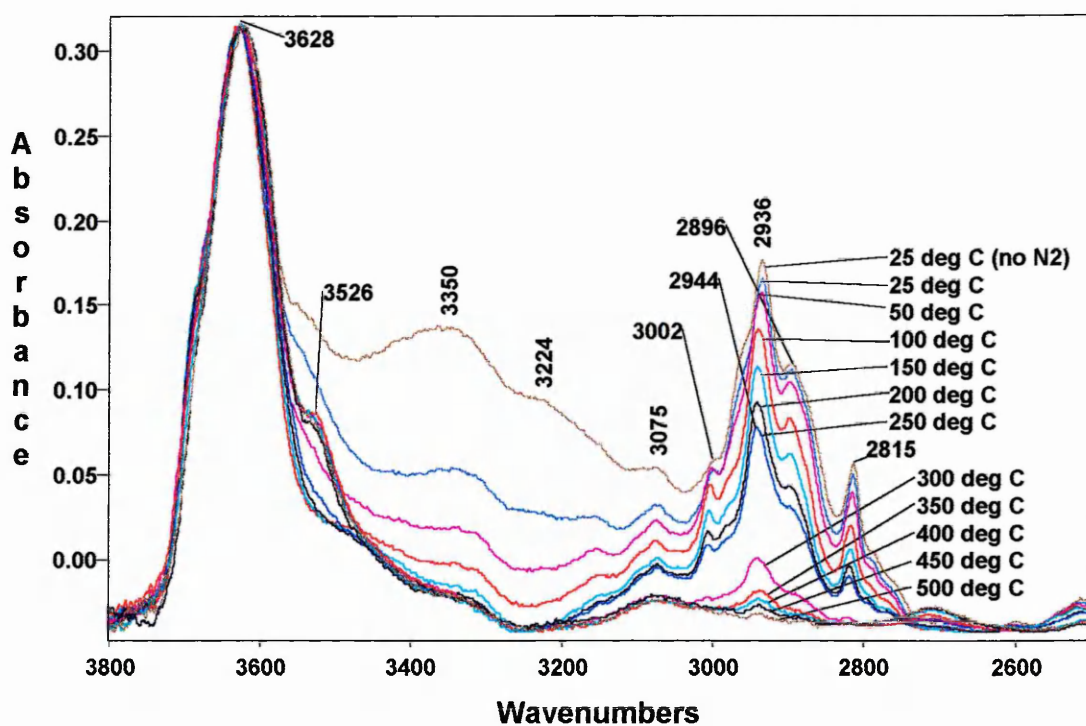
Table 7.4: Assignments of the observed bands in the infrared spectrum of liquid DMF.

Band position (cm^{-1})	Assignment
3538	$\nu(\text{OH})$ water impurity
2929	$\nu_{\text{as}}(\text{CH}_3)$
2859	$\nu(\text{CH})$
2809	$\nu_{\text{s}}(\text{CH}_3)$
2779	
1723 (shoulder)	Amide I $\nu(\text{C}=\text{O})$
1714 (shoulder)	
1675	
1503	$\nu(\text{CN})$
1457 (shoulder)	$\delta_{\text{as}}(\text{CH}_3)$
1439	
1406	$\delta_{\text{s}}(\text{CH}_3)$
1388	$\delta(\text{CH})$

Ca-SWy-2/DMF

Figure 7.45 shows the VT-DRIFTS spectra of Ca-SWy-2 after 16 days in DMF vapour in the region $3800\text{-}2500\text{cm}^{-1}$. The spectra shows a decrease in intensity of the broad bands between $3500\text{-}3100\text{cm}^{-1}$, the shape of these bands are characteristic of water (H-O-H stretching) and therefore indicates its presence in the complex. These bands are removed by 100°C and infers that the water is very weakly bound.

Figure 7.45: VT-DRIFTS spectra of Ca-SWy-2 after exposure to DMF vapour for 16 days ($3800\text{-}2500\text{cm}^{-1}$)

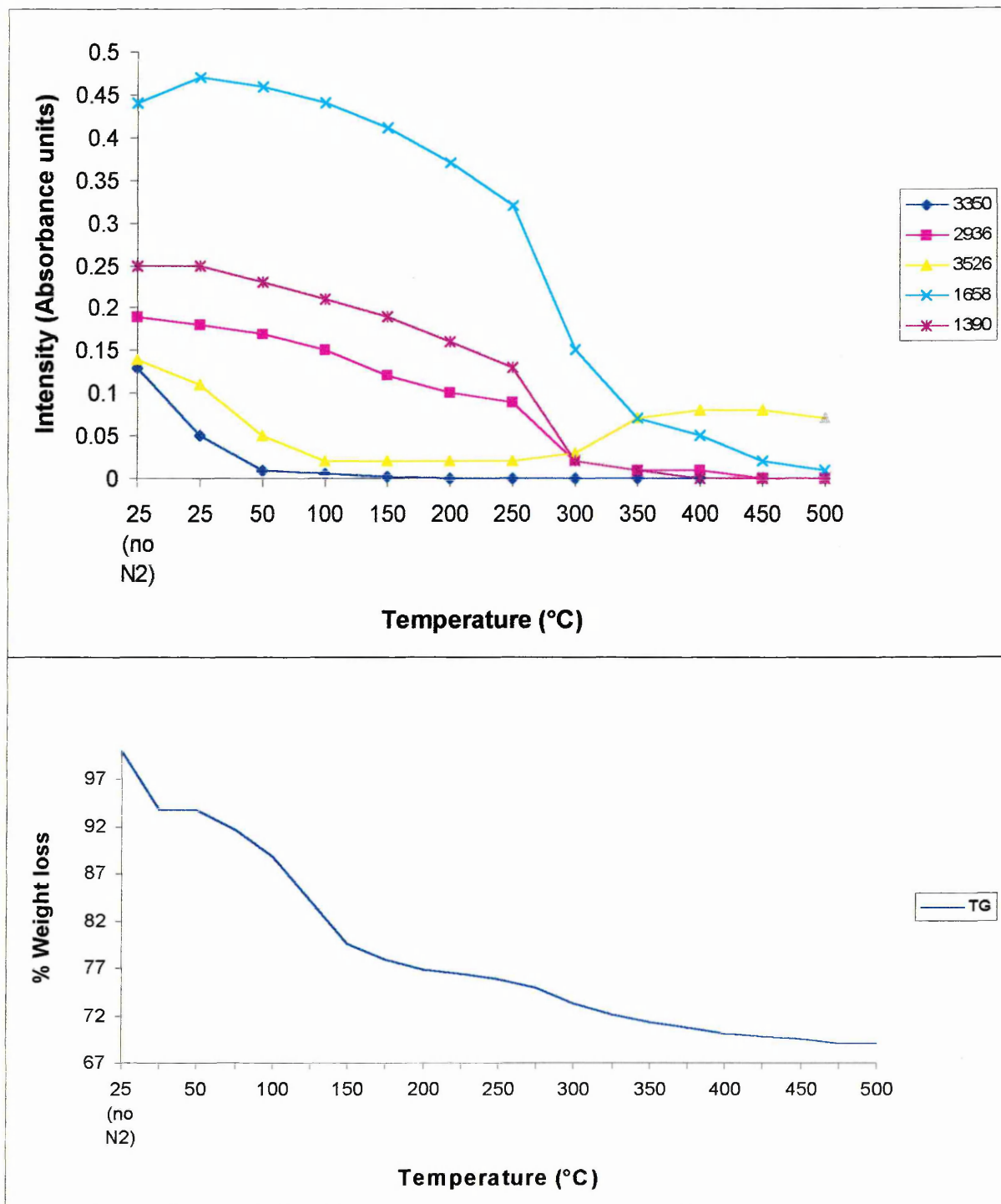


A plot of intensity at 3350cm^{-1} against temperature (figure 7.46) shows this more clearly. This observation also occurs in the Ca-SWy-2/NMF complex in that water is present up to 100°C , this is indicated by the removal of the band at 1625cm^{-1} . The bands observed in the C-H stretching region of the complex do not change significantly as the sample is heated, although a slight shift of approximately 8cm^{-1} to higher frequency occurs in the bands originally positioned at 2929 , 2809 and 3002cm^{-1} . The band originally positioned at 2859cm^{-1} undergoes a huge shift to 2896cm^{-1} . The rate of decrease in intensity of all these bands as the temperature is increased are

approximately the same. Figure 7.46 shows a plot of the intensity of the band at 2936cm^{-1} against temperature. This plot represents the loss of DMF from the complex and is very similar in shape to that of the TG-curve (figure 7.46).

Figure 7.46: A plot of intensity versus temperature of some bands in the VT-DRIFTS spectra of the Ca-SWy-2/DMF complex (16 days in vapour).

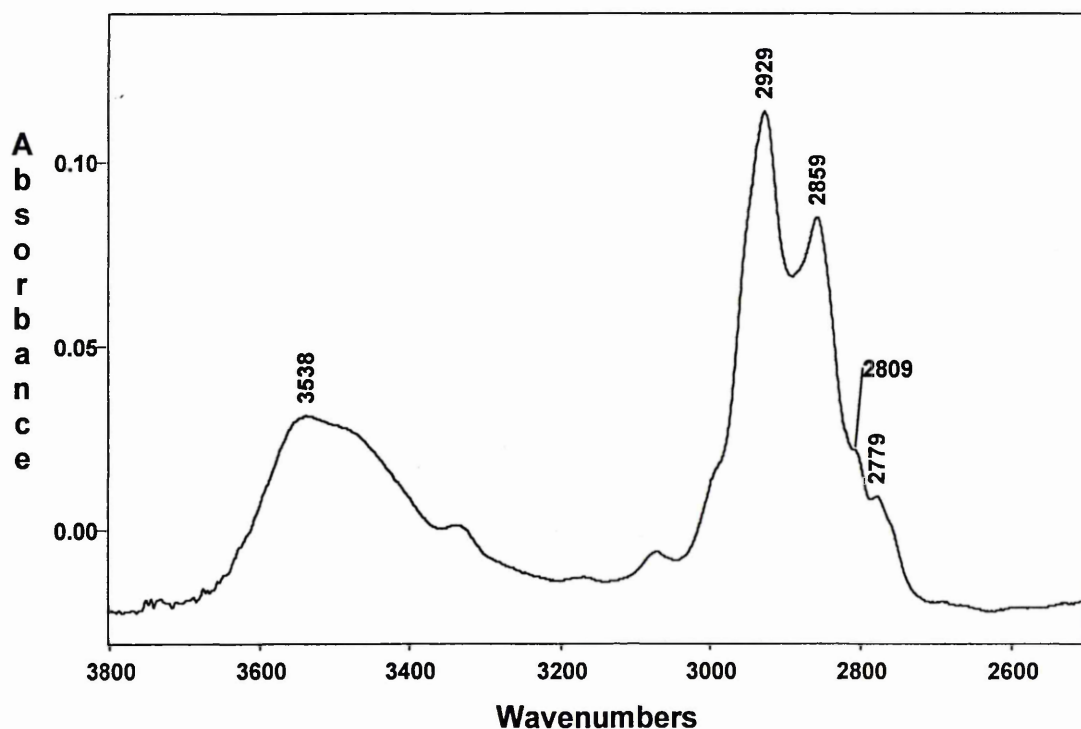
Its TG curve is also shown.



A greater decrease in intensity is observed between 50-150°C in the TG curve than in the intensity of the 2936cm⁻¹ band. Assuming that the extinction coefficient of the band at 2936cm⁻¹ remains constant throughout the spectra, this indicates that the additional decrease in weight between 50-150°C is due to the removal of water. The sharp drop in weight observed after purging for 15 minutes with nitrogen must also be due to the removal of water.

The infrared spectrum of liquid DMF is plotted on the same scale in figure 7.47. The general observation in the C-H stretching bands of DMF when it changes from being in the liquid state to when it is complexed with Ca-SWy-2 is that the bands shift to a higher frequency and become sharper. This may be due to the removal of underlying water but is more likely to be due to a decrease in the number of environments the CH₃ and CH groups are in. The band positioned at 2929cm⁻¹ in the spectrum of liquid DMF is assigned to the antisymmetric vibration of the C-H bond in the CH₃ groups, ($\nu_{as}(\text{CH}_3)$). When complexed to the clay this band shifts to higher frequency (approximately 7cm⁻¹). This indicates that the C-H bonds oscillate at a higher frequency and may be due to the fact the C-H bonds are in a restricted environment.

Figure 7.47: Infrared spectrum (transmission) of DMF (3800-2500cm⁻¹).



The band positioned at 2859cm^{-1} in the spectrum of DMF is assigned to the stretching vibration of the C-H group, $\nu_s(\text{C-H})$. When DMF is complexed to the clay it is likely that this band shifts 37cm^{-1} to a higher frequency. This is a massive shift and indicates the environment of the bond has changed considerably and is in a unique position.

The band positioned at 2809cm^{-1} is due to the C-H stretching vibration of the CH_3 groups. This band appears sharp and is more resolved, its position at higher frequency may indicate that the CH_3 groups are in a restricted environment.

These spectra also show the appearance of a band at 3526cm^{-1} when the temperature of the sample reaches 350°C , this may be the formation of a Ca-hydroxide species.

Figure 7.48 shows the VT-DRIFTS spectra of Ca-SWy-2 after exposure to DMF vapour for 16 days in the region $2000\text{-}1000\text{cm}^{-1}$. The main band in this region is positioned at 1658cm^{-1} which is due to the amide I band (mostly C=O). This band possesses a shoulder at approximately 1627cm^{-1} and is due to the presence of water. This fact coincides with the water bands observed between $3500\text{-}3100\text{cm}^{-1}$ and is removed when the sample is heated to 100°C .

The infrared spectrum of liquid DMF exhibits a very strong band at 1675cm^{-1} and two small bands at 1714 and 1723cm^{-1} (see figure 7.49 for infrared spectrum of DMF on the same scale). The spectrum of vapour DMF exhibits one strong band 1714cm^{-1} . This indicates that the high frequency bands in pure liquid DMF can be attributed to DMF molecules that are undergoing weaker interactions via the carbonyl group. The carbonyl band in the complex is at 17cm^{-1} lower (1658cm^{-1}) than the carbonyl band in pure DMF. This indicates that the carbonyl bond is interacting more strongly, presumably due to interactions with the exchangeable cations in the clay. This shows that the DMF molecules adsorb on to the clay via their carbonyl group. The intensity of this band is plotted as a function of increasing temperature in figure 7.46. A greater decrease is observed between $250\text{-}350^\circ\text{C}$ than $50\text{-}150^\circ\text{C}$, whereas the opposite is observed in the TG-curve. This is due to the removal of water from the clay between $25\text{-}100^\circ\text{C}$. The band at 1658cm^{-1} is asymmetric to the high wavenumber side and indicates that a proportion of the DMF molecules in the clay are more liquid-like (i.e. interacting less strongly through their carbonyl group). A shoulder at

Figure 7.48: VT-DRIFTS spectra of Ca-SWy-2 after exposure to DMF vapour for 16 days (2000-1000 cm^{-1})

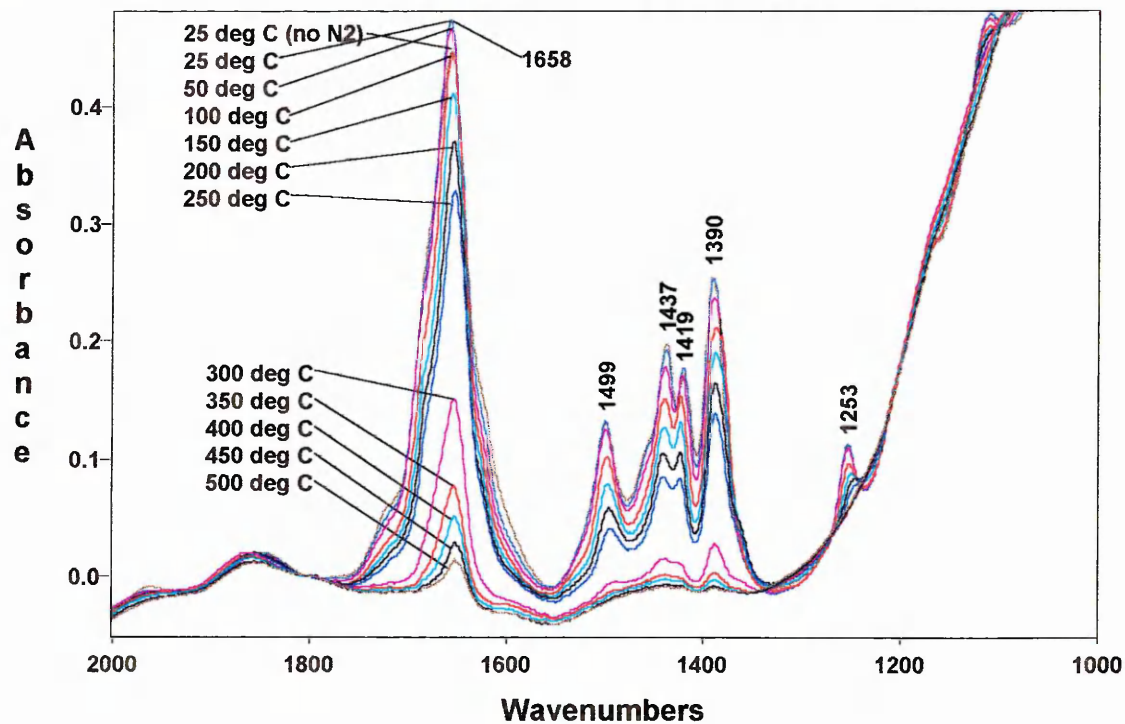
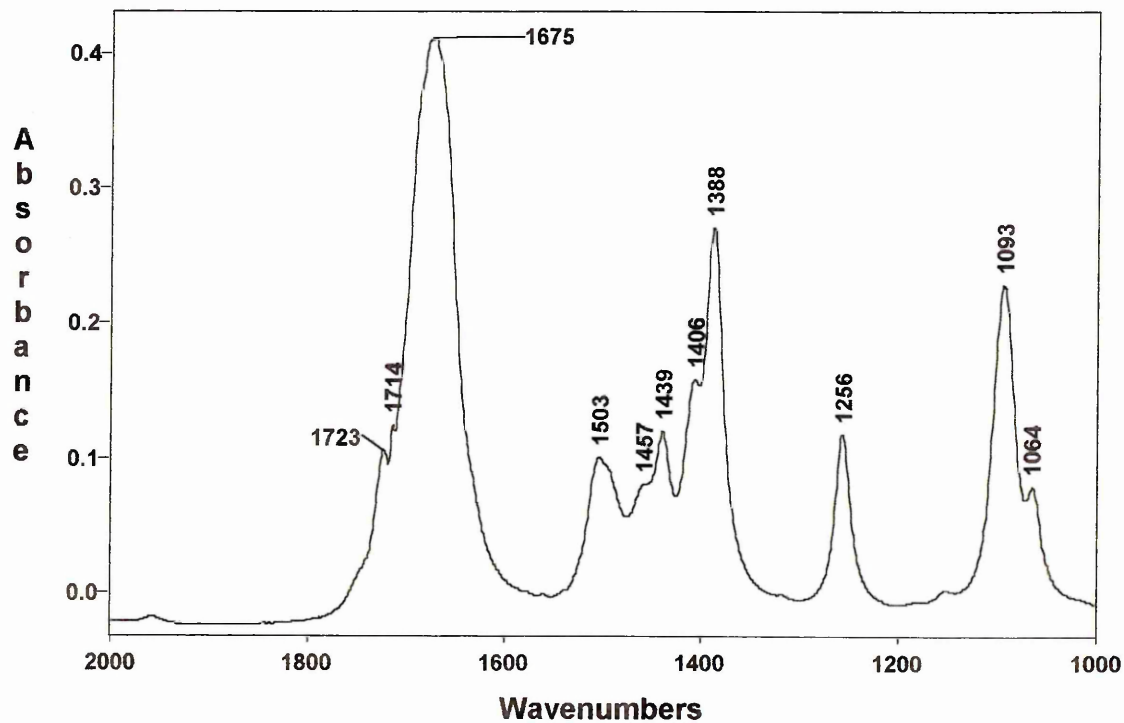


Figure 7.49: Infrared spectrum (transmission) of DMF (2000-1000 cm^{-1}).



approximately 1714cm^{-1} indicates that there are also some vapour-like DMF molecules.

These carbonyl bands will be discussed in more detail with respect to the other cation-exchanged clay complexes later (section 7.5.2).

In the spectrum of pure liquid DMF a band at 1406cm^{-1} is present (figure 7.49). This band shifts to higher frequency when the DMF is complexed to the clay and is positioned at 1419cm^{-1} . This band is assigned to the $\delta_s(\text{CH}_3)$ and shifts to an even higher frequency as the sample is heated to 150°C . Its position then remains constant as the temperature is increased further. The shift to higher frequency could be due to an inductive effect occurring when the DMF is coordinated to the exchangeable cation. As electrons are drawn from the carbon atom the C-H bonds will be affected which will result in a change in the vibrational frequency. Alternatively, the vibrational modes of the groups may be restricted because of their close proximity to the clay layers when intercalated. It is interesting to note that the CH_3 groups in the NMF molecules of the X-SWy-2/NMF molecules showed no significant shifts or band changes. Shifts in the CH_3 vibrational modes of intercalated DMF molecules could therefore occur due to their close proximity because there are twice as many CH_3 groups and is therefore more bulky in size.

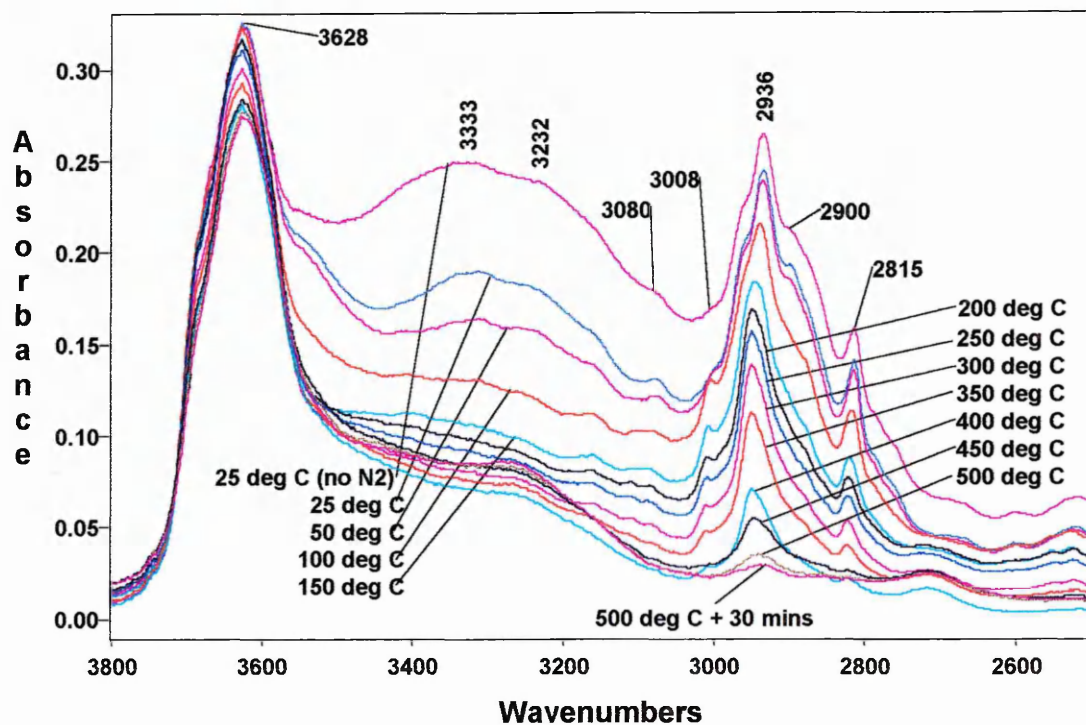
A plot of the intensity of the $\delta(\text{CH})$ band against sample temperature is shown in figure 7.46. The shape of this curve is the same as that of the plots of the carbonyl and $\nu_{\text{as}}(\text{CH}_3)$ bands. Very little change has occurred in the position of the other bands although the C-N stretching band (1503cm^{-1} in liquid DMF) has decreased slightly to a lower frequency (1499cm^{-1}), presumably due to a loss in double bond character upon coordination to the clay.

Mg-SWy-2/DMF

Figure 7.50 shows the VT-DRIFTS spectra of Mg-SWy-2 after exposure to DMF vapour for 16 days in the region $3800\text{-}2500\text{cm}^{-1}$. These spectra show that water is present in the complex, as indicated by the broad bands between $3500\text{-}3100\text{cm}^{-1}$ and that it is removed when the sample is heated to 100°C . This shows that the first

maximum observed in the DTG is partly due to water. Figure 7.51 shows the decrease in intensity of the band at 3333cm^{-1} and shows that it correlates to the decrease in weight observed in the TG between $50\text{-}100^\circ\text{C}$.

Figure 7.50: VT-DRIFTS spectra of Mg-SWy-2 after exposure to DMF vapour for 16 days ($3800\text{-}2500\text{cm}^{-1}$).



The band positioned at 2936cm^{-1} in the spectrum collected at 25°C (prior to purging with nitrogen) is assigned to $\nu_{\text{as}}(\text{CH}_3)$ and is prominent in all the VT-DRIFTS spectra. This band progressively shifts to a higher frequency as the temperature of the sample is increased to 150°C (2949cm^{-1} at 150°C). The band then remains constant upon further increases in temperature. A shift to higher frequency in this band also occurred in the Ca-SWy-2/NMF complex and may be due to the fact the C-H bonds are in a restricted environment.

The band positioned at 2900cm^{-1} is assigned to the C-H stretching vibration and is at a much higher frequency than that in pure liquid DMF. In comparison with the Ca-SWy-2/NMF complex this band is much broader, at a slightly higher frequency, and, is less clearly defined. At 200°C this band becomes the shoulder on the low wavenumber side of the band at 2936cm^{-1} . This is indicated by comparing the increased intensity of

the band at 2936cm^{-1} relative to the band at 2815cm^{-1} . This does not occur in the Ca-SWy-2/NMF complex. The shift to higher frequency indicates the environment of the bond is in a unique environment which presumably results from the coordination of DMF to the exchangeable cations

Figure 7.51: A plot of intensity versus temperature of some bands in the VT-DRIFTS spectra of the Mg-SWy-2/DMF complex (30 days in vapour).

Its TG curve is also shown.

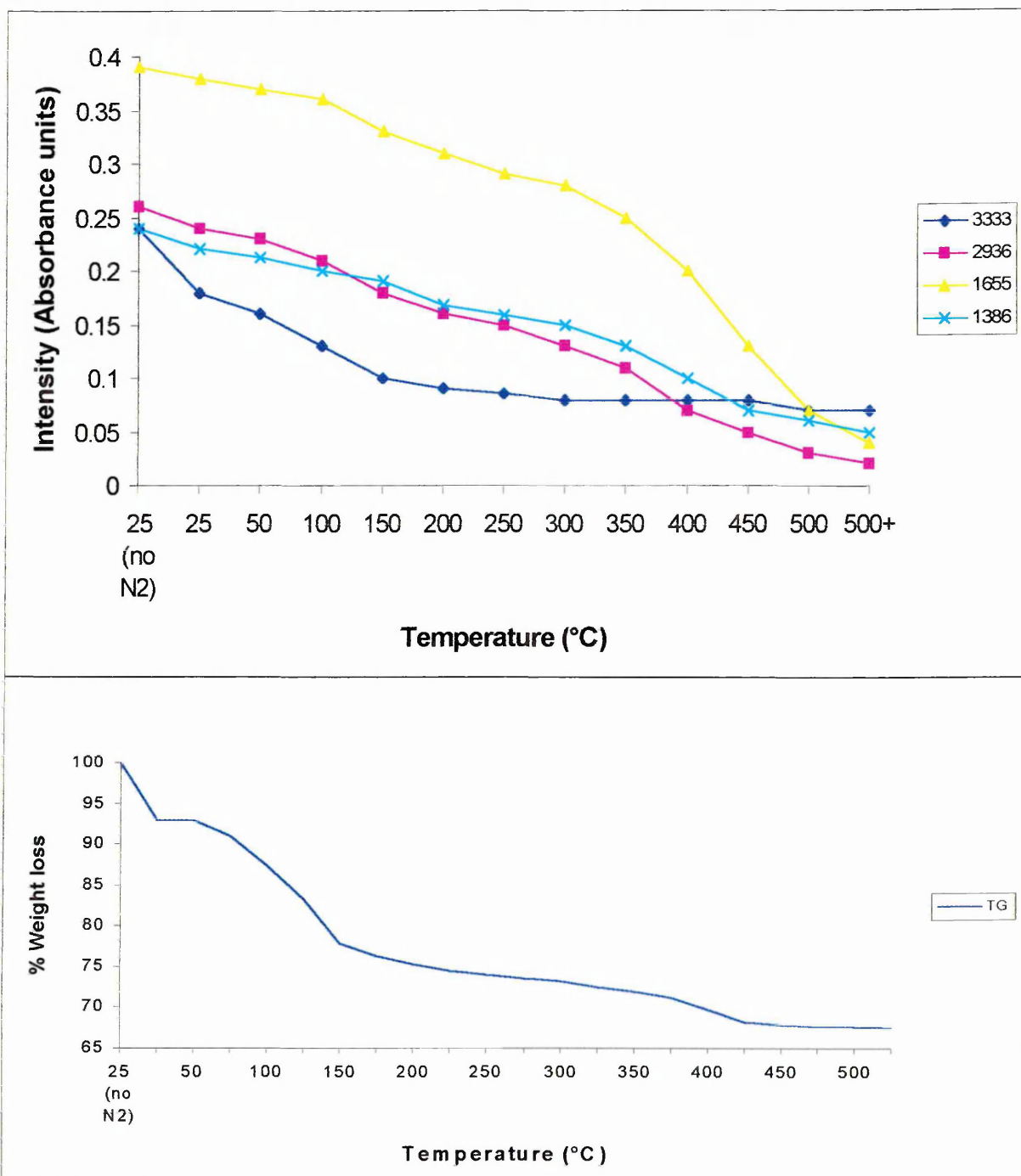
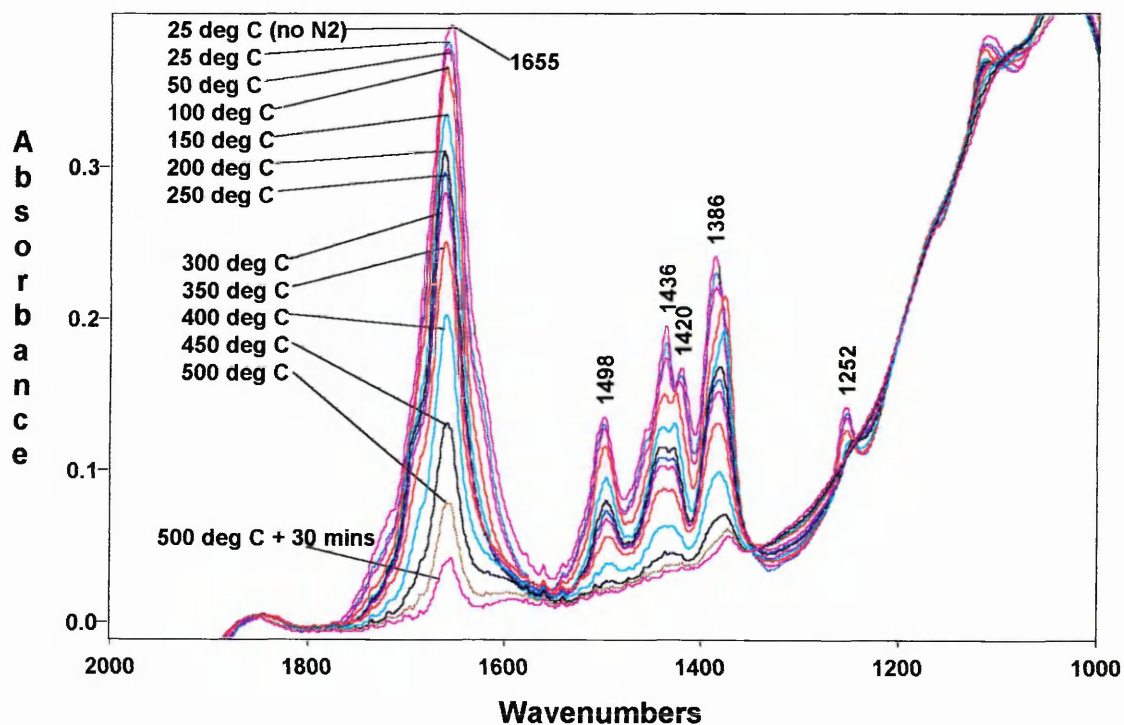


Figure 7.52 shows the 2000-1000 cm^{-1} region of the VT-DRIFTS spectra of Mg-SWy-2 after exposure to DMF vapour for 16 days. These spectra show a shift in the carbonyl band from 1675 (liquid DMF) to 1658 cm^{-1} when the DMF is complexed with the clay. This indicates that the carbonyl bond is interacting more strongly, presumably due to coordination with the clay and shows that the DMF molecules bind to the clay through the carbonyl group, as expected. A plot of intensity of the carbonyl band against temperature is shown in figure 7.51. Here a larger decrease occurs between 350-450 $^{\circ}\text{C}$ than 50-200 $^{\circ}\text{C}$ whereas the opposite happens for the water band (3333 cm^{-1}) indicating that the first maximum in its DTG trace contains water.

Figure 7.52: VT-DRIFTS spectra of Mg-SWy-2 after exposure to DMF vapour for 16 days (2000-1000 cm^{-1})



Similar observations are apparent in the bands observed between 1498-1386 cm^{-1} for both the Ca and Mg-SWy-2/NMF complexes, that is, the band positioned at 1406 cm^{-1} ($\delta_s(\text{CH}_3)$) in pure DMF is now positioned at 1420 cm^{-1} in the complex. This may be due to an inductive effect occurring when DMF is coordinated to the exchangeable cation (i.e. as electrons are drawn away from the carbon atom the vibrational mode of

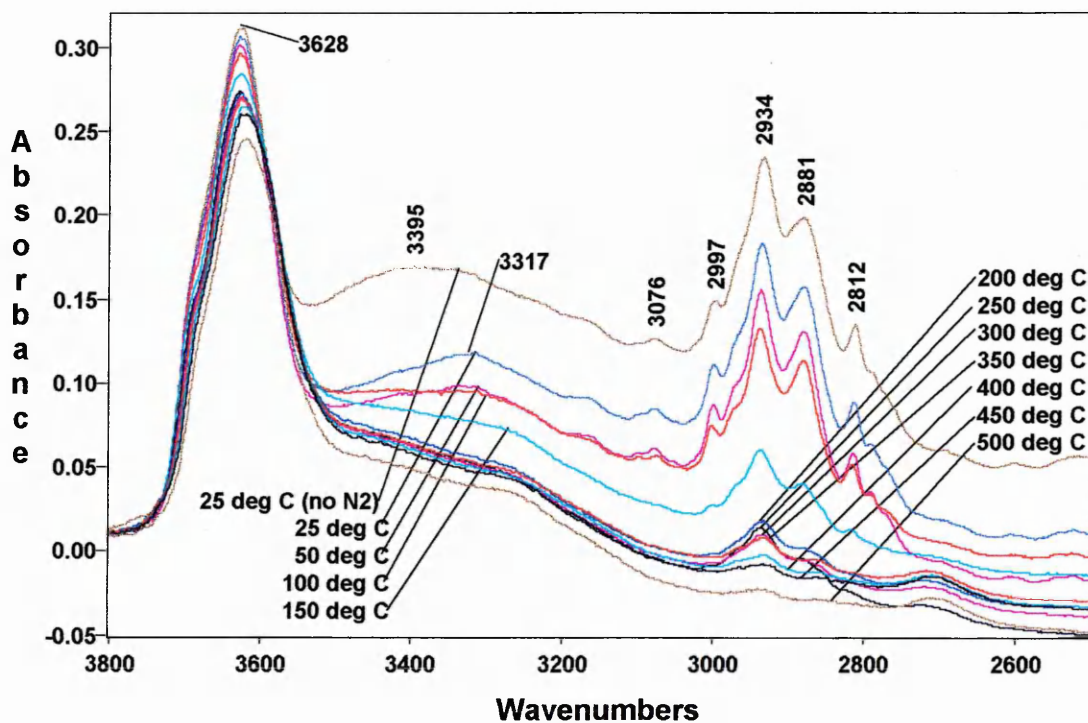
the C-H bonds will be affected) or the vibrational modes will be restricted because of their close proximity to the clay interlayers.

Na-SWy-2/DMF

Figure 7.53 shows the 3800-2500 cm^{-1} region of the VT-DRIFTS spectra of Na-SWy-2 after exposure to DMF vapour for 16 days.

The spectra show that water is lost from the complex between 25-100 $^{\circ}\text{C}$ as indicated by the presence of the broad water bands between 3500-3100 cm^{-1} . The region between 2997-2812 cm^{-1} is very similar to that of the Ca-complex, except that the band due to C-H stretching is at a lower frequency (2881 cm^{-1}).

Figure 7.53: VT-DRIFTS spectra of Na-SWy-2 after exposure to DMF vapour for 16 days (3800-2500 cm^{-1}).



The position of the C-H stretching band in the clay complexes shifts in relation to the polarisability of the exchangeable cation (table 7.5).

Table 7.5: Position of the C-H stretching band in the Ca, Mg and Na-SWy-2/DMF complexes.

X-SWy-2	$\nu_s(\text{C-H}), \text{cm}^{-1}$
Mg	2900
Ca	2896
Na	2881

This is expected since the stronger the electron withdrawing effect of the cation the greater the change in the C-H bond becomes and hence a shift of the band to higher wavenumbers.

Figure 7.54 shows the 2000-1000 cm^{-1} region of the VT-DRIFTS spectra of Na-SWy-2 after exposure to DMF vapour for 16 days. These spectra show that the positions of the bands are similar to those of the Ca and Mg-SWy-2/DMF complexes. The main difference is that the $\delta_s(\text{CH}_3)$ band has not shifted to as high a frequency. There are subtle differences observed in the amide I band, which will be discussed later with respect to the carbonyl band of the other complexes.

Figure 7.54: VT-DRIFTS spectra of Na-SWy-2 after exposure to DMF vapour for 16 days (2000-1000 cm^{-1})

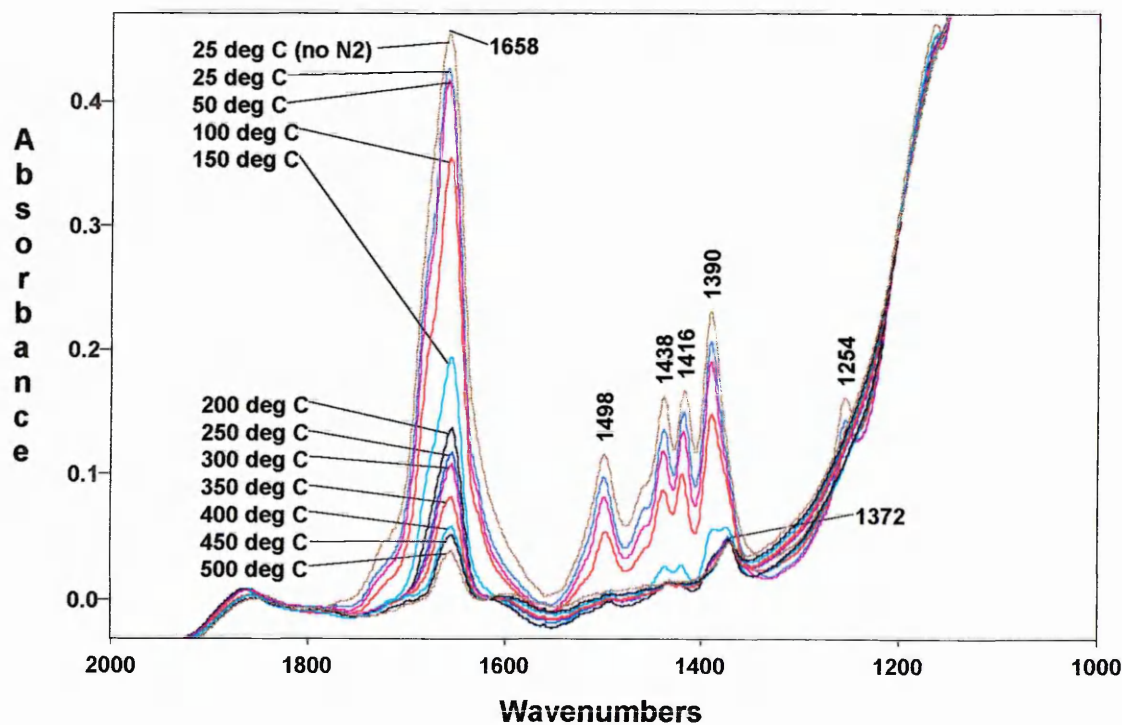
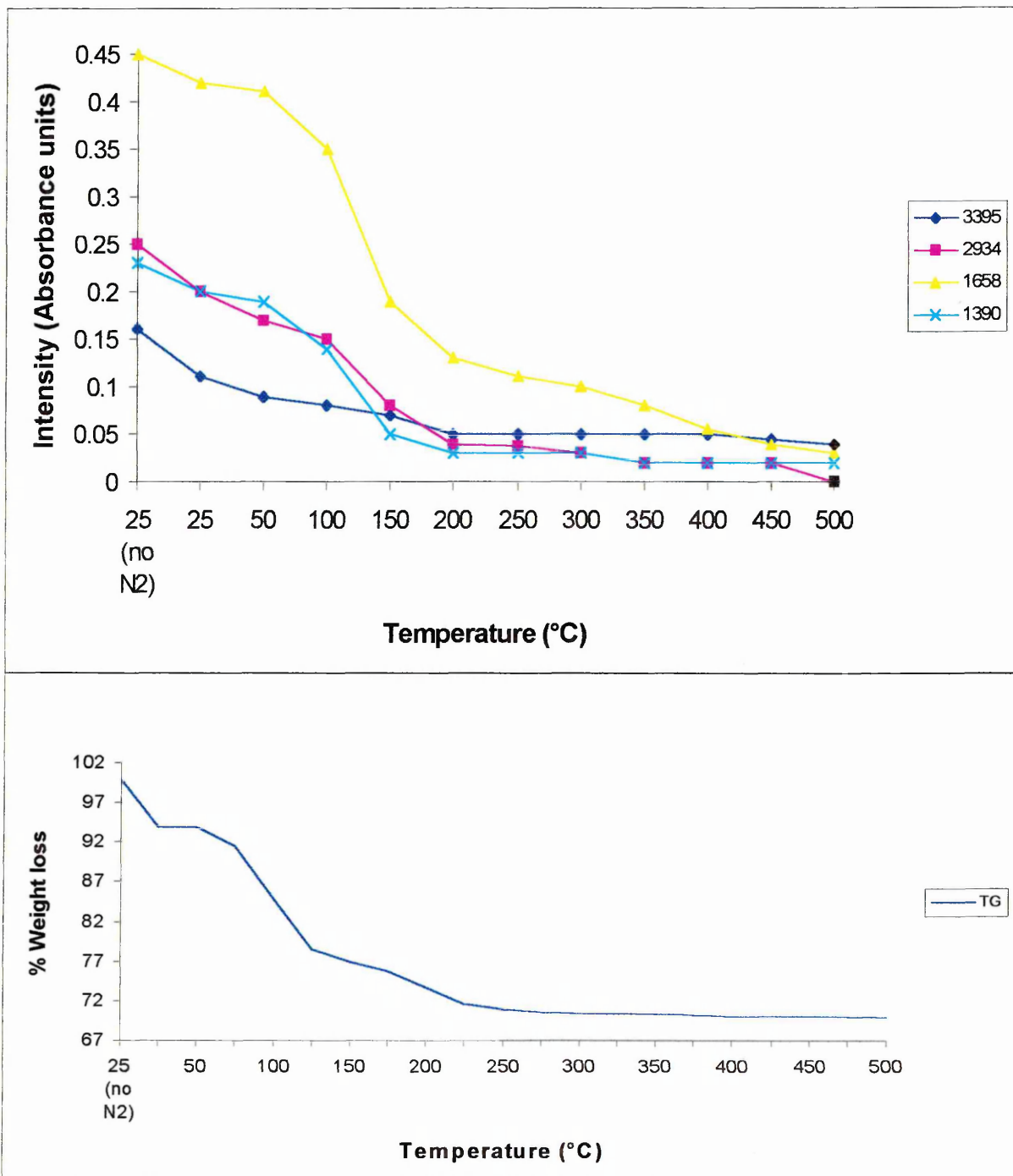


Figure 7.55 shows a plot of intensity of the bands at 3395, 2934, 1658 and 1390 cm^{-1} as the temperature of the sample is increased. These show that DMF is lost during the high temperature maximum observed in the DTG trace and both water and DMF is lost during the low temperature maximum in the DTG trace.

Figure 7.55: A plot of intensity versus temperature of some bands in the VT-DRIFTS spectra of the Na-SWy-2/DMF complex (30 days in vapour).

Its TG curve is also shown.



K-SWy-2/DMF

Figures 7.56 and Figure 7.57 shows the VT-DRIFTS spectra of the K-SWy-2/DMF complex in the regions 3800-2500 and 2000-1000 cm^{-1} , respectively. These spectra show similar changes to those of the Ca, Mg and Na-SWy-2/DMF complexes. The only significant change is that the band at 2880 cm^{-1} is at a slightly lower wavenumber and is broader than in the other complexes. The broadness could be due to the fact Ca is also present as an exchangeable-cation. The changes in the carbonyl band will be discussed in detail later. Figure 7.58 shows that water is lost between 25-100 $^{\circ}\text{C}$ (as shown by the band at 3328 cm^{-1}) and DMF is lost throughout the run (as shown by the bands at 1658 and 1390 cm^{-1}). This indicates that the low temperature maxima observed in the DTG trace are due to the removal of DMF and water, whilst the remainder are due to the removal of DMF.

Figure 7.56: VT-DRIFTS spectra of K-SWy-2 after exposure to DMF vapour for 16 days (3800-2500 cm^{-1})

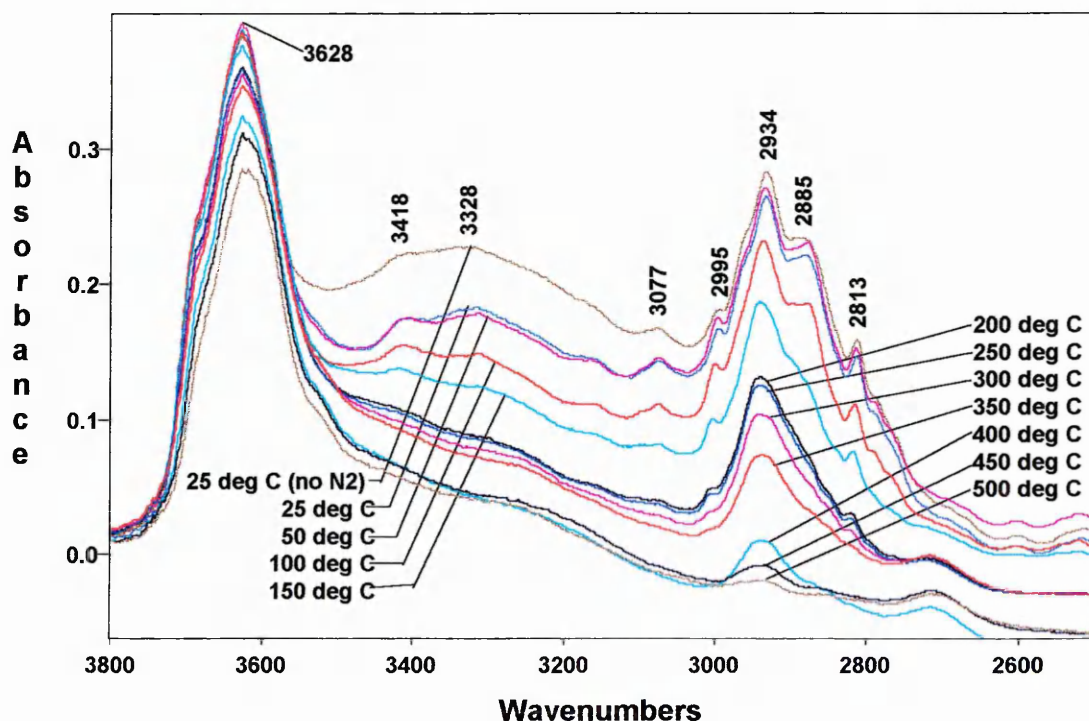
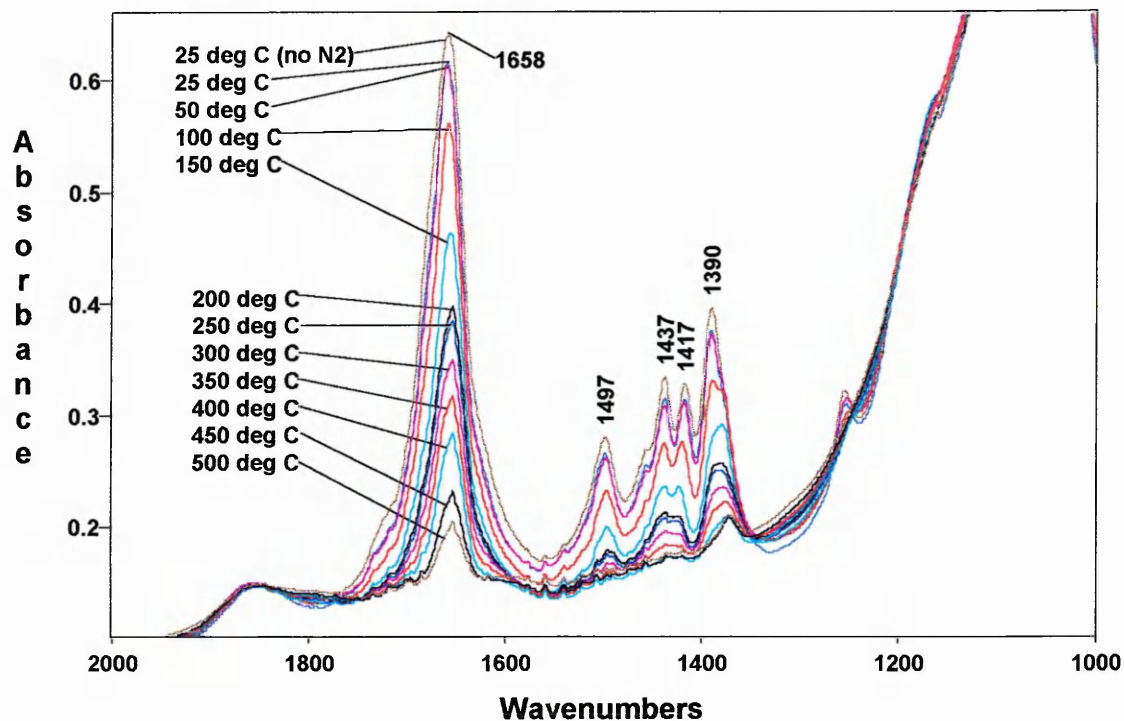


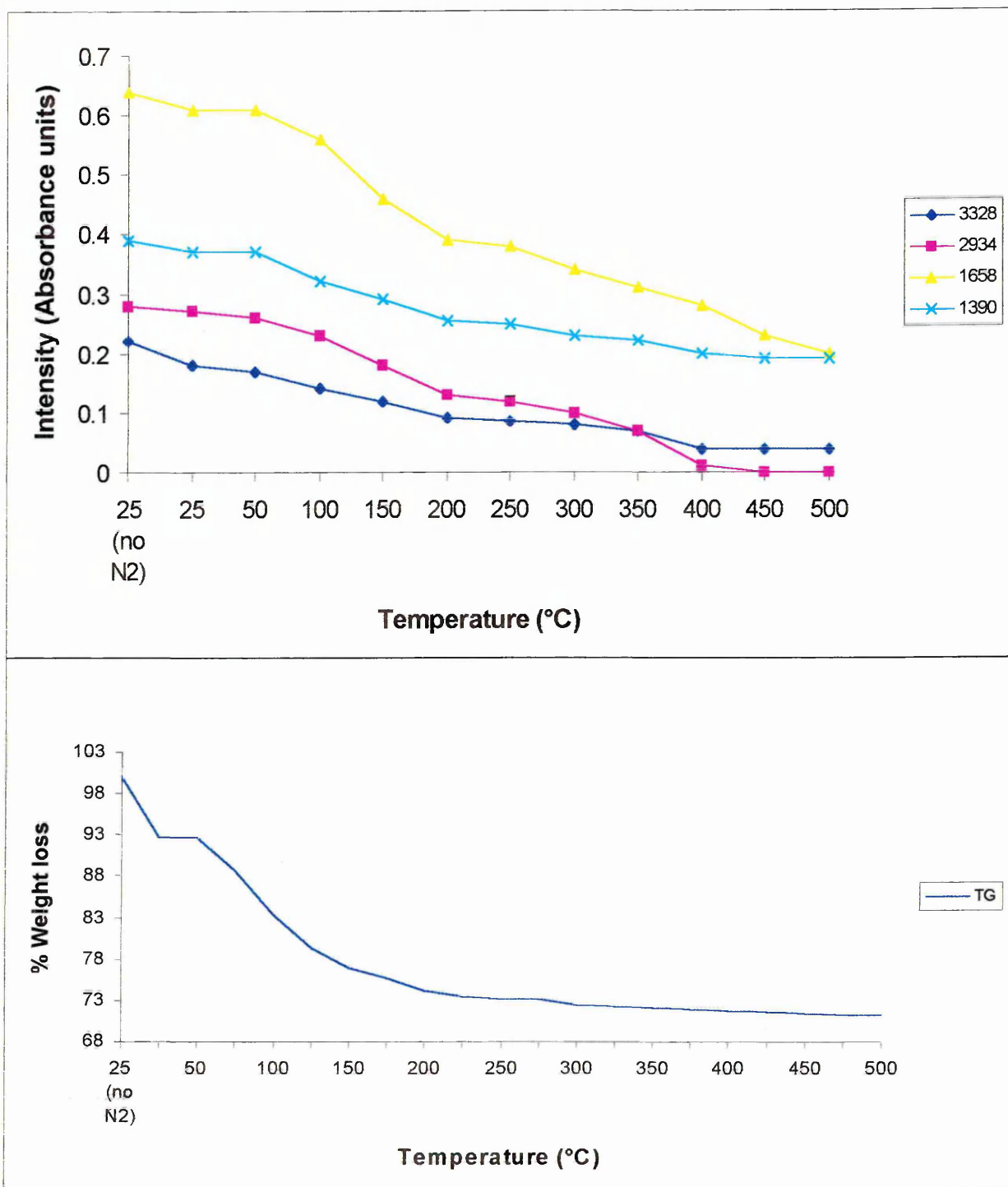
Figure 7.57: VT-DRIFTS spectra of K-SWy-2 after exposure to DMF vapour for 16 days (2000-1000 cm^{-1})



It is interesting to note the carbonyl band in the spectra of all the complexes is still present at temperatures above the temperature of the highest temperature maximum observed in the respective DTG traces. At this stage the layers are likely to have collapsed and the band is present due to trapped DMF molecules, possibly with large extinction coefficients.

Figure 7.58: A plot of intensity versus temperature of some bands in the VT-DRIFTS spectra of the K-SWy-2/DMF complex (30 days in vapour).

Its TG curve is also shown.



7.2.8) Carbonyl stretching region of the X-SWy-2/DMF complexes

Ca-SWy-2/DMF

Figure 7.59A shows the amide I band of the Ca-SWy-2/DMF complex in more detail. It is apparent from the spectra that the band is not symmetric. This is more accentuated in the deconvoluted spectra (figure 7.59B). The aim of this section is to determine trends within the spectra and relate these to the other experimental results.

The first observation to note is that there are at least 4 components to the infrared bands. These are accentuated in the deconvoluted spectra and are positioned at approximately 1720, 1683, 1656 and 1622 cm^{-1} . By referring to past papers and previous discussions these can be assigned to:-

1720 - vapour-like DMF molecules

1683 - DMF molecules (undergoing weaker self intermolecular interactions than liquid-like DMF)

1658 - strongly coordinated DMF molecules (i.e. to cation)

1623 - water molecules

The relative intensity decrease of these bands show that:

i) the strongly coordinated DMF molecules are retained at higher temperatures (i.e. >250°C). This indicates that the high temperature maximum in the DTG trace is due to coordinated DMF molecules. Note that the band progressively shifts to lower frequency as the temperature increases, indicating a progressively stronger interaction between DMF and cation.

ii) The liquid-like DMF molecules undergoing weaker self intermolecular interaction than liquid like DMF decrease in proportion to the cation coordinated DMF molecules between 25-250°C and show that these are assigned to the low temperature maximum (125°C) in the DTG trace. These DMF molecules may be situated in small clusters on clay surfaces, between clay stacks or in the interlayer region.

iii) The band at 1720 cm^{-1} relates to very weakly coordinated DMF molecules, these are removed when the sample reaches approximately 100°C and are probably situated on external clay surfaces.

Figure 7.59A: VT-DRIFTS spectra of the Ca-SWy-2/DMF complex formed after 16 days in DMF vapour (1800-1500 cm^{-1}).

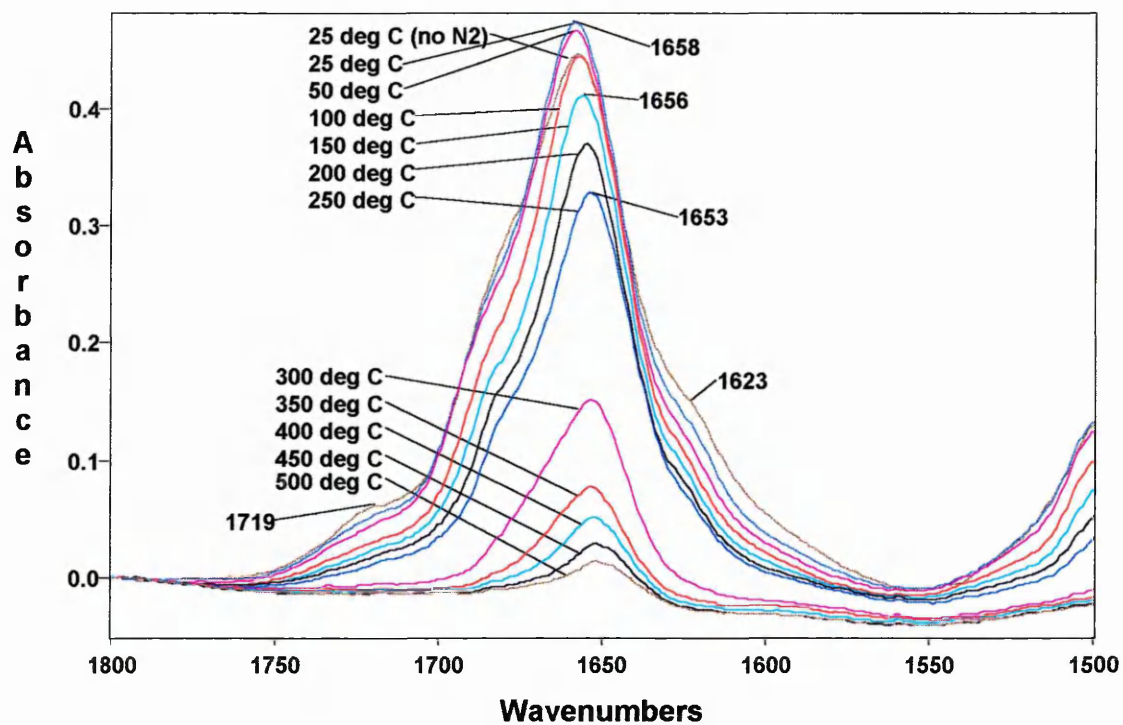
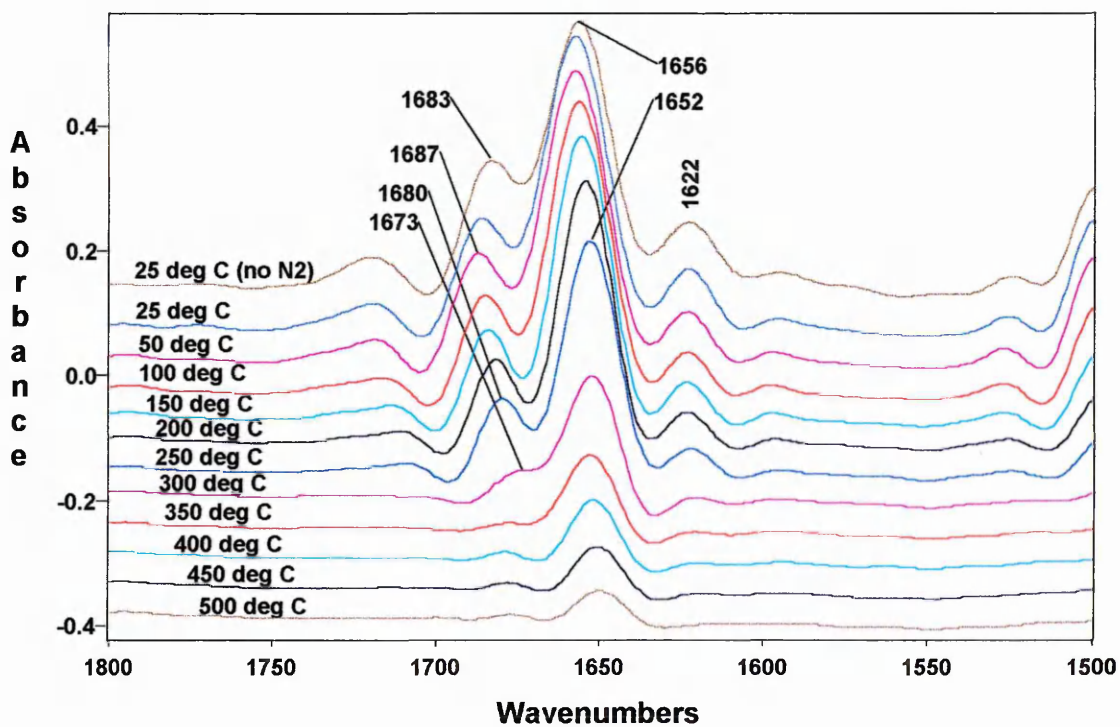


Figure 7.59B: Deconvoluted spectra of the Ca-SWy-2/DMF complex formed after 16 days in DMF vapour (1800-1500 cm^{-1}).



iv) the majority of the water (indicated by the band at 1622cm^{-1}) in the Ca-SWy-2/NMF complex is removed by 100°C and relates to loosely bound water molecules, these are probably found in clusters in the clay layers. The reader should note that a high amount of deconvolution ($K=1.7$) can produce spurious small bands at the edges of large bands. A valley of intensity less than the baseline indicates this is occurring. This occurs between 1622 and 1652cm^{-1} at about 250°C and this shows that water is not actually present above this temperature even though the spectra might suggest this.

Mg-SWy-2/DMF

The infrared spectra (figure 7.60A) and deconvoluted spectra (7.60B) of the carbonyl region in the Mg-SWy-2/DMF complex shows similar trends to that of the Ca-complex. Differences that are apparent are:-

- i) there is no valley between the coordinated DMF molecules (represented by band at $\approx 1656\text{cm}^{-1}$) and the weakly intermolecular-interacting DMF molecules (represented by band at 1692cm^{-1}) in the deconvoluted spectra collected between 25°C (no N_2) and 100°C . This suggests there are more clusters of liquid-like DMF present in the Mg-complex than the Ca-complex since a band positioned at approximately 1677cm^{-1} indicates that liquid-like DMF is present. These clusters are removed by 100°C and show that the low temperature maximum in the DTG trace are created by these.
- ii) the water band (1622cm^{-1}) is removed by 100°C and is not present at higher temperatures.
- iii) the deconvoluted bands at approximately 1657cm^{-1} are retained at higher temperatures (until 500°C) and thus indicates the high temperature maximum in the DTG trace is due to cation-coordinated DMF molecules.

Na-SWy-2/DMF

Figures 7.61A and 7.61B show the carbonyl band in the VT-DRIFTS spectra and deconvoluted spectra of the Na-SWy-2/DMF complex, respectively. Here it is also

Figure 7.60A: VT-DRIFTS spectra of the Mg-SWy-2/DMF complex formed after 16 days in DMF vapour (1800-1500 cm^{-1}).

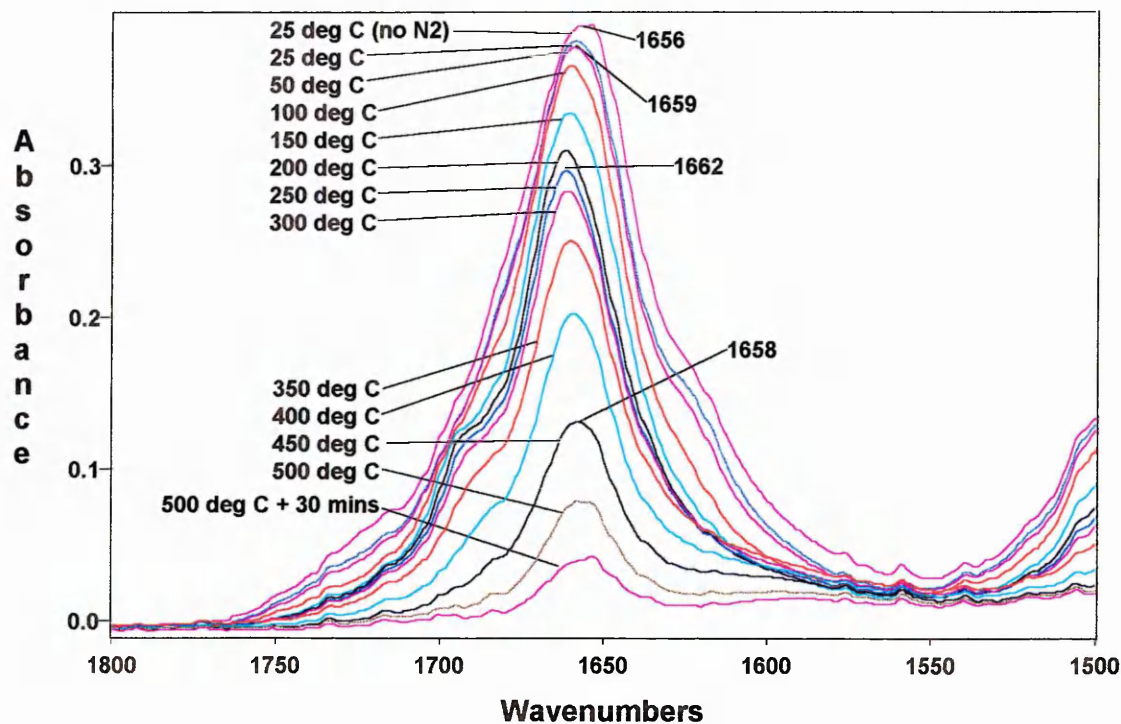


Figure 7.60B: Deconvoluted spectra of the Mg-SWy-2/DMF complex formed after 16 days in DMF vapour (1800-1500 cm^{-1}).

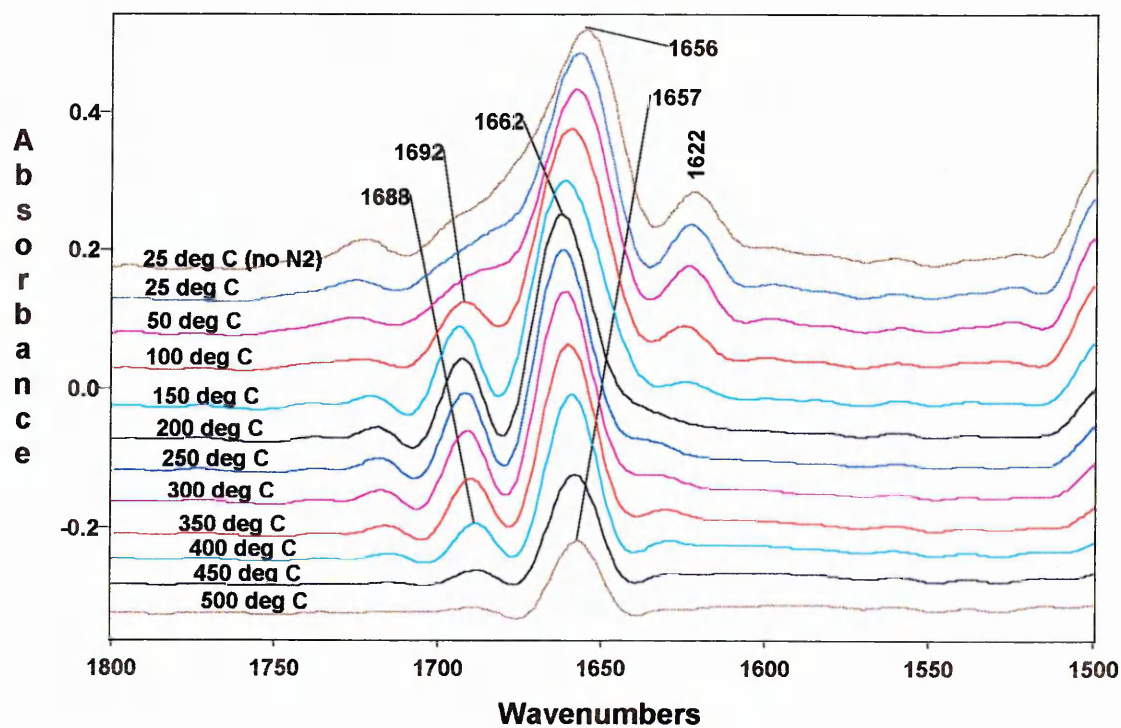


Figure 7.61A: VT-DRIFTS spectra of the Na-SWy-2/DMF complex formed after 16 days in DMF vapour (1800-1500cm⁻¹).

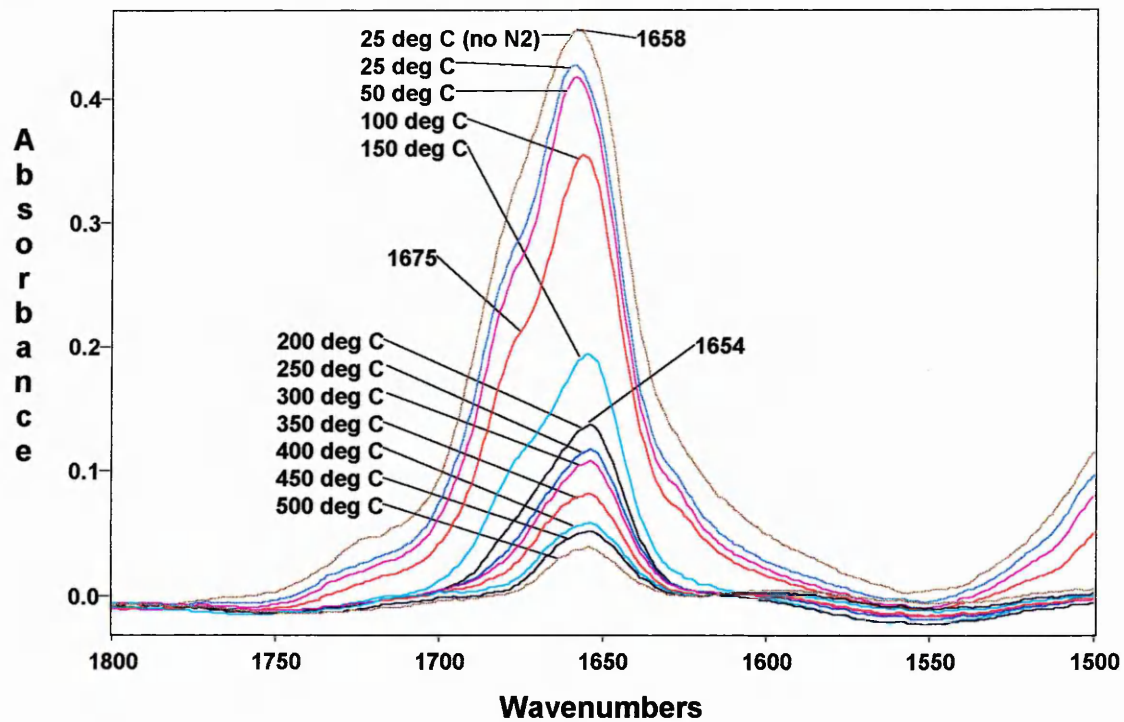
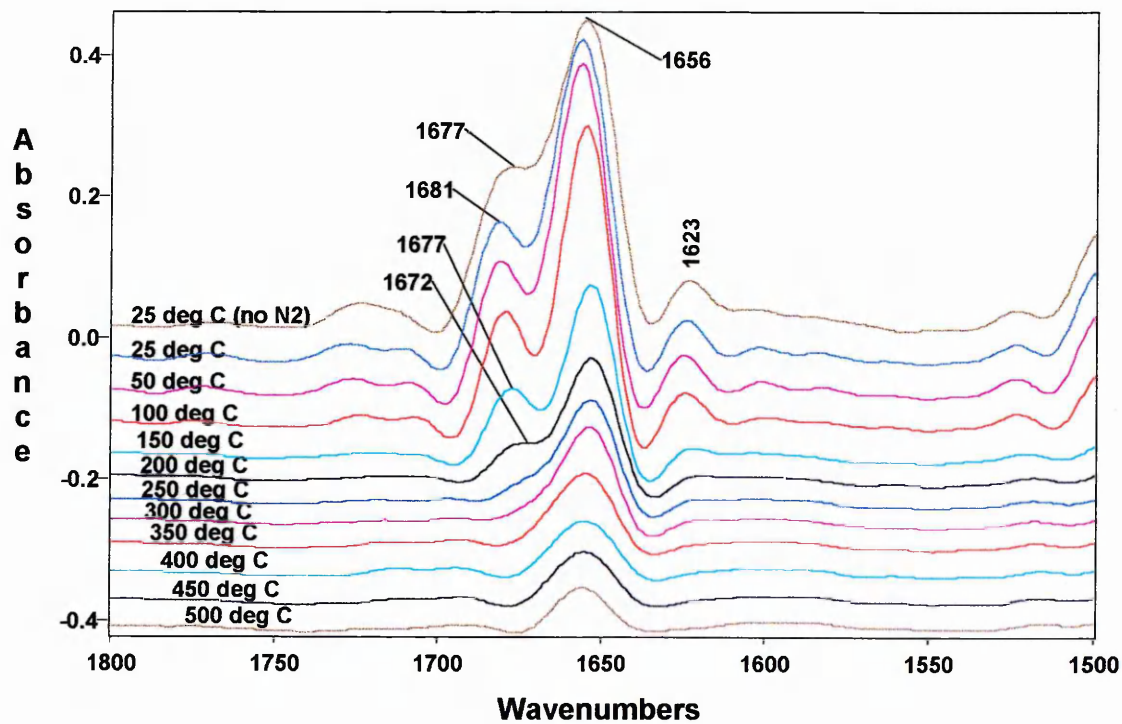


Figure 7.61B: VT-DRIFTS spectra of the Na-SWy-2/DMF complex formed after 16 days in DMF vapour (1800-1500cm⁻¹).



possible to see four components in the deconvoluted spectra. The band positioned at approximately 1677cm^{-1} indicates that liquid-like DMF is present.

K-SWy-2/DMF

Figures 7.62A and 7.62B show the carbonyl band in the VT-DRIFTS spectra and deconvoluted spectra of the K-SWy-2/DMF complex, respectively. At $25\text{-}50^\circ\text{C}$ the spectra appear identical to those of the Na-complex, but above these temperatures the bands at 1680cm^{-1} shifts to even higher frequency (usual trend is to decrease in frequency). This could be due to the effect of the Ca cations in the interlayer. The position of the band when the sample is at 250°C is the same as that in the Ca-complex (1685cm^{-1}) and therefore may account for the difference observed.

Figure 7.62A: VT-DRIFTS spectra of the K-SWy-2/DMF complex formed after 16 days in DMF vapour ($1800\text{-}1500\text{cm}^{-1}$).

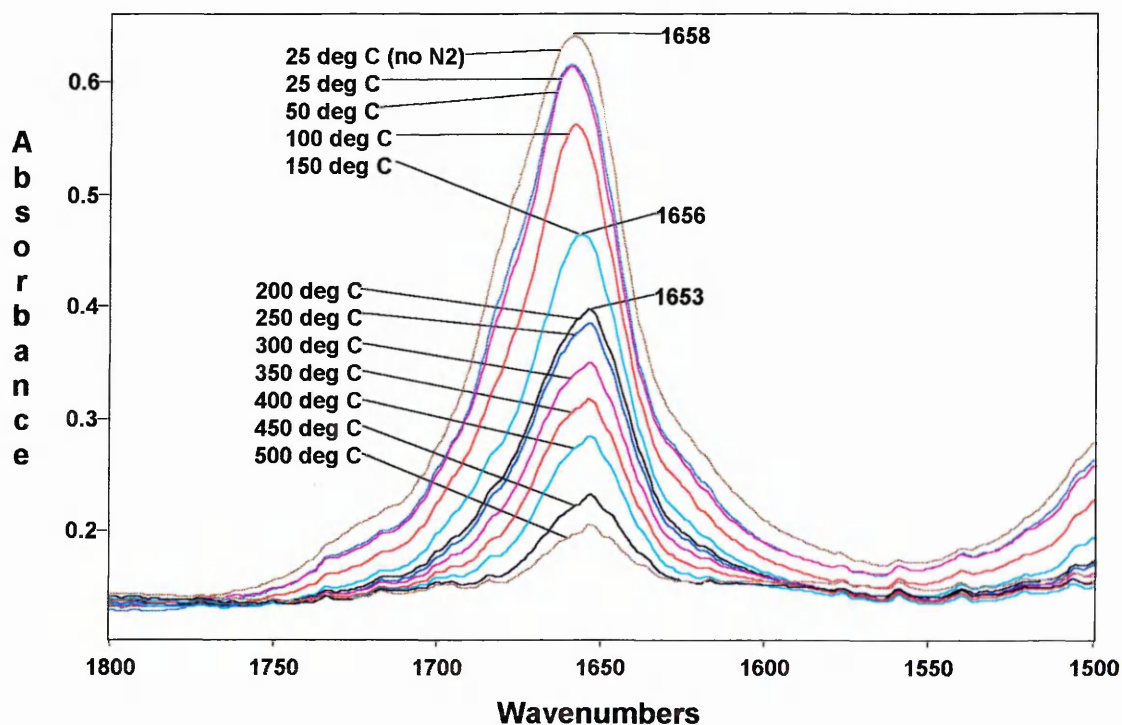
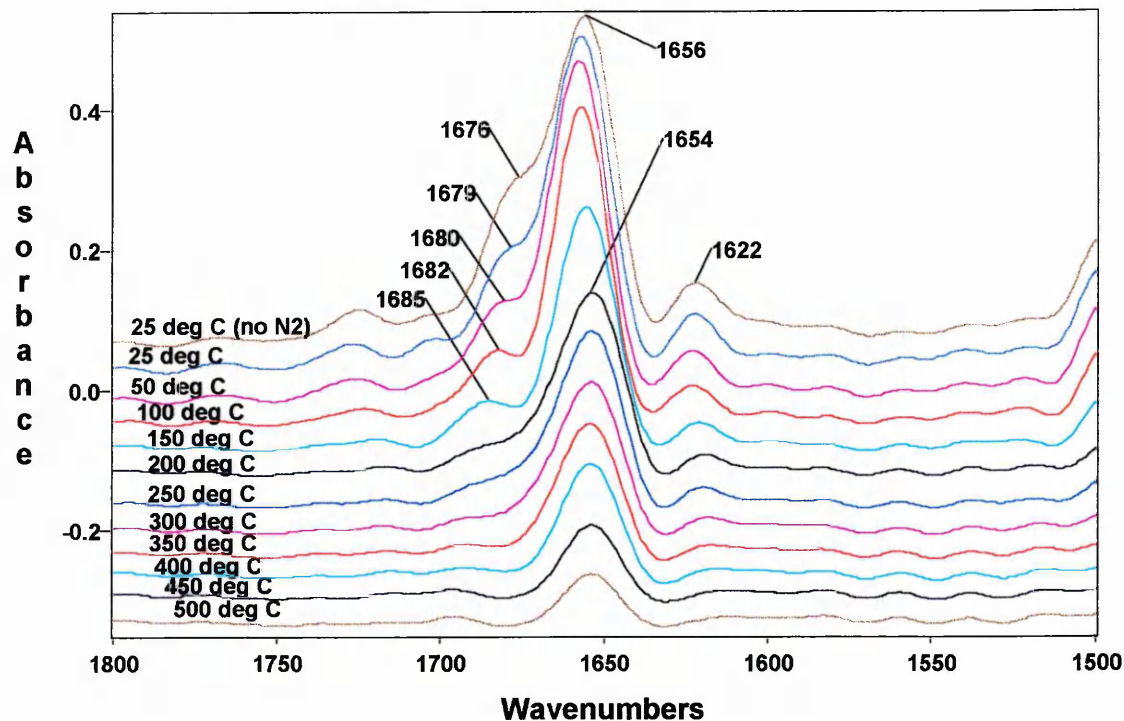


Figure 7.62B: VT-DRIFTS spectra of the K-SWy-2/DMF complex formed after 16 days in DMF vapour ($1800\text{-}1500\text{cm}^{-1}$).



7.2.9) Summary of the X-SWy-2/DMF complexes

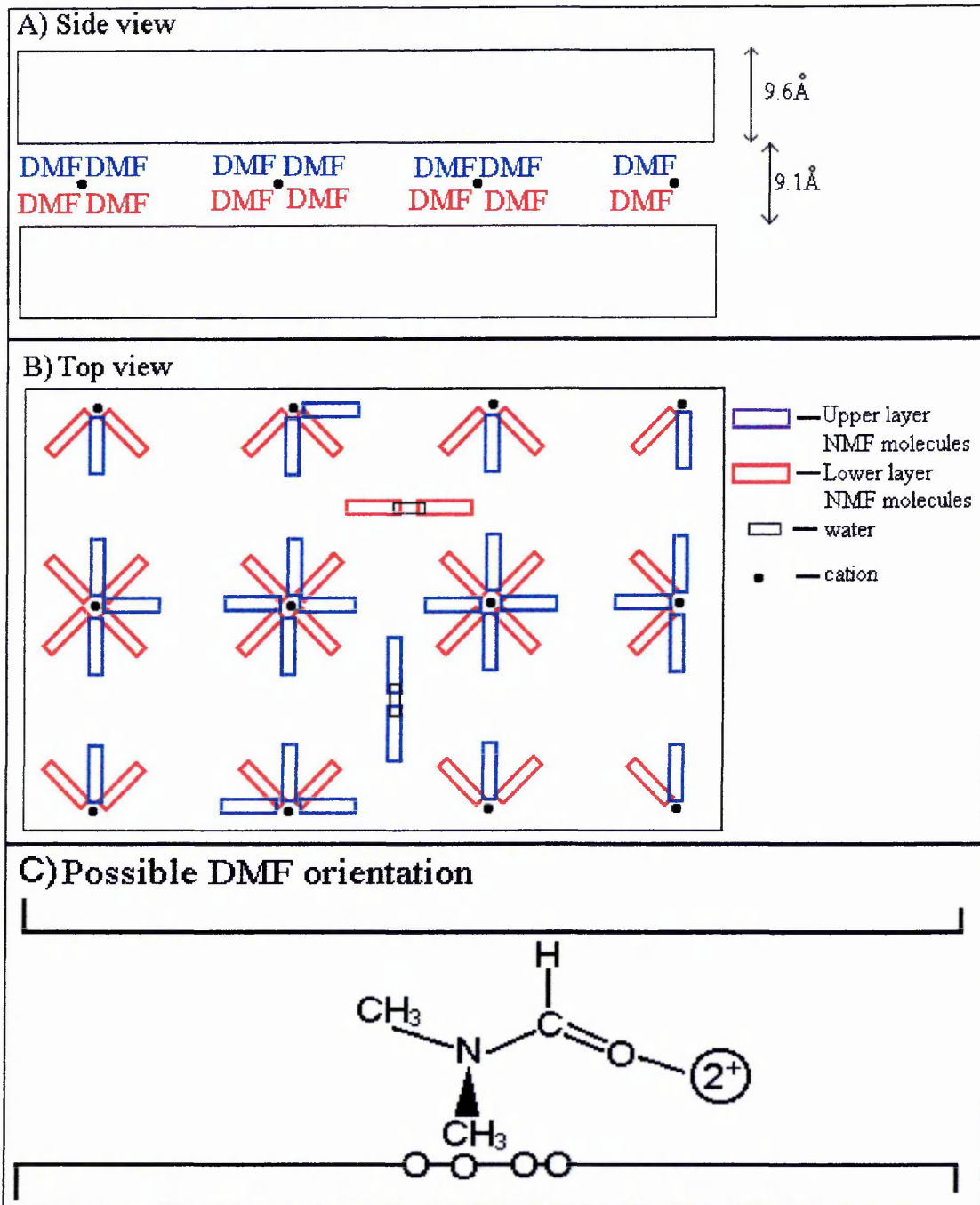
In this section the site distribution of the DMF molecules in the complexes will be discussed in reference to the experimental data.

Ca-SWy-2/DMF

The $d_{(001)}$ -spacing of the complex prior to any thermal treatment is 18.7\AA . This means the interlayer space is 9.1\AA , which is large enough for two DMF layers to be formed. Since DMF molecules do not self-associate to the same strong degree as the NMF molecules then it is unlikely that DMF molecules will interact strongly with the cation-coordinated DMF molecules. Water molecules are known to form hydrogen-bonds with DMF molecules. In fact the association between DMF-water is believed to be stronger than the association between DMF-DMF [287]. It is therefore possible that DMF-water clusters are present between clay stacks, on external clay surfaces and

perhaps in the interlayer region (figures 7.63A and B). Although the VT-DRIFTS spectra do not suggest the formation of DMF-water clusters, it is likely to occur.

Figure 7.63: Diagrammatic representation of the Ca-SWy-2/DMF complex at 35°C



Although no VT-XRD has been performed it is assumed that when the complex is heated and the low temperature maximum in the DTG trace is removed, the $d_{(001)}$ -spacing will decrease so that a single layered complex is formed. Additional evidence to support a single-layered complex is that there are approximately 3.8 DMF molecules

molecules per interlayer cation (amount calculated from TGA data). This is a small enough number to accommodate in a single layer without too much steric hindrance. At this stage (figure 7.63C) the DMF molecules will be coordinated to the cation via the carbonyl group and the C-H and methyl groups will be in close proximity to the clay layers. This is indicated in the VT-DRIFTS spectra, i.e. a shift to higher frequency is observed in the C-H stretching and (CH₃) antisymmetric stretching bands.

Since two methyl groups are present on each DMF molecule it is expected that the $d_{(001)}$ -spacing of the complex will be slightly larger than the corresponding NMF complex. However, VT-XRD experiments on the Ca-SWy-2/DMF complex need to be performed in order to determine this.

Mg-SWy-2/DMF

The $d_{(001)}$ -spacing of the complex prior to any thermal treatment is 19.2Å. This means the interlayer space (9.6Å) is large enough for two layers of DMF molecules to be formed. The site distribution of the DMF and water molecules are likely to be the same as those in the Ca-complex.

It is believed that the complex prior to the removal of the high temperature maximum in the DTG trace will only contain one layer of DMF molecules. This is likely because there are only on average 2.4 DMF molecules per interlayer cation (calculated from TGA data). These could be arranged in a single layer so no steric hindrance occurs.

The VT-DRIFTS data suggests that the $d_{(001)}$ -spacing will be smaller in the Mg-complex than the Ca-complex because the C-H stretching and (CH₃) antisymmetric stretching bands shift to a higher frequency. The shift to higher frequency could be due to the vibrational bonds becoming more restricted due to a closer proximity to the clay layers.

Na-SWy-2/DMF

The $d_{(001)}$ -spacing of the complex prior to any thermal treatment is 19.24Å, thus a

double layered complex is formed. The orientation of the DMF and water molecules will be similar to those in the Ca and Mg-complexes. The number of DMF molecules per cation in the complex prior to the removal of the high temperature maximum in the DTG trace is 1.9 (calculated from TGA data). It is therefore likely that only a single layer will be present.

K-SW_y-2/DMF

The XRD trace (figure 6.19) of the complex prior to any thermal treatment shows two peaks which represents $d_{(001)}$ -spacings of a 17.5 and 13.8Å. The peak representing the $d_{(001)}$ -spacing at 17.5Å is approximately twice as large and therefore indicates the majority of the clay layers are expanded to accommodate a double layer of DMF molecules. The remainder of the clay layers must contain a single layer of DMF molecules.

Summary

The VT-DRIFTS and VT-XRD results presented in this chapter have revealed the site distributions of both NMF and DMF when complexed with different cation-exchanged montmorillonites. In addition some of the bonding mechanisms involved have been determined.

Both NMF and DMF were found to be located in the interlayer region and are associated with exchangeable cations via their carbonyl groups. At room temperature it was found that there are two layers of DMF and NMF in the interlayer region, whereas at higher temperatures (50-170°C) only one is present.

It was expected that shifts in the carbonyl band (of both DMF and NMF) would be directly related to the polarising strength of the exchangeable cations. However such correlations were not observed.

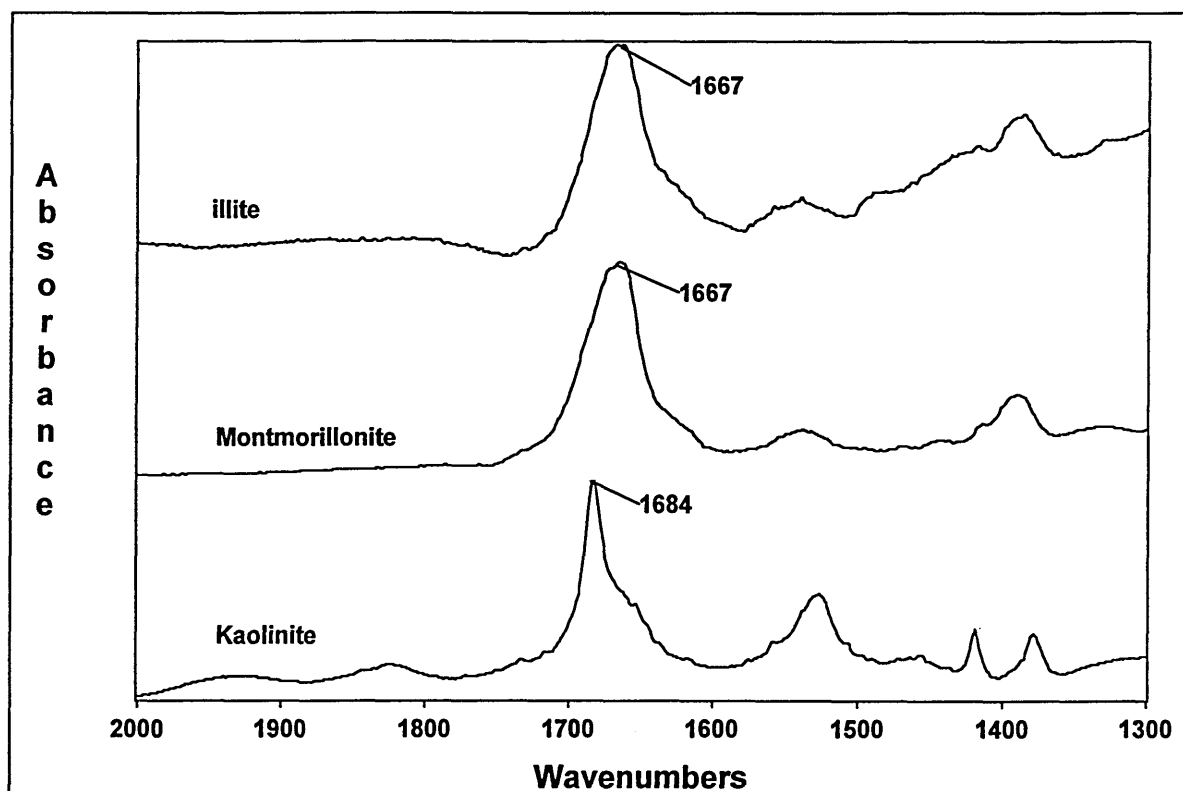
NMF molecules were found to be present associated with other NMF molecules and also as individual species. This was indicated by the position of the N-H stretching band at 3300 and 3420 cm^{-1} , respectively.

The infrared spectra was showed that at higher temperatures the C-H groups were in a restricted environment, this coincided with a reduction in the interlayer space.

7.3) The Use of Infrared Spectroscopy to Map the Surface of Reservoir Rocks

It has been shown that infrared spectroscopy can distinguish montmorillonite/NMF interactions from those involving kaolinite/NMF. This is possible by observing the change in bandwidth of the $\nu(\text{C}=\text{O})$ vibrational bond. Figure 7.64 shows the carbonyl region in the infrared spectra of the complexes formed between kaolinite/NMF, montmorillonite/NMF and illite/NMF. The figure shows that the bandwidth at half height of the kaolinite/NMF complex is much smaller than those of the montmorillonite and illite complexes. It could therefore be possible using infrared microscopy to search for a particular bandwidth at a particular frequency whilst scanning the surface of a reservoir rock in order to detect a particular clay type. The result would be an image of the surface of a reservoir rock that shows the presence and distribution of a clay. This would be similar to an image gained from SEM, but the need for expensive instrumentation and relevant expertise would be avoided. The use of FTIR microscopy and a mapping stage could therefore be used in the future to gain such an image.

Figure 7.64: Infrared spectra (transmission) of the complexes formed between kaolinite/NMF, montmorillonite/NMF and illite/NMF.



8) Conclusions

8.1) Characterisation of Minerals by DRIFTS

It has been shown that by ball milling sandstones, borehole rocks or limestones, and then dispersing in KBr, reproducible DRIFTS spectra of good quality can be obtained. These spectra represent the bulk mineralogy of the samples. It is possible to describe the mineralogy qualitatively using the characteristic infrared bands in the spectra. These descriptions agree with the mineralogy identified by other methods i.e. XRD and SEM.

It has been demonstrated that DRIFTS spectra that are specific to the surface mineralogy can be obtained by sedimentation and ultrasonication techniques. The former technique involves collecting the $<2\mu\text{m}$ fraction of a deconsolidated rock, whereas the latter involves collecting the suspension resulting from ultrasonication of a rock fragment in water after only three minutes.

Analysis of a sandstone that has undergone various degrees of crushing has shown that DRIFTS is a surface weighted technique. This is indicated by the fact a DRIFTS spectrum of a mixture of large quartz grains and clay minerals is dominated by infrared bands of the clay minerals whereas a mixture of ball milled quartz grains and clay minerals is dominated by infrared bands of both components.

The DRIFTS spectra obtained from cut and fractured surfaces are believed to be representative of the surface mineralogy and have been shown to be similar in nature, i.e. the spectra are highly distorted. The distortions for both types of surfaces are more severe in the low wavenumber region ($1800\text{-}500\text{cm}^{-1}$) than the high wavenumber region ($4000\text{-}2000\text{cm}^{-1}$). Since the DRIFTS spectra of the cut rock surfaces are similar to those of the fractured surfaces yet their physical appearance is different it is believed that cut surfaces could be used as a representative of the surface mineralogy. This is advantageous because cut surfaces are easier to prepare and the spectra obtained from these surfaces are more reproducible.

The application of PLS analysis to DRIFTS spectra of ball milled mixtures of standard minerals (dispersed in KBr) in order to gain quantitative analysis has proved to be successful. However, the presence of illite and smectite could not be distinguished as

individual components. These clay minerals needed to be detected as a combination because their DRIFTS spectra are almost identical. The application of PLS to real ball milled rock samples in order to obtain their bulk mineralogy is therefore highly feasible.

The application of PLS analysis to DRIFTS spectra of ball milled mixtures of standard minerals (not dispersed in KBr) in order to gain quantitative analysis has proved to be less successful. This is because distortion due to the collection of a higher amount of specular reflectance is observed in the spectra. It was initially thought that the distorted region ($1800\text{-}500\text{cm}^{-1}$) could not be used to gain quantitative analysis from the spectra and that only the high wavenumber region ($4000\text{-}2000\text{cm}^{-1}$) would be useful. This was not the case since a better prediction was obtained when the whole mid-infrared region ($4000\text{-}500\text{cm}^{-1}$) was used. When the whole region was used it was still not possible to quantify the amount of feldspar in the mixtures.

It is known that if PLS analysis is to be used on the DRIFTS spectra of real sandstones and reservoir rocks then a much larger model needs to be created. This will need to account for the presence of additional minerals found in such samples (e.g. mica and sulphates) and the variability of each mineral type (e.g. the polymorphs of kaolinite which are halloysite, dickite and nacrite).

8.2) Characterisation of Minerals using Chemical Probes.

The TGA results in this thesis have shown that characteristic DTG traces can be obtained from individual clay minerals. This is due to the dehydroxylation of the clay structure or the removal of water occurring in specific temperature ranges. The experimental results in this thesis have also shown that organic molecules (chemical probes) interact with different clay minerals in a variety of ways, and by differing strengths of interaction. This phenomenon has been exploited in order to develop a method of characterising clay minerals contained within sandstones and reservoir rocks. This is because the desorption of chemical probes that complex with clay minerals as they are heated leads to additional characteristic maxima in the corresponding DTG traces. Of the chemical probes studied so far, the one that produces the most characteristic DTG traces is DMF. The DTG traces obtained from

Ca, Mg, Na and K exchanged montmorillonite/DMF complexes all show characteristic maxima due to the desorption of DMF, which could be used to differentiate them in mixtures containing high percentages (>5%). TGA is not a sensitive enough technique to detect levels lower than 5% and so EGA-IR and EGA-MS have been employed to gain sensitivity. The aim of using these techniques is to obtain the same chromatogram-type traces as those of DTG traces. The results have shown that it is possible but complications have arisen due to the breakdown of DMF as it travels from the sample to the detectors. It has been shown that 2% of montmorillonite can be detected within a mixture of illite, kaolinite, chlorite and quartz. The detector responses (for both IR and MS) for this particular sample showed a good signal to noise ratio and showed that lower amounts could easily be detected.

VT-DRIFTS and VT-XRD studies in this thesis cast light on the specific interactions occurring between both NMF and DMF with different cation exchanged montmorillonites. Both molecules are bonded to exchangeable cations via their carbonyl groups. In these specific sites the NMF molecules are also bonded through their N-H group to the clay surface. These are very strong associations. The assignment of these sites have been supported by molecular modelling simulations. Two layers of NMF and DMF molecules are present in the interlayer space of their respective complexes when fully loaded. The two layers are replaced by one layer when the complex is heated at low temperatures (50-100°C).

Additional VT-DRIFTS evidence shows that NMF and DMF molecules are also associated to broken bonds and external surfaces on the exchanged montmorillonites.

8.3) Considerations for Future Work

The most suitable chemical probe studied so far is DMF, however this is not ideal because it breaks down/degrades as it leaves the clay minerals. The next step in the development stage should therefore be to find a chemical probe which is suitable. Whilst reading the literature several other possible chemical probes have been noted. One such possible chemical probe is hydrazine, this is highly volatile and is known to form very stable complexes with kaolinite [287]. Problems may occur because it

oxidises very rapidly with air during heating experiments. Another possible chemical probe could be pyridine-N-oxide since this is also known to form stable complexes with kaolinite [288]. It would be advantageous if chemical probes could be found that are specific to a mineral-type, i.e. one chemical probe for kaolinite, one chemical probe for montmorillonite, and so on. However, this is probably highly unlikely.

It may be necessary to utilise experiments that take into consideration the differences in the time required for a chemical probe to complex with a particular mineral-type. For example, it is known that intercalation of most organic molecules into kaolinite takes longer than it does into montmorillonite clays. If the desorption of a chemical probe from a mixture of montmorillonite and kaolinite was to occur in the same temperature region then it could be exposed for a limited time period so that only the montmorillonite was intercalated, and then exposed for longer so that both montmorillonite and kaolinite was intercalated. Subtraction of the amount desorbed for the limited time period from the total amount desorbed after a longer time would result in the amount of kaolinite present being determined.

The long time periods required to intercalate a chemical probe into kaolinite is a problem that needs to be overcome, since a quick method is essential. This could be achieved by preheating the sample prior to exposure to the chemical probe or heating the sample whilst exposed to the chemical probe. Preliminary TGA experiments concerning preheating Ca-exchanged montmorillonite prior to exposure to DMF have been performed, but no differences in the build up of DMF have been observed.

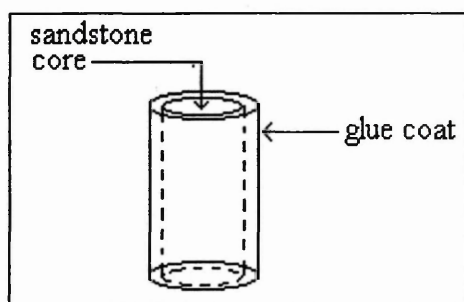
A sample does not necessarily need to be treated with only one chemical probe, two could be used. Perhaps one chemical probe will bind to both kaolinite and montmorillonite, but when in the presence of another chemical probe, the additional chemical probe will preferentially interact with only montmorillonite.

So far only crushed sandstones and powdered minerals have been studied. In the future whole rock cores need to be assessed. A problem that may occur could arise from the chemical probe not being able to be removed from the core at the same speed as from a powder. This could therefore lead to diffusional broadening and a

coalescence of characteristic maxima. The morphology of a crushed clay mineral is different to that when it is in a core (as shown by SEM). This could have an affect on their adsorption properties and this needs to be addressed.

Some of the rocks of interest will be saturated with oil and this may affect the adsorption of a chemical probe on to the clay minerals. It may therefore be necessary to clean the rock prior to exposure. It could be possible to clean the rock with a solvent that will act as a chemical probe. This will also result in a quicker method.

It is possible that the edges and sides of cores could affect the representation of the surface mineralogy within a core. This is because clay minerals that were originally blocked are now free to interact with a chemical probe. This could be overcome by coating the side of a core with some form of heat resistant glue, as shown in the diagram below:-



Once this has been established and a suitable chemical probe has been found then relations between the bulk mineralogy and surface mineralogy need to be ascertained.

8.4) Other methods

A very interesting idea for another method that could be developed is to use a sandstone or reservoir rock core as a chromatography-type column. Pulses of a molecular probe within a carrier gas could then be passed through the core. The extent of retention of the probe could then be detected and related to the minerals present within a core. It would be anticipated that a probe would interact with montmorillonite more strongly than kaolinite, and thus retain the probe in the core for

a longer period of time. Heating of the column may also be needed to help push the probe gas through. This method may have been feasible since clays have been used in High Performance Liquid Chromatography (HPLC) and Gas Chromatography (GC) columns. Tsvetkov et al. [289] used different cation-exchanged clays in HPLC columns to separate substituted benzenes. Rysselberge and Stricht [290] have demonstrated the use of clays as stationary phases in GC columns. Banosz et al. [291] studied the injection of small amounts of alkanes into the stream of a carrier gas flowing through a chromatography column filled with a clay. They studied Na, Al-exchanged montmorillonites and calcined Al-exchanged montmorillonite and showed that the retention times of the alkanes could be related to acidity and surface area. Saada et al. [292] showed that the retention times and retention volumes (volume of carrier gas needed to push a molecule through the column) corresponded to the affinity of molecular probes (alkanes) to the clay mineral in the chromatography column. Despite the limited number of samples they examined, differences between the surface properties of illites and kaolinites were apparent and moreover, larger differences were observed for a given clay mineral.

All of the above studies involved columns filled with a uniform distribution of a clay mineral. Such a distribution may not be present in a core and thus chromatographic traces may not be obtainable.

8.5) Conferences Attended

1) Third UK Colloid and Surface Science Student Meeting (University of Hull), 16-19 July 1995.

2) RSC - Analytical Division, Chemometric Group, Artificial Intelligence Applications (University of Wolverhampton), 12th February 1996.

3) Clay Mineral Group, Autumn Conference (University of Central Lancashire, Preston), 14-25 September 1995.

4) Clay Minerals Group, Spring Meeting (Sheffield Hallam University), 1-2 April 1996.

5) Infrared and Raman Discussion Group (IRDG) Third Martin and Willis Prize Meeting, and, the IRDG 150th Annual Meeting, 16-17 October 1996.

6) Fourth UK Colloid and Surface Science Student Meeting (University of Greenwich), 6-9 July 1997.

9) References

- 1) M. E. Tucker, 'Sedimentary Petrology, An Introduction', Geoscience Texts, Vol. 3, Blackwell Scientific Publications (London), 1981, 10-13.
- 2) K. C. Khilar and H. S. Fogler, Rev. Chem. Eng., 4 (1987), 41-108.
- 3) M. Azari and J. Leimkuhler, SPE 17149 (1988), 61-72.
- 4) A. Parker and C. Davidson, United States Patent, No. 4889563, 26th Dec, (1989).
- 5) Laboratory Testing Guide, (Internal Communication-SCR)(Oct 1987).
- 6) M. M. Herron, Clays Clay Miner., 34 (1986), 204-213.
- 7) H. Blatt, G. Middleton and R. Murray, 'Origin of Sedimentary Rocks', Prentice-Hall, (New Jersey), 1979.
- 8) P. H. Nelson, The Log Analyst (1994) May-June, 38-62.
- 9) D. Borling, K. Chan, T. Hughes and R. Sydanst, 'Oilfield Review-SCR' (April 1994), 44-58.
- 10) L. G. Berry and B. Mason 'Mineralogy-concepts, descriptions, determinations' W. H. Freeman & Company (London), 1959.
- 11) K. G. Cox, N. B. Price and D. Harte, 'Introduction to the Practical Study of Crystals, Minerals and Rocks', revised first edition, Mc-Graw-Hill (London), 1974, 127-134.
- 12) T. F. W. Barth, 'Feldspars', Wiley-Interscience (London), 1969.
- 13) W. F. Hower, SPE paper 4785 (Feb. 1974), New Orleans.
- 14) U. Hofmann, K. Endell and D. Wilm, Z. Kristallogr., 86 (1933), 340-348.
- 15) E. Maegdefrau and U. Hofmann, Z. Kristallogr., 98 (1937), 299-323.
- 16) S. B. Hendricks, J. Geol., 50 (1942), 276-290.
- 17) C. H. Edelman and J. C. L. Favejee, Z. Kristallogr., A102 (1940), 417-431.
- 18) Griffiths and De Hasser, 'Fourier Transform Infrared Spectrometry', John Willey and Sons (New York), 1986.
- 19) Reference 2, pp. 194-202 and 544-563.
- 20) A. M. Saffa and K. H. Michaelian, Appl. Spectrosc., 48 (1994), 871-874.
- 21) P. R. Griffiths and M. P. Fuller, 'Advances in Infrared and Raman Spectroscopy', Vol. 9, Edited by R. J. H. Clark and R. E. Hester, Heyden and Son Ltd (London), 1982.
- 22) J. M. Hollas, 'Modern Spectroscopy', 2nd Edition, John Willey and Sons, 1992.
- 23) M. B. Mitchell, 'Structure-Property relations in Polymers', 1993.
- 24) S. R. Culler, 'Fundamentals of polymer science' (Editors - P.C. Painter and M. M. Coleman), Technomic (Lancaster), 1997.
- 25) D. E. Leyden and R. S. S. Murthy, Spectroscopy, 2 (1987), 28-36.

- 26) W. W. M. Wendlandt and H. G. Hecht, 'Reflectance Spectroscopy', Interscience publishers (London), 1966.
- 27) G. Kortum, 'Reflectance Spectroscopy', Springer-Verlag (Heidelberg), 1969.
- 28) P. J. Brimmer and P. R. Griffiths, *Appl. Spectrosc.*, 42 (1987), 791-797.
- 29) D. M. Hembree and H. R. Smyrl, *Appl. Spectrosc.*, 43 (1989), 267.
- 30) K. A. Martin and J. R. Ferraro, *Appl. Spectrosc.*, 41 (1987), 45-49.
- 31) W. W. Coblenz, *Natl. Bur. Stand. (US) Tech. News Bull.*, 9 (1913), 283.
- 32) J. T. Gier, R. V. Dunkle and J. T. Bevans, *J. Opt. Soc. Am.*, 44 (1954), 558.
- 33) W. R. Blevin and W. J. Brown, *J. Sci. Instrum.*, 42 (1956), 19.
- 34) R. R. Willey, *Appl. Spectrosc.*, 30 (1976), 593.
- 35) R. R. Willey, *Applied Opt.*, 15 (1976), 1124.
- 36) M. P. Fuller and P. R. Griffiths, *Anal. Chem.*, 50 (1978), 1906.
- 37) M. P. Fuller and P. R. Griffiths, *Am. Lab.*, 10 (1978), 69.
- 38) P. J. Brimmer, P. R. Griffiths and N. J. Harrick, *Appl. Spectrosc.* 42 (1986), 258.
- 39) P. J. Brimmer and P. R. Griffiths, *Appl. Spectrosc.*, 42 (1988), 242-247.
- 40) P. W. Yang, H. H. Mantsch and F. Baudais, *Appl. Spectrosc.*, 40 (1986), 974.
- 41) M. P. Fuller, Ph.D. dissertation, Ohio University, Athens, Ohio (1980).
- 42) K. Moradi, C. Depecker and J. Corset, *Appl. Spectrosc.*, 48 (1994), 1491-1497.
- 43) D. J. J. Fraser and P. R. Griffiths, *Appl. Spectrosc.*, 44 (1990), 193-199.
- 44) S. A. Yeboah, S. H. Wang and P. R. Griffiths, *Appl. Spectrosc.*, 38 (1984), 259.
- 45) Z. Krivacsy and J. Hlavay, *Talanta*, 41 (1994), 1143-1149.
- 46) M. L. E. TeVrucht and P. R. Griffiths, *Appl. Spectrosc.*, 43 (1989), 1492-1494.
- 47) Personal communication - T Huhges (SCR).
- 48) T. L. Hughes and C. M. Methven, *SCR Manual:SCR/M/1993/003/WPC/c* (Aug 1993).
- 49) I. M. Hamadeh, S. A. Yeboah, K. A. Trumbull and P. R. Griffiths, *Appl. Spectrosc.* 38 (1984), 486-492.
- 50) R. A. Velapoldi, J. E. Tvedt and A. A. Christy, *Rev. Sci. Instrum.*, 58 (1987), 1126-1128.
- 51) R. G. Messerschmidt, *Appl. Spectrosc.*, 39 (1985), 737-739.
- 52) Z. Krivacsy and J. Hlavay, *J. Mol. Struct.*, 349 (1995), 289-292.
- 53) P. Kubelka and F. Munk, *Z. Tech. Phys.*, 12 (1931), 593.
- 54) P. Kubelka, *J. Opt. Soc. Am.*, 38 (1948), 448.
- 55) A. Tsuge, Y. Uwaminno, T. Ishizuica and K. Suzuki, *Appl Spectrosc.*, 45 (1991), 1377-1380.
- 56) A. A. Christy, O. M. Kvalheim and R. A. Velopoldi, *Vib. Spectrosc.*, 9 (1995), 19-27.

- 57) F. Boroumand, J. E. Moser and H van der Bergh, *Appl. Spectrosc.*, 46 (1992), 1874-1886.
- 58) R. G. Giovanelli, *Opt. Acta*, 2 (1955), 153.
- 59) G. V. Rozenburg, *Dokl. Akad. Nauk. SSSR*, 98 (1954), 201.
- 60) H. G. Hecht, *Appl. Spectrosc.*, 37 (1983), 348-354.
- 61) N. R. Smyrl, E. L. Fuller and G. L. Powell, *Appl. Spectrosc.*, 37 (1983), 38-44.
- 62) T. J. Horr, J. Ralston and R. St. C. Smart, *Colloids Surf.*, 64 (1992), 67-85.
- 63) Z. Krivacsy and J. Hlavay, *Spectrochim. Acta*, 50A (1994), 2197-2202.
- 64) I. M. Mamadeh and P. R. Griffiths, *Appl. Spectrosc.*, 41 (1987), 682-688.
- 65) R. L. White, *Anal Chem.* (1992), 64, 2010-2013.
- 66) R. S. S. Murthy, J. P. Blitz and D. E. Leyden, *Anal. Chem.* 58 (1986), 3167-3172.
- 67) R. L. White and A. Nair, *Chem. Mater.* 2 (1990), 742.
- 68) R. L. White, *Appl. Spectrosc.*, 47 (1993), 1492-1496.
- 69) J. A. de Haseth, *Appl. Spectrosc.*, 36 (1982), 544-552.
- 70) R. L. White, *Anal. Chem.*, 64 (1992), 2010-2013.
- 71) K. W. van Every and P. R. Griffiths, *Appl. Spectrosc.*, 45 (1991), 347-359.
- 72) R. L. White, *Appl. Spectrosc.*, 46 (1992), 1508-1513.
- 73) R. L. White, *J. Anal. Appl. Pyrolysis*, 18, 325-339.
- 74) K. R. Beebe and B. R. Kowalski, *Anal. Chem.*, 59 (1987), 1007-1017A.
- 75) L. J. Janik, J. O. Skjemstand and M. D. Raven, *Aust. J. Soil Res.*, 33 (1995), 621-636.
- 76) P. Geladi and B. R. Kowalski, *Anal. Chim. Acta*, 185 (1986), 1-17.
- 77) D. M. Haaland and E. V. Thomas, *Anal. Chem.*, 60 (1988), 1193-1202.
- 78) G. W. Brindley and G. Brown, 'Crystal Structures of Clay Minerals and their X-ray identification' Mineralogical Society, Monograph No. 5, Spottiswoode Ballantyne Ltd. (London), 1980.
- 79) B. D. Cullity, 'Elements of X-ray Diffraction', Addison Wesley (Reading), 1978.
- 80) M. P. Allen and D. J. Tildesley, 'Computer Simulation of Liquids', Clarendon Press (Oxford), 1987.
- 81) A. M. El-Shabiny, S. M. Hammad. I. A. Ibrahim and A. K. Ismail, *J. Therm. Anal.*, 46 (1996), 1421-1435.
- 82) V. Sucha, I. Kraus and J. Madejova, *Clay Miner.*, 29 (1994), 369-377.
- 83) M. D. R. Cruz and L. M. Real, *Clays Clay Miner.*, 41 (1993), 570-579.
- 84) R. C. Reynolds (Jr.) and C. H. Thomson, *Clays Clay Miner.*, 41 (1993), 66-72.
- 85) C. H. Lim, M. L. Jackson and T. Higashi, *Soil Sci. Soc. Am. J.*, 45 (1981), 433-436.

- 86) G. J. Churchman, J. S. Whitton, G. G. C. Claridge and B. K. G. Theng, *Clays Clay Miner.*, 32 (1990), 241-248.
- 87) G. J. Churchman, *Clays Clay Miner.*, 38 (1990), 591-599.
- 88) V. C. Farmer and J. D. Russel, *Spectrochim. Acta*, 20 (1964), 1149-1173.
- 89) H. W van der Marel, H. Beutelspacher, 'Atlas of Infrared Spectroscopy of Clay Minerals and their Admixtures', Elsevier Scientific publishing Company (Amsterdam), 1976.
- 90) V. C. Farmer, Mineralogical Society Monograph 4, 'The Infrared Spectra of Minerals', Adlard % Son Ltd., (Dorking), 1974.
- 91) A. Matteson and M. M. Herron, *J. Sediment. Petrol.*, 63 (1993), 1144-1148.
- 92) A. Matteson and M. H. Herron, SDR Note: ISD006-90-45, (Dec 1990).
- 93) H. Kodama and K. Oinuma, *Clays Clay Miner.*, 11 (1963), 236-249.
- 94) C. A. Callender and H. M. Dahl, *Scanning Electron Microsc.*, IV (1984), 1501-1514.
- 95) M. D. Wilson and E. D. Pittman, *J. Sediment. Petrol.*, 47 (1977), 3-31.
- 96) S. Hillier, *Clay Miner.*, 29 (1994), 665-679.
- 97) M. E. Crocker, E. C. Donaldson and L. M. Marchin, SPE11973, (1983).
- 98) F. Clegg 'Characterisation of Quarry rocks using Scanning Electron Microscopy' Internal report, Sheffield Hallam University, 1995.
- 99) H. Bennett and R. A. Reed, 'Chemical Methods of Silicate Analysis', Academic Press, (1971).
- 100) W. E. Worrall, *Clays and Ceramic Raw Materials*, 2nd Edition, Elsevier Applied Science Publishers (London), 1986.
- 101) S. J. Van Der Gaast, W. Frankema, T. H. T. Tran and R. L. Frost, *International Laboratory News*, August (1996), p. 8.
- 102) S. St. J. Warne, D. J. Morgan and A. E. Milodowski, *Thermochim. Acta*, 51 (1981), 105-111.
- 103) P. C. Lopez, H. Herrera and G. Bossi, *Thermochim. Acta*, 180 (1991), 331-340.
- 104) D. J. Morgan, S. B. Warrington and S. St. J. Warne, *Thermochim. Acta*, 135 (1988), 207-212.
- 105) A. E. Milodowski, D. J. Morgan, *Nature*, 286 (1980), 248-249.
- 106) A. J. Bloodworth, A. Hurst and D. J. Morgan, *Mem. Sci. Geol. Strasbourg*, 89 (1990), 143-148.
- 107) G. Cai, *J. Therm. Anal.*, 45 (1995), 167-176.
- 108) M. R. Holdiness. *Thermochim. Acta*, 75 (1984), 361-399.
- 109) E. K. Gibson (Jr.) and S. M. Johnson, *Thermochim. Acta*, 4 (1972) 49.
- 110) E. K. Gibson (Jr.), *Thermochim. Acta*, 5 (1973) 243.

- 111) M. Muller-Vonmoos, G. Khar and A. Rub, *Thermochim. Acta*, 20 (1977), 387.
- 112) D. M. Thornley and T. J. Primmer, *Clay Miner.*, 30 (1995), 27-38.
- 113) M. L. McKelvy and T. R. Britt, *Anal. Chem.*, 68, June (1996), 127R- 128R.
- 114) J. P. Blitz and S. M. Augustine, *Spectroscopy*, 9 (1994), 28-34.
- 115) E. A. Cloutis, M. J. Gaffey and T. F. Moslow, *Fuel*, 74 (1995), 874-879.
- 116) A. H. Delgado, R. M. Paroli and J. J. Beaudoin, *Appl. Spectrosc.* 50 (1996), 970-976.
- 117) T. T. Nguyen, L. J. Janik and M. Raupach, *Aust. J. Soil Res.*, 29 (1991), 49-67.
- 118) C. M. Methven and T. L. Hughes, SCR Departmental Note WPC/1994/390 Jan (1995).
- 119) M. J. Wilson, 'A Handbook of Determinative Methods in Clay Mineralogy', Blackie (London), 1987.
- 120) J. P. Blitz, R. S. S. Murthy and D. E. Leyden, *Appl. Spectrosc.*, 40 (1986), 829-831.
- 121) A. L. Smith, 'Applied Infrared Spectroscopy', John Willey & Sons (New York), 1979.
- 122) V. A. Bell, V. R. Citro and G. D. Hodge, *Clays Clay Miner.*, 39 (1991), 290-292.
- 123) A. La Iglesia and A. J. Aznar, *J. Mater. Sci.*, 31 (1996), 4671-4677.
- 124) T. Iwaoka and S. H. Wang and P. R. Griffiths, *Spectrochim. Acta*, 41A (1985), 37.
- 125) B. M. Moudgil, S. Mathur and S. Behl, *Colloids Surf.*, 92 (1994), 183-188.
- 126) V. S. Babu and M. S. Seehra, *Appl. Spectrosc.*, 47, 6 (1993), 830-833.
- 127) R. S. Pandurangi and M. S. Seehra, *Appl. Spectrosc.*, 46 (1992), 1719-1723.
- 128) M. Sobkowiak and P. Painter, *Energy and Fuels*, 9 (1995), 359-363.
- 129) P. C. Painter, M. M. Coleman, R. G. Jenkins, P. W. Whang and P. L. Walker (Jr.), *Fuel*, 57 (1978), 337-344.
- 130) T. Isaksson and T. Naes, *Appl. Spectrosc.*, 42 (1988), 1273-1284.
- 131) H. Martins, S. Jensen and P. Geladi, *Proc. Nordic Symp on Applied Statistics (Stavanger, Stokkand Forky, 1983)*, 205.
- 132) T. Isaksson and B. Kowalski, *Appl. Spectrosc.*, 47 (1993), 702-709.
- 133) P. M. Fredericks, J. B. Lee, P. R. Osborn and D. A. J. Swinkels, *Appl. Spectrosc.*, 39 (1985), 303-310.
- 134) P. M. Fredericks, J. B. Lee, P. R. Osborn and D. A. J. Swinkels, *Appl. Spectrosc.*, 39 (1985), 311-316.
- 135) T. J. Porro and S. C. Pattacini, *Appl. Spectrosc.*, 44, (1990).
- 136) W. Lindberg, J. A. Persson and S. Wold, *Anal. Chem.*, 55 (1983), 643.
- 137) E. Peuchant, C. Salles and R. Jensen, *Anal. Chem.*, 59 (1987), 1816.
- 138) P. Dubois, J. R. Martinez and P. Levillain, *Analyst*, 112 (1987), 1675.
- 139) H. R. Bjorsvik and E. Bye, *Appl. Spectrosc.*, 45 (1991), 771-778.

- 140) T. L. Hughes, C. M. Methven, T. G. L. Jones, S. E. Pelham, P. Fletcher and C. Hall, *Advn. Cem. Bas. Mat.*, 2 (1995), 91-104.
- 141) P. Fletcher and P. Coveney, *Advn. Cem. Bas. Mat.*, 2 (1995), 21-29.
- 142) P. Fletcher, P. V. Coveney, T. L. Hughes and C. M. Methven, SPE 28824 (1994), 1-12.
- 143) T. L. Hughes, C. M. Methven, T. G. J. Jones and S. E. Pelham, *Offshore Technology Conference-7582* (1994), 643-654.
- 144) T. Hughes, C. M. Methven, T. G. J. Jones, S. E. Pelham and P. Franklin, *Recent Advances in Oilfield Chemistry*, (SCR Magazine).
- 145) P. E. Potter, J. B. Maynard and W. A. Pryor, 'Sedimentology of shale', Springer-Verlag (New York), 1980, 7-10.
- 146) E. Leary, 'The building sandstones of the British Isles', Building Research Est. Report.
- 147) C. M. Methven and T. L. Hughes, SCR, Departmental Note:WPC/1994/390 (Jan, 1995).
- 148) D. H. Gray and R. Rex, *Proc. 14th Natl. Conf. Clays and Clay Minerals*, Berkley (1966), 355-366.
- 149) D. M. C. MacEwan, *Trans. Faraday Soc*, 44 (1947), 349-367.
- 150) G. V. Chilingarian and P. Vorabutr, *Drilling and Drilling Fluids*, Elsevier (Amsterdam), 1981.
- 151) C. Rodriguez and D. E. Bugay, *J. Pharm. Sci.*, 86 (1997), 263-266.
- 152) M. E. Essington, *Soil Sci.*, 158 (1994), 181-188.
- 153) N. V. Sastry, J. M. Sequaris and M. J. Schwuger, *J. Colloid Interface Sci.*, 171 (1995), 224-233.
- 154) E. Gonzalez-Pradas, M. Villafranca-Sanchez, M. Perez and M. Viciano, *Agrochimica*, XXXVII, (1993), 104-110.
- 155) V. Luptakova, I. Horvath, A. Perjessy and K. Pukyera, *Chem. Pap.*, 46 (1992), 157-161.
- 156) D. J. Greenland, *Soils Fert.*, XXVIII (1965), 415-425.
- 157) S. Yariv, *International Journal of Tropical Agriculture*, 6 (1988), 1.
- 158) S. Peker, S. Yapar and N. Besun, *Colloids Surf.*, 104 (1995), 249-257.
- 159) T. Barzetti, E. Selli, D. Moscotti and L. Forni, *J. Chem. Soc., Faraday Trans.*, 92 (1996), 1401-1407.
- 160) J. M. Serratosa, *Clays Clay Miner.*, 14 (1966), 385-391.
- 161) J. M. Adam, *Appl. Clay Sci.*, 2 (1987), 309-342.
- 162) J. A. Balantine, 'Chemical Reactions in Organic and Inorganic Constrained Systems', (R. Burton-Editor) Reidel (Dordrecht), 1986, 197-212.
- 163) S. B. Haderlein and R. P. Schwarzenbach, in *Transport and Reactive Processes in Aquifers*, (Editors - T. H. Dracos and F. Stauffer), Balkema (Rotterdam), 1994, 67-72.

- 164) S. B. Haderlein and R. P. Schwarzenbach, *Environ. Sci. Technol.*, 27 (1993), 316-326.
- 165) S. B. Haderlein, K. Weissmahr and R. P. Schwarzenbach, *Environ. Sci. and Technol.* (1994).
- 166) A. Naidja and P.M. Huang, *Appl. Clay Sci.*, 9 (1994), 263-266.
- 167) P. C. Zhang and D. L. Sparks, *Soil Sci. Soc., Am. J.*, 57 (1993), 340-345.
- 168) R. D. Harter and J. L. Ahrichs, *Soil Sci. Soc., Am. proc.*, 33 (1969),
- 169) M. Lacher, N. Lahav and S. Yariv, *J. Thermal Anal.*, 40 (1993), 41-57.
- 170) N. Lahav, M. Lacher and S. Yariv, *J. Thermal Anal.*, 39 (1993), 1233-1254.
- 171) S. Yariv, N. Lahav and M. Lacher, *J. Thermal Anal.*, 42 (1994), 13-30.
- 172) V. Lorprayoon and R. A. Condrate (Sr.), *Clays Clay Miner.*, 29 (1981), 71-71.
- 173) M. Bosetto, P. Arfaioli and P. Fusi, *Soil Sci.*, 155 (1993), 105-113.
- 174) D. A. Laird, E. Barriuso, R. H. Dowdy and W. C. Koskinen, *Soil Sci. Soc. Am. J.*, 158 (1994), 181-188.
- 175) B. K. G. Theng, *The chemistry of clay-organic reactions*, Adam Helgier Ltd. (London), 1974, 211-238.
- 176) M. Harper and C. J. Purnell, *Environ. Sci. Technol.*, 24 (1990), 55-62.
- 177) R. M. Barrer, *Clays Clay Miner.*, 37 (1989), 385-395.
- 178) A. Ruiz-Conde, A. Ruiz-Amil, J. L. Perez-Rodriguez, P. J. Sanchez-Soto and F. A. de la Cruz, *Clays Clay Miner.*, 45 (1997), 311-326.
- 179) T. Dashman and G. Stotzky, *Soil Biol. Biochem.*, 14 (1982), 447-456.
- 180) K. Wada, *Amer. Miner.*, 46 (1961), 78-91.
- 181) P. Sidheswaran, S. V. R. Mohan, P. Ganguli and A. N. Bhat, *Indian J. Chem.*, 26A (1987), 994-998.
- 182) P. Sidheswaran, A. N. Bhat and P. Ganguli, *Clays Clay Miner.*, 38 (1990), 29-32.
- 183) S. Olejnik, L. A. G. Aylmore, A. M. Posner, and J. Quirk, *J. Phys. Chem.*, 72 (1969), 241-249.
- 184) S. Olejnik, A. M. Posner and J. P. Quirk, *Clay Miner.*, 8 (1970), 421-434.
- 185) C. T. Johnston, G. Sposito, D. F. Bocian and R. R. Birge, *J. Phys. Chem.*, 88 (1984), 5959-5964.
- 186) M. S. Camazano and J. S. Martin, *Clays Clay Miner.*, 42 (1994), 221-225.
- 187) J. J. Tunney and C. Detellier, *Clays Clay Miner.*, 42 (1994), 552-560.
- 188) A. S. Reis (Jr.), J. de A. Simoni and A. P. Chagas, *J. Colloid Interface Sci.*, 177 (1996), 1-8.
- 189) R. E. Talbert, O. H. Fletchall, *Weeds*, 13 (1968), 46-52.
- 190) L. A. Pinck, W. H. Holton, F. E. Allison, *Soil Sci.*, 91 (1961), 22-28.

- 191) M. J. Frissel and G. H. Bolt, *Soil Sci.*, 94 (1962), 284-291.
- 192) R. E. Grim, W. H. Allaway and F. L. Cuthbert, *J. Am. Ceram. Soc.*, 30 (1947), 137-142.
- 193) D. E. Ince, C. T. Johnston and B. M. Moudgil, *Langmuir*, 7 (1991), 1453-1457.
- 194) J. V. Smith, 'Surface Chemistry of Feldspars' *Nato ASI SERIES/SERIES C*, 421 (1994), 541-593.
- 195) R. Sokoll, H. Hobert and I. Schmuck, *J. Chem. Soc., Faraday Trans. 1*, 82 (1986), 3391-3399.
- 196) T. I. Titova and L. S. Kosheleva, *Colloids Surf.*, 63 (1992), 97-101.
- 197) S. P. Zhdanov, L. S. Kosheleva and T. I. Titova, *Langmuir*, 3 (1987), 960-967.
- 198) C. M. Koretsky, D. A. Sverjensky, J. W. Salisbury and D. M. D'Aria, *Geochim. Cosmochim. Acta*, 61 (1997), 2193-2210.
- 199) M. K. Lloyd and R. F. Conley, *Clays Clay Miner.*, 18 (1970), 37-46.
- 200) A. Wiewiora and G. W. Brinley, *Proc. Int. Clay Conf., Tokyo* (1969), 723-733.
- 201) T. Mizutani, T. Takano and H. Ogoshi, *Langmuir*, 11 (1995), 880-884.
- 202) M. El-Batouti, A. A. Zaghloul, M. T. Hanna, *J. Colloid Interface. Sci.*, 180 (1996), 106-110.
- 203) J. W. Stuki, D. L. Bish (Technical Editors), and F. A. Mumpton (Managing Editor), *CMS Workshop Lectures, Vol. 3, Thermal Analysis in Clay Science* (1990), Boulder, Colorado.
- 204) B. D. Mitchell and A. C. Birnie, in R. C. Mackenzie (Editor), *Differential Thermal Analysis*, Academic Press (London), 1970, p. 611.
- 205) S. Yariv, *Thermochim. Acta*, 88 (1985), 49-68.
- 206) P. Sidheswaran, P. Ganguli and A. N. Bhat, *Thermochim. Acta*, 118 (1987), 295-303.
- 207) E. Morillo, J. L. Perez-Rodriguez, C. Real and P. J. Sanchez-Soto, *J. Thermal Anal.*, 44 (1995), 313-327.
- 208) S. Inglethorpe and D. J. Morgan, *J. Thermal Anal.*, 40 (1993), 29-40.
- 209) C. H. Rochester, *Chemistry and Industry*, 21, March 1981, 175-179.
- 210) L. H. Little, *Infrared Spectra of adsorbed species*, Academic Press (London), 1966.
- 211) S. Yariv, *Thermochim. Acta*, 274 (1996), 1-35.
- 212) S. Yariv and L. Heller, *Isr. J. Chem.*, 8 (1970), p. 935
- 213) J. A. Lercher, C. Grundling, G. Eder-Mirth, *Catal. Today*, 27 (1996), 353-376.
- 214) C. T. Johnston, T. Tipton, S. L. Trabue, C. Erickson and D. A. Stone, *Environ. Sci. Technol.*, 26 (1992), 382-390.
- 215) H. Knözinger, *Elementary Reaction Steps in Heterogeneous Catalysis*, 398 (1993), 267-285.

- 216) R. W. Parker and R. L. Frost, *Clays Clay Miner.*, 44 (1996), 32-40.
- 217) D. E. Leyden and K. G. Proctor, *The Colloid Chemistry of Silica (ACS)*, 13 (1994) 257-267.
- 218) D. H. Lee, R. A. Condrate (Sr.), J. S. Reed, *J. Mater. Sci.*, 31 (1996), 471-478.
- 219) D. D. Davies, J. E. Kilduff, S. L. Koontz, *Spectrochim. Acta*, 47A (1991), 299-308.
- 220) A. A. Davydov and A. A. Budneva, *Kinet. Catal.*, 36 (1995), 719-724.
- 221) T. J. Horr, J. Ralston and R. St. C. Smart, *Colloids Surf.*, 63 (1992), 21-28.
- 222) C. Breen and B. Rock, *Clay Miner.*, 29 (1994), 179-189.
- 223) J. Cenens and R. A. Schoonheydt, *Clays Clay Miner.*, 36 (1988), 214-224.
- 224) S. Akyuz, T. Akyuz, J. E. D. Davies, K. Esmer and A. E. Ozel, *J. Raman Spectrosc.*, 26 (1995), 883-888.
- 225) D. T. B. Tennakoon, R. Schlogl, T. Rayment, J. Klinowski, W. Jones and J. M. Thomas, *Clay Miner.*, 18 (1983) 357-371.
- 226) M. Lipsicas, C. Straley, P. M. Costanzo and R. F. Giese, *J. Colloid Interface Sci.*, 107 (1985), 221-230.
- 227) M. Cruz, M. Letellier and J. J. Fripiat, *J. Chem. Phys.*, 69 (1978), 2018-2077.
- 228) M. Lipsicas, R. Raythatha, R. F. Giese (Jr.) and P. M. Costanzo, *Clays Clay Miner.*, 34 (1986), 635-644.
- 229) S. Hayashi, *J. Phys. Chem.*, 99 (1995), 7120-7129.
- 230) M. Gabor, M. Toth, J. Kristof, G. K. Hiller, *Clays Clay Miner.*, 43 (1995), 223-228.
- 231) C. Breen, A. T. Deane and J. J. Flynn, *Clay Miner.*, 22 (1987), 169-178.
- 232) G. L. Keldson, J. B. Nicholas, K. A. Carrado and R. E. Winans, *J. Phys. Chem.*, 98 (1994), 279-284.
- 233) E. S. Boek, P. V. Coveney and N. T. Skipper, *Langmuir*, 11 (1995), 4629-4631.
- 234) N. T. Skipper, F-G. C. Chang and G. Sposito, *Clays Clay Miner.*, 43 (1995), 285-293.
- 235) N. T. Skipper, G. Sposito and F-G. C. Chang, *Clays Clay Miner.*, 43 (1995), 294-303.
- 236) A. Delville, *J. Phys. Chem.*, 99 (1995), 2033-2037.
- 237) S. Karaborni, B. Smit, W. Heiding, J. Urai and E. von Oort, *Science*, 271 (1996), 1102-1104.
- 238) E. S. Boek, P. V. Covney and N. T. Skipper, *J. Am. Chem. Soc.*, 117 (1995), 12608-12617.
- 239) S. Olejnik, A. M. Posner and J. P. Quirk, *Clays Clay Miner.*, 22 (1974), 361-365.
- 240) A. Kats, *Philips Res. Repts*, 17 (1962), 133-195.
- 241) T. Delineau, T. Allard, J. P. Muller, O. Barres, J. Yvon and J. M. Cases, *Clays Clay Miner.*, 42 (1994), 308-320.

- 242) S. Petit and A. Decarreau, *Clay Miner.*, 25 (1990), 181-196.
- 243) P. G. Rouxhet, N. Samundacheata, H. Jacobs and O. Anton, *Clay Miner.*, 12 (1977), 171-180.
- 244) J. Madejova, P. Komadel and B. Cícel, *Clay Miner.*, 29 (1994), 319-326.
- 245) A. Matteson and M. M. Herron, 'Quantitative mineral analysis by FT-IR', Research Note (Schlumberger Dowell Research) ISD-004-93-30 May 17 (1993).
- 246) R. J. Barnes, M. S. Dhanoa and S. J. Lister, *Appl. Spectrosc.*, 43 (1989), 772-777.
- 247) M. T. McKenzie and J. L. Koenig, *Appl. Spectrosc.*, 39 (1985), 408-412.
- 248) S. R. Culler, M. T. McKenzie, L. J. Fina, H. Ishida and J. L. Koenig, *Appl. Spectrosc.*, 38 (1984), 791-795.
- 249) Personal communication - T. Hughes (SCR).
- 250) R. T. Graf, J. L. Koenig and H. Ishida, *Appl. Spectrosc.*, 39 (1985), 405-408.
- 251) Personal communication - T. Hughes (SCR).
- 252) R. S. S. Murthy and D. E. Leyden, *Anal. Chem.*, 58 (1986), 1228-1233.
- 253) C. C. Perry, X. Li, *J. Chem. Soc. Faraday Trans*, 87 (1991), 761-766.
- 254) J. L. Post, P. N. Noble, *Clays Clay Miner.*, 41 (1993), 639-644.
- 255) G. R. Hunt, *Geophysics*, 42 (1977), 501-513.
- 256) W. D. Keller, E. E. Pickett and A. L. Reesman, *Proc. Int. Clay. Conf.*, Jerusalem, 1 (1966), 75-85.
- 257) R. C. MacKenzie, *The Differential Thermal Investigations of Clays*, Mineralogical Society (London), 1957.
- 258) R. L. Frost and A. M. Vassallo, *Clays Clay Miner.*, 44, (1996), 635-651.
- 259) A. E. Mildowski, D. J. Morgan and S. St. J. Warne, *Thermochim. Acta*, 152 (1989), 279-297.
- 260) P. J. R. Uwins, I. D. R. Mackinnon, J. G. Thompson and A. J. E. Yago, *Clays Clay Miner.*, 41 (1993), 707-717.
- 261) D. N. Hinckley, *Clays Clay Miner.*, 11 (1963), 229-235.
- 262) A. Plancon and C. Zacherie, *Clay Miner.*, 25 (1990), 249-260.
- 263) C. Breen, *Clay Miner.*, 26 (1991), 487-496.
- 264) C. Breen, *Clay Miner.*, 26 (1991) 473-386.
- 265) J. A. Ballantine, P. Graham, I. Patel, J. H. Purnell, K. J. Williams and J. Thomas, *Proc. of the International Clay Conf.*, Denver, 1985, The Clay Minerals Society, (1987), 311-318.
- 266) R. M. Carr and H. Chih, *Clay Miner.*, 9 (1971), 153-166.
- 267) P. M. Costanzo and R. F. Giese (Jr.), *Clays Clay Miner.*, 38 (1990), 160-190.
- 268) G. J. Churchman and B. K. G. Theng, *Clay Miner.*, 19 (1984), 161-175

- 269) J. L. Bishop, C. M. Pieters and J. O. Edwards, *Clays Clay Miner.*, 42 (1994), 702-716.
- 270) N. I. E. Shewring, T. G. J. Jones, G. Maitland and J. Yarwood, *J. Colloid Interface Sci.*, 176 (1995), 308-317.
- 271) L. Yan, C. B. Roth and P. F. Low, *Langmuir*, 12 (1996), 4421-4429.
- 272) L. Lerot and P. F. Low, *Clays Clay Miner.*, 24 (1976), 191-199.
- 273) C. T. Johnston, G. Sposito and C. Erickson, *Clays Clay Miner.*, 40 (1992), 722-730.
- 274) S. Olejnik, A. M. Posner and J. P. Quirk, *Clays Clay Miner.*, 19 (1971), 83-94.
- 275) D. E. De Graaf and G. B. B. M. Sutherland, *J. Chem. Phys.*, 26 (1957), 716-717.
- 276) G. Forarasi and A. Balaza, *J. Mol. Struct. (Theochem.)*, 133 (1985), 105-123.
- 277) S. A. Tahoun and M. M. Mortland, *Soil Sci.*, 102 (1965), 314-321.
- 278) T. Miyazawa, *J. Mol. Spectrosc.*, 4 (1960), 168-172.
- 279) A. Balaza, *J. Mol. Spectrosc. (Theochem.)*, 153 (1987), 103-120.
- 280) S. Ataka, H. Takeuchi and M. Tasumi, *J. Mol. Struct.*, 113 (1984), 147-160.
- 281) S. A. Tahoun and M.M. Mortland, *Soil Sci.*, 102 (1965), 248-254.
- 282) O. D. Bonner and C. F. Jordan, *Physiol. Chem. Phys.* 8 (1976), 293-301.
- 283) W. E. Waghorne and H. Rubalcava, *J. Chem. Soc. Faraday Trans.*, 1, 78 (1982), 1199-1207.
- 284) S. Affrosman, D. R. Armstrong, D. Robb and J. A. Treverton, *Langmuir*, 11 (1995), 2060-2064.
- 285) A. F. Diorio, E. Lippincott and L. Mandelkern, *Nature*, 195 (1962), 1296-1297.
- 286) T. C. Jao, I. Scott and D. Steele, *J. Mol. Spectrosc.*, 92 (1982), 1-17.
- 287) Y-T. Lee, *J. Raman Spectrosc.*, 28 (1997), 45-51.
- 288) C. T. Johnston, *ACS Symposium Series*, 415 (1989), 432-454.
- 289) S. Olejnik, A. M. Posner and J. P. Quirk, *Spectrochim. Acta*, 27A (1971), 2005-2009.
- 290) F. Tsvetkov, U. Mingelgrin and M. Gal, *J. Thermal Anal.*, 42 (1994), 113-129.
- 291) J. Van Ryselberge and M. Van der Strict, *Nature* 193 (1962), 1281.
- 292) T. J. Badosz, J. Jagiello, B. Anderson and J. A Schwarz, *Clays Clay Miner.*, 40 (1992), 306-310.
- 293) A. Saada, E. Papirer, H. Balard and B. Stiffert, *J. Colloid. Interface. Sci.*, 175 (1995), 212-218.

Appendix 1

A1) DRIFTS spectra of ball milled borehole rocks

Figure A1.1 shows the DRIFTS spectrum of ball milled borehole rock RR3, this is very similar to that of RR2. It has a slightly higher clay/quartz ratio as indicated by the intensity ratios between the bands at 3620 and 1871cm^{-1} , and also has a higher amount of feldspar as indicated by the band at 730cm^{-1} . Residual oil in the rock is also present since C-H stretching bands are observed between 3000 - 2800cm^{-1} . The DRIFTS spectrum of RR4 (figure A1.2) is very similar to that of RR3. A slightly lower amount of illite is present, and no bands due to feldspar are observed indicating it is absent. The DRIFTS spectrum of RR5 (figure A1.3) is very similar to that of RR1 but has a higher clay/quartz ratio (as indicated by the intensity ratios between the bands at 3620 and 1871cm^{-1}). A large amount of kaolinite is present since the bands at 3695 , 3620 , 944 and 915cm^{-1} are very intense. Carbonate is also present as indicated by the band at 1483cm^{-1} . XRD experiments showed a small amount of illite to be present in the rock, this is not observed clearly in the DRIFTS spectrum since no enhancement in the band at 3620 relative to the band at 3695cm^{-1} is observed, however the broad band between 3500 - 3000cm^{-1} is quite intense and thus indicates its presence (Note the difference in this region to the four hydroxyl bands of kaolinite in the spectrum of RR6 which contains no illite). The DRIFTS spectrum of RR6 (figure A1.4) shows a high proportion of kaolinite and quartz.

Figure A1.1: DRIFTS spectrum of ball milled borehole rock RR3

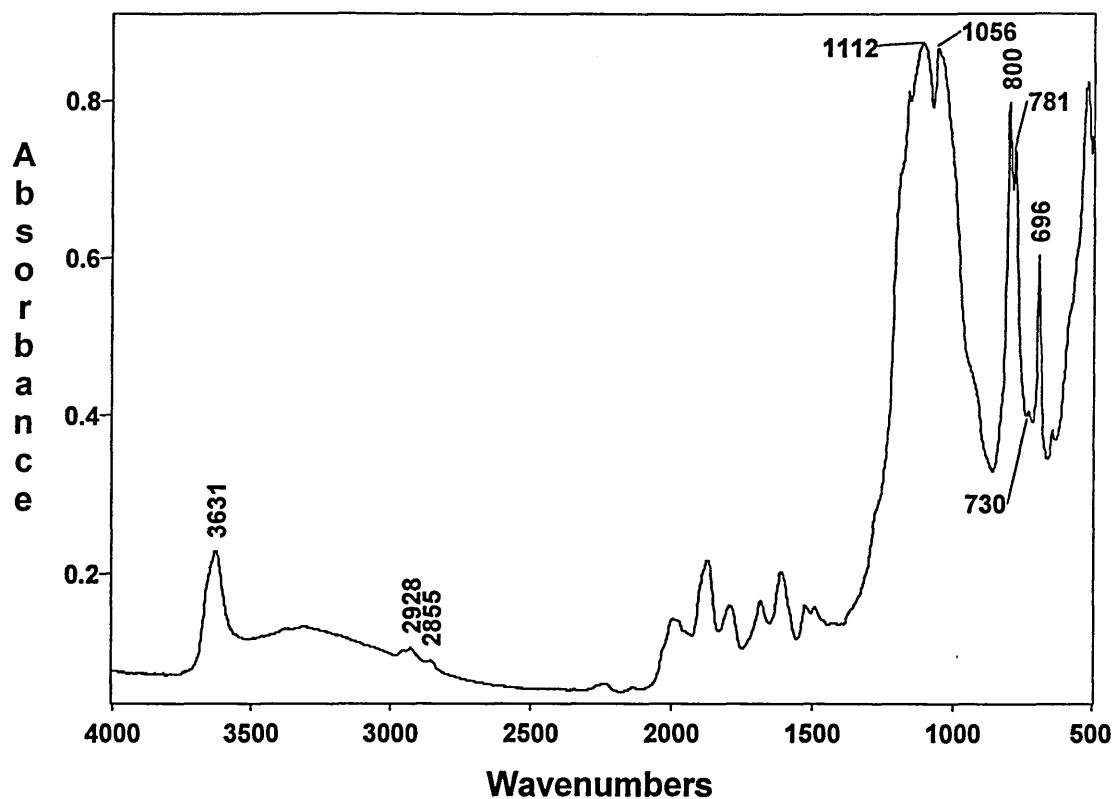


Figure A1.2: DRIFTS spectrum of ball milled borehole rock RR4

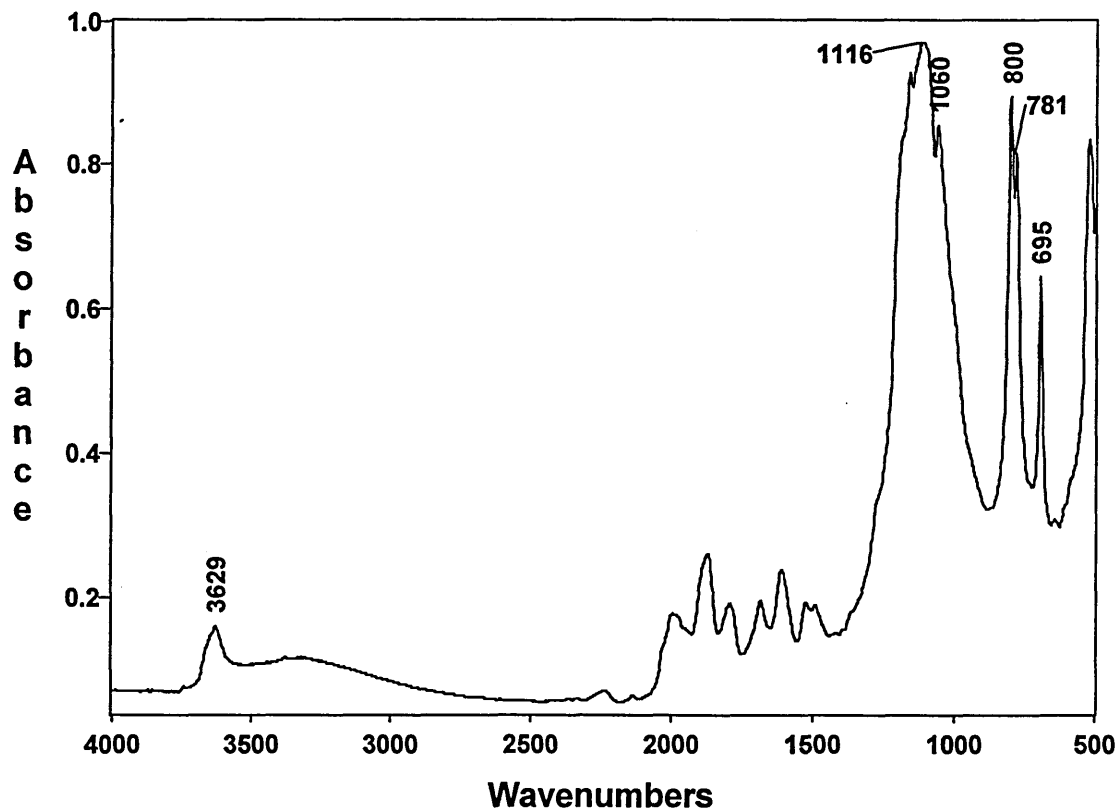


Figure A1.3: DRIFTS spectrum of ball milled borehole rock RR5

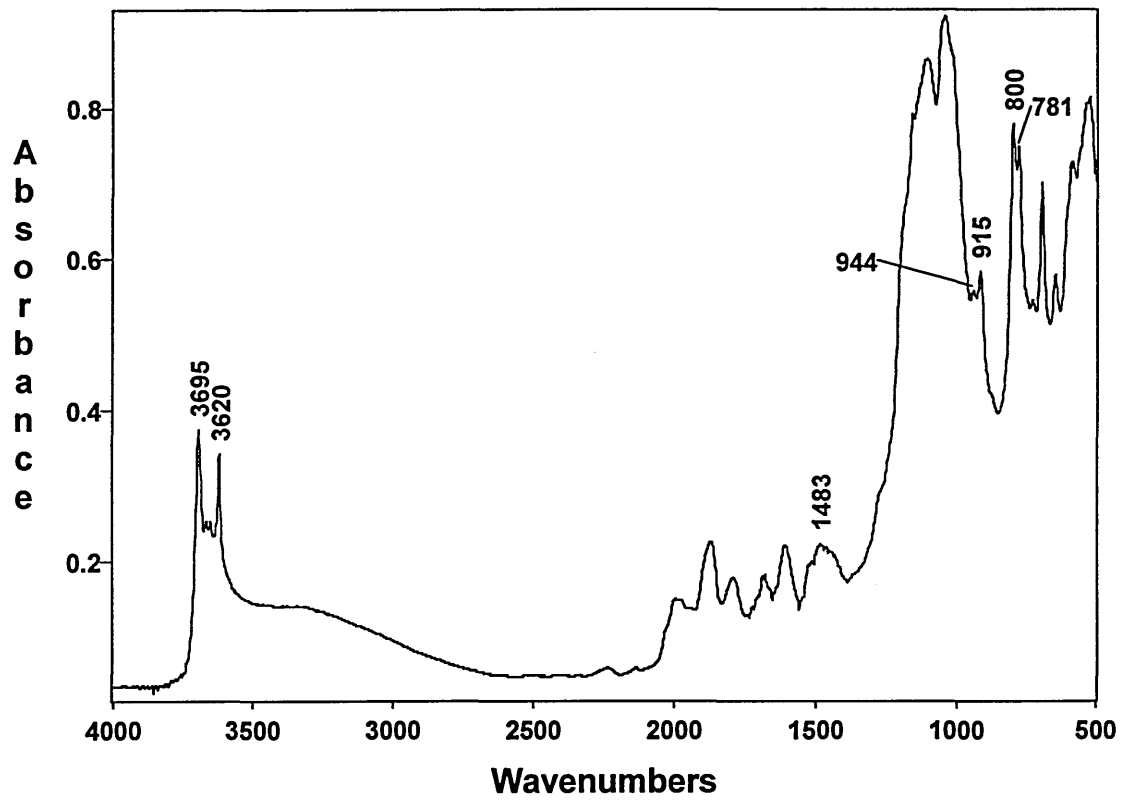


Figure A1.4: DRIFTS spectrum of ball milled borehole rock RR6

